Journal of Biological Regulators & Homeostatic Agents
Volume 28, No. 4, October - December, 2014

CONTENTS

Editorials

R. Jerath, V.A. Barnes and M.W. Crawford. Mind-body response and neurophysiological changes during stress and meditation: central role of homeostasis..... 545

M. Santoni, M. Scarpelli, R. Mazzucchelli, A. Lopez-Beltran, L. Cheng, S. Cascinu and R. Montironi. Targeting prostate-specific membrane antigen for personalized therapies in prostate cancer: morphologic and molecular backgrounds and future promises..... 555

S. Esposito, L. Castellazzi and F. Garbarino. Can probiotic administration during pregnancy and the first year of life effectively reduce the risk of infections and allergic diseases in childhood?..... 565

Original articles

R. Saluja, T. Hawro, J. Eberle, M.K. Church and M. Maurer. Interleukin-33 promotes the proliferation of mouse mast cells through ST2/MyD88 and p38 MAPK-dependent and Kit-independent pathways..... 575

J.S. Keum, M.A. Jaffa, L.M. Luttrell and A.A. Jaffa. Novel mechanism of plasma prekallikrein (PK) activation by vascular smooth muscle cells: evidence of the presence of PK activator..... 587

Y. Yoshino, K. Kohara, M. Abe, S. Ochi, Y. Mori, K. Yamashita, M. Igase, Y. Tabara, T. Mori, T. Miki and S. Ueno. Missense variants of the alanine: glyoxylate aminotransferase 2 gene correlated with carotid atherosclerosis in the Japanese population..... 605

X-C. Xu, Y-H. Zhang, W-B. Zhang, T. Li, H. Gao and Y-H. Wang. MicroRNA-133a functions as a tumor suppressor in gastric cancer..... 615

B. Kempisty, A. Ziółkowska, S. Ciesiółka, H. Piotrowska, P. Antosik, D. Bukowska, M. Nowicki, K.P. Brüssow and M. Zabel. Study on connexin gene and protein expression and cellular distribution in relation to real-time proliferation of porcine granulosa cells..... 625

D. Bukowska, B. Kempisty, P. Zawierucha, K. Jopek, H. Piotrowska, P. Antosik, S. Ciesiółka, M. Woźna, K.P. Brüssow and J.M. Jaśkowski. Microarray analysis of inflammatory response-related gene expression in the uteri of dogs with pyometra..... 637

F-Q. Hu, T. Qiao, X. Xie, R. Hu and H-B. Xiao. Knockdown of the inflammatory factor Pentraxin-3 suppresses growth and invasion of lung adenocarcinoma through the AKT and NF-Kappa B pathways..... 649

J. Pamuła-Piłat, T. Rubel, I.K. Rzepecka, M. Olbryt, R. Herok, A. Dansonka-Mieszkowska, E. Grzybowska and J. Kupryjańczyk. Gene expression profiles in three histologic types, clear-cell, endometrioid and serous ovarian carcinomas..... 659

L. Zhao, W. Guan, Y. Han and Y. Zhao. Comparative study on CT perfusion parameters of different types of lung cancer before and after chemoradiotherapy..... 675

L. Liu, H. Li and X. Lv. The mechanism and significance of E-cadherin, anti-apoptosis B-cell lymphoma-2 protein and sE-cadherin roles in cancer..... 683

N.D. Mattis, J.W. Jay, G.W. Barnett, J.J. Rosaldo, E.W. Howerth, J.C. Means and W.E. Gato. Profile of select hepatic insulin signaling pathway genes in response to 2-aminoanthracene dietary ingestion..... 693

G. Vidotto, A. Catalucci, R. Roncone, M.C. Pino and M. Mazza. Neural correlates of observation of disgusting images in subjects with first episode psychosis and post-traumatic stress disorder..... 705

N.M. Malara, F. Givigliano, V. Trunzo, L. Macrina, C. Raso, N. Amodio, S. Aprigliano, A.M. Minniti, V. Russo, L. Roveda, M.L. Coluccio, M. Fini, P. Voci, U. Prati, E. Di Fabrizio and V. Mollace. *In vitro* expansion of tumour cells derived from blood and tumour tissue is useful to redefine personalized treatment in non-small cell lung cancer patients..... 717

C. Neglia, N. Agnello, A. Argentiero, G. Chitano, G. Quarta, I. Bortone, G. Della Rosa, A. Caretto, A. Distante, A. Colao, C. Di Somma, A. Migliore, R.S. Auriemma and P. Piscitelli. Increased risk of osteoporosis in postmenopausal women with type 2 diabetes mellitus: a three-year longitudinal study with phalangeal QUS measurements..... 733

C.F. Orsi, C. Sabia, A. Ardizzoni, B. Colombari, R.G. Neglia, S. Peppoloni, G. Morace and E. Blasi. Inhibitory effects of different lactobacilli on *Candida albicans* hyphal formation and biofilm development..... 743

M. Fogli, F. Caccuri, ML. Iaria, C. Giagulli, S. Corbellini, F. Campilongo, A. Caruso and S. Fiorentini. The immunomodulatory molecule pidotimod induces the expression of the NOD-like receptor NLRP12 and attenuates TLR-induced inflammation..... 753

F. Mastrangelo, R. Vinci, G. Falco, L. Tettamanti, S. Tetè†, A. Tagliabue and E. Gherlone. Nitric oxide synthase evaluation in oral precancerous and cancerous lesions..... 767

L. Menghini, L. Leporini, G. Pintore, C. Ferrante, L. Recinella, G. Orlando, M. Vacca and L. Brunetti. A natural formulation (Imoviral™) increases macrophage resistance to LPS-induced oxidative and inflammatory stress *in vitro*..... 775

Letters to the Editor

A.A. Chokoeva, G. Tchernev, C. Tana, J. Ananiev and U. Wollina. Sarcoid-like pattern in a patient with tuberculosis..... 783

J. Ananiev, M. Penkova, G. Tchernev, A.A. Chokoeva, S. Philipov, C. Tana, M. Gulubova and U. Wollina. Macrophages and dendritic cells in the development of liver injury leading to liver failure..... 789

D. De Berardis, C. Conti, F. Iasevoli, A. Valchera, M. Fornaro, M. Cavuto, M. Brucchi, G. Perna, M. Pompili, A. Modabbernia, G. Lucidi, M. Mazza, G. Martinotti and M. Di Giannantonio. Alexithymia and its relationships with acute phase proteins and cytokine release: an updated review..... 795

L. Lo Muzio, G. Pannone, A. Santarelli, L. Lo Russo, A. De Lillo, C. Rubini, F. Bambini, P. Bufo, M. Dioguardi and M. Procaccini. Expression of Poly(ADP-ribose) polymerase in bone regeneration.....

JOURNAL OF BIOLOGICAL REGULATORS & HOMEOSTATIC AGENTS Vol. 28, no. 4, 545-554 (2014)

EDITORIAL

MIND-BODY RESPONSE AND NEUROPHYSIOLOGICAL CHANGES DURING STRESS AND MEDITATION: CENTRAL ROLE OF HOMEOSTASIS

R. JERATH[1], V.A. BARNES[2] and M.W. CRAWFORD[1]

[1]Augusta Women's Center, Augusta, GA, USA; [2]Georgia Prevention Institute, Georgia Regents University, Augusta, GA, USA

Received December 17, 2013 – Accepted July 31, 2014

Stress profoundly impacts quality of life and may lead to various diseases and conditions. Understanding the underlying physiological and neurological processes that take place during stress and meditation techniques may be critical for effectively treating stress-related diseases. The article examines a hypothetical physiological homeostatic response that compares and contrasts changes in central and peripheral oscillations during stress and meditation, and relates these to changes in the autonomic system and neurological activity. The authors discuss how cardiorespiratory synchronization, which occurs during the parasympathetic response and meditation, influences and modulates activity and oscillations of the brain and autonomic nervous system. Evidence is presented on how synchronization of cardiac and respiratory rates during meditation may lead to a homeostatic increase in cellular membrane potentials in neurons and other cells throughout the body. These potential membrane changes may underlie the reduced activity in the amygdala, and other cortical areas during meditation, and research examining these changes may foster better understanding of the restorative properties and health benefits of meditation.

Modern life's demands lead to chronic stress and increased prevalence of stress-related conditions and stress has been found to be a contributing factor in human disease (1). Extensive research has been conducted on stress and the anxiety-reducing effects of meditation (2) but very little is known about the underlying processes. This article aims to provide insight into the physiological activity behind the stress response by comparing stress and meditation states in terms of oscillatory activity throughout the body and brain. This activity is then related to the proposed hypothesis of changes in cellular membrane potentials. These changes are suggested to underlie the restorative and health benefits of meditation. This proposed mechanism is similar to the widespread hyperpolarization that may underlie the restorative properties of sleep (3). Deeper knowledge of respiratory homeostasis may foster better understanding of physiological rhythms of the body in various states of consciousness. Additionally, it may further knowledge regarding the efficacy of interventions, such as meditation, for stress-related conditions.

Heart rate variability: influence of respiratory and cardiac oscillations

Respiratory and heart rate variations influence sympathovagal balance which in turn influences

Key words: oscillations, sympathovagal balance, stress, meditation

Mailing address: Dr Ravinder Jerath,
Augusta Women's Center,
2100 Central Ave., Suite 7
Augusta, GA 30904, USA
Tel.: +1 706 736 5378
Fax: +1 706 364 1416
e-mail: rj605r@aol.com

0393-974X (2014)

cardio-respiratory activity and hemodynamics (4). Respiration profoundly influences sympathetic and parasympathetic responses. The shift of low frequency (LF, 0.1 Hz) to high frequency (0.3 Hz) heart rate variability (HRV) is indicative of a parasympathetic shift in sympathovagal balance. It has been established that HRV can be used as a proxy for vagal tone; however, the use of HRV to estimate sympathetic tone has been debated (5). Following *Vipassana* meditation, a mindfulness-based approach, there is a decrease in LF power (6). The increase in normalized high frequency (HF) which is the ratio of HF to LF and the decrease in Traube-Hering Mayer waves (neural oscillations coupled with respiration that are associated with LF power), indicate that the decrease in LF power following *Vipassana* influences overall HRV by increasing the ratio of HF to LF power.

Mind-body interventions such as yoga and mindfulness show significant improvements on stress, sleep quality, and HRV (7). During meditation, slow breathing inhibits sympathetic and limbic activity. Changes in functional connectivity differ between types of meditation and are detectable by fMRI (8).

Influence of oscillations on the autonomic nervous system during stress and meditation

The autonomic nervous system features a feedback loop with the cardiorespiratory system and brain. Under stress, the body shifts to a sympathetic state and cardiorespiratory synchronization decreases (9). However, slow, deep breathing, as in Dharma-Chan meditation, leads to cardiorespiratory synchronization and parasympathetic activation (10). Levels of cardiorespiratory synchronization increase as breathing rates decrease (11). During meditation, cardio-respiratory synchronization is predominantly at a ratio of 4:1 or 5:1, that is, 4 or 5 heartbeats for every 1 breath (12).

Laser Doppler cutaneous blood flow studies show respiration influences BP oscillations at 0.3 Hz (13). Studies have also found spontaneous correlation of slow rhythms of 1 Hz with cardiac and 0.1 Hz with intrinsic myogenic activity. The slowest 0.04 Hz rhythm was attributed to neurogenic factors (14). In another study assessing autonomic control of skin microvessels using a photoplethysmograph, different areas of the body revealed fluctuations of 0.1 Hz that increased in amplitude when subjects were standing. The synchronization between BP and 0.1 Hz oscillations was unrelated to respiration and suggested a common neural, non-local origin (15). During the sympathetic dominant state, BP and HRV are associated with low frequency Mayer waves ranging from 0.05 to 0.15 Hz (16) whereas during the parasympathetic state, HRV is at a higher frequency (0.3 Hz).

According to our model, sympathetic activation during stress and the resulting decrease in membrane potential results in peripheral responses such as increases in skin conductance, heart rate, and BP (Fig. 1). Peripheral microcirculation observed with Doppler flow studies and BP correlates with sympathetic activity (17). Because skin conductance is measured in relation to sweat gland activity innervated by the sympathetic nervous system, it is used as an indicator of sympathetic response (18). During stressed states, peripheral responses are widespread. Skin conductivity (19) and BP (17) increase, and HRV decreases (20). For example during surgery, BP, epinephrine, and norepinephrine levels positively correlate with changes in skin conductance and can be used as an indicator of patient stress (19). Changes in HRV are indicative of autonomic balance and are strongly related to the central nervous system (21). For the purpose of this paper, oscillations in the brain less than 1.5 Hz are referred to as very slow waves and waves from 1.5 – 10 Hz (theta and slow alpha waves) are termed slow waves, while fast oscillations refer to oscillations greater than 10 Hz (beta, gamma, and theta waves.) Slow cardiac, respiratory, and other non-neural waves refer to oscillations less than 1 Hz and fast oscillations refer to oscillations greater than 1 Hz. fMRI brain scans show increased 0.1 Hz oscillations during stress associated with mind wandering and decreased functional connectivity in other brain areas (22) and is also supported by fMRI scans revealing decreased cortical activation during stress (23).

HRV recordings distinguish HF markers of parasympathetic activity (0.15-0.40 Hz), and LF components of sympathetic control (0.04-0.15 Hz). Spectral analysis of microcirculatory blood flow suggests the presence of similar rhythms

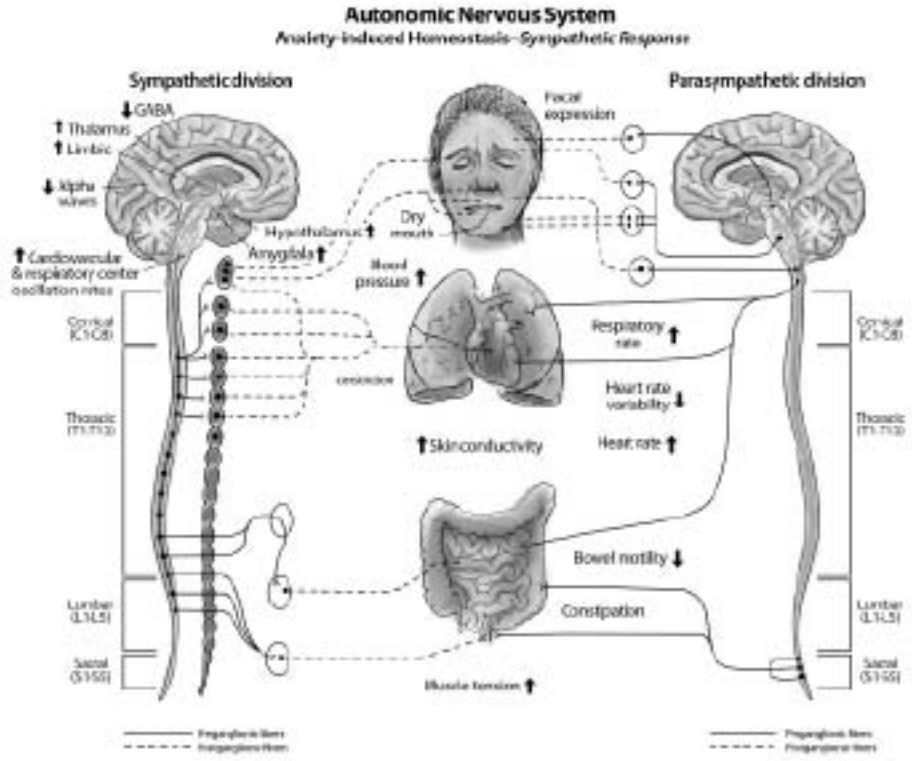

Fig. 1. *Responses associated with sympathetic dominance. The dual-sided autonomic nervous system is shown in which sympathetic activation outweighs the parasympathetic branch. Sympathetic dominance, as seen during the stressed state, leads to a variety of peripheral responses associated with depolarization of target organs. Functional connectivity and alpha waves decrease, while limbic and amygdala activity increase. Brainstem activity also increases, reflected by the increased respiratory center and cardiovascular center rates. Respiration and heart rate increase. Heart rate variability measures are dominated by low frequency components. Blood pressure, skin conductivity, and muscle tension increase. Bowel motility and salivary gland secretion are also hindered. The body is in a relatively depolarized state, including the various target organs and spinal cord. Facial expression depicts a stressed or unpleasant state.*

(24). The pattern characterizing the spectral profile of heart rate and arterial pressure variability consists of LF and HF markers related to vasomotor and respiratory activity, respectively (25). For example, decreased HRV in response to a stressor is related to anxiety and depression (26). Wavelet analysis of HRV reveals the existence of frequencies between 0.145 and 0.6 Hz corresponding to respiration and shows modulation of heart rate by respiration (respiratory sinus arrhythmia) (27). Indeed, Tang et al. (2009) demonstrated sympathetic markers decreased in subjects after training in mind-body techniques compared to a control group (28). In Dharma-Chan meditation, advanced practitioners exhibit a high degree of cardiorespiratory synchronization even during rapid breathing (10). High levels of cardiorespiratory synchronization are also seen during Zen and Kinhin meditation (29). Decreased breathing rate during meditation mediates cardiorespiratory synchronization and a parasympathetic response (30) (Fig. 2) while decreased synchronization of hemodynamic and respiratory rhythms is seen during stress (31). Conversely, meditation has been shown to provide significant benefit for the cardiovascular system (32). Meditation has also been shown to improve anxiety, pain, stress, mental health, and quality of life (33). In addition, after stress, mindfulness meditation results in significantly less neurogenic inflammation than in controls, despite equivalent amounts of stress

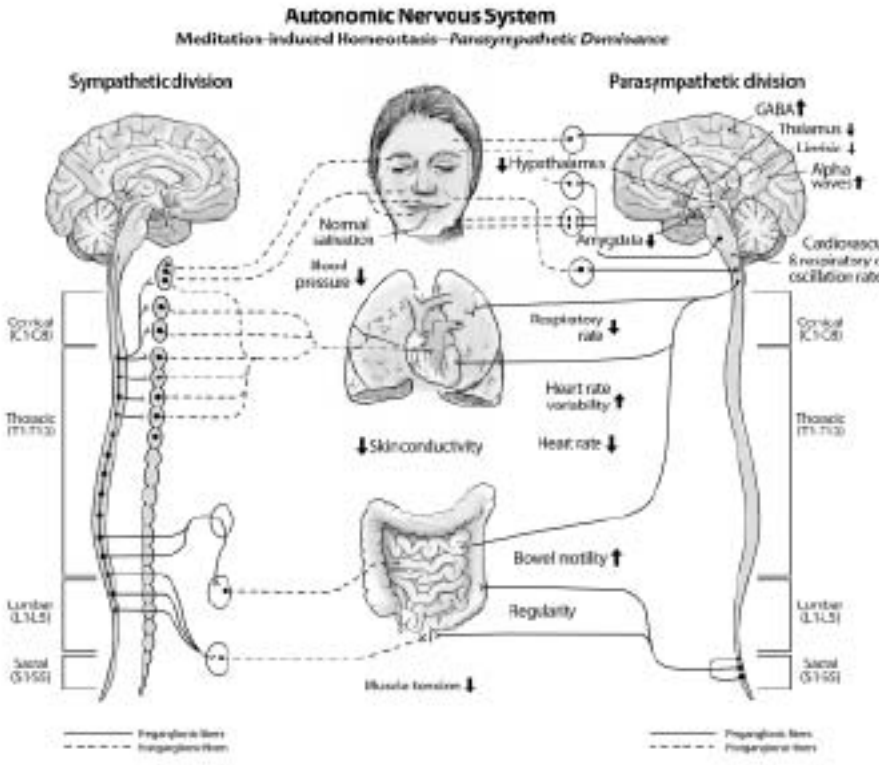

Fig. 2. *Responses associated with parasympathetic dominance. The dual-sided autonomic nervous system is shown, in which parasympathetic activation outweighs the sympathetic branch. In contrast to sympathetic dominance, a shift to prominent parasympathetic activation leads to peripheral responses associated with membrane potential hyperpolarization and the reversal of the effects seen in Fig. 1. In this state, there is an increase in functional connectivity and alpha waves and a decrease in limbic and amygdala activity. Brain stem activity decreases, which is reflected in decreased respiratory center and cardiovascular center rates. Heart rate, respiratory rate, blood pressure, and muscle tension all decrease. High frequency heart rate variability is increased. This parasympathetic shift can be readily achieved through meditation and deep breathing techniques. A pleasant facial expression and widespread hyperpolarization is associated with this state compared to the relatively depolarized state in Fig. 1.*

hormones (34).

Influence of neural oscillations during stress and meditation

Meditation is generally associated with relaxation but many of the changes that occur during meditation do not occur during relaxation alone. For example, relaxation is not associated with the typical hemodynamic changes associated with meditation. Higher levels of cardiorespiratory synchronization that occur during meditation are hypothesized to lead to increases in membrane potential in the cardiovascular system, brainstem, limbic system and higher cortex. The subsequent homeostatic increases in membrane potential may lead to inhibition of emotion centers and increased functional connectivity of the medial prefrontal cortex, thereby increasing focus, memory, and feelings of well-being (35). Another way that mindfulness meditation differs from simple relaxation is that the meditator is aware of moment-to-moment thoughts, feelings, and sensations. We propose that by decreasing stressful or anxious thoughts, that involve greater depolarizations, the practice of mindfulness involves widespread inhibition and membrane hyperpolarization of neurons and in turn contributes to the shift towards parasympathetic activity. Overall, relaxation may be involved in meditation but simply trying to relax does not always relax the mind or stop stressful thoughts. Therefore, we propose that

mindfulness meditation is associated with greater widespread hyperpolarization and inhibition than relaxation alone.

Alpha oscillations have frequencies ranging from 8-13 Hz (36). In a study, using magnetoencephalography, Yamamoto et al. found an increase of alpha wave activity in the medial prefrontal cortex and anterior cingulate cortex during Transcendental Meditation® or automatic self-transcending meditation (TM) (37). Examination of EEGs during automatic self-transcending meditation has shown that there is an increase in alpha-1 wave activity in the brain (38). Alpha waves have been associated with suppressing irrelevant brain activity and improving mental focus (39). Also, it has been suggested that alpha waves play an important role in selective attention and information processing (40). A study by Saggar et al. using EEG found a reduction in beta waves among subjects performing focused attention meditation when compared to the control groups (41). In addition, increases in left hemisphere activity are seen during meditation, which is associated with stronger immunity (42) and increased vaccination response (43).

Meditation practice has been linked to GABAergic cortical inhibition, which has been shown to be associated with improved cognition and regulation of emotions (44). A reduction in GABAergic cortical inhibition has been shown to be linked with memory impairment in schizophrenic patients (45). GABAergic neurons tonically inhibit supraoptic neurons in the hypothalamus and modulate the excitatory effects induced by interleukin-1 (46), suggesting that that the increased cortical GABA modulation associated with meditation (44) may underlie the decreases in interleukins-6 levels (47). GABAergic neurons are important in the process of generating respiratory rhythms and communication between the cardiovascular and respiratory centers in the brainstem. GABAergic neurons have been shown to work as inhibitory neurons that increase their spontaneous firing during inspiration. This suggests that inspiration promotes inhibitory activity in the brainstem and decreases cardiovascular and respiratory center oscillation rates during parasympathetic dominance (48). Injecting GABA into the amygdala increased HRV, consistent with a parasympathetic response, and the injection of glutamate induced a sympathetic response (49). This study suggests that increased levels of GABA in the brain are involved in the parasympathetic response. In addition, stress has been shown to attenuate GABAergic inhibition in the amygdala (50). During stress, there is increased activity in the hypothalamo-pituitary-adrenocortical axis (51) and an increase in activity and stimulation of the amygdala (52). Studies have found a decrease in amygdala activity during mindfulness meditation (53) and during non-meditative states, after participating in mindfulness or compassion meditation training (54). Also, reduced activity in the hippocampus, thalamus, and occipital lobe has been shown after practice of TM (55). During stress, the adrenal medulla increases secretion of the neurotransmitter epinephrine, which reaches the hypothalamus and acts on the central nervous system (56) and elevated cortisol levels from stress (57) may be responsible for decreased serotonin function in the brain during depression (58). During meditation, these neurotransmitters levels reverse. Studies have found decreased levels of stress hormones such as cortisol (59), epinephrine and norepinephrine (60) after meditation. In addition, a stress management study training subjects in deep breathing, relaxation response, and meditation, found reduced anxiety and salivary cortisol levels (61). Levels of the anti-depressant and feel good hormones serotonin (62) and dopamine (60) increase during meditation.

Concentration, Loving-Kindness, and Choiceless Awareness forms of meditation have all been shown to increase functional connectivity in areas involved with self-monitoring and cognition (63). The differences in EEG and neuroanatomical activation in fMRI studies reflect the different meditation approaches being used such as loving kindness, concentration, open monitoring, or focused attention, as well as cardio-respiratory events. For example, in Loving-Kindness meditation, the practitioner focuses on heartfelt compassionate feelings which lead to decreased amygdala activity (63) and activation in the insular and anterior cingulate fMRI signals with associated theta waves. Focused attention meditation leads to activation of more executive function areas and beta/gamma activity (38) supported by cardiorespiratory synchronization, while TM is associated with increased medial

prefrontal cortex activity and alpha wave appearance (64). Autogenic meditation is a practice in which the person uses verbal cues to help induce a feeling of warmth and relaxation.

Do homeostatic changes in neuronal membrane potentials modify the neurotransmitter release that underlies stress, anxiety, and meditation responses?

Membrane potential changes can create currents that synchronize various oscillations throughout the body. The process by which cardiovascular and respiratory rhythms synchronize is not well understood. However, hyperpolarization-activated currents have been shown to synchronize rhythmic cellular activity between the cardiovascular and respiratory centers in the brainstem (65) and within the central nervous system (66). This suggests that cardiorespiratory synchronization is associated with hyperpolarization.

According to our hypothesis, respiration and cardiorespiratory synchronization influence hemodynamic elements, as well as the autonomic nervous system, cerebral blood vessels, and neural elements, by increasing the membrane potential of excitable and non-excitable cells. In animal studies, repetitive parasympathetic stimulation of taste cells led to a hyperpolarization of -9 mV (67) while sympathetic stimulation depolarized toad sinus venosus cells (68). In addition, low-intensity stimulation of the vagus nerve causes long lasting, slow hyperpolarization of cortical neurons. This inhibits neuronal firing and may involve activation of potassium channels by acetylcholine and GABA receptor activity. In humans, inhibition of cortical neurons may be sustained if vagal stimulation is repeated before the last inhibition response has ended (69) suggesting that slow, deep breathing during meditation that stimulates the vagus may sustain this inhibition. These studies suggest that parasympathathetic drive leads to increased cellular membrane potentials and sympathetic drive may lead to decreased membrane potentials, as seen when sympathetic activation during stress leads to decreased membrane potentials of heart cells (70).

Studies monitoring membrane potential changes during sympathetic or parasympathetic states are needed to further understand the homeostatic modulation of cardiac, respiratory, blood pressure (BP) rhythms. An animal study examining the somatosensory cortex found that neurons at -55 mV were almost completely silent while pyramidal neurons at -85 mV had very reliable transmissions (71). This study suggests that cortical neurons with higher membrane potentials may have more reliable transmissions than those with lower membrane potentials. The typical resting state potential of pyramidal neurons is -85 mV to -60 mV (72) therefore if this study had examined transmissions at around -65 mV or -70 mV, we propose that the neurons would have fired more rapidly. We suggest that the increased membrane potentials during meditation in human subjects may increase transmission efficiency and functional connectivity via decreased firing rates while more depolarized neurons fire rapidly, resulting in less efficient and more chaotic transmissions.

We propose hemodynamic de-synchronization leads to a global decrease in membrane potential during stress and hemodynamic synchronization during meditation allows an increased potential to be conducted to all cells. This is reflected peripherally by decreased skin conductivity, BP, heart rate and increased HRV (28) which may be due to the hemodynamic synchronization brought on by the shift to parasympathetic dominance (35) and membrane hyperpolarization.

Our hypothesis focuses on mindfulness meditation but increased levels of cardiorespiratory synchronization are experienced during forms of meditation such as inward-attention (12), Chan (10), Zen, and Kinhin meditation (29), and further research is needed to measure synchronization in other forms of meditation involving slow, deep breathing. Increased levels of synchronization and hemodynamic changes lead to widespread hyperpolarization and inhibition which modulate the autonomic nervous system and brain activity. We propose that eyes closed, open-monitoring, inward-attention, and mindfulness practices may enhance this widespread inhibition.

CONCLUSION

Physiological and behavioral changes differ profoundly between states of meditation and anxiety. During anxiety, heart rate increases, breathing

becomes irregular, and HRV decreases. These changes are accompanied by faster EEG rhythms and changes in neurotransmitters associated with negative emotions. In comparison, the mind-body relaxation response is associated with reverse changes and calm, focused thoughts. What causes these global changes in rhythms and thought processes? Is it a central process regulated by the hypothalamus and brain or by specific neurotransmitters? According to our hypothesis and review of literature, the mechanism is based on homeostatic modulation of intrinsic cellular excitability. Decreases in homeostatic membrane potentials during anxiety increase intrinsic cellular excitability, which in turn brings about changes in neuronal firing, neurotransmitters, and peripheral rhythms. Cardiorespiratory synchronization, during the mind-body response, leads to increases in homeostatic membrane potentials and decreased intrinsic cellular excitability that underlies the changes that modulate the autonomic nervous system and brain activity. Further studies are needed to confirm this hypothesis and elucidate the specific role of the hypothalamus in stabilizing the membrane potential set points of dynamic homeostasis during anxiety and the mind-body response.

ACKNOWLEDGEMENTS

We would like to thank Mike Jensen MSMI, CMI of Georgia Regents University for creating the medical illustrations.

REFERENCES

1. Cohen S, Janicki-Deverts D, Miller GE. Psychological stress and disease. JAMA 2007; 298(14):1685-7.
2. Orme-Johnson DW, Barnes VA. Effects of the transcendental meditation technique on trait anxiety: a meta-analysis of randomized controlled trials. J Altern Complement Med 2014; 20(5):330-41.
3. Jerath R, Harden K, Crawford M, Barnes VA, Jensen M. Role of cardiorespiratory synchronization and sleep physiology: effects on membrane potential in the restorative functions of sleep. Sleep Med 2014; 15(3):279-88.
4. Nattie E, Li A. Respiration and autonomic regulation and orexin. Prog Brain Res 2012; 198:25-46.
5. Reyes del Paso GA, Langewitz W, Mulder LJ, van Roon A, Duschek S. The utility of low frequency heart rate variability as an index of sympathetic cardiac tone: a review with emphasis on a reanalysis of previous studies. Psychophysiology 2013; 50(5):477-87.
6. Krygier JR, Heathers JAJ, Shahrestani S, Abbott M, Gross JJ, Kemp AH. Mindfulness meditation, well-being, and heart rate variability: A preliminary investigation into the impact of intensive Vipassana meditation. Int J Psychophysiol 2013; 89(3):305-13.
7. Wolever RQ, Bobinet KJ, McCabe K, Mackenzie ER, Fekete E, Kusnick CA, et al. Effective and viable mind-body stress reduction in the workplace: a randomized controlled trial. J Occup Health Psychol 2012; 17(2):246-58.
8. Tang YY, Rothbart MK, Posner MI. Neural correlates of establishing, maintaining, and switching brain states. Trends Cogn Sci 2012; 16(6):330-7.
9. Zhang J, Yu X, Xie D. Effects of mental tasks on the cardiorespiratory synchronization. Respir Physiol Neurobiol 2010; 170(1):91-5.
10. Lo PC, Chang CH. Effects of Long-term Dharmachan meditation on cardiorespiratory synchronization and HRV behavior. Rejuvenation Res 2013.
11. Porta A, Guzzetti S, Montano N, et al. Information domain analysis of cardiovascular variability signals: evaluation of regularity, synchronisation and coordination. Med Biol Eng Comput 2000; 38(2):180-8.
12. Wu SD, Lo PC. Cardiorespiratory phase synchronization during normal rest and inward-attention meditation. Int J Cardiol 2010; 141(3):325-8.
13. Brown KW, Ryan RM. The benefits of being present: mindfulness and its role in psychological well-being. J Pers Soc Psychol 2003; 84(4):822-48.
14. Kvernmo HD, Stefanovska A, Bracic M, Kirkebøen KA, Kvernebo K. Spectral analysis of the laser Doppler perfusion signal in human skin before and after exercise. Microvasc Res 1998; 53(3):173-82.
15. Bernardi L, Radaelli A, Solda PL, et al. Autonomic control of skin microvessels: assessment by power spectrum of photoplethysmographic waves. Clin Sci (Lond) 1996; 90(5):345-55.
16. Strik C, Klose U, Kiefer C, Grodd W. Slow rhythmic oscillations in intracranial CSF and blood flow:

registered by MRI. Acta Neurochir Suppl 2002; 81:139-42.
17. Wallin BG. Neural control of human skin blood flow. J Auton Nerv Syst 1990; 30(S):S185-90.
18. Vetrugno R, Liguori R, Cortelli P, Montagna P. Sympathetic skin response: basic mechanisms and clinical applications. Clin Auton Res 2003; 13(4):256-70.
19. Storm H, Myre K, Rostrup M, Stokland O, Lien MD, Raeder JC. Skin conductance correlates with perioperative stress. Acta Anaesthesiol Scand 2002; 46(7):887-95.
20. Brosschot JF, Van Dijk E, Thayer JF. Daily worry is related to low heart rate variability during waking and the subsequent nocturnal sleep period. Int J Psychophysiol 2007; 63(1):39-47.
21. Thayer JF, Ahs F, Fredrikson M, Sollers J Jr, Wager TD. A meta-analysis of heart rate variability and neuroimaging studies: implications for heart rate variability as a marker of stress and health. Neurosci Biobehav Rev 2012; 36(2):747-56.
22. Greicius MD, Krasnow B, Reiss AL, Menon V. Functional connectivity in the resting brain: a network analysis of the default mode hypothesis. Proc Natl Acad Sci U S A 2003; 100(1):253-8.
23. Qin S, Hermans EJ, van Marle HJ, Luo J, Fernandez G. Acute psychological stress reduces working memory-related activity in the dorsolateral prefrontal cortex. Biol Psychiatry 2009; 66(1):25-32.
24. Lino S, Calcagnini G, Censi F, Congi M, De Pasquale F. Cardiovascular neuroregulation and rhythms of the autonomic nervous system: frequency domain analysis. Cardiologia 1999; 44(3):281-7.
25. Montano N, Porta A, Cogliati C, et al. Heart rate variability explored in the frequency domain: a tool to investigate the link between heart and behavior. Neurosci Biobehav Rev 2009; 33(2):71-80.
26. Shinba T, Kariya N, Matsui Y, Ozawa N, Matsuda Y, Yamamoto K. Decrease in heart rate variability response to task is related to anxiety and depressiveness in normal subjects. Psychiatry Clin Neurosc 2008 62(5):603-9.
27. Kenwright DA, Bahraminasab A, Stefanovska A, McClintock PV. The effect of low-frequency oscillations on cardio-respiratory synchronization: Observations during rest and exercise. Eur Phys J B 2008; 65(3):425-33.
28. Tang YY, Ma Y, Fan Y, et al. Central and autonomic nervous system interaction is altered by short-term meditation. Proc Natl Acad Sci U S A 2009; 106(22):8865-70.
29. Cysarz D, Bussing A. Cardiorespiratory synchronization during Zen meditation. Eur J Appl Physiol 2005; 95(1):88-95.
30. Jerath R, Edry JW, Barnes VA, Jerath V. Physiology of long pranayamic breathing: Neural respiratory elements may provide a mechanism that explains how slow deep breathing shifts the autonomic nervous system. Med Hypotheses 2006; 67(3):566-71.
31. Zhang J, Yu X, Xie D. Effects of mental tasks on the cardiorespiratory synchronization. Respir Physiol Neurobiol 2010; 170(1):91-5.
32. Barnes VA, Orme-Johnson DW. Prevention and treatment of cardiovascular disease in adolescents and adults through the transcendental meditation (R) program: a research review update. Curr Hypertens Rev 2012; 8(3):227-42.
33. Goyal M, Singh S, Sibinga EMS, et al. Meditation programs for psychological stress and well-being. Rockville MD 2014.
34. Rosenkranz MA, Davidson RJ, Maccoon DG, Sheridan JF, Kalin NH, Lutz A. A comparison of mindfulness-based stress reduction and an active control in modulation of neurogenic inflammation. Brain Behav Immun 2013; 27(1):174-84.
35. Jerath R, Barnes VA, Dillard-Wright D, Jerath S, Hamilton B. Dynamic Change of awareness during meditation techniques: neural and physiological correlates. Front Hum Neurosci 2012; 6:131.
36. Berger H. Über das Elektrenkephalogramm des Menschen. Archiv für Psychiatrie und Nervenkrankheiten 1929; 87(1):527-70.
37. Yamamoto S, Kitamura Y, Yamada N, Nakashima Y, Kuroda S. Medial profrontal cortex and anterior cingulate cortex in the generation of alpha activity induced by transcendental meditation: A magnetoencephalographic study. Acta Med Okayama 2006; 60(1):51-8.
38. Travis F, Shear J. Focused attention, open monitoring and automatic self-transcending: Categories to organize meditations from Vedic, Buddhist

and Chinese traditions. Conscious Cogn 2010; 19(4):1110-18.
39. Bonnefond M, Jensen O. Alpha oscillations serve to protect working memory maintenance against anticipated distracters. Current Biol 2012; 22(20):1969-74.
40. Klimesch W. α-band oscillations, attention, and controlled access to stored information. Trends Cogn Sci 2012; 16(12):606-17.
41. Saggar M, King BG, Zanesco AP, et al. Intensive training induces longitudinal changes in meditation state-related EEG oscillatory activity. Front Hum Neurosci 2012; 6(256).
42. Sumner RC, Parton A, Nowicky AV, Kishore U, Gidron Y. Hemispheric lateralisation and immune function: a systematic review of human research. J Neuroimmunol 2011; 240-241:1-12.
43. Davidson RJ, Kabat-Zinn J, Schumacher J, et al. Alterations in brain and immune function produced by mindfulness meditation. Psychosom Med 2003; 65(4):564-70.
44. Guglietti CL, Daskalakis ZJ, Radhu N, Fitzgerald PB, Ritvo P. Meditation-related increases in GABAB modulated cortical inhibition. Brain Stimul 2013; 6(3):397-402.
45. Takahashi T, Murata T, Hamada T, et al. Changes in EEG and autonomic nervous activity during meditation and their association with personality traits. Int J Psychophysiol 2005; 55(2):199-207.
46. Li Z, Inenaga K, Yamashita H. GABAergic inputs modulate effects of interleukin-1[beta] on supraoptic neurones *in vitro*. Neuroreport 1993; 5(2):181.
47. Pace TW, Negi LT, Adame DD, Cole SP, Sivilli TI, Brown TD, Issa MJ, Raison CL. Effect of compassion meditation on neuroendocrine, innate immune and behavioral responses to psychosocial stress. Psychoneuroendocrinology 2009; 34(1):87-98.
48. Frank JG, Mendelowitz D. Synaptic and intrinsic activation of GABAergic neurons in the cardiorespiratory brainstem network. PLoS One 2012; 7(5):e36459.
49. Neckel H, Quagliotto E, Casali KR, Montano N, Dal Lago P, Rasia-Filho AA. Glutamate and GABA in the medial amygdala induce selective central sympathetic/parasympathetic cardiovascular responses. Can J Physiol Pharmacol 2012; 90(5):525-36.
50. Rodriguez Manzanares PA, Isoardi NA, Carrer HF, Molina VA. Previous stress facilitates fear memory, attenuates GABAergic inhibition, and increases synaptic plasticity in the rat basolateral amygdala. J Neurosci 2005; 25(38):8725-34.
51. Herman JP, Cullinan WE. Neurocircuitry of stress: central control of the hypothalamo–pituitary–adrenocortical axis. Trends Neurosci1997; 20(2):78-84.
52. Davis M. The role of the amygdala in fear and anxiety. Annu Rev Neurosci 1992; 15:353-75.
53. Creswell JD, Way BM, Eisenberger NI, Lieberman MD. Neural correlates of dispositional mindfulness during affect labeling. Psychosom Med 2007; 69(6):560-65.
54. Desbordes G, Negi LT, Pace TW, Wallace BA, Raison CL, Schwartz E. Effects of mindful-attention and compassion meditation training on amygdala response to emotional stimuli in an ordinary, non-meditative state. Front Hum Neurosci 2012; 1(6):292.
55. Newberg A, Travis F, Wintering N, Nidich S, Alavi A, Schneider R, editors. Cerebral 416 glucose metabolic changes associated with transcendental meditation practice. Neural Imaging 2006; Miami, Fl.
56. Wortsman J. Role of epinephrine in acute stress. Endocrinol Metab Clin North Am 2002; 31(1):79-106.
57. Smyth J, Ockenfels MC, Porter L, Kirschbaum C, Hellhammer DH, Stone AA. Stressors and mood measured on a momentary basis are associated with salivary cortisol secretion. Psychoneuroendocrinology 1998; 23(4):353-70.
58. Dinan TG. Glucocorticoids and the genesis of depressive illness. A psychobiological model. Br J Psychiatry 1994; 164(3):365-71.
59. Vandana B, Vaidyanathan K, Saraswathy LA, Sundaram KR, Kumar H. Impact of integrated amrita meditation technique on adrenaline and cortisol levels in healthy volunteers. Evid Based Complement Alternat Med 2011; 2011:379645.
60. Jung YH, Kang DH, Jang JH, et al. The effects of mind-body training on stress reduction, positive affect, and plasma catecholamines. Neurosci Lett

2010; 479(2):138-42.
61. Iglesias SL, Azzara S, Argibay JC, et al. Psychological and physiological response of students to different types of stress management programs. Am J Health Promot 2012; 26(6):e149-58.
62. Yu X, Fumoto M, Nakatani Y, et al. Activation of the anterior prefrontal cortex and serotonergic system is associated with improvements in mood and EEG changes induced by Zen meditation practice in novices. Int J Psychophysiol 2011; 80(2):103-11.
63. Brewer JA, Worhunsky PD, Gray JR, Tang YY, Weber J, Kober H. Meditation experience is associated with differences in default mode network activity and connectivity. Proc Natl Acad Sci U S A 2011; 108(50):20254-59.
64. Yamamoto S, Kitamura Y, Yamada N, Nakashima Y, Kuroda S. Medial profrontal cortex and anterior cingulate cortex in the generation of alpha activity induced by transcendental meditation: a magnetoencephalographic study. Acta Med Okayama 2006; 60(1):51.
65. Robinson RB, Siegelbaum SA. Hyperpolarization-activated cation currents: from molecules to physiological function. Annu Rev Physiol 2003; 65:453-80.
66. Roberts L, Greene JR. Hyperpolarization-activated current (Ih): a characterization of subicular neurons in brain slices from socially and individually housed rats. Brain Res 2005; 1040(1-2):1-13.
67. Sato T, Nishishita K, Kato Y, Okada Y, Toda K. Tonic activity of parasympathetic efferent nerve fibers hyperpolarizes the resting membrane potential of frog taste cells. Chem Senses 2006; 31(4):307-13.
68. Cousins HM, Bramich NJ. Effects of sympathetic nerve stimulation on membrane potential, [Ca2+]i and force in the arrested sinus venosus of the toad, Bufo marinus. J Physiol 1997; 505(Pt 2):513-27.
69. Zagon A, Kemeny AA. Slow hyperpolarization in cortical neurons: a possible mechanism behind vagus nerve simulation therapy for refractory epilepsy? Epilepsia 2000; 41(11):1382-9.
70. Moreno-Galindo EG, Sánchez-Chapula JA, Sachse FB, Rodríguez-Paredes JA, Tristani-Firouzi M, Navarro-Polanco RA. Relaxation gating of the acetylcholine-activated inward rectifier K+ current is mediated by intrinsic voltage sensitivity of the muscarinic receptor. J Physiol 2011; 589(7):1755-67.
71. Cowan AI, Stricker C. Functional connectivity in layer IV local excitatory circuits of rat somatosensory cortex. J Neurophysiol 2004; 92(4):2137-50.
72. Bean BP. The action potential in mammalian central neurons. Nat Rev Neurosci 2007; 8(6):451-65.

JOURNAL OF BIOLOGICAL REGULATORS & HOMEOSTATIC AGENTS Vol. 28, no. 4, 555-563 (2014)

EDITORIAL

TARGETING PROSTATE-SPECIFIC MEMBRANE ANTIGEN FOR PERSONALIZED THERAPIES IN PROSTATE CANCER: MORPHOLOGIC AND MOLECULAR BACKGROUNDS AND FUTURE PROMISES

M. SANTONI[1], M. SCARPELLI[2], R. MAZZUCCHELLI[2], A. LOPEZ-BELTRAN[3], L. CHENG[4], S. CASCINU[1] and R. MONTIRONI[2]

[1]Medical Oncology, Polytechnic University of the Marche Region, School of Medicine, United Hospitals, Ancona, Italy, [2]Section of Pathological Anatomy, Polytechnic University of the Marche Region, School of Medicine, United Hospitals, Ancona, Italy, [3]Department of Pathology and Surgery, Faculty of Medicine, Cordoba, Spain, and [4]Department of Pathology and Laboratory Medicine, Indiana University School of Medicine, Indianapolis, IN, USA

Received October 20, 2014 – Accepted October 30, 2014

The first two authors contributed equally to this work

Prostate-specific membrane antigen (PSMA) is an integral, non-shed membrane glycoprotein that is highly expressed on prostate epithelial cells and strongly upregulated in prostate cancer (PCa). Prostatic neoplastic transformation results in the transfer of PSMA from the apical membrane to the luminal surface of the ducts. However, the role of PSMA in tumor angiogenesis and carcinogenesis is poorly understood. PSMA is characterized by folate hydrolase and carboxypeptidase activity and internalization function, and its levels are directly correlated to androgen independence, metastasis and PCa progression. As largely substantiated by preclinical and clinical findings, PSMA could represent a promising target for Positron Emission Tomography (PET) radiopharmaceuticals for PCa imaging. Furthermore, PSMA could prove an important target for the development of new therapeutic approaches, including PSMA-based aptamers, peptides, antibody-drug conjugated therapy, as well as radiotherapy and immunotherapy. This review will summarize the role of PSMA in PCa development and progression and its potential role in the diagnosis and treatment of patients with initial and advanced PCa.

Prostate cancer (PCa) is the fifth leading cause of cancer-related mortality worldwide, and the second cause in the male population (1). Due to its insidious behavior, early diagnosis of PCa is difficult, and many patients present metastatic disease at the time of diagnosis (2).

Among cell-surface molecules, the Prostate-Specific Membrane Antigen (PSMA) represents a promising marker of PCa. Its expression profile and other biological properties make it an attractive target for cancer therapy. PSMA is a unique membrane bound glycoprotein that consists of an intracellular domain of 19 amino acids, a transmembrane domain of 24 amino acids, and a glycosylated extracellular

Key words: cancer diagnosis, cancer therapy, positron emission tomography, prostate cancer, PSMA

Mailing address: Prof. Rodolfo Montironi,
Pathological Anatomy,
Polytechnic University of the Marche Region,
School of Medicine, United Hospitals,
Via Conca 71, 60126 Torrette, Ancona, Italy
Tel.: +390715964830 Fax: +39071889985
e-mail: r.montironi@univpm.it

0393-974X (2014)

domain of 707 amino acids (3). Under native conditions, PSMA is expressed as a noncovalent homodimer, for which the ectodomain structure has been solved. In the normal human prostate, PSMA expression and localization is associated with the cytoplasm and apical side of the epithelium surrounding prostatic ducts.

PSMA is a not secretory protein with folate hydrolase and carboxypeptidase activity and internalization function (Fig. 1), and this transport capability can be increased three fold when PSMA is bound to anti-PSMA antibodies. In addition, PSMA is alternatively spliced to produce at least three variants, including PSM', PSM-C and PSM-D, although the implication of such alternative splice variants in PCa cells is unknown at present.

Several studies demonstrated that PSMA is involved in cell biology and plays a crucial role in signal transduction. However, the molecular mechanisms of relating signal transduction still have not been fully clarified. PSMA expression is highest in prostate tissue (secretory acinar epithelium), but detectable levels of PSMA protein are also found in kidney (proximal tubules), nervous system glia (astrocytes and schwann cells), and the small bowel (jejunal brush border) (4,5). PSMA is overexpressed on the malignant epithelial cells that define prostate cancer, as well as neovasculature of a wide range of non-prostatic solid tumors, but not on normal vasculature (6). Prostatic neoplastic transformation results in the transfer of PSMA from the apical membrane to the luminal surface of the ducts (7). However, the role of PSMA in tumor angiogenesis and carcinogenesis is poorly understood.

This review emphasizes the role of PSMA in PCa tumorigenesis and progression, thus underlying its potential in PCa targeted imaging and therapy.

EXPRESSION AND ROLE OF PSMA IN PCa

PSMA was first discovered in the prostate tissue using the monoclonal antibody (mAb) 7E11 derived from the cell membrane of the LNCaP prostate cancer cell line (8). Tissue expression of PSMA increases from normal prostate tissue to high-grade prostatic intraepithelial neoplasia (HGPIN), i.e., the direct precursor of prostate cancer, to PCa (6). Significant correlation exists between higher PSMA expression associated with higher Gleason score (Fig. 2) and PSA at diagnosis, increased tumor angiogenesis, absence of ets-related gene (ERG) expression, lower vitamin D receptor and androgen receptor expression. Notably, in this study PSMA expression was not a predictive biomarker for PCa–specific mortality in surgically treated patients (9).

PSMA expression has been shown to be significantly correlated with prostate growth and differentiation (10). Thus, *in vitro* PSMA expression is associated with increased cellular folate content, conferring a proliferative advantage to PSMA expressing cells (11, 12). Guo et al. showed that PSMA knockdown was associated with the inhibition of the phosphatidylinositol 3-kinase/Akt signaling pathway and consequently with decreased cell proliferation, migration and survival (13). In addition, PSMA seems to stimulate PCa cell proliferation, migration and survival through phospho-p38 (P-p38) MAPK pathway in LNCaP cancer cells (14). Nevertheless, the role of PSMA in promoting PCa cell proliferation remains controversial (15). Additionally, PSMA is involved in the development of PCA metastases. Xu and his colleagues investigated the metastasis-related genes potentially involved in PCa metastasis regulated by PSMA in four prostate cancer cell lines (LNCap, 22RV1, PC-3 and DU145). In this study, CDH6, MMP3, MTSS1 were identified as PSMA-related genes, and their expression was negatively correlated with the stage of prostate cancer, suggesting their possible involvement in the suppression of PCa metastasis by PSMA (16). Interestingly, PSMA can be enriched in exosomes (17), which are nanometer-sized extracellular vesicles of endosomal origin involved in promoting immune suppression and tumor escape (18), as well as PCa invasiveness and stemness (19).

PSMA-BASED IMAGING IN PATIENTS WITH PCa

Accurate assessment is a prerequisite for optimal clinical management and therapy selection of PCa. Conventional imaging techniques, such as bone scintigraphy, CT, ultrasound, and MRI, are currently used to detect primary PCa and metastatic disease. Nevertheless, improved imaging modalities are

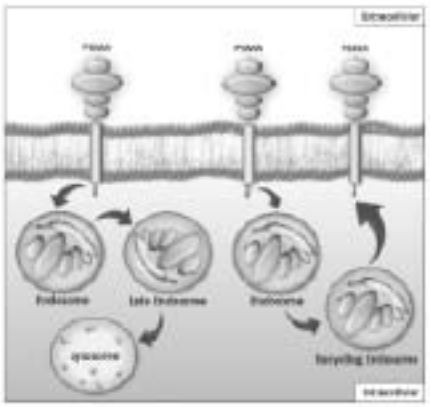

Fig. 1. *Spontaneous or antibody induced internalization of PSMA through clathrin coated pits. PSMA can either go to the lysosomes through late endosomes or be recycled by recycling endosomal compartment (REC). The internalization into endosomal vesicles is enabled by the cytoplasmic tail of PSMA, which contains an internalization signal.*

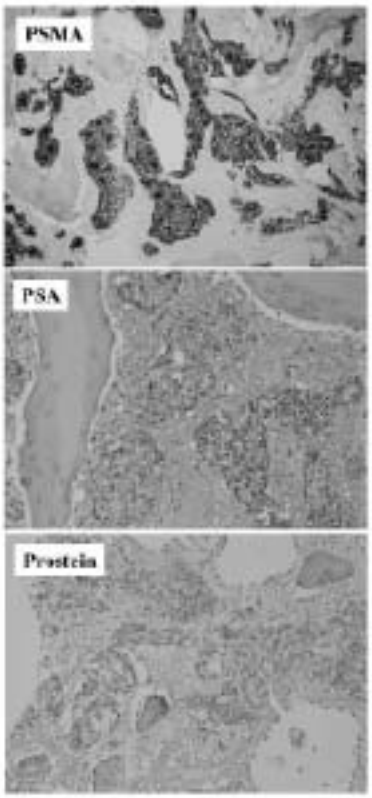

Fig. 2. *Strong and diffuse PSMA immunostaining mostly at the cell membrane level. See for comparison the negativity for PSA and faint and focal positivity for Prostein.*

needed to optimize the management of these patients. In this scenario, Positron Emission Tomography (PET) and single photon emission computed tomography (SPECT) with emerging radiopharmaceuticals may provide an accurate staging of primary disease, restaging of tumor recurrence, and detection of metastatic disease.

PSMA is a well-characterized imaging biomarker of PCa. Several PSMA-based approaches have been developed, including antibodies, nanobodies and small molecule inhibitors.

Antibodies and nanobodies

Indium-111 capromab pendetide (^{111}In-capromab, ProstaScint®) was the first monoclonal antibody against PSMA used in PCa immunoscintigraphy. Correlation of scan results with pathological specimens showed that ^{111}In-capromab was able to detect soft tissue metastases, with an average sensitivity of 60%, a positive predictive value of 60%, and a negative predictive value of 70% (20–22). This not-high-enough sensitivity may be explained by the evidence that ^{111}In-capromab recognizes an intracellular epitope of PSMA, thereby targeting only damaged or necrotic/apoptotic cells.

Unlike its predecessor, J591 is an antibody specific for the extracellular domain of PSMA. ^{111}In-labeled J591 has been evaluated against conventional imaging in the assessment of bone metastases. ^{111}In-labeled J591 localized 93.7% of skeletal lesions detected by conventional imaging, and 13/18 bone lesions detected only with ^{111}In-labeled J591 were later confirmed to be true metastases (23). Most recently, J591 has been radiolabeled with 89Zr (24) and 64Cu (25) for PET imaging in PCa. In 2013, 89Zr J591 PET/CT imaging showed excellent targeting of skeletal, nodal and soft tissue lesions (26).

Presently, a pilot study has been planned to evaluate the use of anti-PSMA antibody MDX1201-A488 in the intra-operative optical imaging in PCa patients treated with robot-assisted laparoscopic surgery (ClinicalTrials.gov Identifier NCT02048150).

An emerging strategy in developing high-contrast nuclear imaging consists is the use of specific antibody fragments, called nanobodies. Nanobodies contain antibody-derived smaller fragments (typically the variable domain alone of heavy chain antibodies)

that largely retain the specific antigen binding properties of original antibodies, but with more rapid pharmacokinetics and lower immunogenic potential. Evazalipour and his colleagues compared the properties of different nanobodies radiolabeled with 99 m-Technetium (99mTc) in $PSMA^+$ LNCaP and $PSMA^-$ PC3 cell lines and in $PSMA^+$ and $PSMA^-$ tumor-bearing xenografts through SPECT/micro-CT imaging and tissue sampling. Among evaluated molecules, nanobody PSMA30 resulted a lead compound for future application in PCa imaging trials (27). Further prospective trials to assess the efficacy of nanobodies in PCa imaging are awaited.

Small molecules

The identification of the structural (28) and functional (29) homology between N-acetylaspartylglutamate peptidase or NAALDase [for which a number of enzymatic inhibitors had been identified (30, 31)] and PSMA has been a major step forward for the development of PSMA-targeted radiotracers. Generally, small molecule PSMA inhibitors consist in zinc binding compounds attached to a glutamate or glutamate isostere. Phosphonate-, phosphate- and phosphoramidates (1) and ureas (2) constitute the two main families of compounds. Based on NAALDase homology, several compounds have been developed and labelled with 123I (32–34), 99mTc (35, 36), 18F (37), 111In (38) and 68Ga (39).

123I-MIP-1072 and 123I-MIP-1095 were the first small molecule inhibitors of PSMA introduced into the clinic. SPECT/CT using these compounds showed a rapid detection of lesions in soft tissue, bone and the prostate glands of males with metastatic PCa (40).

Among emerging PSMA small molecule inhibitors, N-(N-((S)-1,3-dicarboxypropyl) carbamoyl)-4-(18F) fluorobenzyl-L-cysteine (18F-DCFBC) is in course of evaluation in several studies. Using 18F-DCFBC, $PSMA^+$ PC-3 PIP xenografts were visualized early with little radioactivity in the $PSMA^-$ isogenic PC-3 flu xenografts. By 2 hours, the PC-3 PIP xenografts remained clearly visible, with a significant clearance of background radioactivity from blood, liver and kidneys (41, 42).

The use of 18F-DCFBC was investigated in five patients with radiological evidence of metastatic PCa and Gleason scores between 7–9. Bone scans or CT identified 21 lesions (5 bone and 16 lymph node lesions), while 32 lesions were visible with 18F-DCFBC PET. Ten of 11 additional lesions were located in the bone and were suggestive of early bone metastases, indicating the potential of 18F-DCFBC PET in this subpopulation (43). Currently, the use of 18F-DCFBC PET/CT is under evaluation in a phase II study enrolling patients scheduled for surgical prostate (group 1), or with biochemical recurrence after surgery or radiotherapy (group 2), or in metastatic PCa patients (group 3) (NCT02190279). The results are awaited for the end of 2018. In addition, another phase I/II study is ongoing to assess the potential of 18F-DCFBC PET in the detection of primary PCa, bone and nodal metastases in patients at initial diagnosis (NCT01496157).

As for the PSMA inhibitor 18F-DCFPyL (2-(3-{1-carboxy-5-((6-((18)F)fluoro-pyridine-3-carbonyl)-amino)-pentyl}-ureido)-pentanedioic acid), Chen et al. evaluated its use in immunocompromised mice using isogenic PSMA PC3 PIP and PSMA- PC3 flu xenograft models, suggesting that this agent could be viable and effective in this setting (37). Nowadays, a phase I study is assessing the biodistribution and pharmacokinetic of 18F-DCFPyL in patients with advanced PCa (NCT02151760).

The early differentiation between local disease and distant metastasis is crucial for patient management. 18F-choline is able to distinguish PCa lesions with moderate-to-good sensitivity, but its activity is limited to patients with a PSA >1 ng/mL (44). The results obtained by 68Ga-labelled PSMA inhibitors showed a high potential in detecting small recurrent PCa lesions in patients with low PSA levels (45−47). Indeed, 68Ga-labelled PSMA inhibitors are characterized by high accumulation in small metastases and a rapid clearance from background tissue (48). Recently, a comparison between PET/CT and PET/MRI hybrid systems using a 68Ga-labelled PSMA compound for the diagnosis of recurrent PCa was carried out. The results showed that Ga-PSMA PET/MRI was more accurate in the detection of PCa lesions and was associated with lower radiation exposure (39).

Beyond 68Ga-labelled compounds, 99mTc-labelled inhibitors of PSMA have shown a high potential in the detection of PCa lesions. Presently,

a phase II study is testing 99mTc-MIP-1404 PSMA inhibitor in men with high-risk PCa scheduled for radical prostatectomy and extended pelvic lymph node dissection compared to histopathology (ClinicalTrials.gov Identifier NCT01667536).

Furthermore, BAY1075553 (2-PMPA analogs (2S, 4S)-2-18F-fluoro-4-(phosphonomethyl) pentanedioid acid) has demonstrated high uptake in $PSMA^+$ LNCaP tumor xenografts (49). The phase I study showed that BAY1075553 was able to detect primary PCa, lymph node and bone metastases, although its high uptake with degenerative bone lesions may limit its use in assessing bone disease (50).

PSMA-TARGETING STRATEGIES IN PCa THERAPY

PSMA has been extensively used as a target antigen, due to its constitutive or induced internalization property as well as to its high expression in PCa. Several strategies, including aptamers, monoclonal antibodies and peptides have been employed as prodrug or nanoparticles to improve their targeting efficiency to PCa cells.

The discovery and development of anticancer aptamers may provide a relevant contribution to PCa molecular imaging. Aptamers are short DNA, RNA or peptide oligomers able to assume a specific and stable three-dimensional shape *in vivo* (51). Their high affinity and specificity, similar to antibodies, is achieved by folding into a unique three-dimensional conformation that is complementary to the target surface. In this regard, Lupold et al. identified two RNA aptamers (A9 and A10) with high binding affinity to PSMA, leading to the inhibition of its NAALADase/glutamate carboxypeptidase II activity (52). Successively, Xu et al. conjugated A10 aptamer on the surface of micelles, showing high drug uptake in $PSMA^+$ cancer cells both *in vitro* and *in vivo* studies (23).

PSMA can serve as target for delivery of therapeutic agents such as antibody-drug conjugated (ADC) therapy. PSMA ADC consists of a fully human anti-PSMA monoclonal antibody conjugated to monomethylauristatin E through a valine-citrulline linker. Wang and his group assessed the antitumor activity of PSMA ADC in prostate cancer cell lines *in vitro* and in a novel *in vivo* model of taxane-refractory human prostate cancer. They reported that *in vitro* cytotoxic activity was efficient for cells with abundant PSMA expression (>105 molecules/cell; IC50 0.022 nmol/L). In addition, PSMA ADC showed high *in vivo* activity in treating xenograft tumors progressed on previous docetaxel therapy (53).

Recently, Petrylak et al. (54) presented the results from a phase II trial on the use of PSMA-ADC at 2.5 mg/kg in 34 patients with taxane-refractory metastatic castration resistant prostate cancer (CRPC). Of them, 39% had both docetaxel and cabazitaxel, while 58% had received both abiraterone and enzalutamide. Dosing was initiated at 2.5 mg/kg and adjusted at 2.3 mg/kg for tolerability. They showed that PSA decline of ≥30% was noted in 36% (2.3 mg/kg) and 16% (2.5 mg/kg), while circulating tumor cell (CTC) decline of ≥50% was reported in 74% patients in both 2.3 and 2.5 mg/kg. Duration of therapy on 2.3 mg/kg was longer than on 2.5 mg/kg, as well as the rate of serious adverse events (37 vs 59%). Interestingly, PSA and CTC responses were associated with higher PSMA+CTC, while PSA responses alone were correlated with lower NE markers, suggesting that NE differentiation may play a role in this context. Based on these results, this study has been extended and is currently enrolling metastatic CRPC patients (NCT02020135).

In the same view, phage display technology was used by researchers to identify peptide sequences, which can specifically bind to PSMA and inhibit its enzymatic activity.

Denmeade et al. conjugated a PSMA-specific peptide to an inhibitor (thapsigargin) of the sarcoplasmic/endoplasmic reticulum calcium adenosine triphosphate (SERCA) pump. The SERCA pump shares the catalytic properties of ion-motive ATPases of the P-type family and transports calcium ions from the cytoplasm into the sarcoendoplasmic reticulum. Its activity is required by all cell types for viability. The conjugate is inactive until the PSMA-specific peptide is cleaved, thereby initiating SERCA inhibition. In xenograft models, thapsigargin induced PCa tumor regression at doses that were minimally toxic to the host (55). Based on these findings, a phase I study is evaluating the thapsigargin prodrug G-202 in patients with advanced PCa and other solid tumors (NCT01056029).

PSMA could be successfully utilized in immunotherapy and radiotherapy approaches. Adoptive immunotherapy by infusion of designer T cells engineered with chimeric antigen receptors (CARs) to potentiate their antitumor activity is a potentially highly specific modality for the treatment of cancer. Thus, PSMA×CD3 diabody has been shown to be able to retarget human $CD4^+$ and $CD8^+$ lymphocytes to lyse PSMA-expressing C4-2 PCa cells. In addition, other 1st and 2nd generation of anti-PSMA designer T cells have demonstrated their activity in both *in vitro* and *in vivo* studies (56, 57). More recently, mouse-human chimeric IgG1 of 2C9 (KM2777) has been fused with C-terminus interleukin-2 (IL-2). The result of this fusion, KM2812, showed marked antitumor activity, with some complete regressions, in a xenograft tumor model using PSMA-expressing PCa cells.

Currently, a phase I trial is studying the safety of adoptive transfer of autologous T cells targeted to PSMA for the treatment of castrate metastatic PCa (NCT01140373). Vaccine is another very interesting area that utilizes PSMA as a target to potent cellular and humoral immune responses against cancer cells (58).

As for the potential of PSMA targeted antivascular radiotherapy, Bandekar recently evaluated liposomes loaded with the α-particle generator 225Ac to selectively kill $PSMA^+$ PCa cells. In this study, anti-PSMA–targeted liposomes have been able to kill $PSMA^+$ cells, including endothelial cells induced to express PSMA, suggesting their use for selective antivascular α-radiotherapy.

CONCLUSIONS

PSMA represents an attractive target for the detection, diagnosis, and treatment of PCa. PSMA immunohistochemical assessment by pathologists could be further exploited as predictive marker in patients with metastatic PCa, in order to guide clinicians in the selection of the most appropriate imaging technique and therapy in an individual patient.

Since choline PET/CT is unable to detect PCa recurrence at low PSA values, a more sensitive compound based on PSMA-targeted imaging seems to have the characteristics to become the new clinical standard.

A number of PSMA based diagnostic and therapeutic agents are under phase I, II and III clinical trials. Nevertheless, the choice of emerging PSMA-targeted radiotracers and therapeutic agents needs further investigation in order to identify the most specific compound for the different sites and phases of this disease. As our understanding of the precise role of PSMA in prostate carcinogenesis advances and molecular techniques become more refined, PSMA-based strategies will likely play a crucial role in the developing scenario of PCa patients.

REFERENCES

1. Chang SS. Overview of prostate-specific membrane antigen. Rev Urol 2004; 6: S13–S18.
2. Nelson WG, De Marzo AM, Isaacs WB. Prostate cancer. N Engl J Med 2003; 349:366-81.
3. Ananias HJ, van den Heuvel MC, Helfrich W, de Jong IJ. Expression of the gastrin-releasing peptide receptor, the prostate stem cell antigen and the prostate-specific membrane antigen in lymph node and bone metastases of prostate cancer. Prostate 2009; 69:1101-8.
4. Pinto JT, Suffoletto BP, Berzin TM, et al. Clin Cancer Res 1996; 2:1445-51.
5. Carter RE, Feldman AR, Coyle JT. Proc Natl Acad Sci USA 1996; 93:749-53.
6. Ghosh A, Heston WD. Tumor target prostate specific membrane antigen (PSMA) and its regulation in prostate cancer. J Cell Biochem 2004; 91:528-39.
7. Wright GL Jr, Haley C, Beckett ML, Schellhammer PF. Expression of prostate-specific membrane antigen in normal, benign, and malignant prostate tissues. Urol Oncol 1995; 1:18-28.
8. Horoszewicz JS, Kawinski E, Murphy GP. Monoclonal antibodies to a new antigenic marker in epithelial prostatic cells and serum of prostatic cancer patients. Anticancer Res 1987; 7:927-35.
9. Kasperzyk JL, Finn SP, Flavin R, et al. Prostate-specific membrane antigen protein expression in tumor tissue and risk of lethal prostate cancer. Cancer Epidemiol Biomarkers Prev 2013; 22:2354-63.
10. Chang SS, Gaudin PB, Reuter VE, Heston WD. Prostate-specific membrane antigen: present and future applications. Urology 2000; 55:622-29.

11. Yao V, Bacich DJ. Prostate specific membrane antigen (PSMA) expression gives prostate cancer cells a growth advantage in a physiologically relevant folate environment *in vitro*. Prostate 2006; 66:867-75.
12. Yao V, Berkman CE, Choi JK, O'Keefe DS, Bacich DJ. Expression of prostate-specific membrane antigen (PSMA), increases cell folate uptake and proliferation and suggests a novel role for PSMA in the uptake of the non-polyglutamated folate, folic acid. Prostate 2010; 70:305-16.
13. Guo Z, Lai Y, Du T, et al. Prostate specific membrane antigen knockdown impairs the tumorigenicity of LNCaP prostate cancer cells by inhibiting the phosphatidylinositol 3-kinase/Akt signaling pathway. Chin Med J 2014; 127:929-36.
14. Zhang Y, Guo Z, Du T, Chen J, Wang W, Xu K, Lin T, Huang H. Prostate specific membrane antigen (PSMA): a novel modulator of p38 for proliferation, migration, and survival in prostate cancer cells. Prostate 2013; 73:835-41.
15. Ghosh A, Wang X, Klein E, Heston WD. Novel role of prostate-specific membrane antigen in suppressing prostate cancer invasiveness. Cancer Res 2005; 65:727-31.
16. Xu L, Wang Z, Li XF, et al. Screening and identification of significant genes related to tumor metastasis and PSMA in prostate cancer using microarray analysis. Oncol Rep 2013; 30:1920-8.
17. Liu T, Mendes DE, Berkman CE. Functional prostate-specific membrane antigen is enriched in exosomes from prostate cancer cells. Int J Oncol 2014; 44:918-22.
18. Lundholm M, Schröder M, Nagaeva O, Baranov V, Widmark A, Mincheva-Nilsson L, Wikström P. Prostate tumor-derived exosomes down-regulate NKG2D expression on natural killer cells and CD8+ T Cells: mechanism of immune evasion. PLoS One 2014; 9:e108925.
19. Ramteke A, Ting H, Agarwal C. Exosomes secreted under hypoxia enhance invasiveness and stemness of prostate cancer cells by targeting adherens junction molecules. Mol Carcinog 2013; doi: 10.1002/mc.22124.
20. Bermejo CE, Coursey J, Basler J, Austenfeld M, Thompson I. Histologic confirmation of lesions identified by Prostascint scan following definitive treatment. Urol Oncol 2003; 21:349-52.
21. Lau HY, Kindrachuk G, Carter M, Prestage K, Webber D, Stauffer E, Haseman M. Surgical confirmation of ProstaScint abnormalities in two patients with high risk prostate cancer. Can J Urol 2001; 8:1199-202.
22. Hinkle GH, Burgers JK, Olsen JO, Williams BS, Lamatrice RA, Barth RF, Rogers B, Maguire RT. Prostate cancer abdominal metastases detected with indium-111 capromab pendetide. J Nucl Med 1998; 39:650-52.
23. Xu W, Siddiqui IA, Nihal M, et al. Aptamer-conjugated and doxorubicin-loaded unimolecular micelles for targeted therapy of prostate cancer. Biomaterials 2013; 3:5244-53.
24. Holland JP, Divilov V, Bander NH, Smith-Jones PM, Larson SM, Lewis JS. 89Zr-DFO-J591 for immunoPET of prostate-specific membrane antigen expression *in vivo*. J Nucl Med 2010; 51:1293-300.
25. Evans MJ, Smith-Jones PM, Wongvipat J, Navarro V, Kim S, Bander NH, Larson SM, Sawyers CL. Noninvasive measurement of androgen receptor signaling with a positron-emitting radiopharmaceutical that targets prostate-specific membrane antigen. Proc Natl Acad Sci U S A 2011; 108:9578-82.
26. Pandit-Taskar N, O'Donoghue JA, Beylergil V, et al. (89)Zr-huJ591 immuno-PET imaging in patients with advanced metastatic prostate cancer. Eur J Nucl Med Mol Imaging 2014; 4:2093-105.
27. Evazalipour M, D'Huyvetter M, Tehrani BS, et al. Generation and characterization of nanobodies targeting PSMA for molecular imaging of prostate cancer. Contrast Media Mol Imaging 2014; 9:211-20.
28. Luthi-Carter R, Barczak AK, Speno H, Coyle JT. Molecular characterization of human brain N-acetylated alpha-linked acidic dipeptidase (NAALADase). J Pharmacol Exp Ther 1998; 286:1020-25.
29. Tiffany CW, Lapidus RG, Merion A, Calvin DC, Slusher BS. Characterization of the enzymatic activity of PSM: comparison with brain NAALADase. Prostate 1999; 39:28-35.
30. Jackson PF, Cole DC, Slusher BS, Stetz SL, Ross LE, Donzanti BA, Trainor DA. Design, synthesis, and biological activity of a potent inhibitor of the neuropeptidase N-acetylated alpha-linked acidic

dipeptidase. J Med Chem 1996; 39:619-22.
31. Jackson PF, Slusher BS. Design of NAALADase inhibitors: a novel neuroprotective strategy. Curr Med Chem 2001; 8:949-57.
32. Maresca KP, Hillier SM, Femia FJ, et al. A series of halogenated heterodimeric inhibitors of prostate specific membrane antigen (PSMA) as radiolabeled probes for targeting prostate cancer. J Med Chem 2009; 52:347-57.
33. Hillier SM, Maresca KP, Femia FJ, et al. Preclinical evaluation of novel glutamate-urea-lysine analogues that target prostate-specific membrane antigen as molecular imaging pharmaceuticals for prostate cancer. Cancer Res 2009; 69:6932-40.
34. Foss CA, Mease RC, Fan H, et al. Radiolabeled small-molecule ligands for prostate-specific membrane antigen: *in vivo* imaging in experimental models of prostate cancer. Clin Cancer Res 2005; 11:4022-8.
35. Lu G, Maresca KP, Hillier SM, et al. Synthesis and SAR of (99m)Tc/Re-labeled small molecule prostate specific membrane antigen inhibitors with novel polar chelates. Bioorg Med Chem Lett 2013; 23:1557-63.
36. Kularatne SA, Zhou Z, Yang J, Post CB, Low PS. Design, synthesis, and preclinical evaluation of prostate-specific membrane antigen targeted (99m)Tc-radioimaging agents. Mol Pharm 2009; 6:790-800.
37. Chen Y, Pullambhatla M, Byun Y, et al. 2-(3-{1-Carboxy-5-((6-(18F)fluoropyridine-3-carbonyl)-amino)-pentyl}-ureido)-pentanedioic acid, (18F)DCFPyL, a PSMA-based PET imaging agent for prostate cancer. Clin Cancer Res 2011; 17:7645-53.
38. Banerjee SR, Pullambhatla M, Shallal H, Lisok A, Mease RC, Pomper MG. A modular strategy to prepare multivalent inhibitors of prostate-specific membrane antigen (PSMA). Oncotarget 2011; 2:1244-53.
39. Afshar-Oromieh A, Haberkorn U, Schlemmer HP, et al. Comparison of PET/CT and PET/MRI hybrid systems using a 68Ga-labelled PSMA ligand for the diagnosis of recurrent prostate cancer: initial experience. Eur J Nucl Med Mol Imaging 2014; 4:887-97.
40. Barrett JA, Coleman RE, Goldsmith SJ, et al. First-in-man evaluation of two high-affinity PSMA-avid small molecules for imaging prostate cancer. J Nucl Med 2013; 54:380-87.
41. Mease RC, Foss CA, Pomper MG. PET imaging in prostate cancer: focus on prostate-specific membrane antigen. Curr Top Med Chem 2013; 13:951-62.
42. Mease RC, Dusich CL, Foss CA, et al. N-(N-(S)-1,3-Dicarboxypropyl)carbamoyl)-4- (18F)fluorobenzyl-L-cysteine, (18F)DCFBC: a new imaging probe for prostate cancer. Clin Cancer Res 2008; 14:3036-43.
43. Cho SY, Gage KL, Mease RC, et al. Biodistribution, tumor detection and Radiation dosimetry of 18F-DCFBC, a low molecular weight inhibitor of PSMA, in patients with metastatic prostate cancer. J Nucl Med 2012; 53:1883-91.
44. Giovacchini G, Picchio M, Coradeschi E, et al. Predictive factors of ((11)C)choline PET/CT in patients with biochemical failure after radical prostatectomy. Eur J Nucl Med Mol Imaging 2010; 37:301-9.
45. Afshar-Oromieh A, Haberkorn U, Eder M, Eisenhut M, Zechmann C. ((68)Ga)Gallium-labelled PSMA ligand as superior PET tracer for the diagnosis of prostate cancer: comparison with (18)F-FECH. Eur J Nucl Med Mol Imaging 2012; 39:1085-86.
46. Afshar-Oromieh A, Malcher A, Eder M, et al. PET imaging with a ((68)Ga)gallium-labelled PSMA ligand for the diagnosis of prostate cancer: biodistribution in humans and first evaluation of tumour lesions. Eur J Nucl Med Mol Imaging 2013; 40:486-95
47. Eder M, Schafer M, Bauder-Wust U, et al. Ga-complex lipophilicity and the targeting property of a urea-based PSMA inhibitor for PET imaging. Bioconjug Chem 2012; 23:688-97.
48. Eder M, Eisenhut M, Babich J, Haberkorn U. PSMA as a target for radiolabelled small molecules. Eur J Nucl Med Mol Imaging 2013; 40:819-23.
49. Graham, K.; Kettschau, G.; Gromov, A.; Friebe, M.; Gekeler, V.; Dinkelborg, L. (18F)-labeled PET tracer BAY1075553, small molecule inhibitor of PSMA for molecular Imaging of prostate cancer; World Molecular Imaging Conference; Sept. 7-10; San Diego, California. 2011. p. P235
50. Langsteger W, Kunit T, Haim S, et al. BAY 1075553 PET/CT in the assessment of prostate cancer: Safety, tolerability and biodistribution - Phase I first in

human study results. J Nucl Med 2012; 53:1125.
51. Ireson CR, Kelland LR. Discovery and development of anticancer aptamers. Mol Cancer Ther 2006; 5:2957-62.
52. Lupold SE, Hicke BJ, Lin Y, Coffey DS. Identification and characterization of nuclease-stabilized RNA molecules that bind human prostate cancer cells via the prostate-specific membrane antigen. Cancer Res 2002; 62:4029-33.
53. Wang X, Ma D, Olson WC, Heston WD. *In vitro* and *in vivo* responses of advanced prostate tumors to PSMA ADC, an auristatin-conjugated antibody to prostate-specific membrane antigen. Mol Cancer Ther 2011; 10:1728-39.
54. Petrylak DP, Smith DC, Appleman LJ, et al. A phase 2 trial of prostate-specific membrane antigen antibody drug conjugate (PSMA ADC) in taxane-refractory metastatic castration-resistant prostate cancer (mCRPC). 2014 ASCO Annual Meeting; abstract 5023.
55. Denmeade SR, Mhaka AM, Rosen DM, et al. Engineering a prostate-specific membrane antigen-activated tumor endothelial cell prodrug for cancer therapy. Sci Transl Med 2012; 4:140ra86.
56. Ma Q, Safar M, Holmes E, Wang Y, Boynton AL, Junghans RP. Anti-prostate specific membrane antigen designer T cells for prostate cancer therapy. Prostate 2004; 61:12-25.
57. Ma Q, Safar M, Holmes E, Wang Y, Boynton AL, Junghans RP. Anti-prostate specific membrane antigen designer T cells for prostate cancer therapy. Prostate 2004; 6:12-25.
58. Sugimoto Y, Hirota M, Yoshikawa K, et al. The therapeutic potential of a novel PSMA antibody and its IL-2 conjugate in prostate cancer. Anticancer Res 2014; 34:89-97.

JOURNAL OF BIOLOGICAL REGULATORS & HOMEOSTATIC AGENTS Vol. 28, no. 4, 565-573 (2014)

EDITORIAL

CAN PROBIOTIC ADMINISTRATION DURING PREGNANCY AND THE FIRST YEAR OF LIFE EFFECTIVELY REDUCE THE RISK OF INFECTIONS AND ALLERGIC DISEASES IN CHILDHOOD?

S. ESPOSITO, L. CASTELLAZZI and F. GARBARINO

Pediatric Highly Intensive Care Unit, Department of Pathophysiology and Transplantation, Università degli Studi di Milano, Fondazione IRCCS Ca' Granda Ospedale Maggiore Policlinico, Milan, Italy

Received October 23, 2014 – Accepted december 1, 2014

Infections and allergic disorders are common pediatric diseases. It has been reported that probiotics, which are live microorganisms, confer health benefits to hosts when administered in appropriate amounts. Probiotics have been widely used in the treatment of pediatric infections and allergic disorders through modulating the microbial environment of host. However, it is still not clear whether probiotic administration during pregnancy and/or the first year of life is an efficient approach for the prevention of infections and allergic diseases in childhood. The present study aims to address this question through reviewing previous publications on this topic. Analysis of previous studies suggests that probiotic administration during pregnancy and/or the first year of life could reduce the prevalence of infectious diseases in infancy. The effects of probiotic administration during pregnancy and/or the first year of life on the prevention of allergic disorders are still not clear. In addition, the available studies differ in probiotic species, number of probiotics, dosage of probiotics, inclusion and exclusion criteria, outcomes, and diagnostic and follow-up methods. These differences highlight further studies for better understanding the effects of probiotic administration on the prevention of infections and allergic diseases in childhood.

Infectious diseases are common in infants worldwide, leading to a heavy consumption of antibiotics in children (1). In the last decades, the incidence of allergic disorders in Western countries has significantly increased due to antibiotic abuse, hygiene improvement, reduced family size, and dietary changes. According to the "hygiene hypothesis" proposed by Strachan, microbial exposure in childhood is critically important for the development of the immune system (1). Environmental antigens stimulate the host to achieve adequate and appropriate immune competence.

Probiotics are live microorganisms commonly used to modulate the microbial environment in hosts.

A number of studies have reported the usefulness of probiotics in the treatment of infectious diseases (mainly infectious diarrhoea and diarrhoea due to antibiotics) and allergic disorders in childhood (1-5). However, they are often inappropriately prescribed for prevention of infectious diseases (i.e., during administration of any kind of antibiotic therapy or during international travels to prevent diarrhoea). Little is known about the influence of probiotic administration during pregnancy and the first year

Key words: probiotics, infectious diseases, allergic diseases, children, pregnancy

Mailing address: Susanna Esposito, M.D.
Pediatric Highly Intensive Care Unit,
Department of Pathophysiology and Transplantation,
Università degli Studi di Milano, Fondazione IRCCS Ca' Granda,
Ospedale Maggiore Policlinico, Via Commenda 9, 20122 Milano, Italy
Tel.: +39 02 55032498 Fax: +39 02 50320206.
email: susanna.esposito@unimi.it

0393-974X (2014)

DISCLOSURE: ALL AUTHORS REPORT NO CONFLICTS OF INTEREST RELEVANT TO THIS ARTICLE.

of life on the incidence of infectious diseases and allergic disorders in pediatric patients. To address this question, we searched and reviewed the articles published over the last 15 years in PubMed using the key words, "probiotic" and "pregnancy" or "infant" and "infection" or "allergy" and "prevention". Studies on premature newborns and administration of probiotics in the neonatal intensive care unit and treatment of acute diseases using probiotics were excluded from our analyses.

EFFECTS OF PROBIOTICS ADMINISTERED DURING PREGNANCY AND THE FIRST YEAR OF LIFE ON THE PREVENTION OF PEDIATRIC INFECTIOUS DISEASES

The probiotic strains that exhibited infection prevention abilities include *Lactobacillus rhamnosus* GG, *L. rhamnosus* LC705, *Bifidobacterium lactis* Bb-12, *Bifidobacterium breve* Bb99, *Propionibacterium freudenreichii* subsp. *shermani*, *Lactobacillus fermentum* CECT5716, *Lactobacillus reuteri* and *Bifidobacterium longum* BL999 (6-13) (Table I). A number of mechanisms underlying the infection prevention of these probiotics have been proposed. Antimicrobial products released by probiotics can directly kill or inhibit the growth of pathogenic microbes, block toxin-mediated responses, interfere with nutrition acquisition and adhesion of pathogens, and enhance the humoral and cellular immunity of hosts (1).

To the best of our knowledge, there is only one published study evaluating the effects of probiotic administration during pregnancy on the prevention of infectious diseases in pediatric patients. In this study, pregnant mothers received a mixture of four probiotics including *L. rhamnosus* GG, *L. rhamnosus* LC705, *B. breve* Bb99, and *P. freudenreichii* subsp. *shermani* for 4 weeks before delivery (6). The infants received the same probiotics plus a prebiotic daily for 6 months after birth. During the six months of probiotic intervention, antibiotics were less prescribed in the experimental group than in the placebo group. Moreover, respiratory infections occurred less frequently in the experimental than the placebo group during the 24 months of follow-up.

A total of eight studies evaluating the effects of probiotics on the prevention of infectious diseases in infants were identified. Among them, seven studies concluded that probiotic administration in the first year of life was effective for reducing infectious diseases, especially infections of respiratory tracts (7-9, 11-13, 14). Only one study carried out on children aged 7-13 months showed that the use of probiotics (*Streptococcus thermophilus* NCC 2496, *Streptococcus salivarius* DSM 13084, and *L. rhamnosus* LPR CGMCC 1.3724) and prebiotics (Raftilose/Raftiline) did not reduce the risk of acute otitis media (AOM), recurrent AOM, and antibiotic consumption or lower respiratory tract infections during the one year of experiments (14).

However, the studies on the impacts of probiotics in the prevention of pediatric infectious diseases were conducted with different study designs including criteria for inclusion and exclusion subjects, criteria for diagnosis of infectious diseases, follow-up methods, as well as primary and secondary outcomes. Distinct probiotic administration schedules including different probiotic species and administration time were applied in different studies. In addition, the ages of enrolled subjects are also different among these studies. Moreover, the effect of the association prebiotics-probiotics requires further evaluation. Therefore, more studies are highlighted to determine the optimal probiotic administration schedule, although most previous studies suggest that probiotic administration during pregnancy and the first year of life were effective for the prevention of infectious diseases.

IMPACT OF PROBIOTICS ADMINISTERED DURING PREGNANCY AND THE FIRST YEAR OF LIFE ON THE PREVENTION OF PEDIATRIC ALLERGIC DISEASES

The main studies on the impacts of probiotic administration during pregnancy and the first year of life on prevention of pediatric allergic diseases are summarized in Tables II and III. A total of 20 randomized-controlled studies investigating the effects of maternal and/or infant probiotic supplementation on the prevention of allergic diseases were identified and discussed. In eight studies, probiotics were supplemented both prenatally to mothers and postnatally to children (15-22). Mothers' probiotic supplementation was

Table I. *Summary of the published clinical trials on the use of probiotics during pregnancy and the first year of life for the prevention of pediatric infectious diseases.*

Author, year of publication, and country	Type of study	Age range/ duration of intervention	Duration of follow-up	Number of subjects	Probiotic	Main results
Weizman et al. (7), 2005, Israel	Randomized, double-blind, placebo-controlled study	4-10 months/12 wk	12 weeks	201 (60 controls, 73 *Bifidobacterium lactis*, 68 *Lactobacillus reuteri*)	*Bifidobacterium lactis* BB-12 and *Lactobacillus reuteri*, $1x10^7$ CFU in supplemented formula	The experimental group had significantly lower incidence of fever and diarrhea. The subjects who received *L. reuteri* had significantly decreased number of days with fever and antibiotic prescriptions. No significant differences between the two groups in rate and duration of respiratory illness
Puccio et al. (8), 2007, Italy	Prospective, randomized, reference-controlled, double-blinded study	Full-term (≥37 wk), newborn infants whose mothers had decided not to breast feed. From 14 to 112 days of life	7 months	97 (55 controls, 42 in the experimental group)	*Bifidobacterium longum* BL999 $2x10^7$ CFU and prebiotics in supplemented formula	The experimental group had fewer respiratory tract infections than the control group.
Kukkonen et al. (6), 2008, Finland	Randomized, double-blind, placebo-controlled study	4 weeks before delivery to six months	24 months	1810 (512 controls, 506 in the experimental group)	*Lactobacillus rhamnosus* GG, LC705, *Bifidobacterium breve* Bb99, and *Propionibacterium freudenreichii* ssp *Shermani* 8-9x 10^9 CFU plus post-partum galacto-oligosaccharide (capsules)	During the 6 months of probiotic administration, antibiotic were less often prescribed in the experimental group than the placebo group. Moreover, during the 24 months of follow-up, respiratory infections occurred less frequently in the experimental group than the placebo group.
Rautava et al. (9), 2009, Finland	Randomized, double-blind, placebo-controlled study	0-2 months to age of 12 months	12 months	81 (43 controls, 38 in the experimental group)	*Bifidobacterium lactis* BB-12 and *Lactobacillus rhamnosus* GG $1x10^{10}$ CFU in supplemented formula	Probiotics reduced the incidence of early infections (before the age of 7 months) and the incidence of recurrent infections during the first year of life.
Taipale et al. (10), 2011, Finland	Randomized, double-blind, placebo-controlled study	1 month to age of 8 months	8 months	109 (54 controls, 55 in the experimental group)	*Bifidobacterium lactis* BB-12 10 billion CFU released by a novel slow-release pacifier or a spoon	No significant differences between the two groups in gastrointestinal symptoms, otitis media and the connsumtion of antibiotics. The experimental group had less incidence of respiratory infections.
Maldonado et al. (11), 2012, Spain	Randomized, double-blind, controlled study	6 months to age of 12 months	6 months	188 (91 controls, 97 in the experimental group)	*Lactobacillus fermentum* CECT5716 $2x10^7$ CFU and prebiotics in supplemented formula	The experimental group had a significant reduction in the incidence of gastrointestinal, upper respiratory tract infections and total number of infections than the control group.
Gil-Campos et al. (13), 2012, Spain	Randomized, double-blind, controlled study	1 months to 6 months of age	5 months	137 (71 control, 66 in the experimental group)	*Lactobacillus fermentum* CECT5716 $1x10^7$ CFU and prebiotics in supplemented formula	The experimental group had lower incidence of gastrointestinal infections than the control group. No difference in incidence of respiratory tract infections between the two groups.
Luoto et al. (12), 2013, Finland	Randomized, double-blind, placebo-controlled study	3-60 days of life	12 months	94 preterm infants of gestational age ≥ 32+0 and ≤ 36+6 weeks (32 controls, 31 in the prebiotic group as galacto-oligosaccharide and polydextrose mixture, 31 in the probiotic group)	*Lactobacillus rhamnosus* GG, ATCC 53103 $1x10^9$ CFU for 1 to 30 days and $2x10^9$ CFU for 31 to 60 days in supplemented formula	Children in prebiotic and probiotic groups had a significantly lower incidence of respiratory tract infections and a lower incidence of rhinovirus-induced episodes than the control group.
Cohen et al. (14), 2013, France	Randomized, double-blind, placebo-controlled study	7-13 months/12 months	12 months	224 (112 controls and 112 in the experimental group)	*Streptococcus thermophilus* NCC 2496 $1x10^7$ CFU , *Streptococcus salivarius* DSM 13084 $2.5x10^7$ CFU, *Lactobacillus rhamnosus* LPR CGMCC 1.3724 $1x10^7$ CFU and prebiotics (Raftilose/Raftiline) in supplemented formula	No significant differences in incidence of acute otitis media or lower respiratory tract infections between the two groups.

Table II. *Summary of the published clinical trials on the use of probiotics during pregnancy and the first year of life for the prevention of pediatric allergic diseases.*

Author, year of publication, country	Type of study	Age range/duration of intervention	Duration of follow-up	Number of subjects	Infant allergic risk	Probiotic	Main results
Abrahamsson et al. (15), 2013, Sweden	Randomized, double-blind, placebo-controlled trial	36 WG to delivery (mother), birth to 12 months (infant)	7 years	239 mothers (209 infants) (follow-up completed at 7 years : 94 *L.reuteri*, 90 controls)	High (family history)	*Lactobacillus reuteri ATCC 55730 (*1x10^8 CFU)	Prevalence of asthma, allergic rhinoconjunctivitis, eczema and skin prick test reactivity were similar between the probiotic and placebo groups.
Wickens et al. (16), 2013, New Zeland	Randomized, double-blind, placebo-controlled trial	35 WG to 6 month postpartum if breastfeeding (mother), birth to 2 years (infant)	6 years	512 mothers (474 infants) (follow-up completed at 6 years : 144/159 placebo, 134/157 HN001, 144/158 HN019)	High (family history)	2 probiotic groups: *Lactobacillus rhamnosus* HN001 (6x10^9 CFU) or *Bifidobacterium lactis* HN019 (9x10^9 CFU)	HN001 administration led to significant reduction of the cumulative prevalence of eczema and SPT sensitization. HN019 had no significant effects on any outcomes.
Kukkonen et al. (17), 2007, Finland	Randomized, double-blind, placebo-controlled trial	36-38 WG to delivery (mother), birth to 6 months (infant)	2 years	1223 mothers (1018 infants) (610 probiotic group, 613 placebo) (follow-up at 2 years : 461/506 probiotic, 464/512 placebo)	High (family history)	*Lactobacillus rhamnosus GG, Lactobacillus rhamnosus LC 705, Bifidobacterium breve Bb-99, Propionibacterium freudenreichii JS (mothers:* 2,4x10^{10} CFU, infants: 1,2x10^{10} CFU) plus 0.8g of galacto-oligosaccharide	No effects on the cumulative incidence of allergic deseases, but decrease of IgE-associated diseases. Probiotic treatment reduced eczema and atopic eczema.
Kukkonen et al. (18), 2011, Finland	Randomized, double-blind, placebo-controlled trial	36-38 WG to delivery (mother), birth to 6 months (infant)	5 years	160 children (follow-up at 5 years : 64 probiotic, 67 placebo)	High (family history)	*Lactobacillus rhamnosus GG, Lactobacillus rhamnosus LC 705, Bifidobacterium breve Bb-99, Propionibacterium freudenreichii JS (mothers:* 2,4x10^{10} CFU, infants: 1,2x10^{10} CFU) plus 0.8g of galacto-oligosaccharide	Probiotic administration during the first six months of life had no effects on airway infiammation at age 5 years as measured by FENO. No preventive effects of probiotics on atopic eczema and respiratory allergies at 5 years.
Ou et al. (19), 2012, Taiwan	Randomized, double-blind, placebo-controlled trial	24 WG to 6 months postpartum if breastfeeding (mother), weaning to 6 months, (infant)	3 years	191 mothers (151 infants) (follow-up at 3 years : 65/95 LGG, 63/96 placebo)	High (family history)	*Lactobacillus rhamnosus GG (*1x10^{10} CFU)	No significant effects of probiotic supplementation on sensitization, development of allergic disease, or maternal IgE levels.
Kopp et al. (20), 2008, Germany	Randomized, double-blind, placebo-controlled trial	34-36 WG to 3 months postpartum, if breastfeeding (mother), weaning to 6 months, or 3-6 months (infant)	2 years	105 mothers (104 infants) (follow-up completed at 2 years : 50/54 LGG, 44/51 placebo)	High (family history)	*Lactobacillus rhamnosus GG (*1x10^{10} CFU)	*L. rhamnosus* GG had no effects in reducing the incidence and severity of atopic dermatitis, but was associated with an increased rate of recurrent episodes of wheezing bronchitis.

Niers et al. (21), 2009, Netherlands	Randomized, double-blind, placebo-controlled trial	24 WG to delivery (mother), birth to 12 months (infant)	2 years	156 mothers (123 infants) (follow-up at 2 years : 50/78 probiotic, 48/78 placebo)	High (family history)	*Bifidobacterium bifidum W23, Bifidobacterium lactis W52 and Lactobacillus lactis W58* ($3x10^9$CFU)	Eczema during the first 3 months of life was significantly lower in the probiotic group compared with placebo. This effect seemed to be sustained until the age of 2 years, although relative risk reduction decreases with age.
Kalliomaki et al. (22), 2001, 2003, 2007, Finland	Randomized, double-blind, placebo-controlled trial	36-38 WG to 6 months postpartum if breastfeeding (mother), weaning to 6 months, (infant)	7 years	159 mothers (155 infants) (follow up at 7 years : 53/77 probiotic, 62/82 placebo)	High (family history)	*Lactobacillus rhamnosus* GG (/$1x10^{10}$CFU)	At 7 years of age, the risk of eczema was significantly reduced in the Lactobacillus GG group compared with the placebo group. Allergic rhinitis and asthma tend to be more common in the probiotic group. The frequency of atopic sensitization is similar between the two groups.
Huurre et al. (23), 2008, Finland	Randomized, double-blind, placebo-controlled trial	First trimester of pregnancy to the end of exclusive breastfeeding (mother).	12 months	171 mothers (171 infants) (follow-up at 12 months : 140 infants)	High (family history)	*Lactobacillus rhamnosus* GG and *Bifidobacterium lactis* Bb-12 (/$1x10^{10}$CFU)	There was no difference between infant sensitization in the probiotic *vs* the placebo group at the age of 12 months. However, probiotic supplementation had a significant protective effect against sensitization in a subgroup of infants with high hereditary risk due to maternal sensitization
Dotterud et al. (24), 2010, Norway	Randomized, double-blind, placebo-controlled trial	36 WG to 3 months postpartum (mother)	2 years	415 mothers (363 infants) (follow-up at 2 years : 138/211 probiotic, 140/204 placebo)	Unknown, subjects were randomly selected.	*Lactobacillus rhamnosus GG, Bifidobacterium lactis* BB-12, *Lactobacillus acidophilus La-5* (/$1.05x10^{11}$CFU)	Probiotic administration in randomly selected mothers reduced the cumulative incidence of atopic dermatitis, but had no effects on atopic sensitization and asthma.
Rautava et al. (25), 2012, Finland	Randomized, double-blind, placebo-controlled trial	32 WG to 2 months postpartum if breastfeeding (mother)	2 years	241 mothers (250 infants) (follow-up at 2 years : 73/81 LPR + BL999, 70/82 ST11 + BL999, 62/78 placebo)	High (family history)	2 probiotic groups: *Lactobacillus rhamnosus* LPR + *Bifidobacterium longum BL 999* ($1x10^9$ CFU) or *Lactobacillus paracasei ST11* + *Bifidobacterium longum BL 999* ($1x10^9$ CFU)	Either LPR+BL999 or ST11+BL999 supplementation were associated with a reduction of the risk of developing eczema. No effects on the risk of atopic sensitization in the infants.
Boyle et al. (26), 2011, Australia	Randomized, double-blind, placebo-controlled trial	36 WG to delivery (mother)	12 months	250 mothers (250 infants) (follow-up at 12 months : 109/125 probiotic, 103/125 placebo)	High (family history)	*Lactobacillus rhamnosus GG* (/$1x10^8$ CFU)	Prenatal probiotic treatment was not associated with reduced risk of eczema or IgE-associated eczema.

WG: week of gestation.

Table III. *Summary of the published clinical trials on the use of probiotics in the first year of life for the prevention of pediatric allergic diseases.*

Author, year of publication, country	Type of study	Age range/ duration of intervention	Duration of follow-up	Number of subjects	Infant allergic risk	Probiotic	Main results
Taylor et al. (27), 2007, Australia	Randomized, double-blind, placebo-controlled trial	Birth to 6 months (infants)	12 months	226 mothers (218 infants) (follow-up at 5 years : 89/115 probiotic, 89/111 placebo)	High (family history)	*Lactobacillus acidophilus LAVRI-A1* (3x10^9 CFU)	Early supplementation with LAVRI-A1 did not reduce the risk of atopic dermatitis in high-risk infants, but was associated with increased allergen sensitization.
Gruber et al. (28), 2007, Germany	Randomized, double-blind, placebo-controlled trial	Age 7-10 months (infants)	10 months	106 infants (follow-up at 10 months: 54/56 *Lactobacillus rhamnosus* GG, 48/50 placebo)	High (eczema)	*Lactobacillus rhamnosus GG* (1x10^{10}CFU)	No effects of LGG on reducing mild-to-moderate atopic dermatitis in infancy, no differences between the two groups in the use of rescue medication, total serum IgE and development of allergic sensitization against hen's egg or cow's milk
Gore et al. (29), 2012, UK	Randomized, double-blind, placebo-controlled trial	Age 5-8 months (infants)	3 years	137 infants (follow-up at 3 years : 35/45 *Lactobacillus paracasei,* 36/45 *Bifidobacterium lactis,* 40/47 placebo)	High (eczema)	2 probiotic groups: *Lactobacillus paracasei* or *Bifidobacterium lactis* (1x10^{10}CFU)	No benefits from supplementation with *B.lactis* or *L.paracasei* in the prevention of eczema and allergic diseases from age 1 to 3 years.
Van der Aa et al. (30), 2011, Netherlands	Randomized, double-blind, placebo-controlled trial	Age 5-8 months (infants)	18 months	90 infants (follow-up at 12 months : 36/46 probiotic, 39/44 placebo)	High (eczema)	*Bifidobacterium breve M-16V* (1.3x10^9CFU per 100ml) plus 0.8g of a mixture of scGOS and lcFOS	The prevalence of wheezing was significantly lower in the probiotic group than the placebo group. No significant differences in the total IgE levels between the two groups.
West et al. (31), 2009, 2013, Sweden	Randomized, double-blind, placebo-controlled trial	Age 4-13 months (infants)	8-9 year	179 infants (follow-up at 8-9 year : 59/84 probiotic, 62/87 placebo)	Unselected	*Lactobacillus paracasei F19*(1x10^8CFU)	There were no long-term effects of LF19 on any diagnosed allergic disease, airway inflammation, or IgE sensitization.
Hol et al. (32), 2008, Netherlands	Randomized, double-blind, placebo-controlled trial	Age 4-16 months (infants)	16 months	119 infants (follow-up at 12 months : 23/59 probiotic, 25/60 placebo)	High (milk allergy)	*Lactobacillus casei and Bifidobacterium lactis* Bb-12 (2x10^7CFU per g)	The cumulative percentage of tolerance to cow's milk at 6 and 12 months was similar between the two groups. Infants in the placebo group had higher percentages of CD3(+) and CD3(+)CD4(+) lymphocytes than the probiotic-treated infants
Soh et al. (3), 2009, Singapore	Randomized, double-blind, placebo-controlled trial	Birth to 6 months (infants)	12 months	253 infants (follow-up at 12 months : 124/127 probiotic, 121/126 placebo)	High (family history)	*Bifidobacterium longum* BL999 (1x10^7CFU/g) and *Lactobacillus rhamnosus* LPR (2x10^7CFU/g)	At 12 months: early life administration of a cow's milk formula supplemented with probiotics showed no effects on the prevention of eczema and allergen sensitization in the first year of life.
Loo et al. (34) 2014, Singapore	Randomized, double-blind, placebo-controlled trial	Birth to 6 months (infants)	12 months	253 infants (follow-up at 5 years : 112/124 probiotic, 108/121 placebo)	High (family history)	*Bifidobacterium longum* BL999 (1x10^7CFU/g) and *Lactobacillus rhamnosus* LPR (2x10^7CFU/g)	At 5 years: no significant differences between the two groups in developing athsma, allergic rhinitis, eczema, food allergy or sensitization to inhalant allergens.

mostly started in the last trimester of pregnancy, and probiotics were administered to neonates and infants in some cases. In four trials, probiotics were administrated only to mothers during pregnancy (23-26). In the last eight studies, probiotics were supplemented only postnatally to the infants from birth to 16 months of age, and the follow-up lasted for 10 months to 7 years (27-34). In most studies, the study subjects had high-risk of developing allergic disease (i.e., with family history of allergic

disease or had eczema) (15-23, 25-30, 32-34). Only two trials were conducted on randomly selected subjects (24, 31). Various probiotic microorganisms were included in these studies and the daily dose of probiotics ranged from 10^7 to 10^{11} colony-forming units. Overall, *L. rhamnosus* was the most frequently used probiotic, followed by *B. lactis*. In a few cases, prebiotics were administrated with probiotics (17, 18, 30).

Eczema was frequently considered as an index to evaluate the effects of probiotics on the prevention of allergic diseases. Most of these studies showed no significant reduction in incidence of eczema symptoms by probiotic supplementation compared with placebo (15, 18-20, 22, 23, 26-34). However, at least six trials demonstrated that probiotic administration of mothers, infants, or both significantly reduced the incidence of eczema in children (16, 17, 21, 22, 24, 25). Interestingly, in a large cohort study performed by Kukkonen et al., supplementation of four probiotics to mothers from week 36 of pregnancy and to their infants for six months after birth resulted in a reduction of eczema at two years of age compared with the placebo group (17, 18). Nevertheless, follow-up until age five did not show any effects of probiotics on the prevention of atopic eczema and respiratory allergies.

Most of these trials also evaluated the effects of prebiotics on other allergic diseases such as asthma, wheezing, allergic rhinoconjunctivitis, and food allergy (15-19, 21-29, 31-34). In most cases, the incidence and the symptoms of these allergic diseases were not significantly reduced or improved by probiotics. However, van der Aa et al., reported a significant decrease in the prevalence of wheezing in a high-risk group of infants supplemented with a mixture of *B. breve* M-16V, scGOS, and lcFOS compared with the control group (30). In contrast, one study reported an increased risk of recurrent wheezing bronchitis at 2 years of age after a pre- and post-natal supplementation with *L. rhamnosus* GG (20). Furthermore, using the same probiotic strains, Kalliomaki et al. demonstrated that children who received the probiotic had a higher prevalence of allergic rhinitis and asthma at the age of 7 years than the control group (22).

In conclusion, a number of randomized control trials assessed the effects of probiotics on the prevention and improvement of eczema, asthma, wheezing, and allergic rhinoconjunctivitis in pediatric patients, but conflicting results were reported. Similar contradictory findings also emerged from evaluation of atopic sensitization with the majority of probiotic treatments that failed to modify this parameter. A number of factors may contribute to the conflicting findings among these studies, such as the differences in the probiotic strains, dosages, start time and duration of probiotic administration. Therefore, we are unable to draw a conclusion on the effects of probiotic administration during pregnancy or early infancy on the prevention of allergic diseases. Extended follow-up and further trials are needed to better understand the biological function of probiotics.

CONCLUSIONS

Probiotics are an a heterogeneous group of microorganisms that may be effective in the prevention and treatment of a number of human diseases. They have been administrated in pregnacy and/or the first year of life in order to prevent infectious and allergic diseases in childhood. By reviewing previous studies, we found that probiotic administration during pregnacy and the first year of life generally reduced the incidence and improved the symptoms of various infectious diseases in infants. However, the effects of probiotic administration during pregnacy and the first year of life generally on the prevention of allergic diseases are still not clear, mainly due to limited and conflicting studies on this topic. The published studies differred in probiotic species, number and dosage of probiotics, inclusion and exclusion criteria, outcome evaluation, diagnostic criteria of infectious and allergic diseases, and follow-up methods. These differences may explain a number of inconsistent results and conclusions among different studies, which also highlight the necessity for further studies on these topics.

ACKNOWLEDGEMENTS

This study was financially supported by a grant from the Italian Ministry of Health (Ricerca Corrente 2014) to Fondazione IRCCS Ca' Granda Ospedale Maggiore Policlinico, Milan, Italy.

REFERENCES

1. Esposito S, Rigante D, Principi N. Do children's upper respiratory tract infections benefit from probiotics? BMC Infect Dis 2014; 14:194.
2. del Giudice MM, Leonardi S, Ciprandi G, et al. Probiotics in childhood: allergic illness and respiratory infections. J Clin Gastroenterol 2012; 46(S):S69-72.
3. Lionetti E, Francavilla R, Castellazzi AM, et al. Probiotics and *Helicobacter pylori* infection in children. J Biol Regul Homeost Agents 2012; 26(S):S69-76.
4. Miraglia Del Giudice M, Maiello N, Decimo F, et al. Airways allergic inflammation and *L. reuterii* treatment in asthmatic children. J Biol Regul Homeost Agents 2012; 26(S):S35-40.
5. Castellazzi AM, Valsecchi C, Caimmi S, et al. Probiotics and food allergy. Ital J Pediatr 2013; 39:47.
6. Kukkonen K, Savilahti E, Haahtela T, Juntunen-Backman K, Korpela R, Poussa T, Tuure T, Kuitunen M. Long-term safety and impact on infection rates of postnatal probiotic and prebiotic (synbiotic) treatment: randomized, double-blind, placebo-controlled trial. Pediatrics 2008; 122:8-12.
7. Weizman Z, Asli G, Alsheikh A. Effect of a probiotic infant formula on infections in child care centers: comparison of two probiotic agents. Pediatrics 2005; 115:5-9.
8. Puccio G, Cajozzo C, Meli F, Rochat F, Grathwohl D, Steenhout P. Clinical evaluation of a new starter formula for infants containing live *Bifidobacterium longum* BL999 and prebiotics. Nutrition 2007; 23:1-8.
9. Rautava S, Salminen S, Isolauri E. Specific probiotics in reducing the risk of acute infections in infancy--a randomised, double-blind, placebo-controlled study. Br J Nutr 2009; 101:1722-6.
10. Taipale T, Pienihäkkinen K, Isolauri E, Larsen C, Brockmann E, Alanen P, Jokela J, Söderling E. *Bifidobacterium animalis* subsp. *lactis* BB-12 in reducing the risk of infections in infancy. Br J Nutr 2011; 105:409-16.
11. Maldonado J, Cañabate F, Sempere L, et al. Human milk probiotic *Lactobacillus fermentum* CECT5716 reduces the incidence of gastrointestinal and upper respiratory tract infections in infants. J Pediatr Gastroenterol Nutr 2012; 54:55-61.
12. Luoto R, Ruuskanen O, Waris M, Kalliomäki M, Salminen S, Isolauri E. Prebiotic and probiotic supplementation prevents rhinovirus infections in preterm infants: a randomized, placebo-controlled trial. J Allergy Clin Immunol 2014; 133:405-13.
13. Gil-Campos M, López MÁ, Rodriguez-Benítez MV, et al. *Lactobacillus fermentum* CECT 5716 is safe and well tolerated in infants of 1-6 months of age: a randomized controlled trial. Pharmacol Res 2012; 65:231-8.
14. Cohen R, Martin E, de La Rocque F, et al. Probiotics and prebiotics in preventing episodes of acute otitis media in high-risk children: a randomized, double-blind, placebo-controlled study. Pediatr Infect Dis J 2013; 32:810-4.
15. Abrahamsson TR, Jakobsson T, Björkstén B, Oldaeus G, Jenmalm MC. No effect of probiotics on respiratory allergies: a seven-year follow-up of a randomized controlled trial in infancy. Pediatr Allergy Immunol 2013; 24:556-61.
16. Wickens K, Stanley TV, Mitchell EA, Barthow C, Fitzharris P, Purdie G, Siebers R, Black PN, Crane J. Early supplementation with *Lactobacillus rhamnosus* HN001 reduces eczema prevalence to 6 years: does it also reduce atopic sensitization? Clin Exp Allergy 2013; 43:1048-57.
17. Kukkonen K, Savilahti E, Haahtela T, Juntunen-Backman K, Korpela R, Poussa T, Tuure T, Kuitunen M. Probiotics and prebiotic galacto-oligosaccharides in the prevention of allergic diseases: a randomized, double-blind, placebo-controlled trial. J Allergy Clin Immunol 2007; 119:192-8.
18. Kukkonen AK, Kuitunen M, Savilahti E, Pelkonen A, Malmberg P, Mäkelä M. Airway inflammation in probiotic-treated children at 5 years. Pediatr Allergy Immunol 2011; 22:249-51.
19. Ou CY, Kuo HC, Wang L, et al. Prenatal and postnatal probiotics reduces maternal but not childhood allergic diseases: a randomized, double-blind, placebo-controlled trial. Clin Exp Allergy 2012; 42:1386-96.
20. Kopp MV, Hennemuth I, Heinzmann A, Urbanek R. Randomized, double-blind, placebo-controlled

trial of probiotics for primary prevention: no clinical effects of *Lactobacillus* GG supplementation. Pediatrics 2008; 121:e850-6.

21. Niers L, Martín R, Rijkers G, Sengers F, Timmerman H, van Uden N, Smidt H, Kimpen J, Hoekstra M. The effects of selected probiotic strains on the development of eczema (the PandA study). Allergy 2009; 64:1349-58.
22. Kalliomäki M, Salminen S, Poussa T, Isolauri E. Probiotics during the first 7 years of life: a cumulative risk reduction of eczema in a randomized, placebo-controlled trial. J Allergy Clin Immunol 2007; 119:1019-21.
23. Huurre A, Laitinen K, Rautava S, Korkeamäki M, Isolauri E. Impact of maternal atopy and probiotic supplementation during pregnancy on infant sensitization: a double-blind placebo-controlled study. Clin Exp Allergy 2008; 38:1342-8.
24. Dotterud CK, Storrø O, Johnsen R, Oien T. Probiotics in pregnant women to prevent allergic disease: a randomized, double-blind trial. Br J Dermatol 2010; 163:616-23.
25. Rautava S, Kainonen E, Salminen S, Isolauri E. Maternal probiotic supplementation during pregnancy and breast-feeding reduces the risk of eczema in the infant. J Allergy Clin Immunol 2012; 130:1355-60.
26. Boyle RJ, Ismail IH, Kivivuori S, et al. *Lactobacillus* GG treatment during pregnancy for the prevention of eczema: a randomized controlled trial. Allergy 2011; 66:509-16.
27. Taylor AL, Dunstan JA, Prescott SL. Probiotic supplementation for the first 6 months of life fails to reduce the risk of atopic dermatitis and increases the risk of allergen sensitization in high-risk children: a randomized controlled trial. J Allergy Clin Immunol 2007; 119:184-91.
28. Grüber C, Wendt M, Sulser C, Lau S, Kulig M, Wahn U, Werfel T, Niggemann B. Randomized, placebo-controlled trial of *Lactobacillus rhamnosus* GG as treatment of atopic dermatitis in infancy. Allergy 2007; 62:1270-6.
29. Gore C, Custovic A, Tannock GW, et al. Treatment and secondary prevention effects of the probiotics *Lactobacillus paracasei* or *Bifidobacterium lactis* on early infant eczema: randomized controlled trial with follow-up until age 3 years. Clin Exp Allergy 2012; 42:112-22.
30. van der Aa LB, van Aalderen WM, Heymans HS, Henk Sillevis Smitt J, Nauta AJ, Knippels LM, Ben Amor K, Sprikkelman AB; Synbad Study Group. Synbiotics prevent asthma-like symptoms in infants with atopic dermatitis. Allergy 2011; 66:170-7.
31. West CE, Hammarström ML, Hernell O. Probiotics in primary prevention of allergic disease: follow-up at 8-9 years of age. Allergy 2013; 68:1015-20.
32. Hol J, van Leer EH, Elink Schuurman BE, de Ruiter LF, Samsom JN, Hop W, Neijens HJ, de Jongste JC, Nieuwenhuis EE; Cow's Milk Allergy Modified by Elimination and Lactobacilli study group. The acquisition of tolerance toward cow's milk through probiotic supplementation: a randomized, controlled trial. J Allergy Clin Immunol 2008; 121:1448-54.
33. Soh SE, Aw M, Gerez I, et al. Probiotic supplementation in the first 6 months of life in at risk Asian infants-effects on eczema and atopic sensitization at the age of 1 year. Clin Exp Allergy 2009; 39:571-8.
34. Loo EX, Llanora GV, Lu Q, Aw MM, Lee BW, Shek LP. Supplementation with probiotics in the first 6 months of life did not protect against eczema and allergy in at-risk Asian infants: a 5-year follow-up. Int Arch Allergy Immunol 2014;163:25-8.

INTERLEUKIN-33 PROMOTES THE PROLIFERATION OF MOUSE MAST CELLS THROUGH ST2/MyD88 AND p38 MAPK-DEPENDENT AND Kit-INDEPENDENT PATHWAYS

R. SALUJA, T. HAWRO, J. EBERLE, M.K. CHURCH and M. MAURER

Department of Dermatology and Allergy, Charité – Universitätsmedizin Berlin, Germany

Received May 4, 2014 – Accepted August 28, 2014

Interleukin-33 (IL-33), a member of the IL-1 cytokine family, is emerging as a new modulator of immune and inflammatory responses. Although IL-33 and its associated receptor ST2 are reportedly expressed in mast cells (MCs), the precise role of IL-33 in modulating MC function has not been determined. In the present studies, we explored IL-33 effects on MCs *in vivo* and *in vitro*. IL-33 increased the number of peritoneal and skin MCs *in vivo*. IL-33 also resulted in increased proliferation of MCs *in vitro*, as explored by WST assay. Cell cycle analysis further confirmed this result by showing increased G2 cell populations in MCs stimulated with IL-33. We found that IL-33-mediated MC proliferation requires ST2 and MyD88, is independent of Kit, and is mediated through a p38 MAPK-dependent pathway. IL-33 did not induce degranulation and was not cytotoxic for MCs. This novel mechanism for increasing MC proliferation and numbers further defines the role of IL-33 in MC-dependent diseases including allergies and may help to develop novel approaches for the treatment of these disorders.

Mast cells (MCs) are major effector cells in both innate and adaptive immunity (1). Most prominently, MCs are involved in the pathophysiology of allergic diseases, such as allergic rhinitis and asthma (2). MCs are tissue resident cells and may survive for years (3). Their location in the skin, gastrointestinal tract and lung places them strategically as a first line of defence against invading pathogens.

Marked increases in tissue MC numbers have been reported in murine models of several allergic conditions and asthma (4). For example, skin MCs are reportedly increased in murine oxazolone-induced dermatitis (5), and higher numbers of MCs in the bronchial epithelium and airway smooth muscle, associated with pulmonary inflammation, are found in mouse models of allergic airway inflammation (6). Increased MC numbers have also been reported in the bronchi of asthmatic patients after allergen exposure (7). MC hyperplasia seen in these conditions is thought to result, at least in part, from increased proliferation (8). However, the precise mechanisms leading to the increased MC numbers in these settings are still largely elusive and a number of different mechanisms may be involved.

IL-33 is a recently discovered cytokine of the IL-1 family, which is a ligand for T1/ST2/IL-1R4 (9). T1/ST2/IL-1R4 is preferentially expressed on Th2 cells and MCs (10). IL-33 can promote the production of IL-4 (11), IL-5 and IL-13 by Th2 cells and induce NF-κB phosphorylation and MAP kinase activation in MCs (9, 12). IL-33 is reported to have a strong association with MCs in different allergic diseases

Key words: mast cell, IL-33, proliferation, apoptosis, ST2, Kit, p38 MAPK, JNK, ERK

Mailing address:
Dr Rohit Saluja,
Department of Dermatology and Allergy,
Charité – Universitätsmedizin Berlin,
Charitéplatz 1, 10117 Berlin, Germany
Tel.: +4930450518043 Fax: +4930450518972
e-mail: rohit.saluja@charite.de, drrohitsaluja@gmail.com

0393-974X (2014)

(13) and may play a critical role in the regulation of MC proliferation. Recently, IL-33 was described to be up regulated in allergic conditions and to activate MCs (14). Interestingly, increases in MC numbers have repeatedly been linked to MC activation by IgE. For example, in pulmonary inflammation induced by allergen challenge in mice, involvement of IgE was shown to be responsible for the subsequent increase in MCs in the lungs (6). A recent report suggests that MCs themselves can secrete IL-33 after IgE cross-linking (11) and act as target cells for IL-33. We, therefore, hypothesized that IL-33 contributes to the accumulation of MCs at sites of inflammation by inducing the proliferation of MCs, and we tested this hypothesis by using *in vivo* and *in vitro* mouse models.

MATERIALS AND METHODS

Assessment of IL-33 effects on MC numbers in vivo

Mouse rIL-33 (500 ng in 20 µL PBS, Enzo Life Sciences AG, Lausen, Switzerland) or PBS was injected intradermally (once daily) into the ear pinna of mice on three successive days. Mice were sacrificed on day 4, and the ears were excised, fixed in buffered formalin, and processed into paraffin-embedded sections. Specimens were stained with Giemsa stain to identify MCs. Cutaneous MC numbers were assessed by quantitative morphometry in 1 mm^2 areas. Images were captured and analyzed using the AxioVision 4.6 image processing software (Carl Zeiss).

To explore whether IL-33 treatment leads to increased numbers of peritoneal MCs, wild-type C57BL/6 mice were injected intraperitoneally daily with PBS or 500 ng rIL-33 for 3 days. The mice were sacrificed on day 4, and peritoneal lavage was collected. Numbers of peritoneal cells were analyzed by flow cytometry by using MACS Quant (Miltenyi). The following antibodies were used in this study: FITC conjugated anti-mouse FcεRI (MAR-1; Biolegend), PE-Cy7 conjugated anti-mouse CD117 (2B8; BioLegend). All animal care and experimentation were conducted in accordance with current federal, state, and institutional guidelines.

Mast cell cultures, treatment and activation

Bone marrow-derived mast cells (BMMCs) were obtained by culturing bone marrow cells from either C57BL/6 mice, $ST2^{-/-}$ mice, or $MyD88^{-/-}$ mice as previously described (15). $MyD88^{-/-}$ mice on a C57BL/6 genetic background were kindly provided by Dr. Shizuo Akira (Osaka University, Osaka, Japan) by way of Dr. Simon Fillatreau (Deutsches Rheuma-Forschungszentrum, Berlin). $ST2^{-/-}$ mice on a C57BL/6 genetic background were obtained from Dr. Andrew McKenzie (Medical Research Council, Laboratory of Molecular Biology, Cambridge, U.K.) by way of Dr. Max Löhning (Deutsches Rheuma-Forschungszentrum, Berlin). In brief, BMMCs were cultured in medium containing recombinant IL-3 (10 ng/ml; Peprotech, Germany) for a minimum of 4 weeks before they were used. To obtain peritoneal mast cells, peritoneal cells were harvested from euthanized animals by peritoneal lavage with 5 ml saline. These cells were cultured in RPMI containing 10 ng/ml IL-3 and 30 ng/ml SCF (16). The maturity and purity of the cells were examined by toluidine blue staining and flow cytometry analyses for expression of Kit and FcεRI, using FITC-anti-mouse CD117 (Kit) mAb 2B8 or FITC-conjugated rat IgG2b isotype control (both from BD Pharmingen, San Diego, USA), FITC-conjugated anti-mouse FcεRI-α mAb MAR-1, or FITC conjugated Armenian hamster IgG isotype control (eBioscience, Frankfurt, Germany). MCs ($1x10^6$ cells/ml) were treated for 24 or 96 h with different concentrations of IL-33. In separate experiments to investigate the involvement of distinct signalling pathways, MCs were treated with the JNK inhibitor SP600125 (1 µM, Sigma), the ERK inhibitor PD 98059 (1 µM, Calbiochem, Germany) or the p38 MAPK inhibitor SB203580 (10 µM, Calbiochem) in the absence and presence of IL-33 for 24 h to 96 h.

Mast cell proliferation

BMMCs ($1x10^6$ cells/ml) were cultured in RPMI1640 medium containing 10% FCS and rIL-33 (10-100 ng/ml) at 37°C for 24, 48, 72, or 96 h. For monitoring cell proliferation, a colorimetric assay (WST-1, Roche Diagnostics, Mannheim, Germany) was used. 20,000 cells in 200 µl culture medium per well were seeded in 96-well plates and treated for 24 to 96 h with 10, 50, or 100 ng/ml rIL-33, before 10 µl WST-1 reagent was added, followed by incubation of the cells at 37°C for 1 to 3 h until colour changes were seen (17). The optical density of samples was determined at 450 nm in an ELISA plate reader (Dynatech Laboratories). For background correction, the values of untreated controls were subtracted.

Quantification of apoptosis and proliferation by cell cycle analysis

BMMCs ($1x10^6$ cells/ml) were cultured in RPMI1640 medium containing 10% FCS and rIL-33 (10-100 ng/ml) at 37°C for 24, 48, 72, or 96 h. For quantification of apoptosis and proliferation, cell cycle analyses were carried out using propidium iodide staining (17). BMMCs were harvested after treatment with IL-33 at different time points (24 to 96 h), stained with PBS buffer containing

Triton-X 100, sodium citrate and propidium iodide (200 mg/ml, Sigma), centrifuged, washed with PBS and analyzed by flow cytometry in a FACS (BD FACS Calibur).

Mast cell activation and cytokine measurement

For detection of the granular enzyme β-hexosaminidase, an enzymatic colorimetric assay was used as described previously (18). Briefly, 60 µl of supernatant was transferred to a 96-well plate and mixed with an equal volume of substrate solution (7.5 mM p-nitrophenyl-N-acetyl-β-D-glucosaminide dissolved in 80 mM citric acid, pH 4.5). The mixture was incubated on a rocker platform for 2 h at 37°C. After incubation, 120 µl of glycine (0.2 M, pH 10.7) was added to each well, and the absorbance at 405 and 490 nm was measured. Levels of IL-6 in the supernatants were measured by ELISA according to the manufacturer's instructions (eBioscience).

Mast cell viability and cytotoxicity

BMMCs were treated with different concentrations of IL-33 for 24 to 96 h. Cells were re-suspended in 200 µl medium without FCS and penicillin/streptomycin, and 5 µM calcein-AM was added. The cells were then incubated for 1 h (5% CO_2, 37^{0}C), washed and resuspended in PBS, and measured immediately by flow cytometry. Cytotoxicity was determined by measuring LDH activity following the assay manufacturer's instructions (Roche Diagnostics, Basel, Switzerland).

Statistical analyses

All results are expressed as means ± standard errors (SEM) and all statistical analyses were performed using Student's *t*-test. $P < 0.05$ was considered statistically significant.

RESULTS

IL-33 treatment increases mast cell numbers in the skin and peritoneum of mice

When we assessed the effects of IL-33 on MC numbers *in vivo*, we found that intradermal injections of IL-33 markedly increased the numbers of skin MCs at the site of treatment as compared to vehicle injected sites (87±6 *vs* 163±7 / mm^2, $P<0.01$, Fig. 1 A and B). Also, intraperitoneal injections of IL-33 increased peritoneal MC numbers assessed by cytometry (Kimura stain, data not shown) and by FACS staining for Kit and FcεR1, albeit not statistically significantly (Fig. 1C). Together, these data suggest that IL-33 treatment can increase murine MC numbers *in vivo*. It is possible that IL-33 may result in the recruitment of MC progenitors and the migration of mast cells to the peritoneum and their proliferation and that increases in mast cell numbers are due to a combination of these effects. When peritoneal MCs were tested for proliferation in response to IL-33, we found that IL-33 induces significant proliferation at concentrations ranging from 10 to 100 ng/ml (Fig. 1D).

IL-33 induces proliferation, but not degranulation, of mast cells in vitro

To further explore the effect of IL-33 on MC proliferation, we assessed bone marrow- derived MCs and found that they also showed significant dose dependent and sustained proliferation in response to IL-33 (Fig. 2A). IL-33 did not induce MC degranulation as assessed by β-hexosaminidase release assays (Fig. 2B). Furthermore, IL-33 did not exhibit cytotoxic effects, as determined by lactate dehydrogenase (LDH) release assays (Fig. 2C) and Calcein AM staining (to assess cell viability) followed by subsequent flow cytometric analysis at 24 h to 96 h of treatment (Fig. 2D).

IL-33 shifts cell cycling to proliferation, not apoptosis

To delineate the mechanisms of the pro–proliferative effects of IL-33 on MCs, we next examined the effects of IL-33 on cell cycling by propidium iodide (PI) nuclear staining and subsequent flow cytometry (Fig. 3A). IL-33 prominently enhanced the G2 population in BMMCs without affecting the sG1 population within the first 24 h of treatment and for up to 96 h (Fig. 3 B-C). G2 populations were increased 2.8, 3.5, and 4-fold after treatment with 10, 50, and 100 ng/ml, respectively, at 24 hr. Similar effects were observed after 48, 72, and 96 h, indicating that IL-33 induces sustained DNA replication (Fig. 3B). There was no significant increase of sub-G1 cell populations, i.e. no enhancement of apoptosis in BMMCs in response to IL-33 treatment as compared with vehicle-treated cells (Fig. 3C).

IL-33-mediated mast cell proliferation depends on ST2 and MyD88

Since IL-33 is reported to signal through ST2

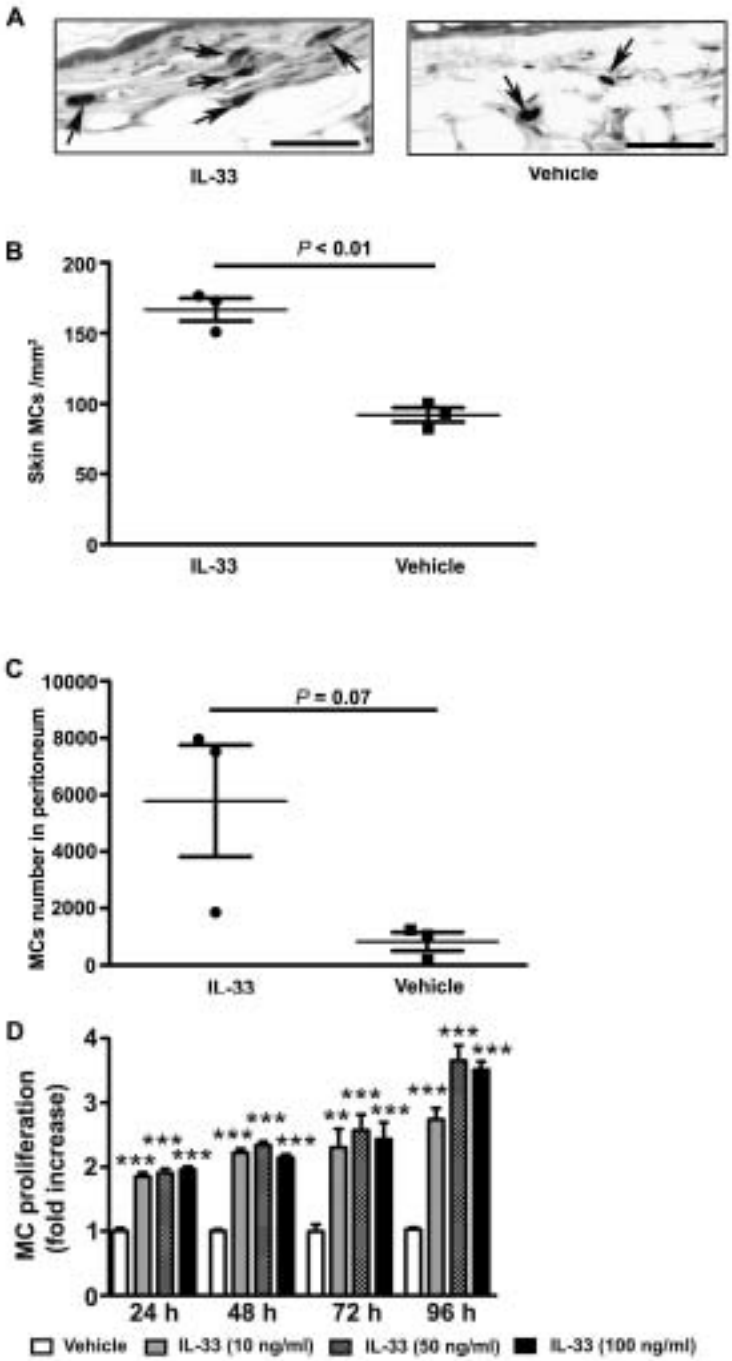

Fig. 1. *IL-33 treatment induces mast cell proliferation in the skin as well as in the peritoneum.* ***A, B****) increased numbers of skin mast cells (arrows in A) in ears of mice treated with IL-33 (left, 500 ng daily for 3 days, intradermal injections) or vehicle (PBS). Sections shown in (A) are stained with Giemsa (magnification 200 X, scale bar 50 µm).* ***C****) Peritoneal MCs as assessed by FACS (Kit⁺ and FcεRI⁺) on day 4 after treatment with IL-33 (500 ng, i.p. daily for three days, n=3 for each group) or vehicle. The data shown are from three independent experiments with 3 mice per group and experiment.* ***D****) Peritoneal MC proliferation was explored by use of the WST-1 assay, and values are expressed as fold increase vs vehicle control. Cells were harvested at different time points e.g. 24, 48, 72 or 96 h after stimulation. **p < 0.01, ***p < 0.001 indicates significant differences from the respective controls. Results are represented as the means ± SEM of 3 independent experiments.*

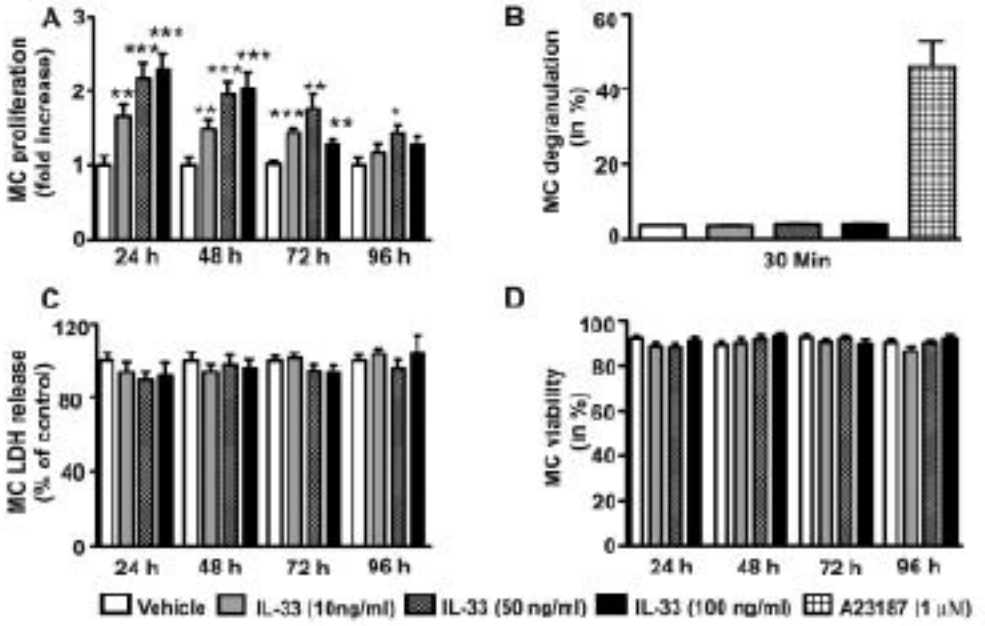

Fig. 2. *Effect of IL-33 in mouse bone marrow-derived mast cells.* ***A)*** *Proliferation of mouse bone marrow-derived mast cells (BMMCs) in response to increasing concentrations (10 - 100 ng/ml) of IL-33 or vehicle. For kinetic analyses, cells were harvested at 24, 48, 72 or 96 h after stimulation. Cell proliferation was determined by WST-1 assay, and values are expressed as fold increase vs. vehicle control. The mean OD values in vehicle treated cells were 0.093, 0.110, 0.068 and 0.061 at 24 h, 48 h, 72 h and 96 h, respectively (**B**). Effects of IL-33 on BMMCs degranulation: BMMCs were cultured for 30 min in the presence or absence of 10-100 ng/ml IL-33. As positive controls, BMMCs were stimulated with 1 µM A23187 (ionomycin). Mast cell degranulation is shown as percentage of β-hexosaminidase release. (C+D) MC treated with increasing concentrations of IL-33 for 24 h to 96 h (**C**) to assess IL-33 cytotoxicity and (**D**) viability in BMMCs. Samples were run in duplicate, results are represented as means ± SEM of 3 independent experiments. *p < 0.05, **p < 0.01, ***p < 0.001 vs vehicle.*

and MyD88, we investigated the involvement of this pathway in IL-33-mediated MC proliferation. We found that BMMCs from mice deficient for ST2 ($ST2^{-/-}$) did not show increased proliferation after treatment with IL-33 (10 - 100 ng/ml) for 24 h to 96 h, whereas SCF, used as positive control, significantly increased proliferation in these cells (Fig. 4A). Nor did ST2-deficient BMMCs show changes in cell cycling in response to IL-33 treatment, in particular no increase of the G2 population proliferation (Fig. 4B). As in WT cells, IL-33 did not induce apoptosis (increase in sG1 populations) in ST2 deficient MCs (Fig. 4C).

Nor did MyD88-deficient BMMCs proliferate in response to IL-33 (Fig. 4D), i.e. G2 cell populations did not increase (Fig. 4E). Similar to $ST2^{-/-}$ BMMCs, IL-33 did not induce apoptosis in $MyD88^{-/-}$ BMMCs (Fig. 4F).

Kit is not needed for IL-33-induced mast cell proliferation

To explore whether IL-33-induced MC proliferation involves Kit, the receptor for stem cell factor, we used BMMC from mast cell deficient $Kit^{W\text{-}sh}/Kit^{W\text{-}sh}$ mice which express ST2 but no functional Kit (19). Kit-deficient BMMCs showed IL-33-induced increases in proliferation that were similar to those of control MCs, indicating that Kit is not critically involved in IL-33-induced MC proliferation (Fig. 5A). To confirm this, we used the specific Kit inhibitor imatinib, which completely abolished MC proliferation induced by SCF but had no effect on

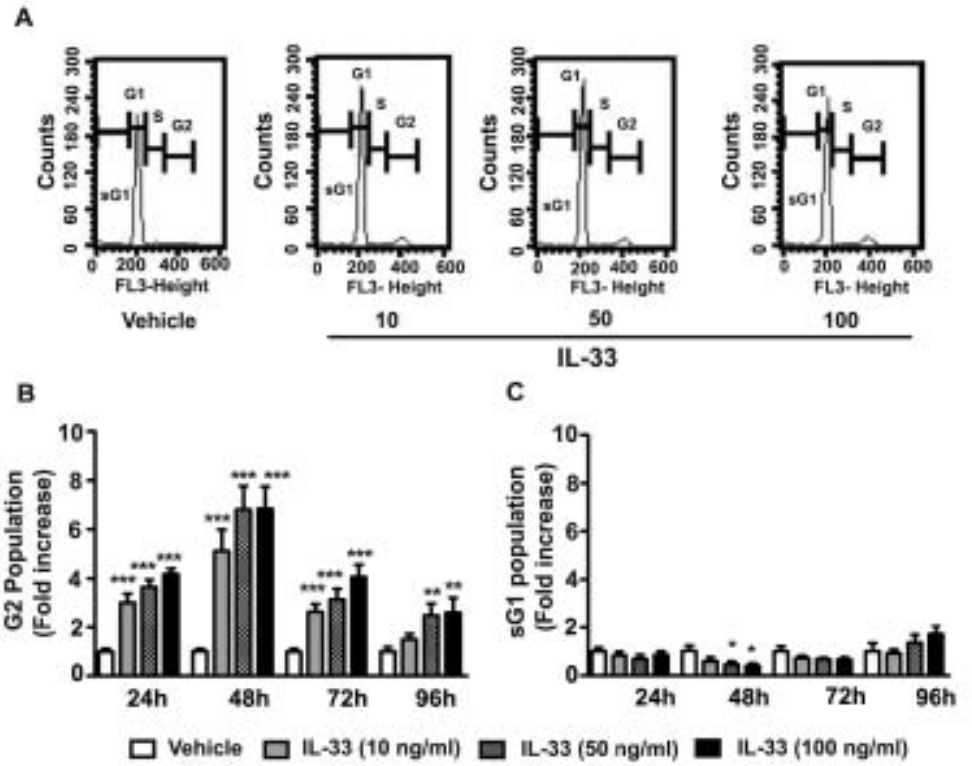

Fig. 3. *IL-33 increases mast cell proliferation and does not induce apoptosis.* ***A)*** *Cell cycle analyses of IL-33-treated BMMCs by propidium iodide (PI) staining and flow cytometry. Representative histograms are shown as compared to the control (vehicle).* ***B)*** *Increase of G2 populations (in fold increase) is shown for IL-33-treated BMMCs (24-96 h). Mean values for G2 populations in vehicle treated cells were 0.59, 0.51, 0.41, and 0.44 at 24 h, 48 h, 72 h, and 96 h respectively.* ***C)*** *Change of size of apoptotic sub-G1 (sG1) cells populations. Mean values for sG1 populations were 0.79, 1.22, 1.61, and 1.71 at 24 h, 48 h, 72 h, and 96 h respectively. *p < 0.05, **p < 0.01, ***p< 0.001 indicates significant differences from the respective controls. Results are represented as the means ± SEM of pooled results of 3 independent experiments.*

IL-33-mediated MC proliferation (Fig. 5B). Imatinib had no effect on IL-33-induced IL-6 production (Fig. 5C). On the other hand, the combination of IL-33 and SCF resulted in significantly increased MC proliferation as compared to the effects of either of them given alone, suggesting that the presence of SCF and IL-33 results in synergistic signals that augment MC proliferation (Fig. 5 D).

IL-33 regulates mast cell proliferation through the p38 MAPK-dependent pathway

Finally, we sought to identify the signal transduction pathways involved in IL-33-induced MC proliferation. When we used specific inhibitors of ERK, JNK and p38 MAP kinases, all of which can be activated by IL-33 binding to ST2, we found that IL-33 (100 ng/ml)-induced MC proliferation was significantly reduced only by the inhibition of p38 but not JNK or ERK (Fig. 6).

DISCUSSION

This study shows that IL-33 can induce murine MC proliferation *in vivo* as well as in *in vitro* via an ST2/MyD88/p38 MAPK-dependent and Kit-independent pathway. In contrast, IL-33 did not induce MC degranulation or affect MC viability.

Treatment with IL-33 increases MC numbers in the skin as well as the peritoneum, which is in support of earlier reports. For example, Hueber et

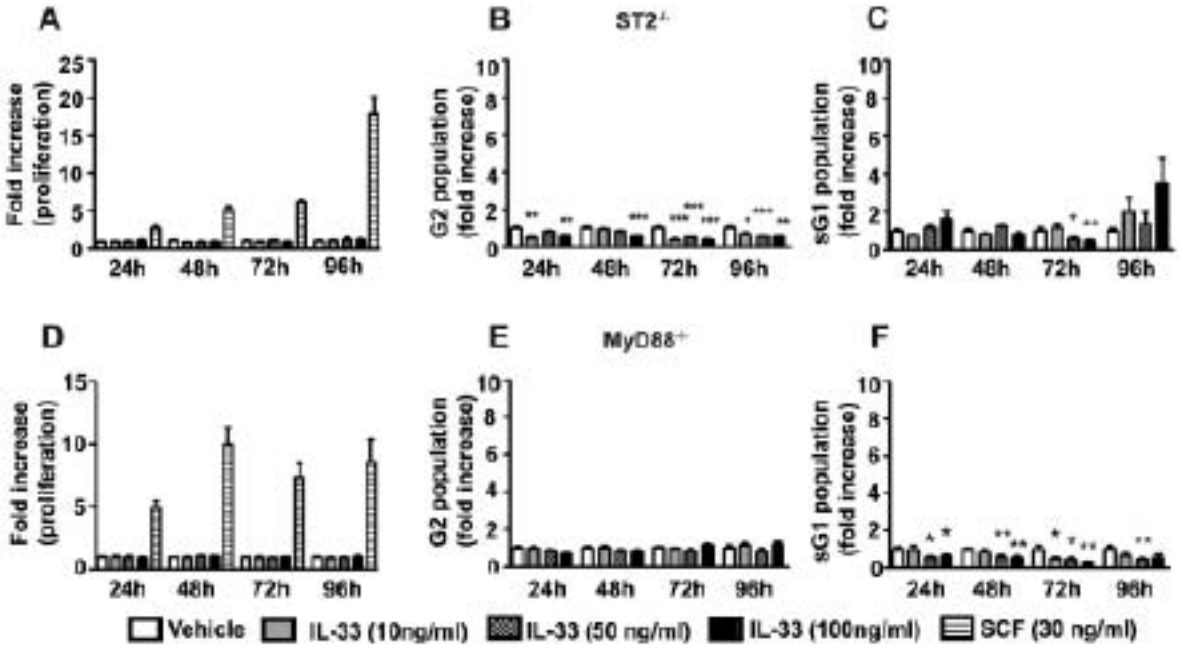

Fig. 4. *IL-33 promotes proliferation of MCs through a ST2- and MyD88-dependent pathway.* ***A)*** *Bone marrow mast cells from ST2-knockout mice treated with IL-33 do not show proliferation as determined by the WST-1 assay. Fold increases of G2 populations (**B**) and sG1 populations (**C**) after treatment with IL-33 or vehicle. The mean values for G2 populations in vehicle treated cells were 0.53, 0.52, 0.39 and 0.38 at 24 h, 48 h, 72 h and 96 h, respectively. The mean values for sG1 populations in vehicle treated cells were 0.45, 0.69, 1.5, and 0.90 at 24 h, 48 h, 72 h and 96 h, respectively.* ***D)*** *BMMCs from MyD88-deficient mice do not proliferate after treatment with IL-33. Fold increases of G2 (E) and sG1 populations (F) of IL-33 treated MCs from MyD88 $^{-/-}$ mice. The mean values for G2 populations in vehicle treated cells were 0.29, 0.20, 0.19, and 0.23 at 24 h, 48 h, 72 h, and 96 h, respectively. The mean values for sG1 populations in vehicle treated cells were 1.44, 4.50, 3.8, and 2.5 at 24 h, 48 h, 72 h and 96 h, respectively. Pooled results are presented as the means ± SEM of 3 independent experiments. *p < 0.05, **p < 0.01, ***p < 0.001.*

al. (20) observed increased MC numbers in the ears of mice after intradermal injection of IL-33 on alternate days up to day 16. In contrast, Enoksson et al. (21) did not observe increased numbers of peritoneal MCs 6 h after treatment with IL-33, which is owed most likely, to the short duration of IL-33 treatment. Our findings suggest that IL-33 could play an important role in the increase of MC numbers and may be involved in the pathogenesis of diseases that are characterized by up regulation of IL-33 such as psoriasis (20) and atopic dermatitis (22). These findings suggest that the increases in MC numbers seen after intradermal and intraperitoneal injections of IL-33 are due to the induction of proliferation by direct effects of IL-33 on local MC populations. However, other effects of IL-33 on MCs, directly or indirectly, could contribute to the accumulation of MCs after IL-33 injections, including increased migration of MC precursors or MCs to site of IL-33 treatment and increased differentiation of MC precursors at such sites.

Our WST-1 results indicate, to our knowledge for the first time, that IL-33 can significantly enhance MC proliferation *in vitro*, which is confirmed by the results of cell cycle analyses. IL-33 increases proliferating G2 populations in a dose-dependent manner, but does not induce apoptosis (sG1 populations). In a recently published article, the role of IL-33 as an inhibitor of apoptosis was explored. In this study, the authors did not detect MC proliferation

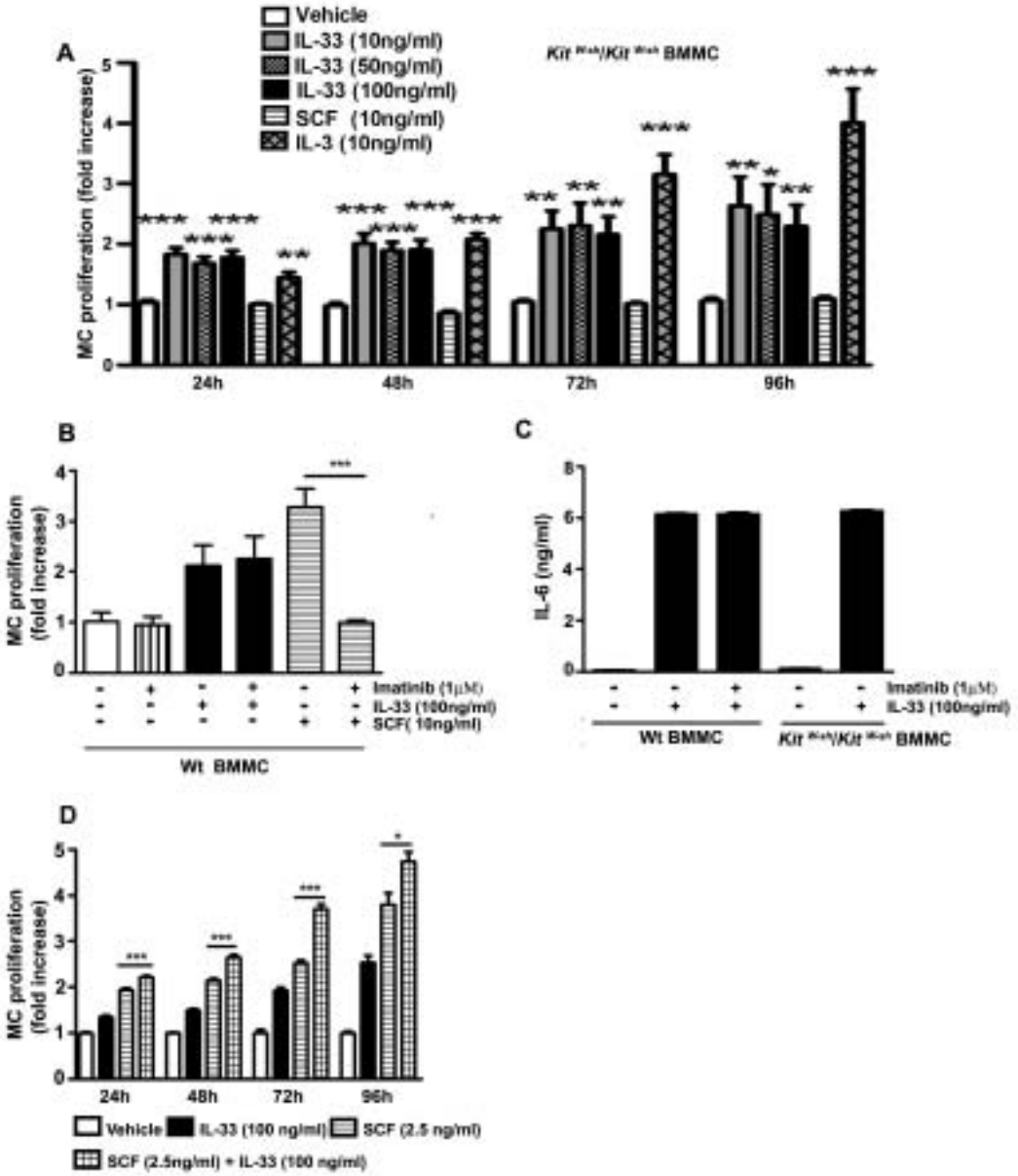

Fig. 5. *IL-33–induced mast cell proliferation does not dependent on the receptor tyrosine kinase Kit. **A)** BMMCs from $Kit^{W\text{-}sh}/Kit^{W\text{-}sh}$ mice show normal proliferation in response to stimulation with increasing concentrations (10-100 ng/ml) of IL-33 as determined by the WST-1 assay. The Kit inhibitor Imatinib does not affect IL-33 induced MC proliferation (**B**) or cytokine production (**C**). **D**) SCF and IL-33 act synergistically to enhance MC proliferation. BMMCs were incubated for 24 h to 96 h with the indicated concentrations of SCF (2.5 ng/ml), in the absence or presence of IL-33 (100 ng/ml). MC proliferation was determined by use of the WST-1 assay. Results are presented as the means ± SEMs for 3 independent experiments and values are expressed as fold change vs control. *p < 0.05, **p < 0.01, ***p < 0.001.*

after stimulation with IL-33 (23). At this point, we can not explain this difference between this finding and our results. Possible explanations include the presence of SCF during BMMC generation, the absence of FCS in the medium during stimulation or the use of different detection methods (CFSE *vs* WST-1/ PI).

IL-33 mediates its known effects through a

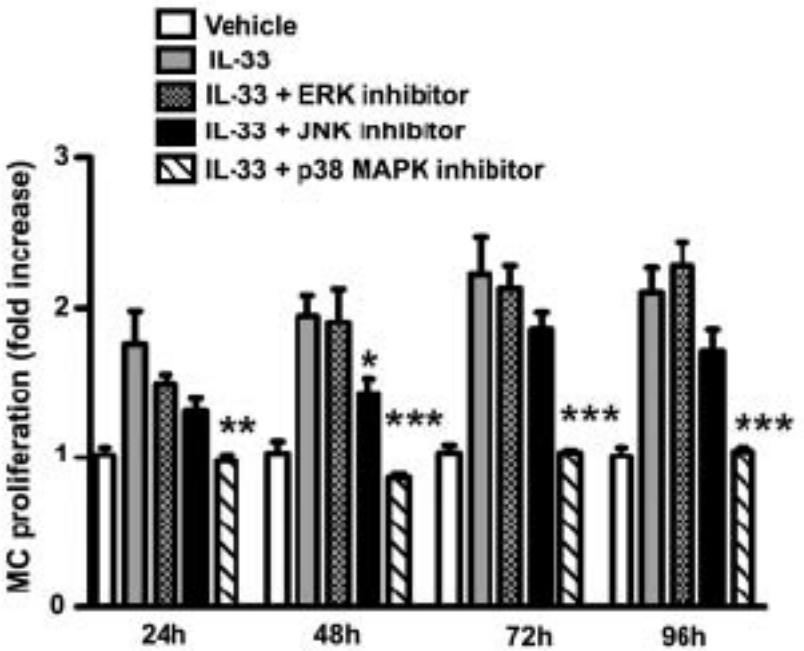

Fig. 6. *IL-33 induced mast cell proliferation is p38 MAPK-dependent. IL-33 (100 ng/ml) induced MC proliferation is inhibited by the p38 MAPK inhibitor SB 203580 (10 μM) but not by the JNK inhibitor SP 600125 (1 μM), or the ERK inhibitor PD 98059 (1 μM). Cell proliferation was determined by WST-1 assay. Samples were run in duplicate and pooled values from 3 independent experiments are expressed as fold change vs control. *p < 0.05, **p < 0.01, ***p < 0.001.*

heterodimeric receptor composed of IL-33R (T1/ST2) and IL1RAP (24). Our results indicate that this receptor is also involved in IL-33-induced MC proliferation. The binding of IL-33 to the ST2 receptor activates a signaling pathway, which involves the recruitment of MyD88 (24). However, the role of MyD88 for IL-33-mediated effects has not previously been investigated. Our results show that MyD88 is a critical step downstream of ST2 engagement by IL-33. Both, genetically ST2 and MyD88-deficient MCs show no induction of proliferation in response to IL-33, whereas, in the same experiments, the Kit ligand SCF (positive control) promoted MC proliferation. ST2 and MyD88 have been demonstrated to be expressed by many cell types other than MCs, e.g. eosinophils and basophils. It would be interesting to test whether IL-33 can induce proliferation in these cells.

Kit receptors form heterodimers with ST2, and these heterodimers have been shown to be involved in the induction of cytokine production (e.g IL-6) by MCs stimulated with IL-33 (19). In contrast to these published results, we did not find differences in the IL-33-induced production of IL-6 between genetically Kit-deficient, imatinib-treated MCs or normal untreated MCs, possibly because of differences in the experimental set-up and conditions (such as concentration of IL-33). We also found that IL-33-induced MC proliferation was unaltered in the absence of Kit. Genetically Kit-deficient MCs from $Kit^{W\text{-}sh}/Kit^{W\text{-}sh}$ mice as well as MCs treated with the Kit-inhibitor imatinib showed normal proliferation in response to IL-33 treatment. On the other hand, SCF and IL-33 appear to induce MC proliferation in synergy as the stimulation of MCs with a combination of both induced more proliferation than either one alone in normal BMMCs.

Finally, we explored the involvement and importance of distinct IL-33 related signalling molecules, i.e. JNK, ERK1/2, and p38 MAPK, in the induction of MCs proliferation by IL-33. Only the inhibition of p38 MAPK, but not of JNK or ERK1/2, significantly inhibited MC proliferation in response to IL-33. Previous reports had indicated that all of these three signalling molecules are involved in the induction of IL-6 (11, 25, 26) and IL-13 production

in BMMCs by IL-33 (27). Taken together, our results suggest that IL-33 may contribute to the accumulation of MCs in diseases characterized by high local levels of this cytokine, such as asthma (28, 29) and allergic rhinitis (30).

One must keep in mind, however, that the effects of IL-33 on human MC proliferation have not yet been investigated. IL-33 has been shown to prolong the survival of human cord blood MCs (31), and just like in murine MCs (26, 32), IL-33 does not induce the release of histamine and PGD_2 in human MCs (31, 33). Thus it appears likely that IL-33 also makes human MCs proliferate, which could be important for the pathogenesis of chronic inflammatory diseases.

ACKNOWLEDGEMENTS

We are grateful to Sina Heydrich, Evelin Hagen and Katja Steinhorst for their excellent technical assistance. We thank Dr. Shizuo Akira (Osaka University, Osaka, Japan), Dr. Andrew McKenzie (Medical Research Council, Laboratory of Molecular Biology, Cambridge, U.K.), and Simon Fillatreau and Max Löhning (Deutsches Rheuma-Forschungszentrum, Berlin) for providing us with $ST2^{-/-}$ and $MyD88^{-/-}$ mice. This work was supported, in part, by grants from DFG to MM (SPP1394; DFG MMA 12/1).

REFERENCES

1. Shelburne CP, Abraham SN. The mast cell in innate and adaptive immunity. Adv Exp Med Biol 2011; 716:162-85.
2. Brown JM, Wilson TM, Metcalfe DD. The mast cell and allergic diseases: role in pathogenesis and implications for therapy. Clin Exp Allergy 2008; 38(1):4-18.
3. Fodinger M, Fritsch G, Winkler K, Emminger W, Mitterbauer G, Gadner H, Valent P, Mannhalter C. Origin of human mast cells: development from transplanted hematopoietic stem cells after allogeneic bone marrow transplantation. Blood 1994; 84(9):2954-59.
4. Nabe T, Matsuya K, Akamizu K, et al. Roles of basophils and mast cells infiltrating the lung by multiple antigen challenges in asthmatic responses of mice. Br J Pharmacol 2013; 169(2):462-76.
5. Hershko AY, Charles N, Olivera A, Alvarez-Errico D, Rivera J. Cutting edge: persistence of increased mast cell numbers in tissues links dermatitis to enhanced airway disease in a mouse model of atopy. J Immunol 2012; 188(2):531-35.
6. Mathias CB, Freyschmidt EJ, Caplan B, et al. IgE influences the number and function of mature mast cells, but not progenitor recruitment in allergic pulmonary inflammation. J Immunol 2009; 182(4):2416-24.
7. Kassel O, de Blay F, Duvernelle C, et al. Local increase in the number of mast cells and expression of nerve growth factor in the bronchus of asthmatic patients after repeated inhalation of allergen at low-dose. Clin Exp Allergy 2001; 31(9):1432-40.
8. Da Silva CA, Reber L, Frossard N. Stem cell factor expression, mast cells and inflammation in asthma. Fundam Clin Pharmacol 2006; 20(1):21-39.
9. Schmitz J, Owyang A, Oldham E, et al. IL-33, an interleukin-1-like cytokine that signals via the IL-1 receptor-related protein ST2 and induces T helper type 2-associated cytokines. Immunity 2005; 23(5):479-90.
10. Moritz DR, Rodewald HR, Gheyselinck J, Klemenz R. The IL-1 receptor-related T1 antigen is expressed on immature and mature mast cells and on fetal blood mast cell progenitors. J Immunol 1998; 161(9):4866-74.
11. Hsu CL, Neilsen CV, Bryce PJ. IL-33 is produced by mast cells and regulates IgE-dependent inflammation. PLoS One 2010; 5(8):e11944.
12. Sabatino G, Nicoletti M, Neri G, et al. Impact of IL -9 and IL-33 in mast cells. J Biol Regul Homeost Agents 2012; 26(4):577-86.
13. Ohno T, Morita H, Arae K, Matsumoto K, Nakae S. Interleukin-33 in allergy. Allergy 2012; 67(10):1203-14.
14. Nakae S, Morita H, Ohno T, Arae K, Matsumoto K, Saito H. Role of interleukin-33 in innate-type immune cells in allergy. Allergol Int 2013; 62(1):13-20.
15. Mrabet-Dahbi S, Metz M, Dudeck A, Zuberbier T, Maurer M. Murine mast cells secrete a unique profile of cytokines and prostaglandins in response to distinct TLR2 ligands. Exp Dermatol 2009; 18(5):437-44.

16. Gomez G, Ramirez CD, Rivera J, et al. TGF-beta 1 inhibits mast cell Fc epsilon RI expression. J Immunol 2005; 174(10):5987-93.
17. Berger A, Quast SA, Plotz M, Hein M, Kunz M, Langer P, Eberle J. Sensitization of melanoma cells for death ligand-induced apoptosis by an indirubin derivative--Enhancement of both extrinsic and intrinsic apoptosis pathways. Biochem Pharmacol 2011; 81(1):71-81.
18. Saluja R, Delin I, Nilsson GP, Adner M. FcepsilonR1-mediated mast cell reactivity is amplified through prolonged Toll-like receptor-ligand treatment. PLoS One 2012; 7(8):e43547.
19. Drube S, Heink S, Walter S, et al. The receptor tyrosine kinase c-Kit controls IL-33 receptor signaling in mast cells. Blood 2010; 115(19):3899-906.
20. Hueber AJ, Alves-Filho JC, Asquith DL, et al. IL-33 induces skin inflammation with mast cell and neutrophil activation. Eur J Immunol 2011; 41(8):2229-37.
21. Enoksson M, Moller-Westerberg C, Wicher G, Fallon PG, Forsberg-Nilsson K, Lunderius-Andersson C, Nilsson G. Intraperitoneal influx of neutrophils in response to IL-33 is mast cell-dependent. Blood 2013; 121(3):530-36.
22. Savinko T, Matikainen S, Saarialho-Kere U, et al. IL-33 and ST2 in atopic dermatitis: expression profiles and modulation by triggering factors. J Invest Dermatol 2012; 132(5):1392-400.
23. Wang JX, Kaieda S, Ameri S, et al. IL-33/ST2 axis promotes mast cell survival via BCLXL. Proc Natl Acad Sci USA 2014; 111(28):10281-86.
24. Kakkar R, Lee RT. The IL-33/ST2 pathway: therapeutic target and novel biomarker. Nat Rev Drug Discov 2008; 7(10):827-40.
25. Enoksson M, Lyberg K, Moller-Westerberg C, Fallon PG, Nilsson G, Lunderius-Andersson C. Mast cells as sensors of cell injury through IL-33 recognition. J Immunol 2011; 186(4):2523-8.
26. Ho LH, Ohno T, Oboki K, et al. IL-33 induces IL-13 production by mouse mast cells independently of IgE-FcepsilonRI signals. J Leukoc Biol 2007; 82(6):1481-90.
27. Tung HY, Plunkett B, Huang SK, Zhou Y. Murine mast cells secrete and respond to interleukin-33. J Interferon Cytokine Res 2014; 34(3):141-7.
28. Yang DX, Li N, Zhang XL, Wang Q. [Serum interleukin 18 and 33 levels and its clinical significance in asthma patients]. Zhonghua Jie He He Hu Xi Za Zhi 2012; 35(7):493-6.
29. Hamzaoui A, Berraies A, Kaabachi W, Haifa M, Ammar J, Kamel H. Induced sputum levels of IL-33 and soluble ST2 in young asthmatic children. J Asthma 2013; 50(8):803-9.
30. Bentley AM, Jacobson MR, Cumberworth V, et al. Immunohistology of the nasal mucosa in seasonal allergic rhinitis: increases in activated eosinophils and epithelial mast cells. J Allergy Clin Immunol 1992; 89(4):877-83.
31. Iikura M, Suto H, Kajiwara N, et al. IL-33 can promote survival, adhesion and cytokine production in human mast cells. Lab Invest 2007; 87(10):971-8.
32. Andrade MV, Iwaki S, Ropert C, Gazzinelli RT, Cunha-Melo JR, Beaven MA. Amplification of cytokine production through synergistic activation of NFAT and AP-1 following stimulation of mast cells with antigen and IL-33. Eur J Immunol 2011; 41(3):760-72.
33. Allakhverdi Z, Smith DE, Comeau MR, Delespesse G. Cutting edge: The ST2 ligand IL-33 potently activates and drives maturation of human mast cells. J Immunol 2007; 179(4):2051-4.

JOURNAL OF BIOLOGICAL REGULATORS & HOMEOSTATIC AGENTS Vol. 28, no. 4, 587-603 (2014)

EDITORIAL

NOVEL MECHANISM OF PLASMA PREKALLIKREIN (PK) ACTIVATION BY VASCULAR SMOOTH MUSCLE CELLS: EVIDENCE OF THE PRESENCE OF PK ACTIVATOR

J.S. KEUM[1], M.A. JAFFA[2], L.M. LUTTRELL[1] and A.A. JAFFA[1,2,3]

[1]Department of Medicine, Division of Endocrinology, Diabetes and Medical Genetics, Medical University of South Carolina, Charleston, USA; [2]Epidemiology and Population Health Department, Faculty of Health Sciences, American University of Beirut, Beirut, Lebanon; [3]Department of Biochemistry and Molecular Genetics, Faculty of Medicine, American University of Beirut, Beirut, Lebanon

Received March 6, 2014 – Accepted September 12, 2014

The contribution of plasma prekallikrein (PK) to vascular remodeling is becoming increasingly recognized. Plasma PK is activated when the zymogen PK is digested to an active enzyme by activated factor XII (FXII). Here, we present our findings that vascular smooth muscle cells (VSMC) activate plasma PK in the absence of FXII. Extracted plasma membrane and cytosolic fractions of VSMCs activate PK, but the rate of PK activation was greater by the membrane fraction. FXII neutralizing antibody did not affect PK activation by extracted proteins of VSMCs. VSMC PKA was inhibited by the serine protease inhibitors such as aprotinin, phenylmethylsulfonyl fluoride, leupeptin and CTI with CI_{50} of 0.78 μM, 1 mM, 3.13 μM and 40 nM on the cultured cells, respectively. No inhibition of PK activation by cysteine, aspartic acid, and metalloprotease inhibitors was observed. This is the first report of the presence of an intrinsic PKA in VSMC. Considering that VSMCs are normally separated from the circulating blood by endothelial cells, direct PK activation by VSMCs may play a role in disease states like diabetes, hyperlipidemia or hypertension where the endothelial layer is damaged.

Atherosclerosis is the leading cause of death in diabetes, and a major source of morbidity and mortality. Early atherosclerotic lesions are characterized by endothelial dysfunction, impaired endothelium-dependent relaxation of blood vessels, accumulation of inflammatory cells, VSMC proliferation and migration and extracellular matrix deposition in the vessel wall (1-3). The role of impaired endothelium-dependent vasodilation and the mechanisms underlying its dysfunction in vascular disease remain unknown, however, evidence indicates that abnormalities in endothelial synthesis and release of nitric oxide may contribute to vascular complications (4).

The localization of kinin receptors within the vascular wall and their activation by bradykinin (BK) implies a role for this system in the regulation of vascular tone and ultrastructure. Two forms of the kallikrein-kinin system (KKS) exist, one in tissue and the other in plasma. Tissue kallikrein, mainly expressed in the pancreas and salivary glands but also in other tissues such as kidney, vasculature (VSMC) and brain, acts on low and high molecular weight kininogen substrate to release Lysyl-BK (5). The plasma KKS, which includes factor XII, prekallikrein

Key words: plasma prekallikrein, vascular cells, serine protease, plasma prekallikrein activator, factor XII

Mailing address: Ayad A Jaffa, Ph.D.
Department of Biochemistry and Molecular Genetics,
Faculty of Medicine,
American University of Beirut,
P.O.Box: 11-0236, Riad El Solh, Beirut 1107 2020
Beirut, Lebanon
e-mail: aj24@aub.edu.lb

0393-974X (2014)

DISCLOSURE: ALL AUTHORS REPORT NO CONFLICTS OF INTEREST RELEVANT TO THIS ARTICLE.

and high molecular weight kininogen (HMWK), has been linked to the activation of the intrinsic pathway of blood clotting. Plasma PK circulates in an inactive form, complexed with HMWK (6). BK, the principal effector of the KKS system, can be generated both systemically and locally within the vessel wall (7-10). Thus, BK can act in a paracrine or autocrine manner to influence vascular function.

The relevance and significance of kinin-mediated vascular growth and dysfunction is greater if there is accelerated kinin generation in populations at risk for vascular disease. Increased circulating levels of KKS components in patients at risk for vascular disease would provide evidence for heightened system activity and may point to a potential role in vascular disease. We have previously shown that type 1 diabetic patients at risk for developing macrovascular disease (those with altered glomerular hemodynamics who are at high risk for subsequent nephropathy) show increased renal kallikrein and kinin production (11). Furthermore, we demonstrated that circulating levels of plasma PK are increased in type 1 diabetic patients who are hypertensive. This increase in plasma PK levels was associated with an increase in albumin excretion rate (12). These observations, together with our recent discoveries that BK promotes VSMC remodeling, provide evidence for the involvement of the plasma KKS as a modulator of vascular disease risk in diabetes (13-17).

In normal plasma, prekallikrein circulates as a bimolecular complex with HMWK (18). Recent studies have identified a binding site or receptor for kininogen on endothelial cells (19). This kininogen binding site was later identified to be a multiprotein kininogen receptor that consists of cytokeratin 1, urokinase plasminogen activator receptor and gC1qR (20). Once kininogen is bound to endothelial cells, it serves as a binding site for prekallikrein. Binding of prekallikrein to endothelial cells results in its activation to kallikrein via propylcarboxypeptidase (PRCP) (21, 22). The generation of active kallikrein on endothelial cells then cleaves its receptor and substrate, HMWK, to release BK, which in turn stimulates the release of modulators of vessel wall function and ultrastructure such as nitric oxide and prostacyclin (22).

Here, we describe a novel mechanism of plasma PK activation by VSMC. Unlike endothelial cells, activation of plasma PK by VSMC occurs irrespective of HMWK binding to the surfaces of VSMC. Furthermore, our data reveal that the plasma PK activator in VSMC is not PRCP, the plasma PK activator identified on endothelial cells. Understanding the processes of activation of plasma prekallikrein may provide insights into the mechanisms through which plasma PK regulates the vasculature and hence lead to novel strategies for intervention.

MATERIALS AND METHODS

Cell culture

Rat aortic VSMC from male Sprague-Dawley rats (Charles-River, Laboratories, Wilmington, MA, USA) were prepared as previously described (13). A 2-cm segment of artery cleaned of fat and adventitia was incubated in 1 mg/ml collagenase for 3 h at room temperature. The artery was then cut into small sections and fixed to a culture flask for explantation in minimal essential media (MEM) containing 10% fetal calf serum (FCS), 1% non-essential amino acids, 100 mU/ml penicillin and 100 µg/ml Streptomycin. Cells were incubated at 37°C in a humidified atmosphere of 95% air -5% CO_2. Medium was changed every 3-4 days and cells were passaged every 6-8 days by harvesting with trypsin-EDTA. VSMC were identified by the following criteria. They stained positive for intracellular cytoskeletal fibrils of actin and smooth muscle cell specific myosin and negative for factor VIII antigens. VSMC isolated by this procedure were homogeneous and were used in all studies between passages 2-6. The studies were carried out in compliance with the Guide for the Care and Use of Laboratory Animals published by the National Institutes of Health (NIH Publication No. 85-23, revised 1996) and approved by the MUSC Institutional Animal Care and Use Committee.

Human aortic vascular smooth muscle cells (HAVSMs), human aortic endothelial cells (HAECs) and human umbilical vein endothelial cells (HUVECs) were purchased from BioWhittaker (Walkersville, MD, USA). They were subcultured in gelatin coated dishes using endothelial basal medium-2 (EBM-2) with SingleQuots (Catalog No. CC4176) from BioWhittaker (Walkersville, MD, USA), containing 2% FBS and 1% AAS. All cells were used from the third passage.

Extraction of cellular proteins

VSMCs were subcultured in the 100-mm culture dishes until 80% confluent. After washing with ice cold PBS, the cells were harvested with 150 ml of isolation buffer (10 mM Tris-HCL, 250 mM sucrose, pH 7.5) on

ice. The cell suspensions were further homogenized using 27-gauge needle and 1-mm syringe. No detergent was used in this procedure. Cell homogenates were centrifuged for 10 min at 40ºC and the supernatants were ultracentrifuged at 45,000 rpm for 60 min at 4°C (Beckman Optima TM TLX ultracentrifuge, TLX-45 Fixed Angle Rotor). The supernatants were collected as the cytosolic fraction of the cellular proteins and kept at -80°C until used. The pellets from ultracentrifugation were resuspended and homogenized in 50 ml of lysis buffer (50 mmol/LTris-HCl, 150 mmol/L NaCl, 0.1% SDS, 0.02% sodium azide,1% NP 40 (IGEPAL), 0.5% sodium deoxycholate, 1mmol/L PMSF, and protease inhibitor cocktail, pH 8.0) on ice. The homogenates were centrifuged at 2,000 rpm for 15 min at 4°C. The supernatants were then centrifuged at 30,000 rpm for 30 min at 4°C. The supernatants were collected for the plasma membrane fraction of cellular proteins and kept at -80°C until used. The protein concentration of each fraction of the cellular protein was measured using bicinchoninic acid (BCA) method.

Western blotting of plasma prekallikrein

VSMCs cultured in 6-well plates to 80% confluence were incubated with plasma prekallikrein and/or factor XII and plasma prekallikrein for various times. Conditioned media from the cells (20 µg protein) was collected and subjected to SDS-PAGE (12%), under reducing conditions and transferred onto nitrocellulose membrane (BioRad, Hercules, CA, USA) with semi-dry transfer method (Biorad, Hercules, CA, USA) at 20V for 50 min. The membranes were immunoblotted with anti-plasma prekallikrein polyclonal antibody (1:1,000 dilution, Enzyme Research Laboratories, South Bend, IN, USA) overnight at 4°C followed by incubating the membranes in a secondary antibody conjugated to horseradish peroxidase (HRP). The immunoreactive bands were visualized using the chemiluminiscence reagent Renaissance (New England Nuclear Life Science Products, Boston, MA, USA), according to the procedure described by the supplier. Membranes were exposed to Kodak LS film and bands were measured by densitometry and quantified by Scion Image program (Scion Corporation, Frederick, MA, USA).

Plasma prekallikrein activation assay

1~2x10^4 VSMCs were subcultured on Falcon® 96-well sterile polystyrene tissue culture plates (Becton Dickinson, Franklin Lakes, NJ, USA) for one to two days for the cells to become greater than 95% confluent. Cells were starved by incubating in 200 µl of serum-free EMEM for 24 h. For endothelial cells, 2x10^4 HUVECs and HAECs were subcultured on the same 96-well tissue culture polystyrene plates with or without gelatin coating. Assays were performed in Hepes buffer (10 mM Hepes, 137 mM NaCl, 4 mM KCl, 11 mM D-glucose, 0.5 mg/ml RIA grade BSA, pH 7.4) at room temperature using 0.4 mM of S-2302 (H-D-Prolyl-L-Phenylalanyl-L-arginine-p-nitroaniline dihydrochloride), a relatively specific chromogenic substrate for plasma kallikrein (Chromogenix, Milano, Italy). After washing the cells with 200 µl of warm Hepes buffer 3x at room temperature, the cells were incubated with 3.58 nM human plasma PK (Enzyme Research Laboratories, South Bend, IN, USA) in Hepes buffer. 2.40 nM human plasma FXII (Enzyme Research Laboratories, South Bend, IN, USA) and 4.28 nM human plasma HMWK (Enzyme Research Laboratories, South Bend, IN, USA) were used in controls. These concentrations were chosen by applying the ratios among the plasma concentrations of the three components of KKS, FXII and HMWK; PK 50 µg/mL (670 nM), FXII 30 µg/mL (375 nM) and HK 80 µg/mL (560 nM). Proper activation of PK on the cultured VSMCs was obtained with these concentrations. The optical density (OD) (absorbance at 405 nm) of *p*-nitroaniline was measured at 2 min intervals using a SpectraMax 340PC (Molecular Devices, Sunnyvale, CA, USA) to follow the kinetics of PK activation. V*max* defined as the maximum slope of the kinetic display of optical density versus time and milli-optical density per minute (mOD/min) was applied in our experiment. In detail, V*max* represents the steepest slope of a segment of 11 contiguous points during the reaction time given; the slopes were calculated by applying linear regression of line segments consisting of time points 1 to 11, 2 to 12, 3 to 13 and so forth. The OD_{max} of our experiment was 0.8 at 405 nm when we used 0.4 mM of S-2302. To characterize the nature of PK activator on VSMCs, PK activation was carried out in the presence or absence of various protease inhibitors such as corn trypsin inhibitor (CTI), aprotinin, phenylmethylsulfonyl fluoride (PMSF), leupeptin, cystatin, pepstatin, ethylenediaminetetraacetic acid (EDTA) and ethylenle glycol-bis(β-aminoethylether)-N,N,N',N'-tetraacetic acid (EGTA). To test the effect of CTI and anti-FXII antibody on the activation of PK on the cells or cell-free systems, CTI and anti-FXII antibody were pretreated with cultured VSMCs or extracted proteins from VSMCs for 30 min at room temperature.

Statistical analysis

Data were expressed as mean±SE and analyzed by analysis of variance for repeated measures. For comparisons involving more than two experimental groups, one way ANOVA using the Tukey-Kramer multiple comparison tests were employed to determine statistical significance using Statistical Analysis Systems (SAS). The rates of PK activation between groups were compared by using V_{max} from kinetic data. The differences of mean V_{max}

between groups were analyzed using the Student's *t* test. Significance was considered if $P<0.05$.

RESULTS

Direct activation of plasma PK by VSMC

We initiated studies to explore the possible mechanisms of plasma PK activation by VSMC. VSMCs cultured on gelatin coated 96-well plates were serum starved by incubating them in 200 µl of serum-free EMEM for 24 h. The cells were washed at least 3 times with HEPES buffer (10 mM HEPES, 137 mM NaCl, 4 mM KCl, 11 mM D-glucose, 0.5 mg/ml RIA grade BSA, pH 7.4) followed by the addition of 0.4 mM of S-2302 and 3.58 nM human plasma PK (ERL, South Bend, IN, USA). The optical density (OD) (absorbance at 405 nm) of *p*-nitroaniline was measured at 2-min interval to follow the kinetics of plasma PK activation. The results shown in Fig. 1A demonstrate the conversion of plasma PK to active kallikrein upon its contact with VSMC as evidenced by its ability to cleave S-2302. In contrast, the chromogenic substrate S-2302 was not cleaved by plasma PK in a cell free system, thus excluding the possibility of PK autoactivation.

Activation of plasma PK by VSMC was also determined by Western blot analysis. VSMC were incubated with a known concentration of plasma PK (3.58 nM) for various times. The appearance of cleaved fragments of PK in conditioned media is indicative of the conversion of prekallikrein to kallikrein. Fig. 1B demonstrates the detection of cleaved fragments of PK in the conditioned media as early as 1 h that corresponds to one heavy chain (52kD) and two light chains (36 and 33 kDs). As a positive control, PK activated with FXII in cell-free system for 4 h, resulted in a similar pattern of PK cleaved fragments as that generated by VSMC.

The rate of plasma PK activation between VSMC and endothelial cells was compared in the absence of added HMWK. The results shown in Fig. 2 demonstrate that both human aortic VSMC and rat VSMC can directly activate plasma PK to active kallikrein. In contrast, no activation of plasma PK occurred when plasma PK was added to human aortic endothelial cells (HAEC) and/or human umbilical vein endothelial cells (HUVEC).

To assess whether VSMC can hydrolyze S2302 in the absence of PK, rat aortic VSMCs were incubated with 0.4 mM of S-2302 in the presence and absence of 3.58 nM of PK either alone or in the presence of FXII or HMWK. The results in Fig. 3A show that cleavage of S2302 by VSMC was observed only in the presence of PK, PK+FXII and PK+HMWK. No cleavage of S2302 was observed by VSMC in the absence of PK (NO PK). We next determined whether VSMC release factors into the conditioned media that may result in the hydrolysis of S2302. Conditioned media collected 24 h after incubation with VSMC was incubated with 0.4 mM of S-2302 and 3.58 nM of PK in the presence and absence of FXII. The results in Fig. 3B show that no hydrolysis of S2302 by PK was observed in conditioned media (PK+Cell Media) collected from VSMC and in PK+ Media. Hydrolysis of S2302 by PK was observed only in the presence of FXII.

Activation of plasma PK by cellular proteins extracted from VSMCs

We next determined whether the putative plasma PK activator we discovered on the surfaces of VSMC is mainly associated with the plasma membrane or with the cytosol. We extracted the cellular protein from cultured VSMCs without using any detergent, which might affect the activity of enzymes involved in activation of the KKS, and separated each fraction using ultracentrifugation. The results shown in Fig. 4 A and B demonstrate that incubation of plasma PK (3.58 nM) and 0.4 mM S-2302 with either cytosolic or plasma membrane fractions resulted in a concentration-dependent increase in plasma PK chromogenic activity. The higher the protein concentration the faster the rate of conversation of plasma prekallikrein to active kallikrein

The next series of studies compared V_{max} between the membrane and cytosolic fractions. The results in Fig. 5A demonstrate that both the cytosolic and plasma membrane fraction showed activation of plasma PK when 40 µg protein of each fraction was used. As a control, the results were compared to activation of plasma PK by FXII in a cell free system. The V_{max} of the PK activation using 40 µg of plasma membrane protein was significantly higher ($P<0.016$) than that for cytosolic fraction of the same protein concentration (Fig. 5B). Furthermore, the V_{max} of 40 µg of plasma membrane fraction was significantly

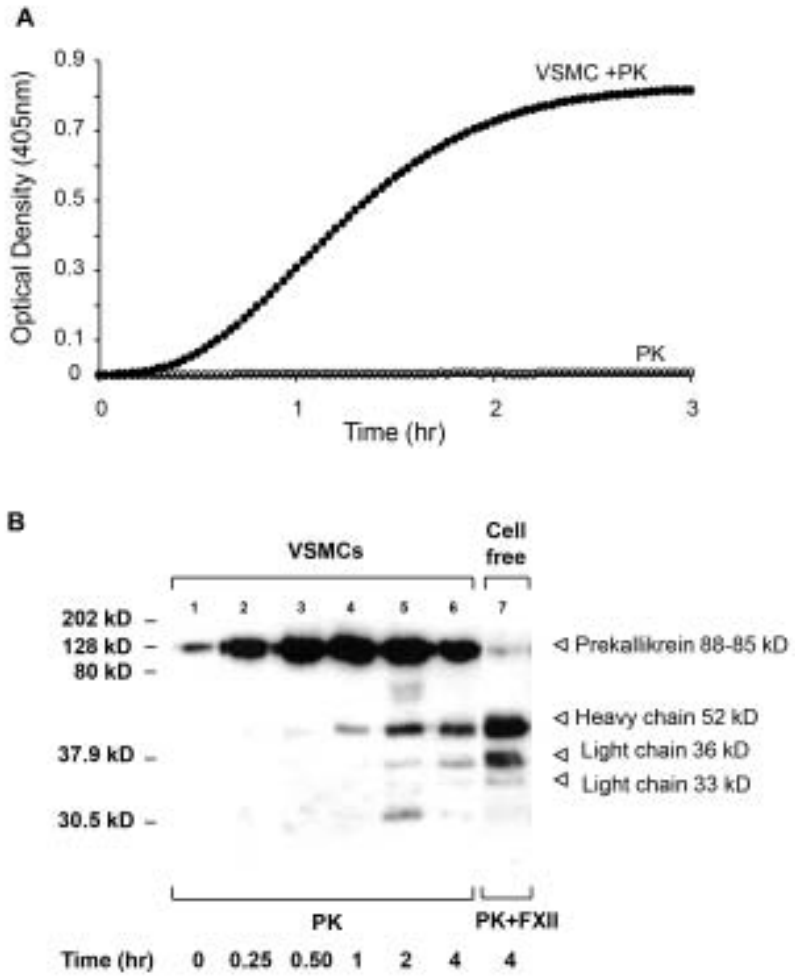

Fig. 1. *Prekallikrein activation by cultured VSMC in the absence of FXII.* ***A)*** *VSMC were subcultured in the 96-well microplate. Optical densities (OD) were recorded at 405 nm at 2-min intervals for 3 h using SpectraMax® 340 PC laser microplate reader. No activation of PK was present by using 3.85 nM of PK and 0.4 mM of kallikrein substrate S-2302® in the cell-free system (open circle). When the same amount of PK was added to VSMC, activation of PK was detected in the absence of FXII (closed circle). The graphs are from a representatives set of 10 experiments.* ***B)*** *Immunoblot analysis of conditioning media of VSMC incubated with 3.58 nM of prekallikrein shows the conversion of PK into various digestion fragments including those corresponding to heavy chain (52 kD) and light chains (36 and 33 kD) of the PK as a function of time. PK digestion fragments by FXII in cell-free system are shown for comparison.*

higher ($P<0.035$) than that observed for FXII (2.40 nM) activation of plasma PK in this experiment. The Vmax of the reaction was significantly greater for plasma membrane at any given protein concentration, indicating that the rate of conversion of prekallikrein to kallikrein is higher in plasma membrane fractions than the cytosolic fractions, indicating that the concentration of PK activator is higher (as a fraction of total protein) in plasma membrane than in cytosol. No activation of plasma PK was observed in a cell-free system (Fig. 5A).

Characterization of the plasma PK activator in VSMC

Role of factor XII in plasma PK activation. To exclude the possibility that activation of plasma PK by VSMC may be due to contamination by FXII that is present as part of the FBS used to culture VSMC,

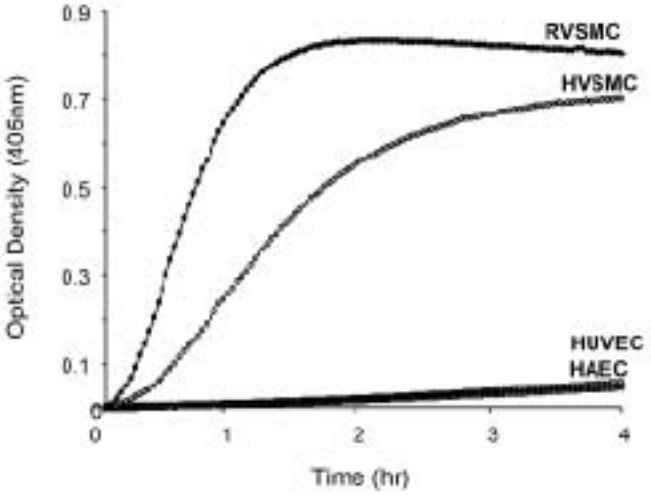

Fig. 2. *Comparison of PK activation by endothelial and VSMC. Rat aortic VSMCs, human aortic VSMC (HVSMC), human umbilical vein endothelial cells (HUVECs) and human aortic endothelial cells (HAECs) were subcultured in different wells and incubated with 3.58 nM of PK and 0.4 mM of S-2302. Optical densities were recorded at 405 nm every 2 min for 2 hrs. While HUVECs and HAECs did not show PK activation, rat VSMC (closed circle) and HVSMC (open circle) showed remarkable activation of PK in the absence of FXII. Graphs are from a representative set of 3 experiments.*

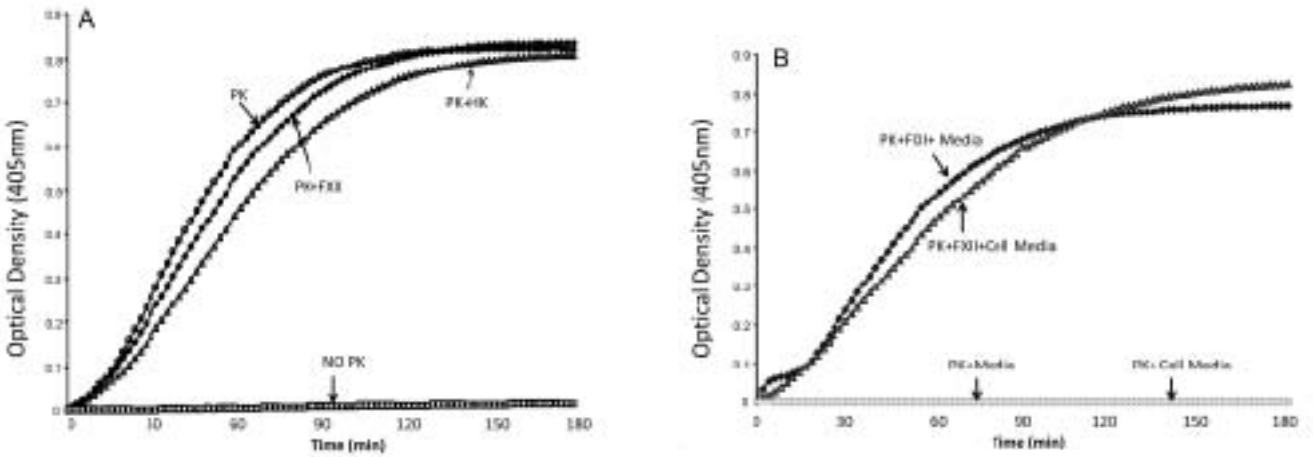

Fig. 3. ***A****) Cleavage of S2303 by PK in VSMC. Rat aortic VSMC were incubated with 0.4 mM of S-2302 in the presence and absence of 3.58 nM of PK alone and in the presence of FXII and/or HK. Optical densities were recorded at 405 nm at every 2 min for 3 h. Cleavage of S2302 by VSMC was observed only in the presence of PK, PK+FXII and PK+HK. No cleavage of S2302 was observed by VSMC in the absence of PK (NO PK). Graphs are from a representative set of 4 experiments.* ***B****) Effect of cell culture media on PK activation. 0.4 mM of S-2302 and 3.58 nM of PK were incubated with conditioned media collected 24 h after incubation with VSMC in the presence and absence of FXII. No hydrolysis of S2302 by PK was observed in conditioned media (PK+Cell Media) collected from VSMC and in PK+ Media. Hydrolysis of S2302 by PK was observed only in the presence of FXII. Graphs are from a representative set of 4 experiments.*

we determined whether activation of plasma PK is sensitive to inhibition with corn trypsin inhibitor (CTI), a select inhibitor of factor XII.

Our first experiments determined the inhibitory profile in our assay conditions of CTI on plasma PK activation by FXII in a cell free system. The inhibitory profile of CTI on plasma PK activation by FXII was assessed by performing a concentration-response

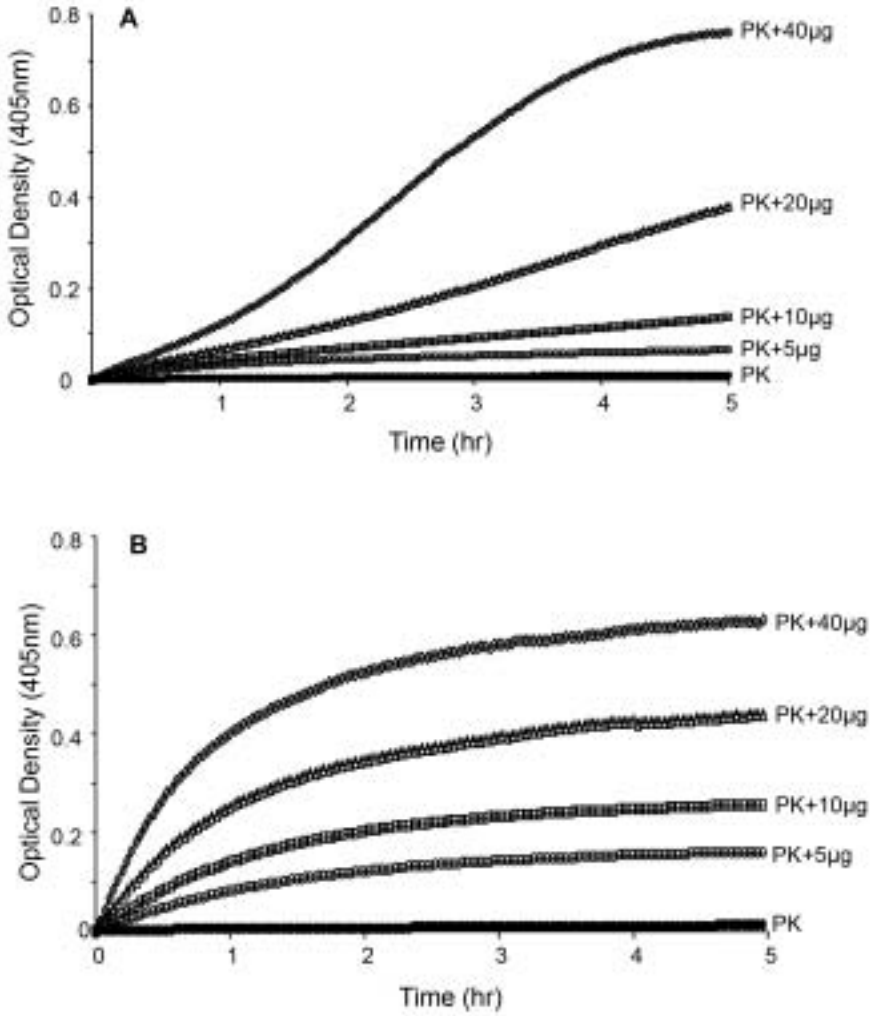

Fig. 4. *Dose-response prekallikrein activation by cytosolic and plasma membrane fractions. **A)** Dose response of cytosolic fractions (5, 10, 20 and 40 µg) on PK activation (3.58 nM of PK, closed circles). **B)** Dose response of plasma membrane fraction (Pmb) on PK activation in a cell- free system. The results are representative of 4 separate experiments.*

curve using various concentrations of CTI (0.5nM-10µM). A concentration-dependent inhibition of plasma PK activation by FXII was observed in response to CTI treatment. The IC_{50} was between 0.312 µM and 0.156 µM, with peak inhibition of about 80% by 10 µM of CTI (Fig. 6A). Based on this finding we elected to use two concentrations of CTI (0.156 µM and 10 µM) to assess whether these concentrations would inhibit plasma PK activation to response to proteins extracted from the plasma membrane or cytosol of VSMC.

Plasma membrane and cytosolic protein extracts (40 µg) were incubated in the presence or absence of 0.156 µM or 10 µM of CTI for 30 min prior to performing the activation assay. The results shown in Fig. 6A, demonstrate that activation of plasma PK by FXII was significantly inhibited in the presence of CTI. Both concentrations of CTI (0.156 µM and 10 µM) significantly inhibited plasma PK activation by FXII (54% and 80% inhibition in V_{max}, $P<0.05$ and $P<0.0001$, respectively). Incubation of plasma PK with either the plasma membrane or cytosolic fraction resulted in significant activation of plasma PK (Fig. 6, B and C). However, no inhibition of PK

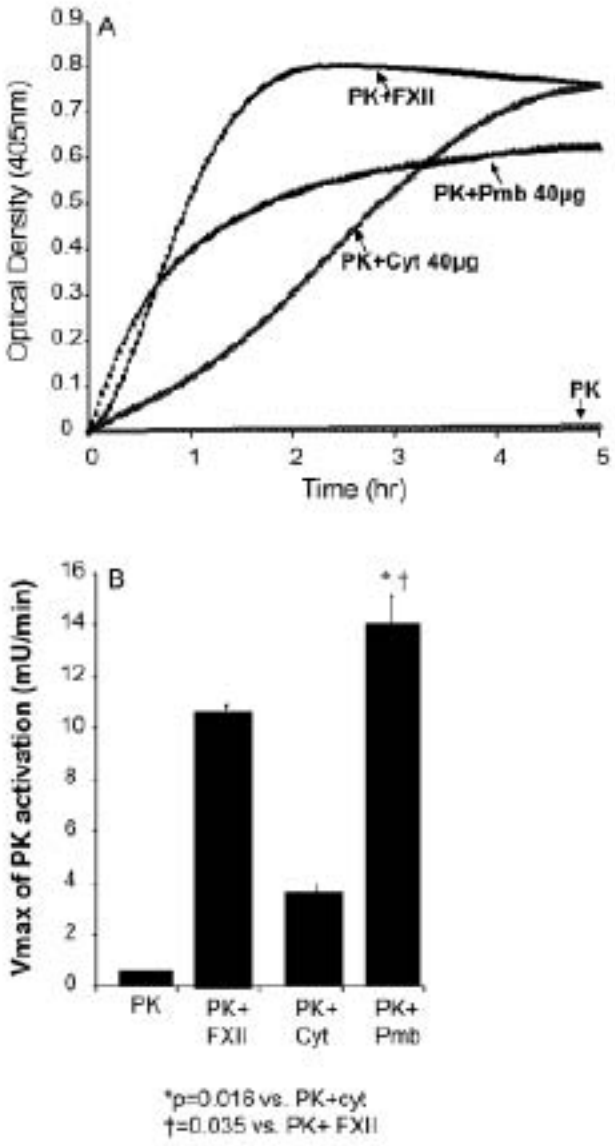

Fig. 5. *Prekallikrein activation by extracted proteins from VSMC in cell-free system.* ***A****) 40 µg of cytosolic (Cyt) and/or plasma membrane (Pmb) protein fractions extracted from VSMC were used to assess activation of PK in cell-free system. Optical densities were read at 405 nm at 2-min intervals for 5 h. Autoactivation of PK was not observed in the absence of cellular protein (open circle). Both cytosolic fraction (open triangle) and plasma membrane fraction (closed triangle) activated PK.* ***B****) The rate of PK activation by plasma membrane fraction was faster than that by cytosolic protein based on the maximum rate of the kinetic profile (V_{max}). The V_{max} of plasma membrane was even higher than that by factor XII (FXII) (closed circle in A). The results are averages from 3 experiments, each with triplicates.*

activation was observed by either concentration of CTI (0.156 µM and 10 µM) when plasma membrane and cytosolic fractions were used to activate PK (11% increase and 2.4% decrease in Vmax, respectively, P=0.08 and P=0.66, respectively, Fig. 6, B and C).

To explore further the involvement of FXII in plasma PK activation by VSMC, plasma PK activation by VSMC alone and/or by FXII and VSMC was determined in the presence and absence of neutralizing anti-FXII antibodies (100µg/mL). The results shown in Fig. 7A demonstrate that VSMC alone and/or VSMC+FXII resulted in plasma PK activation. However, in the presence of anti-FXII antibodies, the activation of plasma PK that was observed in response to FXII and VSMC was significantly reduced compared to FXII-treated VSMC (34% inhibition in Vmax, P<0.001). On the other hand, pretreatment of VSMC with anti-FXII antibodies had no significant effect on plasma PK activation by VSMC alone (9% inhibition in V_{max}, P=0.254, Fig. 7A).

To assess whether the concentration of anti-FXII antibody we used was effective in neutralizing the effects of FXII, we measured the rate of plasma PK activation by FXII in a cell free system in the presence and absence of anti-FXII antibody (100µg/mL). The results in Fig. 7B show that the increase in plasma PK activation in response to FXII was significantly inhibited in the presence of neutralizing anti-FXII antibodies (88% inhibition in V_{max}, P<0.0001).

The effect of neutralizing anti-FXII antibodies on plasma PK activation in response to plasma membrane and cytosolic fractions extraction from VSMC was also assessed. The results shown in Fig. 7, C and D demonstrate that anti-FXII antibodies had no significant effect on plasma PK activation in response to either the membrane fraction or the cytosolic fraction (3% increase each in V_{max}; P=0.578). Taken together, these findings rule out a role for the involvement of FXII in activation of plasma PK by VSMC.

Effect of protease inhibitors on VSMC plasma PK activator

To characterize the plasma PK activator in VSMC, the inhibitory profile of the plasma PK activator was assessed by using a panel of protease inhibitors. In these studies plasma PK (3.58 nM)

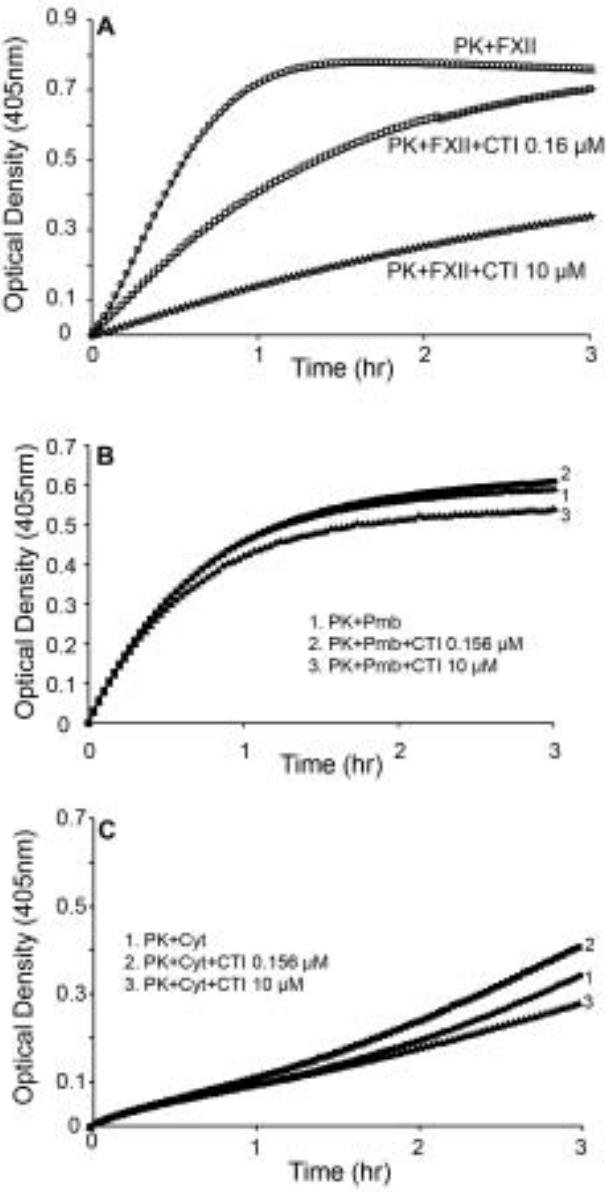

Fig. 6. *Inhibitory profile of PK activation BY CTI in cell-free system.* ***A****) PK activation by FXII in the absence of CTI is shown. Using 0.156 μM and 10 μM, CTI inhibited activation of PK by factor XII (FXII) in dose-dependent manner (p=0.0161 and p=0.000176 for 0.156 μM and 10 μM, respectively, n=3).* ***B****) 40 μg of plasma membrane fraction (Pmb) of VSMC activated PK was not inhibited by 0.156 μM and 10 μM of CTI (p=0.996 and p=0.906 for 0.156 μM and 10 μM, respectively, n=3).* ***C****) Cytosolic fraction also activated PK, which did not show a significant inhibition by 0.156 μM and 10 μM of CTI (p=0.165 and p=0.765 for 0.156 μM and 10 μM, respectively, n=3).*

was added to VSMC cultured on 96 well-plates in the presence and absence of high concentrations of i) serine protease inhibitors (aprotinin 0-100 μM; phenylmethylsulfonyl chloride 0-10 mM; leupeptin 0-100 μM) and antipain 0-100 μM); ii) cysteine protease inhibitor (cystatin 0-100μg/ml); iii) aspartic acid protease inhibitor (pepstatin 0-1.56μg/ml); iv) metalloprotease inhibitors (bestatin 0-250 μg/ml) and v) calcium-dependent proteases (EDTA-Na_2 0-3.125 mM, EGTA 0-12.5 mM). The amount of kallikrein activity formed in the presence of the above inhibitors was determined by the hydrolysis of 0.4 mM S-2302 and compared with an uninhibited control. In addition to assessing the effect of these inhibitors on the chromogenic activity of PK, we also determined whether these inhibitors would block the conversion of PK to active kallikrein. This was assessed by SDS-PAGE, an event that is independent of kallikrein amidolytic activity.

The results shown in Fig. 8 demonstrate that aprotinin (Fig. 8A), PMSF (Fig. 8B) and leupeptin (Fig. 8C), inhibited the chromogenic activity of PK in a concentration dependent manner with an IC50 0f 0.78 **μM,** 1 mM and 3.12 **μM, respectively**. We next determined whether aprotinin, PMSF and leupeptin would block the conversion of PK to kallikrein as assessed by SDS-PAGE, an event that is independent of kallikrein amidolytic activity. PK migrated as a thick band between 85-88kD (Fig. 8, A-C). Incubation of PK with VSMC for 4 h resulted in the generation of multiple breakdown products of PK that migrated at 52 and 36 and 33KD. However, in the presence of increasing concentrations of aprotinin, PMSF and leupeptin, no breakdown products of PK were observed, indicating that the PK activating enzyme(s) associated with VSMC is sensitive to inhibition with aprotinin, PMSF and leupeptin.

The cysteine protease inhibitor cystatin (Fig. 9A) and an aspartic acid protease inhibitor pepstatin (Fig. 9B) did not inhibit the chromogenic activity of plasma PK, nor did they block the conversion of plasma PK to kallikrein as assessed by SDS-PAGE. Furthermore, the metalloprotease inhibitor bestatin (Fig. 10A) and the calcium-dependent proteases, EDTA-Na_2 (Fig. 10B) and EGTA (Fig. 10C) also had no significant effect on the chromogenic activity of plasma PK or the conversion of plasma PK to

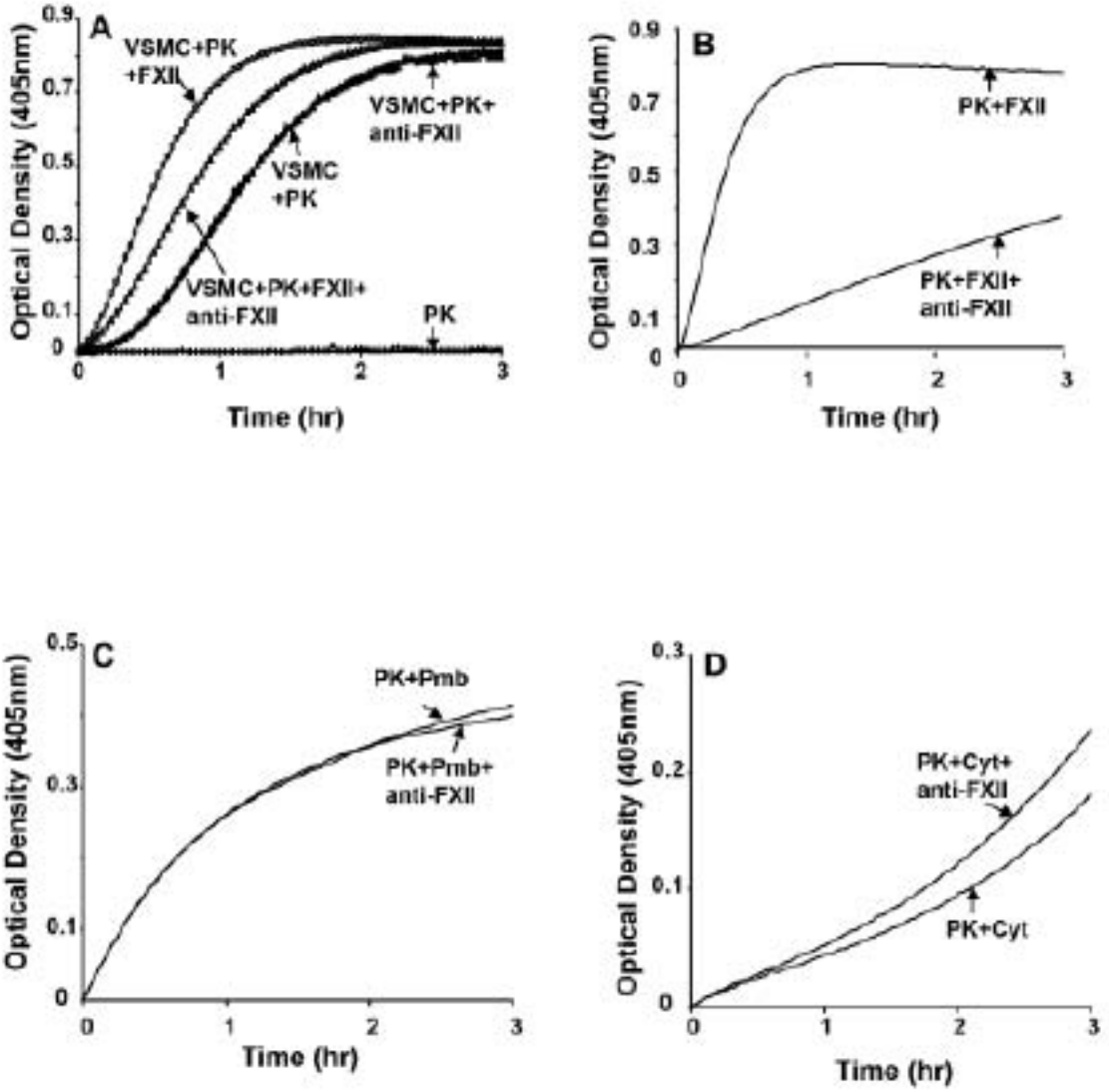

Fig. 7. *The effect of anti-FXII antibody on the activation of PK.* ***A****) VSMC incubated with anti-FXII antibody for 30 min at room temperature. Anti-FXII (100µg/ml) antibody inhibited PK activation by FXII (p=0.00674). However, activation of PK by the VSMC in the absence of FXII was not inhibited by 100µg/mL of anti-FXII (closed circles and closed triangles).* ***B****) Anti-FXII inhibited PK activation by FXII (p=0.0144).* ***C****) Anti-FXII did not inhibit PK activation by plasma membrane fraction (Pmb, 40 µg) of VSMC. D) Anti-FXII did not inhibit PK activation by cytosolic fraction (Cyt, 40 µg) of VSMC. The graphs are representative sets from 4 separate experiments.*

kallikrein as assessed by SDS-PAGE.

Effect of angiotensin II and bradykinin

We next evaluated whether the putative plasma PK activator in VSMC is the endothelial cell plasma PK activator propylcarboxypeptidase (PRCP). Plasma PK (3.58 nM) was added to VSMC in the presence and absence of 10 µM angiotensin II (Ang II) and/or 100 µM of BK. Both Ang II and BK are substrates for PRCP that inhibit PRCP activity (20). The amount of kallikrein activity formed in the presence of Ang II and BK was determined by the hydrolysis of 0.4 mM S-2302 and compared with an uninhibited control. The results shown in Fig. 11 demonstrate that neither AngII nor BK inhibited the chromogenic activity of PK, thus ruling out PRCP as

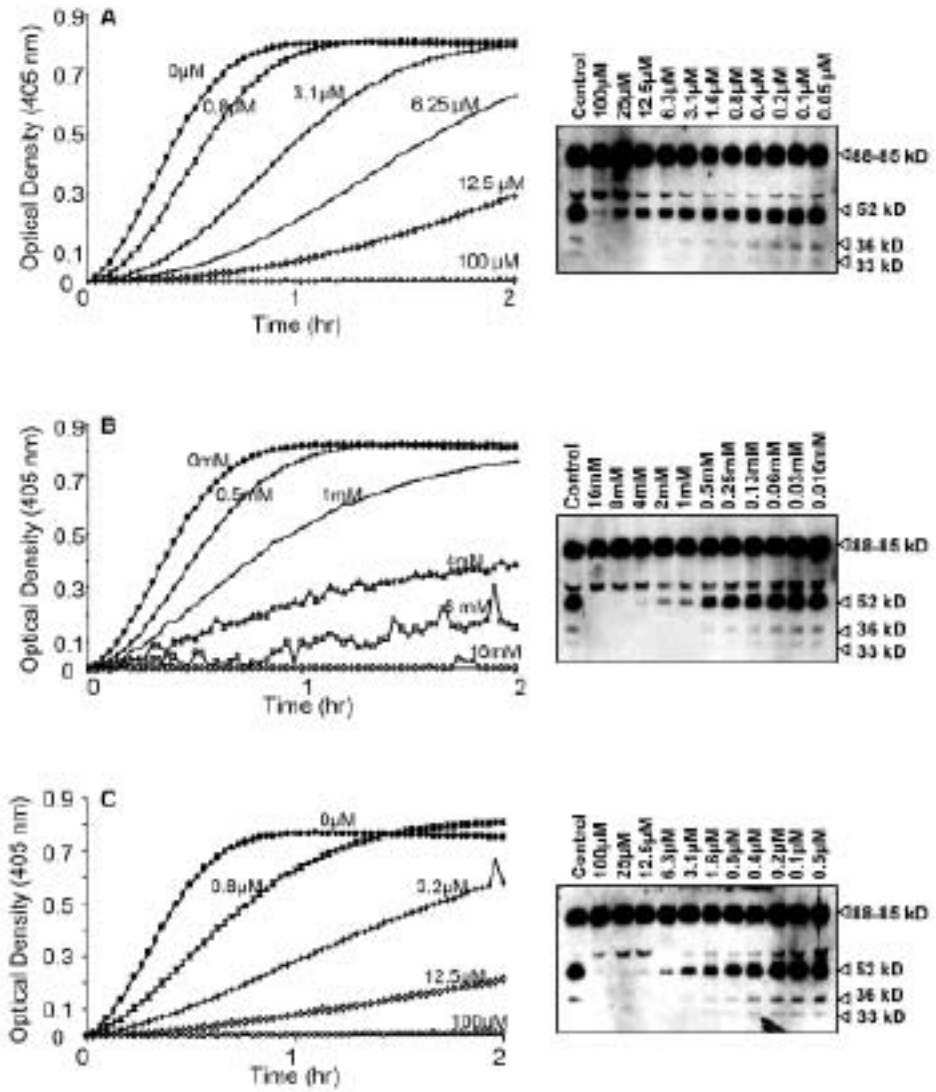

Fig. 8. *Inhibition profile of PK activation on surfaces of VSMCs by serine protease inhibitors.* ***A-C****) PK activation by VSMCs was dose-dependently inhibited by aprotinin (A), phenylmethylsulfonyl fluoride (PMSF) (B) and leupeptin (C). Each graph of PK activation and the bands obtained by Western blotting represent the effect of serial dilution of protease inhibitors used (n=3).*

the putative PK activator in VSMC (4.3% increase and 4.7% decrease in Vmax, respectively; P=0.547 and P=0.651, Fig.11B).

DISCUSSION

The pathophysiological significance of plasma PK independent of its role in blood coagulation is just beginning to be realized. Plasma PK has recently been shown to be associated with high blood pressure and albuminuria in type 1 diabetic patients, to modulate thrombosis risk and to promote vascular remodeling (12, 18). The plasma PK gene KLKB1 is encoded by a single gene that is mapped to the q34-q35 region of chromosome 4 and is composed of 15 exons and 14 introns that correspond to the coding regions of

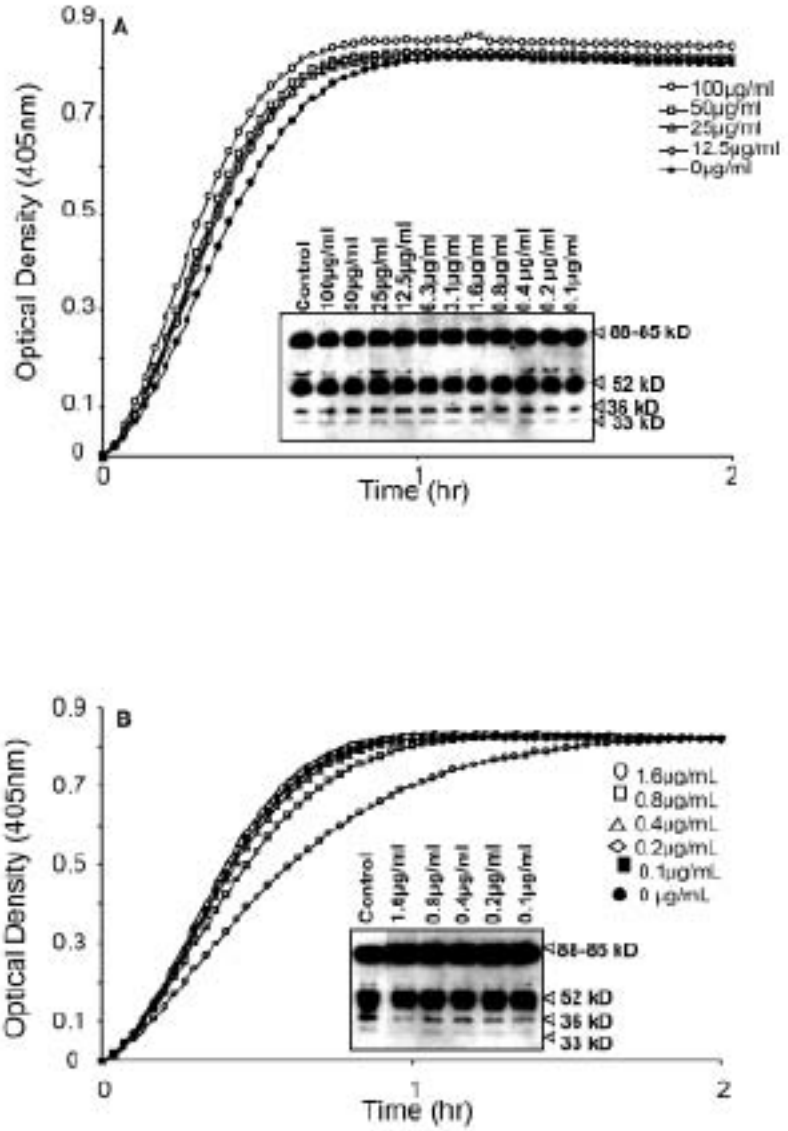

Fig. 9. *Inhibitory profile of PK activation by cysteine and aspartic acid protease inhibitors.* ***A)*** *PK activation by VSMC was not inhibited by cystatin, a cysteine protease inhibitor.* ***B)*** *PK activation by VSMC was not inhibited by pepstatin, an aspartic acid protease inhibitor (n=3 experiments).*

the heavy and light chains of plasma kallikrein. The heavy chain consists of four tandem repeat sequences called "apple" domains (named A1-A4) that are responsible for binding PK to HMWK. The catalytic domain of PK is in the light chain (23). Plasma PK is predominately synthesized in the liver and secreted into the circulation where it circulates as a bimolecular complex bound to its substrate HMWK (5). Under physiological conditions, the assembly of the plasma PK-HMWK complex on the surfaces of endothelial cells is facilitated by the binding of domains 3, 4 and 5 of HMWK to a multiprotein receptor complex that consists of cytokeratin 1 (CK1), the receptor for globular head of the C1q (gC1qR) and the urokinase plasminogen activator receptor (u-PAR) (19-21). Once assembled on the surfaces of endothelial cells,

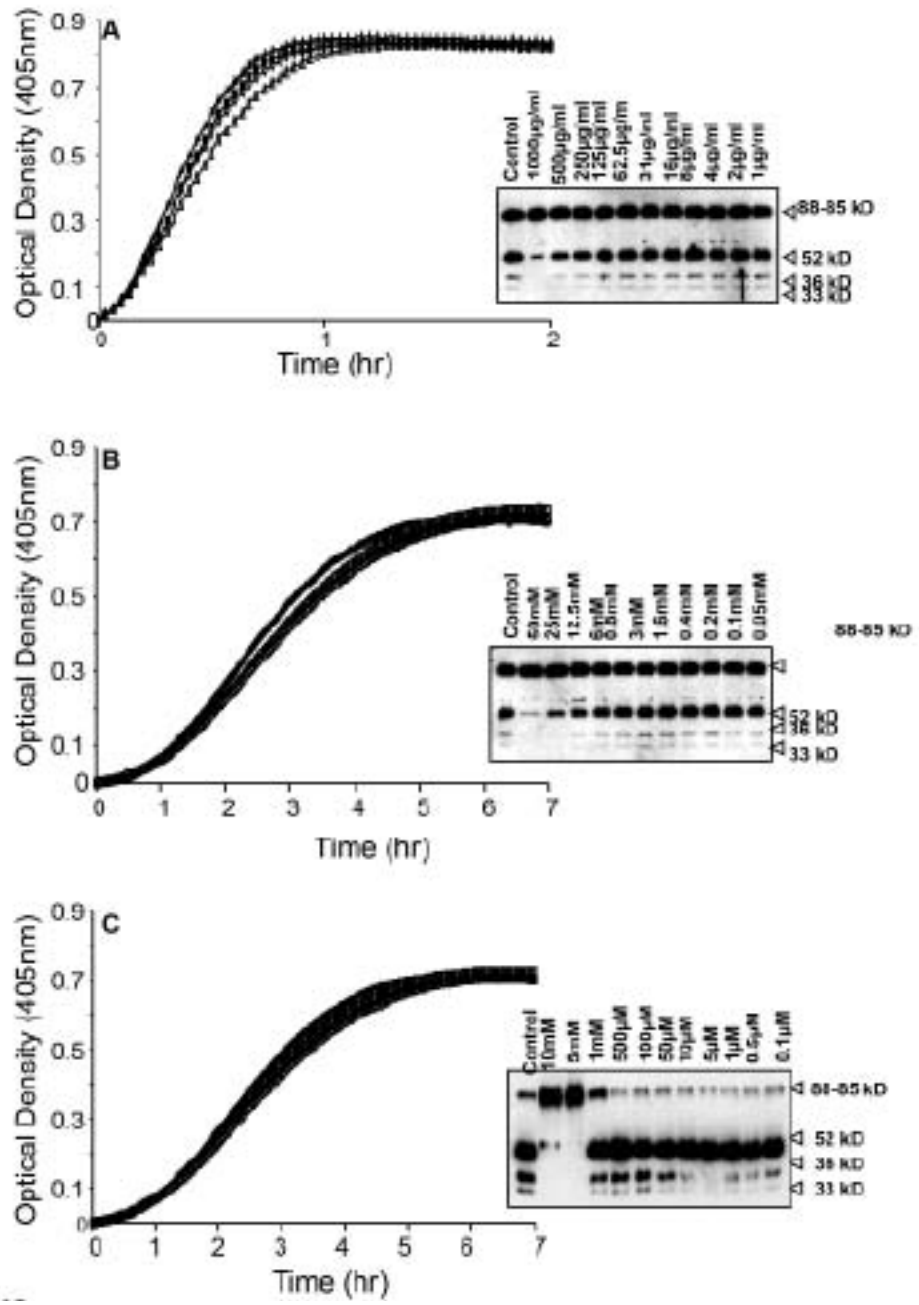

Fig. 10. *Inhibition profile of PK activation by metalloprotease inhibitors. **A-C**) PK activation by VSMC was not inhibited by bestatin (A), EDTA-Na_2 (B) and EGTA (C). Activation assays and Western blot analysis showed similar results (n=3 experiments).*

PRCP, which is bound to the complex, activates plasma PK to activate kallikrein, which in turn cleaves HMWK to release BK (22). The generated BK can act on its B2-receptors in an autocrine and or paracrine manner to initiate a multitude of cellular signals that influence vascular structure and tone. For instance, activation of B2 receptors on endothelial cells by BK results in the generation of nitric oxide, which promotes vasodilatation of the vessel wall and inhibits proliferation of the underlying VSMC (24). Interestingly, flow-dependent dilation of carotid arteries in response to perfused kininogen

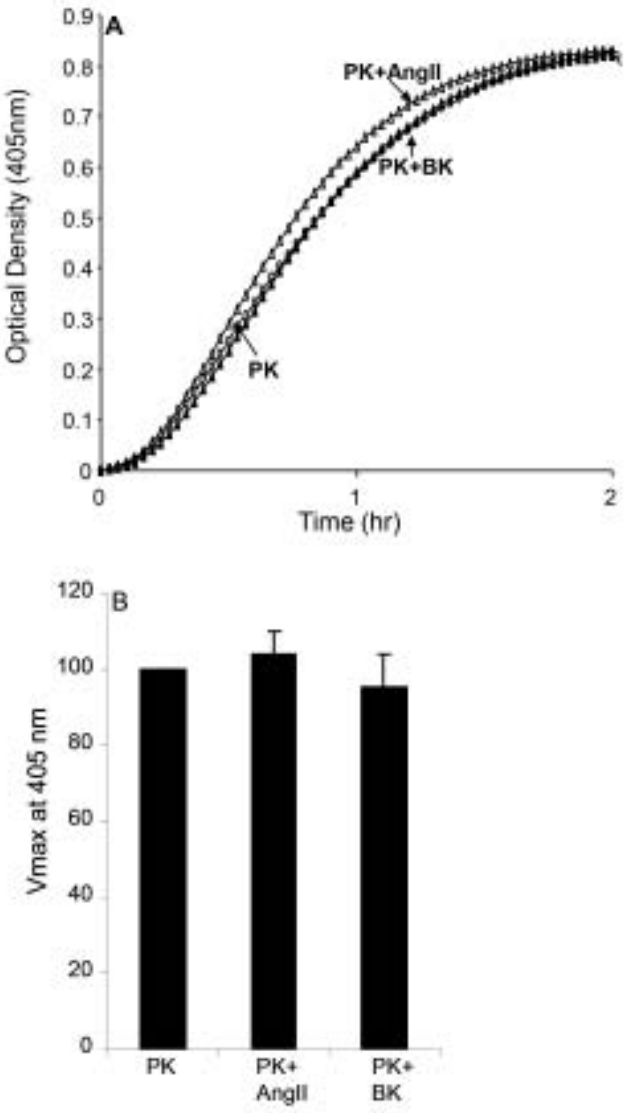

Fig. 11. *Effect of angiotensin II (AngII) and bradykinin (BK) on prekallikrein (PK) activation by VSMC. PK activation was carried out in the absence (open circle) or presence of AngII (10 μM, open triangle) and BK (100 μM, closed triangle) for 2 h at room temperature. No inhibition of PK activation by VSMC was observed by incubating PK in the presence of AngII or BK. The graphs were representative of 3 separate experiments.*

was diminished in tissue kallikrein knockout mice, implicating a direct role for tissue kallikrein in vascular remodeling (25).

However, when the endothelium is denuded or injured, as a result of the diabetic state, plasma PK will be in direct contact with VSMC leading to its activation and initiation of its signal transduction mechanisms. Furthermore, VSMC comprise the main cellular component in atherosclerotic lesions and their number and activity largely determines the thickness of the intima. In this regard, circulating levels of plasma PK are in constant contact with the atherosclerotic plaque leading to its activation by VSMC and initiation of PK signaling pathways that may ultimately alter the pathophysiology of the atherosclerotic plaque. Moreover, our recent findings have implicated a role for plasma PK in vascular remodeling by promoting growth of vascular smooth muscle cells (26). Plasma PK, activated on the surface of exposed VSMC, not only can generate bradykinin, but can cause direct activation of protease activated receptors 1 and 2, leading to transactivation of epidermal growth factor (EGF) receptors and the release of proinflammatory cytokines (26). Trans-activation of EGF receptors has been shown to play an important role in vascular injury response, promoting VSMC hypertrophy and hyperplasia (27). In addition, exciting new information was recently generated that implicate the plasma PK system as a modulator of diabetic microvascular complications (nephropathy and retinopathy). Abnormalities in plasma PK activity were associated with increased blood pressure and greater albumin excretion rate in type 1 diabetic patients (12). Furthermore, activation of plasma PK in the vitreous has been shown to increase retinal vascular permeability, and in the presence of diabetes can cause retinal edema, implicating a role for plasma PK in diabetic retinopathy (28). Furthermore, plasma PK which also increases renin angiotensin system activity by activating prorenin, may be an attractive therapeutic target for the treatment of vascular disease in high risk settings (29). Given the pivotal role of plasma PK in promoting vascular disease in diabetes, identifying the factors that lead to plasma prekallikrein activation is of high significance and can provide insights into new therapeutic targets that can modulate the rate of plasma PK activity at targets sites.

Although HMWK plays a pivotal role in PK activation by HSP90 or PRCP, HMWK was not essential for activation of PK on surfaces of VSMCs in our experiments (20, 30). When HMWK was added together with PK, the rate of PK activation

was slightly lower than PK alone. This finding is in contrast to a previous report by Fernando et al. showing that addition of PK and HMWK to VSMC did not result in PK activation as evidenced by hydrolysis of S2302 (31). In addition, anti-factor FXII antibody, did not inhibit the activation of PK by VSMCs themselves or extracted proteins from the VSMC. Additionally, using extracted VSMC proteins, CTI did not show a dramatic inhibition as is seen with CTI's inhibition of PK activation by FXII. Thus, the direct activation of PK on VSMC cannot be attributed to contaminating FXII arising from some trace amounts of remaining FXII that might be present in FBS used in the culture media.

The direct activation of PK by PK activator of VSMC seen in this study was inhibited by other serine protease inhibitors such as aprotinin, phenylmethylsulfonyl fluoride (PMSF), and leupeptin. No inhibition of PK activation was observed in response to inhibitors of cysteine and aspartic acid proteases and metalloproteases. Angiotensin II (AngII) and BK are known substrates for PRCP and both inhibit PK activation by PRCP in endothelial cells (20, 30). However, when we examined AngII and BK, they did not inhibit the activation of PK by VSMC. This suggests that the activator of VSMC in this experiment may be different from PRCP, a known endothelial PK activator.

Furthermore, the pattern of kinetics of PK activation by the cytosolic fraction of extracted protein was quite different from that by plasma membrane fractions. The rate of PK activation measured using V_{max} was much faster with the plasma membrane fraction than with the cytosolic fraction. In the early phase, PK activation by plasma membrane fraction was even faster than that by FXII on the same plate. This suggests that the PK activator is not FXII and that it constitutes a larger fraction of plasma membrane protein than cytosolic protein. It is important to note here that the kinetics of activation of Prekallikrein to kallikrein by VSMC is slow in the face of enriched substrate, and is similar in pattern to the activation of prekallikrein by endothelial cells and by heat shock protein 90 (30, 32).

As possible alternate pathway for activation of PK by vascular cells, a number of studies in cell free systems implicated a role for proteoglycans in the autoactivation of PK and factor XII (33-35). However, a number of recent studies using endothelial cells have shown that negatively charged proteoglycans inhibit the binding of HMWK to endothelial surfaces and limit the liberation of BK from kininogen cleavage (36). Moreover, heparin was shown not to affect the activation of PK on endothelial cells (37). These results are in agreement with our studies showing that when PK was added to either HAEC or to HUVECS, no activation of PK was observed, thus ruling out a potential role of proteoglycans in PK activation. Since VSMC synthesize and secrete proteoglycans, we tested whether the culture medium collected from the cell layer of cultured VSMC will stimulate PK activation (38, 39). No PK activation was observed when incubated with culture media collected from VSMC. PK activation was observed only in the presence of Factor XII, thus ruling out a potential role for cell surface proteoglycans in PK activation by VSMC. However, the data presented in the current manuscript do not rule out a possible role of activation of PK by proteoglycans that are not rapidly secreted by VSMC.

In summary, the findings of this manuscript point to a novel mechanism of plasma PK activation by VSMC. Unlike endothelial cells, activation of plasma PK by VSMC occurs irrespective of HMWK binding to the surfaces of VSMC. Future studies will aim to purify, characterize and identify the nature of this putative plasma PK activator present in VSMC.

ACKNOWLEDGEMENTS

This work was supported by the National Institutes of Health Grants HL077192 and HL087986 (AAJ).

REFERENCES

1. Ross R. Atherosclerosis: An inflammatory disease. NEJM 1999; 340:115-26.
2. Clowes AW, Karnovsky MJ. Suppression by heparin of smooth muscle cell proliferation in injured arteries. Nature 1977; 265:625-26.
3. Jackson CL, Schwartz SM. Pharmacology of smooth muscle cell replication. Hypertension 1992; 20:713-36.
4. Luscher TF, Tanner FC, Tschudi MR, Noll G. Endothelial dysfunction in coronary artery disease. Annu Rev Med 1993; 44:395-18.

5. Shaw Jl, Diamandis EP. Distribution of 15 human kallikreins in tissues and biological fluids. Clin Chem 2007; 53:1423-32.
6. Colman RW, Schamier AH. Contact System: A vascular biology modulator with anticoagulant, profibrinolytic, antiadhesive and proinflammatory attributes. Blood 1997; 90:3819-43.
7. Margolius HS. Kallikrein and Kinins. Some unanswered questions about system characteristics and roles in human disease. Hypertension 1995; 26:221-29.
8. Mombouli JV, Vanhoutte PM. Kinins and endothelial control of vascular smooth muscle. Ann Rev Pharmacol Toxicol 1995; 35:679-705.
9. Saed G, Carretero OA, MacDonald RJ, Scicli GA. Kallikrein messenger RNA in arteries and viens. Circ Res 1990; 67:510-16.
10. Sakakibara T, Hintze TH, Nasjletti A. Determinants of kinin release in isolated rat hindquarters. Am J Physiol 1998; 274:R120-25.
11. Harvey JN, Edmundson AW, Jaffa AA, Martin LL, Mayfield RK. Renal excretion of kallikrein and eicosanoids in patients with type I diabetes: relationship to glomerular and tubular function. Diabetolgia 1992; 35:857-62.
12. Jaffa AA, Durazo-Arvizu R, Zheng D, Lackland DT, Srikanth S, Garvey WT, Schmaier AH and the DCCT/EDIC Study Group. Plasma prekallikrein: a marker for hypertension and nephropathy in type 1 diabetes. Diabetes 2003; 52:1215-21.
13. Velarde V, Ullian ME, Morinelli TA, Mayfield RK, Jaffa AA. Mechanisms of MAPK activation by bradykinin in vascular smooth muscle cells. Am J Physiol 1999; 277:C253-61.
14. Naidu P, Velarde V, Kappler C, Young RC, Mayfield RK, Jaffa AA. Calcium and calmodulin mediate bradykinin induced MAPK phosphorylation and c-fos induction in vascular cells. Am J Physiol 1999; 277:H1061-8.
15. Greene EL, Velarde V, Jaffa AA. Role of reactive oxygen species in bradykinin induced MAPK and c-fos induction in vascular cells. Hypertension 2000; 35:942-47.
16. Douillet CD, Velarde V, Christopher JT, Mayfield RK, Trojanowska ME, Jaffa AA. Mechanisms by which bradykinin promotes fibrosis in vascular smooth muscle cells: role of TGF-β and MAPK. Am J Physiol 2000; 279:H2829-37.
17. Webb J, Tan Y, Jaffa MA, Jaffa AA. Evidence for prostacyclin and cAMP upregulation by bradykinin and insulin-like growth factor 1 in vascular smooth muscle cells. J Recept Signal Transduct Res 2010; 30:61-71.
18. Schmaier AH. Assembly, activation and physiologic influence of plasma kallikrein/kinin system. Int Immunopharmacol 2008; 8:161-65.
19. Motta G, Rojkjaer R, Hasan A, Cines D, Schmaier AH. High molecular weight kininogen regulates prekallikrein assembly and activation on endothelial cells: A novel mechanism for contact activation. Blood 1998; 91:516-28.
20. Shariat-Madar Z, Mahdi F, Schmaier AH. Identification and characterization of prolylcarboxypeptidase as an endothelial cell prekallikrein activator. J Biol Chem 2002; 277:17962-69.
21. Shariat-Madar Z, Mahdi F, Schmaier AH. Recombinant prolylcarboxypeptidase activates plasma prekallikrein. Blood 2004; 103:4554-61.
22. Zhao Y, Qiu Q, Mahdi F, Shariat-Madar, Z, Rojkjer R, Schmaier AH. Assembly and activation of HP-HK complex on endothelial cells results in bradykinin liberation and NO formation. Am J Physiol 2001; 280:H1821-H29.
23. Yu H, Anderson PJ, Freedman BI, Rich SS, Bowden DW. Genomic structure of the human plasma prekallikrein gene, identification of allelic variants and analysis in end stage renal disease. Genomics 2000; 69:225-34.
24. Briner VA, Tsai P, Schrier RW. Bradykinin: potential for vascular constriction in the presence of endothelial injury. Am J Physiol 1993; 264:F322-27.
25. Berga S, Menton P, Bloch-Faure M, Mathieu E, Alhenic-Gelas F, Levy IB, Boulanger CM. Decreased flow-dependent dilation in carotid arteries of tissue kalikrein-knockout mice. Circ Res 2001; 88:593-99.
26. Abdullah R, Keum J, El-Shewy HM, et al. Plasma kallikrein promotes bradykinin-independent signaling in aortic vascular smooth muscle through direct activation of protease-activated receptors**.** J Biol Chem 2010; 285:35206-15.
27. Ohtsu H, Dempsey PJ, Frank GD, et al. ADAM17 mediates epidermal growth factor receptor

transactivation and vascular smooth muscle cell hypertrophy induced by angiotensin II. Arterioscler Thromb Vasc Biol 2006; 26:e133-e37.

28. Clemont A, Chilcote TJ, Kita T, Liu J, Sinha S, Feener FP. Plasma kallikrein mediates retinal vascular dysfunction and induces retinal thickening in diabetic rats. Diabetes 2011; 60:1590-98.
29. Derkx FH, Schalekamp MP, Bouma B, Kluft C, Schalekamp MA. Plasma kallikrein-mediated activation of the renin-angiotensin system does not require prior acidification of prorenin. JCEM 2013; 54:343-47.
30. Joseph K, Tholanikunnel B, Kaplan A. Heat shock protein 90 catalyzes activation of the prekallikrein-kininogen complex in the absence of factor XII. Proc Natl Acad Sci USA 2002; 99:896-900.
31. Fernando AN, Fernando LP, Fukuda Y, Kaplan AP. Assembly, activation, and signaling by kinin-forming proteins on human vascular smooth muscle cells. Am J Physiol Heart Circ Physiol 2005; 289: H251-57.
32. Joseph K, Tholanikunnel B, Kaplan A. Factor XII-independent cleavage of high molecular weight kininogen by prekallikrein and inhibition by C1 inhibitor. J Allergy Clin Immunol 1999; 124:143-49.
33. Hojima Y, Cochrane CG, Wiggins RC, Austin KF, Stevens RL. *In vitro* activation of the contact (Hageman Factor) system of plasma by heparin and chondroitin sulfate E. Blood 1984; 63:1453-59.
34. Tankersley DL, Finlayson JS. Kinetics of activation and autoactivation of human factor XII. Biochemistry 1984; 23:273-79.
35. Tans G, Rosing J, Berrettini M, Lammle B, Griffin JH. Autoactivation of human plasma prekallikrein. J Biol Chem 1987; 262:11308-14.
36. Renne T, Schuh K, Muller-Esterl W. Local bradykinin formation is controlled by glycosaminoglycans. J Immunology 2005; 175:3377-85.
37. Gozzo AJ, Motta G, Cruz-Silva I, et al. Heparin affects the interaction of kininogen on endothelial cells. Biochimie 2001; 93:1839-45.
38. De Dois ST, Frontanilla KV, Nigro J, Ballinger ML, Ivey ME, Cawson EA, Little PJ. Regulation of the atherogenic properties of vascular smooth muscle proteoglycans by anti-hyperglycemic agents. J Diabetes Complications 2007; 21:108-17.
39. Oohira A, Wight TN, Bornstein P. Sulfacted proteoglycans synthesized by vascular endothelial cells in culture. J Biol Chem 1983; 258:2014-21.

MISSENSE VARIANTS OF THE ALANINE: GLYOXYLATE AMINOTRANSFERASE 2 GENE CORRELATED WITH CAROTID ATHEROSCLEROSIS IN THE JAPANESE POPULATION

Y. YOSHINO[1], K. KOHARA[2], M. ABE[1], S. OCHI[1], Y. MORI[1], K. YAMASHITA[1], M. IGASE[2], Y. TABARA[3], T. MORI[1], T. MIKI[2] and S. UENO[1]

[1]Department of Neuropsychiatry, Molecule and Function, Ehime University Graduate School of Medicine, Shitsukawa, Toon, Ehime, Japan; [2]Department of Geriatric Medicine, Ehime University Graduate School of Medicine, Shitsukawa, Toon, Ehime, Japan; [3]Department of Clinical Genetics, Kyoto University Graduate School of Medicine, Kyoto, Japan

Received July 31, 2014 – Accepted October 27, 2014

Alanine:glyoxylate aminotransferase 2 (AGXT2; EC 2.6.1.44) degrades asymmetric dimethylarginine (ADMA), a competitive inhibitor of nitric oxide (NO) synthase. Increased ADMA, reduced NO, and hypertension are shown in Agxt2 knockout mice. There are four single nucleotide polymorphisms (rs37370, rs37369, rs180749, and rs16899974) with which AGXT2 activity changes in humans and may be related to vulnerability of vascular sclerosis. To examine the relationship between them, we studied the functional haplotypes of the AGXT2 gene and decided their relationship with arteriosclerotic changes via carotid intima-media thickness (carotid IMT) in Japanese subjects. Genotyping of those polymorphisms and the carotid IMT in 1,426 Japanese subjects were then evaluated. Subjects with C-A-A-A haplotype (rs37370, rs37369, rs180749, rs16899974) showed low AGXT2 activity ($P < 0.0001$; Pearson's correlation coefficients: 0.497). The C-A-A-A haplotype was significantly associated with mean carotid IMT ($P = 0.049$) and max carotid IMT ($P = 0.004$). Subjects with two C-A-A-A haplotypes exhibited thicker mean carotid IMT ($P = 0.022$) and maximum carotid IMT ($P = 0.001$). In multiple regression analysis, subjects with two C-A-A-A haplotypes were independently and positively associated with mean carotid IMT ($P = 0.02$) and maximum IMT ($P = 0.005$) after correction. There was a significant correlation between the functional variants in the AGXT2 gene and carotid IMT in Japanese. The AGXT2 genotype may be an important factor underlying atherosclerosis.

Alanine:glyoxylate aminotransferase 2 (AGXT2; EC 2.6.1.44) is the only aminotransferase that metabolizes D-3-aminoisobutyrate (AIB), an intermediate product of thymine (1, 2). The amount of D-AIB excretion in the urine is related to AGXT2 activity (3). Recently, four functional single nucleotide polymorphisms (SNPs; rs37370, rs37369, rs180749, and rs16899974) of the AGXT2 gene, which are independently associated with urinary D-AIB excretion, have been reported including from our group (3-6). AGXT2 also degrades asymmetric dimethylarginine (ADMA) *in vivo* (7). Recently,

Key words: D-3-aminoisobutyrate, alanine:glyoxylate aminotransferase 2, asymmetric dimethylarginine, carotid atherosclerosis

Mailing address: Dr Yuta Yoshino
Department of Neuropsychiatry,
Molecule and Function,
Ehime University Graduate School of Medicine,
Shitsukawa, Toon, Ehime 791-0295, Japan
Phone: +81-89-960-5315; Fax: +81-89-960-5317;
e-mail: whisperoftheheart2@yahoo.co.jp

0393-974X (2014)

Caplin et al. (8) demonstrated AGXT2 knockout mouse showed increased circulating levels of ADMA with reduced NO concentration, and hypertension. They also indicated an association between the AGXT2 gene and diastolic blood pressure (8). High ADMA concentration in blood is related to several cardiovascular diseases including hypertension (9), congestive heart failure (10), chronic kidney disease (11), atherosclerosis (12), and human metabolome (4).

Carotid intima-media thickness (IMT) testing via ultrasound is a safe and inexpensive method for evaluating atherosclerosis risk and was established as an index of structural change in the artery (13). Bai et al. (14) reported that the circulating level of ADMA is positively related to carotid IMT, an index for systemic atherosclerosis and which reflects future risk of cardiovascular events (15, 16). Similarly, Riccioni et al. (17) reported that high serum levels of ADMA were associated with asymptomatic atherosclerosis in the common carotid arteries and internal carotid arteries. These findings indicate that the AGXT2 gene could affect atherosclerosis via ADMA metabolism. It is important to know the individual AGXT2 activity, which is indicated by either urinary D-AIB excretion or its four known functional SNPs independently, because it affects the concentration of ADMA in relation to future cardiovascular events. One-third of Japanese lack AGXT2 activity genetically (22), so they will be vulnerable to them. However, to our knowledge, no studies have evaluated the association between known SNPs of AGXT2 and carotid atherosclerosis in addition to urinary D-AIB excretion.

In the present cross-sectional study, we examined the association between the AGXT2 SNPs and their haplotype with carotid IMT and urinary excretion of D-AIB in the Japanese general population.

MATERIALS AND METHODS

Subjects

All subjects in this study were of unrelated Japanese origin and all signed written informed consent approved by the institutional ethics committees of Ehime University Graduate School of Medicine.

AGXT2 activity and urinary excretion of D-AIB

We enrolled 85 Japanese subjects (41 males, 44 females; mean age = 48.3±21.0 years) (5) recruited from Ehime Prefecture, Japan. The cohort were volunteer hospital workers, students, and citizens living in the same prefecture, who did not have any urinary disorders checked by blood examination. Subjects with renal failure related to D-AIB excretion were excluded.

Carotid arteriosclerosis study

We enrolled 1,426 Japanese subjects recruited from among visitors to the Anti-Aging Center at Ehime University Hospital. Inclusion criteria were free of any history of symptomatic cardiovascular events including stroke, transient ischemic attack, coronary heart disease, and congestive heart failure. All subjects were physically and mentally independent in their daily lives (18, 19).

Risk factor evaluation

Lifestyle, medical history, and prescription drug use were evaluated by questionnaire. Anthropometric measurements were carried out by a trained nurse. Venous blood for measurement of serum lipids, plasma glucose, and insulin was collected in the morning after at least 11 h fasting (18, 19). Homeostasis model assessment-insulin resistance (HOMA-IR) was calculated as an index of insulin resistance. Blood pressure was measured in the sitting position after at least 5 min of rest on the right brachium with an oscilometric device (HEM-9000AI; Omron Healthcare Co. Ltd, Kyoto, Japan). Mean blood pressure (BP) was obtained with the following formula: mean BP=(systolic BP + diastolic BP × 2)/3.

Measurement of D-AIB in the urine

Urine samples were frozen at −30°C until measuring D-AIB concentrations by SRL (Tokyo, Japan) with high-performance liquid chromatography (20).

Carotid ultrasonography

The carotid arteries were evaluated using an SSD-3500SV (Aloka Co., Ltd., Tokyo, Japan) with a 7.5-MHz probe equipped with a continuous flow Doppler and phase-locked echo-tracking system. IMT of the far wall of the common carotid artery (CCA) was measured using computerized software, which simultaneously measured the IMT at three points in 1-cm intervals, with three separate cursors positioned optimally on a B-mode image. Nine IMTs of the far wall were measured at three contiguous sites at 1-cm intervals proximal to the bulb from the anterior, lateral, and posterior approaches on each side, and then averaged to obtain the mean IMT. Max-IMT was determined as the greatest thickness measured on both sides of the CCA and bulbus. The reproducibility (CV) of IMT was 3.3±1.6% in the intra-measurement and 5.8±3.3% in between measurements in our laboratory (18).

Genotyping

EDTA tubes were used for collection of blood samples. Venous blood was collected and genomic DNA was extracted from whole blood leukocytes according to standard procedures. Briefly, after gathering the blood samples, DNA was extracted from frozen white blood cells using a blood mini kit with QIAcube (Qiagen, Tokyo, Japan). The purified DNA was stored at 4°C until genetic analyses. Genotyping of SNPs (rs37370, rs37369, rs180749, and rs16899974) in the AGXT2 gene was conducted using the TaqMan 5′-exonuclease allelic discrimination assay (Assay ID: rs37369; C___11162986_1, rs37370; C__1018750_1, rs180749; C__1018795_1, and rs16899974; C__25742181_10, respectively) using a StepOnePlus real-time PCR system (Applied Biosystems, Foster City, CA, USA). The genotyping call rate for urinary D-AIB measurements of 85 Japanese control subjects was 96.5% (rs16899974). The genotyping call rates for the carotid arteriosclerosis study were 97.5% (rs37370), 97.8% (rs37369), 97.8% (rs180749), and 98.9% (rs16899974). No deviation from the Hardy–Weinberg equilibrium (HWE) in the examined SNPs was detected ($P > 0.05$).

Haplotype analysis

Haplotype analysis was performed with commercially available software (SNPAlyze; Dynacom, Tokyo, Japan), which allowed estimation of individual diplotype (21). Haplotype analysis call rates were 94.1% for the 85 Japanese control subjects and 97.5% for the 1,426 subjects.

Statistical analysis

Associations between a polymorphism and urinary D-AIB excretion, a haplotype, and D-AIB excretion were compared by correlation analysis. Associations between the four SNPs and carotid atherosclerosis, or between specific haplotype and carotid atherosclerosis, were compared by one-way ANOVA. Further multiple regression analyses were performed to ascertain whether SNPs and haplotype were associated with carotid IMT and max-IMT independently of other possible confounding parameters such as age, body mass index (BMI), mean BP, lipid profile, HOMA-IR, use of antihypertensive drugs, antidyslipidemic drugs, antidiabetic drugs, and current smoking status. Hardy–Weinberg equilibrium and minor allele frequency were tested with the HWE calculator including analysis for ascertainment bias (http://www.oege.org/software/hwe-mr-calc.shtml). Statistical significance was defined at the 95% level ($P = 0.05$).

RESULTS

Correlation of AGTX2 SNPs and D-AIB urinary excretion

Because we previously reported that three SNPs of the AGXT2 gene (rs37370, rs37369, and rs180749) are correlated with urinary D-AIB excretion (5), we performed genotyping rs16899974 in 85 Japanese subjects, and the association with D-AIB urinary excretion was evaluated. Results showed that SNP was significantly correlated with D-AIB urinary excretion ($r = -0.39$, $P < 0.0001$; Fig. 1). The characteristics of the SNP are shown in Table I.

Specific AGXT2 haplotype affect the urinary excretion of D-AIB

The results of haplotype analyses of 85 Japanese subjects are shown in Table III. We assumed that subjects who had two alleles of C-A-A-A haplotype (rs37370, rs37369, rs180749, rs16899974) were D-AIB high excretors. We conducted correlation analysis of non-career, one-career, and two-career of a C-A-A-A allele haplotype (Fig. 2). The haplotype was significantly correlated with D-AIB excretion ($P < 0.0001$). The Pearson's correlation coefficient was 0.497.

Correlation of AGXT2 SNPs and carotid arteriosclerosis

The clinical characteristics of the study population are summarized in Table V. The characteristics of the four tagging SNPs (rs37370, rs37369, rs180749, and rs16899974) are shown in Table II. All SNPs were in HWE ($P > 0.05$ for all). SNP rs37370 was significantly associated with mean carotid IMT ($P = 0.037$) and maximum carotid IMT ($P = 0.012$) (Table VI). In allelic model analysis, CC in rs37370 was significantly associated with maximum carotid IMT ($P = 0.015$), and AA in rs16899974 was significantly associated with mean carotid IMT ($P = 0.036$) and maximum carotid IMT ($P = 0.019$) (Table VI).

Specific AGXT2 haplotype affect the carotid atherosclerosis

The haplotype frequency in the carotid atherosclerosis study is shown in Table IV. The C-A-A-A haplotype (rs37370, rs37369, rs180749, rs16899974) was significantly associated with mean carotid IMT ($P = 0.049$) and maximum carotid IMT ($P = 0.004$) (Table VII). Subjects with two C-A-A-A haplotypes had a significantly higher mean carotid IMT ($P = 0.022$) and carotid max-IMT ($P = 0.001$) than subjects with one or no C-A-A-A haplotype.

Table I. *Main characteristics of the selected tagging SNPs in the AGXT2 gene for urinary D-AIB measurements of control subjects.*

SNP (major/minor allele)	Localization	HWE *P*-value	MAF
rs16899974 (C/A)	exon 14 (V498L)	>0.05	0.40

SNP: Single Nucleotide Polymorphism; AGXT2: Alanine:glyoxylate aminotransferase 2; D-AIB: D-3-aminoisobutyrat; HWE: Hardy–Weinberg equilibrium test; MAF: minor allele frequency.

Table II. *Haplotype analysis for urinary D-AIB measurements of 85 Japanese control subjects.*

No.	rs37370	rs37369	rs180749	rs16899974	Frequency
1	C	A	A	A	0.1903
2	T	A	G	C	0.1683
3	T	G	A	C	0.1676
4	C	A	A	C	0.1298
5	T	A	A	A	0.0839
6	T	G	A	A	0.0694
7	C	G	A	C	0.0477
8	T	A	A	C	0.0433
9	T	G	G	C	0.0358
10	C	G	A	A	0.0272
11	T	A	G	A	0.0202
12	T	G	G	A	0.0164
13	C	G	G	A	4.77E-17
14	C	G	G	C	2.97E-30
15	C	A	G	C	2.53E-33
16	C	A	G	A	3.26E-38

D-AIB: D-3-aminoisobutyrate.

Table III. *Main characteristics of the selected tagging SNPs in the AGXT2 gene for subjects in the carotid atherosclerosis study.*

No.	SNP (major/minor allele)	Localization	HWE *P*-value	MAF
1	rs37370 (T/C)	exon 3 (S102N)	>0.05	0.45
2	rs37369 (A/G)	exon 4 (V140I)	>0.05	0.35
3	rs180749 (A/G)	exon 6 (T212I)	>0.05	0.20
4	rs16899974 (C/A)	exon 14 (V498L)	>0.05	0.44

SNP: Single Nucleotide Polymorphism; AGXT2: Alanine:glyoxylate aminotransferase 2; HWE: Hardy–Weinberg equilibrium test; MAF: minor allele frequency.

Multiple regression analysis for carotid atherosclerosis

To investigate whether C-A-A-A haplotype was independently related to carotid atherosclerosis, multiple regression analyses were performed (Table VIII). Results revealed that subjects with two C-A-A-A haplotype had a significantly higher carotid mean IMT (p=0.02) and maximum IMT (p=0.005) compared with those with one or no C-A-A-A haplotype, independently.

Table IV. *Haplotype analysis for subjects for the carotid atherosclerosis study.*

No.	rs37370	rs37369	rs180749	rs16899974	Frequency
1	C	A	A	A	0.2266
2	T	G	A	C	0.1974
3	C	A	A	C	0.1476
4	T	A	G	C	0.1058
5	T	A	A	A	0.0744
6	T	G	A	A	0.0637
7	T	A	G	A	0.0499
8	C	G	A	C	0.0376
9	T	A	A	C	0.0355
10	C	G	A	A	0.0172
11	T	G	G	C	0.0169
12	C	G	G	C	0.0116
13	T	G	G	A	8.90E-03
14	C	A	G	C	6.91E-03
15	C	A	G	A	4.07E-08
16	C	G	G	A	3.93E-08

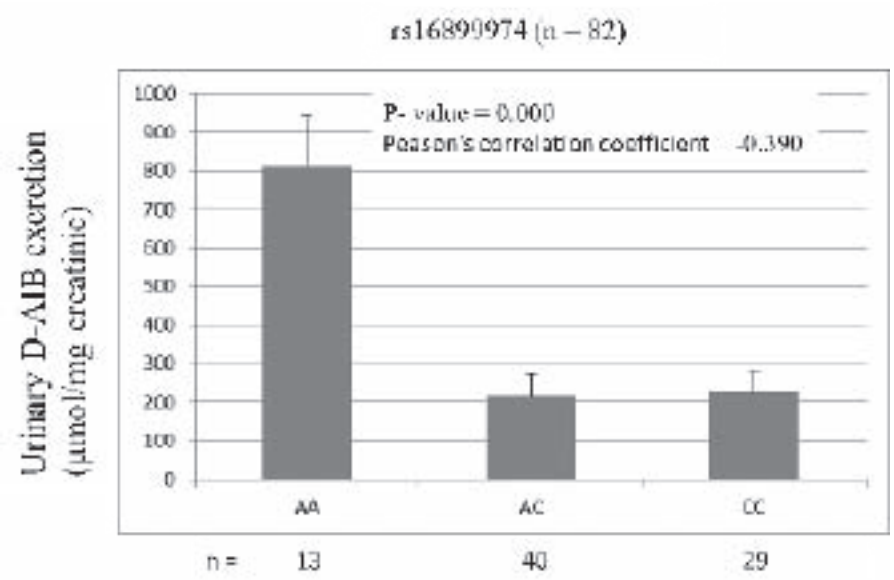

Fig. 1. *D-AIB excretion in the urine for each genotype (average ± standard error). D-AIB: D-3-aminoisobutyrate.*

DISCUSSION

In this study, we carried out two experiments to clarify the genetics of the AGXT2 gene with carotid IMT in Japanese subjects. At first, we recruited 85 subjects to decide the relationship between the haplotypes of the AGXT2 gene and urinary D-AIB concentration that will be almost equal to the AGXT2 activity. Then, the correlation between the functional variants in the AGXT2 gene and carotid IMT with

Table V. *Clinical characteristics of subjects for the carotid atherosclerosis study.*

N	1426
Men, n (%)	559 (39)
Age, years	66.3±9.0
Body height, cm	157.4±8.5
Body weight, kg	57.7±10.3
BMI, kg/m^2	23.2±3.1
Visceral fat area, cm^2	103.5±60.1
Systolic BP, mmHg	135.6±19.5
Diastolic BP, mmHg	77.1±11.2
Mean BP, mmHg	96.6±12.7
Heart rate, beats/min	66.2±10.1
Total cholesterol, mg/dL	218.9±36.8
HDL cholesterol, mg/dL	67.7±18.4
Triglyceride, mg/dL	107.5±60.0
Glucose, mg/dL	103.8±19.2
Insulin, μU/mL	5.8±4.1
HOMA-IR	1.54±1.46
Antihypertensive drugs, n (%)	425 (30)
Antidyslipidemic drugs, n (%)	331(23)
Antidiabetic drugs, n (%)	83 (6)
Current smoking, n (%)	92 (6)
Hypertension, n (%)	760 (53)
Dyslipidemia, n (%)	705 (49)
Diabetes mellitus, n (%)	260 (23)
Carotid mean IMT, mm	0.802±0.155
Carotid maximum IMT, mm	1.020±0.279

BMI: Body Mass Index; BP: Blood Pressure; HDL: High Density Lipoprotein; HOMA-IR: Homeostasis model assessment-Insulin Resistance; IMT: Intima-media thickness.

1,426 Japanese subjects was indicated.

We found that a functional SNP of the AGXT2 gene (rs16899974) was significantly correlated with D-AIB excretion in the urine of 85 Japanese subjects ($P < 0.0001$), similar to that reported by Kittel et al. (6) in non-Asian people. We also conducted haplotype analysis of the four functional polymorphisms of the AGXT2 gene in 85 Japanese subjects with urinary D-AIB excretion, and found that the AA homozygote in exon 14 of the AGXT2 gene (rs16899974) was related to high D-AIB excretion and low AGXT2 activity (Fig. 1). Furthermore, there was a significantly high correlation of specific haplotype of the AGXT2 gene, C-A-A-A haplotype (rs37370, rs37369, rs180749, rs16899974), with high urinary D-AIB excretion, suggesting that the homozygote with this haplotype is a D-AIB high excretor. Approximately 20–30% of the Japanese population are thought to lack AGXT2 activity and are D-AIB excretors (5, 22). The allelic frequency of the C-A-A-A haplotype in our study was 22.5%, suggesting that this is the major haplotypic allele responsible

Table VI. *Four SNPs and carotid atherosclerosis (average ± standard error).*

A	**rs37370**				**rs37370**			**rs37370**		
	CC	CT	TT	P	C	TT	P	CC	T	P
	n=287	N=680	n=438		n=967	n=438		n=287	n=1118	
Mean carotid IMT, mm	0.811±0.166	0.791±0.147	0.813±0.147	0.037	0.797±0.153	0.813±0.159	0.072	0.811±0.166	0.799±0.152	0.27
Maximum carotid IMT, mm	1.055±0.328	0.999±0.567	1.028±0.261	0.012	1.016±0.281	1.028±0.261	0.42	1.055±0.328	1.011±0.259	0.015
B	**rs37369**				**rs37369**			**rs37369**		
	GG	GA	AA	P	G	AA	P	GG	A	P
	n=176	n=658	n=587		n=834	n=587		n=176	n=1245	
Mean carotid IMT, mm	0.800±0.148	0.804±0.161	0.800±0.150	0.91	0.803±0.159	0.800±0.150	0.76	0.800±0.148	0.802±0.156	0.86
Maximum carotid IMT, mm	1.008±0.228	1.026±0.298	1.018±0.271	0.71	1.022±0.284	1.018±0.271	0.77	1.008±0.228	1.022±0.285	0.52
C	**rs180749**				**rs180749**			**rs180749**		
	AA	AG	GG	P	A	GG	P	AA	G	P
	n=919	n=434	n=66		n=1353	n=66		n=919	n=500	
Mean carotid IMT, mm	0.802±0.157	0.799±0.149	0.811±0.177	0.81	0.801±0.154	0.811±0.177	0.62	0.802±0.157	0.800±0.153	0.80
Maximum carotid IMT, mm	1.028±0.294	1.001±0.239	1.027±0.302	0.25	1.020±0.278	1.027±0.302	0.83	1.028±0.294	1.00±0.248	0.13
D	**rs16899974**				**rs16899974**			**rs16899974**		
	CC	CA	AA	P	C	AA	P	CC	A	P
	n=454	n=682	n=278		n=1136	n=276		n=454	n=960	
Mean carotid IMT, mm	0.801±0.161	0.796±0.150	0.820±0.160	0.098	0.798±0.154	0.820±0.160	0.036	0.801±0.161	0.803±0.153	0.79
Maximum carotid IMT, mm	1.019±0.293	1.008±0.257	1.056±0.309	0.053	1.012±0.272	1.056±0.309	0.019	1.019±0.293	1.022±0.274	0.83

SNP: Single Nucleotide Polymorphism; IMT: Intima-media thickness.

Table VII. *Number of C-A-A-A haplotypes and carotid atherosclerosis (average ± standard error).*

	Haplotype 1				**Haplotype 1**			**Haplotype 1**		
	0	1	2	P	0	1+2	P	0+1	2	P
	n=767	n=552	n=70		n=767	n=622		n=1319	n=70	
Mean carotid IMT, mm	0.803±0.155	0.796±0.152	0.844±0.179	0.049	0.803±0.155	0.801±0.156	0.79	0.800±0.154	0.844±0.179	0.022
Maximum carotid IMT, mm	1.016±0.263	1.014±0.266	1.126±0.427	0.004	1.016±0.263	1.026±0.290	0.47	1.015±0.264	1.126±0.427	0.001

IMT: Intima-media thickness.

for loss of function in D-AIB excretion in the urine.

In knockout mice, a high D-AIB excretor was reported to lack AGXT2 activity and indicate higher ADMA in the body (8). Because ADMA is a competitive inhibitor of nitric oxide synthase (NOS) (11, 12), the amount of ADMA will change the concentration of NO in tissues. Endothelial NOS regulates constriction of blood vessels and blood pressure (23). High serum levels of ADMA can decrease release of NO, resulting in atherosclerosis (24). Serg et al. (25) reported higher ADMA levels in patients with atherosclerosis and a strong positive correlation with IMT. In healthy subjects, high serum levels of ADMA were associated with asymptomatic atherosclerosis (17). ADMA is produced from the methylated arginine residue of protein and is freely distributed in tissues including the central nervous system (26). Martens-Lobenhoffer et al. (27) reported that high levels of ADMA were related to the course of hospital stay after subarachnoid hemorrhage. AGXT2 is also distributed in the brain (28). Thus, AGXT2 activity may be related to cerebrovascular

Table VIII. *Multiple regression analyses for carotid atherosclerosis.*

	IMT		IMT Maximum	
	β	P	**β**	P
n	1258		1258	
Sex	0.07	0.006	0.12	<0.0001
Age, years	0.36	<0.0001	0.23	<0.0001
BMI, kg/m^2	0.16	<0.0001	0.16	<0.0001
Visceral fat area, cm^2	−0.08	0.046	−0.10	0.018
Systolic BP, mmHg	0.32	<0.0001	0.27	<0.0001
Diastolic BP, mmHg	−0.20	<0.0001	−0.17	<0.0001
Total cholesterol, mg/dL	0.07	0.01	0.08	0.007
HDL cholesterol, mg/dL	−0.10	0.0009	−0.09	0.005
Triglyceride, mg/dL	−0.05	0.11	−0.06	0.06
Glucose, mg/dL	0.06	0.03	0.03	0.28
Insulin, μU/mL	−0.01	0.76	0.02	0.45
Antihypertensive drugs, n (%)	0.04	0.15	0.04	0.17
Antidyslipidemic drugs, n (%)	0.04	0.15	0.07	0.017
Antidiabetic drugs, n (%)	0.07	0.011	0.09	0.0009
Current smoking, n (%)	0.04	0.06	0.03	0.19
*Haplotype1 2 *vs.* 0+1	0.05	0.02	0.09	0.0005

BMI: Body Mass Index; BP: Blood Pressure: HDL: High Density Lipoprotein; IMT: Intima-media thickness.

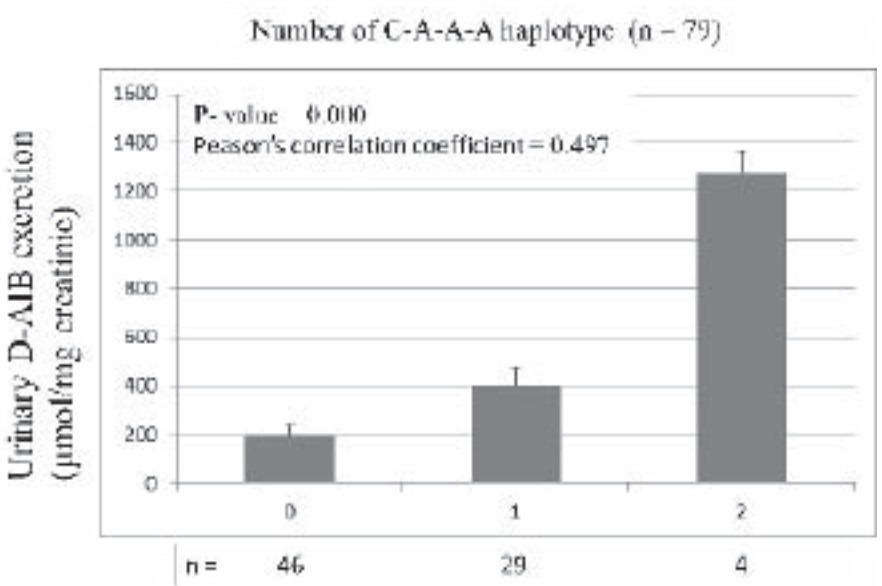

Fig. 2. *D-AIB excretion in the urine for the number of C-A-A-A haplotypes (average ± standard error). D-AIB: D-3-aminoisobutyrate.*

events.

We also investigated the correlation of the four functional SNPs and haplotype with carotid IMT. In our genotypic analysis model, both mean carotid IMT and maximum carotid IMT were thicker in CC homozygous than other groups for the functional

SNP in exon 3 (rs37370). In the allelic analysis model, CC homozygous in exon 3 was also a risk genotype. This CC homozygote was previously confirmed to be related to high D-AIB excretion (5). In the allelic model of the functional SNP in exon 14 (rs16899974), subjects with AA homozygous exhibited thicker mean carotid IMT and maximum carotid IMT when compared with other genotypes. In addition, the C-A-A-A haplotype of the AGXT2 gene was a risk haplotype for both mean carotid IMT and maximum carotid IMT (Tables V and VI).

AGXT2 activity is known to be dependent on ethnicity. For example, 86% of Micronesians are high excretors of D-AIB (29), compared with less than 10% of Caucasians (30). Yanai et al. (22) reported that 35.8% of Japanese lack AGXT2 activity, while we reported that 24.7% of Japanese lack AGXT2 activity (5). As AGXT2 activity correlates with the NO system via ADMA, Japanese have a higher risk of atherosclerosis than Caucasians, but less than Micronesians. Further studies with other ethnic groups are required.

Several studies are needed in the future. Although we indicate these four functional SNPs are due to the AGXT activity and related to carotid IMT in Japanese subjects, it should be investigated whether our results are also useful for the other races, such as Caucasians and Micronesians. To compare serum ADMA and NO with haplotypes of the AGXT2 gene will also provide much information.

In conclusion, we found a significant correlation between the AGXT2 activity and carotid IMT in the Japanese population. It may be possible to predict future cardiovascular vulnerability by using blood samples. Thus, AGXT2 activity may be an underlying mechanism of atherosclerosis.

ACKNOWLEDGEMENTS

We thank Ms. Mayumi Doi for technical assistance, and the healthy volunteers for participating in this study. This work was partially supported by a Health and Labour Science Research Grant from the Japanese Ministry of Health, Labour and Welfare, a Grant-in-Aid for Scientific Research from the Japanese Ministry of Education, Culture, Sports, Science and Technology, and the Ehime Graduate University of Medicine's Good Practice Fund.

REFERENCES

1 Kakimoto Y, Armstrong MD. The preparation and isolation of D-(-)-beta-aminoisobutyric acid. J Biol Chem 1961; 236:3283-86.

2 Kakimoto Y, Taniguchi K, Sano. D-beta-aminoisobutyrate:pyruvate aminotransferase in mammalian liver and excretion of beta-aminoisobutyrate by man. J Biol Chem 1969; 244:335-40.

3 Suhre K, Wallaschofski H, Raffler J, et al. A genome-wide association study of metabolic traits in human urine. Nat Genet 2011; 43:565-9.

4 Rhee EP, Ho JE, Chen MH, Shen D, et al. A genome-wide association study of the human metabolome in a community-based cohort. Cell Metab 2013; 18:130-43.

5 Yoshino Y, Abe M, Numata S, et al. Missense variants of the alanine:glyoxylate aminotransferase 2 gene are not associated with Japanese schizophrenia patients. Prog Neuropsychopharmacol Biol Psychiatry. 2014; 53:137-41.

6 Kittel A, Müller F, König J, et al. Alanine-glyoxylate aminotransferase 2 (AGXT2) polymorphisms have considerable impact on methylarginine and β-aminoisobutyrate metabolism in healthy volunteers. PLoS One 2014; 9(2): e88544.

7 Ogawa T, Kimoto M, Watanabe H, Sasaoka K. Metabolism of NG,NG-and NG,N'G-dimethylarginine in rats. Arch Biochem Biophys 1987; 252:526-37.

8 Caplin B, Wang Z, Slaviero A, Tomlinson J, Dowsett L, Delahaye M, Salama A; International Consortium for Blood Pressure Genome-Wide Association Studies, Wheeler DC, Leiper J. Alanine-glyoxylate aminotransferase-2 metabolizes endogenous methylarginines, regulates NO, and controls blood pressure. Arterioscler Thromb Vasc Biol 2012; 32(12):2892-900.

9 Kayrak M, Bacaksiz A, Vatankulu MA, Ayhan SS, Taner A, Unlü A, Yazici M, Ulgen MS. Association between exaggerated blood pressure response to exercise and serum asymmetric dimethylarginine levels. Circ J 2010; 74:1135-41.

10 Wilson, Tang WH, Tong W, et al. Differential effects of arginine methylation on diastolic dysfunction and disease progression in patients with chronic systolic heart failure. Eur Heart J 2008; 29:2506-13.
11 Vallance P, Leone A, Calver A, Collier J, Moncada S. Accumulation of an endogenous inhibitor of nitric oxide synthesis in chronic renal failure. Lancet 1992; 339:572-5.
12 Leiper JM, Santamaria J, Chubb A, MacAllister RJ, Charles IG, Whitley GSJ, Vallance P. Identification of two human dimethylarginine dimethylaminohydrolases with distinct tissue distributions and homology with microbial arginine deiminases. Biochem J 1999; 343:209-14.
13 Honda O, Sugiyama S, Kugiyama K, et al H. Echolucent carotid plaques predict future coronary events in patients with coronary artery disease. J Am Coll Cardiol 2004; 43(7):1177-84.
14 Bai Y, Sun L, Du L, Zhang T, Xin W, Lan X, Du G. Association of circulating levels of asymmetric dimethylarginine (ADMA) with carotid intima-media thickness: evidence from 6168 participants. Ageing Res Rev 2013; 12(2):699-707.
15 O'Leary DH, Polak JF, Kronmal RA, et al. Distribution and correlates of sonographically detected carotid artery disease in the Cardiovascular Health Study. The CHS Collaborative Research Group. Stroke 1992; 23(12):1752-60.
16 Mannami T1, Konishi M, Baba S, Nishi N, Terao A. Prevalence of asymptomatic carotid atherosclerotic lesions detected by high-resolution ultrasonography and its relation to cardiovascular risk factors in the general population of a Japanese city: the Suita study. Stroke 1997; 28(3):518-25.
17 Riccioni G, Scotti L, D'Orazio N, Gallina S, Speziale G, Speranza L, Bucciarelli T. ADMA/SDMA in elderly subjects with asymptomatic carotid atherosclerosis: values and site-specific association. Int J Mol Sci 2014; 15(4):6391-98.
18 Ochi N, Kohara K, Tabara Y, et al. Association of central systolic blood pressure with intracerebral small vessel disease in Japanese. Am J Hypertens 2010; 23:889-94.
19 Ohara M, Kohara K, Tabara Y, Ochi M, Nagai T, Igase M, Miki T. Sarcopenic obesity and arterial stiffness, pressure wave reflection and central pulse pressure: the J-SHIPP study. Int J Cardiol 2014; 174:214-17.
20 Shimbo K, Kubo S, Harada Y, et al. Automated precolumn derivatization system for analyzing physiological amino acids by liquid chromatography/mass spectrometry. Biomed Chromatogr 2010; 24:683-91.
21 Awata T, Neda T, Iizuka H, et al. Endothelial nitric oxide synthase gene is associated with diabetic macular edema in type 2 diabetes. Diabetes Care 2004; 27(9):2184-90.
22 Yanai J, Kakimoto Y, Tsujio T, Sano I. Genetic study of beta aminoisobutyruc acid excretion by Japanese. Am J Hum Genet 1969; 21:115-32.
23 Wood KC, Cortese-Krott MM, Kovacic JC, et al. Circulating blood endothelial nitric oxide synthase contributes to the regulation of systemic blood pressure and nitrite homeostasis. Arterioscler Thromb Vasc Biol 2013; 33(8):1861-71.
24 Leiper J, Vallance P. Biological significance of endogenous methylarginines that inhibit nitric oxide synthases. Cardiovasc Res 1999; 43(3):542-48.
25 Serg M, Kampus P, Kals J, et al. Association between asymmetric dimethylarginine and indices of vascular function in patients with essential hypertension. Blood Press 2011; 20(2):111-6.
26 Ueno S, Sano A, Kotani K, Kondoh K, Kakimoto Y. Distribution of free methylarginines in rat tissues and in the bovine brain. J Neurochem 1992; 59(6):2012-6.
27 Martens-Lobenhoffer J, Sulyok E, Czeiter E, Büki A, Kohl J, Firsching R, Tröger U, Bode-Böger SM. Determination of cerebrospinal fluid concentrations of arginine and dimethylarginines in patients with subarachnoid haemorrhage. J Neurosci Methods 2007; 164(1):155-60.
28 Abe M, Ochi S, Mori Y, et al. Distribution of D-3-aminoisobutyrate-pyruvate aminotransferase in the rat brain. BMC Neurosci 2014; 15(1):53.
29 Blumberg BS, Gartler SM. High prevalence of high-level β-amino-isobutyric acid excretors in Micronesians. Nature 1959; 184:19909-2.
30 Armstrong MD, Yates K, Kakimoto Y, Taniguchi K, Kappe T. Excretion of β-aminoisobutyric acid by man. J Biol Chem 1963; 238:1447-55.

MicroRNA-133a FUNCTIONS AS A TUMOR SUPPRESSOR IN GASTRIC CANCER

X-C. XU[1], Y-H. ZHANG[2], W-B. ZHANG[1], T. LI[1], H. GAO[1] and Y-H. WANG[1]

[1]Department of Gastrointestinal Surgery, The First Affiliated Hospital of Xinjiang Medical University, Urumqi, Xinjiang Uygur Autonomous Region, China; [2]Department of Pathology, Affiliated Tumor Hospital of Xinjiang Medical University, Urumqi, Xinjiang Uygur Autonomous Region, China

Received August 8, 2014 – Accepted October 2, 2014

The first two authors contributed equally to this article

MicroRNAs (miRNAs) are small and highly conserved non-coding RNAs that regulate gene expression of target mRNAs through posttranscriptional inhibition involved in the tumorigenesis and progression of multiple malignancies. Although miR-133a has been shown to function as a tumor suppressor in some cancers, the clinical significance and function of miR-133a in gastric cancer remain unclear. Hence, we were focused on the expression and mechanisms of miR-133a in the development of gastric cancer in this study. It was found that the expression of miR-133a was downregulated (P<0.001), while transgelin-2 (TAGLN2) was upregulated (P<0.05) in primary gastric cancer tissues, compared to the adjacent non-cancerous tissues (ANCT). Furthermore, decreased expression of miR-133a and increased expression of TAGLN2 were both associated with lymph node metastases in patients with gastric cancer (P<0.001; P=0.011). Functional analysis studies revealed that ectopic expression of miR-133a reduced cell proliferation and invasion, and induced cell apoptosis and cycle arrest via suppressing the level of TAGLN2 from transcriptional and translational levels and downregulated the expression of proliferating cell nuclear antigen (PCNA) and matrix metalloproteinase-2 (MMP-2) in gastric cancer cells. In conclusion, these results demonstrate that decreased expression of miR-133a is associated with the lymph node metastases of patients with gastric cancer. Overexpression of miR-133a inhibits cell growth and invasion and induces cell apoptosis and cycle arrest through repressing TAGLN2 gene, suggesting that miR-133a might be used as a biomarker or therapeutic target for the treatment of gastric cancer.

Gastric cancer is one of the most common malignancies worldwide, with an estimated 934,000 cases reported globally in 2002 (1), and is the second most common cause of death from cancer. The prognosis of gastric cancer is poor with an estimated relative five-year survival rate of less than 20% (2). Gastric cancer is also a genetic disease developing from a multi-step process. Single or multiple mutations in genes related to growth control, invasion and metastasis form the molecular genetic basis of malignant transformation and tumor progression (3). Thus, identification of predictive biomarkers remains a fundamental challenge in the treatment of patients with gastric cancer.

Key words: microRNA-133a, TAGLN2, gastric cancer, invasion, apoptosis

Mailing address: Prof. Yun-Hai Wang,
Dept. of Gastrointestinal Surgery,
The First Affiliated Hospital of Xinjiang Medical University,
No. 137 South Liyushan S. RD,
Urumqi 830011, Xinjiang Uygur Autonomous Region China
Tel.: +86 0991 4365545 Fax: +86 0991 4324139
e-mail: wangyunhai007948@163.com

0393-974X (2014)

DISCLOSURE: ALL AUTHORS REPORT NO CONFLICTS OF INTEREST RELEVANT TO THIS ARTICLE.

MiRNAs are non-coding RNAs capable of regulating gene expression at the post transcriptional level, and miRNAs and their target genes have been implicated in the development of many cancers. The miRNAs differentially expressed in cancer tissues including miR-133a, have been identified to be downregulated in multiple tumor types (4-8). The decreased expression of miR-133a may be the candidate to develop a biomarker with sufficient sensitivity and specificity for the diagnosis of colorectal cancer (CRC) (8). Loss of miR-133a is also associated with lymph node metastasis, clinical stages and shorter relapse-free survivals of patients with breast cancer, suggesting detection of miR-133a may serve as a novel biomarker for cancer progression and patient prognosis (9). Furthermore, miR-133a functions as a tumor suppressor inhibiting tumor cell proliferation and invasion by targeting oncogenic fascin homolog 1 (FSCN1) gene (9-11). MiR-133a is a direct regulator of CD47, and significantly inhibits tumorigenesis and growth, which may provide new insights into cancer progression, and a is promising candidate for target therapy in esophageal squamous cell carcinoma (ESCC) (12).

However, the clinical significance and function of miR-133a have not been comprehensively understood in gastric cancer. In the present study, we analyzed the clinical significance of miR-133a and TAGLN2 expression by quantitative RT-PCR and immunohistochemistry (IHC) assays in gastric cancer, and investigated the effects of miR-133a overexpression on cell proliferation, invasive potential, apoptosis and cycle distribution in gastric cancer cells, uncovering the essence of miR-133a as a potential therapeutic target in gastric cancer.

MATERIALS AND METHODS

Materials

The human gastric cancer SGC-7901 cell line used in the experiments was from Institute of Biochemistry and Cell Biology (Shanghai, China). Forty cases of gastric cancer tissues and corresponding ANCT were collected from the Department of Gastrointestinal Surgery of the First Affiliated Hospital of Xinjiang Medical University. MiR-133a mimic and negative control vector were from Genechem (Shanghai, China). The primers of miR-133a and TAGLN2 were synthesized by ABI (Framingham, USA). All antibodies were from Cell Signaling Technologies (Boston, USA).

Drugs and reagents

Dulbecco's Modified Eagle medium (DMEM) and fetal bovine serum (FBS) were from Thermo Fisher Scientific Inc (Waltham, MA, USA); TRIzol Reagent and Lipofectamine 2000 were from Invitrogen (Carlsbad, CA, USA); M-MLV Reverse Transcriptase was from Promega (Madison, WI, USA); SYBR Green Master Mixture was from Takara (Otsu, Japan). ECL-PLUS/Kit was from GE Healthcare (Piscataway, NJ, USA).

Clinical samples and data

Human gastric cancer tissues and the corresponding ANCT were obtained from biopsy prior to chemotherapy in a total of 40 consecutive cases of gastric cancer admitted to our hospital between January 2008 and December 2012. The study was approved by the Medical Ethics Committee of Xinjiang Medical University, and written informed consent was obtained from the patients or their parents before sample collection. Two pathologists respectively reviewed all of the cases.

IHC staining

TAGLN2 antibody was used for IHC detection of protein expression in tissue microarrays. RAGE antibody was used at 1:100 dilutions. Endogenous peroxidase was inhibited by incubation with freshly prepared 3% hydrogen peroxide with 0.1% sodium azide. Non-specific staining was blocked with 0.5% casein and 5% normal serum. Tissue microarrays were incubated with biotinylated antibodies and horseradish peroxidase. Staining was developed with diaminobenzidine substrate and sections were counterstained with hematoxylin. PBS replaced TAGLN2 antibody in negative controls.

Quantification of protein expression

The expression of TAGLN2 was semiquantitatively estimated as the total immunostaining scores, which were calculated as the product of a proportion score and an intensity score. The proportion and intensity of the staining was evaluated independently by two observers. The proportion score reflected the fraction of positive staining cells (score 0, <5%; score 1, 5%-10%; score 2, 10%-50%; score 3, 50%-75%; score 4, >75%), and the intensity score represented the staining intensity (score 0, no staining; score 1, weak positive; score 2, moderate positive; score 3, strong positive). Finally, a total expression score was given ranging from 0 to 12. Based on the analysis in advance, TAGLN2 was regarded as negative expression in gastric cancer tissues if the score

<2, and positive expression if the score ≥2.

Regular and real-time RT-PCR

Regular RT-PCR was used to detect the expression of primary transcript and mature product of miR-133a, and real-time PCR was also used for the expression of miR-133a and TAGLN2. Briefly, for primary transcript, 11 μg of total RNA was reversely transcribed using oligo-dT primer (Takara, Tokyo, Japan), and 2 μL of the reverse transcription reaction mix was amplified by PCR with denaturation at 95°C for 2 min and 25 cycles at 95°C for 30 s, 55°C for 30 s, and 72°C for 1 min. For mature product, 1 μg of total RNA was reversely transcribed using miR-133a-specific stem-loop RT primer, and 2 μL of the reverse transcription mix was amplified by PCR with denaturation at 95°C for 2 min and 25 cycles (semiquantitative RT-PCR) or 50 cycles (quantitative real-time PCR) at 95°C for 10 s and 60°C for 1 min. The average level of U6 snRNA was used as an internal control. Each data point was in triplicate. The SYBR green (Takara) method and the IQ5 Real-time PCR detection system (BioRad, Hercules, CA) were used for real-time PCR.

Cell culture and transfection

SGC-7901 cells were cultured in DMEM medium supplemented with 10% heat-inactivated FBS, 100U/ml of penicillin and 100μg/ml of streptomycin. They were all placed in a humidified atmosphere containing 5% CO_2 at 37°C. MiR-133a mimic and negative control were used to transfect SGC-7901 cells. Cells were subcultured at a 1:5 dilution in 300 μg/ml G418-containing medium. Positive stable transfectants were selected and expanded for further study. The clone in which the miR-133a mimic transfected was named as miR-133a mimic group, the negative control transfected was named as NC group and SGC-7901 cells were named as CON group.

Western blot assay

Gastric cancer cells were harvested and extracted using lysis buffer (Tris-HCl, SDS, Mercaptoethanol, Glycerol). Cell extracts were boiled for 5 min in loading buffer and then equal amount of cell extracts were separated on 15% SDS-PAGE gels. Separated protein bands were transferred into polyvinylidene fluoride (PVDF) membranes and the membranes were blocked in 5% skim milk powder. The primary antibodies against TAGLN2, PCNA and MMP-2 were diluted according to the instructions of antibodies and incubated overnight at 4°C. Then, horseradish peroxidase-linked secondary antibodies were added at a dilution ratio of 1:1000, and incubated at room temperature for 2 h. The membranes were washed with PBS for three times and the immunoreactive bands were visualized using ECL-PLUS/Kit according to the kit's instruction. The relative protein level in different cell lines was normalized to GAPDH concentration. Three separate experiments were performed for each clone.

Cell proliferation assay

Cell proliferation was analyzed using the MTT assay. Briefly, cells infected with miR-133a virus were incubated in 96-well-plates at a density of 1×10^5 cells per well with DMEM medium supplemented with 10% FBS. Cells were treated with 20 μl of MTT dye at 0, 24 h, 48 h, 72 h, and subsequently incubated with 150 μl of DMSO for 5 min. The color reaction was measured at 570 nm using an Enzyme Immunoassay Analyzer (Bio-Rad, Hercules, CA). The proliferation activity was calculated for each clone.

Transwell invasion assay

Transwell filters were coated with matrigel (3.9 mg/ml, 60-80 ml) on the upper surface of a polycarbonic membrane (diameter 6.5 mm, pore size 8 mm). After incubating at 37°C for 30 min, the matrigel solidified and served as the extracellular matrix for analysis of tumor cell invasion. Harvested cells (1×10^5) in 100 ml of serum-free DMEM were added into the upper compartment of the chamber. A total of 200 ml conditioned medium derived from NIH3T3 cells was used as a source of chemoattractant, and was placed in the bottom compartment of the chamber. After 24-h incubation at 37°C with 5% CO_2, the medium was removed from the upper chamber. The non-invaded cells on the upper side of the chamber were scraped off with a cotton swab. The cells that had migrated from the matrigel into the pores of the inserted filter were fixed with 100% methanol, stained with Hematoxylin, and mounted and dried at 80°C for 30 min. The number of cells invading through the matrigel was counted in three randomly selected visual fields from the central and peripheral portion of the filter using an inverted microscope (200×magnification). Each assay was repeated three times.

Cell apoptosis analysis

To detect cell apoptosis, gastric cells were trypsinized, washed with cold PBS and resuspended in binding buffer according to the instructions of the apoptosis kit. FITC-AnnexinV and PI were added to the fixed cells for 20 min in darkness at room temperature. Then, Annexin V binding buffer was added to the mixture before the fluorescence was measured on FAC sort flow cytometer. The cell apoptosis was analyzed using the Cell Quest software (Becton Dickinson, USA). Three separate experiments were performed for each clone.

Cell cycle analysis

To detect cell cycle variation, gastric cancer cells were

trypsinized, washed by PBS and fixed with 80% cold ethanol overnight at -20°C. After PBS washing,the fixed cells were stained with PI in the presence of RNase A for 30 min at room temperature in darkness. Each sample was filtered through a 50-μm nylon filter to obtain single-cell suspension. The samples were then analyzed on FACsort flow cytometer (Becton Dickinson, Mountain View, CA, USA). ModFit3.0 software (Verity Software House, Topsham, ME, USA) was used for cell cycle analysis. Three separate experiments were performed for each clone.

Statistical analysis

SPSS 21.0 was used for the statistical analysis. Kruskal-Wallis H test and *Chi*-squared test were used to analyze the expression rate in all groups. One-way analysis of variance (ANOVA) was used to analyze the differences between groups. The LSD method of multiple comparisons was used when the probability for ANOVA was statistically significant. Statistical significance was $P<0.05$.

RESULTS

The expression of miR-133a and TAGLN2 in gastric cancer tissues

The RNA expression levels of miR-185 and TAGLN2 were evaluated in gastric cancer tissues by Real-time PCR assay. As shown in Fig. 1, miR-133a expression was significantly decreased, while that of TAGLN2 was increased in cancer tissues compared to the ANCT (each, ** $P<0.01$). MiR-133a had a negative correlation with TAGLN2 expression in gastric cancer tissues ($P<0.05$).

The expression of TAGLN2 protein was examined in gastric cancer tissues by IHC staining. As shown in Fig. 2, the positive expression of TAGLN2 protein was detected in 65.0% (26/40) of the gastric cancer tissues, and 37.5% (15/40) in a small fraction of ANCT. There was a significant difference between them ($P<0.05$).

Correlation of TAGLN2 and miR-133a expression with clinicopathologic characteristics

Correlation of TAGLN2 and miR-133a expression with clinicopathologic characteristics of patients with gastric cancer was further analyzed. As shown in Table I, the decreased expression of miR-133a was negatively associated with lymph node metastasis of gastric cancer ($P<0.05$), but did not correlate with the age, gender of patients, and the size, degree of differentiation and TNM stage of the tumors ($P>0.05$). As indicated in Table II, no significant link was found between TAGLN2 expression with the factors including age and gender of the patients, or the size, tumor differentiation and TNM staging of the tumors (each $P>0.05$). However, TAGLN2 expression was positively correlated with lymph node metastases ($P=0.011$).

Modulation of miR-133a on TAGLN2 expression

To monitor the expression of miR-133a in target cells, the miR-133a mimic and scrambled control were delivered into SGC-7901 gastric cancer cells. The expression levels of miR-133a and TAGLN2 were then detected after miR-133a mimic infection for 48 h by Real-time PCR. We found that the RNA expression of miR-133a was upregulated (Fig. 3A), while that of TAGLN2 was downregulated (Fig. 3B) in the miR-133a mimic group compared with the NC group and CON groups (each $^{**}P<0.01$). As for the expression of TAGLN2 protein indicated by Western blot assay (Fig. 3C, D), TAGLN2 was reduced in the miR-133a mimic group in comparison with the NC group and CON groups (each $^{**}P<0.01$).

The effect of miR-133a overexpression on cell proliferation

To verify the effect of miR-133a overexpression on tumor growth, we examined cell proliferative activities by MTT assay. The results showed that miR-133a overexpression markedly diminished the proliferative activities of gastric cancer cells in a time-dependent manner compared to the CON and NC groups (Fig. 4A). In addition, the expression level of PCNA protein, examined by Western blot assay (Fig. 4 B, C), was found significantly down-regulated in the miR-133a group compared with the CON and NC groups.

Effects of miR-133a overexpression on cell invasion

To determine the effects of miR-133a overexpression on invasive potential of gastric cancer cells, Transwell assay was performed. The invasive and metastatic potential in Transwell assay was determined on the basis of the ability of cells to invade a matrix barrier containing laminin and type IV collagen, the major components of the basement

Table I. *Correlation of miR-133a expression with clinicopathologic characteristics of patients with gastric cancer.*

Total	40		
Age (years)			
≥60	14	2.31 ~ 8.47	
<60	26	4.17 ~ 17.65	NS
Sex			
Male	27	2,79 ~ 11.71	
Female	13	4.09 ~ 13.43	NS
Tumor size (cm)			
≥5	18	3.12 ~ 9.87	
<5	22	4.37 ~ 12.91	NS
Degree of differentiation			
Well/Moderately	16	3.44 ~ 14.84	
Poorly	24	2.01 ~ 7.31	NS
TNM stage			
I+II	21	1.24 ~ 10.57	
III+IV	19	3.20 ~ 12.94	NS
Lymph node metastasis			
Negative	15	5.30 ~ 21.57	
Positive	25	1.91 ~ 8.53	**<0.05**

NS: no significance

Table II. *Correlation of TAGLN2 expression with clinicopathologic features of patients with gastric cancer.*

Variables	Cases (n)	TAGLN2 expression -	+	*P* value
Number of patients	40	14	26	
Age (years)				
≤60	14	6	8	
> 60	26	8	18	0.450
Sex				
Male	27	9	18	
Female	13	5	8	0.753
Tumor size (cm)				
≤3.5	18	8	10	
> 3.5	22	6	16	0.263
Tumor differentiation				
Well+Moderately	16	7	9	
Poorly	24	7	17	0.350
TNM staging				
I+II	21	6	15	
III+IV	19	8	11	0.376
Metastatic lymph node				
Negative	15	9	6	
Positive	25	5	20	0.011

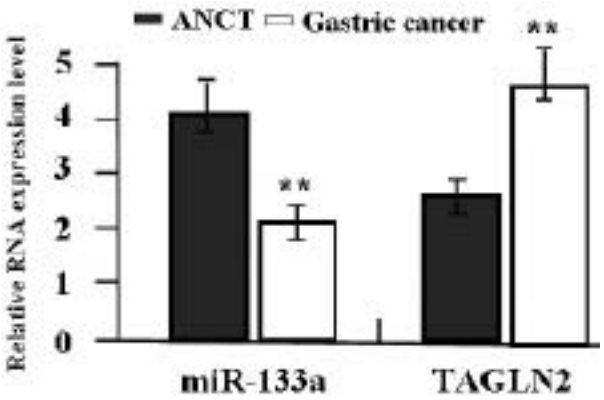

Fig. 1. *The RNA expression of miR-133a and TAGLN2 in gastric cancer tissues. The RNA expression levels of miR-185 and TAGLN2 were detected in gastric cancer tissues by Real-time PCR assay. MiR-133a expression was significantly decreased, while that of TAGLN2 was increased in cancer tissues compared to the ANCT (each, ** P<0.01).*

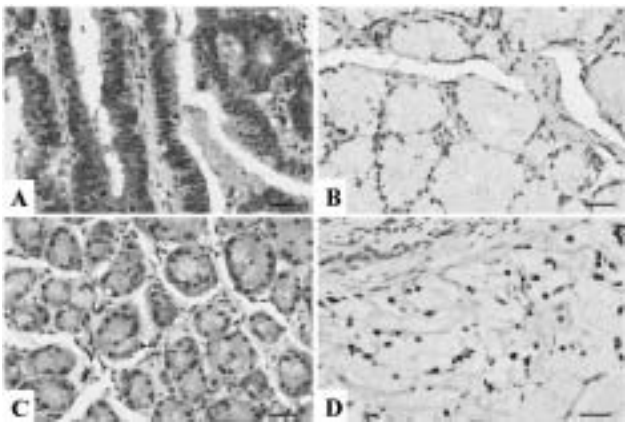

Fig. 2. *The expression of TAGLN2 protein in gastric cancer tissues (×200). Gastric cancer tissues and adjacent non-cancer tissues (ANCT) were immunohistochemically stained with an anti-TAGLN2 antibody and classified as low expression and high expression. A) High expression of TAGLN2 in gastric cancer. B) Low expression of TAGLN2 in gastric cancer. C) High expression of TAGLN2 in ANCT. D) Low expression of TAGLN2 in ANCT. Scale bars: 75 □m.*

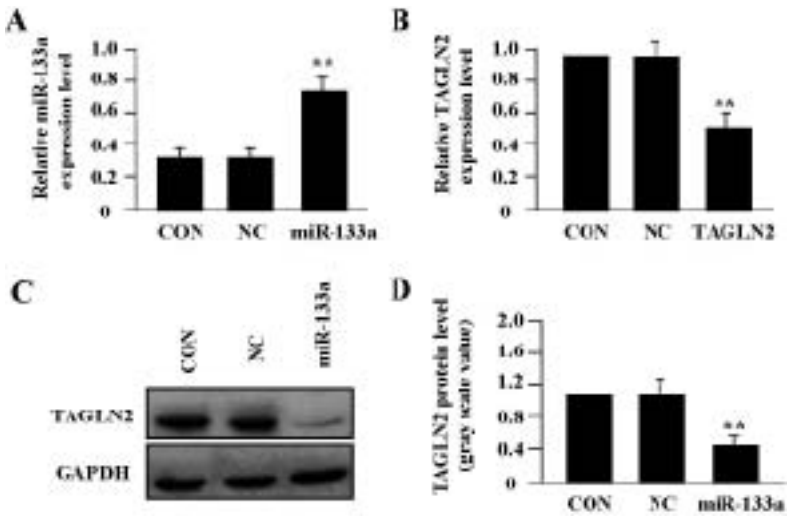

Fig. 3. *Modulation of miR-133a on TAGLN2 expression. After gastric cancer SGC-7901 cells were transfected with miR-133a mimic for 24 h, the expression levels of miR-133a and TAGLN2 were examined by (A, B) Real-time PCR and (C, D) Western blot assays. The expression of miR-133a was significantly increased, but that of TAGLN2 was decreased in miR-133a mimic group compared with the CON and NC groups (each **P<0.01).*

membrane (Fig. 5A). The invasive potential of SGC-7901 cells was markedly weakened in the miR-133a mimic group compared with the CON and NC groups (**P<0.01, Fig. 5B). In addition, the expression level of MMP-2 protein examined by Western blot assay (Fig. 5C, D) was found significantly down-regulated in the miR-133a group compared with the CON and NC groups.

Effects of miR-133a overexpression on cell apoptosis and cycle distribution

To determine the effects of miR-133a

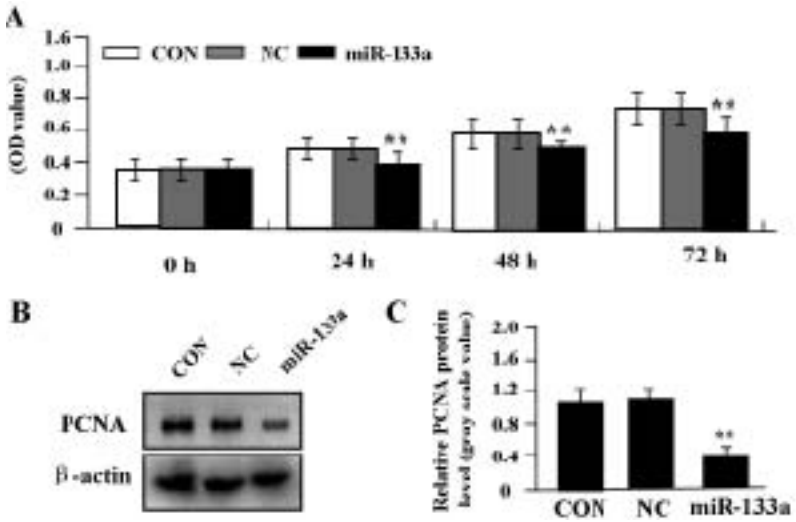

Fig. 4. *Effect of miR-133a overexpression on cell proliferation. A) MTT assay was used to examine cell proliferative activity for consecutive 3 days, and indicated that cell proliferative activities were remarkably diminished in a time-dependent manner in miR-133a group compared with the CON and NC groups (**P<0.01). B, C) The expression level of PCNA protein was found significantly down-regulated in miR-133a group compared with the CON and NC groups in gastric cancer cells.*

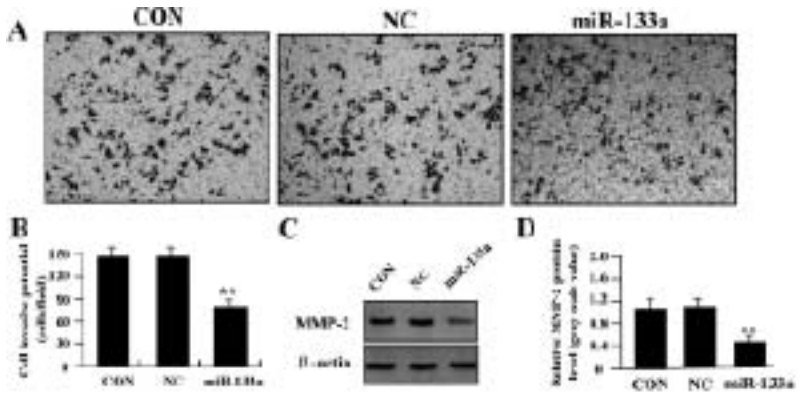

Fig. 5. *Effects of miR-133a overexpression on cell invasion(×200). A, B) After gastric cancer SGC-7901 cells were transfected with miR-133a mimic, Transwell assay was performed to determine cell invasive potential. Cell invasive potential was markedly weakened in miR-133a mimic group compared with the CON and NC groups (each **P<0.01). C, D) The expression level of MMP-2 protein was found significantly down-regulated in miR-133a group compared with the CON and NC groups in gastric cancer cells.*

overexpression on apoptosis and cycle distribution, flow cytometric analysis was performed. The apoptotic indexes of SGC-7901 cells were significantly higher in the miR-133a mimic group than those in NC and CON groups (**$P < 0.01$) (Fig. 6A, C). Cell cycle kinetics showed that, the G_0/G_1 and G_2/M phase fractions were decreased, while S phase was increased. Cell cycle was arrested in S phase in the miR-133a mimic group compared with the NC and CON groups (Fig. 6B, D).

DISCUSSION

MiRNAs are small non-coding RNA molecules

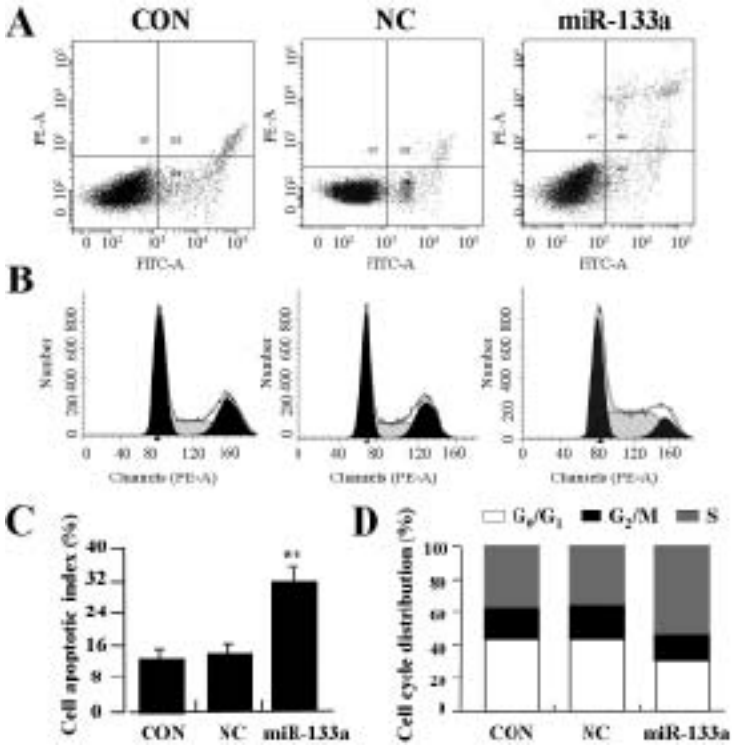

Fig. 6. *Effects of miR-133a overexpression on cell apoptosis and cycle distribution. Flow cytometric analysis was performed to assess cell apoptosis and cycle distribution. A, C) The apoptotic indexes of SGC-7901 cells in miR-133a mimic group were significantly higher than those in NC and CON groups (**P < 0.01). B, D) Cell cycle kinetics showed that, the G0/G1 and G2/M phase fractions were decreased, while S phase was increased. Cell cycle was arrested in S phase in miR-133a mimic group compared with the NC and CON groups.*

that play important roles in the multistep process of cancer development. MiR-1-133a has been shown to display significantly low expression in CRC tissue and liver metastatic tissues (13), and correlate with lymph node metastases and prognosis of patients with CRC (8) and breast cancer (9). MiR-133a is also downregulated in osteosarcoma cell lines and tissues, and is significantly correlated with tumor progression and prognosis of the patients (14). However, the expression and clinical significance of miR-1-133a have not been reported. Our present study, consistent with the results of others (8, 9, 13, 14), indicated that the expression of miR-133a was decreased in gastric cancer compared to the ANCT, and correlated with lymph node metastases of the patients, suggesting that miR-133a might act as a promising therapeutic target for cancer therapy.

The function of miR-133a has been studied in many types of cancers. It has been found that miR-133a as a tumor suppressor reduces tumor cell proliferation, migration, and invasion by targeting oncogenic genes (9, 15), and induces cell apoptosis and cycle arrest (16, 17). In addition, miR-133a sensitizes CRC cells to doxorubicin and oxaliplatin by enhancing apoptosis and inhibiting cell proliferation (17). However, the function of miR-133a in gastric cancer has not been explored. Our present study showed that ectopic expression of miR-133a suppressed cell proliferation and invasion through downregulation of PCNA and MMP-2 expression, and induced cell apoptosis and cycle arrest at S phase in gastric cancer SGC-7901 cells, which was supported by other studies (18, 19). No direct study has shown the regulation of miR-133a on PCNA expression in cancer cells, but few reports indicate that MMP-2/-9 are identified as potential targets for miR-29a and miR-133a (20). Thus, miR-133a may inhibit the invasion of gastric cancer cells

through downregulation of MMP-2 expression. These findings demonstrate that miR-133a might function as a tumor suppressor in gastric cancer.

Furthermore, the regulatory mechanisms of miR-133a on the downstream genes in gastric cancer cells need be further confirmed. The genome-wide gene expression analysis has been used to identify the molecular targets of miR-133a regulation in lung cancer, and revealed several candidate genes, including GSTP1, EGFR and TAGLN2 and so on (21). Some studies then validated the target genes of miR-133a in cancer. Tumor suppressive miR-133a directly regulates oncogenic GSTP1 gene in bladder cancer (22), and targets EGFR in prostate and breast cancers (23, 24) and TAGLN2 in maxillary sinus squamous cell carcinoma (25) and bladder cancer (26). Although it has been indicated that TAGLN2 is involved in the expression and regulation in some cancers (27, 28), different from TAGLN2 as a result of the tumor suppressor (28), our present study showed that the expression of TAGLN2 was increased in gastric cancer tissues and correlated with lymph node metastases. MiR-133a might act as a tumor suppressor in gastric cancer through down-regulation of TAGLN2 expression, indicating the underlying molecular mechanisms of miR-133a in gastric cancer carcinogenesis.

In conclusion, our findings indicate that these results demonstrate that decreased expression of miR-133a is associated with the lymph node metastases of patients with gastric cancer. Overexpression of miR-133a inhibits cell growth and invasion and induces cell apoptosis and cycle arrest through repressing TAGLN2 gene, suggesting that miR-133a might be used as a biomarker or therapeutic target for the treatment of gastric cancer.

ACKNOWLEDGEMENTS

This work was supported by Xinjiang Graduate research and innovation projects (XJGR12013080).

REFERENCES

1. Parkin DM, Bray F, Ferlay J, Pisani P. Global cancer statistics, 2002. CA Cancer J Clin 2005; 55:74-108.
2. Neugut AI, Hayek M, Howe G. Epidemiology of gastric cancer. Semin Oncol 1996; 23:281-91.
3. Farthing MJ, Fitzgerald R, Zhang ZW. Acid, helicobacter and immunity: a new paradigm for oesophagogastric cancer. J Physiol Paris 2001; 95:423-27.
4. Chan M, Liaw CS, Ji SM, et al. Identification of Circulating MicroRNA Signatures For Breast Cancer Detection. Clin Cancer Res 2013; 19:4477-87.
5. Fleming JL, Gable DL, Samadzadeh-Tarighat S, Cheng L, Yu L, Gillespie JL, Toland AE. Differential expression of miR-1, a putative tumor suppressing microRNA, in cancer resistant and cancer susceptible mice. PeerJ 2013; 1: e68.
6. Wu X, Ajani JA, Gu J, et al. MicroRNA expression signatures during malignant progression from Barrett's esophagus to esophageal adenocarcinoma. Cancer Prev Res (Phila) 2013; 6:196-205.
7. Hsu CM, Lin PM, Wang YM, Chen ZJ, Lin SF, Yang MY. Circulating miRNA is a novel marker for head and neck squamous cell carcinoma. Tumour Biol 2012; 33:1933-42.
8. Ma Y, Zhang P, Yang J, Liu Z, Yang Z, Qin H. Candidate microRNA biomarkers in human colorectal cancer: systematic review profiling studies and experimental validation. Int J Cancer 2012; 130:2077-87.
9. Wu ZS, Wang CQ, Xiang R, et al. Loss of miR-133a expression associated with poor survival of breast cancer and restoration of miR-133a expression inhibited breast cancer cell growth and invasion. BMC Cancer 2012; 12:51.
10. Chiyomaru T, Enokida H, Tatarano S, et al. miR-145 and miR-133a function as tumour suppressors and directly regulate FSCN1 expression in bladder cancer. Br J Cancer 2010; 102:883-91.
11. Kano M, Seki N, Kikkawa N, et al. miR-145, miR-133a and miR-133b: Tumor-suppressive miRNAs target FSCN1 in esophageal squamous cell carcinoma. Int J Cancer 2010; 127:2804-14.
12. Suzuki S, Yokobori T, Tanaka N, et al. CD47 expression regulated by the miR-133a tumor suppressor is a novel prognostic marker in esophageal squamous cell carcinoma. Oncol Rep 2012; 28:465-72.
13. Chen WS, Leung CM, Pan HW, Hu LY, Li SC, Ho MR, Tsai KW. Silencing of miR-1-1 and miR-133a-2 cluster expression by DNA hypermethylation in colorectal cancer. Oncol Rep 2012; 28:1069-76.
14. Ji F, Zhang H, Wang Y, et al. MicroRNA-133a,

downregulated in osteosarcoma, suppresses proliferation and promotes apoptosis by targeting Bcl-xL and Mcl-1. Bone 2013; 56:220-26.

15. Nohata N, Hanazawa T, Kikkawa N, et al. Caveolin-1 mediates tumor cell migration and invasion and its regulation by miR-133a in head and neck squamous cell carcinoma. Int J Oncol 2011; 38:209-17.
16. Kawakami K, Enokida H, Chiyomaru T, et al. The functional significance of miR-1 and miR-133a in renal cell carcinoma. Eur J Cancer 2012; 48:827-36.
17. Dong Y, Zhao J, Wu CW, et al. Tumor suppressor functions of miR-133a in colorectal cancer. Mol Cancer Res 2013; 11:1051-60.
18. Kinoshita T, Nohata N, Watanabe-Takano H, et al. Actin-related protein 2/3 complex subunit 5 (ARPC5) contributes to cell migration and invasion and is directly regulated by tumor-suppressive microRNA-133a in head and neck squamous cell carcinoma. Int J Oncol 2012; 40:1770-78.
19. Yamasaki T, Yoshino H, Enokida H, et al. Novel molecular targets regulated by tumor suppressors microRNA-1 and microRNA-133a in bladder cancer. Int J Oncol 2012; 40:1821-30.
20. Jones JA, Stroud RE, O'Quinn EC, et al. Selective microRNA suppression in human thoracic aneurysms: relationship of miR-29a to aortic size and proteolytic induction. Circ Cardiovasc Genet 2011; 4:605-13.
21. Moriya Y, Nohata N, Kinoshita T, et al. Tumor suppressive microRNA-133a regulates novel molecular networks in lung squamous cell carcinoma. J Hum Genet 2012; 57:38-45.
22. Uchida Y, Chiyomaru T, Enokida H, et al. MiR-133a induces apoptosis through direct regulation of GSTP1 in bladder cancer cell lines. Urol Oncol 2013; 31: 115-23.
23. Tao J, Wu D, Xu B, Qian W, Li P, Lu Q, Yin C, Zhang W. microRNA-133 inhibits cell proliferation, migration and invasion in prostate cancer cells by targeting the epidermal growth factor receptor. Oncol Rep 2012; 27:1967-75.
24. Cui W, Zhang S, Shan C, Zhou L, Zhou Z. microRNA-133a regulates cell cycle and proliferation of breast cancer cells by targeting epidermal growth factor receptor through EGFR/Akt signaling pathway. FEBS J 2013; 280: 3962-74.
25. Nohata N, Hanazawa T, Kikkawa N, et al. Identification of novel molecular targets regulated by tumor suppressive miR-1/miR-133a in maxillary sinus squamous cell carcinoma. Int J Oncol 2011; 39:1099-107.
26. Yoshino H, Chiyomaru T, Enokida H, et al. The tumour-suppressive function of miR-1 and miR-133a targeting TAGLN2 in bladder cancer. Br J Cancer 2011; 104:808-18.
27. Lin H, Chen QL, Wang XY, Han W, He TY, Yan D, Chen K Su LD. Clinical significance of pituitary tumor transforming gene 1 and transgelin-2 in pancreatic cancer. Int J Immunopathol Pharmacol 2013; 26:147-56.
28. Leung WK, Ching AK, Chan AW, Poon TC, Mian H, Wong AS, To KF, Wong N. A novel interplay between oncogenic PFTK1 protein kinase and tumor suppressor TAGLN2 in the control of liver cancer cell motility. Oncogene 2011; 30:4464-75.

STUDY ON CONNEXIN GENE AND PROTEIN EXPRESSION AND CELLULAR DISTRIBUTION IN RELATION TO REAL-TIME PROLIFERATION OF PORCINE GRANULOSA CELLS

B. KEMPISTY[1,2], A. ZIÓŁKOWSKA[1], S. CIESIÓŁKA[1], H. PIOTROWSKA[3], P. ANTOSIK[4], D. BUKOWSKA[4], M. NOWICKI[1], K.P. BRÜSSOW[5] and M. ZABEL[1,6]

[1]Department of Histology and Embryology, Poznań University of Medical Sciences, Poznań, Poland; [2]Department of Anatomy, Poznań University of Medical Sciences, Poznań, Poland; [3]Department of Toxicology, Poznań University of Medical Sciences, Poznań, Poland; [4]Institute of Veterinary Sciences, Poznań University of Life Sciences, Poznań, Poland; [5]Institute of Reproductive Biology, Leibniz Institute for Farm Animal Biology, Dummerstorf, Germany; [6]Department of Histology and Embriology, Wroclaw Medical University, Wroclaw, Poland

Received August 20, 2014 – Accepted October 27, 2014

Granulosa cells (GCs) play an important role during follicle growth and development in preovulatory stage. Moreover, the proteins such as connexins are responsible for formation of protein channel between follicular-cumulus cells and oocyte. This study was aimed to investigate the role of connexin expression in porcine GCs in relation to their cellular distribution and real-time cell proliferation. In the present study, porcine GCs were isolated from the follicles of puberal gilts and then cultured in a real-time cellular analyzer (RTCA) system for 168 h. The expression levels of connexins (Cxs) Cx36, Cx37, Cx40 and Cx43 mRNA were measured by RQ-PCR analysis, and differences in the expression and distribution of Cx30, Cx31, Cx37, Cx43 and Cx45 proteins were analyzed by confocal microscopic visualization. We found higher level of Cx36, Cx37, and Cx43 mRNA expression in GCs at recovery (at 0 h of *in vitro* culture, IVC) compared to all analyzed time periods of IVC (24, 48, 72, 96, 120, 144 and 168 h; P<0.001). On the other hand, the expression level of Cx40 transcripts was higher after 24 h of IVC compared to 0 h and the other times of IVC (P<0.001). Similarly to mRNAs, the expression levels of Cx31, Cx37 and Cx45 proteins were higher before (0 h) compared to after 168 h of IVC. The expression of Cx30 and Cx43, however, did not vary between the groups. In all, the proteins were distributed throughout the cell membrane rather than in the cytoplasm both before and after IVC. After 24 h of IVC, we observed a significant increase in the proliferation of GCs (log phase). We found differences in the proliferation index between 72-96 and 96-140 h within the same population of GCs. In conclusion, the decrease in the expression of Cx mRNAs and proteins following IVC could be associated with a breakdown in gap-junction connections (GJCs), and leads to the decreased of their activity, which may be a reason of non-functional existence of connexon in follicular granulosa cells. These data indicated that the differentiation and proliferation of GCs and lutein cells are regulated by distinct mechanisms in pigs.

Key words: pig, granulosa cells, connexins, real-time proliferation

Mailing address: Bartosz Kempisty PhD,
Department of Histology and Embryology,
Department of Anatomy,
Poznań University of Medical Sciences,
6 Święcickiego St., 60-781 Poznań, Poland
Tel./Fax: +48 61 8546419 / +48 61 8546440,
e-mail: etok@op.pl

0393-974X (2014)

During folliculogenesis, the follicular cells surrounding the mammalian oocyte form a single flattened layer which proliferates and differentiates into cells called granulosa cells (GCs). In the mature follicle, GCs form the corona radiata, a region of cumulus cell layers around the oocyte. It is well recognized that the maturation and proliferation of GCs are complex processes of biochemical and morphological changes (1-3). This process is also dependent on secreted gonadotropins and steroids that modulate the differentiation of GCs (4-6). Testosterone, progesterone and estradiol are responsible for GC proliferation and the suppression of LH receptor (LHR) synthesis (7-11). Although the influence of steroids and other hormones or growth factors on the differentiation and proliferation of GCs has been documented in humans and rodents (12, 13), the maturation process of GCs is still not entirely understood. The final maturation of cumulus-oocyte complexes (COCs) goes along with multipart biochemical and morphological changes, including changes in gene expression profile and cumulus cell expansion, to reach the MII stage. The maturation of COCs is also associated with the activity of gap junction connections (GJCs) that are primarily formed by proteins called connexins (Cxs). It has been shown that the expression of Cxs is related to proper oocyte maturation (14, 15).

Cxs form the protein structure responsible for bi-directional communication between the oocyte and the surrounding somatic cumulus cells. Therefore, the relationship between full COC maturation and GJC activity lead to assume that Cxs can be regarded as markers of oocyte maturation. Moreover, Melton et al. (16) and Itahana et al. (17) investigated the expression of several connexins, including Cx26, Cx30.3, Cx32 and Cx43 in developing follicles of prepubertal porcine ovaries. They showed that substantial amounts of Cx43 are expressed in GCs following activation of follicle development as well as GJC being associated with follicular growth and development. It was assumed that not only Cx43 is a key GJC protein but several others, such as Cx32, CX30.3 and Cx26 are expressed in the follicle and their expression is regulated differentially. The role of Cx43, the most important connexin during the maturation of COCs, has been recognized in several mammalian species, including bovine, pigs and rodents (18-21). However, the expression and cellular distribution of other connexin proteins has not been studied in porcine GCs. In a recent experiment using cultivation of separated porcine cumulus or granulosa cells we observed that several proteins changed their cellular localization between the nucleus and the cytoplasm. The differential distribution of cyclin-dependent kinase (Cdk4) and Cx43 was dependent on the time of cultivation. It is not yet known whether the real-time proliferation of GCs is associated with the expression and cellular distribution of Cxs, which may affect the GJC activity during GC maturation.

Therefore, in this study we used a model where the expression and cellular localization of connexins, in relation to the real-time proliferative potential of porcine GCs was measured. It is one of the new aspects of the experiment, where the porcine GCs proliferation was evaluated in real-time with measured of each 15 min of electrical impedance during 168 h of cultivation, which demonstrated the cell division cycle activity. The expression of Cxs in cumulus cells (CCs) is well recognized, however expression of these genes and proteins in GCs still needs further investigation. Since Melton et al. (16) demonstrated for the first time expression of Cx43 mRNA in porcine GCs, it was suggested that Cxs may play the crucial role not only in CCs-oocyte cross-talk but also in follicle growth and development.

MATERIALS AND METHODS

Animals

A total of 24 crossbred Landrace gilts with a median age of 135 days and weight of 98 kg were used in this study. All of the animals were kept under identical conditions.

Collection of porcine ovaries and in vitro culture of granulosa cells

The ovaries (n=48) and reproductive tracts were recovered at slaughter and transported to the laboratory at 38ºC in 0.9% NaCl within 30 min. To provide optimum conditions for subsequent oocyte maturation *in vitro*, the ovaries of each animal were placed in PBS plus or supplemented with fetal bovine serum (FBS; Sigma-Aldrich Co., St. Louis, MO, USA) (22, 23). Thereafter, single preovulatory large follicles with diameter estimated

more than 5 mm (n=130) were opened into a sterile Petri dish by puncturing using a 5 ml syringe and 20-G needle, and the COCs and follicular fluid (FF) were recovered. Then, the follicular fluid was used to isolate GCs, whereas the COCs were discarded.

Medium consisted of Dulbecco's Modified Eagle's Medium (DMEM/F12, Sigma-Aldrich, USA), 2% fetal calf serum (FCS) *(*PAA, Linz, Austria), 10 mg/ml ascorbic acid (Sigma-Aldrich, USA), 0.05 µM dexamethasone (Sigma-Aldrich, USA), 200 mM L-glutamine (Invitrogen, USA), 10 mg/ml gentamycine (Invitrogen, USA), 10,000 units/ml penicillin and 10,000 µg/ml streptomycin (Invitrogen, USA). Cells were cultivated at 38.5°C under aerobic conditions (5% CO_2). Once the adherent cells were more than 80% confluent, they were detached with 0.05% trypsin-EDTA (Invitrogen, USA) for 10 min and counted using a Z2 counter or cell viability analyzer (Vi-Cell XR 2.03; both Beckman Coulter, USA). We used $3x10^6$ cells per dish for culture and $5x10^3$ cells per one E-Plate in RTCA system.

In vitro GC culture using a real-time cellular analyzer (RTCA)

The recovered GCs from follicular fluid (after puncturing of single follicles) were transferred into an E-Plate 48 of a real-time cell analyzer (RTCA, Roche-Applied Science, GmbH, Penzberg, Germany), which consisted of an RTCA Analyzer, an RTCA SP Station and RTCA Software. The GCs were then cultured in 200 µl of standard culture medium that consisted of DMEM/F12 (Sigma-Aldrich, USA) as mentioned above. The GCs were cultured for 0-168 h at 38.5°C under 5% CO_2 in air. The cultivation medium was replaced every 44 h. The pool of GCs before IVC and after 168 h of IVC was treated with trypsin (0.25% trypsin in a balanced salt solution, Sigma-Aldrich, St. Louis, MO, USA) and used for further confocal microscopy analysis. Additionally, after each step of cell culture, the cell index (CI) and the normalized cell index were used to evaluate the relative and quantitative changes in electrical cell impedance. The cell status was determined using RTCA software. Once the cells were attached (lag phase, first 24 h of culture) the electrical impedance was measured. Since the cells start with log phase (logarithmic increase of proliferation, next 24-48 h of culture), after several cell divisions the electrical impedance was increased. The cell index or cell normalized index was measured from electrical impedance of proliferative cells.

Confocal microscopic observations of protein distribution

At recovery and during 168 h of *in vitro* culture, GCs were collected and fixed using an acetone-methanol (1:1, v/v) solution for 10 min at -20ºC and washed three times in PBS/PVP (0.2%). To block non-specific binding, the samples were incubated in 3% BSA in PBS with 0.1% Tween-20 for 30 min at room temperature (RT). GCs were incubated for 1 h at RT with a rabbit polyclonal anti-Cx30 antibody (Ab) (C-20), rabbit polyclonal anti-Cx31 Ab (H-43), goat polyclonal anti-Cx37 Ab (N-14), mouse monoclonal anti-Cx43 Ab (F-7) and goat polyclonal anti-Cx45 Ab (N-19) from Santa Cruz Biotechnology (Santa Cruz, CA, USA). The antibodies were diluted 1:500 in PBS with 1.5% BSA and 0.1% Tween-20. After several washes with PBS containing 0.1% Tween-20, the samples incubated with anti-Cx30, anti-Cx31, anti-Cx37, anti-Cx43 and anti-Cx45 primary antibodies were treated with a fluorescein isothiocyanate (FITC)-conjugated goat anti-rabbit IgG Ab diluted 1:500 in PBS with 0.1% Tween-20 for 1 h at RT. After washing in PBS with 0.1% Tween-20, the GCs were stained with 0.1 µg/ml 4,6-diamino-2-phenylindole (DAPI, UltraCruz Mounting Medium, sc-24941; Santa Cruz Biotechnology, Santa Cruz, CA, USA) in 10 ml of mineral oil containing 1.5µg/ml of DAPI, mounted in an anti-fade medium on glass slides and examined by an LSN 510 confocal system with an Olympus Fluoview 10i microscope. Additionally, the GCs were stained with goat polyclonal anti-vimentin antibody (C-20). FITC was excited at 488 nm using an argon laser, and the emission was imaged through a 505-530 nm filter. All confocal microscopic images were analyzed using Imaris 7.2 (BitPlane, Zurich, Switzerland) software. The protein expression pattern was estimated as the fluorescence intensity measured by Imaris 7.2 program.

Real-time quantitative polymerase chain reaction (RQ-PCR) analysis

Total RNA was isolated from GCs before and after IVC using an RNeasy mini column from Qiagen GmbH (Hilden, Germany). The RNA samples were re-suspended in 20 µl of RNase-free water and stored in liquid nitrogen. RNA samples were treated with DNase I and reverse-transcribed (RT) into cDNA. RQ-PCR was conducted in a LightCycler real-time PCR detection system (Roche Diagnostics GmbH, Mannheim, Germany) using SYBR® Green I as a detection dye, and target cDNA was quantified using the relative quantification method. The relative abundance of Cx36, Cx37, Cx40 and Cx43 transcripts in each sample was standardized to the internal standard glyceraldehyde-3-phosphate dehydrogenase (GAPDH). For amplification, 2 µl of cDNA solution was added to 18 µl of QuantiTect® SYBR® Green PCR (Master Mix Qiagen GmbH, Hilden, Germany) and primers (Table I). One RNA sample of each preparation was processed without the RT-reaction to provide a negative control for subsequent PCR.

To quantify the specific genes expressed in the GCs,

the expression levels of specific oocyte mRNAs in each sample were calculated relative to PBGD and ACTB. To ensure the integrity of these results, the additional housekeeping gene 18S rRNA was used as an internal standard to demonstrate that PBGD and ACTB mRNAs were not differentially regulated in the groups of GCs. The gene for 18S rRNA expression has been identified as an appropriate housekeeping gene for use in quantitative PCR studies. Expression of PBGD, ACTB and 18S rRNA mRNA was measured in cDNA samples from isolated GCs.

Statistical analysis

A one-way ANOVA followed by Tukey's post-hoc test was used to compare the results of the real-time quantification of the proliferation index. The experiments were carried out in at least two replicates. The results quantifying the cell proliferation index were obtained using an RTCA system. The differences were considered to be significant at $*P<0.05$, $**P<0.01$ and $***P<0.001$ for the RQ-PCR and RTCA analyses. The RTCA results were evaluated by comparing the results obtained in six replicates of the same recovered granulosa cell population. Statistical calculations were applied to the highest normalized proliferation index at each time point for each investigated group to compare the results. The software program GraphPad Prism version 4.0 (GraphPad Software, San Diego, CA, USA) was used for the statistical calculations.

All of the experiments were approved by the local Ethics Committee of the Poznan University of Life Sciences, Poland (permission no. 32/2012).

RESULTS

Spindle-shaped porcine granulosa cell morphology was observed during the *in vitro* cultivation period. To analyze the expression and subcellular protein distribution of Cx30, Cx31, Cx37, Cx43 and Cx45, four images were obtained using confocal microscopy: phase contrast, DAPI stained cell nucleus, fluorescence observation of antibody staining, and both DAPI and antibody stained granulosa cells. The granulosa cells analyzed prior to IVC were centrifuged and resuspended immediately after collagenase treatment; however, after IVC, the cells were studied during the cultivation phase, where a spindle-shaped porcine granulosa cell morphology was observed. The expression of Cx30 in porcine granulosa cells (Fig.1 A, B) did not differ significantly before and after IVC and was detectable at low levels. The highest level of Cx31 expression in porcine granulosa cells was observed prior to IVC ($P<0.001$) (Fig. 2 A, B). The expression of Cx37 (Fig. 3 A, B) and Cx45 (Fig. 4 A, B) was increased in cells before compared to after IVC ($P<0.001$). A high expression level of Cx43 was found both before and after IVC (Fig. 5 A, B). Overall, Cx proteins were distributed in the cytoplasm and membranes of porcine granulosa cells. An antibody against vimentin was used as the positive control (Fig. 6). Semi-quantitative analysis of protein expression showed no differences in Cx30 and Cx43 protein levels before and after IVC (Fig. 7A, D). However, the expression levels of Cx31, Cx37 and Cx45 were higher ($P<0.001$) before IVC compared to thereafter (Fig. 7 B, C, E).

The proliferative ability of GCs was analyzed in real-time by using an RTCA system over an *in vitro* cultivation period of 168 h. Over the entire interval (0-140 h), we found a difference between the proliferation indices of cells in one of six analyzed pools of cells ($P<0.05$), (Fig. 8A). An increased proliferation index in one of six analyzed pools of cell cultures ($P<0.05$) was also observed during the first 24 h (Fig. 8B) (lag phase), the next 24 h-48 h (Fig. 8C) (log phase) and the subsequent 48 h-72 h (Fig. 8D). When we analyzed the next periods of cultivation, i.e., 72 h-96 h and 96 h-140 h, we observed greater differences in the proliferation index within three of six analyzed cell cultures (Fig. 8 E, F) ($P<0.01$, $P<0.001$, respectively).

The expression levels of Cx43, Cx40, Cx37 and Cx36 mRNA were analyzed by using RQ-PCR (Fig. 9 A, B, C, D). We observed an increased expression of Cx43, Cx37 and Cx36 in porcine GCs before IVC (0 h) compared to all later time points (24 h to 168 h; $P<0.001$), (Fig. 9 A, C, D). Regarding Cx40, a higher expression level was observed after 24 h of IVC compared to 0 h and other time periods ($P<0.001$; Fig. 9B).

DISCUSSION

Connexins (Cxs) are well known as the proteins that permit bi-directional communication between the oocyte and the surrounding somatic granulosa-cumulus cells. This "cross-talk" has been suggested

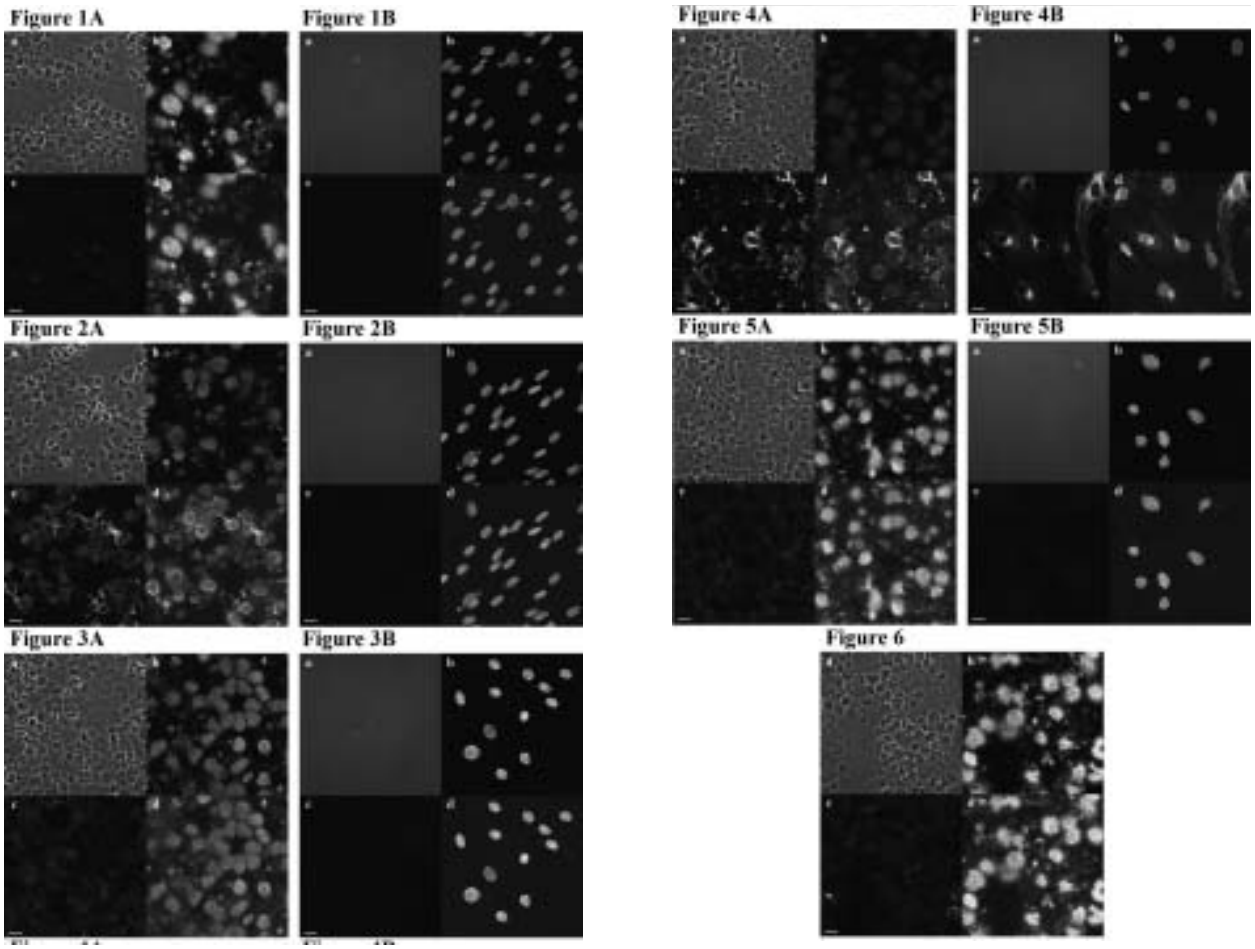

Figs. 1-6. *Confocal microscopic observation of Cx30, Cx31, Cx37, Cx43, Cx45 and vimentin protein levels and cellular distribution in porcine GCs before (at 0 h) and after (at 168 h) IVC. The GCs that were collected before (Fig. 1A, 2A, 3A, 4A, 5A) and after 168 h (Fig. 1B, 2B, 3B, 4B, 5B) of IVC were stained with 0.1 µg/ml 4,6-diamino-2-phenylindole (DAPI; Santa Cruz Biotechnology, Santa Cruz, CA, USA) in mineral oil following staining for porcine Cx30 (rabbit polyclonal anti-Cx30 Ab) (Fig. 1A, 1B), Cx31 (rabbit polyclonal anti-Cx31 Ab) (Fig. 2A, 2B), Cx37 (goat polyclonal anti-Cx37 Ab) (Fig. 3A, 3B), Cx43 (mouse monoclonal anti-Cx43 Ab) (Fig. 4A, 4B), and Cx45 (goat polyclonal anti-Cx45 Ab) (Fig. 5A, 5B). Secondary antibodies were labeled with FITC (fluorescence isothiocyanate), which emits a green fluorescent signal after excitation at 488 nm. The arrows indicate the cytoplasmic localization of investigated proteins in GCs in both before and after IVC. The scale bars represent 20 µm. Arrows shows membrane distribution of investigated proteins. The GCs were stained with 0.1 µg/ml 4,6-diamino-2-phenylindole (DAPI; Santa Cruz Biotechnology, Santa Cruz, CA, USA) in mineral oil following staining for porcine vimentin (goat polyclonal anti-vimentin Ab) (Fig. 6). a-Nomarski, b-DAPI stained nucleus, c-antibody stained cells, d-merge.*

to be the main mechanism that enables the proper maturation of oocytes, and furthers embryonic growth and development. Although Cx genes and encoded protein expression has been recognized in both oocytes and granulosa cells (15, 24, 25), there is still a lack of data indicating the possible association between the real-time proliferation of granulosa cells *in vitro* and the expression/cellular distribution of Cxs in porcine GCs. Therefore, this study was aimed to investigate the expression and localization of Cxs in porcine granulosa cells before and after IVC in relation to proliferation *in vitro*.

We showed that the expression levels of Cx transcripts were significantly higher before

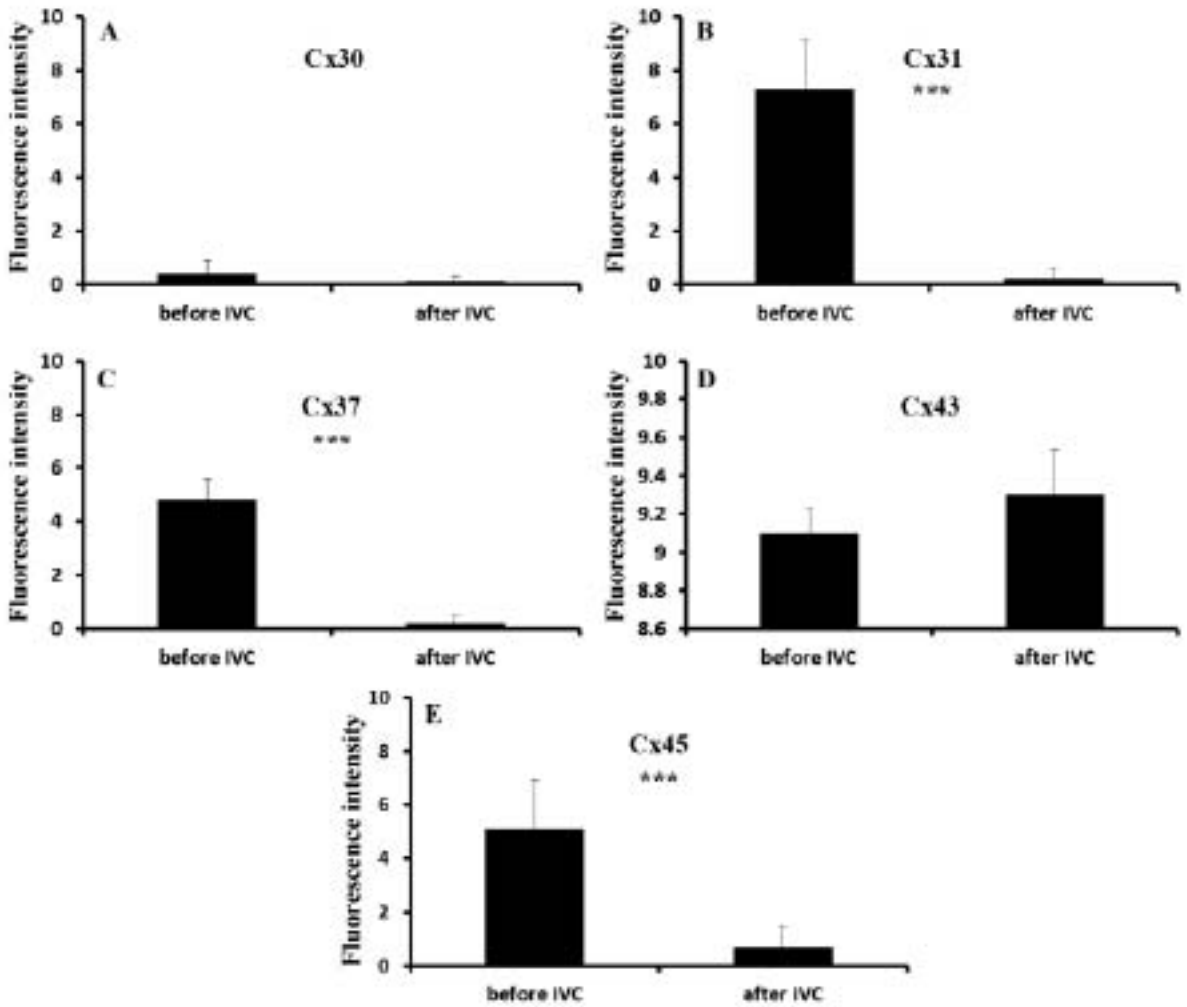

Fig. 7. *Fluorescence intensity of porcine GCs stained with anti-Cx30, anti-Cx31, anti-Cx37, anti-Cx43 and anti-45 antibodies. The quantitative expression of Cx30, Cx31, Cx37, Cx43, and Cx45 proteins in porcine GCs were analyzed before or after IVC (**A, B, C, D, E**), respectively. The fluorescence intensity was measured using Imaris software. The differences were considered to be significant at P<0.05, P<0.01 and P<0.001. GraphPad Prism version 4.0 (GraphPad Software, San Diego, CA) was used for statistical calculations. All confocal microscopic images were analyzed using Imaris 7.2 (BitPlane, Zurich, Switzerland) software.*

cultivation compared to thereafter. It is suggested that during the IVC period, these cells lose the ability to form gap junction connections. Moreover, it may be suggested that a change in GCs phenotype during culture as well as differentiation of these cells into lutein cells may also be the main reason of changes in Cxs gene and protein profile. However, regarding our RTCA assay results, we observed an increase in the proliferation of GCs during the log phase, which started from 24 h of IVC. Since the proliferation of porcine GCs is not associated with the activity of GJCs, the existence of separate mechanisms regulating the proliferation of GCs can be assumed, which are apart from the main function of GJCs to provide the transfer of small molecules between oocytes and GCs (24, 26). Moreover, we did not observe association between genes and/or protein expression pattern and proliferative activity of GCs measured by electrical impedance and Cell Index. It was previously described that formation of GJCs are highly correlated with expression pattern of Cxs. However, since in our study it was found that the

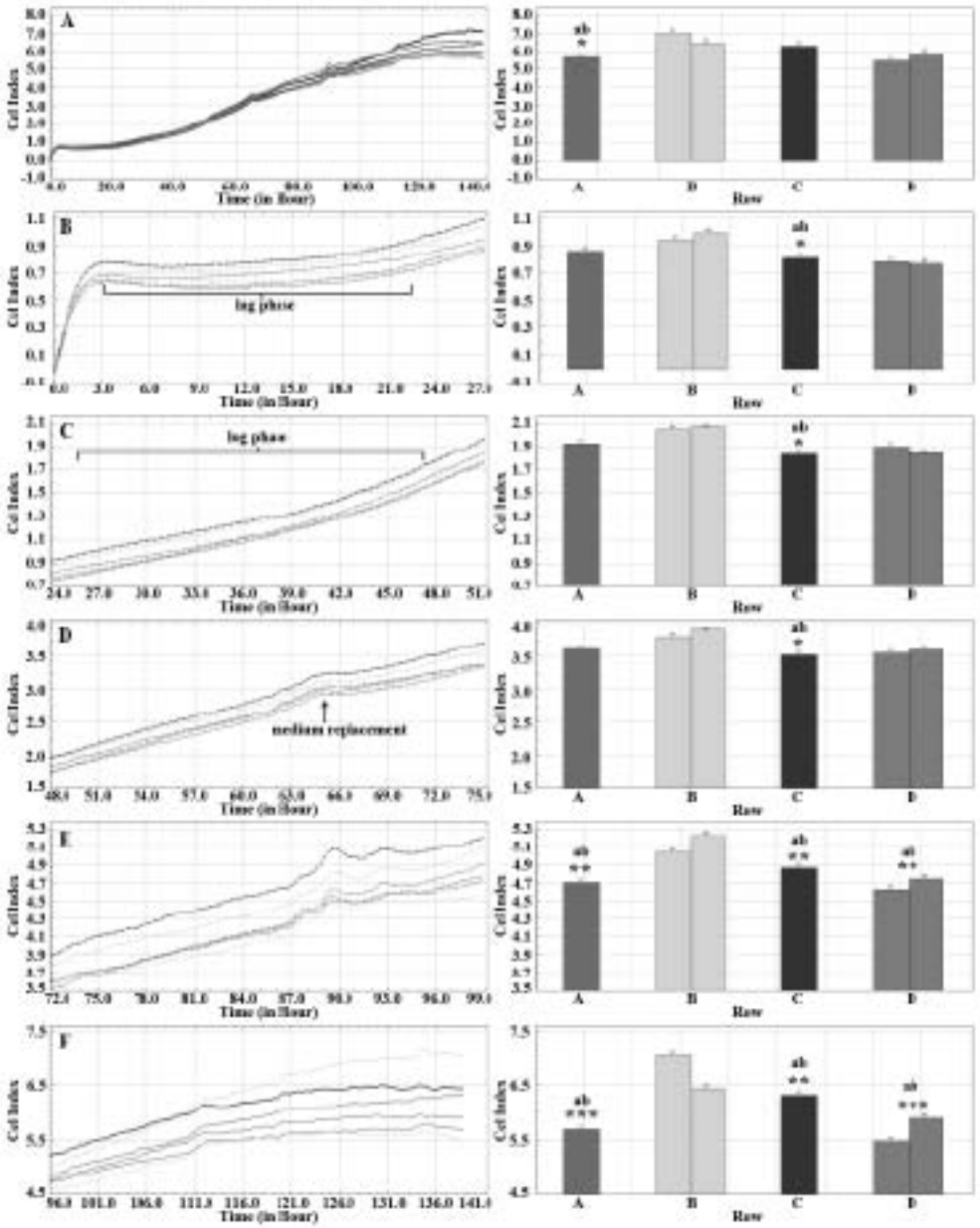

Fig. 8. *Cell proliferation index of porcine GCs cultivated for 140 hours. Porcine granulosa cells were recovered from follicles of puberal gilts and treated with collagenase for 10 min at 38.5ºC. The cells were immediately transferred into an E-Plate 48 of a real-time cell analyzer (RTCA, Roche-Applied Science, GmbH, Penzberg, Germany). The experiment consisted of six replicates involving the cultivation of the same population of collected cells. At each step of the experiment, the cell proliferation index was assessed for real-time in vitro cultivation for the time periods of 0-140 h (**A, B, C, D, E, F**), (for 0-24 h, 24-48 h, 72-96 h, and 96-140 h, respectively). The differences were considered to be significant at the level of $^{*}P<0.05$, $^{**}P<0.01$ and $^{***}P<0.001$. The different superscripts described significant differences (ab).*

expression patterns are reversible correlated with growth of Cell Index, we suggest that this is not a good model for connexin formation *in vivo*.

Our observations are partially supported by Santiquet et al. (20), who have shown that the expression, degradation and localization of primary connexins in oocytes are dynamic processes that change during the first hours of IVM. The important

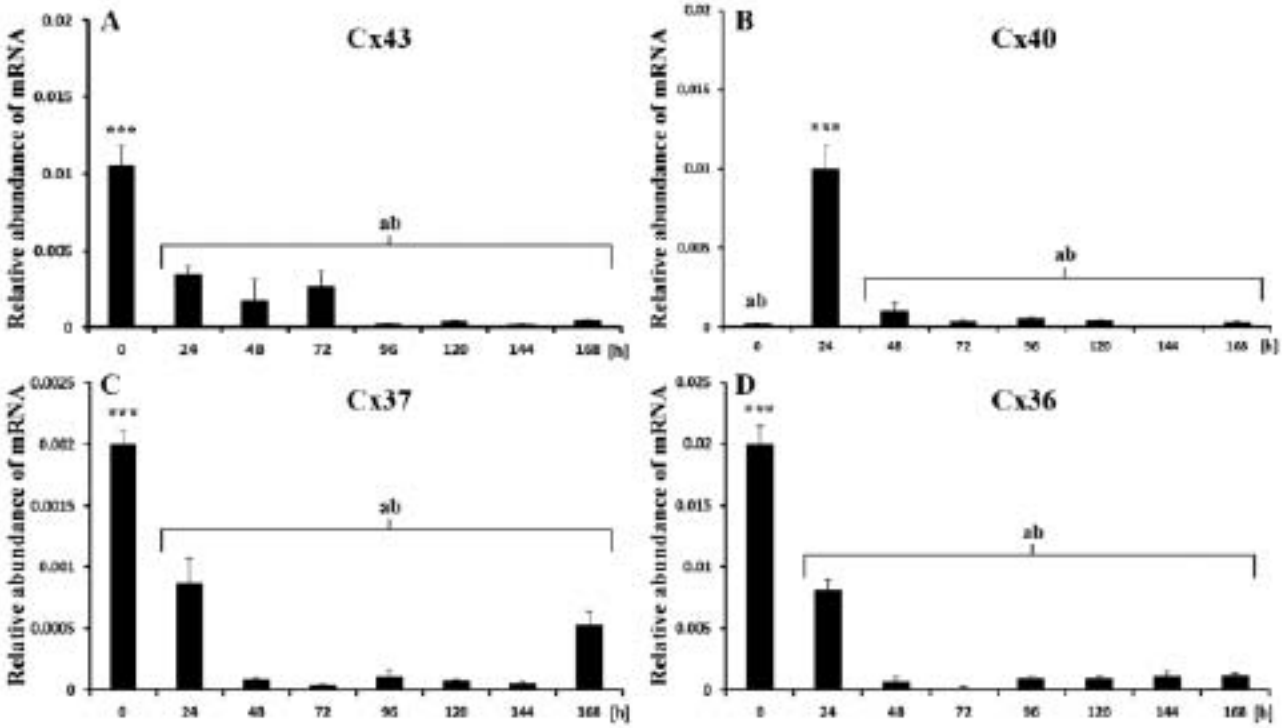

Fig. 9. *Relative abundance of Cx43, Cx40, Cx37 and Cx36 transcripts in porcine GCs analyzed before (at 0 h) and after (at 168 h) IVC. Porcine GCs were isolated from follicles of pubertal gilts and immediately used to isolate RNA, which was reverse-transcribed into cDNA. The relative abundance of Cx43 (**A**), Cx40 (**B**), Cx37 (**C**), and Cx36 (**D**) mRNAs was evaluated by RQ-PCR analysis before and after IVC. The results are presented as the mean ± SEM with the level of significance shown as * P<0.05, ** P<0.01, *** P<0.001. The different superscripts described significant differences (ab).*

role of Cxs in follicle growth and development was recently investigated by Knapczyk-Stwora et al. (27), who used porcine fetal female and male gonads as a model for the observation of Cx43 expression and cellular distribution. Similar to our results, they found Cx43 expression in pre-granulosa and granulosa cells of primordial and primary follicles, and they concluded that Cx43-mediated GJC activity corresponds to fetal gonadal development. However, in opposition to these results, we suggest that Cxs expression and/or GJC activity are reversely correlated with the proliferation of GCs and follicular development during oocyte maturation. Another hypothesis on the breakdown of Cxs was previously suggested by Sasseville et al. (24), who proposed that GJC disruption is achieved by a gonadotropin-dependent mechanism involving the recruitment of Cx43 to clustered lipid rafts. Moreover, they found that GJC breakdown is regulated by the accumulation of connexins in lipid raft microdomains. This hypothesis supports a pivotal role for lipid rafts in the activity of GJCs and the function of connexins. Another hypothesis regarding the function of Cxs and follicular development was based on an observation by Cheng et al. (28). They found a strong increase in the expression of Cx43 in granulosa cells of tertiary follicles and a much lower level of expression of this protein in early and progressed atretic follicles. Together, these findings indicate that the expression of Cx43 is downregulated during follicular atresia. The authors also concluded that the expression of Cx43 is highly involved in the apoptosis observed during atresia of porcine follicles. These observations were supported by experiments of Melton et al. (16). Using *in situ* hybridization and immunohistochemical examination, they observed Cx43 mRNA and protein expression in porcine granulosa cells during different

Table I. *Oligonucleotide sequences used for RQ-PCR analysis.*

Gene	Gene accesion number	Primer sequence (5'-3')	Produkt size (bp)
Cx43	NM_001244212.1	CAGCACTTTTCTTTCATTAGGGGC CTAAGGCACTCCAGTCACC	194
Cx37	NM_001244224.1	GTGTGTCCGCACCGCCACCGATGA ACAGGACCGTCAGCCAGA	155
Cx36	XM_001924757.4	AGCAGCACTCCACTATGATCGG TGTTGCACACAAACATGGTCT	123
Cx40	XM_003130802.2	ATCGCTTTCACCTGCAAGTCCT CGCCATCCTCAGCAGAACCAT	220
ACTB	XM_003124280.3	CCCTTGCCGCTCCGCCTTC GCAGCAATATCGGTCATCCAT	69
PBGD	NM_001097412.1	GAGAGTGCCCCTATGATGCT ATGATGGCACTGAACTCCT	214
18S rRNA	AB117609	GTGAAACTGCGAATGGCTC CCGTCGGCATGTATTAGCT	105

stages of follicular growth. Their findings show that Cx43 mRNA was detectable in the GCs of primary follicles but not in dominant primordial follicles. Furthermore, the expression of Cx43 mRNA was correlated with the progressive stage of follicle growth. Taking into account both of these results, we can conclude that the expression and distribution of connexins are highly associated with porcine follicle development. Although we found that the expression of certain connexins was increased only before IVC, a much higher level of expression of Cx40 at 24 h of IVC was also noted. Our observation supports experimental results obtained by Itahana et al. (17), who analyzed the expression of Cx26, Cx30.0, Cx32 and Cx43 mRNAs in porcine ovarian follicles. They found that Cx43 is not the only GJC protein expressed during ovarian follicle development; other connexins, such as Cx32, 30.3 and 26, are also expressed, and their expression levels are regulated differentially.

It is hypothesized that the breakdown in Cxs during IVC is related to a decreased GJC activity. Moreover, our results demonstrate that the activity of GJCs is not a compulsory factor that determines the proliferation of GCs and activation of oocyte maturation mechanisms in pigs. Moreover, we suggested the existence of different mechanisms of regulation of porcine GCs into lutein cell differentiation.

ACKNOWLEDGEMENTS

This study was made possible by grants number 2011/03/B/NZ4/02411 "OPUS" from the Polish National Centre of Science.

REFERENCES

1. Sessions-Bresnahan DR, Carnevale EM. The effect of equine metabolic syndrome on the ovarian follicular environment. J Anim Sci 2014; 92:1485-94.
2. Gaytán F, Morales C, Manfredi-Lozano M, Tena-Sempere M. Generation of multi-oocyte follicles in

the peripubertal rat ovary: link to the invasive capacity of granulosa cells? Fertil Steril 2014; 101:1467-76.
3. Hatzirodos N, Irving-Rodgers HF, Hummitzsch K, Harland ML, Morris SE, Rodgers RJ. Transcriptome profiling of granulosa cells of bovine ovarian follicles during growth from small to large antral sizes. BMC Genomics 2014; 15:24. doi: 10.1186/1471-2164-15-24.
4. Tetsuka M, Nishimoto H, Miyamoto A, Okuda K, Hamano S. Gene expression of 11β-HSD and glucocorticoid receptor in the bovine (Bos taurus) follicle during follicular maturation and atresia: the role of follicular stimulating hormone. J Reprod Dev 2010; 56:616-22.
5. Olatinwo MO, Bhat GK, Stah CD, Mann DR. Impact of gonadotropin administration on folliculogenesis in prepubertal ob/ob mice. Mol Cell Endocrinol 2005; 245:121-27.
6. Luo CW, Kawamura K, Klein C, Hsueh AJ. Paracrine regulation of ovarian granulosa cell differentiation by stanniocalcin (STC) 1: mediation through specific STC1 receptors. Mol Endocrinol 2004; 18:2085-96.
7. Evans JR, Schreiber NB, Williams JA, Spicer LJ. Effects of fibroblast growth factor 9 on steroidogenesis and control of FGFR2IIIc mRNA in porcine granulosa cells. J Anim Sci 2014; 92:511-19.
8. Riaz H, Dong P, Shahzad M, Yang L. Constitutive and follicle-stimulating hormone-induced action of somatostatin receptor-2 on regulation of apoptosis and steroidogenesis in bovine granulosa cells. J Steroid Biochem Mol Biol 2014; 141:150-59.
9. Aardema H, Roelen BA, van Tol HT, Oei CH, Gadella BM, Vos PL. Follicular 17β-estradiol and progesterone concentrations and degree of cumulus cell expansion as predictors of in vivo-matured oocyte developmental competence in superstimulated heifers. Theriogenology 2013; 80:576-83.
10. Baufeld A, Vanselow J. Increasing cell plating density mimics an early post-LH stage in cultured bovine granulosa cells. Cell Tissue Research 2013; 354:869-80.
11. Monga R, Sharma I, Datta TK, Singh D. Characterization of serum-free buffalo granulosa cell culture and analysis of genes involved in terminal differentiation from FSH- to LH-responsive phenotype. Domest Anim Endocrinol 2011; 41:195-206.
12. Ding T, Luo A, Yang S, et al. Effects of basal media and supplements on diethylstilbestrol-treated immature mouse primary granulosa cell growth and regulation of steroidogenesis *in vitro*. Reprod Domest Anim 2012; 47:355-64.
13. Maillard V, Froment P, Ramé C, Uzbekova S, Elis S, Dupont J. Expression and effect of resistin on bovine and rat granulosa cell steroidogenesis and proliferation. Reproduction 2011; 141:467-79.
14. Kempisty B, Ziółkowska A, Piotrowska H, et al. Short-term cultivation of porcine cumulus cells influences the cyclin-dependent kinase 4 (Cdk4) and connexin 43 (Cx43) protein expression--a real-time cell proliferation approach. J Reprod Dev 2013; 59:339-45.
15. Kempisty B, Ziółkowska A, Piotrowska H, et al. Real-time proliferation of porcine cumulus cells is related to the protein levels and cellular distribution of Cdk4 and Cx43. Theriogenology 2013; 80:411-20.
16. Melton CM, Zaunbrecher GM, Yoshizaki G, Patiño R, Whisnant S, Rendon A, Lee VH. Expression of connexin 43 mRNA and protein in developing follicles of prepubertal porcine ovaries. Comp Biochem Physiol B Biochem Mol Biol 2001; 130:43-55.
17. Itahana K, Morikazu Y, Takeya T. Differential expression of four connexin genes, Cx-26, Cx-30.3, Cx-32, and Cx-43, in the porcine ovarian follicle. Endocrinology 1996; 137:5036-44.
18. Racedo SE, Wrenzycki C, Herrmann D, Salamone D, Niemann H. Effects of follicle size and stages of maturation on mRNA expression in bovine *in vitro* matured oocytes. Mol Reprod Dev 2008; 75:17-25.
19. Calder MD, Caveney AN, Sirard MA, Watson AJ. Effect of serum and cumulus cell expansion on marker gene transcripts in bovine cumulus-oocyte complexes during maturation *in vitro*. Fertil Steril 2005; 83:1077-85.
20. Santiquet N, Robert C, Richard FJ. The dynamics of connexin expression, degradation and localisation are regulated by gonadotropins during the early stages of *in vitro* maturation of swine oocytes. PLoS One 2013; 8:e68456.
21. Teilmann SC. Differential expression and localisation of connexin-37 and connexin-43 in follicles of

different stages in the 4-week-old mouse ovary. Mol Cell Endocrinol 2005; 234:27-35.
22. Al-aghbari AM, Menino AR. Survival of oocytes recovered from vitrified sheep ovarian tissues. Anim Reprod Sci 200 ; 71:101-10.
23. Nascimento AB, Albornoz MS, Che L, Visintin JA, Bordignon V. Synergistic effect of porcine follicular fluid and dibutyryl cyclic adenosine monophosphate on development of parthenogenetically activated oocytes from pre-pubertal gilts. Reprod Domest Anim 2010; 45:851-9.
24. Sasseville M, Gagnon MC, Guillemette C, Sullivan R, Gilchrist RB, Richard FJ. Regulation of gap junctions in porcine cumulus-oocyte complexes: contributions of granulosa cell contact, gonadotropins, and lipid rafts. Mol Endocrinol 2009; 23:700-10.
25. Sato E, Yokoo M. Morphological and biochemical dynamics of porcine cumulus-oocyte complexes: role of cumulus expansion in oocyte maturation. Ital J Anat Embryol 2005; 110:205-17.
26. Chang HM, Cheng JC, Leung PC. Theca-derived BMP4 and BMP7 down-regulate connexin43 expression and decrease gap junction intercellular communication activity in immortalized human granulosa cells. J Clin Endocrinol Metab 2013; 98:E437-45.
27. Knapczyk-Stwora K, Durlej-Grzesiak M, Duda M, Slomczynska M. Expression of connexin 43 in the porcine foetal gonads during development. Reprod Domest Anim 2013; 48:272-77.
28. Cheng Y, Inoue N, Matsuda-Minehata F, Goto Y, Maeda A, Manabe N. Changes in expression and localization of connexin 43 mRNA and protein in porcine ovary granulosa cells during follicular atresia. J Reprod Dev 2005; 5:627-37.

MICROARRAY ANALYSIS OF INFLAMMATORY RESPONSE-RELATED GENE EXPRESSION IN THE UTERI OF DOGS WITH PYOMETRA

D. BUKOWSKA[1], B. KEMPISTY[2,3], P. ZAWIERUCHA[2,3], K. JOPEK[2], H. PIOTROWSKA[4], P. ANTOSIK[1], S. CIESIÓŁKA[2], M. WOŹNA[1], K.P. BRÜSSOW[5] and J.M. JAŚKOWSKI[1]

[1]Institute of Veterinary Sciences, Poznan University of Life Sciences, Poznan, Poland; [2]Department of Histology and Embryology, Poznan University of Medical Sciences, Poznan, Poland; [3]Department of Anatomy, Poznan University of Medical Sciences, Poznan, Poland; [4]Department of Toxicology, Poznan University of Medical Sciences, Poznan, Poland; [5]Institute of Reproductive Biology, Leibniz Institute for Farm Animal Biology, Dummerstorf, Germany

Received August 13, 2014 – Accepted October 31, 2014

Pyometra, which is accompanied by bacterial contamination of the uterus, is defined as a complex disease associated with the activation of several systems, including the immune system. The objective of the study was to evaluate the gene expression profile in dogs with pyometra compared with those that were clinically normal. The study included uteri from 43 mongrel bitches (23 with pyometra, 20 clinically healthy). RNA used for the microarray study was pooled to four separated vials for control and pyometra. A total of 17,138 different transcripts were analyzed on the uteri of female dogs with pyometra and of healthy controls. From 264 inflammatory response-related transcripts, we found 23 transcripts that revealed a 10- to 77-fold increased expression. Thereby, the expression of interleukin 8 (IL8), interleukin-1-beta (IL1B), interleukin 18 receptor (IL18RAP), interleukin 1-alpha (IL1A), interleukin receptor antagonist (IL1RN) and interleukin 6 (IL6) increased 77-, 20-, 17-, 13-, 13- and 11-fold, respectively. Furthermore, the expression of the calcium binding proteins S100A8 was 44-fold higher, and that of S100A12 and S100A9 37-fold, respectively, in the uteri of canines with pyometra compared with that of the controls. Moreover, the expression of the transcripts of toll-like receptors (TLR8 and TLR2), integrin beta 2 (ITGB2), chemokine ligand 3 (CCL3), semaphorin 7A (SEMA7A), CD14 and prostaglandin-endoperoxide synthase 2 (PTGS2) was increased between 10- and 18-fold. Furthermore, after using RT-qPCR we found an increased expression of AOAH, IL1A, IL8, CCL3, IL1RN and SERPINE 1 mRNAs which can be served also as markers of the occurrence of pyometra in domestic bitches. In summary, it is concluded that up-regulation of interleukins may be used as a marker of the inflammatory response in dogs with pyometra. Moreover, all of the 23 up-regulated transcripts may be novel molecular markers of the pathogenesis of canine pyometra. Several proteins – products of these genes - may be recognized as potential biomarkers of this disease or as therapeutic targets in other mammalian species, including humans.

Key words: canine pyometra, microarray, inflammation

Mailing address: Bartosz Kempisty PhD, Department of Histology and Embryology, Department of Anatomy, Poznan University of Medical Sciences, 6 Święcickiego St., 60-781 Poznań, Poland Tel./Fax: +48 61 8546419/+48 61 8546440, e-mail: etok@op.pl

0393-974X (2014)

Canine pyometra is the accumulation of pus within the uterine lumen. It mostly occurs in the progesterone dominant phase metestrus (diestrus). It begins with endometritis and/or cystic endometrial hyperplasia (CEH) (1-4). It was called the endometritis/cystic endometrial hyperplasia/pyometra complex (CEH/P) (5) but some authors consider cystic endometrial hyperplasia a secondary phenomenon that occurs following endometritis (6, 7).

The spontaneous appearance of pyometra in bitches involves estrogen stimulation of the uterus, followed by prolonged intervals of progesterone dominance (1, 2, 10). In many cases, the clinical cause of pyometra in bitches appears also as a result of a previous treatment with estrogens or progestins. These hormonal therapies, including the use of either progestins for estrus suppression or estrogens for either estrus induction or pregnancy termination, are factors that strongly favor pyometra induction (11-13). There are two theories regarding possible pathomechanism of canine pyometra, (1) triggering of the response by *E. coli* and the influence of other microorganism infections and (2) an old hypothesis of the basic role of hormonal influence and exacerbation of the condition through the infection.

Sugiura et al. (14) showed that suppression of cellular immunity is associated with higher progesterone concentrations, and these levels are accompanied by increased glandular secretion and decreased myometrial activity. The authors suggested that a combination of these events favors bacterial colonization. Since the clinical diagnostic criteria for pyometra are not always clear, it would be helpful to find new specific molecular markers of these diseases.

Several studies found that inflammatory response factors, such as cytokines, chemokines, CD molecules, integrins (ITG), tumor necrosis factor (TNF) and toll-like proteins, are proteins that regulate several immune-related processes as well as the inflammatory response (15-17). Hagman et al. (18) identified in their study an up-regulation of expression of almost 800 genes in canine uterus with bacterial infection. These genes included chemokine and cytokine, as well as genes associated with inflammatory cell extravasation, anti-bacterial action, the complement system and innate immune responses, as well as proteoglycan-associated genes.

This study aims to identify potential molecular biomarkers by identifying those genes that are up regulated to the greatest degree in the endometrium. Moreover, we indicated genetic predisposition and potential role of biomarkers in early recognition at preclinical state of endometritis, in prognosis and establishment of the probability of occurrence of pyometra in the future life of the animal. This may also provide insights into the pathogenesis of pyometra.

MATERIALS AND METHODS

Animals

A total of 23 mongrel bitches with pyometra (median age of 4.5 years, range 2.5-6) and 20 mongrel healthy controls (median age of 4 years, range 2-7) were used in this study after having undergone a routine ovariohysterectomy in diestrus. Pyometra was identified by a fluid-filled uterus and positive bacterial cultures from the uterine content. All animals included in the research were in diestrus, defined using morphological criteria as the examination of vaginal smear and serum progesterone level. The clinical history and symptoms indicated that most patients suffered from genital or systemic disease. Several bitches displayed purulent or purulent–hemorrhagic discharge, lethargy, polyuria, polydipsia, anorexia, vomiting, dehydration, abdominal pain, temperature disturbances, changes in the mucous membrane colors, and increased heart and respiratory rates. In the group of bitches with pyometra, hematological and blood biochemistry changes were observed, including leukocytosis with neutrophilia, a left shift in the differential white blood cell count, normocytic or normochromic anemia and thrombocytopenia. Increased concentrations of C–reactive protein, alkaline phosphatase, bilirubin, cholesterol, markers of renal profile and electrolytes were found. The history was evaluated, clinical signs and uterine pus were measured, and diagnostic symptoms were identified. The experiments were approved by the Local Ethics Committee.

The uterus and reproductive organs were removed by an ovariohysterectomy while the animals were under general anesthesia using 3 mg/kg ketamine hydrochloride (Bioketan Vetoquinol, Biowet, Poland), which was given iv after pre-anesthetic treatment with 0.05 mg/kg atropine sulfate given sc (Polfa S.A., Poland) and 1-3 mg/kg xylazine hydrochloride given im (Xylavet 2%, Scanvet, Poland). General anesthesia was maintained using an inhaled mixture of halothane, nitrous oxide and oxygen.

Bacteriological culture was carried out and in 78%

it was *Escherichia coli*, in 13% *Staphyllococcus* spp., 4.5 % *Streptococcus* spp. in 4.5 % it *was Pseudomonas aeruginosa* (8, 9).

Sample collection

The samples were isolated from the middle of the left horn of each animal, and the horns were cut longitudinally. The dissection was performed with microsurgical (ophtalmological) instruments as scissors using stereomicroscope Discovery V-20 (Zeiss). The endometrium was washed with PBS (Sigma-Aldrich, St. Louis, MO, USA) and separated from the myometrium under a microscope (Olympus). Immediately after collection, endometrial slides were stored in RNAlater (Qiagen, Hilden, Germany) at -80°C. Then the set of collected endometrium samples were immediately defrosted and used for extraction of the total RNA.

RNA extraction from tissues

Total RNA was extracted from samples using TRI Reagent (Sigma, St Louis, MO, USA), and RNeasy MinElute cleanup Kit (Qiagen, Hilden, Germany). The amount of total mRNA was determined from the optical density at 260 nm, and the RNA purity was estimated using the 260/280 nm absorption ratio (higher than 1.8) (NanoDrop spectrophotometer, Thermo Scientific, ALAB, Poland). The RNA integrity and quality were checked on a Bioanalyzer 2100 (Agilent Technologies, Inc., Santa Clara, CA, USA). The resulting RNA integrity numbers (RINs) were between 8.5 and 10 with an average of 9.2 (Agilent Technologies, Inc., Santa Clara, CA, USA). The RNA in each sample was diluted to a concentration of 100 ng/µl with an OD260/OD280 ratio of 1.8/2.0. RNA used for microarray study was pooled to four separated vials for control and pyometra. The first three pooled pyometra samples were obtained by the sum of subsequent six RNA samples. The fourth sample was obtained by pooling the last five pyometra RNA samples. Due to the fact that the total number of control RNA samples equaled 20, they were pooled by the sum of subsequent five control RNA samples. From each RNA sample, 500 ng of RNA were taken for pooled vials. The remaining amount of isolated RNA was used for RT-qPCR study (23 pyometra and 20 control RNA).

Microarray expression analysis and statistics

The Affimetrix procedure was previously described by Tyczewska et al. (2012). Total RNA (100 ng) from each pooled sample was subjected to two round sense cDNA amplifications (Ambion® WT Expression Kit). The obtained cDNA was used for biotin labeling and fragmentation by Affymetrix GeneChip® WT Terminal Labeling and Hybridization (Affymetrix). Biotin-labeled fragments of cDNA (5.5 µg) were hybridized to Affymetrix® Canine Gene 1.1 ST Array Strip (48°C/20 h). Each array was comprised of 590.097 unique 25-mer oligonucleotide probes, which include 27.681 genes. Twenty-four unique probe sequences were hybridized to single transcript. After hybridization, every array strip was washed and stained by Fluidics Station of GeneAtlas System (Affymetrix). The array strips were scanned by Imaging Station of GeneAtlas System. The preliminary analysis of the scanned chips was performed using Affymetrix GeneAtlasTM Operating Software. The quality of gene expression data was checked according to quality control criteria provided by the software. The obtained CEL files were imported into downstream data analysis software. If not otherwise stated, all the presented analyses and graphs were performed by Bioconductor and R programming language (20). Each CEL file was merged with a description file. For background correction, normalization and summarization of results, we used Robust Multiarray Averaging (RMA) algorithm (21). Statistical significance of analyzed genes was performed by moderated *t*-statistics from empirical Bayes method. Obtained p value was corrected for multiple comparisons using the Benjamini and Hochberg's false discovery rate 22). The selection of significantly changed gene expression was based on p value lower than 0.05 and expression fold higher than +2 or lower than -2 (fold ±2).

Differentially expressed genes were subjected to the election of genes involved in the inflammatory response. The term "inflammatory response" was used as a query for searching in Gene Ontology Biological Process (GO BP) description tag for each analyzed gene. The set of genes involved in the inflammatory response were subsequently subjected to clustering by the hierarchical clustering algorithm. Microarray data were analyzed using the cluster analysis of William Shannon. The obtained data were presented as the heat map graph.

Validation by RT-qPCR

Reverse transcription was performed using AMV reverse transcriptase (Promega) with Oligo dT (PE Biosystems, Warrington, UK) as primers at a temperature of 42°C for 60 min (thermocycler UNO II, Biometra). The primers used were designed by Primer 3 software (Whitehead Institute for Biomedical Research, Cambridge, MA) (Table I). The primers were purchased from the Laboratory of DNA Sequencing and Oligonucleotide Synthesis, Institute of Biochemistry and Biophysics, Polish Academy of Sciences, Warsaw. RT-qPCR was performed by means of the Lightcycler 2.0 instrument (ROCHE) with the 4.05 software version. Using the above-mentioned primers, SYBR green detection system was applied. Each 20 µl reaction mixture contained

Table I. *Gene names and primer sequence used for RT-qPCR assay.*

Gene name	Gene symbol	Gene bank accession number	Orientation (sense, antysense)	Sequence	Position	Product size
interleukin 8	IL8	NM_001003200	S A	AAAATGGGTACAAAAGGTT TTGAAGTCTCATTGGCATC	252-270 358-376	125
interleukin 1 receptor antagonist	IL1RN	NM_001003096.1	S A	CCGTGTTCTTGGGGATCCAT GCAGGCAGCAGACTCAAAGC	284-303 449-468	185
chemokine (C-C motif)	CCL3	NM_001003297.1	S A	TCTGCCTGCTGCTCATAGCC CTTCTTTGGGACACTTGCTG	24-43 169-188	165
serpin peptidase inhibitor,	SERPINE1	NM_001197095	S A	CTTCCACAAATCTGACGGTA CTGCCTGGTCATATTCCCT	633-652 858-876	244
interleukin 1, alpha	IL1A	NM_001003157	S A	TCATGAAGCCCAGATCAGT TTCTGATGTGTAAGCTCCC	399-417 583-601	203
acyloxyacyl hydrolase	AOAH	XM_539519	S A	AGCCAGCAAGAAATTTACGAAC GATTCTCCTTCCCCAGAACCT	1569-1590 1763-1783	215
S100 calcium binding protein A12	S100A12	XM_003434905	S A	TCCCTGCTCAGTAGTCCTC GAAGACATCAACGATCCCCTC	24-42 124-144	121
interleukin 6	IL6	AF275796.1	S A	CTCCAGAACAACTATGAGGGT AACAGCCCTCAGACTGAAC	427-447 651-669	243
Beta 2 microglobulin	B2M	NM_001284479.1	S A	CTGGTTTCCTGGCCTTGCTC TCTGCTTTCATCTCCTTTCCGTT	29-48 205-227	199

Table II. *Fold change of inflammatory related genes expression in canine with pyometra.*

Gene Symbols	Gene Names	Fold Change	Inflammatory response	Positive regulation
IL8	interleukin 8	76.822828	≥	
S100A8	S100 calcium binding protein A8	43.517853	≥	
S100A9	S100 calcium binding protein A9	37.157093	≥	
S100A12	S100 calcium binding protein A12	37.052523	≥	
PTGS2	prostaglandin-endoperoxide synthase 2	28.972019	≥	≥
IL1B	interleukin 1, beta	19.806744	≥	≥
CCL3	chemokine (C-C motif) ligand 3	16.763958	≥	≥
IL18RAP	interleukin 18 receptor accessory protein	16.709828	≥	
CHI3L1	chitinase 3-like 1	15.686272	≥	
PIK3CG	phosphatidylinositol-4,5-bisphosphate 3-kinase	14.815404	≥	≥
SEMA7A	semaphorin 7A	14.522514	≥	
TLR8	toll-like receptor 8	14.428546	≥	
AOAH	acyloxyacyl hydrolase	14.427443	≥	
IL1A	interleukin 1, alpha	12.871239	≥	
IL1RN	interleukin 1 receptor antagonist	12.818872	≥	
FCER1G	Fc fragment of IgE	12.046116	≥	≥
VCAM1	vascular cell adhesion molecule 1	11.935321	≥	
ITGB2	integrin, beta 2	11.135444	≥	
IL6	interleukin 6	10.939659	≥	≥
SPP1	secreted phosphoprotein 1	10.678636	≥	
SERPINE1	serpin peptidase inhibitor	10.599662	≥	≥
CD14	CD14 molecule	10.561551	≥	
TLR2	toll-like receptor 2	10.413059	≥	≥

4 µl template cDNA (standard or control), 0.5 µM of every gene-specific primer and a previously determined optimum $MgCl_2$ concentration (3.5 µM for one reaction). LightCycler FastStart DNA Master SYBR Green I mix (ROCHE) was used. The real-time PCR program included a 10 min denaturation step to activate the Taq DNA Polymerase, followed by a three-step amplification program: denaturation at 95°C for 10 s, annealing at 56°C for 5 s, and extension at 72°C for 10 s. Specificity of reaction products was checked by determination of melting points (0.1°C/s transition rate).

RT-qPCR data were expressed as means ± SE, and the statistical significance of differences between control and experimental groups was estimated using Student's *t*-test. The verification of PCR product specification was performed by the restriction enzyme cutting analysis (data not shown).

RESULTS

In order to obtain a complete view of the gene dynamics profile in the uteri of female dogs with pyometra in relation to healthy controls, we performed a whole gene expression analysis by Affymetrix® Canine Gene 1.1 ST Array by which we examined the expression of nearly 18,000 different genes. The dynamics profile of the whole gene expression is shown in the scatter plot and bar plot graphs (Fig. 1 A, B). Each dot in Fig. 1A represents mean expression value of the unique gene, black dots corresponding to genes whose expression did not differ between groups (fold change of expression is lower than 2). Genes, where the fold change was higher than cut off value and differences were significant ($p<0.05$), were considered as differentially expressed genes. The green color corresponds to genes up-regulated in pyometra, whilst the red dots correspond to genes down-regulated in pyometra. Of 17,138 different transcripts, 1,360 were up-regulated in pyometra (green dots), and 1,005 were down-regulated (red dots). There were 14,773 unchanged genes in the analyzed groups (cut-off of ±2). Graph 1B concerns the gene expression profile with different cut off values. In order to select the most potent expression changes, the cut-off value was set to ±10. For this criterion, 134 genes were up-regulated in pyometra, and only 8 were down-regulated (Fig. 1B). There were 16,996 unchanged genes in the groups analyzed.

Using GO BP (Gene Ontology biological process) data, we subset genes involved in the inflammatory response. The GO BP data were part of the Affymetrix description file and were previously merged with expression-level data. Subsequently, the "inflammatory response" term was used as a query to select a list of genes whose description in GO BP included "inflammatory response". The resulting data are shown as a scatter plot (Fig. 2). Of the 264 genes that were selected, 98 genes were up-regulated in pyometra (green dots) and only 10 were down-regulated (red dots). The remaining genes were unchanged.

From genes which belong to the inflammatory response group, we selected a set of genes with the highest differences in the expression between pyometra and healthy controls, i.e., by the selection of genes with a fold change larger than 10 or smaller than <10 (cut off >10). All of the selected transcripts (n=23) were up-regulated in pyometra (10- to 77-fold). Each of the raw expression values from those genes was grouped by means of hierarchical clustering algorithm. The result of such an analysis is presented as a heat map (Fig. 3). The raw expression value from the 23 strongest up-regulated transcripts in pyometra are shown also as a dot plot (Fig. 4).

Six genes were selected for results validation by RT-qPCR. Those analyses were performed on AOAH, IL1A, IL8, CCL3, IL1RN, SERPINE1 genes by applying primers presented in Table II. Results from RT-qPCR validation are presented in Fig. 5. The exact fold change value obtained from the microarray in comparison to the fold change from RT-qPCR was slightly differing, but the tendency of the gene expression was exactly the same. However, all of the analyzed genes were expressed much higher in dogs with pyometra. From microarray data the highest fold was observed in IL-8 (fold =76.82). Fold for IL-8 obtained by RT-qPCR was also the highest of all analyzed genes but the value of the fold was much higher (fold = 6060). On the other hand, the fold of IL1RN obtained by the microarray = 12.82 whilst RT-qPCR revealed fold = 2.72.

DISCUSSION

Pyometra is a uterine disease, which may be associated with an increased immune response against the infections of the uterine fluid as well as a pro-inflammatory response (14, 23, 24). There is

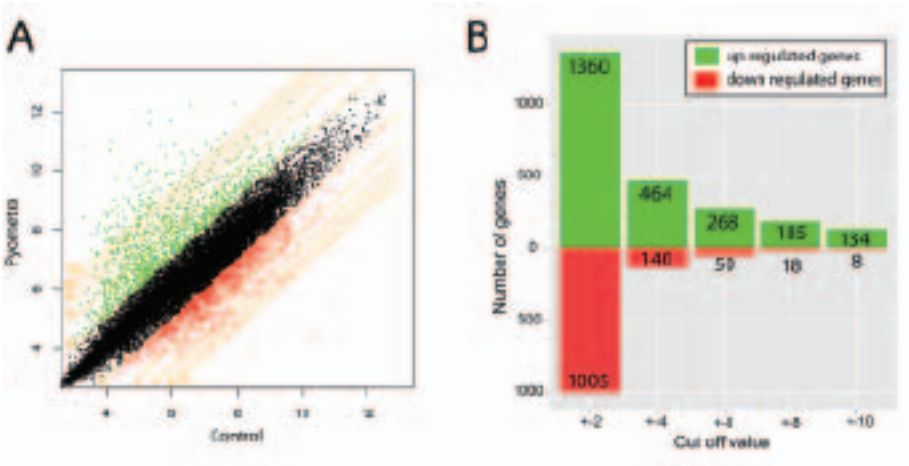

Fig. 1.

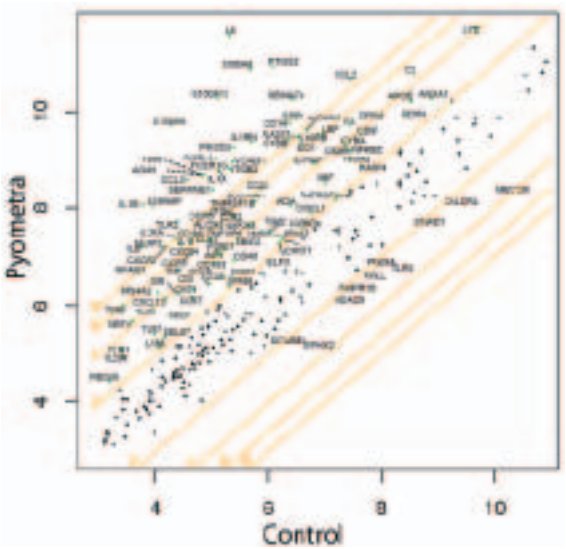

Fig. 2.

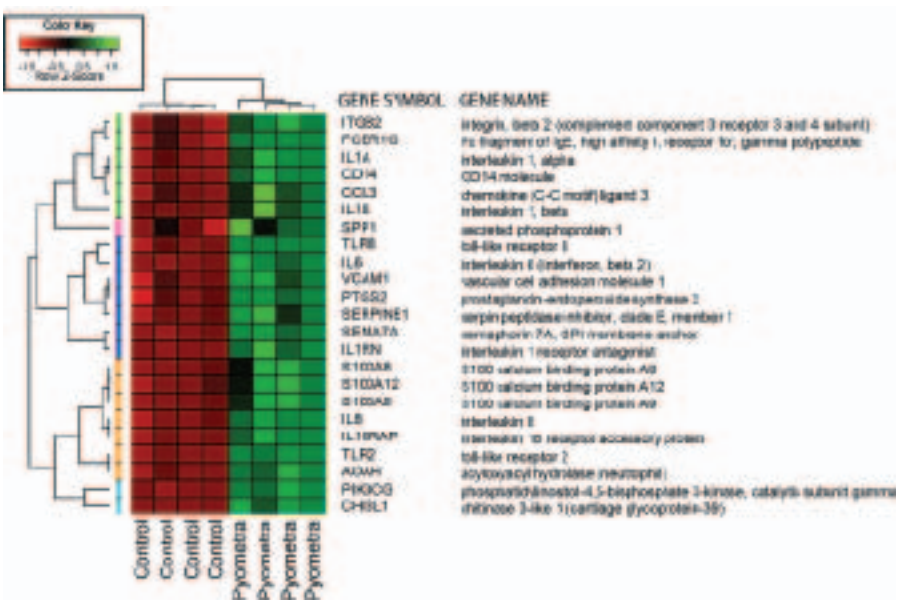

Fig. 3.

Fig. 1. *Expression profile of genes analyzed by Affymetrix®* Canine Gene 1.*1 ST Array.* ***A)*** *Scatterplot of the genes that are differentially expressed in subjects with pyometra compared with the expression in the control group. The orange lines mark the cut-off values (2-, 4-, 6-, 8-fold change of expression). The green dots represent transcripts whose expression is up-regulated more than 2-fold in pyometra (p<0.05). The red dots represent transcripts whose expression is down-regulated less than 2-fold in pyometra (P<0.05). Names of genes have not been shown.* ***B)*** *Expression profile of differentially expressed genes. Upper green part of graph represent number of genes which expression fold - pyometra to control group, is higher than cut-off value (x axis), whilst lower red part of graph: number of genes which expression fold - pyometra to control group is lover then cut-off value.*

Fig. 2. *Scatterplot of genes that are differentially expressed in the inflammatory response process in pyometra relative to the expression in the control group. The orange lines mark the cut-off values (2-, 4-, 6-, and 8-fold changes in expression). The green dots represent transcripts whose expression is up-regulated more than 2-fold in pyometra (p<0.05). The red dots represent transcripts whose expression is down-regulated less than 2-fold in pyometra (p<0.05). For genes below cut-off expression levels, names of genes have not been shown. Detailed data for differentially expressed genes are presented in supplementary tables.*

Fig. 3. *Heat map representation of the strongest differences of expressed genes involved in inflammatory response process. Expression of all of selected genes was more the 10-fold higher pyometra in relation to control group (n=4). The arbitrary signal intensity acquired from the microarray analysis is represented by colors (see color bar). The studied genes were clustered by means of a hierarchical clustering algorithm. The expression level of each gene was scaled in such a manner that the intense green color represents the highest expression and the intense red color represents the lowest expression level in pyometra.*

certainly an inflammatory response and, depending on the stage and cause of the pyometra, there may be a significant immune component of this disease. Pyometra is caused by the infection of the uterus and the infection triggers an immune response. Molecular markers for pyometra could be helpful for its diagnosis. Products of genes with the increased expression in the uterus of a bitch with pyometra could function as specific molecular biomarkers. The most recently published studies evaluated several immune and inflammatory response-related proteins in the blood serum (17, 23). However, to date there have been only few reports indicating alterations in the transcript expression in the uterus of a dog with pyometra after using microarray assays (18). Our study concentrated exactly on the gene expression in endometrium in dogs severely affected by pyometra. The bacteriological culture was performed and in 78% it was *Escherichia coli*, in 13% *Staphyllococcus* spp., 4.5% *Streptococcus* spp. and in 4.5% it was *Pseudomonas aeruginosa*. After using microarray assay, we identified 17,138 differentially expressed transcripts in the uterus with pyometra. A total of 264 genes were related to the inflammatory response, 98 of which increased in the expression, 10 decreased, and the remaining were unchanged. Furthermore, we analyzed 23 transcripts whose expression increased between 10- and 77-fold.

The aim of the present study was to select potent variable genes from a group of the inflammatory response, so we set the high cut-off value +-10. At the assumed cut-off value 23 genes are overexpressed in pyometra; using the same assumptions we do not obtain genes down regulated in pyometra.

Interleukins are factors that are closely related to the immune system activity as well as to immune and inflammatory responses. In our study, we found that the expression of interleukin-8 (IL-8), interleukin-1-beta (IL-1b), interleukin-18 receptor (IL-18RAP), interleukin-1-alpha (IL-1a), interleukin receptor (IL-1RN) and interleukin-6 (IL-6) increased 77-, 20-, 17-, 13-, 13- and 11-fold, respectively. In the study of Hagman (18) the cytokines IL-6 and IL-1 were upregulated to the largest reach and IL-18 and IL-33 were also evident. To date there have been several studies on interleukins measured in the

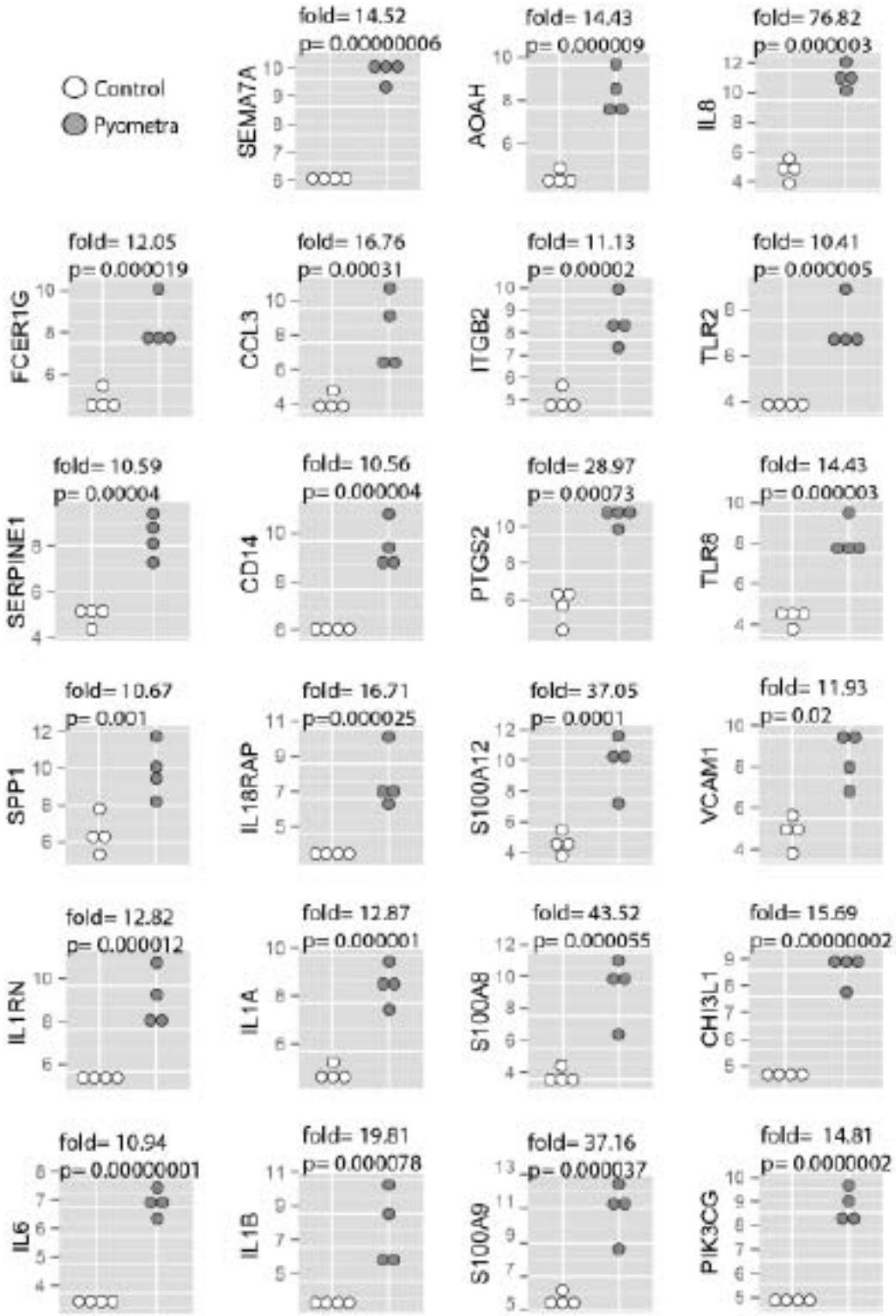

Fig. 4. *Dot plot of the most different expressed genes involved in inflammatory response process. Expression of all of selected genes was more the 10-fold higher pyometra in relation to control group (n=4). Fold changes and p values are shown for each of the graph.*

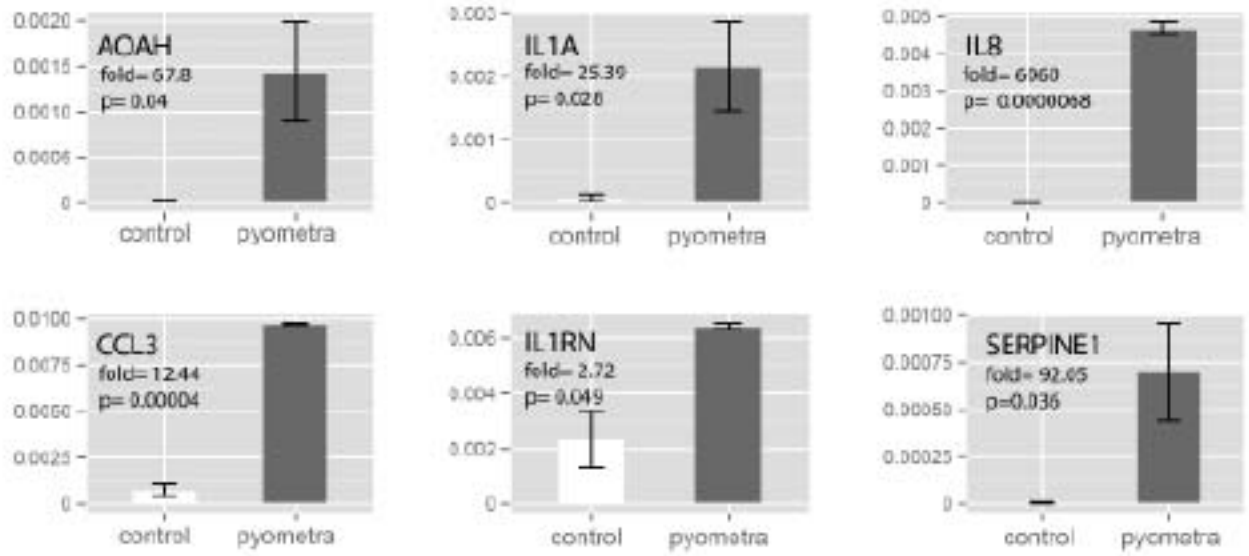

Fig. 5. *Results of RT-qPCR validation for selected genes (AOAH, IL1A, IL8, CCL3, IL1RN, SERPINE1) involved in inflammatory response process. Expression was calculated in relation to B2M reference gene. Y-axis – relative expression level. Bar plots present means ± SE. In each group n = 4. Fold changes and p values are shown for each of the graph.*

blood serum of bitches with pyometra (17, 23, 25-27). Kjelgaard-Hansen et al. (23) found an increased concentration of interleukin-10 (IL-10) in the canine serum with an inflammatory response, which was also associated with a higher level of C-reactive protein (CRP). However, dogs with an acute-phase response were characterized by a low level of IL-10 and no correlation with the CRP level was found even when there was a marked inflammatory response. Similar to these observations, our results confirmed an increased mRNA level of several interleukins that are involved in the inflammatory response, indicating that these interleukins could be molecular markers of canine pyometra. Particularly, the expression of IL-8 was 77-fold higher in the infected uterus compared to healthy controls. IL-8 may play a central role in the pro-inflammatory response and mediate the activation and migration of neutrophils into the tissue from peripheral blood. The differential expression profiling of IL-8 between groups of bitches with pyometra may be associated with a different activity of pro-inflammatory response, which is case-dependent, or a different activation of the immune response specific cells, e.g. neutrophils as a results of the uterine bacterial infection. Kjelgaard-Hansen et al. (23) investigated the IL-10 serum concentration in healthy dogs, in that with a naturally-occurring acute phase reaction and in dogs following surgical stimulus. They found an increased level of IL-10 in the serum of bitches with pyometra compared to others. Moreover, IL-10 showed a higher degree of variation in females with the increased inflammatory response and higher concentration of CRP. Bitches with an acute phase response were characterized by IL-10 levels with no clear relationship to CRP concentrations, with the observed low IL-10 level even when there was a marked inflammatory response. Other data of Tamada et al. (28) showed a correlation between the IL-8 mRNA level measured by RT-PCR and other inflammatory response markers, such as collagen concentration, collagenase activity in the endometrial tissue, and morphological changes in collagenous fibers determined by a histological assay. It was found that the IL-8 mRNA level was positively correlated with the cervical patency and the number of neutrophils in the cervical stroma. They suggested that the local expression of IL-8 may be involved in connective tissue remodeling as a result of the collagen degradation in the uterus of bitches with pyometra. Our study revealed strong overexpression of IL-8 genes measured both by the microarray and RT-qPCR. The fold change, for example IL-8 calculated by the microarray was 76.82 and after

using RT-qPCR was estimated as 6060 higher than control. Although both fold changes were different, a similar tendency was significantly noted. The competition of results obtained by RT-qPCR and microarray belongs to frequently used methods of the statistical analysis of the gene expression, and differences in fold changes calculated by those two techniques are quite common.

After using microarray assays, we found a 44-fold increased expression for the calcium binding protein S100A8, and a 37-fold increase in S100A12 and S100A9, respectively. Recently, Hofmann et al. (29) found that the central cell surface receptor (RAGE) for calcium binding proteins (S100) interacts with the newly identified extracellular RAGE-binding protein (ENRAGE) in the endothelium, mononuclear phagocytes and lymphocytes. Thereby, RAGE plays a central role in immune cell activation and the generation of pro-inflammatory mediators. They also found that a murine knock-out model for ENRAGE/RAGE displayed the arresting activation of important immune signaling pathways and down-regulated the expression of inflammatory-related gene mediators. Our results also indicated the role of S100As genes in the inflammatory response, presumably by the activation of immune-response specific cells, e.g., lymphocytes in canines with pyometra. We may suggest that this process could be associated with the inflow of activated inflammatory response cells as well as with further accumulation of this bacteria-contaminated fluid.

In the present study, we also observed that additional transcripts, such as toll-like receptors 2 and 8 (TLR2 and TLR8), the CD14 molecule, integrin beta 2 (ITGB2), chemokine ligand 3 (CCL3), prostaglandin-endoperoxide synthase 2 (PTGS2) or semaphorin 7A (SEMA7A), were also increased 10- to 18-fold in the infected canine uterus. All of these molecules play a central role in the immune and pro-inflammatory responses or are associated with the activation of immune-specific cells and the activation of immune-related signaling pathways (30, 31). Several of these proteins are also involved in the response to bacterial contamination, for example TLRs have specificity for different bacterial components. This function of TLRs could explain the manifold increased expression of TLR8 and TLR2, respectively, during bacterial contamination in closed-cervix canine pyometra. Other molecules, such as CCL3, which is also known as macrophage inflammatory protein-1, are involved in the acute inflammatory response as well as in the recruitment and activation of polymorphonuclear leukocytes (32). Moreover, Silva et al. (7, 15) investigated the transcriptional profiles of genes encoding the Toll-like receptors (TLR1-TLR7 and TLR9) as well as the protein expression of TLR2 and TLR4 in canine endometrium over the course of the oestrous cycle. They observed an increased expression of TLR2, TLR4 mRNAs and proteins at the late dioestrus and anoestrus, and they were decreased in the follicular phase and early dioestrus. It was suggested that the low level of TLRs transcripts or proteins observed at early dioestrus may be associated with the high prevalence of pyometra at this stage of the oestrous cycle. Contrary to these results, we found up-regulation of investigated TLRs transcripts in bitches with pyometra. However, differences in expression profiling may be explained by various oestrous cycle stages when the endometrium was recovered. Taking together both of these results, it may be suggested that TLRs are involved in the activation of the inflammatory response associated with pyometra in the bitch, and, therefore, may be used as a marker of bacterial infections in canine uterus. In the study of Hagman (18) caspase-8 was upregulated and contributed to NF-κB stimulation through TLR4. In the study of Chotimanukul et al. (33), the immunohistochemical localization of Toll-like receptor (TLR) in the canine reproductive tract was analyzed. They observed a different expression of TLR4 in the endometrial stroma, the endometrial surface epithelium and glandular epithelium. They found that TLR4 was expressed higher in the uterus of bitches with pyometra compared to other groups. It was concluded that increased expression of TLR4 is highly associated with uterine bacterial infections. On the other hand, differential expression of TLR4 may be the reason for physiological processes in distinct cell types of endometrium in bitches at various stages of oestrous cycle.

In conclusion, the expression of all investigated pro-inflammatory response-related transcripts was increased in the uterus of canines with pyometra compared to healthy controls, which suggested that inflammation is a main pathological stage

of canine pyometra. The increased expression of inflammatory-related transcripts in canines with pyometra revealed that inflammation in the uterus is also associated with the activation of specific immune cells that are involved in the pathogenesis of canine pyometra. Moreover, all of the 23 up-regulated transcripts may be novel molecular markers of the detection of pyometra in female dogs. Although some of the genes, such as interleukins were previously described as molecular marker of proinflammatory response specific for pyometra complex in domestic bitches, several of them are first described in this study, and therefore may be used as new markers of this disease. Since AOAH and SERPINE1 were highly expressed in bitches with pyometra as compared to controls, they may serve as markers of this disease, different from pro- inflammatory related genes. The expression of immune and inflammatory response genes was found to be associated with the occurrence of pyometra. Since in most of the available findings the serum concentration of immune-response proteins was studied, the identified molecular factors of this study, which are associated with the induction and development of pyometra, may be used as biomarkers. In future studies the unique upregulated transcripts should be examined also in the serum or perhaps vaginal discharge in dogs with pyometra. These biomarkers may be used in the future as a target for the anti-inflammation therapeutic strategy in many species of mammals. Since dogs and humans reflect many genetic similarities, there exists the possibility of common treatment of the induced similar disease also including inflammatory response-related diseases.

The research on pathological changes in bitches' uteri is limited by a plethora of factors to a high degree - endogenous hormonal disorders, the specificity of the heat cycle, secondary bacterial infections, variety of pathogens, variety of histological changes, the animal condition, the clinical stage, the quick pace of changes.

ACKNOWLEDGEMENTS

This study was made possible by grant numbers 2013/09/N/NZ5/01835, and 5279/B/P01/2011/40 from the Polish Ministry of Scientific Research and Higher Education and National Centre of Science.

REFERENCES

1. Dow C. The cystic endometrial hyperplasia-pyometra complex in the bitch. Vet Rec 1958; 70:1102-8.
2. Sandholm M, Vasenius H, Kivistö AK. Pathogenesis of canine pyometra. J Am Vet Med Assoc 1975; 167:1006-10.
3. Bartoskova A, Vitasek R, Leva L, Faldyna M. Hysterectomy leads to fast improvement of haematological and immunological parameters in bitches with pyometra. J Small Anim Pract 2007; 48:564-8.
4. Fieni F. Clinical evaluation of the use of aglepristone, with or without cloprostenol, to treat cystic endometrial hyperplasia-pyometra complex in bitches. Theriogenology 2006; 66:1550-6.
5. Arora N, Sandford J, Browning GF, Sandy JR, Wright PJ. A model for cystic endometrial hyperplasia/pyometra complex in the bitch. Theriogenology 2006; 66:1530-6.
6. De Bosschere H, Ducatelle R, Vermeirsch H, Van Den Broeck W, Coryn M. Cystic endometrial hyperplasia-pyometra complex in the bitch: should the two entities be disconnected? Theriogenology 2001; 55:1509-19.
7. Silva E, Henriques S, Brito S, Ferreira-Dias G, Lopes-da-Costa L, Mateus L. Oestrous cycle-related changes in production of Toll-like receptors and prostaglandins in the canine endometrium. J Reprod Immunol 2012; 96:45-57.
8. Krekeler N, Lodge KM, Anderson GA, Browning GF, Charles JA, Wright PJ. Effect of simulated stages of the canine oestrous cycle on *Escherichia coli* binding to canine endometrium. Reprod Domest Anim 2012; 47(S):331-4.
9. Siqueira AK, Ribeiro MG, Leite Dda S, et al. Virulence factors in *Escherichia coli* strains isolated from urinary tract infection and pyometra cases and from feces of healthy dogs. Res Vet Sci 2009; 86:206-10.
10. Smith FO. Canine pyometra. Theriogenology 2006; 66:610-12.
11. Corrada Y, Arias D, Rodríguez R, Tortora M, Gobello C. Combination dopamine agonist and prostaglandin agonist treatment of cystic endometrial hyperplasia-pyometra complex in the bitch. Theriogenology

2006; 66:1557-59.
12. Gobello C, Castex G, Klima L, Rodríguez R, Corrada Y. A study of two protocols combining aglepristone and cloprostenol to treat open cervix pyometra in the bitch. Theriogenology 2003; 60:901-8.
13. Breitkopf M, Hoffmann B, Bostedt H. Treatment of pyometra (cystic endometrial hyperplasia) in bitches with an antiprogestin. J Reprod Fertil Suppl 1997; 51:327-31.
14. Sugiura K, Nishikawa M, Ishiguro K, et al. Effect of ovarian hormones on periodical changes in immune resistance associated with estrous cycle in the beagle bitch. Immunobiology 2004; 209:619-27.
15. Silva E, Leitão S, Henriques S, Kowalewski MP, Hoffmann B, Ferreira-Dias G, da Costa LL, Mateus L. Gene transcription of TLR2, TLR4, LPS ligands and prostaglandin synthesis enzymes are up-regulated in canine uteri with cystic endometrial hyperplasia-pyometra complex. J Reprod Immunol 2010; 84:66-74.
16. Payan-Carreira R, Pires MA, Ström Holst B, Rodriguez-Martinez H. Tumour necrosis factor in the canine endometrium: an immunohistochemical study. Reprod Domest Anim 2011; 46:410-8
17. Karlsson I, Hagman R, Johannisson A, Wang L, Karlstam E, Wernersson S. Cytokines as immunological markers for systemic inflammation in dogs with pyometra. Reprod Domest Anim 2012; 47(S):337-41.
18. Hagman R, Rönnberg E, Pejler G. Canine uterine bacterial infection induces upregulation of proteolysis-related genes and downregulation of homeobox and zinc finger factors. PLoS One 2009; 4:e8039.
19. Tyczewska M, Rucinski M, Trejter M, Ziolkowska A, Szyszka M, Malendowicz LK. Angiogenesis in the course of enucleation-induced adrenal regeneration--expression of selected genes and proteins involved in development of capillaries. Peptides 2012; 38:404-13.
20. Gentleman RC, Carey VJ, Bates DM, et al. Bioconductor: open software development for computational biology and bioinformatics. Genome Biol 2004; 5:R80.
21. Irizarry RA, Hobbs B, Collin F, et al. Exploration, normalization, and summaries of high density oligonucleotide array probe level data. Biostatistics 2003; 4:249-64.
22. Benjamini Y, Hochberg Y. Controlling the false discovery rate: a practical and powerful approach to multiple testing. J R Stat Soc Series B 1995; 57:28 -300.
23. Kjelgaard-Hansen M, Luntang-Jensen M, Willesen J, Jensen AL. Measurement of serum interleukin-10 in the dog. Vet J 2007; 173:361-5.
24. Tecles F, Subiela SM, Petrucci G, Panizo CG, Cerón JJ. Validation of a commercially available human immunoturbidimetric assay for haptoglobin determination in canine serum samples. Vet Res Commun 2007; 31:23-36.
25. Fransson BA, Karlstam E, Bergstrom A, et al. C-reactive protein in the differentiation of pyometra from cystic endometrial hyperplasia/mucometra in dogs. J Am Anim Hosp Assoc 2004; 40:391-9.
26. Fransson BA, Bergström A, Wardrop KJ, Hagman R. Assessment of three automated assays for C-reactive protein determination in dogs. Am J Vet Res 2007; 68:1281-6.
27. Fransson BA, Lagerstedt AS, Bergstrom A, et al. C-reactive protein, tumor necrosis factor **α**, and interleukin-6 in dogs with pyometra and SIRS. J Vet Emerg Crit Care 2007; 17:373-81.
28. Tamada H, Kawata N, Kawate N, et al. Factors associated with patency of the uterine cervix in bitches with pyometra. Res Vet Sci 2012; 93:1203-10.
29. Hofmann MA, Drury S, Fu C, et al. RAGE mediates a novel proinflammatory axis: a central cell surface receptor for S100/calgranulin polypeptides. Cell 1999; 97:889-901.
30. Hagman R. Clinical and molecular characteristics of pyometra in female dogs. Reprod Domest Anim 2012; 47(S):323-25.
31. Coggan JA, Melville PA, de Oliveira CM, Faustino M, Moreno AM, Benites NR. Microbiological and histopathological aspects of canine pyometra. Braz J Microbiol 2008; 39:477-83.
32. Wolpe SD, Davatelis G, Sherry B, et al. Macrophages secrete a novel heparin-binding protein with inflammatory and neutrophil chemokinetic properties. J Exp Med 1988; 167:570-81.
33. Chotimanukul S, Sirivaidyapong S. Differential expression of Toll-like receptor 4 (TLR4) in healthy and infected canine endometrium. Theriogenology 2011; 76:1152-61.

KNOCKDOWN OF THE INFLAMMATORY FACTOR PENTRAXIN-3 SUPPRESSES GROWTH AND INVASION OF LUNG ADENOCARCINOMA THROUGH THE AKT AND NF-KAPPA B PATHWAYS

F-Q. HU, T. QIAO, X. XIE, R. HU and H-B. XIAO

Department of Cardiothoracic Surgery, Xinhua Hospital, Shanghai Jiao Tong University School of Medicine, Shanghai, China

Received September 9, 2014 – Accepted October 17, 2014

The first two authors contributed equally to this article

Pentraxin-3 (PTX3), a modulator of tumor-associated inflammation, is known to be positively correlated with tumor grade and severity of malignancies, but the function and molecular underlying mechanisms of PTX3 remain unclear. In the present study, the expression of PTX3 in human lung adenocarcinoma (LAC) was examined by immunohistochemical assay using a tissue microarray procedure. A loss-of-function experiment was performed to explore the effects of lentiviral vector-mediated PTX3 shRNA (Lv-shPTX3) on cell growth and invasive potential in LAC cell lines (A549 and LETPα-2), assessed by MTT and Transwell assays, respectively. We found that the expression of PTX3 protein was significantly increased in LAC tissues compared with that in adjacent non-cancerous tissues (ANCT) (60.42% vs. 29.17%, *P*=0.004), and positively correlated with lymphatic invasion of the tumor (*P*=0.006). Furthermore, knockdown of PTX3 suppressed tumor proliferation and invasion of LAC cells, followed by decreased expression of p-AKT, p-NF-kappa B, PCNA, and MMP-9. Taken together, our findings demonstrate that upregulation of PTX3 expression is correlated with tumor metastasis of LAC patients, and knockdown of PTX3 blocks the development of LAC through inhibition of the AKT and NF-kappa B pathways, suggesting that PTX3 may serve as a potential therapeutic target for the treatment of cancer.

Lung cancer is the most commonly diagnosed type of cancer and the primary cause of cancer-related deaths worldwide (1). The current best approach for the treatment of cancer is complete surgical removal of the tumor and adjacent lymph nodes. However, the efficacy of this therapeutic approach alongside hormone, radio, and chemo-therapy is very limited (2). Therefore, identification of key genes or targets related to tumorigenesis is critical for prevention and treatment of cancer.

Pentraxin-3 (PTX3) is an inflammatory mediator synthesized in a variety of cells and tissues including heart, vascular endothelial cells, smooth muscle cells, macrophages and adipocytes (3, 4). The level of PTX3 has been found increased in patients with polycystic ovary syndrome (3), irradiated arteries and veins (4), pulmonary fungal infections (5) and febrile neutropenia (6), and predictive of septic shock and bacteremia at the onset of febrile neutropenia (7). Moreover, inflammatory mediators play decisive roles in different stages of tumour development, of which PTX3 is identified to be

Key words: pentraxin-3, lung adenocarcinoma, growth, invasion, apoptosis

Mailing address: Prof. Hai-Bo Xiao,
Department of Cardiothoracic Surgery,
Xinhua Hospital, Shanghai Jiao Tong University
School of Medicine, 1665 Kongjiang Road,
Shanghai, 200092 China
Tel.: +86 21 25078051 Fax: +86 21 65048015
e-mail: xiaohaibo2013@163.com

0393-974X (2014)

expressed in breast cancer using coupling proteomics and transcriptomics and has a potential prognostic value (8). PTX3 is highly expressed in human soft tissue liposarcomas (9), prostate cancer (10, 11) and acute lymphoblastic leukemia (12), contributes to the oncogenesis (9) and serves as diagnostic, prognostic or predictive serological markers for cancer (11).

However, some studies show that PTX3 is down-regulated due to promoter hypermethylation in esophageal squamous cell carcinoma (13), which inhibits migration of multiple myeloma (MM) plasma cells and fibroblast growth factor-2-mediated MM angiogenesis (14). Moreover, activation of nuclear factor-kappa B or AKT signaling promotes the aggressiveness and survival of lung adenocarcinoma (LAC) cells (15, 16). To elucidate the function and molecular mechanisms of PTX3 in human LAC, we examined the expression of PTX3 by immunohistochemical assay using a tissue microarray procedure in LAC tissues, and constructed lentiviral vector-mediated Lv-shPTX3 to observe the effects of PTX3 knockdown on the biological behaviors of LAC cells *in vitro* and *in viv*o. We hypothesized that knockdown of PTX3 might repress growth and invasion of LAC cells through regulation of the AKT and nuclear factor-kappa B pathways.

MATERIALS AND METHODS

Materials

The LAC cell lines (A549 and LETPα-2) used for our experiments were obtained from the Institute of Biochemistry and Cell Biology (Shanghai, China). Lentivirus-mediated PTX3 shRNA (Lv-shPTX3), negative control vector, and virion-packaging elements were purchased from Genechem (Shanghai, China). Human LAC tissues and the corresponding ANCT were collected from the Department of Cardiothoracic Surgery, Xinhua Hospital. The tissue microarray of LAC was made by Shanghai Outdo Biotech CO.LTD (Shanghai, China). All the antibodies were purchased from Cell Signaling Technologies (Boston, USA). PTX3 primer was synthesized by ABI (Framingham, USA).

Drugs and reagents

Dulbecco's Modified Eagle medium (DMEM) and fetal bovine serum (FBS) were purchased from Thermo Fisher Scientific Inc. (Waltham, MA, USA); TRIzol Reagent and Lipofectamine 2000 were obtained from Invitrogen (Carlsbad, CA, USA); M-MLV Reverse Transcriptase was purchased from Promega (Madison, WI, USA); SYBR Green Master Mix was obtained from Takara (Otsu, Japan); and the ECL Plus Kit was obtained from GE Healthcare (Piscataway, NJ, USA).

Clinical samples and data

Tissue microarray was prepared for IHC test. Human LAC tissues and the corresponding ANCT were obtained from biopsy in a total of 48 consecutive LAC cases admitted to our hospital from January 2011 to December 2013. The baseline characteristics of the patients before neo-adjuvant chemotherapy were summarized. The study was approved by the Medical Ethics Committee of Shanghai Jiao Tong University and written informed consent was obtained from the patients or their parents before sample collection. Two pathologists respectively reviewed all of the cases.

Tissue microarray

The advanced tissue arrayer (ATA-100, Chemicon International, Tamecula, CA, USA) was used to create holes in a recipient paraffin block and to acquire cylindrical core tissue biopsies with a diameter of 1 mm from the specific areas of the "donor" block. The tissue core biopsies were transferred to the recipient paraffin block at defined array positions. The tissue microarrays contained tissue samples from 48 formalin-fixed paraffin-embedded cancer specimens with known diagnosis, and corresponding ANCT from these patients. The block was incubated in an oven at 45°C for 20 min to allow complete embedding of the grafted tissue cylinders in the paraffin of the recipient block, and then stored at 4°C until microtome sectioning.

Immunohistochemical staining

Tissue microarray sections were processed for IHC analysis of PTX3 protein as follows. Immunohistochemical examinations were carried out on 3-mm thick sections. For anti-PTX3 immunohistochemistry, unmasking was performed with 10 mM sodium citrate buffer, pH 6.0, at 90°C for 30 min. For anti-PTX3 immunohistochemistry, antigen unmasking was not necessary. Sections were incubated in 0.03% hydrogen peroxide for 10 min at room temperature, to remove endogenous peroxidase activity, and then in blocking serum [0.04% bovine serum albumin, A2153 (Sigma-Aldrich, Shanghai, China) and 0.5% normal goat serum X0907, (Dako Corporation, Carpinteria, CA, USA) in PBS] for 30 min at room temperature. Anti-PTX3 antibody was used at a dilution of 1:200. The antibody was incubated overnight at 4°C. Sections were then washed three times for 5 min in PBS. Non-specific staining was blocked with 0.5% casein and

5% normal serum for 30 min at room temperature. Finally, staining was developed using diaminobenzidine substrate, and sections were counterstained with hematoxylin. Normal serum or PBS was used to replace anti-PTX3 antibody in negative controls.

Quantification of protein expression

The expression of PTX3 was semiquantitatively estimated as the total immunostaining scores, which were calculated as the product of a proportion score and an intensity score. The proportion and intensity of the staining was evaluated independently by two observers. The proportion score reflected the fraction of positive staining cells (0, none; 1, ≤10%; 2, 10% to ≥25%; 3, >25% to 50%; 4, >50%), and the intensity score represented the staining intensity (0, no staining; 1, weak; 2, intermediate; 3, strong). Finally, a total expression score was given ranging from 0 to 12. Based on the analysis in advance, PTX3 expression was categorized into two groups: negative expression and positive expression. The scoring was independently assessed by two pathologists.

Cell culture and transfection

LAC cell lines were cultured in DMEM medium supplemented with 10% heat-inactivated FBS, 100U/ml of penicillin, and 100 μg/ml of streptomycin. Cells in this medium were placed in a humidified atmosphere containing 5% CO_2 at 37°C. Cells were subcultured at a 1:5 dilution in medium containing 300μg/ml G418 (an aminoglycoside antibody, commonly used stable transfection reagent in molecular genetic testing). On the day of transduction, LAC cells were replated at 5×10^4 cells/well in 24-well plates containing serum-free growth medium with polybrene (5 mg/ml). When 50% confluence was reached, cells were transfected with recombinant experimental virus or control virus at the optimal MOI (multiplicity of infection) of 50, and cultured at 37°C and 5% CO2 for 4 h. Then supernatant was discarded and serum containing growth medium was added. At 4 days of post-transduction, transduction efficiency was measured by the frequency of green fluorescent protein (GFP)-positive cells. Positive and stable transfectants were selected and expanded for further study. The Lv-shPTX3 vector-infected clone and the negative control vector-infected cells were named as Lv-shPTX3 group and NC group.

Quantitative Real-time PCR

To quantitatively determine the mRNA expression level of PTX3 in LAC cells, Real-time PCR was performed. Total RNA was extracted for each clone using TRIzol according to the manufacturer's protocol. Reverse transcription was carried out using M-MLV and cDNA amplification was performed using the SYBR Green Master Mix kit according to the manufacturer's guidelines. The PTX3 gene was amplified using a specific oligonucleotide primer and the GAPDH gene was used as an endogenous control. The PCR primer sequences were as follows: PTX3 Forward, 5'-TGGCCAAAACAAAAATAACCAG-3' and Reverse 5'-GTGCTTTCAGATGAATGCTGT-3'; GAPDH Forward, 5'-CCTTCTCTTGCTGG GTGATTG-3' and Reverse 5'-GACAATGAATTTGGCTACAGCA-3'. Data were analyzed using the comparative Ct method ($2^{-\square\square Ct}$). Three separate experiments were performed for each clone.

Western blot assay

LAC cell lines were harvested and extracted using lysis buffer (Tris-HCl, SDS, mercaptoethanol, and glycerol). Cell extracts were boiled for 5 min in loading buffer, and then an equal amount of cell extracts was separated on 15% SDS-PAGE gels. Separated protein bands were transferred onto polyvinylidene fluoride (PVDF) membranes, which were subsequently blocked in 5% skim milk powder. Primary antibodies against PTX3, p-AKT, p-NF-kappa B, PCNA, and MMP-9 were diluted according to the manufacturer's instructions and incubated overnight at 4°C. Subsequently, horseradish peroxidase-linked secondary antibodies were added at a dilution of 1:1000 and incubated at room temperature for 2 h. The membranes were washed 3 times with PBS, and the immunoreactive bands were visualized using the ECL Plus Kit according to the manufacturer's instructions. The relative protein levels in different cell lines were normalized to the concentration of GAPDH. Three separate experiments were performed for each clone.

Cell proliferation assay

Cell proliferation was analyzed using the MTT assay. Briefly, cells infected with Lv-shPTX3 virus were incubated in 96-well-plates at a density of 1×10^5 cells per well with DMEM medium supplemented with 10% FBS. Cells were treated with 20 μl of MTT dye at 0, 24 h, 48 h, 72 h, and subsequently incubated with 150 μl of DMSO for 5 min. The color reaction was measured at 570 nm using an Enzyme Immunoassay Analyzer (Bio-Rad, Hercules, CA, USA). The proliferation activity was calculated for each clone.

Transwell invasion assay

Transwell filters were coated with Matrigel (3.9 mg/ml; 60–80 ml) on the upper surface of a polycarbonate membrane (diameter, 6.5 mm; pore size, 8 mm). After incubating at 37°C for 30 min, the Matrigel solidified and served as the extracellular matrix for analysis of tumor cell invasion. Harvested cells (1×10^5) in 100 ml of serum-

free DMEM were added into the upper compartment of the chamber. A total of 200 ml of conditioned medium derived from NIH3T3 cells was used as a source of chemoattractant, which was placed in the bottom compartment of the chamber. After 24 h of incubation at 37°C with 5% CO_2, the medium was removed from the upper chamber. The non-invaded cells on the upper side of the chamber were scraped off with a cotton swab. Cells that had migrated from the Matrigel into the pores of the inserted filter were fixed with 100% methanol, stained with hematoxylin, then mounted and dried at 80°C for 30 min. The number of cells invading through the Matrigel was counted in 3 randomly selected visual fields from the central and peripheral portion of the filter by using an inverted microscope (200× magnification). Each assay was repeated 3 times.

Statistical analysis

SPSS 20.0 was used for the statistical analysis. Kruskal-Wallis H test and *Chi*-squared test were used to analyze the expression rate in all groups. One-way analysis of variance (ANOVA) was used to analyze the differences between groups. The LSD method of multiple comparisons was used when the probability for ANOVA was statistically significant. Statistical significance was set at $P < 0.05$.

RESULTS

The expression of PTX3 in LAC tissues

The expression of PTX3 protein was examined by IHC staining in LAC tissues. The different levels of positive expression of PTX3 protein were detected in LAC and ANCT tissues (Fig. 1). Positive PTX3 immunostaining was mainly localized in the nucleus and cytoplasm of LAC tissue cells. According to the PTX3 immunoreactive intensity, the positive expression of PTX3 was significantly increased in LAC tissues compared with that in ANCT (P=0.004) (Table I).

Correlation of PTX3 expression with clinicopathologic parameters

The association between PTX3 expression and several clinical and pathologic factors was analyzed. As shown in Table II, increased expression of PTX3 was closely correlated with lymph node metastases of LAC (P=0.006). However, no significant link was found between PTX3 expression and other factors including age, gender of the patients, and histology and tumour size, degree of differentiation and TNM stage of LAC (P>0.05, respectively).

Effect of PTX3 on the expression of AKT and NF-kappa B

After Lv-shPTX3 was transfected into LAC cell lines (A549 and LETPα-2) for 24 h, the expression levels of PTX3 and AKT mRNA (Fig. 2A, B) and those of PTX3, p-AKT and p-NF-kappa B proteins (Fig. 2 C, D) were detected by Real-time PCR and Western blot assays, which indicated a decreased expression of PTX3, p-AKT and p-NF-kappa B in Lv-shPTX3 group compared with the NC group in LAC cells (**$P < 0.01$).

Effect of PTX3 on cell proliferation

Deregulated cell proliferation is a hallmark of cancer. To verify the effect of PTX3 on cell growth, we evaluated cell proliferative activities by MTT assay. The results showed that knockdown of PTX3 could decrease the proliferative activities of LAC cell lines (A549 and LETPα-2) in a time-dependent manner compared to the NC group (**$P < 0.01$) (Fig. 3A, B). The expression level of PCNA mRNA, examined by Real-time PCR assay (Fig. 3 C, D), was found significantly down-regulated in Lv-shPTX3 group compared with the NC group (**$P < 0.01$).

Effect of PTX3 on cell invasion

To determine the effect of PTX3 on cell invasion, a Transwell assay was performed. The invasive potential of tumor cells in Transwell assay was determined by the ability of cells to invade a matrix barrier containing laminin and type IV collagen, the major components of the basement membrane. Representative micrographs of Transwell filters can be seen in Fig. 4A. It was found that the invasive potential of LAC cells was apparently lowered in Lv-shPTX3 group compared to the NC group (**$P < 0.01$) (Fig. 4B). The expression level of MMP-9 mRNA, examined by Real-time PCR assay (Fig. 4C), was found significantly reduced in Lv-shPTX3 group compared with the NC group (**$P < 0.01$).

DISCUSSION

Lung cancer is prevalent worldwide and improvements in timely and effective diagnosis are needed. To assess the clinical value of Pentraxin-3 (PTX3) in diagnosis and prognosis,

Table I. *Expression of PTX3 proteins in LAC tissues.*

Target	Group	Total	N				Positive rate (%)	χ^2	*P*
			-	+	++	+++			
PTX3	LAC	48	19	15	9	5	60.42		
	ANCT	48	34	7	5	2	29.17	8.525	0.004

PTX3: pentraxin-3; LAC: lung adenocarcinoma ; ANCT: adjacent non-cancerous tissues.

Table II. *The correlation of PTX3 expression with clinicopathologic characteristics of LAC patients.*

Variables	Cases (n)	PTX3 expression		*P* value
		-	+	
Total	48	19	29	
Age (years)				
≥60	31	12	19	
<60	17	7	10	0.869
Sex				
Male	35	14	21	
Female	13	5	8	0.924
Tumor size (cm)				
≥5	39	13	26	
<5	9	6	3	0.068
Degree of differentiation				
Well/Moderate	8	3	5	
Poor	40	16	24	0.896
TNM stage				
I+II	16	9	7	
III+IV	32	10	22	0.099
Lymph node metastasis				
Negative	26	15	11	
Positive	22	4	18	0.006

Zhang et al. (17) detected the serum level of PTX3 in a total of 1,605 patients with lung cancer, benign lung diseases and healthy controls and revealed the elevated level of PTX3 in lung cancer, suggesting a potential biomarker for lung cancer. The diagnostic sensitivity and specificity of serum PTX3 is validated similar to clinically used lung cancer biomarkers, indicating that PTX3 has clinical utility for lung cancer diagnosis and management (18). The proteomics analysis of conditioned media of lung cancer cell lines is also utilized to identify PTX3 as the candidate lung cancer biomarker (19). In the present study, we examined the expression of PTX3 in LAC tissues and found that PTX3 was up-regulated in the nucleus and cytoplasm in LAC tissue cells compared with the ANCT, suggesting that intracellular accumulation of PTX3 might be associated with the tumorigenesis of LAC. Furthermore, the expression of PTX3E was positively correlated with lymphatic invasion of the tumor, indicating that LAC patients with high PTX3 expression might have a poor prognosis.

PTX3 is a tumor necrosis factor and interleukin-1beta-stimulated gene that encodes a long PTX with pro-inflammatory activity. Microglia, as the

phagocytes of the central nervous system, plays an important role in the recognition, engulfment, and clearance of apoptotic cells and invading microbes. Glia-derived PTX3 can modulate phagocytic functions of microglia and have important implications in the regulation of microglial activity in health and disease (20). The function of PTX3 in cancer has been explored. Some studies show that administration of PTX3 promotes tumor migratory potential and the mobilization of macrophages in breast cancer cells, while PTX3 silencing prevents tumor migration, macrophage chemotaxis, and bone metastases (21). However, PTX3 binds FGF2 with high affinity and specificity, preventing the binding of fibroblast growth factor 2 (FGF2) to its cognate tyrosine kinase receptors and leading to inhibition of the tumor angiogenesis and growth (22). PTX3-overexpressing has a powerful anti-FGF2 activity and leads to the reduction of tumor growth *in vivo* (23). To clarify the function of PTX3 in cancer, we investigated the biological behaviors in Lv-shPTX3-transfected LAC cells and found that knockdown of PTX3 could inhibit the proliferation and invasion of LAC cells and induce cell apoptosis and cycle arrest, suggesting a tumor-promoting role in LAC.

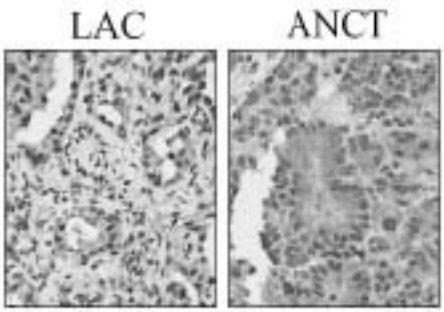

Fig. 1. *The expression of PTX3 in LAC tissues (× 200). Expression of PTX3 protein was evaluated using IHC staining. Positive expression of PTX3 protein was found increased in LAC tissues but decreased in ANCT.*

AKT is frequently activated in various cancers, and is involved in lung tumor development and progression (24). Specific targeting of AKT pathway in combination with radiotherapy or chemotherapy

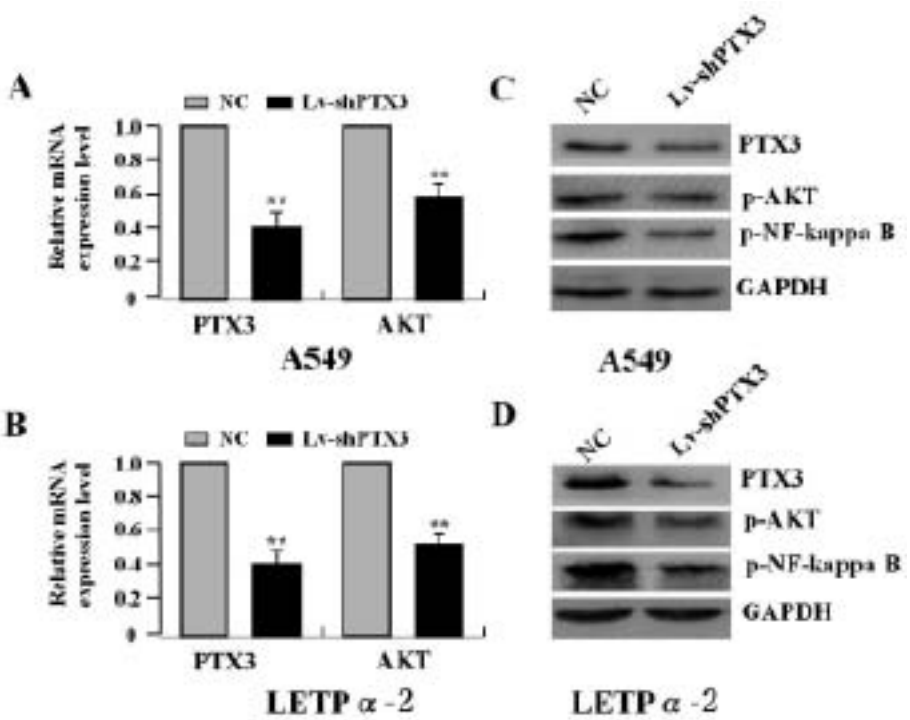

Fig. 2. *Effect of PTX3 on AKT and NF-kappa B expression.* ***A, B****) The mRNA expression of PTX3 and AKT indicated by Real-time PCR assay was decreased in Lv-shPTX3 group compared with the NC group in LAC cells (each **P < 0.01).* ***C, D****) The protein expression of PTX3, p-AKT and p-NF-kappa B indicated by Western blot assay was reduced in Lv-shPTX3 group compared with the NC group in LAC cells.*

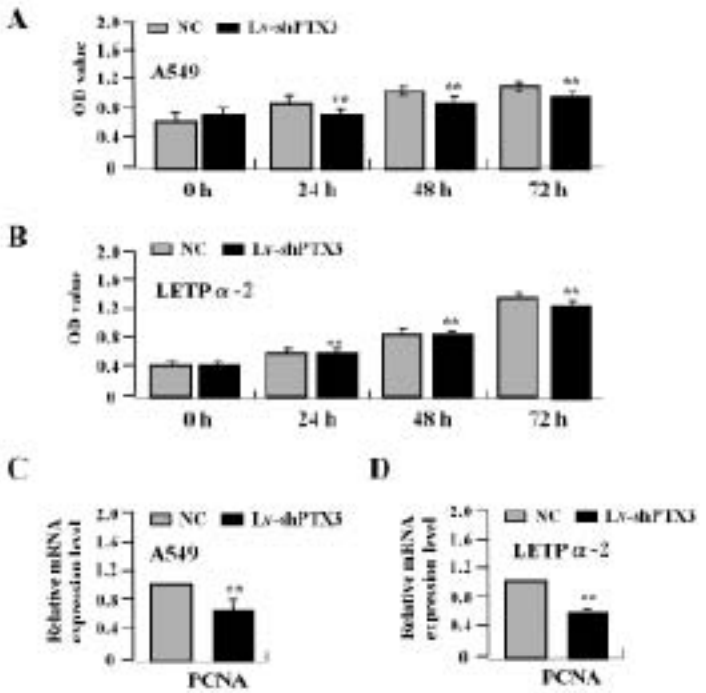

Fig. 3. *Effect of PTX3 on cell proliferation.* ***A, B****) We investigated the growth of LAC cells by MTT. Knockdown of PTX3 significantly diminished proliferative activities of LAC cells in a time-dependent manner compared with the NC group (each **P < 0.01).* ***C, D****) The mRNA expression of PCNA was examined by Real-time PCR indicating a significant decrease in Lv-shPTX3 group compared to the NC group (each **P < 0.01).*

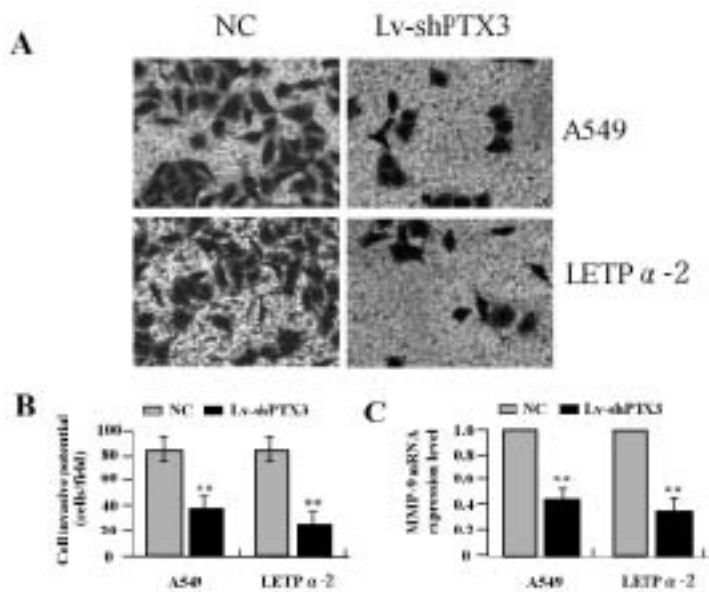

Fig. 4. *Effect of PTX3 on cell invasion.* ***A****) The invasive potential assessed by Transwell assay was determined on the basis of the ability of cells to invade a matrix barrier containing laminin and type IV collagen, the major components of the basement membrane.* ***B****) The invasive capabilities of LAC cells were weakened in Lv-shPTX3 group compared with the NC group (**P < 0.01).* ***C****) The mRNA expression of MMP-9 indicated by Real-time PCR assay was significantly decreased in Lv-shPTX3 group compared with the NC group (**P < 0.01).*

can enhance tumor control in lung cancer (25). In addition, NF-kappaB has been proved to play an important role in anchorage-independent growth and metastatic growth of lung carcinoma cells (26). Moreover, activation of the AKT or NF-kB pathway results in augmented invasiveness in lung cancer cells and plays a key role in the development of lung cancer (27). In the present study, we found that PTX3 could significantly downregulate the expression of p-AKT and p-NF-kappaB, suggesting that PTX3 might participate in the progression of LAC through the AKT and NF-kB pathways.

PCNA, as a nuclear protein that is expressed in proliferating cells, may be required for maintaining cell proliferation, and used as a marker for lung cancer cell proliferation (28). MMPs are important molecules involved in tumor metastasis. They are expressed on the tumor cell surface, activate pro-MMP to exacerbate the malignancy, and are considered a powerful indicator of distant metastasis of lung cancer (29). Previous studies have reported that, AKT or NF-kB pathway is correlated with cell proliferation marker PCNA (30), and results in the upregulation of MMP-9 (31) in lung cancer. Our finding showed that knockdown of PTX3 suppressed LAC growth and invasion and induced cell apoptosis and cycle distribution with the decreased expression of PCNA, MMP-9 and cyclinD1 and increased expression of caspase-3, suggesting that AKT and NF-kB pathways might mediate the regulation of PTX3 on the expression of PCNA and MMP-9 in LAC cells.

In conclusion, increased expression of PTX3 is correlated with tumor invasion of LAC patients, and knockdown of PTX3 blocks the development of LAC through inhibition of the AKT and NF-kappa B pathways, suggesting that PTX3 may serve as a potential therapeutic target for the treatment of cancer.

ACKNOWLEDGEMENTS

This work was partially supported by the National Natural Science Foundation of China (30901476).

REFERENCES

1. Siegel R, Naishadham D, Jemal A. Cancer statistics, 2013. CA Cancer J Clin 2013; 63:11-30.
2. William WN Jr, Glisson BS. Novel strategies for the treatment of small-cell lung carcinoma. Nat Rev Clin Oncol 2011; 8:611-19.
3. Aydogdu A, Tasci I, Tapan S, et al. High plasma level of long Pentraxin 3 is associated with insulin resistance in women with polycystic ovary syndrome. Gynecol Endocrinol 2012; 28:722-25.
4. Christersdottir Björklund T, Reilly SJ, Gahm C, Bottazzi B, Mantovani A, Tornvall P, Halle M. Increased long-term expression of pentraxin 3 in irradiated human arteries and veins compared to internal controls from free tissue transfers. J Transl Med 2013; 11:223.
5. Biagi E, Col M, Migliavacca M, et al. PTX3 as a potential novel tool for the diagnosis and monitoring of pulmonary fungal infections in immuno-compromised pediatric patients. J Pediatr Hematol Oncol 2008; 30:81-5.
6. Juutilainen A, Vänskä M, Pulkki K, Hämäläinen S, Nousiainen T, Jantunen E, Koivula I. Pentraxin 3 predicts complicated course of febrile neutropenia in haematological patients, but the decision level depends on the underlying malignancy. Eur J Haematol 2011; 87:441-7.
7. Vänskä M, Koivula I, Hämäläinen S, Pulkki K, Nousiainen T, Jantunen E, Juutilainen A. High pentraxin 3 level predicts septic shock and bacteremia at the onset of febrile neutropenia after intensive chemotherapy of hematologic patients. Haematologica 2011; 96:1385-9.
8. Pavlou MP, Dimitromanolakis A, Diamandis EP. Coupling proteomics and transcriptomics in the quest of subtype-specific proteins in breast cancer. Proteomics 2013; 13:1083-95.
9. Willeke F, Assad A, Findeisen P, et al. Overexpression of a member of the pentraxin family (PTX3) in human soft tissue liposarcoma. Eur J Cancer 2006; 42:2639-46.
10. Ravenna L, Sale P, Di Vito M, et al. Up-regulation of the inflammatory-reparative phenotype in human prostate carcinoma. Prostate 2009; 69:1245-55.
11. Sardana G, Jung K, Stephan C, Diamandis EP. Proteomic analysis of conditioned media from the PC3, LNCaP, and 22Rv1 prostate cancer cell lines: discovery and validation of candidate prostate cancer biomarkers. J Proteome Res 2008; 7:3329-38.

12. Sulicka J, Surdacki A, Mikołajczyk T, et al. Elevated markers of inflammation and endothelial activation and increased counts of intermediate monocytes in adult survivors of childhood acute lymphoblastic leukemia. Immunobiology 2013; 218:810-6.
13. Wang JX, He YL, Zhu ST, Yang S, Zhang ST. Aberrant methylation of the 3q25 tumor suppressor gene PTX3 in human esophageal squamous cell carcinoma. World J Gastroenterol 2011; 17:4225-30.
14. Basile A, Moschetta M, Ditonno P, et al. Pentraxin 3 (PTX3) inhibits plasma cell/stromal cell cross-talk in the bone marrow of multiple myeloma patients. J Pathol 2013; 229:87-98.
15. Chen PM, Wu TC, Wang YC, Cheng YW, Sheu GT, Chen CY, Lee H. Activation of NF-κB by SOD2 promotes the aggressiveness of lung adenocarcinoma by modulating NKX2-1-mediated IKKβ expression. Carcinogenesis 2013; 34:2655-63.
16. Togano T, Watanabe M, Itoh K, Umezawa K, Masuda N, Higashihara M, Horie R. Activation of Akt involves resistance to NF-κB inhibition and abrogation of both triggers synergistic apoptosis in lung adenocarcinoma cells. Lung Cancer 2014; 83:139-45.
17. Zhang D, Ren WH, Gao Y, Wang NY, Wu WJ. Clinical significance and prognostic value of pentraxin-3 as serologic biomarker for lung cancer. Asian Pac J Cancer Prev 2013; 14:4215-21.
18. Diamandis EP, Goodglick L, Planque C, Thornquist MD. Pentraxin-3 is a novel biomarker of lung carcinoma. Clin Cancer Res 2011; 17:2395-9.
19. Planque C, Kulasingam V, Smith CR, Reckamp K, Goodglick L, Diamandis EP. Identification of five candidate lung cancer biomarkers by proteomics analysis of conditioned media of four lung cancer cell lines. Mol Cell Proteomics 2009; 8:2746-58.
20. Jeon H, Lee S, Lee WH, Suk K. Analysis of glial secretome: the long pentraxin PTX3 modulates phagocytic activity of microglia. J Neuroimmunol 2010; 229:63-72.
21. Choi B, Lee EJ, Song DH, et al. Elevated Pentraxin 3 in bone metastatic breast cancer is correlated with osteolytic function. Oncotarget 2014; 5:481-92.
22. Alessi P, Leali D, Camozzi M, Cantelmo A, Albini A, Presta M. Anti-FGF2 approaches as a strategy to compensate resistance to anti-VEGF therapy: long-pentraxin 3 as a novel antiangiogenic FGF2-antagonist. Eur Cytokine Netw 2009; 20:225-34.
23. Margheri F, Serratì S, Lapucci A, et al. Systemic sclerosis-endothelial cell antiangiogenic pentraxin 3 and matrix metalloprotease 12 control human breast cancer tumor vascularization and development in mice. Neoplasia 2009; 11:1106-15.
24. Balsara BR, Pei J, Mitsuuchi Y, Page R, Klein-Szanto A, Wang H, Unger M, Testa JR. Frequent activation of AKT in non-small cell lung carcinomas and preneoplastic bronchial lesions. Carcinogenesis 2004; 25:2053-9.
25. Schuurbiers OC, Kaanders JH, van der Heijden HF, Dekhuijzen RP, Oyen WJ, Bussink J. The PI3-K/AKT-pathway and radiation resistance mechanisms in non-small celllung cancer. J Thorac Oncol 2009; 4:761-7.
26. Jiang Y, Cui L, Yie TA, Rom WN, Cheng H, Tchou-Wong KM. Inhibition of anchorage-independent growth and lung metastasis of A549 lung carcinoma cells by IkappaBbeta. Oncogene 2001; 20:2254-63.
27. Akca H, Demiray A, Tokgun O, Yokota J. Invasiveness and anchorage independent growth ability augmented by PTEN inactivation through the PI3K/AKT/NFkB pathway in lung cancer cells. Lung Cancer 2011; 73:302-9.
28. Fontanini G, Pingitore R, Bigini D, Vignati S, Pepe S, Ruggiero A, Macchiarini P. Growth fraction in non-small cell lung cancer estimated by proliferating cell nuclear antigen and comparison with Ki-67 labeling and DNA flow cytometry data. Am J Pathol 1992; 141:1285-90.
29. Minamoto H, Antonângelo L, da Silva AG, et al. Tumour cell and stromal features in metastatic and non-metastatic non-small cell lung carcinomas. Histopathology 2003; 43:427-43.
30. Zhang J, Xu YJ, Zhang ZX, DU CL, Qiao LF, Ni W, Chen SX. Nuclear factor-kappaB activity and its correlation with cell proliferation in non-small cell lung cancer tissues. Zhonghua Jie He He Hu Xi Za Zhi 2007; 30:771-75.
31. Andela VB, Schwarz EM, Puzas JE, O'Keefe RJ, Rosier RN. Tumor metastasis and the reciprocal regulation of prometastatic and antimetastatic factors by nuclear factor kappaB. Cancer Res 2000; 60:6557-62.

GENE EXPRESSION PROFILES IN THREE HISTOLOGIC TYPES, CLEAR-CELL, ENDOMETRIOID AND SEROUS OVARIAN CARCINOMAS

J. PAMUŁA-PIŁAT[1], T. RUBEL[2,3], I.K. RZEPECKA[4], M. OLBRYT[1], R. HEROK[1,5], A. DANSONKA-MIESZKOWSKA[4], E. GRZYBOWSKA[1] and J. KUPRYJAŃCZYK[4]

[1]Center for Translational Research and Molecular Biology of Cancer Maria Skłodowska-Curie Memorial Cancer Center and Institute of Oncology, Gliwice Branch, Poland; [2]Institute of Radioelectronics, Warsaw University of Technology, Warsaw, Poland; [3]Laboratory of Bioinformatics and Systems Biology, Maria Sklodowska-Curie Memorial Cancer Center and Institute of Oncology, Warsaw, Poland; [4]Department of Molecular Pathology, Maria Skłodowska-Curie Memorial Cancer Center and Institute of Oncology, Gliwice, Poland; [5]EURx Ltd. Gdansk, Poland

Received August 6, 2014 – Accepted December 5, 2014

Ovarian carcinoma is the most lethal type of gynecologic malignancy in the Western world. Majority of early stage ovarian cancers are asymptomatic and this is the main reason that more than two-thirds of patients are diagnosed with advanced disease. Ovarian tumors are heterogeneous and the different histologic subtypes are further classified as benign, borderline (low-grade) and malignant (high-grade) to reflect their behavior. The aim of the study was to analyze gene expression profiles in three histologic types of ovarian carcinoma in an attempt to find the molecular differences among serous, endometrioid and clear cell subtypes. The analysis of gene expression was performed on 57 samples of ovarian carcinoma. RNA was isolated from the ovarian cancer tissues. The gene expression changes were determined by microarray analysis and quantitative real time polymerase chain reaction (qRT-PCR). Measurement of relative gene expression levels was used to identify molecular differences among three histologic types of ovarian carcinoma (clear-cell, endometrioid and serous). Unsupervised statistical analysis revealed four biological subtypes among three histotypes under study. The endometrioid ovarian carcinoma was divided into two molecular subtypes. The biggest molecular differences were observed between clear-cell and serous carcinomas (1070 genes, FDR 0.05), the smallest between endometrioid and serous carcinomas (81 genes, FDR 0.05). The biggest group of differentially expressed genes was involved in transport and metabolism. This finding can explain the differences in the response to chemotherapy observed among different histologic types of ovarian carcinomas. In conclusion, we found TCF2 (HNF1B) gene as a suitable marker for ovarian clear cell carcinoma. Gene expression profiling also shed light on the molecular mechanisms of different chemoresistance among the analyzed histotypes.

Ovarian carcinoma is the most lethal type of gynecologic malignancy in the Western world. In Poland it is the fifth leading malignancy diagnosed in women and the seventh leading cause of cancer

Key words: gene expression, ovarian cancer, adhesion, motility, invasion, TCF2 (HNF1B), WT1, COL, IGF, HLA, ABC, SLC genes

Mailing address: Prof. E. Grzybowska,
Center for Translational Research and Molecular Biology of Cancer,
Maria Skłodowska-Curie Memorial Cancer Center
and Institute of Oncology, Gliwice Branch, PL 44-101 Gliwice,
ul. Wybrzeże Armii Krajowej 15 44-101 Gliwice, Poland
tel. +48 32 2789762 fax. +48 32 2313512
e-mail: ewagrzybowska@yahoo.com

0393-974X (2014)

mortality in women (1). The majority of early stage ovarian cancers are asymptomatic and this is the main reason that more than two-thirds of patients are diagnosed with advanced disease. Ovarian tumors are heterogeneous and the different histologic subtypes are further classified as benign, borderline (low-grade) and malignant (high-grade) to reflect their behavior. Serous carcinomas account for about 50% of all epithelial ovarian carcinomas (EOC); endometrioid carcinomas comprise about 25% of EOC; clear-cell and mucinous adenocarcinomas are less frequent, each accounting for less than 10% of all EOC (2).

Ten to fifteen percent of ovarian carcinomas are diagnosed in the carriers of germline mutations in *BRCA1/2* genes. It was found (3, 4) that tumors associated with *BRCA1* and *BRCA2* genes displayed distinct gene expression profiles and that the genes responsible for this distinction segregated sporadic tumors into either "BRCA1-like or BRCA2-like" phenotypes. Loss of *BRCA1* or *BRCA2* function is a later event than *TP53* mutation (5).

Despite the significant progress we have witnessed during the last decade, the mechanisms of tumorigenesis in the ovary are largely unknown. Two major ways of ovarian cancer development have been described (6). Ovarian carcinomas may develop from preexisting benign or borderline tumors of various histological types (including serous cysts and endometriosis). On the other hand, they develop *de novo* from the ovarian surface epithelium or its derivatives. Recently, a concept of serous cancer development from tubal epithelium adhesive to the ovary has been presented (7). The first route leads predominantly to formation of well or moderately differentiated carcinomas, while the other two to poorly differentiated carcinomas. The differences in tumor grade may be determined by underlying molecular changes, among which several have been already identified. Among alterations that have been found in less differentiated carcinomas are *TP53* mutations (in 80-100% of poorly differentiated/ undifferentiated tumors), various mechanisms of BRCA1/2 dysfunction (in nearly 80% of ovarian carcinomas) (4), LOH at *RB* locus (in about 60% of carcinomas), and amplification of *PI3KCA* gene (in about 24% of ovarian carcinomas) (8). Among molecular lesions found in better differentiated carcinomas are the mutations in *KRAS, PTEN, PI3K* and beta-catenin genes, and their frequency is largely determined by the histological type.

The application of DNA microarray technology has enabled the analysis of the whole transcriptome from one cancer tissue sample. It allowed to find molecular signatures for different cancers which revealed the presence of several molecular subtypes which differed in the outcome of disease. Microarray-based profiling technologies have provided an opportunity to simultaneously examine the relationship between thousands of genes and clinical phenotypes (9).

In this study we analyzed gene expression profiles in three histologic types of ovarian carcinoma (serous, endometrioid and clear-cell carcinoma) in order to find the molecular subtypes of ovarian carcinoma and the genes that are characteristically deregulated in different histologic types of ovarian cancer among thousands of normally expressed genes.

MATERIALS AND METHODS

Tissue specimens

Ovarian cancer specimens were obtained from patients during the initial surgical treatment prior to chemotherapy. Tumor fragments (1-10, depending on the tumor size), were snap-frozen and stored at -72°C until further use. Histological evaluation of the group of 110 tumors and over 300 of their fragments was performed to control the relative content of non-tumor tissue. Cryostat sections were prepared from different fragments of each tumor. Upper and lower sections from each cryosection collection were evaluated by the pathologist (JK), and the rest of tissue material was used for DNA microarray analysis if it contained up to 10% of stromal cell fraction (range: <1% -10%, median 1%, see Table I). For qRT-PCR validation analysis, the cryosections contained up to 30% of stromal cell fraction (range: <1% - 30%, median 5%, see Table IA). Altogether, we analyzed 57 carcinomas: 28 were selected for cDNA microarray analyses and 29 were collected for independent validation. The study was approved by the Bioethics Committee at the Maria Skłodowska-Curie Memorial Institute of Oncology in Warsaw, Poland.

The tumors were classified according to the criteria set by the World Health Organization (10). Altogether, there were 22 serous, 18 endometrioid and 17 clear-cell carcinomas. Histological grade was evaluated on a

4-grade scale according to Broders' criteria (11) by using one of the sections taken for the microarray analysis. Two tumors were well differentiated (G1, 3.4%), 19 showed moderate differentiation (G2, 32.8%), 28 were poorly differentiated (G3, 50%), and 8 were mostly or completely undifferentiated (G4, 13.8%). Evaluation of poorly differentiated carcinomas as endometrioid ones was based on the presence of areas typical of the endometrioid type in other tumor sections, including foci of abortive squamous metaplasia. The tumors were staged according to the criteria set by the International Federation of Gynecologists and Obstetricians (FIGO). Sixteen tumors (28%) were in stage I; 6 (10.2%) were in stage II; 32 were in stage III (56.1%) and 3 (5.3%) were in stage IV.

All tumors were characterized with reference to the *TP53* mutational status and p53 immunohistochemical accumulation. Six exons in *TP53* gene were examined by a sequencing method. For 28 samples chosen for microarray analysis, BRCA1 mutation status was evaluated. Clinical and molecular characteristics of the tumor samples analyzed in this study are presented in Tables I and IA.

RNA isolation

The RNA was isolated from 63 frozen samples of ovarian cancer tissues (Tables I and IA). Frozen tissues were homogenized in RLT buffer (Qiagen). Total RNA was extracted using RNeasy Mini Kit (Qiagen) according to the manufacturer's protocol including digestion step with DNAse I. Yield quality was estimated using the ND-1000 Spectrophotometer (NanoDrop Technologies). RNA quality was controlled by microcapillary electrophoresis measurements in the Agilent 2100 Bioanalyser using the RNA 6000 Nano LabChip Kit, and analyzed with RNA Integrity Number software (Agilent). The probes with high efficiency of RNA isolation were chosen to microarray analyses and qRT-PCR (Tables I and IA). Four from sixty-three RNA isolated samples were not qualified for the analyses because of low efficiency or RNA degradation (low RNA Integrity Number). Two tissue samples were not isolated because of unclear histological type description (Table I).

Microarray data analysis

Amplification and hybridization were performed according to the protocols recommended by Affymetrix, using 8 mg of total RNA as a template. Double-strand cDNA was synthesized with Reverse Transcriptase II (Invitrogen). Half of the volume of cDNA was used for the synthesis of biotynylated cRNA using BioArray High Yield RNA Transcript Labeling Kit (Enzo Life Sciences). Fragmented cRNA was hybridized first to Affymetrix control Test3 microarray and then, after evaluation of the sample quality, to the Human Genome U133 Plus 2.0 Gene Chip array (containing »47.000 transcripts) (Affymetrix) for 16 h at 45°C. After washing and staining, arrays were scanned with GeneChip Scanner 3000 (Affymetrix).

The probe set data were generated with MAS 5.0 software (Affymetrix). Hybridization signals obtained from different microarrays were pre-processed and normalized with Robust Multi-Array Analysis (RMA) algorithm implemented in the R/BioConductor package (*affy*), and the signal intensities were transformed to a logarithmic scale (base 2). Probe sets exhibiting signal intensities below a preselected threshold in more than 75% of samples were filtered out. The threshold value was established as the 98th percentile of the expression levels detected in Y-chromosome-linked probe sets. The total number of remaining probe sets after the filtration step was 27387. To select differentially expressed genes, the *t*-test (for pairwise comparisons) and ANOVA (to compare all histotypes) were employed. The resulting *p*-values were adjusted for multiple hypothesis testing by the Benjamini-Hochberg procedure in order to control the false discovery rate (FDR). Only probe sets with adjusted *p*-values $\leq$ 0.05 and fold change (FC) values $\geq$ 2.0 were considered as significantly changed. Hierarchical clustering with Pearson's correlation coefficient as the distance metric and principal component analysis (PCA) were used to evaluate the relationship between three histological types of ovarian cancer. Before clustering and PCA, the expression levels of each gene were standardized by subtracting the mean value and dividing by the standard deviation. The statistical analysis was performed using proprietary software working in MATLAB environment (MStat, available at http://proteom.ibb.waw.pl/mstat). One sample of ovarian cancer was eliminated from the statistical analysis because of significant differences in gene expression between the examined molecular histological subtypes of ovarian cancer.

qRT-PCR validation of microarray data

Nineteen genes were selected to confirm microarray data. The validity of gene expression was verified by qRT-PCR. Quantitative PCR was preformed using Chromo4^{TM}System (software Opticon Monitor-BioRad) according to the manufacturer's recommendation. cDNA was synthesized using 0.7 mg total RNA and iScript Reverse Transcriptase (BioRad) using Eppendorf Mastercycler S (Hamburg, Germany). The real–time PCR assays were conducted using an iQSYBR Green Supermix (BioRad). The temperature profile was as follows: initial denaturation at 95°C for 4 min., followed by 55 cycles at 95°C/56°C/72°C for 30 s, and a final extension step at 72°C for 5 min. All PCR reactions were repeated three times and average values were taken to analysis. All results were normalized to the expression

of reference genes such as glyceraldehyde-3-phosphate dehydrogenase (*GAPDH*), β-actin (*ACTB*) and ribosomal protein L41 (*RPL41*). The comparative threshold cycle (C_T) method was used to assess relative quantitation of three histologic types of ovarian cancer. Data analyses were performed using the 2^{-DDCT} (Pfaffl method) with *ACTB* as a reference gene. Primers were designed with *Primer3* freeware available at http://frodo.wi.mit.edu/cgi-in/primer3/primer3. Sequences of the primers are available upon request.

The data discussed in this publication have been deposited in NCBI's Gene Expression Omnibus (Edgar et al., 2002) and are accessible through GEO Series accession number GSE63885 (http://www.ncbi.nlm.nih.gov/geo/query/acc.cgi?acc=GSE63885.

RESULTS

Comparison of all histotypes

Microarray analysis was carried out to compare gene expression in 28 samples of ovarian carcinoma, including three distinct histotypes: clear-cell, endometrioid and serous carcinoma. The analysis was carried out to find out whether morphological features which enabled to distinguish the histotypes corresponded with biologic differences found among them. Supervised ANOVA-based analysis of all histotypes under study showed significant differences in expression for 1469 genes (FDR=0.05, FC≥2.0). Principal Component Analysis (PCA) and Hierarchical Clustering (HC) performed on the set of differentially expressed genes revealed four distinct groups among three histotypes under study, regardless of the tumor grade (Figs. 1 and 2). The analysis showed that the endometrioid carcinoma can be divided into two clusters. One of them was very similar to serous carcinoma and in PCA analysis it localized closely to this histotype.

Hierarchical clustering analysis carried out at FDR 1% also revealed two subtypes of endometrioid carcinoma. The same analysis carried out at more stringent conditions (FDR 0.1%) showed only three main histologic types (Fig. 3).

The most frequently represented genes belonged to the groups involved in metabolism, signal transduction, transcription and transport (Table II). We observed deregulated expression of genes involved in energy metabolism belonging to insulin-like growth factor system (*GBA3*-glucosidase; *RXFP1* - relaxin/insulin-like family peptide receptor 1; *FOXO1A* - forkhead box O1A; *IGFBP1* - insulin-like growth factor binding protein 1; *IGF2BP3* - insulin-like growth factor mRNA binding protein3 (acting as tumor suppressor in breast, prostate, lung and colon cancers); *IGF1* - insulin-like growth factor1; *GRB10* - growth factor receptor-bound protein 10; *DOK5* - docking protein 5; *STXBP4* - syntaxin binding protein 4; *DOK7* - docking protein 7; *PIK3R3* - phosphoinositide-3-kinase, regulatory subunit 3; and *IGF2*- insulin-like growth factor 2). IGF axis can be of importance for the therapy of cisplatin-resistant ovarian carcinomas. Also, 5 different HLA genes (*HLA-DRA, HLA-DRB1, HLA-DQB1, HLA-DMA* and *HLA-DMB*) were differentially expressed in the studied ovarian cancer histotypes.

Comparison of clear-cell carcinoma vs serous and endometrioid carcinoma

Histotypes under study were also compared pairwise (Fig. 4). When clear-cell carcinoma subset was compared to the rest of the histotypes, two distinct subgroups of tumors emerged in non-supervised clustering. Seven hundred and fifty-four genes were found to be differentially expressed at FDR=0.05.

The differences in *ESR1* expression were the most significant in comparisons between clear-cell carcinoma *vs* other histotypes. It was downregulated in clear-cell carcinoma (FC=0.038). The same trend was observed for *PGR* gene (FC=0.227), however, the gene is at the bottom of the list of significantly differentially expressed genes. *TCF2* (*HNF1B)* (potential marker of clear-cell carcinoma) was upregulated in this histotype (FC=3.76).

The differences in expression were also found for *TCF3* (FC=0.47) and *TCF7L2* (FC=0.33) genes which encode transcription factors that influence glucose metabolism and regulate the expression of immunoglobulin genes. Both genes were downregulated in clear-cell carcinoma.

A significant upregulation of *ABCC3* gene (FC=4.25) was also noted in this comparison, as well as in other ones. The gene, which belongs to the family of ABC transporters, encodes cystic fibrosis transmembrane regulator as canalicular multispecific organic anion transporter. This protein is a member

Table I. *Characteristics of histological subtypes of ovarian cancer studied.*

Sample No.	Histologic type	% of stroma	Grade	FIGO	Status of BRCA1 mutation	Status of p53 mutation	p53 accumulation
94	CC	3	3	IC	0	0	0
199	CC	5	3	IIC	0	0	0
208	CC	1	2	IC	ND	0	0
285	CC	3	2	IIIC	ND	1	1
304	CC	1	3	IIIC	ND	1	1
339	CC	5	2	IIB	0	0	0
365	CC	5	3	IIIC	ND	1	0
445	CC	1	4	IA	ND	ND	0
456	CC	1	3	IIA	ND	ND	0
153	**E**	**2**	**2**	**IA**	**0**	**0**	**0**
159	E	3	1	IC	1	0	0
165	**E**	**1**	**4**	**IIIC**	**0**	**1**	**1**
169	E	3	3	IC	ND	0	0
179	E	<1	4	IB	0	1	1
193	**E**	**10**	**4**	**IA**	**0**	**0**	**1**
254	E	<1	4	IIIB	0	1	1
309	**E**	**2**	**4**	**IIIC**	**1**	**0**	**0**
428	E	ND	4	IIIC	0	1	0
436	E	5	2	IA	0	ND	1
444	E	2	2	IC	0	ND	0
605	**E/S**	**1**	**3**	**IIIC**	**0**	**1**	**1**
609	E	<5	3	IIIC	0	1	1
188BT	E	1	1	IA	0	0	0
188CA	E	1	1	IA	0	0	0
602	**E/CC**	**ND**	**3**	**IIIC**	**1**	**1**	**1**
314	S	10	3	IIIC	0	1	1
316	S	<2	3	IIIB	0	1	1
328	S	5	3	IIIA	1	1	0
331	S	1	4	IIIC	1	1	0
340	S	<1	3	IIIC	0	0	0
351	S	5	3	IIIC	1	1	1
352	S	1	4	IIIC	0	1	0
353	S	<1	2	IIIC	0	0	0
369	S	5	3	IIIC	0	1	1
360	S	5	3	IIIC	0	1	0

Samples marked in bold were eliminated form microarray analysis because of low yields of RNA or RNA degradation (low RNA Integrity Number). CC: clear-cell ovarian cancer; E denotes endometrioid ovarian cancer; S: serous ovarian cancer; ND: no data.

of the multidrug resistance-associated protein (MRP) subfamily which is involved in multi-drug resistance and may play a role in the transport of biliary and intestinal excretion of organic anions.

We also found differentially expressed genes which belong to the CYP and SLC gene families. Among them were *CYP2C18* (FC=6.54) and *CYP2C9* (FC=5.11), both upregulated in clear-cell carcinoma. The cytochrome P450 proteins are monooxygenases which catalyze many reactions involved in drug metabolism and synthesis of lipids. The enzymes are known to metabolize many xenobiotics.

The expression differences were observed in the genes from SLC family (*SLC16A3* (FC=2.65),

Table IA. *Characteristics of additional ovarian tissue samples used for validation of microarray results by qRT–PCR.*

Sample No.	Histologic type	% of stroma	Grade	FIGO
507	CC	1	2	IIIC
549	CC	1	2	IIIC
566	CC	8	3	IIA
635	CC	1	2	IC
564	CC	3	2	IIIC
544	CC	30	2	IA
529	CC	1	2	BD
514	CC	8	2	IA
511	E	1	3	IIIC
555	E	1	2	IIIC
565	E	1	4	IIIC
567	E	1	2	IB
642	E	1	2	BD
546	E	5	2	IIIC
309	E	2	4	IIIC
472	E	5	3	IIB
543	E	10	3	IB
562	E	20	2	IA
610	S	5	3	IIIA
197	S	5	3	IIIC
206	S	10-12	3	IIIC
300	S	2	3	IIIC
319	S	8	3	IV
382	S	2	3	IIIC
389	S	10	3	IV
398	S	10	3	IIIC
322	S	8	3	IIB
415	S	8	3	IV
547	S/CC	5	2	IIIC

CC: clear-cell ovarian carcinoma; E: d endometrioid ovarian carcinoma: S: serous ovarian carcinoma; ND: no data.

SLC25A15 (FC=6.03), *SLC25A30* (FC=2.4), *SLC35F5* (FC=4), *SLC1A3* (FC=4.95), *SLC7A2* (FC=4.2), *SLC8A1* (FC=4.71), *SLC15A2* (FC=0,.6), *SLC16A9* (FC=0.14), *SLC26A7* (FC=0.22), *SLC27A6* (FC=0.18), *SLC9A3R1* (FC=0.46) and *SLC5A3* (FC=0,.49).

Comparison of clear-cell carcinoma vs serous carcinoma

The most pronounced biological differences were found, regardless of the grade, between clear-cell and serous carcinomas. Differential expression of 1070 genes distinguished both histotypes at FDR=0.05. Among them were homeobox family upregulated genes (*HOXA1* (FC=2.49), *HOXA2* (FC=13.42) located on 7p15 chromosome, *HOXB6* (FC=7.8), *HOXB7* (FC=4.81) and *HOXB8* (FC=8.06) located on chromosome 17q22), which are not expressed in normal ovarian surface epithelium. They are typically found in an organized cluster. They were upregulated in serous carcinoma as opposed to clear-cell carcinoma.

Table II. *Statistical analyses of molecular differences among studied ovarian cancer histotypes.*

Statistical analysis of biologic differences among ovarian cancer histotypes	FDR	No of significantly expressed genes, FC>2
All histotypes	0.05	1469
	0.01	690
	0.001	170
Clear-cell carcinoma *vs* serous and endometrioid carcinoma	0.05	754
	0.01	260
Clear-cell carcinoma *vs* serous carcinoma	0.05	1070
	0.01	290
Clear-cell carcinoma *vs* endometrioid carcinoma	0.05	200
	0.01	35
Serous carcinoma *vs* endometrioid carcinoma	0.05	81
	0.01	9
Endometrioid carcinoma 1 *vs* endometrioid carcinoma 2	0.01	87

Statistical significance of probesets was analyzed using t-test and Whitney-Mann U-test. FDR: False Discovery Rates (%); FC: Fold-Change.

We also found differentially expressed genes which enable tumor cells to disseminate, connected with motility, invasion and adhesion. There were 10 genes belonging to collagen family (*COL8A1* (FC=0.11), *COL4A1* (FC=2.55), *COL4A3BP* (FC=3.95), *COL16A1* (FC=0.32), *COL4A2* FC=2.72), *COL27A1* (FC=2.14), *COL8A2* (FC=0.26), *COL10A1* (FC=0.32), *COL12A1* (FC=0.26), *COL1A1* (FC=0.38)), and collagenase *MMP2* (FC=0.42), laminin *LAMC1* (FC=3.27), fibronectin *FNDC3B* (FC=2.41), integrins *ITGA7* (FC=0.38), *ACTN1* (FC=0.45), *VAV3* (FC=6.57) and four kallikreins (*KLK11* (FC=0.1), *KLK7* (FC=0.125), *KLK10* (FC=0.12), *KLK5* (FC=0.12)) which degrade matrix components.

Three differentially expressed genes: *WT1* (FC=0.079), *WIT1* (FC=0.29) and *DIRC2* (FC=2.29) had been earlier recognized in renal carcinoma, especially the tumor suppressor gene *WT1*. There were also fourteen genes connected with functioning of the nervous system: *NPAS3* (FC=0.07), *NET1* (FC=0.32), *ST6GALNAC5* (FC=0.053), *SYNCRIP* (FC=0.44), *PTN* (FC=0.097), *MYEF2* (FC=0.44), SYT12 (FC=0.49), *SCHIP1* (FC=3.16), *AUTS2* (FC=0.28), *OPTN* (FC=0.44), *PVR* (FC=3.42), *HN1* (FC=2.19) and *MCPH1* (FC=2.68).

Comparison of clear-cell carcinoma vs endometrioid carcinoma

Five-fold less differences were found between clear-cell and endometrioid carcinoma, where only 200 genes were differentially expressed at FDR=0.05.

Among differentially expressed genes, some of them had been found earlier to be important in carcinogenesis, having tumor suppressor or putative tumor suppressor status. Among these differentially expressed genes are: *ANXA4* (FC=4.42) which belongs to annexin family of calcium-dependent phospholipid binding proteins; *MUC16* gene (downregulated, FC=0.12) which encodes CA125 antigen, the only routine biomarker in ovarian cancer screening and monitoring of disease progression); *KLK11* (FC=0.067) belonging to the family of kallikreins, a subgroup of serine proteases having diverse physiological functions; *PBX1* (FC=0.37) regulating expression of valosin-containing protein involved in cancer growth

Table III. *Gene ontology classification of genes from statistical analysis in respect to biological processes (FDR 1%).*

Biological process	No. of genes (%)
Transport	126 (18.26)
Transcription	88 (12.75)
Metabolism	87 (12.60)
Signal transduction	86 (12.46)
Adhesion	40 (5.79)
Cell proliferation	37 (5.36)
Apoptosis	32 (4.63)
Proteolysis	23 (3.33)
Cell cycle regulation	22 (3.18)
Immune response	15 (2.17)
Cell growth regulation	8 (1.16)
Angiogenesis	6 (0.86)
Function unknown	120 (17.39)

as negative regulator of transcription, linked mainly to leukemias; *NET1* oncogene (FC=0.45) [downregulated in clear cellcarcinoma (CCC)], expressed also in human hepatocellular carcinoma and having a role in promotion of invasion and proliferation, key phenotypic hallmarks of cancer cells; *NFIL3* (FC=3.42) downregulated (following irradiation) in ovarian carcinoma; for two commonly co-expressed receptors, *EGFR* and *HER2,* differential overexpression (earlier reported for ovarian cancer) was found to be significant only for EGFR (FC=0.49) *DAPK1* (FC=2.47), a death-associated protein kinase 1, a positive mediator of gamma-interferon-induced programmed cell death; *DOCK8* (FC=3.7), the downregulation of which was observed in lung cancer; *RHOF* (FC=3.29) involved in the regulation of cytoskeleton and found

Table IV. *ANOVA analysis of qRT-PCR validation of microarray data.*

	Ist series of samples			IInd series of samples			Ist and IInd series of samples		
Gene	df	F	p	df	F	P	df	F	p
ABCC3	25	8,40161	0.001619	23	4,42890	0.023599	51	4.44324	0.016640
ANXA4	25	19,41615	0.000008	23	21,46181	0.000006	51	42.93458	0.000000
ARHGAP2	25	13,19472	0.000123	23	10.01888	0.000742	51	22.53429	0.000000
BBOX	25	17,98502	0.000014	23	8,96883	0.001320	51	26.83253	0.000000
CCNYL	*25*	*2,12184*	*0,140880*	*22*	*0,66485*	*0.524385*	50	1.24856	0.295708
ESR1	26	26.73868	0.000000	23	28.65034	0.000001	52	56.39660	0.000000
EYA2	24	26.51666	0.000001	23	13,12322	0.000158	50	37.37034	0.000000
FREM2	25	10.12734	0.000600	22	9.11273	0.001310	50	15.54200	0.000006
GAS6	25	14.16779	0.000077	*23*	*1.24877*	*0.305589*	51	9.95253	0.000224
KLK11	26	17.06452	0.000018	*23*	*1,68512*	*0.207520*	52	12.42335	0.000039
LAMC1	25	7.09231	0.003633	23	11.10175	0.000422	51	16,98709	0.000002
MUC16	26	12.65035	0.000146	23	6.79403	0.004803	52	19.14883	0.000001
NET1	25	4.65769	0.019083	23	5.06455	0.015047	51	8.84344	0.000504
OCC1	25	8.69122	0.001363	23	5.11267	0.014554	51	14.16391	0.000013
PGR	26	21.78120	0.000003	23	7.38337	0.003335	52	26.40348	0.000000
PTHLH	25	6.78113	0.004438	23	10.74629	0.000506	51	16,.2234	0.000003
SLC35F5	25	14.16219	0.000077	23	10.45551	0.000589	51	24.01382	0.000000
TCF2	25	15.89603	0.000035	23	19.68726	0.000010	51	37.11465	0.000000
WT1	26	16.92847	0.000020	23	7.11618	0.003929	52	21.56812	0.000000
ACTB	*26*	*0.12395*	*0.883945*	23	1.02437	0.374829	52	0.19969	0.819612
GAPDH	*26*	*0.69762*	*0.506850*	0			29	0.82327	0.448994
RPL41	*25*	*1.59568*	*0.222742*				25	1.59568	0.222742

The validity of gene expression was verified by qRT-PCR. Ist series of samples - the same samples which were analyzed with microarray GeneChip method; IInd series of samples - samples taken to verify the results of the Ist series of samples; df: degree of freedom; F: F-distribution; p: P value.

Table V. *Comparison of gene expression differences between studied histotypes analyzed by microarray genechip method and qRT-PCR.*

Gene	Comparison of histologic types	FC value		
		Microarray analysis	qRT-PCR 1	qRT-PCR 2
ABCC3	CC *vs* S	4.179	3.60	2.44
	CC *vs* E	-	10.12	3.20
	S *vs* E	-	2.81	1.31
ANXA4	CC *vs* S	5.805	10.31	10.15
	CC *vs* E	4.419	6.04	6.12
	S *vs* E	-	0.59	0.60
ARHGAP26	CC *vs* S	0.194	0.35	0.27
	CC *vs* E	0.164	0.12	0.23
	S *vs* E	-	0.34	0.88
BBOX1	CC *vs* S	0.065	0.01	0.01
	CC *vs* E	-	0.05	0.07
	S *vs* E	4.082	3.72	5,38
CCNYL1	CC *vs* S	5.117	1.74	0,80
	CC *vs* E	-	1.52	1,16
	S *vs* E	-	0.87	1.46
ESR1	CC *vs* S	0.043	0.05	0.07
	CC *vs* E	0.033	0.03	0.03
	S *vs* E	-	0.54	0,44
EYA2	CC *vs* S	0.115	0.06	0.06
	CC *vs* E	0.062	0.03	0.06
	S *vs* E	-	0.42	1.01
FREM2	CC *vs* S	20.564	37.30	22.21
	CC *vs* E	-	0.74	7.11
	S *vs* E	-	0.02	0.32
GAS6	CC *vs* S	0.281	0.31	0.48
	CC *vs* E	-	0.89	1.02
	S *vs* E	2.88	2.88	2.12
KLK11	CC *vs* S	0.108	0.06	0.20
	CC *vs* E	0.067	0.04	0.25
	S *vs* E	-	0.56	1.29
LAMC1	CC *vs* S	3.271	3.15	1.91
	CC *vs* E	2.461	3.35	2.59
	S *vs* E	-	1.06	1.35
MUC16	CC *vs* S	0.093	0.08	0.08
	CC *vs* E	0.122	0.16	0.28
	S *vs* E	-	1.95	3.67
NET1	CC *vs* S	0.333	0.40	0.44
	CC *vs* E	0.447	0.59	0.44
	S *vs* E	-	1.48	1.01
OCC-1	CC *vs* S	8,492	6.64	4.85
	CC *vs* E	-	3.64	2.53
	S *vs* E	-	0.55	0.52
PGR	CC *vs* S	-	0.60	0.60
	CC *vs* E	0.123	0.05	0.14
	S *vs* E	5.959	0.08	0.23
PTHLH	CC *vs* S	72.325	11.63	17.09
	CC *vs* E	-	10.53	16.54
	S *vs* E	3.52	0.91	0.97
SLC35F	CC *vs* S	4.503	6.0	2.94
	CC *vs* E	-	2.97	3.28
	S *vs* E	-	0.46	1.12
TCF2	CC *vs* S	3.959	161.28	157.83
	CC *vs* E	3.549	38.03	34.09
	S *vs* E	-	0.24	0.22
WT1	CC *vs* S	0.053	0.05	0.12
	CC *vs* E	-	0.33	0.92
	S *vs* E	-	6.08	7.77

The genes for validation were chosen from the list of genes where all three histotypes were compared at FDR<0.001. Not all of them were significant in the lists of pair comparisons. CC: clear-cell carcinoma; E: endometrioid carcinoma; S: serous carcinoma; FC: Fold Change.

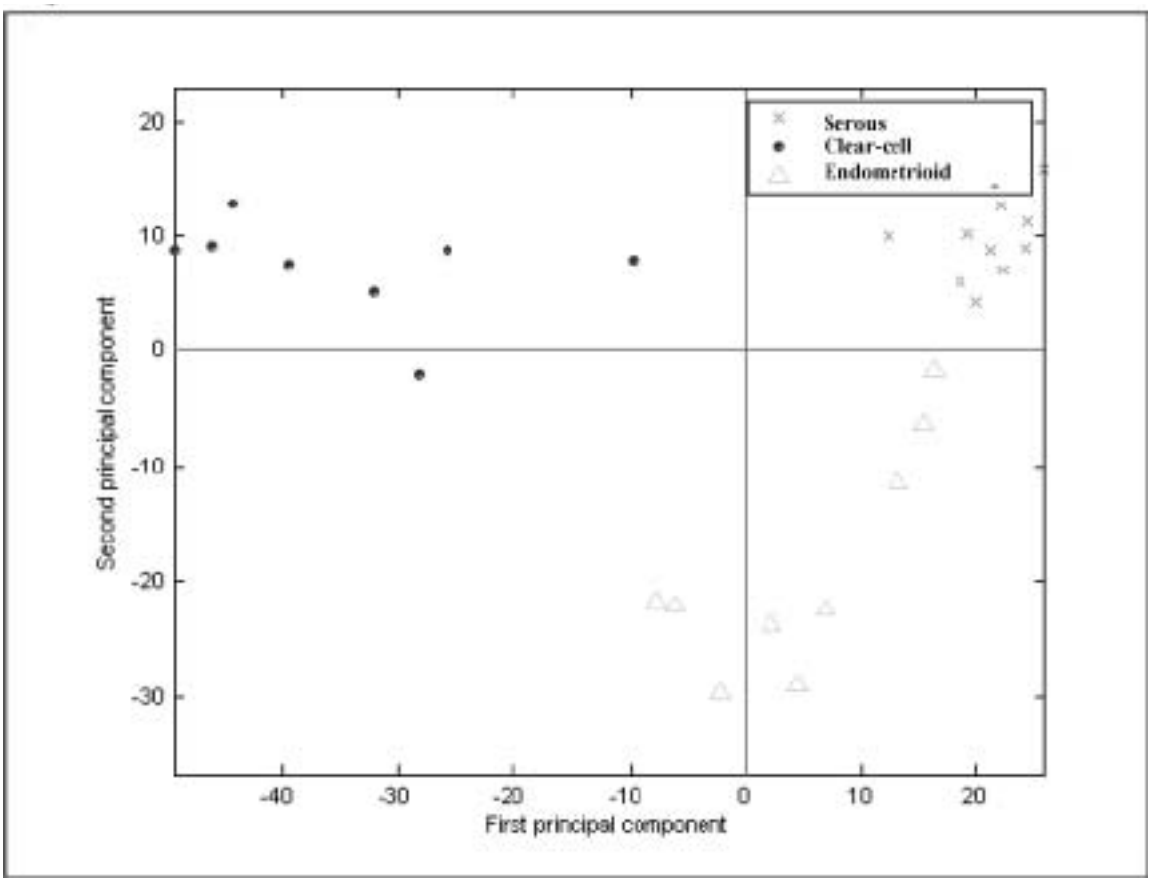

Fig. 1. *Principal Component Analysis (PCA) of three studied histotypes at FDR≤ 0.05. The first two principal components were computed from 1469 probe sets discriminating 9 endometrioid (triangles Δ), 11 serous (x) and 8 clear-cell carcinoma (circles o) histologic subtypes.*

to be upregulated in follicular lymphomas; *PDCD4* (FC=0.41) encoding a protein localized to the nucleus of proliferating cells and the expression of which is modulated by cytokines in natural killer and T cells; *FGFR3* (FC=7.44), a member of the FGFR family of receptor tyrosine kinases, implicated in diverse biological processes, including cell proliferation, differentiation, survival, and tumorigenesis; finally, *PTTG1IP* (FC=2.44) encoding a protein which directly binds to pituitary tumor-transforming gene 1 protein (*PTTG1*), facilitating nuclear translocation of PTTG1 and potentation of the transcriptional activation of basic fibroblast growth factor by PTTG1.

Comparison of serous carcinoma vs endometrioid carcinoma

The least pronounced biologic differences were observed between serous and endometrioid carcinoma. Only 81 genes were differentially expressed at FDR=0.05. However, few genes which are already known to be connected with ovarian carcinogenesis were differentially expressed in both histotypes. The most important among them was *PGR* (FC=5.95). Another differentially expressed gene was *MUC5AC* (FC=0.46) which has a function of extracellular matrix structural constituent. *ABCA3* (FC=0.38) belongs to ATP-binding cassette (ABC) transporters. The full transporter encoded by this gene may be involved in the development of resistance to xenobiotics and engulfment during programmed cell death. *CEACAM1* gene (FC=4.43) was described as upregulated in endometrioid carcinomas. The same was observed in our analysis. The gene belongs to the immunoglobulin superfamily. It is a transmembrane glycoprotein that

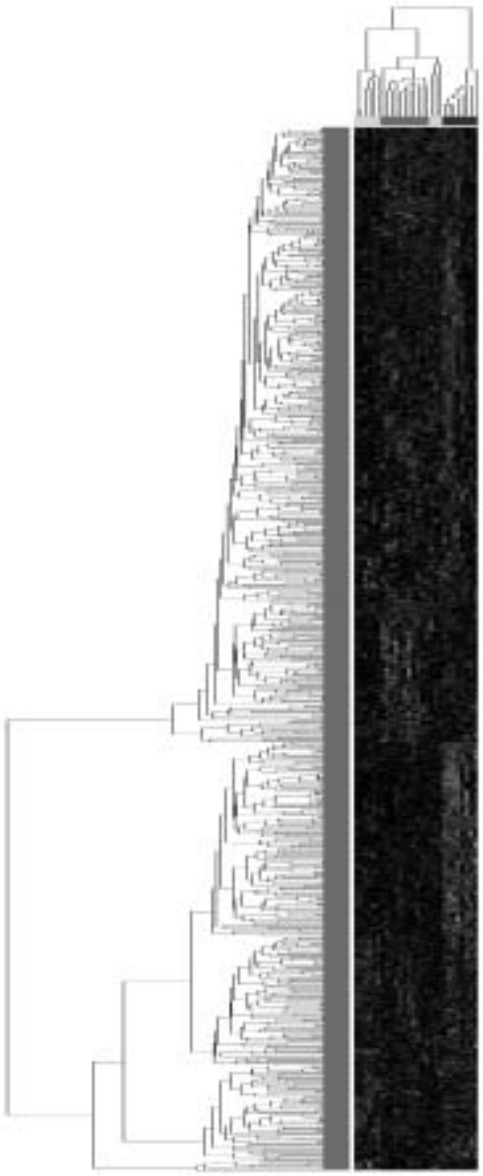

Fig. 2. *Hierarchical clustering analysis of three studied histotypes at FDR≤0.01. Hierarchical clustering of gene expression data revealed a relationship between the three histotypes studied. Color in each cell reflects expression level of the corresponding probe set in the array sample relative to its mean expression level estimated for the entire set of samples. Grey indicates expression levels greater than the mean, light grey indicates expression levels lower than the mean; black denotes no change in expression level. The analysis clusters clear-cell (black) carcinoma samples on one side and serous (grey) and endometrioid (light grey) carcinomas on the other side. The analysis reveals also two molecular subtypes of endometrioid carcinoma which localize on both sides of serous carcinoma histotype.*

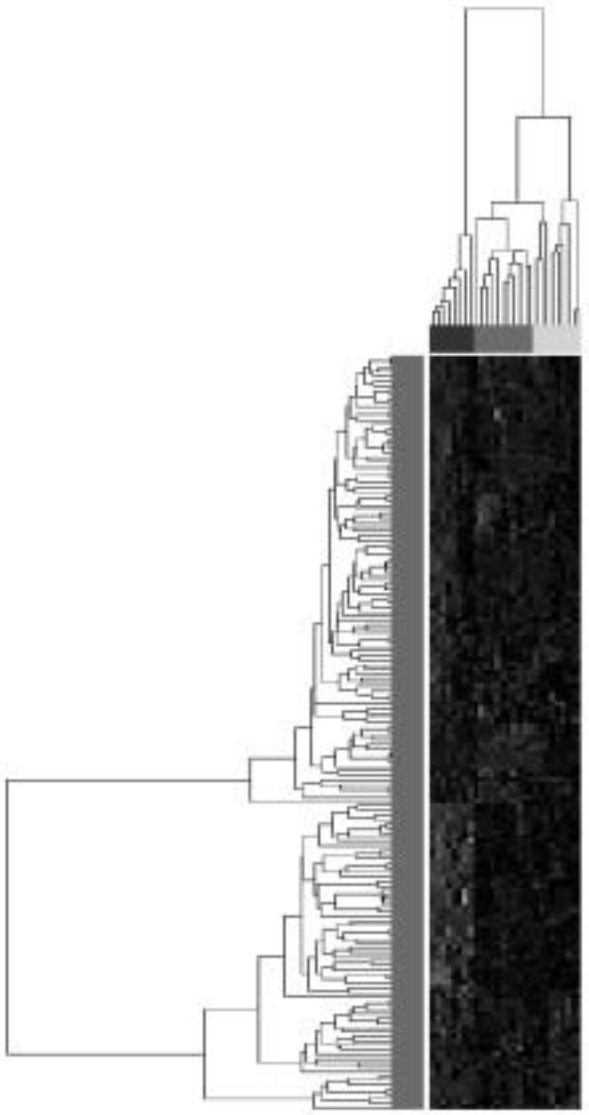

Fig. 3. *Hierarchical clustering (HC) analysis of three studied histotypes at FDR≤ 0.001 performed on 170 probe sets discriminating 8 clear-cell (black), 11 serous (grey) and 9 endometrioid (light grey) carcinoma samples*

mediates homophilic intercellular growth, immune cell activation and tissue morphogenesis. It is a putative tumor suppressor. Overexpression of *TGFα* (FC=3.15) was observed in endometrioid carcinoma and is related to the biological aggressiveness of breast cancer. *SERPINA1* (FC=5.03) has an invasion-promoting effect in anaplastic large cell lymphoma. *ITGA7* (FC=0.47) regulates cell growth and proliferation. Mutations in this gene are associated

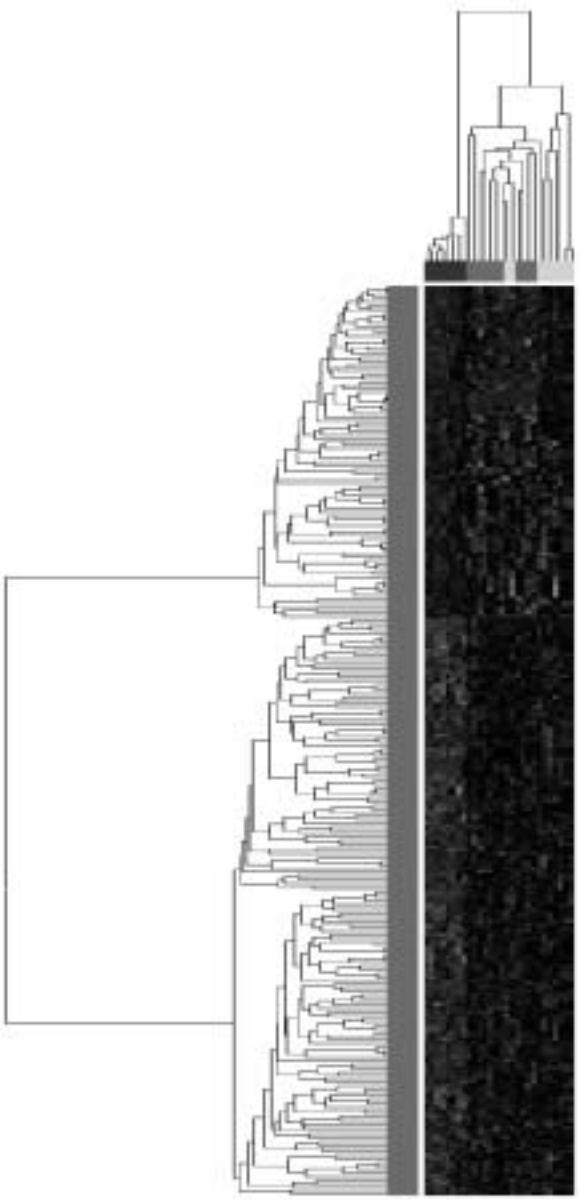

Fig. 4. *Pair-wise hierarchical clustering analysis of clear-cell vs endometrioid or serous carcinomas at FDR≤0.05 performed on 754 probe sets discriminating 8 clear-cell (black) carcinoma samples from 20 serous (grey) and endometrioid (light grey) carcinoma samples.*

with prostate, liver cancer, glioblastoma multiforme and leiomyosarcoma.

Subclasses of endometrioid carcinoma

Nine samples of endometrioid carcinoma were divided by unsupervised statistical analysis into two subgroups consisting of 3 and 6 samples. Three samples belonging to one subgroup were of high grade (4), had no germline mutation in *BRCA1* gene. Two of them had somatic mutation in *TP53* gene which resulted in the accumulation of p53 protein in ovarian cancer cell. Significance Analysis of Microarrays (SAM) method was applied for the statistical analysis of these subgroups, and revealed 87 genes which were differentially expressed at FDR=0.1 (12). Among them there were the following genes: *SALL1* (FC=0.029), a zinc finger transcriptional repressor, a part of the NuRD histone deacetylase complex (HDAC) connected with gonad development; *TFF3* (FC=0.01) encoding stable secretory proteins expressed in gastrointestinal mucosa, connected with defense response; *UVRAG* (FC=2.67), a DNA repair gene which complements the ultraviolet sensitivity of xeroderma pigmentosum group C cells and encodes a C2 domain-containing protein which activates the Beclin1-PI(3)KC3 complex promoting autophagy and suppressing the proliferation and tumorigenicity of human colon cancer cells (mutations in this gene have been associated with colon cancer); *GDA* (FC=0.04) encoding an enzyme that catalyses the hydrolytic deamination of guanine, producing xanthine and ammonia, connected with nervous system development; *OCC-1* (FC=0.17) overexpressed in colon cancer; and *PGRMC2* (FC=0.45) a progesterone receptor membrane component 2.

qRT-PCR validation of microarray data

The results of gene chip microarray analysis were validated with quantitative qRT-PCR. For the PCR-based analysis, we selected 19 transcripts that were differentially expressed among three different histologic types of ovarian carcinoma under study, and 3 reference transcripts which showed the most stable expression in microarray analysis (Table IV). The same samples were used for microarray analysis and qRT-PCR to validate the microarray data. An additional set of samples from three histologic types was also analyzed with qRT-PCR method to validate the gene expression profiling differences on another set of ovarian cancer samples. *ACTB* gene showed the most stable expression in qRT-PCR analysis and was chosen as a reference transcript. Statistical analysis showed that only the expression of *CCNYL*

gene was not significant. Thus, quantitative PCR validated significant differences in the levels of 18 out of 19 selected transcripts among the three different histotypes. The analysis of the second set of samples with qRT-PCR confirmed the results of the analysis of the first set (Table IV). The same transcript (*CCNYL*) was not significant in either set of the samples. Table V compares the fold change (FC) analysis for all histotypes under study. For 18 genes, the same trend (upregulation or downregulation) was observed for both methods: microarray and qRT-PCR.

DISCUSSION

Microarray analysis revealed significant biological differences among the studied histotypes, more excessive than either grade or stage. The samples used in analysis were at different stages and grades, but unsupervised statistical methods emphasized the histotypes as the main factor of stratification into different groups. The largest biological difference was found for clear-cell carcinoma when compared with serous histotype. These data provide evidence that clear-cell carcinoma has distinct biological features that differentiate it from the other histotypes.

Analysis of genes that were differentially expressed in clear-cell carcinoma when compared to other histologic subtypes emphasized two major biologic processes: transport and metabolism which were disregulated among the histotypes under study. It is possible then that these particular processes are connected with intrinsic resistance and poor response to anticancer drugs of CCC. Modified activity of proteins involved in active and passive transport of xenobiotics and their metabolism must exert effect on the response to chemotherapy. Other affected pathways, such as IGF axis, can also influence the response to chemotherapy as the alterations in the metabolism of glucose modify the proliferation rates of cancer cells. IGFBPs are circulating transport proteins for IGF. They can regulate cell growth and death, either dependent or independent of its interaction with IGF (13). IGFBP-3 is directly involved in the suppression of cancer invasion and metastasis in endometrioid ovarian carcinoma.

These findings may corroborate with a distinctive observation that patients with CCC of the ovary have a lower response rate to anticancer drugs. The chemotherapeutic effect was observed in 29% of patients who received adjuvant chemotherapy. Oncologists have noted that subtypes respond differentially to chemotherapy (14). The dismal response rate of CCCs (15%) contrasts sharply with that of high-grade serous (80%), resulting in a lower 5-year survival for CCC compared to high-grade serous carcinoma in patients with advanced-stage tumors (20% vs 30%) (15).

In our analysis, CCC was identified to exhibit a distinct behavior, as compared with other histologic subtypes of ovarian neoplasms. However, the number of genes involved in transport and metabolism in ovarian cancer tissue before chemotherapy indicates that this is an intrinsic feature of cancer tissue which is linked to low response to treatment. It shows also that it is impossible to find a reliable biomarker of transport or metabolism because these are most likely coordinated by a huge number of genes.

Our findings have been confirmed by other authors [e.g. reviewed by Itamochi et al. (16)], in respect to the mechanism of drug resistance emphasized as deregulation of proteins belonging to the family of ABC transporters. Their action leads to decreased accumulation of drugs in clear carcinoma cells and therefore to chemoresistance to conventional platinum- or taxane-based chemotherapy.

Motility, adhesion and invasion

Differences in the spread by local extension or intra-abdominal dissemination of tumor cells between serous and CCC histotypes are reflected by the differential expression of genes connected with motility, invasion and adhesion. The proportion between connective tissue and epithelial tissue is related to the degree of malignancy: the more connective tissue, the better the differentiation. Collagen expression has also been linked specifically to outcome and chemoresistance in ovarian cancer (17). Kallikreins degrade matrix components, including fibronectin, vitronectin, laminin and collagens I, II, III and IV, thereby increasing ovarian cancer cell invasiveness and contributing to the pathways connected with the resistance to cisplatin (18). We observed differential expression of these genes in our analysis and it could be the intrinsic feature of ovarian carcinoma histotypes as in our samples there was only 2% of stroma.

Estrogen and progesterone receptor genes are expressed in various types of ovarian carcinoma but their role in ovarian carcinogenesis is not as clear as in breast cancer (19). Estrogens are implicated as causative factors of ovarian carcinogenesis by contrast to progesterone which has a role as a protective factor against ovarian cancer. In our analysis, *ESR1* gene was one of the most significantly differentiating genes for pairwise comparisons of the histotypes under study. The *ESR1* gene expression was downregulated in clear-cell carcinoma. This gene encodes an estrogen receptor 1, a ligand-activated transcription factor. Estrogen and its receptors are essential for sexual development and reproductive function, but also play a role in other tissues such as bone. Estrogen receptors are also involved in pathological processes including breast cancer, endometrial cancer and osteoporosis. Estrogens may play an important role in ovarian carcinogenesis and significant dysregulation of expression of *ERα* and *PGR* genes observed in the studied histotypes confirms this observation. The expression of *PGR* gene was also significantly different between histotypes in pairwise comparisons but it was not so pronounced as for *ESR1* gene. The *PGR* has long been hypothesized as a candidate gene for ovarian cancer susceptibility and its variation has been widely studied (20, 21). Variation in expression of *PGR* (upregulated in endometriod carcinoma) encoding a member of steroid receptor superfamily, was found to be associated with higher risk of ovarian cancer.

In our study, the expression of only 200 genes differentiated clear-cell from endometrioid carcinoma. It is in agreement with the evidence that both carcinomas may develop from ovarian endometriosis, although there are suggestions that clear-cell carcinoma develops from endometriosis occurring through implantation of the endometrium (TCF2-positive), while the endometrioid carcinoma arises from endometriosis occurring in the mechanism of mullerian metaplasia of ovarian surface epithelium (TCF2-negative) (22). In this analysis, *TCF2* (*HNF1B)* showed highly significant differential expression in the histotypes under study, both in microarray analysis and in qRT-PCR validation. In other studies TCF2 was considered as a putative molecular marker and a possible target for therapy of ovarian clear-cell carcinoma (23, 24). TCF2 is also a biomarker of importance for renal carcinoma. Matsumura et al. (25) suggests a new therapy with sorafenib, designed for renal carcinoma, which significantly reduces clear-cell carcinoma tumor size in nude mice, due to the molecular similarities between renal carcinoma and ovarian clear-cell carcinoma (OCCC).

Other important processes and genes which were affected in the histotypes under study include homeobox family, genes connected with immune response, with kidney tumors and with the nervous system. The same dysfunctional products of the genes may have multiple pathogenic roles. Devine et al. (26) discussed pathogenic pathways of the same genes which can lead either to inappropriate neuronal death in Parkinson's disease when present in germline, or to inappropriate cell survival in cancer when present in somatic cells. Tumor suppressor gene *WT1* which is connected with Wilm's tumor in kidneys is thought also as a putative gynecologic marker (27-28).

Interestingly, SAM method revealed several genes that differentiated two subgroups of endometriod carcinoma. Two of them: *TFF3* and *UVRAG* were earlier connected with colon and colon cancer. However, these results should be taken with caution because the group under study consisted of 9 samples only and they were unevenly distributed (3 and 6 samples). Three samples in one subgroup could be outliers as well. The molecular difference between two subtypes of endometrioid carcinoma is similar (in number of genes that were differentially expressed) to the biological difference found between endometrioid and serous carcinomas. Molecular subclasses of endometrioid carcinoma were also found by another group where they were able also to distinguish the low-grade and advanced stage and high grade endometrioid subtypes (29).

TP53 gene is known as the most frequently mutated in many cancers and *BRCA1* gene, when mutated in germline, is the strongest risk factor for breast and ovarian cancer (3). In this study, statistical analyses did not reveal differential expression of *BRCA1, 2* or *TP53* genes being in the same signaling pathway, even though some tissues under study were from carriers of germline mutations in *BRCA1* gene. This can be explained that the gene expression at the mRNA level is not the only difference observed between normal and tumor cells. The histologic

subtypes under study differed also in respect to the frequency of somatic mutations in *TP53* gene. The highest percentage of *TP53* mutation or p53 accumulation was observed in serous and the lowest percentage was seen in clear-cell ovarian carcinoma (30).

Another analysis of different histotypes using tissue microarrays showed also that biomarker expression profile within the same histotype was consistent across stage. Early and advanced ovarian carcinomas differed primarily based on subtype, while within a subtype there was no difference between early and advanced stage tumors. A study by Köbel et al. suggested that ovarian carcinoma subtypes were different diseases (31). Our results corroborate with further analyses of these authors (32) in which they elaborated a 9-gene calculator for the classification of different ovarian histotypes on the protein level. In our analysis, 5 out of 9 genes (*TCF2, PGR, TFF3, VIM* and *WT1*) were also differentially expressed when studied histotypes are compared.

In conclusion, the expression levels of *TCF2* (*HNF1B)* gene in three histotypes confirm earlier findings that it can be taken into consideration as a molecular marker for CCC.

Identification of two molecular subtypes of endometrioid carcinoma needs to be further confirmed by analysis of more samples.

Chemoresistance can be studied using certain classes of less expensive gene chips. High-density microarray analysis performed in this study sets the directions for more detailed future analysis of molecular markers in ovarian carcinoma.

ACKNOWLEDGEMENTS

The study was supported by MNiSW grant No PBZ-KBN-091/P05/2003/56

REFERENCES

1. Zemla BFP, Kolosza Z, Banasik TR. Atlas of Cancer Incidence and Mortality within Katowice District in the Years 1985-1993. Gliwice: Cancer Epidemiology Department, Centre of Oncology, Maria Sklodowska-Curie Memorial Institute, Gliwice Branch, 1999.
2. Canevari S, Gariboldi M, Reid JF, Bongarzone I, Pierotti A. Molecular predictors of response and outcome in ovarian cancer. Clin Rev Oncol/Hematol 2006; 60:19-37.
3. Menkiszak J, Gronwald J, Górski B, et al. Hereditary ovarian cancer in Poland. Int J Cancer 2003; 106:942-45.
4. Jazaeri AA, Yee CJ, Sotiriou C, Brantley KR, Boyd J, Liu ET. Gene expression profiles of BRCA1-linked, BRCA2-linked, and sporadic ovarian cancers. J Natl Canc Inst 2002; 94:990-1000.
5. Bowtell DD. The genesis and evolution of high-grade serous ovarian cancer. Nat Rev Cancer 2010; 10:803-8.
6. Scully RE. Pathology of ovarian cancer precursors. J Cell Biochem Suppl 1995; 23:208-18.
7. Vang R, Shih I-M, Kurman R. Ovarian low-grade and high-grade serous carcinoma: Pathogenesis, clinicopathologic and molecular biologic features, and diagnostic problems. Adv Anat Pathol 2009: 16:267-82.
8. Plisiecka-Hałasa J, Dansonka-Mieszkowska A, Kraszewska E, Dańska-Bidzińska A, Kupryjańczyk J. Loss of heterozygosity, microsatellite instability and TP53 gene status in ovarian carcinomas Anticancer Res 2008; 28:989-96.
9. Jochumsen KM, Tan Q, Høgdall EV, Høgdall C, Kjær SK, Blaakær J, Kruse TA, Mogensen O. Gene expression profiles as prognostic markers in women with ovarian cancer. Int J Gynecol Canc 2009; 19:1205-13.
10. Tavassoli FA, Devilee P [edit.]. Tumors of the Breast and Female Genital Organs. Pathology & Genetics. Lyon, France: IARC Press; 2003 World Health Organization Classification of Tumours.
11. Broders AC, Carcinoma: Grading and practical application, Arch Pathol, 1926, 2:376-81.
12. Tusher VG, Tibshirani R, Chu G, Significance analysis of microarrays applied to the ionizing radiation response. Proc Natl Acad Sci USA 2001; 98:5116-21.
13. Torng PL Lee YC, Huang CY, Ye JH, Lin YS, Chu YW, Huang SC, Cohen P, Wu CW, Lin CT. Insulin-like growth factor binding protein-3 (IGFBP-3) acts as an invasion-metastasis suppressor in ovarian endometrioid carcinoma. Oncogene 2008; 27:2137-47.

14. Jazaeri AA, Awtrey CS, Chandramouli GVR, et al. Gene expression profiles associated with response to chemotherapy in epithelial ovarian cancers. Clin Cancer Res 2005; 11:6300-10.
15. Du Bois A, Lück H-J, Meier W, et al. A randomized clinical trial of cisplatin/paclitaxel versus carboplatin/paclitaxel as first-line treatment of ovarian cancer. J NCI 2003: 95:1320-30.
16. Itamochi H, Kigawa J, Terakawa N. Mechanisms of chemoresistance and poor prognosis in ovarian clear-cell carcinoma. Cancer Sci 2008: 99:653-58.
17. Bast RC, Hennessy B, Mills GB. The biology of ovarian cancer: new opportunities for translation. Nat Rev Cancer 2009; 9:415-28.
18. Prezas P, Arlt MJ, Viktorov P, et al. Overexpression of human tissue kallikrein genes KLK4, 5, 6 and 7 increases the malignant phenotype of ovarian cancer cells. Biol Chem 2006: 387:807-11.
19. Ho SM. Estrogen, progesterone and epithelial ovarian cancer Reprod Biol Endocrinol 2003; 1:73.
20. Pearce CL, Wu AH, Gayther SA, et al. Progesterone receptor variation and risk of ovarian cancer is limited to the invasive endometrioid subtype: results from the ovarian cancer association consortium pooled analysis. Br J Cancer 2008; 98:282-88.
21. Lazennec G. Estrogen receptor beta, a possible tumor suppressor involved in ovarian carcinogenesis. Cancer Lett 2006; 231:151-7.
22. Kajihara H, Yamada Y, Shigetomi H, Higashiura Y, Kobayashi H. The dichotomy in the histogenesis of endometriosis-associated ovarian cancer: clear-cell-type versus endometrioid-type adenocarcinoma. Int J Gynecol Pathol 2012; 31:304-12.
23. Tsuchiya A, Sakamoto M, Yasuda J, et al. Expression profiling in ovarian clear-cell carcinoma, Identification of hepatocyte nuclear factor -1β as a molecular marker and a possible molecular target for therapy of ovarian clear-cell carcinoma. Am J Pathol 2003; 163:2503-12.
24. Shen H, Fridley BL, Song H, et al. Epigenetic analysis leads to identification of HNF1B as a subtype-specific susceptibility gene for ovarian cancer. Nat Commun 2013; 4:1628.
25. Matsumura N, Mandai M, Okamoto T, et al. Sorafenib efficacy in ovarian clear-cell carcinoma revealed by transcriptome profiling. Cancer Sci 2010; 101:2658-63.
26. Devine MJ, Plun-Favreau H, Wood NW. Parkinson's disease and cancer: two wars, one front. Nat Rev Can 2011; 11:812-23.
27. Madore J, Ren F, Filali-Mouhim A, Sanchez L, Köbel M, Tonin PN, Huntsman DM, Mes-Masson A-M. Characterization of molecular differences between ovarian endometrioid carcinoma and ovarian serous carcinoma. J Pathol 2010; 220:392-400
28. Netinatsunthorn W, Hanprasertpong J, Dechsukhum C, Leetanaporn R, Geater A. WT1 gene expression as a prognostic marker in advanced serous epithelial ovarian carcinoma: an immunohistochemical study. BMC Can 2006; 11; 6:90.
29. Tothill RW, Tinker AV, George J, et al. Novel molecular subtypes of serous and endometrioid ovarian cancer linked to clinical outcome. Clin Canc Res 2008; 14:5198-208.
30. Kupryjańczyk J, Thor AD, Beauchamp R, Merritt V, Edgerton SM, Bell DA, Yandell DW. p53 gene mutations and protein accumulation in human ovarian cancer. Proc Natl Acad Sci U S A 1993; 90:4961-5.
31. Köbel M, Kalloger SE, Boyd N, et al. Ovarian carcinoma subtypes are different diseases: Implications for biomarker studies. PLoS Medicine 2008; 5:1749-60.
32. Kalloger SE, Köbel M, Leung S, et al. Calculator for ovarian carcinoma subtype prediction. Modern Pathol 2011; 24:512-21.

COMPARATIVE STUDY ON CT PERFUSION PARAMETERS OF DIFFERENT TYPES OF LUNG CANCER BEFORE AND AFTER CHEMORADIOTHERAPY

L. ZHAO[1], W. GUAN[2], Y. HAN[1] and Y. ZHAO[3]

[1]Department of Radiology, First Affiliated Hospital of Henan University of Science and Technology, Henan University of Science and Technology, Luoyang, China; [2]Department of Nuclear Medicine, First Affiliated hospital of Henan University of Science and Technology, Henan University of Science and Technology, Luoyang, China; [3]Department of Neurosurgery, First Affiliated Hospital of Henan University of Science and Technology, Clinical Medicine Henan University of Science and Technology, Luoyang, China

Received November 22, 2014 – Accepted December 15, 2014

The aim of this paper was to observe the changes in computed tomography (CT) perfusion parameters of patients with lung cancer in early stage before and after chemoradiotherapy. Twenty-five previously treated lung cancer patients underwent a first CT perfusion scan and then a following one before the second course of chemotherapy. CT images of the fourth course of treatment were compared with the initial images. The cases were divided into a remission group and a non-remission group according to Response Evaluation Criteria In Solid Tumors (RECIST). Blood flow (BF), blood volume (BV), Patlak permeability Surface (PS) and Pallak blood volume (PBV) in the different groups were respectively compared before and after treatment. In addition, SPSS17.0 was applied for statistical analysis. $P < 0.05$ signified that the difference had statistical meaning. CT perfusion parameters were all found to be changed compared to before the treatment. BV and PBV parameters decreased twice. BV and PBV parameters in the non-remission group showed an increasing trend. The difference before and after the treatment of these parameters had the highest statistical significance, as well as the difference of remission rate of PBV increasing group and decreasing group. Through the contrasting χ^2 test of remission rate of BV and PBV, it was found that the remission rate of the BV increasing group and the decreasing group had no statistical difference; the remission rate in the PBV decreasing group was higher than the increasing group. All the findings suggest that the change in size of the damaged tissue had no statistical meaning in the early stage of CT perfusion parameter change; CT perfusion parameter of the remission group in the early stage after chemotherapy decreased while the non-remission group increased; the change of BV and PBV was significant.

Lung cancer is one of the most common malignant cancers. It was reported that the incidence of lung cancer has exceeded breast cancer and colorectal cancer and has become the malignant cancer with the highest incidence and mortality in the world (1-3). Lung cancer not only threatens the patient's life but also brings heavy economical burden for the patient. Although new chemotherapeutic drugs and therapeutic

Key words: CT perfusion, normality test, RECIST criteria, blood flow, blood volume

Mailing address: Dr. W. Guan,
No. 24 Jinghua Road,
First Affiliated Hospital of Henan
University of Science and Technology,
Luoyang, 471003, China
Tel.: +86 0379 69823199 Fax: +86 0379 69823399
e-mail: whgguan@163.com

0393-974X (2014)

DISCLOSURE: ALL AUTHORS REPORT NO CONFLICTS OF INTEREST RELEVANT TO THIS ARTICLE.

methods are constantly being proposed, their curative effects are not definite (4). Immunohistochemical determination has verified that microvessel density (MVD) count can reflect the generation of new vessels in tumor and is closely related to the malignant characteristics of tumor. Evaluation of MVD is of important reference value to distinguish grading and prognosis of benign and malignant tumors (5). However, MVD detection of tumor is carried out on the viable tissue and is hard to perform in the clinic, since it is an invasive examination (6). With the development of spiral CT technology and the data processing ability of computer technology, a proper mathematical model can transform information about the increase of tumor vessel with the injection time of contrast agent into peer CT value time density curve (TDC) and information that reflects capillary permeability. Therefore, physiological indexes such as BF, BV and PS change (7).

To date, treatment of lung cancer still focuses on operation and radiotherapy in the early stage as well as chemotherapy and palliative radiotherapy in the advanced stage, but the prognosis of advanced lung cancer is still poor (8, 9). Chemotherapy becomes the first choice for those patients who have central-type lung cancer and can not tolerate radiotherapy or an operation. It is of great importance to select an effective therapeutic schedule and then correct that schedule as soon as possible if there is a poor outcome. Any morphological assessment can only be made through repeated measurements and comparing with those taken prior to treatment. CT perfusion value of focus before and after treatment may change before morphology changes. Thus, CT perfusion imaging can provide an objective base to understand whether the treatment is effective in a short period of time from the beginning of treatment and assist the clinician to formulate the next step in treatment. We applied the latest dual-source CT equipment and non-invasive technology of CT perfusion imaging on 25 patients with lung cancer who were being treated with regular chemicals. Also, we explored the change of blood supply in short term before and after the treatment with regular chemicals. The blood supply characteristics can be used in predictive analysis of the therapeutic effects on a tumor, thereby providing a new method for the clinical diagnosis of a tumor and to decide on the type of treatment (10).

MATERIALS AND METHODS

Materials

A total of 27 patients who were diagnosed with lung cancer at the first visit but had not been treated and who were admitted to the First Affiliated Hospital of China Medical University, Shenyang, China from May 2009 to November 2009, were enrolled in this study. Of these patients, 22 were male and 5 were female, with a mean age of 52 years and size of lesion varying from 2.0 to 6.5 cm. The patients whose lesions were close to the diaphragmatic surface (easily affected by respiratory movement) and who could not hold their breath over 30 s were excluded.

Method of acquisition and processing of data

The patients were followed-up for 100 days during which CT scanning was carried out three times. The first CT perfusion scan was carried out before chemotherapy treatment, and the results were taken as the initial data of CT scanning and perfusion parameter. The second CT scan was carried out before the second treatment (about 21 to 25 days) and the results were compared to the initial data. A cycle of chemotherapy (about 100 days) was fulfilled after the fourth course of treatment. Then the patients underwent regular CT plain scanning, and the results were compared to the initial data.

Response evaluation criteria in solid tumors (RECIST) (10) was adopted as the detection and evaluation method on the therapeutic effect of tumor. The evaluation criteria can be divided into:

Complete remission (CR): all targeted damaged tissue (focus) disappeared.

Partial remission (PR): major axis of baseline focus reduced $\geq 30\%$.

Progress of disease (PD): major axis of baseline focus increased by 20% or the new focus appeared.

Stability of disease (SD): major axis of baseline focus reduced but did not reach the standard of PR or increased but did not reach PD.

CR and PR were defined as remission, SD and PD as non-remission. Patients who had to undergo radiotherapy or who died after two courses of treatment were classified as the non-remission group.

CT perfusion data scanning method

Firstly, regular plain scanning was performed on the whole lung. The focus in the lung was selected as

the dynamic scanning center horizon by plain scanning image. Thorax perfusion CT 7 mm was applied to carry out continuous dynamic scanning on the selected focus, with 120kV, 100mAs, 0.7cm×4 horizons, that is, effective scanning scope of 2.8 cm, matrix of 512×512, scanning delay time of 6 s, data acquisition time of 53 s. Finally, 196 images were acquired. A total of 40 ml non-ionic contrast medium [iohexol, 300 mgI/ ml, General Electric Pharmaceutical (Shanghai) Co., Ltd] was injected into the forearm i.v. through preset trocar by high pressure syringe with double pumps (patients whose focus were close to the precava adopted lower-limb venous injection), with an injection rate of 6 ml/s. Also, 50 ml of normal saline was injected at the same rate.

Data analysis

Of the 27 cases, 1 case of adenosquamous carcinoma was excluded, since metastasis had occurred at the second lung scanning, with a large area of necrotic primary focus and excessively thin wall. Also, one case of squamous carcinoma in the II b period was excluded, as the patient had heavy breathing movements during the second scan, leading to inexact data. Therefore, 25 cases of patients were finally selected.

The first CT perfusion image was compared to the prior CT plain scanning image. All data were divided into a remission group and a non-remission group according to the RECIST. We respectively compared the variation difference of BF, BV, PS and PBV in the different groups before and after treatment. SPSS 17.0 software was used for statistical analysis. Firstly, the normality test was performed, and if the data conformed, then the paired *t* test method was applied; the results applied a two-sided test ($\alpha = 0.05$); $P < 0.05$ meant that the difference had statistical significance (value of *t* was expressed as significance test value of regression parameter; value of P was the significance test value of regression equation).

RESULTS

Change of tumor size in lung cancer patients before and after chemotherapy

There were 15 cases in the remission group and 10 cases in the non-remission group according to RECIST. Two cases in the non-remission group were combined with radiotherapy after the second chemotherapy. One patient died in the middle stage of the third course of chemotherapy. Three patients were found to have no change after comparison of CT perfusion images. The change of focus size after two CT perfusions is shown in Table I.

Table I shows that the change of focus size had no statistical significance in the early stage of CT perfusion parameter change. Also, the changes of focus size in early stage in the remission group and the non-remission group were without statistical

Table I. *Comparison of the largest diameter of tumor after two CT perfusion before and after treatment (unit: cm).*

Group	Cases	Before treatment	After treatment	*t* value	P value
All cases	25	4.07±1.17	3.85±0.98	1.725	0.096
Remission group	15	4.01±1.25	3.86±1.70	1.068	0.303
Non-remission group	10	4.15±1.13	3.85±0.87	1.346	0.211

Table II. *Comparison of parameters in remission group before and after treatment.*

Group	Cases	Before treatment	After treatment	*t* value	P value
BF(ml/100ml/min)	15	52.4±33.2	34.6±27.4	1.695	0.112
BV(ml/1000ml)	15	71.1±20.3	49.8±31.4	2.558	0.023
PS(0.5ml/100ml/min)	15	38.7±26.3	41.3±18.9	-0.427	0.676
PBV(ml/1000ml)	15	73.0±34.2	45.1±19.1	3.325	0.005

Table III. *Comparison of parameters in non-remission group before and after treatment.*

Group	Cases	Before treatment	After treatment	*t* value	P value
BF(ml/100ml/min)	9	41.2±53.3	51.2±33.1	-0.804	0.445
BV(ml/1000ml)	9	50.4±61.1	120.2±16.0	-3.062	0.016
PS(0.5ml/100ml/min)	10	30.2±16.6	37.2±16.6	-1.491	0.170
PBV(ml/1000ml)	10	38.1±9.4	62.0±38.1	-2.471	0.036

Table IV. *Comparison of PBV parameter of small cell lung cancer and non-small cell lung cancer before and after treatment.*

Group	Cases	Before treatment	After treatment	*t* value	P value
Small cell lung cancer	13	56.0±18.9	64.5±20.4	-1.679	0.119
Non-small cell lung cancer	12	62.3±42.0	53.5±35.5	0.964	0.356

significance.

Change of CT perfusion parameter of tumor patients before and after chemotherapy

Of the 25 cases, BF and BV of one patient with adenocarcinoma metastasis in bone in the non-remission group could not be detected. The statistical analysis data is shown in Tables II and III.

Table II shows that parameters of BV and PBV of the remission group before and after treatment all decreased, and the decrease of PV and PBV parameters before and after treatment had statistical significance.

It can be seen from Table III that BF, BV and PBV parameters in the non-remission group increased after treatment and the changes of BV and PBV parameters all had statistical significance.

Comparison of PBV parameter of patients with different pathological patterns of tumor before and after chemotherapy

In this group, there were 13 cases of small cell lung

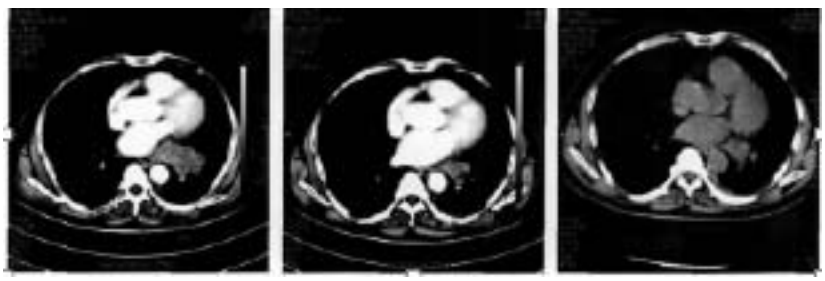

Fig. 1. *Comparison of focus in CT average perfusion level before and after treatment.*

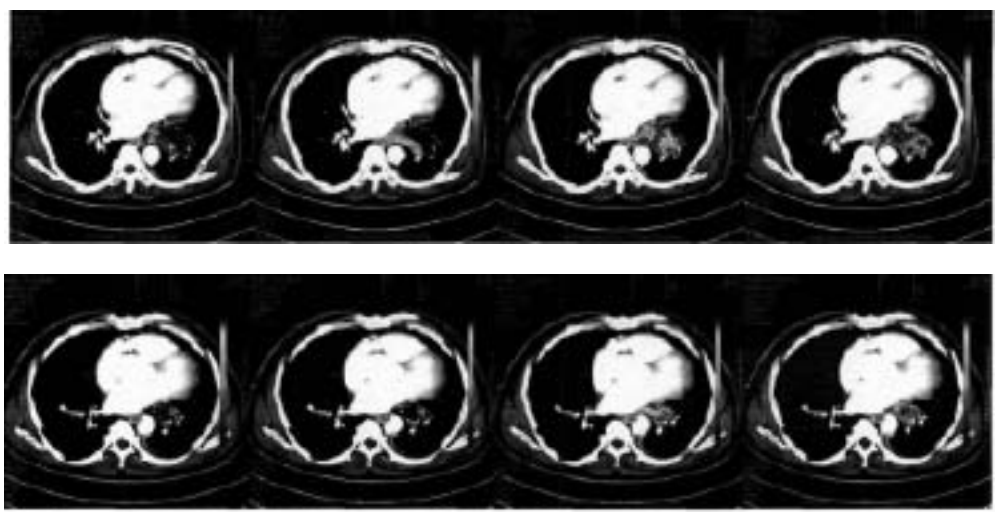

Fig. 2. *Comparison of rheography and numerical value of BF, BV, PS and PBV parameters before and after treatment in remission group.*

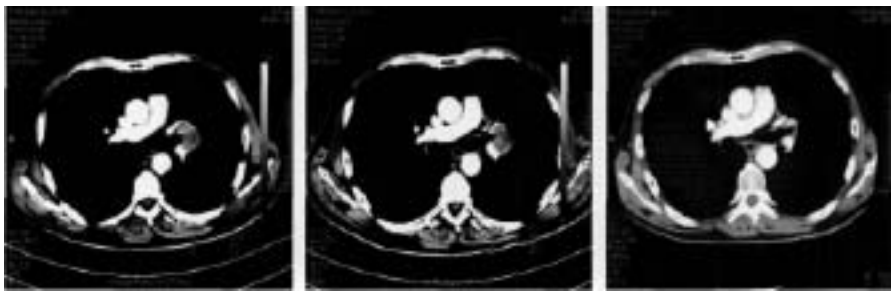

Fig. 3. *Comparison of focus in CT average perfusion level before and after treatment in non-remission group.*

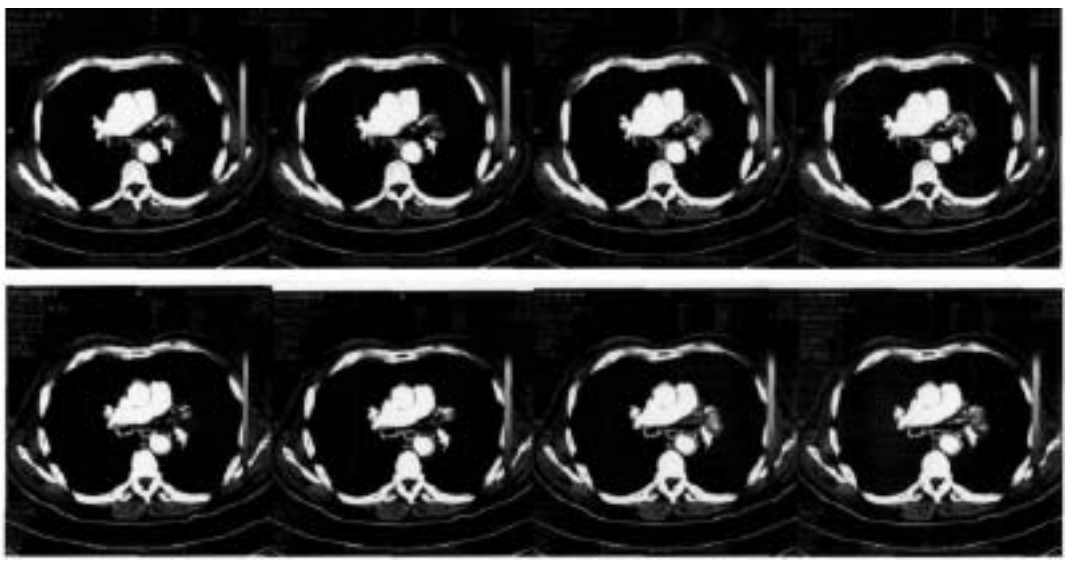

Fig. 4. *Comparison of rheography and numerical value of BF, BV, PS and PBV parameters before and after treatment.*

cancer, of which 7 cases were in remission, and 12 cases of non-small cell lung cancer, of which 8 were in remission. PBV parameters of these two cancers were compared before and after the treatment, as shown in Table IV.

It can be seen from Table IV that PBV parameters of lung cancer in pathological types before and after treatment had no statistical significance. In addition, there was little difference between PBV parameters of different pathological types before and after treatment.

Typical cases and illustration

Case 1: a 65-year-old male patient with stage IV small cell lung cancer with cerebellar metastasis. Focus in the second test decreased significantly compared to the first test; the decreasing amplitude was more than 30%; the two results of PBV were 49.0ml/1000ml and 54.6ml/1000ml. After four months, liver metastasis had occurred as shown in the abdominal CT review. The pulmonary focus was roughly equal to that at the second scan. The patient was classified in the non-remission group because new focus had appeared. Fig. 1 shows the comparison of focus in the CT average perfusion level before and after treatment. Fig. 2 is the comparison of rheography and numerical value of BF, BV, PS and PBV parameters before and after treatment.

Case 2: a male patient with stage IIb small cell lung cancer. Focus before and after the treatment were compared. The two results of PBV were 92ml/1000ml and 60.6ml/1000ml; the focus had disappeared in the CT review after four months, therefore, the patient was classified as belonging to the remission group. Fig. 3 is the comparison of focus in the CT average perfusion levels before and after treatment. Fig. 4 is the comparison of rheography and numerical value of BF, BV, PS and PBV parameters before and after treatment.

DISCUSSION

CT perfusion imaging (11, 12) refers to performing continuous scanning on the selected level after injecting a contrast agent in the vein to obtain TDC of every pixel in that level. Abscissa is time and ordinate is the increased CT value after injection (it is generally recognized that 1mg/ml of iodine concentration corresponds to 25HU, i.e., 1 mg iodine can increase 25HU of CT value of 1 ml). The curve reflects the change of increased CT value over time in artery and tissue after injecting the contrast agent, which directly reflects concentration change of contrast agent in those organs, thereby indirectly reflecting the change of perfusion volume of tissue organs (13).

In order to analyze a specific area of an image, image post processing in this experiment adopted the body PCT software of Siemens Syngo Multimodality workplace. This software selects and sketches the region of interest in the maximum horizon. The selection of the region of interest must be a rectangle and include the whole focus. Aorta, bone tissue and lung tissue included were automatically removed through pre-setting the range of CT value (-50~150).

The effect of breathing of patients was corrected by 3D. As to the influence of breathing movement, the computer selected the most similar horizon to replace. Through the comparative analysis, it was found that the best data measurement area, i.e., region of interest reported in most literature, could be selected from the average CT horizon map.

It was known from the image analysis and comparative research on the size of lesion before and after the chemotherapy that, twice lesions in the remission group and the non-remission group had no significant change in size and the change of tumor size in the early stage after chemotherapy was not suitable as the index of curative effect judgment (14). In order to study the curative effect of chemotherapy in the early stage more effectively, this experiment applied CT perfusion in the early-stage curative effect evaluation after chemotherapy. The result showed that BV and PBV in the remission group and the non-remission group all changed before and after treatment, with a decrease in the remission group and an increase in the non-remission group; the change of PBV was more significant. The increase of PBV in the early stage after chemotherapy demonstrated that the MVD of tumor tissue was richer compared to that before treatment. Among these cases, the size of lesion can be regarded as having no significant change as well as being enlarged or reduced compared to before treatment. In the non-remission group, although the volume of tumor reduced in the early stage after treatment, the effect of medication was often not satisfactory. The decrease of PBV showed that MVD of tumor tissue decreased compared to before treatment. In the remission group, although the volume of tumor had no change compared to before treatment, the effect of medication was often satisfactory. Kiessling et al. pointed out that lung cancer with a volume larger than 50 cm^3 had low perfusion; central type lung cancer had low perfusion compared to peripheral lung cancer; parameters of small cell lung cancer and non-small cell lung cancer had no significant difference. They also thought that the perfusion and peak of lung cancer depended on the position and size of tumor rather than histological type (15, 16). In this experiment, two CT perfusion values of one case of lung cancer were significantly higher than those of the other patients while the PBV perfusion parameter between different pathological types had no statistical significance. In the early stage after chemotherapy, the size of focus had no significant change while the CT perfusion parameter changed significantly. The CT perfusion parameter of the remission group after chemotherapy in the early stage decreased while that of the non-remission group increased; meanwhile, the change of BV and PBV value had statistical significance.

This study included previously treated patients, with interference factors such as drug resistance of tumor excluded, and studied early-stage assessment

of the chemotherapeutic effect on lung cancer by CT perfusion. Early-stage CT perfusion parameter of the remission group after chemotherapy had a decreasing trend, while that of the non-remission group had an increasing trend, and changes of BV and PBV had statistical significance. Increases of PBV in the early stage after chemotherapy indicates that prognosis of patients is weak and they are not sensitive to treatment with chemical drugs; decrease of PBV just the reverse. Therefore, change of PBV is valuable for assessment of the curative effect of chemotherapy.

REFERENCES

1. Chen WQ, Zhang SW, Zou XN. Estimation and projection of lung cancer incidence and mortality in China. Chinese J of Lung Cancer 2010; 13(5):488-93.
2. Ferlay J, Shin HR, Bray F, Forman D, Mathers C, Parkin DM. Estimates of Worldwide Burden of Cancer in 2008: GLOBOCAN 2008. Int J Cancer 2010; 127(12):2893-917.
3. Shan F. Clinical application research on lung cancer 64 layer spiral CT volumetric perfusion. Shanghai: Fudan University 2009.
4. Sun Y, Shi YK. Clinical Medical Oncology Manual. Beijing: People's Medical Publishing House 2009; 79-83.
5. Ding N. Bibliometric analysis of research status and hotspot related to lung cancer in our country. Biom Infon Res 2014; 4(23):67-72.
6. Wu BB. The Relationship of TNM staging peripheral non-small cell lung cancer with strengthening index of 16 row spiral CT perfusion imaging and tumor MVD. 2010.
7. Xiong Z, Liu JK, Hu CP, Zhou H, Zhou ML, Chen W. Role of immature microvessels in assessing the relationship between CT perfusion characteristics and differentiation grade in lung cancer. Arch Med Res 2010; 41:611-7.
8. Zhang Z, Han SH, Zhang XT, Wu XS, Ma XZ. Expression level of serum CD44v6 before and after chemotherapy and its clinical meaning. J Med Res 2013; 7(42):112-4.
9. Fraioli F, Anzidei M, Zaccagna F, et al. Whole-tumor perfusion CT in patients with advanced lung adenocarcinoma treated with conventional and antiangiogenetic chemotherapy: initial experience. Radiology 2011; 259(2):574-82.
10. Liu K. Correlation research on non-small cell lung cancer CT perfusion parameter, EGFR and MMP-9. Guangzhou: Southern Medical University. 2013.
11. Wu BB. The relationship of TNM staging peripheral non-small cell lung cancer with strengthening index of 16 row spiral CT Perfusion Imaging and Tumor MVD. Guangxi: Guangxi Medical University. 2010.
12. Garcia FR, Goh VJ, Padhani AR, Gonzalez SB, Garrido M, Leon L, Caamano AG. CT Perfusion in oncologic imaging: a useful tool. AJR Am J Roentgenol 2013; 200(1):8-19.
13. Li Y, Yang ZQ, Chen TW, Chen HJ, Lu YR. Peripheral lung carcinoma: correlation of angiogenesis and first-pass perfusion parameters of 64-detector row CT. Lung Cancer 2008; 61(1):44-53.
14. Jain R, Poisson L, Narang J, Scarpace L, Rosenblum ML, Rempel S, Mikkelsen T. Correlation of perfusion parameters with genes related to angiogenesis regulation in glioblastoma: a feasibility study. AJNR Am J Neuroradiol 2012; 33(7):1343-8.
15. Bellomi M, Petralia G, Sonzogni A, Zampino MG, Rocca A. CT perfusion for the monitoring of neoadjuvant chemotherapy and radiation therapy in rectal carcinoma: initial experience. Radiology 2007; 244(2):486-93.
16. Spira D, Gerlach JD, Spira SM, Schulze M, Sauter A, Horger M. Effect of scan time on perfusion and flow extraction product (K-trans) measurements in lung cancer using low-dose volume perfusion CT (VPCT). Acad Radiol 2012; 19(l):78-83.

THE MECHANISM AND SIGNIFICANCE OF E-CADHERIN, ANTI-APOPTOSIS B-CELL LYMPHOMA-2 PROTEIN AND SE-CADHERIN ROLES IN CANCER

L. LIU, H.X. LI and X.Q. LV

Pathology Department, the First Affiliated Hospital of Zhengzhou University, Zhengzhou, China

Received November 22, 2014 – Accepted December 15, 2014

Women are most likely to suffer from breast cancer of all the malignant tumors. Its incidence is growing rapidly, which severely threatens the health of females. E-cadherin (E-cad), as the mediator of tumor tissue cells, when adhesion between the cells decreases, can improve the wettability and migration ability of cells, and help cell growth and proliferation in the new area. E-cad serves not only as a cancer inhibitor but also as a cancer promoter. sE-cadherin (sE-cad) is formed as a result of the degradation and exfoliation of N-end extracellular domain of E-cad and its level is closely related to the invasion and metastasis of tumor cells. B-cell lymphoma-2 protein (Bcl-2 protein) is the key regulatory factor for the mitochondria apoptosis pathway during the apoptosis of cells, and it plays an important role in the signal transduction pathway of cell apoptosis. Its abnormal expression may induce disorder of the mechanism. This paper, through the study of the expression and relationship of E-cad, Bcl-2 protein and sE-cad, attempts to explain their expression changes during the development of breast cancer, providing clues clinically useful for further recognition of occurrence and development, early diagnosis, interference and early treatment of breast cancer.

Breast cancer is a constant threat to the physical and mental health of females. In China, the incidence of breast cancer is increasing year by year. Early inspection and treatment is the key to lowering the risk of death (1). In addition, proper diagnosis is of positive significance for both individualized and clinical treatment. Research has found that: cell adhesion molecules play an important function in tumor process; E-cad is one of the important representatives; generally the structure of molecules includes intracellular domain, transmembrane domain and extracellular domain and abnormal change can induce the deterioration of a carcinoma (2-3).

E-cad, which widely exists in epithelial cells of mature tissue, is one of the important representatives of multiple adhesion molecules. Besides regulating the maturity of embryonic tissue, formation of tissue and being involved in message exchange between cells, it also plays an important role in the integration and polarity of the morphological structure of epithelial cells, the differentiation of epithelial cells, and the aggregation and adhesion between homologous epithelial cells (4). There is research that reports that E-cad also plays an important function in the occurrence of tumors, and its abnormal expression can activate multiple carcinogenic signal paths, induce cell apoptosis mechanisms, thereby leading to the occurrence of oncocytes (5).

sE-cad is formed as a result of the degradation

Key words: breast cancer, E-cad, anti-apoptosis Bcl-2 protein, sE-cad

Mailing address: Dr Huixiang Li,
Pathology Department,
the First Affiliated Hospital
of Zhengzhou University,
No.1, Jianshe Road, Zhengzhou, China
Telephone/Fax: +86 0371 67354312
e-mail: lliuleil@163.com

0393-974X (2014)

and exfoliation of the N-end extracellular domain of E-cad (6). Rapid proliferation and growth of tumor cells can speed up E-cad metabolism and protein degradation, thereby increasing concentration of sE-cad, and finally affecting signal transmission of tumors and the loss of adhesion between cells. The existence of sE-cad enhances invasiveness and metastasis. Its presence increases the invasion and metastasis capabilities of tumor cells (7).

Anti-apoptosis Bcl-2 protein participates in the development of a series of cancers during cells apoptosis (8), which is biologically one of the basic characteristics of tumor cells. It plays an important function in both the occurrence and development of tumors (9). Its normal expression and regulation is the key factor for cell apoptosis. Research has indicated that in the pathological expression of breast cancer, the more deteriorated the carcinoma is, the poorer the biological behavior of tumor cells will be, as Bcl-2 increases its expression (10).

During research on the relationship between E-cad and inflammatory breast cancer, Tan Miduo et al. (11) found that E-cad shows intense positive expression that is identical with its function, in inflammatory breast cancer tissue and cell lines, and it is closely related to the wettability and metastasis of inflammatory breast cancer. Through research on the predictors for the effect of neoadjuvant chemotherapy on TNBC patients, Kraus et al. (12) found that the pathologic complete remission rate for people with decreased E-cad expression is obviously higher than normal (P=0.001). Aomatsu et al. (13) held that E-cad may serve as a predictive factor of curative effect of neoadjuvant chemotherapy on breast cancer patients, and such prediction is of great value. This paper mainly studies the reaction mechanism and indicator significance of E-cad in breast cancer, and explores the expression and relationship of them in order to create a new breakthrough for the diagnosis and prognosis of breast cancer.

MATERIALS AND METHODS

Tissue samples

Experiment 1: the tissues of all the samples collected from hospitals were embedded in paraffin. After an operation, breast tissues were removed and pathologically diagnosed, and the related clinical materials were collected. The results showed that: in group A there were 30 cases of normal breast tissues adjacent to tumors; in group B there were 30 cases of breast hyperplasia tissue (breast hyperplasia tissue group); in group C there were 70 cases of breast cancer tissue (breast cancer group). The subjects were strictly chosen: patients should not have previously had malignant cancer or breast cancer operations; patients must not have other malignant tumors; the breast cancer tissue must be without inflammation or skin diseases. The collected materials were as follows (Table I).

Experiment 2: experimental samples were prepared for groups A, B and C, by collecting the serum respectively from 30 healthy adult females, 30 patients of benign breast disease and 30 patients of breast cancer. The ELISA method was adopted to detect the expression of sE-cad in the above serum.

Immunohistochemical staining

The tissue slices received heat treatment and were then cooled down. They were washed with PBS buffer solution and then 3% H_2O_2 was added. They were then washed with PBS again after standing for 10 min. The remaining water was removed. After that, goat serum was added, confining the liquid to the tissue slices, which was then incubated at room temperature for 10 min. The confining liquid was absorbed and primary antibody incubation was conducted at 4°C overnight; the slices were then washed with PBS. They then underwent the 2nd incubation for 20 min, they were washed with PBS, but not dried. Then DAB coloration was used for testing. The redundant PBS was removed. The tissues were examined under a microscope to find the claybank particles, which do not absorb coloration; 31% hematoxylin staining liquid was used to counterstain for 3 min. They were then differentiated using hydrochloric acid for 1 s; then they were washed, dried and sliced. They were mounted in neutral balsam and then observed under the microscope.

ELISA

Serum samples at the ratio of 1:2 were diluted. 100 µl of standard diluents was added and the plate was sealed. They were incubated at 37°C for 120 min, before opening the plate. They were absorbed twice and spun-dried; 0.1 ml biotin antibody working liquid was added and they were incubated for 60 min at 37°C. They were then washed three times and spun-dried; 0.1 ml ABC working liquid was added and they were incubated for 30 min at 37°C, then washed 5 times and spun-dried. TMB color-substrate solution was added on an Elisa plate. They were removed from light and left to react at 37°C. The solution was shaken. Fifteen min later, 50 µl TMB stop buffer was added. Absorbance OD value of every space was measured at wave length of 450 nm. Then the standard curves were elaborated.

Findings on the result of Bcl-2 protein immunologic tissue experiment: if the cytomembrane or cytoplasm takes the shape of claybank, it is positive, which can be estimated through cancer cell count and the use of staining-intensity semi-quantitative integral method, negative (<4 points) and positive (≥4 points).

Findings on the result of Bcl-2 protein immunologic tissue experiment: if cytoplasm has claybank particles, there is positive staining, which can be estimated by the percentage of positive staining and staining-intensity semi-quantitative integral, negative (0-2 points), weak positive (3 points), positive (4-5 points) and strong positive (6 points).

Statistical method

χ^2 was used to examine E-cad and Bcl-2, and to analyze the correlation of them with pathological features of breast cancer. Spearman's rank correlation was used to analyze the correlativity of the expression of E-cad and Bcl-2 in breast cancer tissue and the change of concentration of sE-cad. Variance analysis was adopted for the calculation of the concentration of sE-cad in serum. The *t*-test was used for examining correlation between the samples of the two groups.

RESULTS

The expression of E-Cad and Bcl-2 in normal adjacent tissue, hyperplasia tissue and cancer tissue

The assessment of E-cad and Bcl-2 protein in the results of immunohistochemical experiments is shown in Fig. 1, of which A, B and C are the expression levels of E-cad protein in normal adjacent tissue, hyperplasia tissue and cancer tissue, respectively. D, E, and F are the expression levels of Bcl-2 protein in normal adjacent tissue, hyperplasia tissue and cancer tissue, respectively.

Under the high-power microscope, positive staining of E-cad could be seen in part of the breast cancer cell nucleus area (Fig. 1). It might result from the abnormal expression or abnormal accumulation of E-cad in cancer cells with the occurrence and development of cancer cells, which was consistent with previous reports that cells of some tumors such as gastric carcinoma, esophagus cancer, breast cancer also show phenomenon of nucleus displacement of E-cad. Abnormally expressed E-cad not only leads to the accumulation, differentiation of cells and even invasion and metastasis, but also can influence the expression of cancer gene or cancer suppressor gene. All in all, the results demonstrated that, E-cad is closely related to the differentiation and metastasis of breast cancer cells.

Comparison of statistics and scores: the positive expression rate of E-cad in normal and hyperplasia tissue have no statistical differences while it shows abnormal reduction in breast cancer tissue ($p<0.01$). The positive expression rate of group A, B and C are 93.3%, 76.7% and 47.1%, respectively. The positive expression rate of Bcl-2 protein in normal and hyperplasia tissues has no statistical difference while it shows abnormal increase in breast cancer tissue ($p<0.01$). The positive expression rates of group A, B and C are 16.7%, 23.3% and 57.1%, respectively. The specific comparison is as shown in Table II. Group A presents normal breast tissue adjacent to tumors; group B presents hyperplasia tissue of breast cancer; group C presents breast cancer tissue. Group A and B will be compared to group C.

As shown in Table II, it was found that the positive expression rate (47.1%) of E-cad in breast cancer tissue was remarkably lower than in adjacent abnormal tissue (93.3%) and in hyperplasia tissue (76.7%), moreover, the positive expression of the tissues tended to decline as the lesion became worse. This demonstrates that, the expression of E-cad gradually decreased as the normal mammary epithelial cells evolved into breast cancer tissue.

Relationship of the expression of E-Cad and Bcl-2 protein with the pathological factors of breast cancer patients

During this research, we found that the expression of E-cad, Bcl-2 protein has no connection with the age of patients or the size of tumors ($p>0.05$). However, it is closely related to the grading of histopathology, the metastasis of lymphonodus and the clinical TNM staging ($p<0.05$). Detailed research results are shown in Table III.

As shown in Table III, when $p<0.05$, the two are closely related; when $p>0.05$, hardly related; in histopathological differentiation, metastasis of lymphonodus and clinical TNM staging, the positive expression rates of E-cad and Bcl-2 protein show opposite phenomenon.

It can be concluded from the experimental results (Tables II and III) that the positive expression rates of Bcl-2 are 57.1%. 23.1% and 16.7%, respectively

Table I. *Clinical features of breast cancer patients.*

Clinicopathologic feature		Cases (n)	%
Age	<50	46	65.7
	≥50	24	34.3
Size of tumor(cm)	<2	38	54.3
	≥2	32	45.7
Grading of histopathology	High-medium differentiation	36	51.4
	Low differentiation	34	48.6
Lymphatic metastasis	yes	47	67.1
	no	23	32.9
Clinical TNM stage	I~II stage	43	61.4
	III stage	27	38.6

Table II. *Comparison of expression of E-cad and Bcl-2 protein in breast cancer tissue in each group.*

group	Case (n)	E-cad					Bcl-2 protein				
		-	+	Positive rate (%)	χ^2	P	–	+	Positive rate (%)	χ^2	P
A	30	2	28	93.3	20.345	0.01	25	5	16.7	17.521	0.01
B	30	7	23	76.7	7.985	0.005	23	7	23.3	12.423	0.001
C	70	37	33	47.1			30	40	57.1		

in the breast cancer tissue, breast hyperplasia tissue and adjacent normal breast cancer tissue groups, are of statistical significance (χ^2=17.521, p<0.01; χ^2=12.423, p<0.001); the expression of Bcl-2 was correlated to breast pathological grading, differentiation of tumor tissue and metastasis of lymphonodus, and its correlation with pathological grading was positive.

Correlation of the expression of E-Cad and Bcl-2 protein

The positive expression rate of E-cad and Bcl-2 protein in breast cancer tissue shows that the two are apparently negatively correlated (r=-0.709, P<0.05). The results of the specific analysis is shown in Table IV.

Through analyzing the correlation between the positive expression rate of E-cad and Bcl-2 in breast cancer tissue (Table IV), it was found that, they were in significant negative correlation (r= -0.713, p< 0.05). Thus, it was speculated that, E-cad might be involved in the regulation of cell cycles and influence on cell apoptosis through acting on Bcl-2, thereby disrupting the mechanism of breast cancer cells, but the actual function and mechanism need further verification.

Table III. *Relationship of the expression of E-cad and Bcl-2 protein with the clinicopathologic feature of breast cancer.*

Clinical index		Case (n)	E-cad			χ^2	P value	Bcl-2 protein			X^2	P value
			positive	negative	Positive rate (%)			positive	negative	Positive rate (%)		
Age	<50	41	18	22	43.9	2.010	0.154	30	11	73.2	1.028	0.332
	≥50	29	17	12	58.6			19	10	65.5		
Size of tumor (cm)	<2	41	26	15	63.4	2.016	0.149	23	17	56.1	0.316	0.541
	≥2	29	15	12	51.7			18	11	62.1		
Grading of histopatology	High-medium differentiation	37	12	25	32.4	4.821	0.027	20	17	54.1	4.953	0.028
	Low differentiation	33	22	11	66.7			10	23	30.3		
Metastasis of lymphonodus	yes	46	13	32	28.2	4.012	0.046	39	7	84.8	8.572	0.003
	no	24	14	8	58.3			12	12	50.0		
Clinical TNM staging	I□II stage	39	25	14	64.1	7.612	0.007	21	18	53.8	4.425	0.038
	III stage	31	10	20	32.3			24	7	77.4		

As shown in the table above, when p<0.05, it indicates the two are closely related; when p>0.05, hardly related; in histopathological differentiation, metastasis of lymphonodus and clinical TNM staging, the positive expression rates of E-cad and Bcl-2 protein show opposite phenomenon.

Detection result of sE-cad in different groups

The detection result of sE-cad in groups A, B and C are shown in Table V, which shows that, sE-cad levels in serum had statistical significance (groups C and A: t=-19.456, p<0.001); groups B and A: t=-2.623, p<0.05), while the difference between the normal breast cancer group and the breast hyperplasia group had no statistical significance (P> 0.05).

Table IV. *Comparison of the relationship of E-cad and Bcl-2 in breast cancer tissue.*

E-cad	Cases (n)	Bcl-2		X^2	r	P value
		positive	negative			
positive	33	5	28	35.687	-0.713	0.001
negative	37	31	6			

Table V. *Comparison of the detection result of sE-cad level in serum (mg/ml).*

Grouping	Case (n)	Mean ± SD (mg/ml)	t	P value
Group A	30	1.812±0.208		
Group B	30	2.219±0.254	-2.623	0.03*
Group C	30	6.215±0.625	-19.456	0.000***

Group A: group of healthy female serum; group B: group of serum from breast cancer hyperplasia patient; group C: group of serum from breast cancer patient

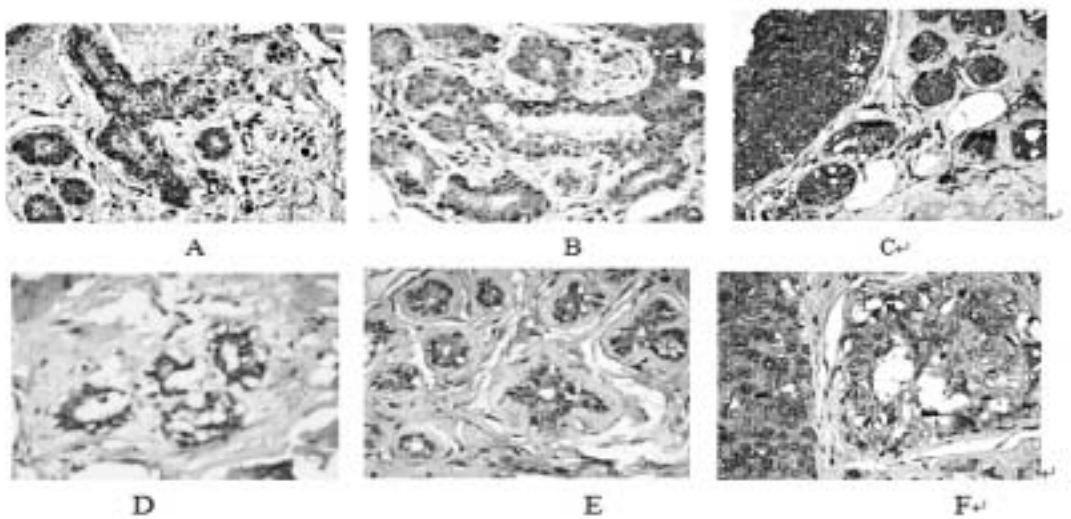

Fig. 1. *The expression of E-cad and Bcl-2 in breast cancer in each group.*

Correlation of Se-Cad level in serum with the expression of E-Cad in breast tissue

As shown in Fig. 2, the positive expression rates of the level of sE-cad in serum and the level of E-cad in breast tissue are negatively correlated. sE-cad was negatively correlated to the positive expression rate of E-cad in breast tissue ($r = -0.766$, $p < 0.05$), as shown in Fig. 2. It demonstrated that, the expression of the two proteins had both statistical significance and high correlation. When tumor occurs, the rapid proliferation and growth of cancer cells leads to the increase in apoptotic cancer cells, and then speeds up

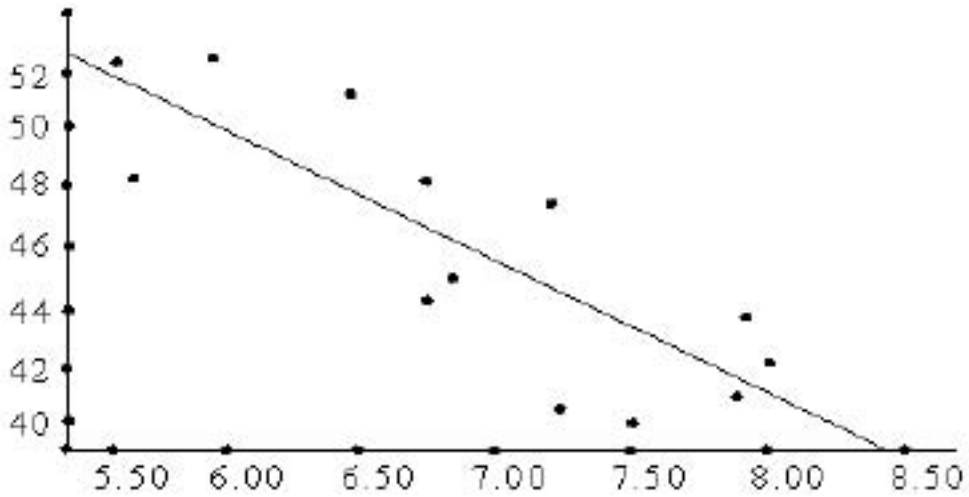

Fig. 2. *Positive expression rates of the level of sE-cad in serum and the level of E-cad in breast tissue are negatively correlated.*

E-cad metabolism and protein dissolution, finally, the concentration of sE-cad in serum rises abnormally.

DISCUSSION

E-cad, a transmembrane glycoprotein, is an important member of the cadherin family. E-cad mainly exists in non-neurological epithelial tissues such as those of the breasts (14), thyroid and gastric epithelium. Its structure is made up of transmembrane domain, extracellular domain (N-amino terminal) and intracellular domain (C-carboxyl terminal). Transmembrane domain is the hydrophobic domain, containing 32 amino acid molecules. Extracellular domain is a calcium binding domain. Intracellular domain is a series of catenin (3), which adjust the polymerization and depolymerization of adhesion molecules (15) and also mediates endocytosis, degradation, transduction of intracellular signals, transcription of genes and adjustment of partial cytoskeletal proteins (16). A number of studies indicate that the positive expression of E-cad can inhibit the expression of cancer. However, the abnormal decrease or deficiency of E-cad expression can decrease cell adhesion and speed up the invasion and metastasis of tumor cells (17). It can also cause disorder of cell apoptosis mechanisms and promote the generation of tumors, as proved by some studies (18). In addition, the expression of E-cad has nothing to do with the age of a patient or the size of a tumor, while it is closely related to the degree of histopathology, metastasis of lymphonodus and the clinical TNM stage. When the cancer cells differentiate normally, then the expression of E-cad is normal, invasion between cells is less and adhesion is good, whereas the cells react to the phenomenon of an invasive attack and adhesive dispersion (19). Therefore, the degree of invasion and the adhesion ability of tumor cells could be viewed to judge the seriousness of cancer.

sE-cad protein is created due to the degradation of the extracellular structure of E-cad protein or the death of cells in normal epithelial tissue (20). They participate in the invasion and metastasis of tumor cells, conditioning the biological behavior and prognosis of a tumor (21). A healthy human body contains a small amount of sE-cad. However, when E-cad split abnormally and the content of sE-cad abnormally rises, the symptoms of tumor are more obvious. Experimental research illustrates that in various epithelial malignant tumors such as breast cancer, gastric cancer (22) and bladder cancer (23), the level of sE-cad in serum increases and it participates in abnormal activities of non-epithelial

tumors such as the activation of signals, failure of cell connection, invasion and metastasis. The level of sE-cad does not obviously change in non-epithelial tumors. Therefore, we can judge epithelial tumors by detecting the content of sE-cad. This research indicates that the level of sE-cad in serum and the positive expression rate of E-cad in breast tissue are negatively correlated.

As an important component of cell apoptosis and inhibition, anti-apoptosis Bcl-2 protein plays an important part in the pathogenesis of cells. This research shows that the positive expression rate of Bcl-2 protein is positively correlated with pathological grading and metastasis of lymphonodus. It is in agreement with the conclusion of the research on the expression of ASAH1 and Bcl-2 Protein Expression in Breast Cancer and Its Clinical Meaning by Cui Kai et al. (24). Expression of Bcl-2 protein and E-cad are negatively correlated. The abnormal expression of E-cad can affect or inhibit the expression of tumor genes. Therefore, we deduce that E-cad may affect the expression of Bcl-2 in genes and thus influence the periodical change of tumor cells and the expression of cells. It prospects great application in the judgment of the pathogenesis of breast cancer.

In conclusion, the positive expression of E-cad and anti-apoptosis Bcl-2 protein are negatively related in breast cancer. The positive expression obviously decreases in breast cancer tissue, rather than normal breast cancer and breast cancer hyperplasia tissue. However, the expression of Bcl-2 is exactly contrary. Both E-cad and Bcl-2 are related to the pathological grading and metastasis of lymphonodus. sE-cad levels in serum from breast cancer patients are significantly higher than that from normal and benign hyperplasia patients. The experiments in this research prove that, the change in the serum levels of sE-cad in breast cancer tissue is negatively correlated to the positive expression rate of E-cad in normal breast tissue, therefore, it can be taken as an important index of occurrence and development of tumors and can provide a powerful tool in assessing treatment and prognosis. Therefore, it is clear that E-cad can play an important role in the occurrence, development and metastasis of breast cancer cells and can become one of the indexes for determining the biological behavior of breast cancer. Moreover, sE-cad level changes may become an index of tumor marker, used for diagnosing biological behavior of breast cancer, thereby providing an important basis for early diagnosis and monitoring of breast cancer.

ACKNOWLEDGEMENTS

This project was supported by the National Natural Science Foundation of China.

REFERENCES

1. Zhang H, Xiang MJ, Mao SL, Wu Y, Li YX, Li MQ, Chen H. The clinical value of the combined measurement of three serum tumor markers in breast cancer. Chin J Lab Diagn 2011; 22(1):22.
2. Li L, Yang HY. Abnormal expression and meaning of adhesion molecule E-cadherin in breast cancer. J Oncol 2008; 6(2):135-40.
3. Rodriguez FJ, Lewis-Tuffin LJ, Anastasiadis PZ. E-cadherin's dark side: possible role in tumor progression. Biochim Biophys Acta 2012; 1826(1):23-31.
4. Liu YB, Zhong J, Wen GB. research progress of molecular regulatory mechanism of E-cad in breast cancer. J Mod Med Health 2014; 30(8):1190-1192.
5. Li LX, Hu WH, Liu GY, Zhang Y. The expression and its significance of EGFR, ER and E-cadherin in breast cancer. China Mod Doc 2013; 51(20):30-31
6. Xu J, Zhang S, Zhang YJ, Jin K, Gu XH. Relationship of C-erbB-2 and E-cadherin Expressions in breast cancer and lymph node metastasis. Jiangsu Med J 2013; 39(1):85-87.
7. Weiss JV, Klein-Scory S, Kubler S, Reinacher-Schick A, Stricker I, Schmiegel W, Schwarte-Waldhoff S. Soluble E-cadherin as a serum biomarker candidate: elevated levels in patients with late-stage colorectal carcinoma and FAP. Int J Cancer 2011; 128:1384.
8. Fang JG, Feng RT. Inhibitive factors of Apoptosis Protein (IAP) and Bcl-2 protein family and tumor immunity treatment. Clin Misdiagn Mistherapy 2010; 23(7):673-75.
9. Douglas Hanahan, Robert A. Weinberg. Hallmarks of cancer: the next generation. Cell 2011; 144(5):646-74.
10. Gu WW, Shi T, Gu YH, Yang J. Research progress

of programmed cancer cell death regulated through interaction between Bcl-2 and IP3R. Tumor 2013; 33(8):743-746.
11. Tan MD, Li L, Liu GW. Research progress on relationship between E-Cadherin and inflammatory breast cancer. Anti-Tumor Pharm 2012; 2(4):249-52.
12. Kraus MD, James A, David J, et al. Predictors of pathologic complete response after standard neoadjuvant chemotherapy in triple-negative breast carcinoma. Appl Immunohistochem Mol Morphol 2012; 14(8):334-38.
13. Makhoul I, Kiwan E. Neoadjuvant systemic treatment of breast cancer. J Surg Oncol 2011; 103(4):348-57.
14. Shi ZM, Liu JX, Liu HM, Wang L, Yang XX. Expression and significance of EBP50, β-catenin and E-cadherin in human breast cancer tissue and its significance. Chin J Lab Diagn 2010; 14(10):1558-60.
15. Parsons JT, Horwitz AR, Schwartz MA. Cell adhesion: integrating cytoskeletal dynamics and cellular tension. Nat Rev Mol Cell Biol 2010; 11(9):633-44.
16. Hartsock A, Nelson WJ. Adherens and tight junctions: structure, function and connection to the actin cytoskeleton. Biochim Biophys Acta 2008; 1778(3):660-69.
17. Tan MD, Huang G, Zhou DG, Liu Guowen. The role of E-cadherin in tumor. Anti-Tumor Pharm 2013; 3(4):255-58.
18. Fausto J. Rodriguez, Laura J. Lewis-Tuffin, Panos Z.Anastasiadis. E-cadherin's dark side: Possible role in tumor progression. Biochim Biophys Acta 2012; 1826(1):23-31.
19. Dong JY, Li QC. EMT, embryonic development and tumor invasion and metastasis. Mod Oncol 2010; 18(02):0396-98.
20. Xu YY. Clinical significance of determining serum level of soluble epithelia cell cadherin in the treatment of acute lymphocyte leukemia. J Shihezi Univ (Nat Sci) 2013; 31(1):3-15.
21. Gao SY, Song R, Li SL, Liu JJ, Huang KL, Li LY. The expression and significance of E-cadherin and sE-cadherin in 42 cases of prostate cancer. Chongqing Med J 2010; 39(27):3240-41.
22. Li X, Zhang JF, Zhan Z, Yang YP. TCM syndrome research on relations of serum-soluble epithele E-cad with stomach cancer. Chin J Info Trad Chin Med 2014; 21(1):30-32.
23. Jäger T, Becker M, Eisenhardt A, et al. The prognostic value of cadherin switch in bladder cancer. Oncol Rep 2010; 23(4):1125-32.
24. Cui K, Wang H, Qi P, Zai SF, Xu ZW. Research on the expression of ASAH1 and Bcl-2 protein expression in breast cancer and its clinical significance. Chin J Coal Ind Med 2012; 15(4):496-98.

PROFILE OF SELECT HEPATIC INSULIN SIGNALING PATHWAY GENES IN RESPONSE TO 2-AMINOANTHRACENE DIETARY INGESTION

N.D. MATTIS[1], J.W. JAY[1], G.W. BARNETT[1], J.J. ROSALDO[1], E.W. HOWERTH[2], J.C. MEANS[3] and W.E. GATO[1]

[1]Department of Chemistry, Georgia Southern University, Statesboro, GA USA; [2]Department of Pathology, College of Veterinary Medicine, The University of Georgia, Athens, GA, USA; [3]Bren School of Environmental Science & Management, UC Santa Barbara, Santa Barbara, CA, USA

Received June 11, 2014 - Accepted October 3, 2014

Some genes that regulate various processes such as insulin signaling, glucose metabolism, fatty acid, and lipid biosynthesis were profiled. The objective of the current investigation is to examine the mRNA expression of some genes that mediate insulin signaling due to 2AA toxicity. 2AA is a polycyclic aromatic hydrocarbon (PAH) that has been detected in broiled food and tobacco smoke. Twenty-four post-weaning 3-4-week-old F344 male rats were exposed to 0mg/kg-diet, 50mg/kg-diet, 75mg/kg-diet, and 100mg/kg-diet 2AA for 2 weeks and 4 weeks. The mRNA expression of AKT1, G6PC, GCK, GLUT4, INSR, IRS1, PP1R3C, PAMPK, SOCS2, and SREBF1 was determined by qRTPCR followed by the quantification of G6PC and AMPK via ELISA. The results suggest that 2AA modulates these genes depending on the length of exposure. Up-regulation of AMPK and SOCS2 genes in animals treated with 100mg/kg-diet and 50mg/kg-diet, respectively, during 14 days of feeding was noted. G6PC expression was inhibited in the 2-week group while being dose-dependently increased in the 4-week group. Hepatic activity of G6PC was enhanced significantly in the livers of rats that ingested 2AA. It appears that 2AA intoxication leads to the activation of irs1 and akt1 genes in the liver. Quantified AMPK amounts increased significantly in the short-term treatment group. Dose-dependent rise of AMPK in animals treated to 2AA showed an increased production of hepatic AMPK in response to the toxicity of 2AA in order to maintain cellular homeostasis. In contrast, the reduction in AMPK concentration in treated animals within the 4-week set indicated an adaptive recovery.

Recent population studies found a link between certain types of environmental chemical exposures and changes in the insulin signaling pathway. This evidence can be seen in the correlation between rising diabetes rates and the production of organic chemicals via linking of these chemicals and obesity (1). Polycyclic aromatic hydrocarbons (PAHs) are one type of environmental contaminants that is specifically linked to changes in insulin-related processes. Environmental exposure to PAHs modulates various cellular and biochemical processes in the cell in an insulin-dependent manner (2). A recent study by Khalil and coworkers (3) found that exposure to benzo[a]pyrene, in addition to a high fat diet, reduced the expression of genes related to insulin secretion. They are formed from

Key words: liver, insulin signaling pathway, AMP-activated protein kinase (AMPK), glucose-6-phosphatase (G6PC), gene regulation, 2-aminoanthracene

Mailing address: Dr. Worlanyo E. Gato,
Assistant Professor of Biochemistry,
Department of Chemistry,
Georgia Southern University
Statesboro, GA 30458, USA
Tel.: +1 912 478 5922
e-mail: wgato@georgiasouthern.edu

0393-974X (2014)

the "incomplete combustion of organic materials" (3) and can be found in a wide range of products including coal, tar, crude oil, cereals, grains, flour, vegetables, and pickled foods (4).

A recent investigation by Gato et al. (5) found that 2-aminoanthracene (2AA), a polycyclic aromatic hydrocarbon, may alter the expression of important genes in the liver of Fisher 344 rats in relation to the insulin signaling pathway. 2AA belongs to a class of aromatic amines, arylamines, that are naturally and synthetically occurring mutagens that undergo metabolic activation in the liver (5, 6). They occur from burning tobacco and broiling meat, but may also be produced synthetically for industrial purposes. Compared to other PAHs, 2AA is thought to be more harmful and also has a greater probability of human exposure (4).

This present study explored the effects of 2AA on the insulin signaling pathway, primarily focusing on the gene expression of AKT1, G6PC, GCK, GLUT4, INSR, IRS1, PP1R3C, PRKAB1 (AMPK), SOCS2, and SREBF1 in the liver of Fisher 344 rats. These hepatic genes were chosen because each plays an important role in the insulin pathway and they are vital to its normal function. Investigation of the exposure of 2AA on these genes could lead to advances in understanding why some populations are more prone to developing type 2 diabetes. A brief description of these mRNA transcripts is shown in Table I.

MATERIALS AND METHODS

Experimental design

Rats were purchased from Harlan Laboratories. The animals were 3-4 weeks old at the time of treatment. The animals were randomly assigned into dose regimens of 0mg/kg-diet (control), 50mg/kg-diet (low dose), 75mg/kg-diet (medium dose), and 100mg/kg-diet (high dose) 2AA for either 14 or 28 days. There were three animals in each treatment group. The animals were housed in individual cages at the Southern Illinois University Animal Facility with a 12h/12h light/dark cycle. The rats had access to distilled water ad libitum. The animals were handled according to the guidelinesof the National Institute of Health (NIH) and Southern Illinois University Guide for Care and Use of Laboratory Animals [IACUC protocol # 09-039]. At the end of treatment, the rats were euthanized and blood was collected by cardiac puncture. Excised livers were immediately frozen in liquid nitrogen.

Diet preparation

2AA (CAS # 613-13-8) [98+% pure] was obtained from Sigma-Aldrich, St Louis, MO, USA). Diet preparation involved the immersion of 1 kg diet obtained from PMI (Nutrition International, LLC Brentwood, MO, USA) in 1-L molecular grade ethyl alcohol containing the appropriate amount of 2AA. The alcohol was then evaporated under the hood with periodic mixing. This was followed by storage of the diet in a freezer, protecting it from light.

Histopathology

The frozen liver samples were quickly thawed and post-fixed overnight in normal buffered formalin. The samples were paraffin-embedded and sectioned at 5 □ onto glass slides and stained with hematoxylin and eosin (H&E). A histopathology of selected 2AA exposed liver tissues is shown in Fig. 3.

Total RNA extraction

Total RNA was extracted from the livers of the rats using a Qiagen RNA Isolation kit (Qiagen, Valencia, CA, USA). Approximately 30 mg of liver was homogenized in RLT buffer to denature and inactivate RNases. The RNA was then allowed to bind to a silica-gel membrane and was finally eluted with RNase-free water according to the manufacturer's guidelines (Qiagen RNeasy mini handbook, 2011, Valencia, CA, USA). Total RNA was quantified using the UV-vis spectrophotometer and 260 and 280 nm absorbance. RNA electrophoretic gels were run to determine the RNA quality. The quality of the extracted RNA was also examined using Bio-Rad Laboratories' Experion™ RNA StdSens Analysis Kit (Bio-Rad Laboratories Inc., Hercules, CA, USA).

mRNA quantification of selected insulin signaling pathway genes by RT-PCR

The expression of key gene transcripts reported to be important in mediating insulin signaling processes was examined via quantitative RT-PCR. Two classes of transcripts were analyzed. They included genes (G6PC, GCK, PP1R3C, PRKAB [AMPK], SOCS2, and SREBF1 measured with GAPDH as the control gene) that were previously reported to respond to 2AA toxicity via microarray and DAVID bioinformatics analytical tool (5). In addition, four major insulin signaling pathway genes: AKT1, INSR, IRS1, and GLUT4 were quantified. FASTA mRNA sequences for these selected genes were obtained for Rattus norvegicus from the National Center for the Biotechnology Information (NCBI). Using NCBI Primer-Blast, forward and reverse primers were designed for each mRNA transcript. These oligonucleotide sequences, obtained from Integrated DNA Technologies Inc. (IDT;

Table I. *Description of mRNA transcripts.*

Gene	Description	References
AKT1	AKT is a component of the PI-3 kinase pathway and is activated by phosphorylation at Ser 473 and Thr 308. AKT is a key regulator of many signal transduction pathways including insulin and glucose metabolism.	(7)
G6PC	G6PC codes for glucose-6-phosphatase, which is an integral membrane protein that catalyzes the hydrolysis of D-glucose 6 phosphate to D-glucose and orthophosphate. It is a key enzyme in glucose homeostasis, functioning in gluconeogenesis and glycogenolysis.	(8, 9)
GCK	GCK codes for glucokinase, which is an enzyme that facilitates phosphorylation of glucose to glucose-6-phosphate.	(10)
GLUT4	Glucose transporter type 4 is primarily responsible for insulin-regulated glucose transport into cells. Impairment of GLUT4 trafficking and translocation has been observed in insulin-dependent diabetes.	(11)
INSR	The insulin receptor belongs to a class of proteins referred to as tyrosine kinase receptors. Insr is activated by insulin. This gene plays a key role in the regulation of glucose homeostasis. Deficiency in this protein will ultimately result in clinical manifestations including diabetes.	(12)
IRS1	Insulin receptor substrate 1 mediates signal transfer from insulin and insulin-like growth factor to intracellular pathways including insulin signaling pathway. Mutation in Irs1 has been implicated in type 2 diabetes and insulin resistance.	(13)
PPP1R3C	PPP1R3C codes for protein phosphatase-1 (PP1), which participates in the regulation of a wide variety of cellular functions by reversible protein phosphorylation.	(14)
PRKAB1	PRKAB1 codes for 5'-AMP-activated protein kinase subunit beta-1, which is a regulatory subunit of the AMP-activated protein kinase (AMPK). AMPK is an important energy-sensing enzyme that monitors cellular energy status.	(15)
SOCS2	SOCS2 codes for a member of the STAT-induced STAT inhibitor (SSI) family, which is cytokine-inducible negative regulators of cytokine signaling.	(16)
SREBF1	SREBF1 codes for Sterol regulatory element-binding transcription factor 1, which is a transcription factor that binds to a sequence in the promoter of different genes and plays a key role in sterol biosynthesis.	(17)

Coralville, IA, USA), are shown in Table II.

First strand synthesis of cDNA was accomplished using the iScript reverse transcription supermix for RT-qPCR (Bio-Rad Laboratories Inc., Hercules, CA, USA). Synthesized cDNA was mixed with the primer set and SsoFast EvaGreen supermix for the RT-qPCR reaction. The product was quantified via a Bio-Rad CFX96™ instrument (Bio-Rad Laboratories Inc.) according to the manufacturer's guidelines. The normalized gene expression values were determined via relative (delta Cq) gene expression and are represented in Figs. 4 and 5.

ELISA G6PC assay

The level of glucose-6-phosphatase catalytic (G6PC)

Table II. *Nucleotide sequences designed as forward and reverse primers of each specific gene.*

AKT1	Forward	5' TACCATGAACGACGTAGC 3'
	Reverse	5' CCACTGAGAAGTTGTTGAGT 3'
G6PC	Forward	5' CTACTCTCGCTATCTTTCGT 3'
	Reverse	5' AGGTGATGAGACAGTACCTC 3'
GCK	Forward	5' CAGAGATGGCTATGGATACT 3'
	Reverse	5' AGGTGGGTAACATCTTTACA 3'
GLUT4	Forward	5' GGGACACTATACCCTATTCA 3'
	Reverse	5' CAATGTTATAGCCAAACTGA 3'
INSR	Forward	5' ACAGTGTTGCTTGCAG 3'
	Reverse	5' AGGTTGTTCCGGATGT 3'
IRS1	Forward	5' AGTGAGGATTTAAGCACCTA 3'
	Reverse	5' GTACCCATGAGTTAAAAAGG 3'
PPP1R3C	Forward	5' CTGCATCCGCTAAGTG 3'
	Reverse	5' CATGACTGAACTTGTCAAAG 3'
PRKAB1 (AMPK)	Forward	5' TATTTGATGCTTTAATGGTG 3'
	Reverse	5' ATCCTTGATAGAGAGTGCAT 3'
SOCS2	Forward	5' AATTTGGAGAGAAACAACC 3'
	Reverse	5' TGGCTTCATTAACAGTCATA 3'
SREBF1	Forward	5' TATCAATGACAAGATTGTGG 3
	Reverse	5' TTTCTACCACTTCAGGTTTC 3'

protein in liver tissues was quantified using an enzyme-linked immunosorbent assay (ELISA). This assay is based on the biotin double antibody sandwich technology (Human G6PC Elisa Kit Operating Manual, MyBiosource Inc., San Diego, CA, USA). Samples containing G6PC were added to wells that were pre-coated with G6PC monoclonal antibodies and then incubated for 60 min at 37°C. Anti-G6PC antibodies labeled with biotin were added to the wells after incubation. The wells were washed to remove unbound enzymes. Chromogen solutions were added to the mixture to enhance color development. The extent of coloration is proportional to the amount of G6PC in each standard and sample. Absorbance (OD) values were measured on a microplate reader (Spectra Max 190, Molecular Devices Corporation, Sunnyvale, CA, USA) at 450 nm. The standard curve employed to quantify the level of G6PC in liver tissues is shown in Fig. 1.

Hepatic quantification of AMPK-α via ELISA

Hepatic adenosine monophosphate-activated protein kinase was quantified using 5' AMP-activated protein kinase catalytic subunit enzyme-linked immunosorbent assay following guidelines provided by the manufacturer (AMPKa pThr172 ELISA kit, Abcam Inc., Cambridge, MA, USA). Plates were pre-coated with specific mouse monoclonal antibody. Samples and standards were pipetted into the wells along with a rabbit monoclonal primary detector antibody, and then incubated for 3 h at room temperature. The plates were washed to remove all excess protein and unbound detector antibody followed by addition of an HRP-conjugated secondary detector to the wells. After 1 more hour of incubation, the plate was thoroughly washed and TMB solution was added to each well. A color change, that was directly proportional to the amount of AMPK-a pT172 that remained bound to the plate, was noted. After 15 min of color development, 100 µL of 1N HCl was added to terminate the reaction. Absorbance was measured at 450 nm on a microplate reader (Spectra Max 190, Molecular Devices Corporation, Sunnyvale, CA, USA). Standard curve (Fig. 2) was generated to calculate the hepatic amounts of AMPK.

Data analysis

Statistical significant differences in the hepatic

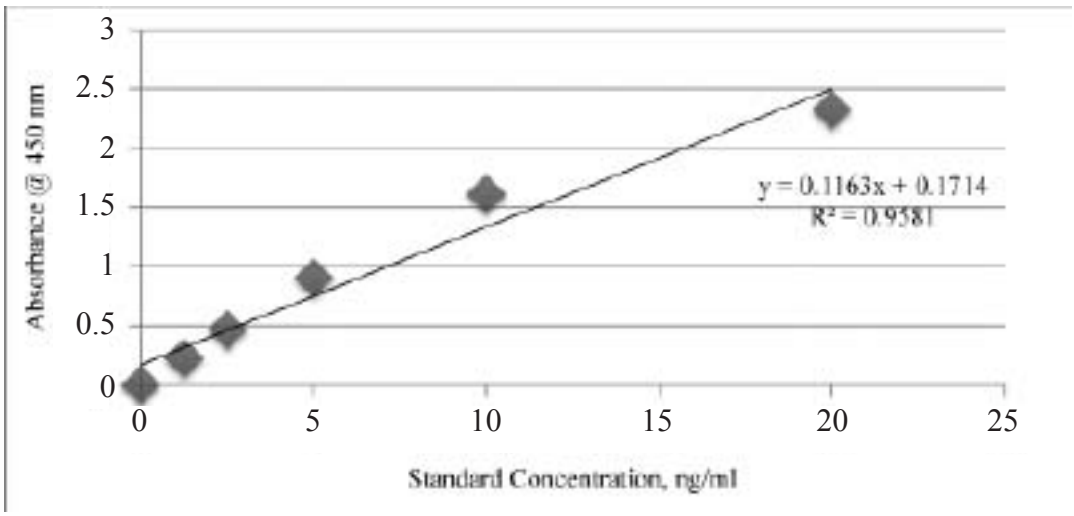

Fig. 1. *Standard curve for quantifying hepatic G6PC via ELISA. Dilution of 20 ng/ml G6PC solution was performed to generate several standard concentrations. Standard solutions were treated in similar fashion as the samples. Absorbance of standards and samples were determined at 450 nm using a microplate reading instrument.*

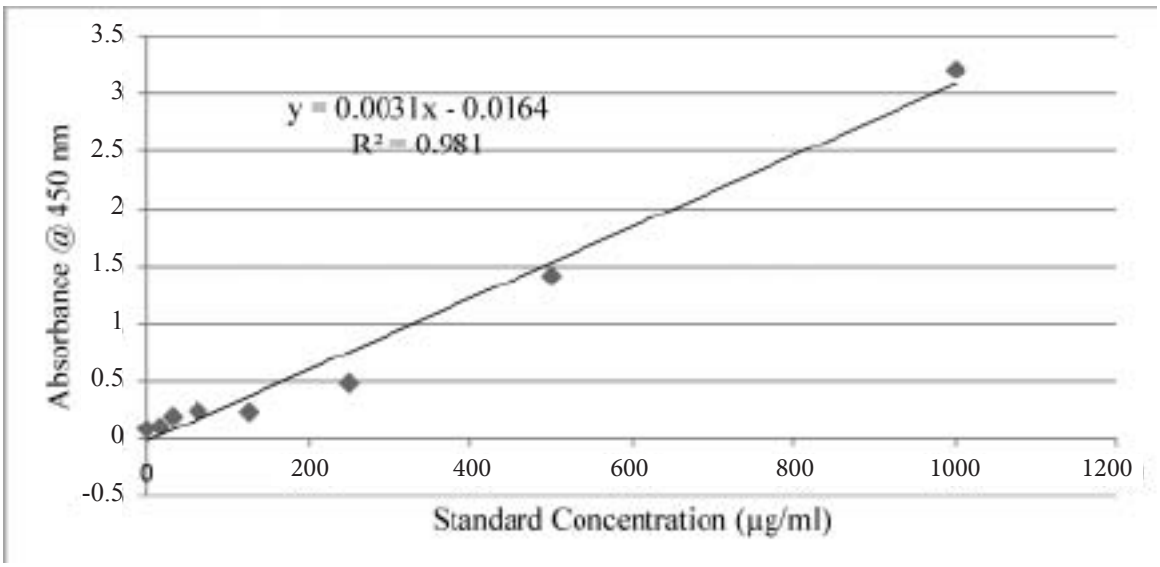

Fig. 2. *Standard curve showing plot of absorbance versus concentration employed to quantify hepatic ampk protein concentration. A standard concentration of 1000 µg/ml was further diluted to create a working dynamic range that was employed to link concentrations with absorbance. Absorbance was measured at 450 nm on a microplate reader.*

amounts of G6PC and AMPK proteins in the 2AA treated and untreated animals were calculated via analysis of variance (ANOVA). Data was presented at mean±SE. Significant differences were indicated as either * $P<0.05$ or ** <0.01.

RESULTS

Histopathology

Microscopic changes were dose- and time-dependent. When compared to the control group, the 2-week group exhibited minimal, mild, or moderate periportal hepatocellular cytologic alteration consistent with hypertrophy characterized by enlarged hepatocytes with intensely eosinophilic slightly granular cytoplasm and variably enlarged nuclei in the 2LD, 2MD, and 2HD groups, respectively (Fig. 1). By 4 weeks, periportal hepatocellular changes were more pronounced in all treatment groups; being mild in the 4LD group and moderate to severe, sometimes panlobular, in the 4MD and

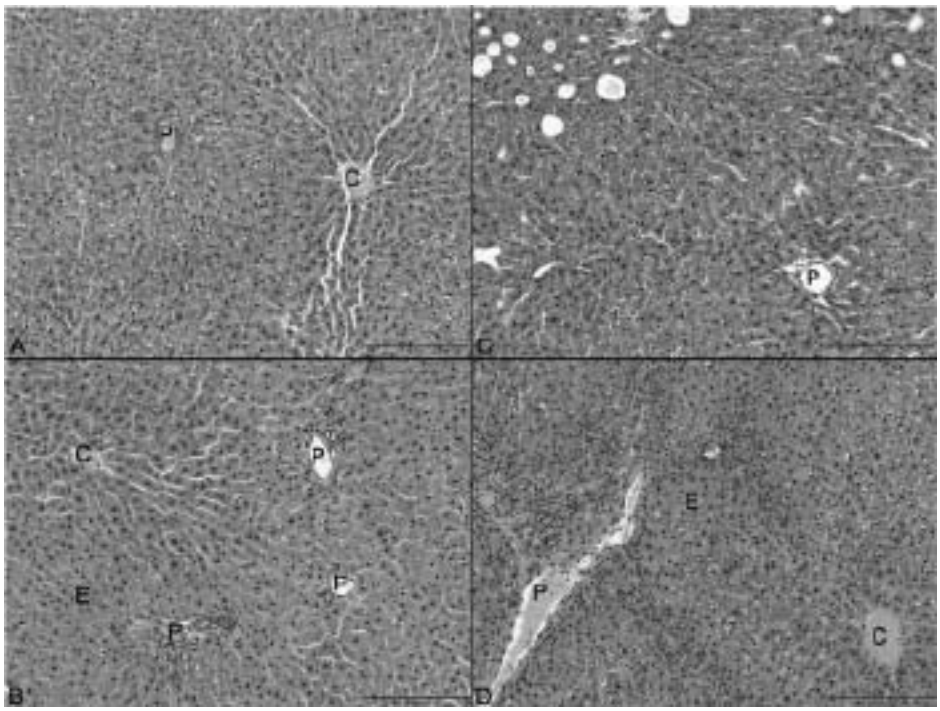

Fig. 3. *Histopathology of Selected 2AA exposed liver tissues from F344 Rats fed a contaminated diet for two and four weeks. A) Two weeks, control (0 mg/kg); no changes are observed. C=central vein; P=portal area. B) Two weeks, high-dose (100 mg/kg); a rim of hypertrophied hepatocytes surrounding portal areas (P) is hypereosinophilic (E) as compared to the hepatocytes surrounding the central vein (C) that look more similar to the control. Portal areas are more prominent than the control due to mild oval cell hyperplasia. C) Four weeks, control (0mg/kg); scattered lipid-filled cells are present. P=portal area. D) Four weeks, high-dose (100 mg/kg); the periportal hypereosinophilic zone of hypertrophy (E) is wider than at two weeks. Portal areas (P) are much more prominent and cellular than the control due to moderate oval cell hyperplasia which dissects around periportal hepatocytes, some of which are shrunken and apoptotic. A thin rim of hepatocytes that are similar in appearance to the control surrounds the central vein (C). HE stain, 200X.*

4HD groups. At this time, oval cell hyperplasia was mild in the 4LD group and moderate in the 4MD and 4HD groups with oval cells encircling individual periportal hepatocytes that appeared apoptotic in the 4MD and 4HD groups.

mRNA quantification of selected insulin signaling pathway genes by RT-PCR

We previously observed the expression of some genes that mediate insulin signaling through global gene expression analysis in animals that consumed 2AA (4). The relative gene expression (ΔCq) of G6PC, GCK, PP1R3C, AMPK, SOCS2, and SREBF1 were quantified by quantitative PCR. The rats fed 2AA for 2 weeks showed an overexpression of AMPK and SOCS2 in high-dose and low-dose animals, respectively. The rest of the genes were down-regulated. With respect to the 4-week 2AA treatment group, G6PC was highly expressed in treated animals relative to controls. Similar mRNA expression of PP1R3C in rats that ingested 2AA was observed. Srebf1 was at least 2-fold expressed in low-dose and medium-dose groups. Also, GCK was at least 4-fold changed in animals that were in the 75 mg/kg 2AA set. AMPK gene was barely expressed in the 4-week group (Fig. 4).

The next set of genes analyzed were transcripts that regulate the insulin signaling pathway but have not been previously reported to be modulated by arylamine chemical exposure. The genes examined in the rat livers after exposure to 2AA were AKT1, INSR, IRS1, and GLUT4. GLUT4 and INSR were

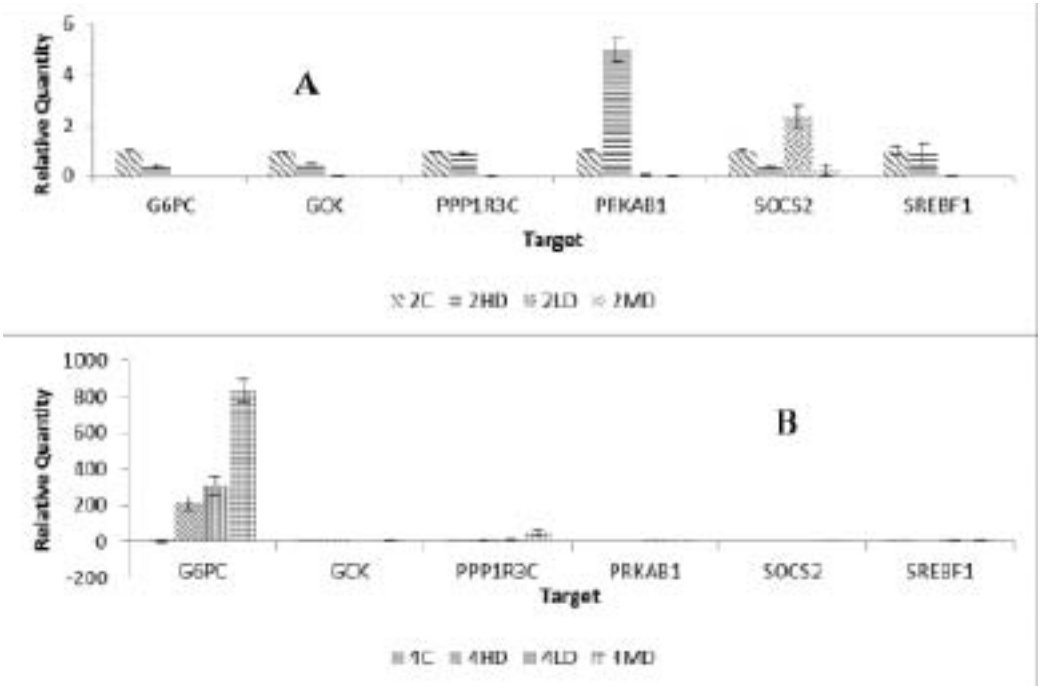

Fig. 4. *Relative hepatic gene expression of some insulin signaling pathway genes. These transcripts were previously noted via pathway analysis tool to be likely regulated by 2AA. Rats were fed a diet contaminated with 2-aminoathracene for 2 weeks (A) and 4 weeks (B).*

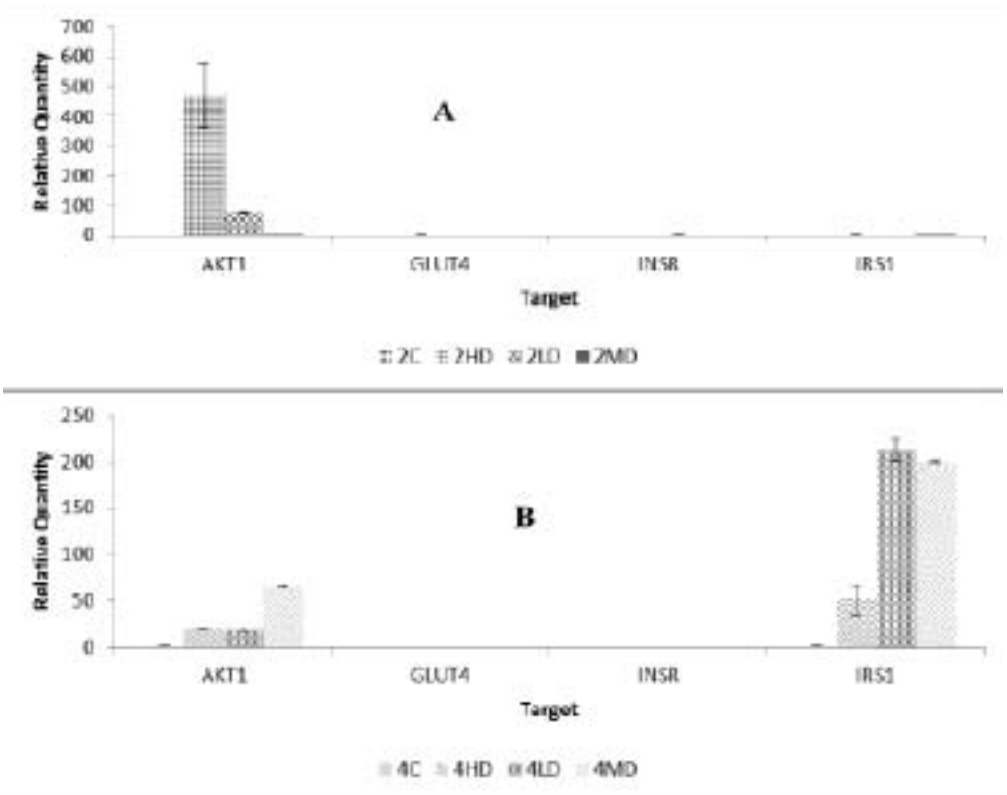

Fig. 5. *Gene expression (ΔCq) of selected insulin signaling pathway mRNA transcripts by quantitative real-time PCR. A) 14-day treatment group and B) 28-day exposure group. These genes have not been previously noted to be affected by 2AA.*

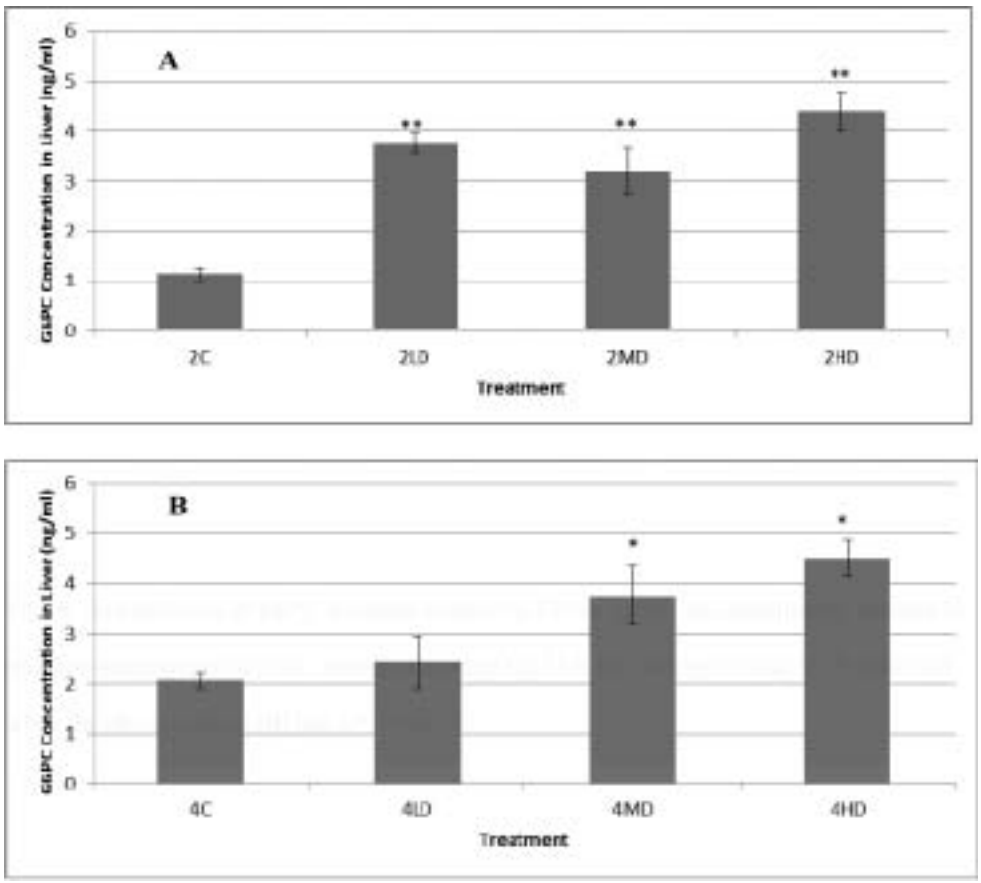

Fig. 6. *Quantification of G6PC in hepatic tissues via ELISA. G6PC was significantly elevated in rats that were exposed to 2AA. Animals that were fed 2AA for 14 days (A) had **, P<0.000564 while the 28-days Group (B) had a *, P<0.0135.*

not expressed at all in both treatment groups. IRS1 was up-regulated in a concentration-dependent manner in the 28-day group. Expression of IRS1 was not observed in the 14-day animals exposed to 2AA. AKT1 transcript was expressed dose-dependently in both the 14-day and 28-day animals that ingested 2AA (Fig. 5).

Quantification of G6PC and AMPK levels in liver tissues via ELISA

Hepatic G6PC levels were quantified. G6PC levels were reported to be involved in glucose homeostasis. This enzyme catalyzed the final steps of glycogenolysis and gluconeogenesis (18). G6PC levels in both treatment groups were significantly greater in the animals exposed to 2AA. For the 14-day rats, G6PC amounts were greatest in the high-dose group, followed by the low-dose and medium-dose respectively. With respect to the 28-day set, G6PC concentration was dose-dependent (Fig. 6). Although the low-dose rats indicated higher G6PC levels, they were not significant.

The amounts of AMPK in livers of F344 rats that ingested 2AA were measured. Protein AMPK is an important energy-sensing enzyme that monitors cellular energy status (15). The concentration of AMPK in the 2-week group increased in a dose-dependent fashion. That is, the high-dose animals indicated an average AMPK concentration of 658 µg/ml, followed by medium-dose animals (516 µg/ml), and low-dose animals (249 µg/ml). On the contrary, the 4-week set showed a dose-dependent reduction in AMPK levels in liver tissues. For instance, the AMPK in the low-dose animals reduced by 84% relative to the AMPK in the control rats. Similarly, AMPK levels in the medium- and high-dose sets

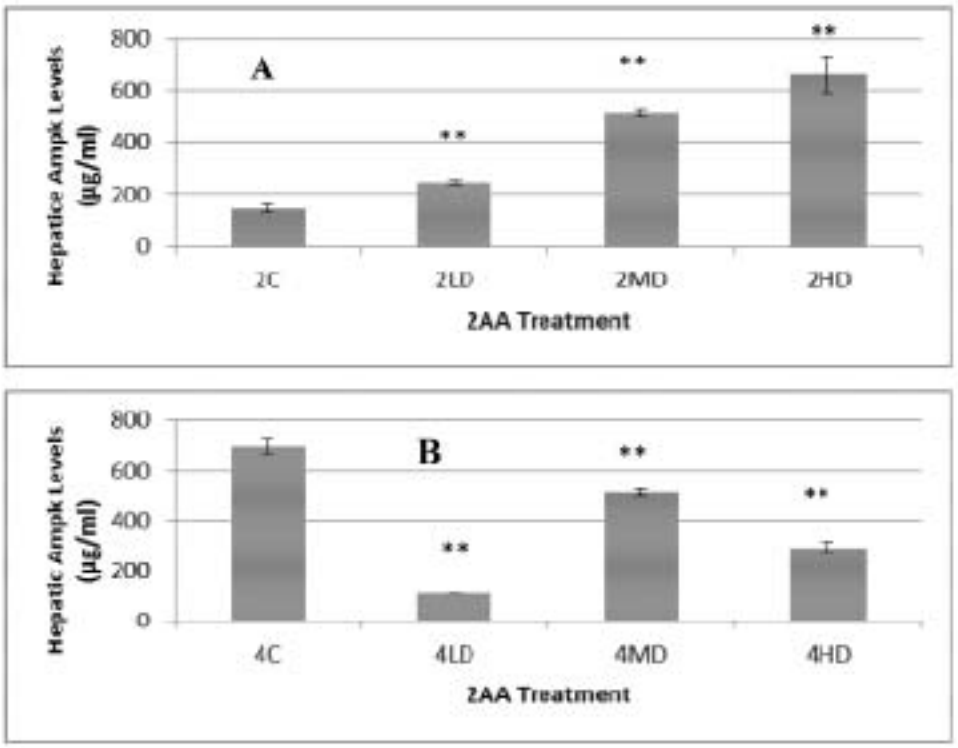

Fig. 7. *Hepatic concentration of AMPK (PRKAB1) in F344 rats fed various levels of 2AA for 2 weeks (**A**) and 4 weeks (**B**). For both treatment periods, rats ingested control – 0 mg/kg-, 50 mg/kg- (low-lose – LD), 75 mg/kg- (medium-dose – MD), and 100 mg/kg-2AA diet (high-dose – HD. Treated animals showed significantly (**, P<0.001) altered AMPK levels compared to control groups.*

reduced by 27% and 58% respectively (Fig. 7).

DISCUSSION

Insulin is a mediator of a wide range of biological processes including stimulation of glucose uptake, modulation of cell growth and differentiation, glycogen, lipid, and protein synthesis, antilipolysis, and activation of specific genes. The general mechanism of the insulin signaling pathway involves protein phosphorylation and dephosphorylation, and the insulin receptor itself is partly a tyrosine kinase that undergoes ligand-dependent activation (19). The metabolism of glucose in the blood is regulated by the release of insulin and glucagon. Insulin stimulates glucose uptake in muscle or fat cells because it moves GLUT4 vesicles to the plasma membrane of the cell. All insulin secreted by the pancreatic beta cells pass through the liver before entering the bloodstream, so the liver has the ability to regulate the amount of insulin in the blood (20, 21).

The goal of the present study was to profile the expression of some insulin signaling genes in the liver of F344 rats exposed to 2AA. Understanding the nature of the architecture of the liver in treated animals is essential to interpreting gene and protein expression data. Microscopic examination of liver post-2AA exposure indicated periportal hepatocellular hypertrophy; oval cell hyperplasia; and periportal apoptosis in treated animals when compared with control rats, the severity of changes increasing with increasing dose. In a previous study, we examined the link between 2AA exposure and apoptosis. Our findings suggest a dose-dependent increase in mRNA expression of apoptotic-related genes such as AEN (apoptosis enhancing nuclease) and BAX (Bcl2-associated X protein) (22).

Six genes intimately connected with the insulin signaling pathway were previously observed to be potentially modulated by 2AA in the liver (5). The

transcripts G6PC, GCK, PP1R3C, AMPK, SOCS2, and SREBF1 play various roles in metabolic processes (Table I). Relative quantification of these mRNA products indicated an up-regulation of the AMPK and SOCS2 genes in animals treated with the 100 mg/kg-diet and the 50 mg/kg-diet, respectively, during 14 days of feeding. The rest of the mRNA transcripts were down-regulated in the treated rats relative to the control group. In contrast, the G6PC gene was highly up-regulated in all animals that ingested 2AA for 28 days. PP1 protein was also up-regulated in the rats treated with the 75 mg/kg-diet. The other genes tested were not differentially altered in the 28-day animals. Whereas most of the gene transcripts were down-regulated in the 14-day group, the 28-day group did not indicate any expression of these same genes at all. Clearly, dietary exposure to 2AA both enhances and inhibits the activity of these gene products depending on the length of exposure.

The next four genes examined in response to 2AA toxicity namely AKT1, INSR, IRS1, and GLUT4 also played direct roles in regulating insulin signaling pathway. GLUT4 and INSR were not expressed at all in either of the treatment groups. Non-expression of GLUT4 was not unexpected since this gene is mostly expressed in skeletal muscle. In contrast, AKT1 was up-regulated in animals treated with 2AA for both 2 weeks and 4 weeks. However, IRS1 mRNA was only expressed in the treatment group that was exposed to 2AA for 4 weeks. Insulin receptor substrate (IRS) is essential in regulating hepatic metabolic activity. Binding of insulin to this receptor, initiates the insulin signaling cascade via phosphorylation type mechanisms (23, 24). Glucose and lipid metabolism by IRS protein is achieved through the phosphinositide-3 (PI-3) kinase-Akt pathway and activation of the mitogen-activated protein kinase. It appears that 2AA intoxication leads to the activation of the IRS1 and AKT1 genes in the liver.

To validate the current observations, immunoblot assay was employed to quantify the protein expression of G6PC. Glucose-6-phosphatase regulates the rate limiting step of gluconeogenesis. The ability to of this enzyme to catalyze the hydrolysis of glucose-6-phosphate to glucose and phosphate (Pi) indicates its key role in mediating glucose homeostasis (25). Quantified mRNA expression of G6PC seems to be inhibited in the 2-week group while dose-dependently increased in the 4 weeks 2AA-treated rat liver. The hepatic protein activity of G6PC was enhanced significantly in the livers of rats that ingested 2AA. This hepatic G6PC activity was almost 3-fold enhanced in the treated groups during 2 weeks of feeding on 2AA-contaminated diet. Similarly, rats fed 2AA for 28 days showed at least a 1.5-fold increase in G6PC activity, suggesting G6PC as a target for 2AA toxicity. This observation might explain why in the past, animals that consumed 2AA diet ingested more diet than animals in control groups while still gaining less accumulated weight in the process (26), therefore, it appears, an increased G6PC activity leads to a corresponding rise in glucose utilization.

We also quantified the amounts of AMPK in livers of F344 rats exposed to 2AA via ELISA assay kit. AMPK is reported to be able to sense energy and modulate cellular homeostasis. This process occurs through binding to the g subunit that leads to conformational changes and then phosphorylation of Thr172 at the subunit when ADP or AMP is present. Activation of AMPK through phosphorylation leads to the protein producing a series of effects related to increased catabolic pathways and suppression of anabolic pathways to generate optimal ATP levels. For example, AMPK suppresses gluconeogenesis in the liver while promoting glucose uptake in peripheral tissues (27). Quantified AMPK amounts were significantly increased in the short-term treatment group. Dose-dependent rise of AMPK in animals treated with 2AA suggest an increased production of hepatic AMPK in response to the toxicity of 2AA in order to maintain cellular homeostasis. In contrast, the reduction in AMPK concentration in treated animals within the 4-week set indicated an adaptive recovery over a longer period of exposure to 2AA. The level of AMPK in the 4-week group was fairly inconsistent. Compared with the 2-week control group, AMPK concentration was greater in the 4-week animals. The medium-dose group had similar levels of AMPK for both time points. A recent study suggested the influence of age on the activation of AMPK in muscular tissues. This particular study compared 8-month-old rats with 30-month-old rats and found varied levels of AMPK depending on the particular isoform of AMPK. Because our study did not focus on any specific isoform of AMPK, but rather on AMPK protein levels, we cannot attribute

the increase in AMPK levels in the 4-week group to differences in age (28).

In conclusion, the expression of a select insulin signaling genes in the liver of rats exposed to 2AA was quantified by qRT-PCR. AMPK and SOCS2 genes in animals that ingested 100 mg/kg-2AA diet and 50 mg/kg-2AA diet, respectively, during 14 days of feeding were up-regulated. Glut4 and INSR were not expressed at all in either treatment group. In contrast, AKT1 was up-regulated in animals treated with 2AA for both 2 weeks and 4 weeks. However, IRS1 mRNA was only expressed in the treatment group that was exposed to 2AA for 4 weeks. It appears 2AA intoxication leads to the activation of the IRS1 and AKT1 genes on the insulin signaling pathway genes in the liver. Quantified mRNA expression of G6PC was inhibited in the 2-week group while dose-dependently increased in the 4-week 2AA-treated rat liver. The hepatic activity of G6PC determined via ELISA assay was enhanced significantly in the livers of rats that ingested 2AA. This hepatic G6PC activity was almost 3-fold enhanced in the treated groups during two weeks of feeding on 2AA contaminated diet. Similarly, rats fed 2AA for 28 days showed at least a 1.5-fold increase in G6PC activity, suggesting G6PC as a target for 2AA toxicity. Quantified AMPK amounts were significantly increased in the short-term treatment group. The dose-dependent rise of AMPK in animals treated to 2AA suggest an increase production of hepatic AMPK in response to the toxicity of 2AA in order to maintain cellular homeostasis. In contrast, the reduction in AMPK concentration in treated animals within the 4-week set indicates an adaptive recovery over a longer period of exposure to 2AA.

ACKNOWLEDGEMENTS

We would like to thank the Southern Illinois University-Carbondale's Laboratory Animal Program staff for their help in training, and caring for the animals. We are also grateful to Ms. Emilia Zargham for helping with the feeding study.

The project was supported by funding from Georgia Southern University's Research and Economic Development.

REFERENCES

1. Sargis RM, Neel BA, Brock CO, Lin Y, Hickey AT, Carlton DA, Brady MJ. The novel endocrine disruptor tolylfluanid impairs insulin signaling in primary rodent and human adipocytes through a reduction in insulin receptor substrate-1 levels. Biochim Biophys Acta 2012; 1822:952-60.
2. Castorena-Torres F, Bermúdez de León M, Cisneros B, Zapata-Pérez O, Salinas JE, Albores A. Changes in gene expression induced by polycyclic aromatic hydrocarbons in the human cell lines HepG2 and A549.Toxicol *In Vitro* 2008; 22:411-21.
3. Khalil A, Villard PH, Dao MA, ET AL. Polycyclic aromatic hydrocarbons potentiate high-fat diet effects on intestinal inflammation. Toxicol Lett 2010; 196:161-67.
4. Agency for Toxic Substances and Disease Registry (ATSDR) (1995) Toxicological profile for polycyclic aromatic hydrocarbons (PAHs). US Department of Health and Human Services, Public Health Service. Atlanta GA. <http://www.atsdr.cdc.gov/ToxProfiles/tp69.pdf>
5. Gato WE, Hales DB, Means JC. Hepatic gene expression analysis of 2-aminoanthracene exposed Fisher-344 rats reveal patterns indicative of liver carcinoma and type 2 diabetes. J Toxicol Sci 2012; 37:1001-16.
6. Baker D, Taylor H, Lee S, Barker S, Goad M, Means J. Hepatic toxicity and recovery of Fischer 344 rats following exposure to 2-aminoanthracene by intraperitoneal injection. Toxicol Pathol 2001; 29:328-32.
7. Korkolopoulou P, Levidou G, Trigka EA, et al. A comprehensive immunohistochemical and molecular approach to the PI3K/AKT/mTOR (phosphoinositide 3-kinase/v-akt murine thymoma viral oncogene/mammalian target of rapamycin) pathway in bladder urothelial carcinoma. BJU Int 2012; 110(11 Pt C):1237-48.
8. Chou JY and Mansfield BC. Mutations in the glucose-6-phosphatase-alpha (G6PC) gene that cause type Ia glycogen storage disease. Hum Mutat 2008; 29:921-30.
9. Froissart R, Piraud M, Boudjemline AM, et al. Glucose-6-phosphatase deficiency. Orphanet J Rare Dis 2011; 6:27.
10. Rees MG, Davis MI, Shen M, et al. A panel of diverse assays to interrogate the interaction between

glucokinase and glucokinase regulatory protein, two vital proteins in human disease. Plos ONE 2014; 9:1-14.

11. Jaiswal N, Maurya CK, Venkateswarlu K, Sukanya P, Srivastava AK, Narender T, Tamrakar AK. 4-Hydroxyisoleucine stimulates glucose uptake by increasing surface GLUT4 level in skeletal muscle cells via phosphatidylinositol-3-kinase-dependent pathway. Eur J Nutr 2012; 51:893-98.
12. Okamoto H, Accili D. *In vivo* mutagenesis of the insulin receptor. J Biol Chem 2003; 278:28359-62.
13. Guo S. Insulin signaling, resistance, and the metabolic syndrome: insights from mouse models into disease mechanisms. J Endocrinol 2014; 220(2):1-23.
14. Montori-Grau M, Guitart M, García-Martínez C, Orozco A, Gómez-Foix AM. Differential pattern of glycogen accumulation after protein phosphatase 1 glycogen-targeting subunit PPP1R6 overexpression, compared to_PPP1R3C_and PPP1R3A, in skeletal muscle cells. BMC Biochem 2011; 12:57.
15. Mount PF, Gleich K, Tam S, et al. The outcome of renal ischemia-reperfusion injury is unchanged in AMPK-β1 deficient mice. PLoS One 2012; 7(1):e29887.
16. Krebs DL, Hilton DJ. SOCS proteins: negative regulators of cytokine signaling. Stem Cells 2001; 19:378-87.
17. Laggai S, Kessler SM, Boettcher S, et al. The IGF2 mRNA binding protein p62/IGF2BP2-2 induces fatty acid elongation as a critical feature of steatosis. J Lipid Res 2014; 55:1087-97.
18. Carlin MP, Scherrer DZ, De Tommaso AM, Bertuzzo CS, Steiner CE. Determining mutations in G6PC and SLC37A4 genes in a sample of Brazilian patients with glycogen storage disease types Ia and Ib. Genet Mol Biol 2013; 36:502-6.
19. Sabio G, Das M, Mora A, et al. A stress signaling pathway in adipose tissue regulates hepatic insulin resistance. Science 2008; 32:1539-43.
20. Field JB. Role of liver in insulin physiology. Diabetes Care 1980; 3:255-60.
21. Joffe D, McMahon, A, Mitrano B. How the liver affects insulin and vice versa: Part 1 carbohydrate metabolism. Diabetes In Control 2012; 653 (http://www.diabetesincontrol.com/articles/53-/13881-how-the-liver-affects-insulin-and-vice-versa-part-1-carbohydrate-metabolism; Accessed April 28, 2014).
22. Gato WE, McGee SR, Hales DB, Means JC. Time-dependent regulation of apoptosis by AEN and BAX in response to 2-aminoanthracene dietary consumption. Toxicol Int 2014; 21:57-64.
23. Fritsche L, Weigert C, Häring H-U, Lehmann R. How insulin receptor substrate proteins regulate the metabolic capacity of the liver - implications for health and disease. Curr Med Chem 2008; 15:1316-29
24. Taniguchi CM, Emanuelli B, Kahn CR. Critical nodes in signalling pathways: insights into insulin action. Nat Rev Mol Cell Biol 2006; 7:85-96.
25. Barfell A, Crumbly A, Romani A. Enhanced glucose 6-phosphatase activity in liver of rats exposed to Mg^{2+}-deficient diet. Arch Biochem Biophys 2011; 509:157-63.
26. Gato WE, Means JC. Pancreatic gene expression altered following dietary exposure to 2-aminoanthracene:links to diatobegenic activity. J Pharmacol Toxicol 2011; 6:234-48.
27. Steinberg GR, Kemp BE. AMPK in health and disease. Physiol Rev 2009; 89:1025-78.
28. Hardman SE, Hall DE, Cabrera AJ, Hancock CR, Thomson DM. The effects of age and muscle contraction on AMPK activity and heterotrimer composition. Exp Gerontol 2014; 55:120-28.

NEURAL CORRELATES OF OBSERVATION OF DISGUSTING IMAGES IN SUBJECTS WITH FIRST EPISODE PSYCHOSIS AND POST-TRAUMATIC STRESS DISORDER

G. VIDOTTO[1], A. CATALUCCI[2], R. RONCONE[3], M.C. PINO[3] and M. MAZZA[3]

[1]Department of General Psychology, University of Padua, Padova, Italy; [2]Department of Neuroradiology, University of L'Aquila, L'Aquila, Italy; [3]Department of Life, Health and Environmental Sciences, University of L'Aquila, L'Aquila, Italy

Received August 12, 2013 – Accepted August 28, 2014

The aim of this study was to analyze neural responses to disgusting images in individuals with first episode psychosis and post-traumatic stress disorder (PTSD). Although anhedonia is a common symptom in both disorders we expected that they would be associated with different neurophysiological abnormalities and patterns of activation. We recruited three groups of participants: 13 individuals with first episode psychosis, 10 individuals with PTSD who had survived the April 2009 L'Aquila earthquake and 25 healthy controls matched for age and education. All individuals participated in a functional imaging experiment in which they watched six alternating blocks of disgusting and scrambled images whilst undergoing scanning with a General Electric 1.5T whole-body scanner. We estimated individuals' beta-weights, extracting 22 clusters corresponding to 22 significant areas. Findings were consistent with other neuroimaging studies; the active areas (i.e. amygdala, insula, inferior and medial frontal gyrus) have consistently been associated with emotional experiences. Statistical analysis revealed important group differences in intensity and direction (positive or negative) of signal from baseline during disgusting condition. Although these results are preliminary they show that functional neuroimaging techniques may make a valuable contribution to differential diagnosis of first episode psychosis and PTSD.

Anhedonia is the loss of the capacity to experience pleasure, i.e. the inability to feel and understand pleasure. It has been proposed that anhedonia is the result of a dysfunction in a basic neurophysiological function and a trait marker of vulnerability that precedes and contributes to development of schizophrenia (1). Anhedonia is also known to inhibit successful rehabilitation from schizophrenic disorder and impair social functioning (2). In humans the ability to experience the pleasant or unpleasant nature of stimuli and situations has evolved beyond immediate survival and supports a variety of social behaviours (3). Disgust is a very basic emotion which has an important survival value for conspecifics. In its most basic and primitive form, disgust ('core disgust') (4) indicates that something (e.g. food) that the individual tastes or smells is bad and, perhaps, dangerous (5). Recent studies suggest that the subcortical systems, particularly the insula, contain neural populations that become active when individuals experience disgust or observe it in others. These studies also show that hedonic processes (e.g. expression of pleasure and appreciation of beauty) play an important role in social interaction

Key words: anhedonia, first episode psychosis, functional neuroimaging, post-traumatic stress disorder

Mailing address: Prof. Giulio Vidotto,
Department of General Psychology,
University of Padua,
Via Venezia 8,
35137 Padova, Italy
Tel.: +39 0498276683 Fax: +39 0498276600
e-mail: giulio.vidotto@unipd.it

0393-974X (2014)

DISCLOSURE: ALL AUTHORS REPORT NO CONFLICTS OF INTEREST RELEVANT TO THIS ARTICLE.

(6, 7) and it has been suggested that human social interactions depend on hedonic processing (8). Recent neuroimaging studies have revealed that abnormalities in several brain networks in patients with schizophrenia are related to anhedonia (9). More recently, symptoms of anhedonia have also been observed in individuals with post-traumatic stress disorder (PTSD) (10-13). Several studies suggest that certain negative symptoms, such as anhedonia, aboulia, alogia, lack of motivation and social withdrawal are characteristics of both schizophrenia and PTSD (14-17), however the underlying cognitive profile associated with anhedonia and related symptoms differs between these patient groups. Given that anhedonia is common to schizophrenia and PTSD (18, 19) understanding the underlying neural mechanisms may be useful in understanding the comorbidity of the two psychiatric disorders. The high comorbidity (i.e. the presence of overlapping symptoms) compromises a diagnostic process based only on clinical symptoms at the onset of illness. Furthermore, psychotic symptoms (e.g. hallucinations and delusions) and experiences associated with a diagnosis of psychosis (e.g. involuntary hospitalization, seclusion, restraint, forced medications) may constitute a traumatic event and contribute to PTSD (20, 21). Disgust stimuli have been used frequently in studies of emotional response in healthy subjects and subjects with psychiatric disorders (12). The neural response to disgusting stimuli seems to involve frontal lobe areas (inferior frontal cortex, medial prefrontal cortex etc.) and subcortical structures such as the amygdale, insula, basal ganglia and hippocampus (22, 23). Individuals with schizophrenia showed a reduced neural response to disgust stimuli compared with healthy subjects, particularly in frontal and subcortical areas (8, 11, 22-24). It is only recently that emotional numbing and anhedonia in PTSD have been the subjects of empirical research (24, 25). In this clinical population, as in schizophrenia, negative symptoms and anhedonia may be important aspects of the psychopathology (25-27). We wanted to evaluate anhedonia, a clinical feature of schizophrenia and PTSD, through investigating processing of disgust. We consider that in schizophrenia social incompetence is related to deficits associated with the core symptoms of the disorder, whereas in PTSD the social impairments and anhedonia depend on fear or anger related to the traumatic event. We predicted that individuals with first episode psychosis and PTSD would show different patterns of neural activation although anhedonia symptom is common to both disorders.

MATERIALS AND METHODS

Participants

We recruited three groups of participants, G1: 13 first episode psychosis individuals (6 males, 7 females); G2: 10 patients with PTSD (2 males, 8 females) who had survived the 6.3 magnitude earthquake in L'Aquila on April 6, 2009; G3: 25 healthy subjects (11 males, 14 females), matched for age and education. Socio-demographic and clinical data for the three groups are summarized in Table I.

First episode psychosis group

The first episode psychosis group consisted of individuals who were no more than 3 months from first diagnosis (i.e. first hospitalization or first clinical assessment) and had been clinically assessed before of the 2009 L'Aquila earthquake. They were drug-naïve and free from other medical conditions or substance abuse. The educational level of participants varied, 34% had not completed high school education, 18% had completed high school, 34% had some post-high school training and 14% had obtained a university degree. The group included patients with various diagnoses, schizophrenia (n = 4), schizoaffective disorder (n = 3) and psychosis not otherwise specified (n = 6). All participants were outpatients treated consecutively in the Outpatients Department of the San Salvatore Hospital, L'Aquila, Italy.

All patients had received a diagnosis before the start of the study. Diagnoses of schizophrenia or schizoaffective disorder according to DSM-IV-TR (28) (APA, 2000) were based on the Structured Clinical Interview for DSM IV Patient Edition (SCID-II) (29) and confirmed at a consensus meeting attended by at least two senior psychiatrists. Clinical assessment of symptoms in the month leading up to the evaluation was carried out using an Italian version of the Positive and Negative Syndrome Scale (PANSS) (30) which has similar psychometric properties to the original version.

PTSD group

The Davidson Trauma Scale (DTS) (31) was completed by participants in the PTSD group to assess trauma exposure and PTSD status. The DTS was developed as a measure of the severity and frequency of

symptoms described as characteristic of PTSD in DSM-IV-TR and can be used to assess response to treatment. It consists of three sub-scales assessing Intrusion (criterion B; items 1-5), Avoidance/Numbing (criterion C; items 6-12) and Hyper-arousal (criterion D; items 13-17). Each item assesses one of the 17 symptoms of PTSD listed in DSM-IV, respondents rate the severity and frequency of the symptom described in each item during the previous week using five-point Likert scales.

After this preliminary screening all participants were assessed using the Clinician Administered PTSD Scale (CAPS, Version DX) (32). The CAPS is designed to investigate the seventeen PTSD symptoms described in DSM-IV plus eight additional symptoms.

Exclusion criteria were: past neurological diseases, epilepsy, head trauma and mental retardation.

All subjects provided informed consent to participate in the study. In all three groups anhedonia was evaluated using the Italian version of the Snaith-Hamilton Pleasure Scale (SHAPS) (33). The SHAPS is a self-report scale consisting of 14 items covering four domains of pleasure responses and estimates the degree to which the respondent is able to experience pleasure or anticipate a pleasurable experience. Summary scores were used in the analysis.

Stimuli and procedure

Forty colour pictures from the International Affective Picture System rated as 'highly disgusting' were obtained from NIMH Center for Emotion and Attention (University of Florida, USA). The disgusting images included images of mutilated bodies, wounds, disgusting animals (e.g. snakes, spiders, cockroaches, and rats) in contact with parts of the face or body, and body waste products. Forty pictures of scrambled scenes were used as control stimuli. Stimuli were presented using Superlab software according to a 'boxcar' single-subject design in which the two conditions (disgusting and scrambled) were alternated over the course of a scan.

Stimuli were presented in blocks of five images. There were eight blocks of disgusting images and eight blocks of scrambled images. Each image was presented for 2 s followed by a 1.5 s inter-stimulus interval during which participants were required to fixate a cross on the screen. After two blocks (alternating disgusting and scrambled images) there was a 14 s resting phase during which participants fixated a cross on the screen. All participants viewed six alternating blocks of disgusting and scrambled

Table I. *Socio-demographic and clinical data on participants.*

	Schizophrenia	Healthy	PTSD	F	p-value
Age in years	24.2 (2.8)	27.5 (9.3)	35.2 (14.1)	22.10	0.0001
Education in years	14.20 (0.42)	14.64 (0.81)	14.53 (0.66)	1.38	0.261
SHAPS	7.6 (0.8)	1.84 (0.74)	8.38 (3.33)	53.39	0.0001
PANSS General Psychopathology	36.9 (10.8)				
PANSS Negative Symptoms	16.6 (6.5)				
PANSS Positive Symptoms	9.1 (2.8)				
Axis I Current Comorbidity Schizophrenia Schizoaffective disorders Psychosis Delirium	 33% 25% 33% 8%				
Davidson Trauma Scale (DTS) total score	9.30 (4.32)	33.9 (13.7)	69.7 (27.9)	95.59	0.0001
DTS Intrusion score	4.30 (3.36)	11.1 (5.5)	19.2 (8.1)	40.35	0.0001
DTS Avoidance score	2.10 (1.44)	8.8 (6.4)	23.2 (11.8)	66.25	0.0001
DTS Hyperarousal score	2.50 (11.52)	14.0 (6.0)	25.7 (10.1)	86.46	0.0001
SAM picture valence ratings	6.80 (0.79)	6.76 (0.72)	6.38 (0.87)	1.18	0.316

Values are means or percentages, standard deviations are in parentheses. PANSS: Positive and Negative Syndrome Scale; SHAPS: Snaith-Hamilton Pleasure Scale; DTS: Davison Trauma Scale; SAM: Self- Assessment Manikin scale.

Table II. *For each group out a Random Effects Analysis was carried to calculate and subject beta-weights for predictors and 22 significant clusters corresponding to 22 areas identified with Talairach coordinates (x, y, z) were extracted.*

		BRAIN AREAS	X	Y	Z	T
1	RTJ	Right Temporoparietal Junction	60	-40	7	-6
2	RITG	Right Inferior Temporal Gyrus	54	-58	10	-4.2
3	RTP	Right Temporal Pole	51	-4	-26	-4.4
4	RST	Right Superior Temporal Gyrus	51	-49	16	-4.5
5	RIPL	Right Inferior Parietal Lobe	48	-58	34	-4.8
6	RIFG	Right Inferior Frontal Gyrus	54	29	-2	-4.1
7	RPI	Right Posterior Insula	36	-22	10	-4.8
8	RAI	Right Anterior Insula	39	-13	10	-4.1
9	RPG	Right Parahippocampal Gyrus	36	-4	-35	-4.6
10	RSFG	Right Superior Frontal Gyrus	30	17	61	-4.5
11	LC	Lateral Cerebellum	21	-55	-23	-4.2
12	MFG	Medial Frontal Gyrus	12	-13	49	-4.8
13	PC	Precuneo	-3	-73	28	-4.4
14	RA	Right Amygdala	13	-19	-14	-4.2
15	LPL	Left Paracentral Lobule	-3	-34	52	-4.4
16	LCN	Left Caudate Nucleus	-12	11	13	-4.8
17	DP	Left Dorsolateral Prefrontal	-27	41	13	-5.5
18	LIC	Left Insula/Claustrum	-33	-1	10	-4.3
19	LI	Left Insula	-45	-28	-2	-4.3
20	LIFG	Left Inferior Frontal Gyrus	-48	17	7	-4.1
21	LIFC	Left Inferior Frontal Cortex	-51	20	4	-4.4
22	LST	Left Superior Temporal Sulcus	-57	-49	4	-4.6

images for the functional imaging experiment. Participants lay in the scanner in a dimly lit environment. The stimuli were displayed on a screen with a black background and made visible by a mirror mounted on the interior of the head coil. At the beginning of each session visual instructions lasting 5 s informed participants about the task.

Participants were asked to observe all images carefully. At the end of the fMRI session participants evaluated the valence of each disgusting image on the Self- Assessment Manikin scale (SAM). The SAM valence scale consists of a cartoon-type figure with a nine-point scale (34). They were also required to complete a recognition test.

Image acquisition

Patients and control participants were scanned with a General Electric 1.5T whole-body scanner, at the Department of Neuroradiology, San Salvatore Hospital, L'Aquila, Italy. For whole-brain structural volumes we used a T1-weighted 3D FSPGR with a voxel size of $1mm^3$. The blood oxygen level-dependent (BOLD) signal was obtained using echo planar imaging sequences (23 contiguous transversal sections, covering all the cerebral hemispheres; slice thickness, 4 mm; TE 60 ms; flip angle, 60°; matrix 64 x 64; TR volume 2 s). Acquisition of functional data was based on presentation of 15 stimulation blocks lasting 16 s each. Six rest interval blocks lasting 14 s each interrupted stimulation blocks.

Image analysis

After discarding the first 4 frames, images were corrected for section acquisition time, warped into

standard space, re-sampled into 3-mm isotropic voxels, corrected for head motion and slow frequency drifts, and smoothed using an 8-mm full-width at half-maximum Gaussian kernel (BrainVoyager QX 1.4; Brain Innovation BV, Maastricht, The Netherlands). The anatomical and functional series were then co-registered in order to map the fMRI activity to high-resolution images. Three-dimensional statistical maps were overlaid on the Talairach-transformed Montreal Neurological Institute T1-weighted brain template (http://www.brededatabase.com).

Using a general linear model approach with an equation $y = \beta X + \varepsilon$, where y was a time series associated with signal change, X was a matrix of the postulated predictor variables, and ε the related error, the calculated beta-weights are the relative heights, or amplitudes, of the various predictor variables. To analyze the fMRI time series we performed a random effects group analysis using a correction for temporal autocorrelation to extract 22 clusters corresponding to 22 significant areas (Table II). Three predictors of interest were considered (i.e. disgusting and scrambled conditions, with fixation of the cross during the inter-stimulus intervals as the baseline). We proceeded with an interpolation of tabular data to define an acceptable threshold for cluster sizes. The Cluster-Level Statistical Estimator Threshold algorithm, via a Monte Carlo simulation was used to identify probable clusters. The Cluster Threshold plug-in enabled us to correct for multiple measurements using a cluster size as a threshold value. This method was based on the fundamental assumption that activated areas tended to show signal changes on groups of spatially contiguous voxels.

Finally, our procedure provided the computation of beta-weights for each single subject and each single cluster related to the three postulated predictors (i.e. baseline, disgusting, and scrambled conditions).

RESULTS

Clinical measures

Group differences in clinical variables were evaluated using ANOVA (Table I). The ANOVA revealed group differences in DTS total score ($F_{2,45}$=95.59; p=0.0001), and scores on the three subscales: Intrusion ($F_{2,45}$=40.35; p=0.0001), Avoidance ($F_{2,45}$=66.25; p=0.0001), and Hyperarousal ($F_{2,45}$=86.46; p=0.0001). Post-hoc comparisons indicated that the PTSD participants reported significantly higher score in all DTS measures compared to two groups.

There was a significant group difference in SHAPS score ($F_{2,45}$=53.39; p=0.0001). Post-hoc comparisons showed that the clinical sample (participants with PTSD or first episode psychosis) had significantly higher SHAPS scores than controls (Table II). The PANSS was only administered to the first episode psychosis group, the results are reported in Table I.

Picture valence ratings

ANOVA revealed no group differences in valence ratings for the disgusting stimuli ($F_{2,45}$=1.18; p=0.316).

Patterns of neural activation

Disgust condition. Second-level statistical analyses were carried out using R packages (R Development Core Team, 2011). ANCOVA with Bonferroni correction (α = 5%) was used to assess group difference in the mean beta-weights of the 22 relevant clusters across the disgust and scrambled conditions; the mean beta-weights in the baseline condition were used as covariates. Planned comparisons were used to explore group differences.

In the following sentences, F-value refers to ANOVA while z-value refers to contrast in plan comparison. p-value was equally significant both for F and z. There were differences between the groups for mean beta-weights. The PTSD group showed a higher mean value than the other two groups in right inferior parietal lobe (RIPL; $F_{2,43}$=8.63; z=-2.88; p<.001), right inferior frontal gyrus (RIFG; $F_{2,43}$=7.63; z=-2.71; p<.001), right anterior insula (RAI; $F_{2,43}$= 10.03; z=-3.67; p<.001), medial frontal gyrus (MFG; $F_{2,43}$= 11.82; z=3.19; p<.001), left inferior frontal gyrus (LIFG; $F_{2,43}$= 9.03; z=-3.56; p<.001), and right amygdala (RA; $F_{2,43}$= 16.42; z=3.59; p<.001). No other significant differences were found in the disgust condition.

Images of the transversal sections for data averaged across participants for RIPL, RIFG, RAI, MFG, LIFG, and RA with the associated mean beta-weights (± SE) for the first episode psychosis, PTSD and control groups are shown in Fig.1.

Scrambled condition. There were differences between the groups for mean beta-weights. The PTSD group showed a higher mean value than the other two groups in right temporoparietal junction (RTJ; $F_{2,43}$=9.55; z=-4.26; p<.001), right parietal

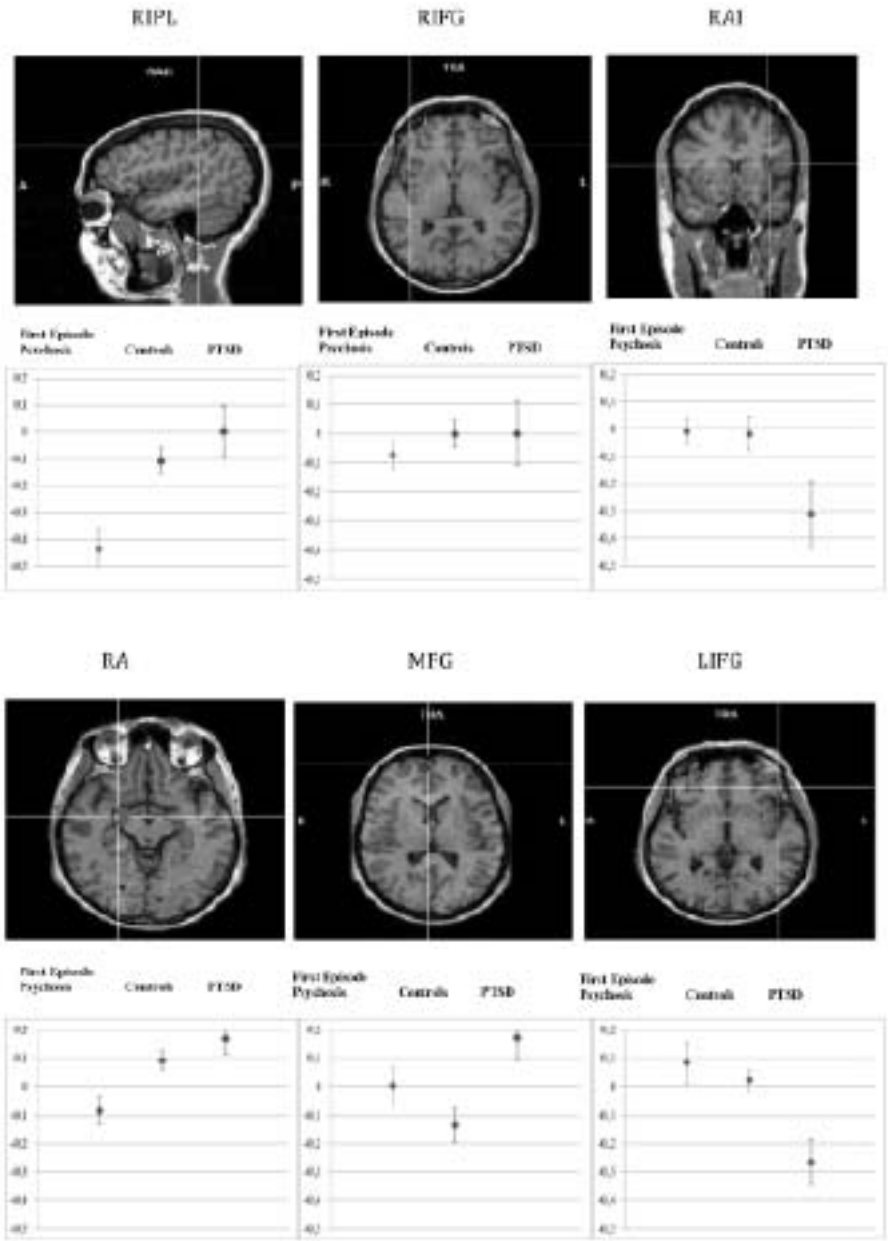

Fig. 1. *In the disgust condition, LIFG, RIFG, RAI, RIPL, MFG and RA showed increase activation in the PTSD group compared to the other two groups. Images are transversal sections for the data averaged across participants. The right hemisphere of the brain corresponds to the right side of the image.*

gyrus (RPG; $F_{2,43}$=18.98; z=-5.29; p<.001), MFG ($F_{2,43}$=17.87; z=-5.77; p<.001), left inferior frontal gyrus (LIFG; $F_{2,43}$=12.7; z=-3.65; p<.001), left inferior frontal cortex (LIFC; $F_{2,43}$=13.4; z=4.15; p<.001), and lateral cerebellum (LC; $F_{2,43}$=9.7; z=4.32; p<.001). No other significant differences were found in the scrambled condition.

Images of the transversal sections for data averaged across participants for RTJ, RPG, MFG, LIFG, and LC with the associated mean beta-weights (± SE) for first episode psychosis individuals, PTSD and control groups are shown in Fig. 2.

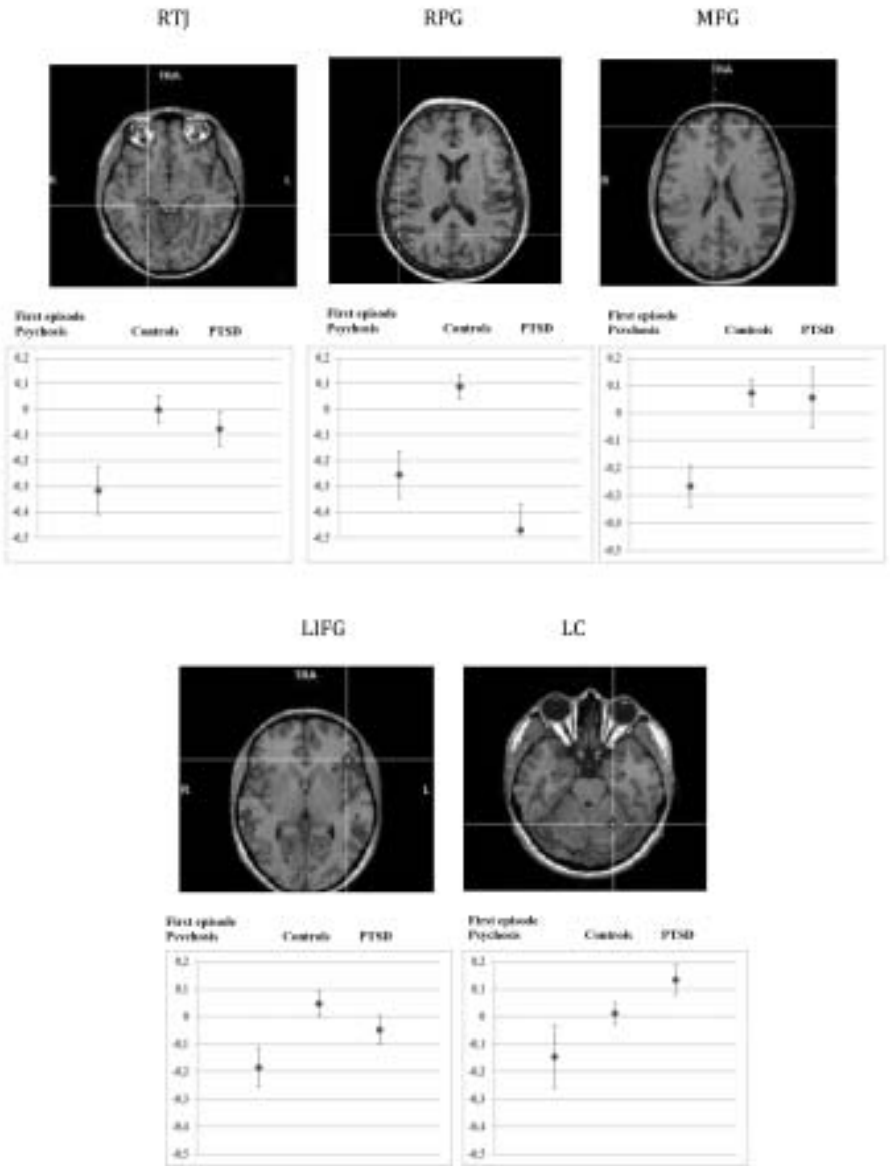

Fig. 2. *In scrambled condition RTJ, LIFG, and RPG showed decreased activation in participants with first episode psychosis and PTSD compared to controls; MGF and LC showed increase activation in the PTSD group. Images are transversal sections for the data averaged across participants. The right hemisphere of the brain corresponds to the right side of the image.*

Multinomial analysis

Multinomial logistic regression is usually used to analyze a relationship between one non-metric dependent variable and one or more metric and/or non-metric independent variables. The probability of belonging to a specific group can be estimated from the raw data using a likelihood function. The fit between the resulting model and the empirical data can be estimated using goodness of fit tests. In this study we attempted to uncover areas in which activity (i.e. using the related mean beta-weights as independent variable) could be used to classify our participants into one of the three groups (first episode psychosis individual, PTSD, control).

Three different equations were used to define the probabilities that a participant belonged to each

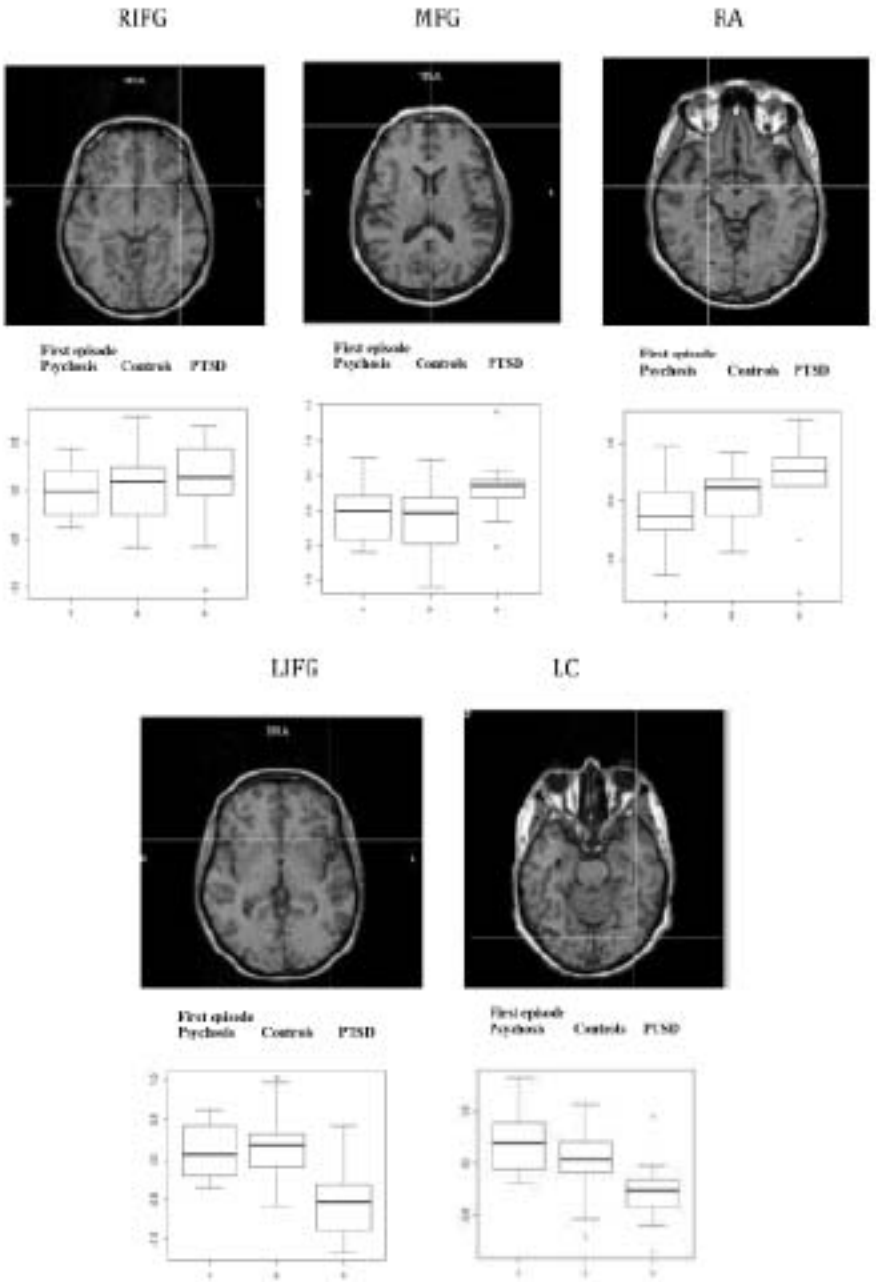

Fig. 3. *PTSD group had higher beta-weights than the first episode psychosis group and healthy controls: (**a**) identifies first episode psychosis participants, (**b**) healthy controls and (**c**) PTSD participants.*

one of the three groups; the participant is predicted to belong to the group associated with the highest probability. The model revealed five neuroanatomical areas associated with differential activation following disgust images: RIFG (χ^2 =9.66; p<.001), MFG (χ^2=26.59; p<.001), RA (χ^2=16.27; p<.001), LIFC (χ^2=22.86; p<.001), and LCN (χ^2=26.64; p<.001).

There were significant differences between amplitude of activation in the PTSD group and the other two groups for the following areas: RIFG, MFG, RA, LIFC, and LCN. In comparison with the other groups, PTSD participants showed hyperactivation in response

to the disgusting images in all these areas (Fig. 3).

DISCUSSION

To the best of our knowledge, this is the first study to compare the relationship between anhedonia and neural correlates of disgust in two clinical populations (first episode psychosis individual and PTSD).

Several studies have demonstrated that the areas in which we observed the greatest activation following disgusting images (i.e. amygdala, insula, inferior and medial frontal gyrus) play a key role in processing emotions; they have often been associated with emotional experiences and emotion recognition (12, 13). These results are consistent with those of other neuroimaging studies (12-15) which showed that viewing disgusting images activates the anterior insula and the frontal cortex. Some authors (8) have suggested that the strength of activation in insula and inferior frontal cortex when looking at disgusting stimuli indicates that these areas have a dual function, (1) translating observations of other people's facial expressions into similar visceral states in oneself and (2) making the individual conscious of this visceral state such that he or she becomes aware of the emotional state of others.

Another area which was activated by the disgusting stimuli was the ventral medial prefrontal cortex which is linked to limbic structures such as the amygdala through a complex set of interconnections. This anatomical relationship might indicate that the medial prefrontal cortex mediates the integration of visceromotor aspects of emotion with information gathered from the internal and external environments. Frith and Frith (35) proposed that in humans ventral medial prefrontal cortex might contribute to the integration of emotional and cognitive processes by incorporating emotional biasing signals or markers into decision-making processes, they also postulated that medial prefrontal regions are concerned with explicit representations of states of the self that are attenuated during (non-self-referential) goal-directed behaviour.

Healthy group

The data from our healthy controls are consistent with recent literature indicating that the LAI and LIFG are preferentially activated by pleasant and unpleasant stimuli (22). The role of the inferior frontal gyrus (pars opercularis) in coding experience and social observation of disgusting experiences is well-established; the inferior frontal gyrus is involved in imagination, and the functional connectivity between this region and the rest of the brain differs according to experience, observation and imagination of disgust (4). The medial frontal cortex seems to play a critical role in the perception of disgust; a recent study showed that medial prefrontal cortex represents perceived emotions at an abstract, modality-independent level, and thus may play a critical role in understanding and categorization of other emotional mental states.

It has been suggested (12-14) that emotional self-regulation is normally implemented by a neural circuit consisting of several regions of the prefrontal cortex and the subcortical limbic structures.

First episode psychosis group

Individuals with first episode psychosis showed less activation in RIPL, RIFG, RAI, MFG, RA, and LIFG in response to disgusting images than the other two groups. Our results provided support for the hypothesis that individuals with schizophrenia have significant difficulties in the emotion processing (11), reflected in anhedonia, which is one of the core symptoms of the disease and may be associated with hypofrontality in schizophrenia. Our findings provide further evidence for the relationship between functional hypofrontality in schizophrenia and possible involvement of a functional imbalance in cortico-cerebellar-thalamic-cortical circuits in the resting state associated with first episode psychosis. First episode psychosis individuals show a less intense response to emotional stimuli and a significant reduction in baseline activity in areas such as amygdala, insula, inferior frontal operculum and medial frontal cortex. Many previous studies (8) have reported that schizophrenic patients showed reduced limbic system activation during processing of negative emotions, such as fear and disgust. This particular lower response of limbic system, since the onset of the illness confirms the hypothesis that the activation of limbic areas, in particular right insula (RA) and inferior frontal gyrus (LIFG and RIFG), is correlated with the presentation of emotional stimuli.

PTSD group

Individuals with PTSD showed higher activation in RIPL, RIFG, RAI, MFG, RA, LIFG and RA in

response to disgusting images than the other two groups. Whereas individuals with PTSD showed greater activation in these areas during the disgust condition than healthy controls, first episode psychosis individuals showed lower activation in that same brain areas.

The relatively greater activation of medial prefrontal cortex in response to disgusting images in the PTSD group which is consistent with previous studies (12, 13) which reported a significant increase in blood flow to the medial prefrontal cortex in PTSD patients which correlated at trend levels with psychophysical indices of stress response. These data provide evidence for the involvement of the medial prefrontal cortex in the pathophysiology of PTSD. PTSD patients' high psychophysiological reactivity to negative stimuli (e.g. the disgusting images in this study) may be related to high reactivity to memories of the trauma. Stronger activation of the limbic (RAI, RA) and frontal areas (RIFG, LIFG, MFG) in individuals with PTSD in the presence of emotionally negative stimuli might prompt participants to use coping behaviours intended to protect them from re-experiencing the pain related to traumatic events (13).

Interpretation of the patterns of activation

We observed changes of activity in different directions in our two clinical samples. According to Gusnard and Raichle (28) the direction (positive or negative) change in activity relative to baseline is important in cognitive neuroscience. These authors introduced the concept of a physiological baseline, the metabolic and circulatory parameters associated with the brain during a resting, awake state. Brain activation can be produced experimentally and changes in brain activity are depicted graphically as an increase or decrease with respect to baseline. Deactivation is defined as a pattern of metabolic and circulatory changes in the opposite direction to those associated with activation. Both excitation and local inhibition should be seen as increases in activity (activation).

In conclusion, neuroimaging techniques could make a valuable contribution to differential diagnosis of psychiatric disorders, as the clinical symptoms are not always specific to a particular disease, particularly in the early stages of a disorder.

Disgusting images induced different responses in the two clinical groups although both groups had difficulty in processing emotions and symptoms such as anhedonia (2) which are common to PTSD and first episode psychosis individuals. The differences in the response to disgusting images could be used for differential diagnosis. The areas for which significant group differences in activation were observed (inferior frontal cortex bilaterally, ventromedial prefrontal cortex, amygdala and caudate nucleus) may be involved in processing emotional communicative signals. Both the PTSD group and first episode psychosis group showed a different pattern of activation from the control group in response to disgusting images.

The hyperactivation of frontal areas in the PTSD group may be associated with emotional pain, resulting in individuals avoiding the social context in which the hyperactivation occurred. The frontal hypoactivity shown by the first episode psychosis group appears to be associated with the same behavioural result as the PTSD frontal hyperactivity, namely social isolation. This isolation is not voluntary; rather it is a consequence of an inability to experience pleasure in being with others (8).

All these findings seem to have substantial diagnostic value; our multinomial analysis suggested that beta values related to crucial areas were a significant predictor of the group to which individual participants belonged. In conclusion, although fMRI is still a long way from being used as a diagnostic tool for psychiatric disorders in a clinical context, this preliminary investigation suggests that it has potential as a tool for the differential diagnosis of first episode psychosis and PTSD. Our results show that the direction of relative changes in the pattern of activation (compared with healthy controls) are an interesting indication in the early stages of the illness (first episode psychosis and PTSD), and analysis of neural responses to emotionally significant stimuli could contribute to a better understanding of social and emotional impairments that would have value in developing curative and preventive interventions. As a matter of fact, the small sample group is an important limitation to our study. For this reason, cautions has to be used in generalizing some of the discussed statistical results.

REFERENCES

1. Kwapil TR. Social anhedonia as a predictor of the

development of schizophrenia-spectrum disorders. J Abnorm Psychol 1998; 107:558-65.
2. Blanchard JJ, Mueser KT, Bellack AS. Anhedonia, positive and negative affect, and social functioning in schizophrenia. Schizophrenia Bull 1998; 24:413-24.
3. Seeman MV. Symptoms of schizophrenia: normal adaptations to inability. Med Hypotheses 2007; 69:253-57.
4. Rozion P, Bauer R, Catanese D. Food and life pleasure and worry, among American college students: gender differences and regional similarities. J Pers Soc Psychol 2003; 85:132-41.
5. Carr L, Iacoboni M, Dubeau MC, Mazziotta JC, Lenzi GL. Neural mechanisms of empathy in humans: a relay from neural systems for imitation to limbic areas. Proc Natl Acad Sci USA 2003; 100:5497-502.
6. Di Dio C, Macaluso E, Rizzolatti G. The golden beauty: brain response to classical and renaissance sculptures. PLoS One 2007; 2:1197-201.
7. Jenkins AC, Macrae CN, Mitchell JP. Repetition suppression of ventromedial prefrontal activity during judgments of self and others. Proc Natl Acad Sci USA 2008; 105:4507-12.
8. Crespo-Facorro B, Paradiso S, Andreasen NC, O'Leary DS, Watkins L, Ponto LLB, Hichwa RD. Neural mechanisms of anhedonia in schizophrenia: A PET study of response to unpleasant and pleasant odors. JAMA 2001; 4:427-35.
9. Lee JS, Han K, Lee SK, Seok JH, Kim JJ. Altered structural connectivity and trait anhedonia in patients with schizophrenia. Neurosci Lett 2014; 579C:7-11.
10. Frewen PA1, Dozois DJ, Lanius RA. Assessment of anhedonia in psychological trauma: psychometric and neuroimaging perspectives. Eur J Psychotraumatol 2012; Epub 2012.
11. Burbridge JA, Barch DM. Anhedonia and the experience of emotion in individuals with schizophrenia. J Abnorm Psychol 2007; 116:30-42.
12. Mazza M, Giusti, L, Albanese A, Mariano M, Pino MC, Roncone R. Social cognition disorders in military police officers affected by posttraumatic stress disorder after the attack of An-Nasiriyah in Iraq 2006. Psychiat Res 2012; 198(2):248-52.
13. Mazza M, Tempesta D, Pino MC, Catalucci A, Gallucci M, Ferrara M. Regional cerebral changes and functional connectivity during the observation of negative emotional stimuli in subjects with post-traumatic stress disorder. Eur Arch Psy Clin N Epub 2013.
14. Nietlisbach G, Maercker A, Rossler W, Haker H. Are empathic abilities impaired in posttraumatic stress disorder? Psychol Rep 2010; 106:832-44.
15. Lanius RA, Vermetten E, Loewenstein RJ, Brand B, Schmahl C, Bremner JD. Emotion modulation in PTSD: clinical and neurobiological evidence for a dissociative subtype. Am J Psychiat 2010; 167:640-47.
16. Loas G, Boyer P, Legrand A. Anhedonia and negative symptomatology in chronic schizophrenia. Compr Psychiat 1996; 37:5-11.
17. Kashdan TB, Elhai JD, Frueh BC. Anhedonia and emotional numbing in combat veterans with PTSD. Behav Res Ther 2006; 44:457-67.
18. Mazza M, Lucci G, Pacitti F, Pino MC, Mariano M, Casacchia M, Roncone R. Could schizophrenic subjects improve their social cognition abilities only with observation and imitation of social situations? Neuropsychol Rehabil 2010; 20(5):675-703.
19. Litz BT, Schlenger WE, Weathers FW, Caddell JM, Fairbank JA, La Vange LM Predictors of emotional numbing in posttraumatic stress disorder. J Trauma Stress 1997; 10:607-18.
20. Buckley PF, Miller BJ, Lehrer DS, Castle DJ. Psychiatric comorbidities and schizophrenia. Schizophr Bull. 2009; 35(2):383-402.
21. Chapleau KM1, Bell MD, Lysaker PH. The relationship between post-traumatic symptom severity and object relations deficits in persons with schizophrenia. Br J Clin Psychol 2014; 53(2):157-69.
22. Jabbi M, Bastiaansen J, Keysers C. A common anterior insula representation of disgust observation, experience and imagination shows divergent functional connectivity pathways. PLoS One 2008; 3:29-39.
23. Williams LM, Das P, Liddell BJ, Olivieri G, Peduto AS, David AS, Gordon E, Harris AW. Fronto-limbic and autonomic disjunctions to negative emotion distinguish schizophrenia subtypes. Psychiat Res 2007; 155:29-44.
24. Penn DL, Sanna LJ, Roberts DL. Social cognition in schizophrenia: an overview. Schizophrenia Bull 2008; 34:408-11.

25. Putnam KM, Pizzagalli DA, Gooding DC, Kalin NH, Davidson RJ. Neural activity and diurnal variation of cortisol: evidence from brain electrical tomography analysis and relevance to anhedonia. Psychophysiology 2008; 45:886-95.
26. Kashdan TB, Elhai JD, Frueh BC. Anhedonia, emotional numbing, and symptom overreporting in male veterans with PTSD. Pers Indiv Differ 2007; 43(4)725-35.
27. Gusnard DA, Raichle ME. Searching for a baseline: functional imaging and the resting human brain. Nat Rev Neurol 2001; 2:685-94.
28. American Psychiatric Association (APA). Diagnostic and statistical manual of mental disorders (4th ed.). Washington, DC: APA. 2001.
29. First MB, Gibbon M, Spitzer RL, Williams JBW, Benjamin LS. Structured Clinical Interview for DSM-IV Axis II Personality Disorders, (SCID-II). Washington, D.C.: American Psychiatric Press, Inc., 1997.
30. Pancheri P, Brugnoli R. Valutazione dimensionale della sintomatologia schizofrenica. Validazione della versione italiana della Scala per la valutazione dei Sintomi Positivi e Negativi (PANSS). Ital J Psychopathol 1995; 60:1-3.
31. Davidson JR, Book SW, Colket JT, et al. Assessment of a new self-rating scale for post-traumatic stress disorder. Psychol Med 1997; 27:153-60.
32. Palmieri PA, Weathers FW, Difede J, King DW. Confirmatory factor analysis of the PTSD Checklist and the Clinician-Administered PTSD Scale in disaster workers exposed to the World Trade Center Ground Zero. J Abnorm Psychol 2007; 116:329-41.
33. Snaith RP, Hamilton M, Morley S, Humayan A, Hargreaves D, Trigwell P. A scale for the assessment of hedonic tone the Snaith-Hamilton Pleasure Scale. Brit J Psychiat 1995; 167:99-103.
34. Bradley MM, Lang PJ. Measuring emotion: the self-assessment manikin and the semantic differential. J Behav Ther Exp Psy 1994; 25:49-59.
35. Frith CD, Frith U. Interacting minds - a biological basis. Science 1999; 286:1692-95.

IN VITRO EXPANSION OF TUMOUR CELLS DERIVED FROM BLOOD AND TUMOUR TISSUE IS USEFUL TO REDEFINE PERSONALIZED TREATMENT IN NON-SMALL CELL LUNG CANCER PATIENTS

N.M. MALARA[1], F. GIVIGLIANO[2], V. TRUNZO[3], L. MACRINA[4], C. RASO[5], N. AMODIO[6], S. APRIGLIANO[7], A.M. MINNITI[7], V. RUSSO[3], L. ROVEDA[8], M.L. COLUCCIO[9], M. FINI[10], P. VOCI[2], U. PRATI[8], E. DI FABRIZIO[11] and V. MOLLACE[12]

[1]Italian Institutes of Technology, Arnesano, Lecce, Italy; [2]Thoracic Surgery, Cancer Centre of Excellence, University "Magna Graecia" of Catanzaro, Italy; [3]Cellular Toxicological Laboratory, Department of Health Science, Salvatore Venuta Campus, University "Magna Graecia" Catanzaro, Italy; *[4]University of Medicine San Raffaele, Milano, Italy; [5]Systems Biology, University College of Dublin, Belfied, Republic of Ireland; [6]Department of Experimental and Clinical Medicine, Salvatore Venuta Campus, University "Magna Graecia" of Catanzaro, Italy; [7]Association ExChanger: Share your Science,Catanzaro, Italy; [8]Oncology Surgery, Cancer Centre of Excellence, University "Magna Graecia" of Catanzaro, (Italy); [9]Bionem Laboratories, Department of Experimental and Clinical Medicine, Salvatore Venuta Campus, University "Magna Graecia" of Catanzaro, Italy; [10] IRCCS San Raffaele Pisana, Rome, Italy; [11]Physical Science and Engineering Division, King Abdullah University of Science and Technology, Kingdom of Saudi Arabia; [12]Interregional Research Center for Food Safety and Health (IRC-FSH), Catanzaro, Italy*

Received March 28, 2014 – Accepted June 17, 2014

The clinical development of locally and advanced non-small cell lung cancer (NSCLC) suffers from a lack of biomarkers as a guide in the selection of optimal prognostic prediction. Circulating Tumour Cells (CTCs) are correlated to prognosis and show efficacy in cancer monitoring in patients. However, their enumeration alone might be inadequate; it might also be critical to understand the viability, the apoptotic state and the kinetics of these cells. Here, we report what we believe to be a new and selective approach to visually detect tumour specific CTCs. Firstly, using labelled human lung cancer cells, we detected a specific density interval in which NSCL-CTCs were concentrated. Secondly, to better characterize CTCs in respect to their heterogeneous composition and tumour reference, blood and tumour biopsy were performed on specimens taken from the same patient. The approach consisted in comparing phenotype profile of CTCs, and their progenitor Tumour Stem Cells, (TSCs). Moreover, NSCL-CTCs were cultivated in short-time human cultures to provide response to drug sensitivity. Our bimodal approach allowed to reveal two items. Firstly, that one part of a tumour, proximal to the bronchial structure, displays a predominance of CD133+. Secondly, specific NSCL-CTCs Epithelial Cell Adhesion Molecule (EpCAM)+CD29+ can be used as a negative prognostic factor as well the high expression of CTCs EpCAM +. These data were confirmed by drug-sensitivity tests, *in vitro*, and by the survival curves, *in vivo*.

Key words: NSCLC short-term cultivation, cultivated circulating tumour cells, stem cell niche, TUNEL-assay

Mailing address: Prof. Vincenzo Mollace,
Institute of Research for Food Safety and Health (IRC-FSH),
Department of Health Science, University of Magna Graecia,
Campus S. Venuta, Germaneto,
Viale Europa, 88100 Catanzaro, Italy
Tel.: +39 0961 3694381 Fax: +39 0961 3695025
e-mail: mollace@libero.it

0393-974X (2014)

Lung cancer is the main worldwide cause of death among patients with malignant tumours (1). For locally advanced non-small cell lung cancer (NSCLC), multimodal therapy including chemotherapy, radiotherapy and surgery can improve the survival of patients compared to single-treatment modalities. While surgical resection after induction therapy is not currently considered an established standard approach, better identification of biomarkers to define prognosis through targeted chemotherapy to be associated to surgery is considered an imperative goal and has recently been suggested by experienced worldwide institutions (1).

Recently, characterization of tumour stem cells (TSCs) within tumour bulk and correspondent circulating tumour cells (CTCs) in peripheral blood has been shown to be relevant for monitoring the development of many cancer diseases. Characterization of both TSCs and/or CTCs, in the same patient, has been suggested as a promising tool for studying quiescence state underlying potential metastases "en route" to a secondary site (2, 3). However, the relationship between TSCs and/or CTCs and its impact on NSCLC prognosis and treatment must still be adequately standardised. The number of CTCs has been found to correlate with prognosis and show the translation of efficacy monitoring in patients. However, their enumeration alone might be inadequate; it might also be critical to understand the viability, apoptotic state and kinetics of these cells. Although interest in employing CTCs is high, underestimation of the need to understand their functional state and kinetics has led to inconsistent interpretation of data.

Similar problems may be issues when evaluating TSCs derived from the tumour bulk, though some controversies still remain (4). The TSCs, similar to normal stem cells, are capable of self-renewal and can also produce differentiated progeny. Thus, TSCs represent a relevant source of bio-markers which appear essential for monitoring the development of both primary cancer and metastases. One of the main features of TSCs is represented by their precise location in close relationship to one or more surrounding differentiated tissues, or niche cells that, along with the extra cellular matrix and various secreted molecules, could provide a peculiar microenvironment able to regulate key adult stem cell functions (5). Signals derived from the niche microenvironment strongly modulate intrinsic adult stem cell signalling and regulate stem cell proliferation and cell fate decisions (6). The microenvironment surrounding normal and tumour stem cells, which provides the stem cell niche, plays multiple roles: it is a mechanical anchorage for the stem cells and provides cross-talk communication mediated by direct contact and/or indirect extracellular factors. The microenvironment may also provide signalling via the cell receptor integrin as suggested by its expression in prostatic TSCs (7) and its co-expression with AC133 (CD133) in the epidermal basal cells (8), as well as metalloprotease-mediated lysophospholipid signaling (9).

Besides this evidence, the specific mechanism by which cancer cells form from differentiated cell compartments or from stem or progenitor cells has not been understood. Studies regarding human lung tumour tissues focused on $CD133^{+}$ as stem cell markers (10), and on CK7 or CK19 as cytokeratin (CK) differentiation markers (11). CD29 has been suggested as a candidate as tumour marker. This integrin is involved in lung tumourigenesis (12) and in the wound-repair process of airway epithelium (13), and it is expressed by human lung carcinoma cells of different isotopes (14). It is directly involved in the cell-matrix and cell-cell interactions with dominant expression in most epithelial lung carcinomas cells. Thus, CD29 seems to play an important role in *in vivo* regulation of proliferation and differentiation of epithelial cells through the basement membrane (15). In this study we report what we believe to be a new and selective approach to visually detect live CTCs. We reported previously an isolation and expansion strategy of CTCs from patients affected by colon cancer (3). In this study, we carried out a specific method to selectively capture the CTCs in a patient's blood which were produced by NSCLC. Simulation experiments using labelled human lung cancer cells permitted to identify the density interval where NSCL-CTCs are concentrated. Our approach consisted in comparing the phenotype profile of NSCL-CTCs, and their progenitor TSCs in the same patient using blood and tumour biopsies. Moreover, NSCL-CTCs were cultivated in short-term human cultures to provide dose-response data able to detect heterogenic response to drug sensitivity consistent

with clinical experience. Our bimodal approach enabled to find that, within the tumour bulk, there is an area, proximal to the bronchial structure, displaying a predominance of the $CD133^+$ cell population. Moreover, this area is characterized for the expression of CK7 and CD29 and EpCAM positive cells. We used the resulting profile of TSC as a guideline to identify corresponding NSCL-CTCs in liquid biopsies. This approach identified an interesting NSCL-CTCs phenotype, EpCAM+CD29+. The combination strategies used for isolation and typing NSCL-CTCs allowed precise definition of a personalized prognosis.

MATERIALS AND METHODS

Patient selection

The "Oncologic Excellent Centre" Thoracic Surgery Unit enrolled patients suffering from NSCLC. Each individual patient entering the study signed an informed consensus on the general content of study methodology and objectives. In addition, the study design was carried out according to local and international institutional guidelines and received formal approval by our referred Ethics Committee (Bioethics Expert, University Hospital "Mater Domini", Project Number: 2013.34)

Peripheral blood samples were collected (5 ml of blood in a tube containing Ethylenediaminetetraacetic acid (EDTA), as well as healthy and tumour tissues samples from patients who underwent therapeutic radical tumour resection without previous anticancer treatment. Two independent pathologists confirmed the histological diagnosis of cancer in all cases involved. The stage of cancer disease was determined in agreement with Tumour-Node-Metastasis (TNM) (UICC-2009). stage

Design of tissue map image of the removed specimens

For each individual patient, the zone was isolated and mapped where the cancer stem cells (CSCs) were in the area undergoing surgical removal in order to identify where the biopsy should be carried out. We did this using knowledge gained from the studies of embryonic cellular development in the lung. We removed healthy autologous epithelium tissue alongside the tumour tissue as a normal control.

Primary cell cultures from solid tissue specimens

We extracted specimens of both healthy and cancerous pieces of tissues and kept them in a solution of Phosphate-Buffered Saline (PBS) 1X, (Dilution buffer, Invitrogen) with 10% of penicillin-streptomycin and 1% Amphotericin B solution. Using a scalpel we cut the tissue up as fine as possible and then filtered it through a 100-µm-nylon cell strainer (BD Falcon, USA). This procedure resulted in a heterogeneous cell population. We cultured tissue samples in a specific medium to allow cancer cells to be better identified (M). The procedure for cultivating healthy cells was the same as the one used for cancer cells in presence of a supplement of 10% of serum.

Primary cell cultures from blood samples

Five to 10 ml peripheral blood samples were taken from each patient and put into tubes containing EDTA and then centrifuged using Ficoll-Paque Plus (GE Healthcare) to separate the cancer cells from the remaining cellular blood components. The CTC suspension was isolated from cell layer comprised between 1080÷1090 (g/m) density gradient values (3) according to the heterogeneous size and relative cell density of the cancer cells. Using conditions similar to the ones used for tumour specimens the CTCs were cultivated; however, individual growth factor (EGF) and Fibroblast Growth Factor (FGF) were added to the complete growth medium which improved the adherent monolayer cellular yield, discouraging the survival of normal leukocytes. At 10% the use of 0.83% Tris/NH_4Cl solution was necessary to dissolve contaminating erythrocytes.

Validation of NSCL-CTCs gradient phase

Human cancer colon cell lines A549 were cultured in RPMI1640 medium containing 10% fetal bovine serum (FBS), and 30 mg penicillin G/0.05 g streptomycin. Cells were plated at $1X10^6$ per well onto a six-well plate 24 h before infection, and were infected with adenoviral vector. In order to perform infections, A549 cells were incubated with pAdenoVator-CMV5(CuO)-IRES-GFP (Qbiogene, Carlsbad, CA) in serum free medium for 1 h at 37°C. Both vectors were used at a multiplicity of infection (m.o.i.) of 3000 physical particles/cell, determined experimentally as the lowest m.o.i. at which the majority of the cellular population become infected (assessed by EGFP expression). Twenty-four hours later, both adherent and floating cells were harvested, washed with PBS and counted. GFP was evaluated through cytometric analysis. Five hundred infected cells were put in 5 ml of entire peripheral blood of healthy subjects. The blood sample was submitted to the above-described protocol to isolate NSCL-CTCs.

Cell culture medium

The culture medium (M) used contained DMEM/F12 supplemented with several factors to enhance stem cell growth. In particular, we added basic fibroblast growth factor (bFGF), epidermal growth factor (EGF) and Fetal Bovine Serum (FBS) (D-MEM/F12- Heparin 25000

u/5ml (fc: 0.5 U/ml) EGF 200 µg/ml (fc: 50 ng/ml) - FGF 25 µg/ml (fc: 25 ng/ml)- BSA 1%- penicillin-streptomycin solution 1%. The complete fresh medium used to enhance cell adhesion was prepared with Ham′s Nutrient Mixture F12 (Sigma-Aldrich, Inc.) solution: 10% FBS (Fetal Bovine Serum), 1% penicillin-streptomycin solution, 1% Amphotericin B solution (BioReagent, sterile-filtered, 250 µg/mL in deionised water, suitable for cell culture, from Sigma-Aldrich, Inc.).

Cytometry

The cells were washed in PBS and incubated in PBS + 10 mmol EDTA at 37°C for 15 min. Cell suspension, pelleted by centrifugation at 200 g for 5 min was re-suspended in 0.5 ml PBS and 1% foetal calf serum (FCS; Sigma). The cells were then incubated at 4°C with primary antibodies (EpCAM EpCAM-FITC Miltenyi Biotec), Fibronectin (Fibronectin-FITC SouthernBiotech), CD4-Fluorescein, CD8-PE, CD56-PE (BD Pharmigen), Cytokeratin 7, CD56 (primary Biocare Medical and relative secondary in PE and Fluorescein by Southern Biotech) for 30 min then were centrifuged and pelleted before washing in 2 ml PBS and 1% FCS. After the cultivation phase, cancer cell suspensions were analysed using 1500 events as threshold in each acquisition.

All antibodies used for flow cytometry had a dilution of 1:100 in PBS+ 1% FCS. The secondary antibody was used for cytokeratin expression analysis before the final wash for 15 min in 2 ml PBS and 1% FCS. Flow cytometry was carried out using flow cytometry apparatus (Becton Dickinson, San Diego, CA, USA) and the results were analysed with Cellquest and Flow JO software.

Cell cycle analysis

The cells ($2x10^5$) were washed with cold PBS and fixed with 70% ethanol at -20°C overnight. The cell pellets were re-suspended in 500 µl PBS containing 2 mg/ml RNAse A (Sigma) and incubated at 37°C for 60 min. Then the cell pellets were stained as previously reported (16). Using Fluorescence activated Cell sorting (FACS) (Becton and Dickinson San Jose, CA, USA). The DNA content was analyzed. The cell population was determined in each cell-cycle phase using Modfit 3.1 Software (Becton and Dickinson San Jose, CA, USA).

Apoptosis and cell viability assays

Using 96-well black plates, the individual wells were prepared in parallel for the ViaLight and TUNEL assay. All the plates were seeded with a density of 40,000 cells/ml in triplicate, for each treatment concentration and incubated for 24 h to achieve 60–70% confluence. The cultivated cancer cells were treated with Half Maximal Inhibitory Concentration (IC50) dose of Adriblastin and Taxotere diluted in culture medium (with FBS 0.1%) immediately before use. Two types of controls were used, untreated cells and cells treated with 0.1% FBS.

Terminal Deoxyribonucleotidyl Transferase (TdT)-mediated fluorescin dUTP Nick-End Labeling (TUNEL) assay

The optimal fixation for the detection of the fluorescein-dUTP nick-end labeling and simultaneous DNA content analysis was obtained with 70% ethanol at -20° for at least 12 h. The cells were treated as previously reported (17) Briefly, 3×10^5 cells/well were cultured and treated with Docetaxel and Adriablastina alone for 96 h. Then the cells were fixed in 4% paraformaldehyde in PBS (pH 7.4) for 15-30 min at room temperature and permeabilized for 2-5 min.

The acquisition of data was carried out using Cell Quest program and each measurement of fluorescin related to the DNA content was obtained. Each analysis was carried out on at least 30,000 events.

Statistical analysis

Using Student's two-tailed *t* test, the data was analyzed to identify statistically significant differences between groups. Results reported as mean ± SEM. *P* values less than 0.05 were considered statistically significant. Wilcoxon-Mann-Whitney U test was used to examine the null hypothesis of rank identity between 2 sets of data. IBM SPSS Statistics 20 software was used for all statistical analysis and graphing.

RESULTS

Patient characteristics

The average age of the patients, who were all male, was 66.9 years (range 51-84 years). In brief, six patients (43%) were diagnosed with adenocarcinoma and eight cases (57%) with squamous cell carcinoma. Ten patients (71.4%) had a well or moderately differentiated histological grade, three patients (21.4%) were in stages IIIA to IIIB and one (7.2%) was in stage IV. Further details about the clinical pathological features of the patients can be found in Table I.

Blood biopsy: identification of circulating lung cancer cells (NSCL-CTCs)

The team collected blood samples one day before surgery. We identified the specific interval of density to isolate lung cancer cells through a simulation procedure using a secondary human lung cancer cell

Table I. *Clinical pathological features of the patients.*

NUMBER PATIENTS	AGE	GENDER	STADIUM (TNM)	HISTOLOGY	GRADING
P1	61	M	IV	Adenoca	3
P2	67	M	I	Squamous	3
P3	68	M	I	Squamous	3
P9	76	M	II	Squamous	3
P10	74	M	II	Squamous	2
P11	76	M	II	Adenoca	3
P13	74	M	I	Adenoca	3
P14	58	M	III	Squamous	3
P15	84	M	I	Squamous	2
P16	58	M	III	Squamous	2
P20	51	M	I	Adenoca	2
P21	77	M	III	Squamous	2
P12	57	M	I	Adenoca	1
P4	56	M	I	Adenoca	3

Patients affected by adeno (adenoca) and squamous cell carcinoma were selected. The stage of cancer disease was determined in agreement with TNM stage (Tumour-Node-Metastasis, UICC-2009).

line (A549). We put A549 stably expressing GFP in the peripheral blood in increasing numbers. Then the blood samples were divided, and one part was centrifuged to separate the density phases and the second part was analyzed after the lysis procedure of the red blood cells. Fig. 1 shows all the experimental procedure phases.

A549-expressing-GFP cells were more concentrated (3.3±1) in the density interval of 1089-1090 gr/m^3 compared with the concentration of A549-expressing-GFP cells recovered from the peripheral blood sample.

We applied the protocol of isolation to the blood samples of the healthy subjects (n = 15) and the

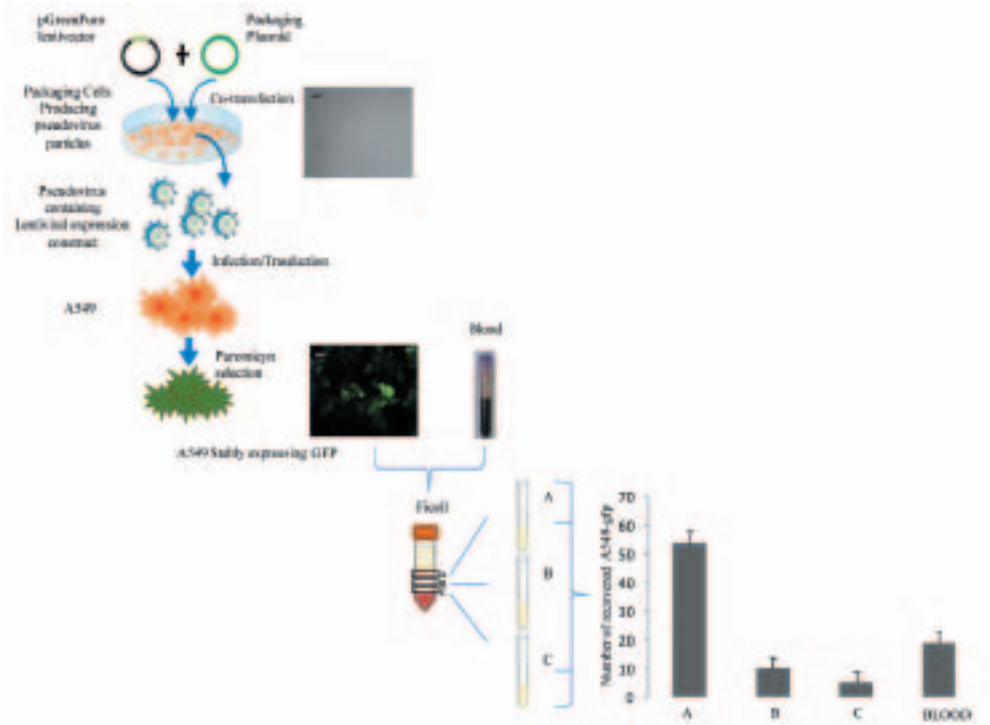

Fig. 1. *Graphical description of the procedure to recover lung cancer cells put in peripheral blood. Secondary lung cancer cell line A549 was transfected to express GFP-protein reporter. A549-GFP were put in the peripheral blood of a healthy subject. Flow cytometry analysis highlighted that the number of A549 recovered directly from the blood was 10±1 (media%±SEM) after red blood cell lyses. If the blood sample is submitted to gradient separation the number of recovered cells increases. In the density phase A, density interval of 1089-1090 gr/m3, 30±1 was recovered (media%±SEM). The experiments were repeated at least 5 times.*

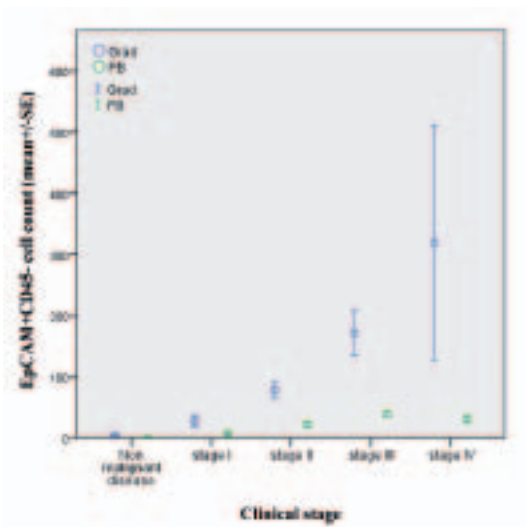

Fig. 2. *Distribution of EpCAM +CD45- isolated by gradient separation (blue) (corresponding to density interval of 1089-1090 gr/m3) and peripheral blood PB (green) of patients with nonmalignant lung diseases (*n = *14) and primary lung cancer patients (*n = *14) classified according to their clinical stage. Data are expressed as mean ± SE.*

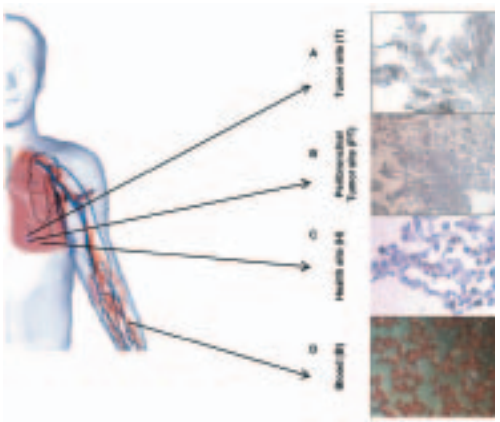

Fig. 3. *Schematic representation of samples collected from lung cancer patients. In panels **A**, **B** and **C**: E&E staining of lung biopsies from different tumour areas (A) tumour site alongside the tumour distant from bronchial structure, (B) peribronchial tumour site near bronchial structure, (C). Healthy site epithelium removed alongside the tumour bulk. In (**D**) thin blood smear. Tissue section A, B, and C was stained with anti-CD133 antibody. In the sections PT zone, (B), CD133+ staining showed a focal reinforcement of the positive cytoplasmic cell number .*

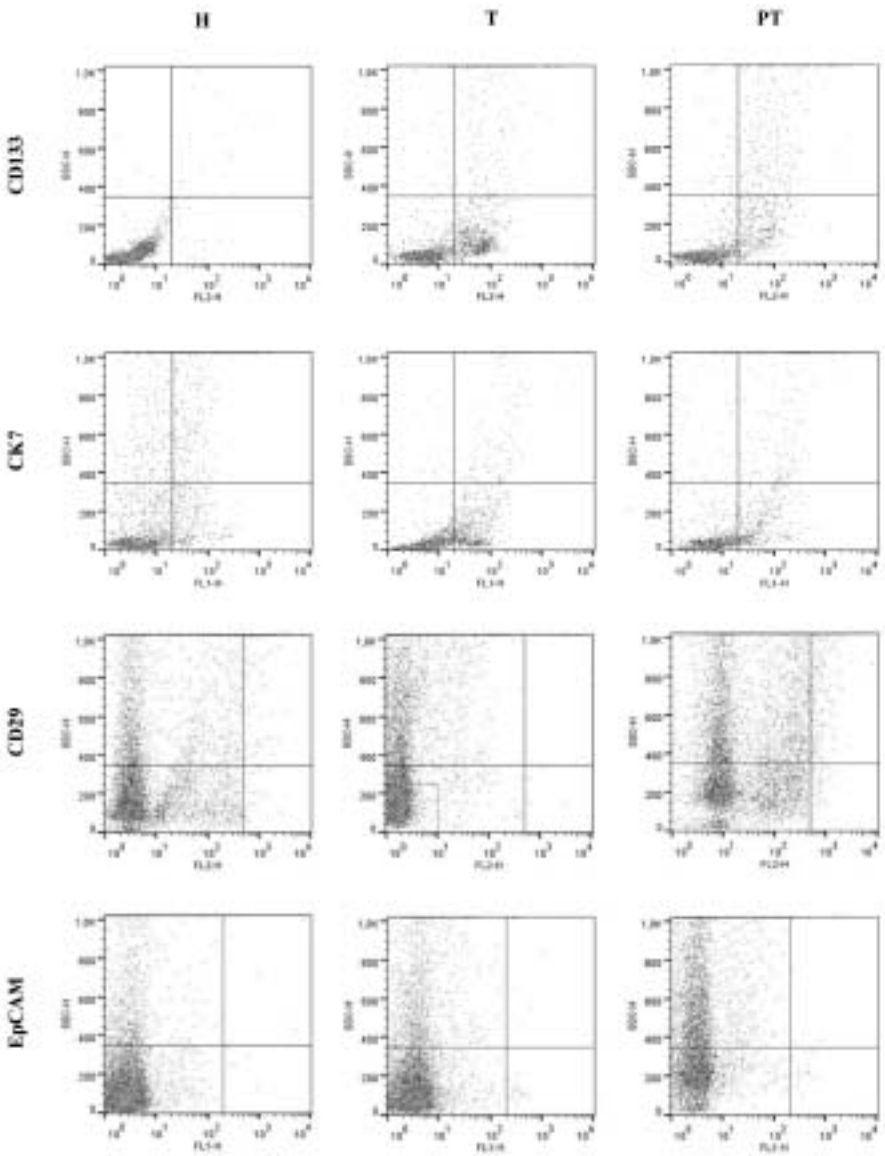

Fig. 4. *Flow cytometry plots showing the percentage of CD133+, CK7, CD29 and EpCAM gated cells within the three biopsies (H, T, and PT). The plot shows a line which is representative of 14 patients. Data was acquired using Fluorescence activated Cell sorting (FACS) cytometer and analyzed using Flow Jo data analysis software.*

NSCLC patients (n = 15).

The NSCL-CTCs- EpCAM $^{+}$ yield from the identified density phase was compared with the NSCL-CTCs- EpCAM $^{+}$ collected from the entire blood using cytometry analysis.

The mean of recovered NSCL-CTCs- EpCAM $^{+}$CD45^{-} was 13.5±3.1 (data are expressed as mean ± SEM) from the sample of peripheral blood treated only for red blood cell lysis. The mean of recovered NSCL-CTCs- EpCAM $^{+}$CD45^{-} was 76±25 from the sample collected at the density phase of 1089-1090gr/m^3. Fig. 2 shows the distribution of EpCAM $^{+}$CD45^{-} isolated from the density interval and the peripheral blood of patients with non-malignant lung diseases (n = 14) and primary lung cancer patients (n = 14) classified according to clinical stage TNM. In particular, 28.6±9.1 NSCL-CTCs EpCAM $^{+}$CD45^{-} was found in the density phase and 8±2.5

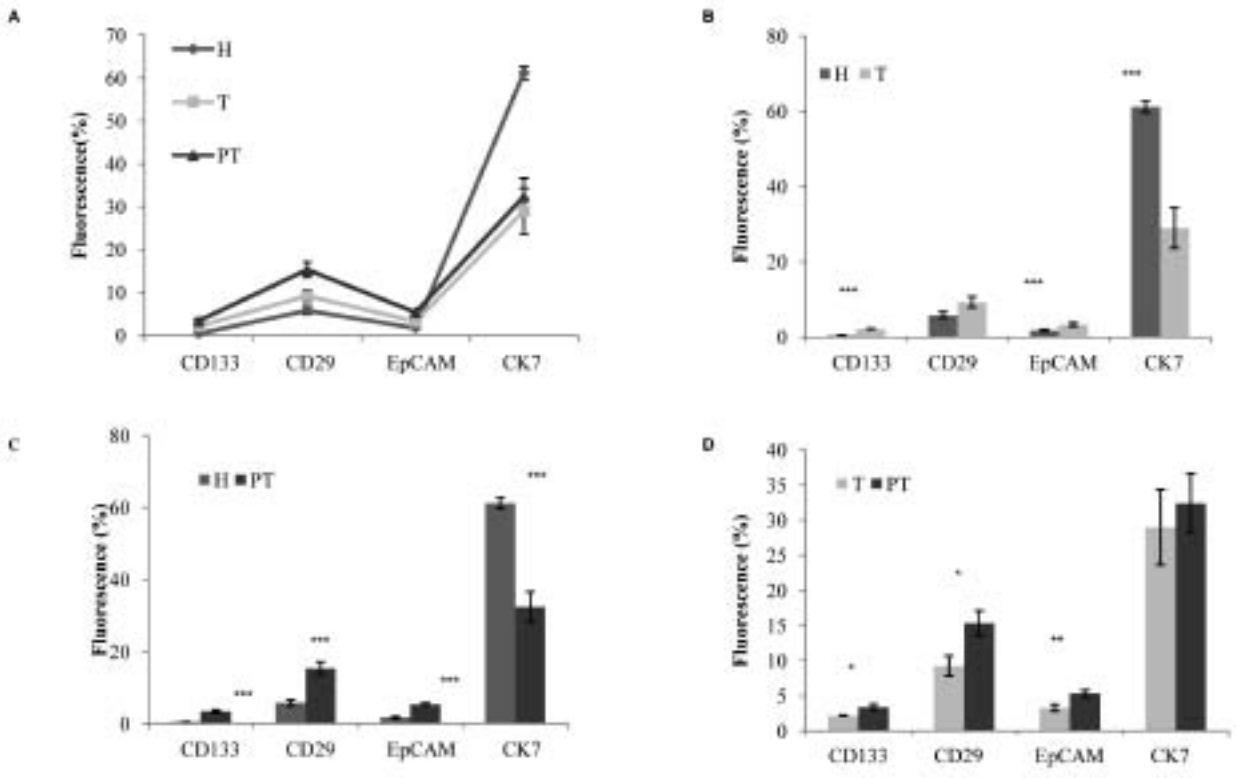

Fig. 5. ***A****) Data from Fig. 2, expressed as the mean±SEM, n=14. Comparison of the phenotypic profile of cancer cells isolated from different zones of the tumour tissue.* ***B***, ***C***, ***D****) Bar diagrams represent mean ± SEM,* n *= 14, data were analyzed by Student's t test. ***, P < 0.001; **, P < 0.01;* *******, P <0. 05.*

NSCL-CTCs EpCAM $^{+}$CD45^{-} in the peripheral blood of patients affected by NSCLC at stage I; 78±13.9 NSCL-CTCs EpCAM $^{+}$CD45^{-} in the density phase and 22.8±4.3 NSCL-CTCs EpCAM $^{+}$CD45^{-} in the peripheral blood of patients at stage II, 171.8±36.6 NSCL-CTCs EpCAM $^{+}$CD45^{-} in the density phase and 39±5.3 NSCL-CTCs EpCAM $^{+}$CD45^{-} in the peripheral blood of patients at stage III; 319±190.5 NSCL-CTCs EpCAM $^{+}$CD45^{-} in the density phase and 31.7±6.3 NSCL-CTCs EpCAM $^{+}$CD45^{-} in the peripheral blood of patients at IV stage. Finally, 5.3±1 NSCL-CTCs EpCAM $^{+}$CD45^{-} was found in the density phase and 0.07±0.04 NSCL-CTCs EpCAM $^{+}$CD45^{-} in the peripheral blood of healthy subjects.

Tissue biopsy: surface profile of primary non small cell lung cancer and normal lung epithelial cell

The hypothesis of niche model searching for a distinct anatomical location of the progenitor, TSCs, within the primary tumour was tested. The tumour area in different fragments (Fig. 3 A, B) from the same surgical specimen and in parallel were classified and mapped, as a normal control, also healthy epithelium removed alongside the tumours were analyzed (C).

Starting with fresh primary tumour tissues directly harvested from human patients undergoing surgery, the NSCLC tumours were surgically excised from patients and rapidly transported to the laboratory (within a few minutes from the moment of excision to preserve cell vitality), where the samples were quickly processed to obtain representative cellular suspension from different tumour zones. The tumour tissues biopsied (n = 14) in zone T (alongside the tumour distant from bronchial structure) showed a CD133+ frequency of 2.18±0.07 (mean±SEM). The tumour tissues biopsied in Zone PT (within the tumour near to bronchial structure) showed a CD133+ frequency of 3.41±0.4 (mean±SEM). The

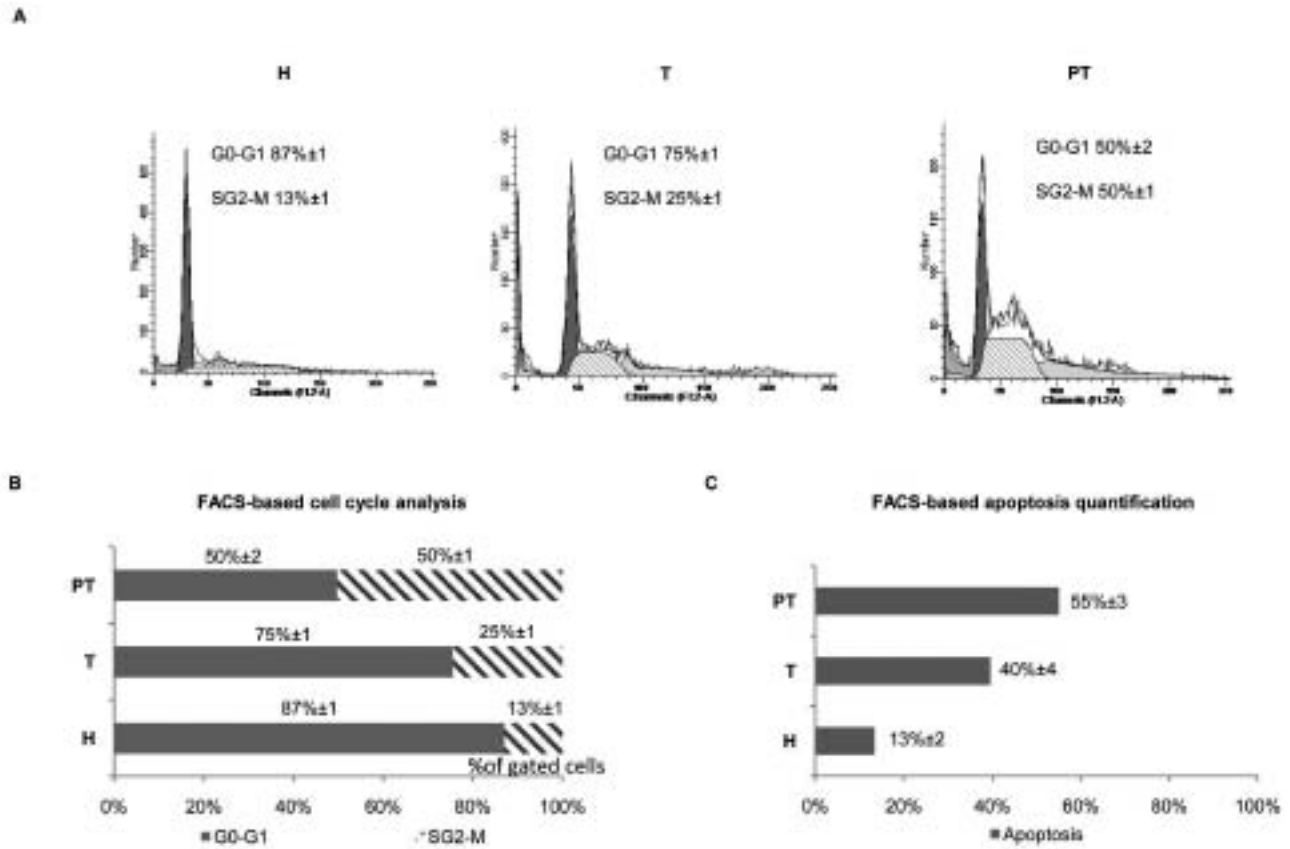

Fig. 6. ***A)*** *FACS-based cell cycle analysis of the cells derived from three different biopsies (H, T, PT). The plot shows a line which is representative of 14 patients. The values represent the number of cells in each phase of the cell cycle as a percentage of total cells.* ***B)*** *Bar diagrams of the cell cycle showing the percentage distributions of the cell cycle phases in the three cell groups, mean±SEM, n=14. Difference between the cell cycle phases among the three groups were analyzed by Student's t test. ***, P < 0.001;* ***C)*** *Pre-G0/G1 peaks quantification for the evaluation of apoptosis in the three cell groups. Data are expressed as mean ± SEM,* n = *14. Student's t test was applied to find significant differences between the three groups P< 0.001.*

tumour tissues biopsied in Zone H (normal lung tissue) showed a CD133+ frequency of 0.45±0.05. To ensure consistency and reproducibility in the set-up of experimental procedures, we decided to address the CD133+ in tissue sections. Immunohystochemical analysis with anti-CD133 antibody staining confirmed a variable cellular cytoplasm positivity in the corresponding Zone T (Fig. 3 A). In particular, the pneumocyte of type II exhibit cytoplasmic stain more than the pneumocytes of type I. In the sections of Zone PT the CD133+ staining showed a focal reinforcement of the positive cytoplasm cell numbers, as shown in Fig. 3. The representative cellular suspensions from different tumour zones were also investigated for the expression of CK7, CD29 and EpCAM antigens as shown in Fig. 4.

CK7 frequency was 29±5.3 (mean±SEM) for T zones, 32.43±4 for PT zones and 61.2±1.5 for H zones. CD29 frequency was 9.26±1.4 (mean±SEM) for T zones 15.34±1.7 for PT zones and 5.79±0.8 for H zones. EpCAM frequency was 3.29±0.4 (mean±SEM) for T zones, 5.36±0.4 for PT zones and 1.74±0.2 for H zones. Mean ±SEM of the fluorescence measured is reported in Fig. 5 (A). Moreover, comparing the fluorescence mean measured between the zones, H and tumour tissue

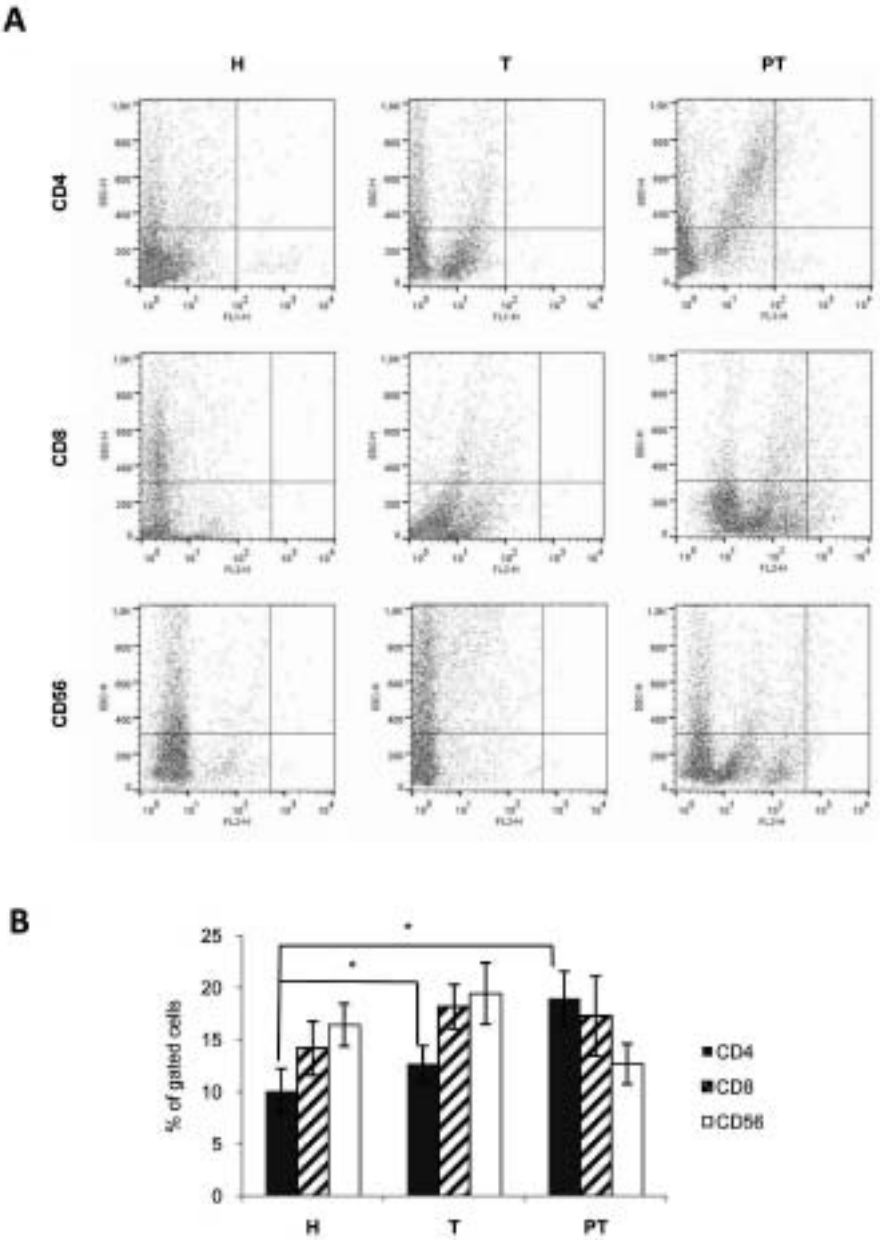

Fig. 7. ***A)*** *Flow cytometry plots showing the percentage of the CD4⁺, CD8⁺ and CD56⁺ infiltrating cells within the three biopsies (H, T, and PT). Results are from 14 patients, showing one representative plot of gated CD4⁺, CD8⁺ and CD56⁺ cells.* ***B)*** *Data from A, expressed as the percentage of CD4⁺, CD8⁺ and CD56⁺ gated cells. Bar diagrams represent mean ± SEM,* n *= 14, data were analyzed by Student's t test. *, P <0. 05.*

(T and PT) (Fig. 5 A, B) we highlighted that CD133 positive cancer cells are more concentrated in the tumour tissue with significant differences, (T) *vs* (H) and (PT) *vs* (H), P<0.001, respectively. Within the tumour tissue the CD133 positive cancer cells are more present in the peribronchial areas (PT) with significant difference (p<0.05). The same behavior was found for the antigens CD29 and EpCAM. The expression of CK7 was significantly different in the tumour compared with the healthy tissue, but without any difference within the tumour bulk. The results of statistical evaluation for each antigen is

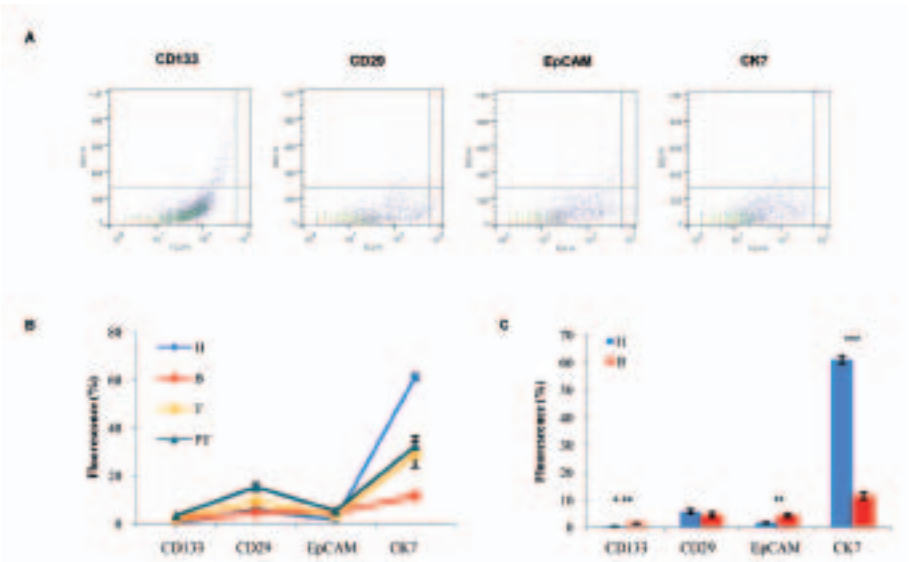

Fig. 8. ***A)*** *Dot plots representative of cytomerter evaluation of expression of CD45-CD133+(1,44±0.1 (mean ± SEM) CD45-CK7+ (11±1) and CD45- EpCAM + (4.5±0.7) CD45-CD29+(4.7±0.8) antigens as plotted in (**B**). **C**) Statistical comparison between healthy tissue (H) and blood biopsy, reveals higher amounts in the blood of CD133 (p<0.001) and EpCAM (p<0.01). An inverse relation was found for the CK7 expression (p<0.001). No statistically significant difference was reported for CD29.*

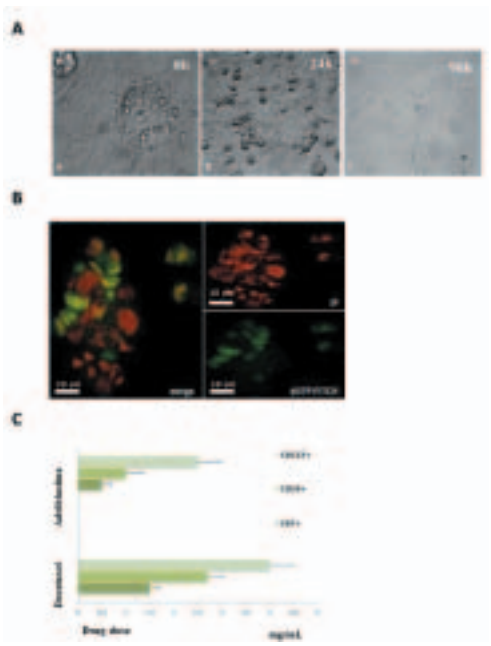

Fig. 9. ***A)*** *Pharmacological treatments: the panel shows the cancer cell cultures at time 0 (A), 24 (**B**) and 96 hours (**C**) of treatment. The graph shows the IC50 of anticancer chemotherapeutic agents able to induce 50% of apoptosis. Docetaxel was used with a dose ranging from 1.5 to 2 mg/ml: Adriblastina was used with a dose ranging from 1 to 2.5 mg/ml. These data show a "gradient of chemo-sensibility" within the same cancer cellular population, in particular CD133>CD29>CK7.*

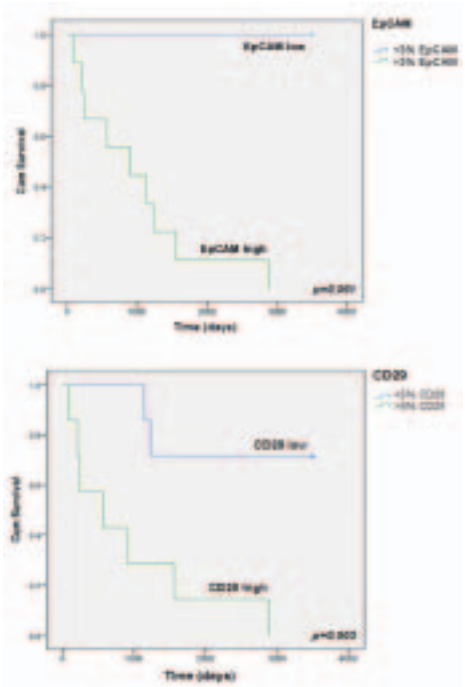

Fig. 10. *EpCAM (**A**) and CD29 (**B**) status in NSCLC patients (n=21). The y-axis represents the percentage of patients; the x-axis, their survival in days. The Kaplan–Meier plots demonstrate significant (Log rank = 10.208; p = 0.001) lower survival in NSCLC patients with high EpCAM expression (green line (A) and also in NSCLC with high CD29 expression [(green line (B)] and significant (Log rank = 13,94; p < 0.001).*

shown graphically in Fig. 5 A, B, C.

Cell cycle phases distribution and tumour infiltrating lymphocytes (TIL) within primary non-small cell lung cancer

To determine whether there are differences in cell cycle phase distribution of fresh cancer cell suspension derived from specific regions of the tumour tissue (Fig. 3 C zones 1,2,3), cell cycle distribution was analyzed by using flow cytometry of cells isolated from tumour and healthy biopsies. Fig. 6 shows the difference between normal H tissue and cancer tissue T and PT biopsies, all of which are statistically significant ($p<0.001$ (n=14). Moreover, Pre-G0/G1 peak quantification was considered to calibrate spontaneous apoptosis fractions in the three cell groups. The Student's *t* test applied found significant differences between the three groups $P< 0.001$. The PT tumour area is characterized by an elevated SG2-M phase and by 55%±3 of cancer cells in spontaneous apoptosis compared with the T and H tissues.

The cellular suspension obtained from each tissue biopsy was also analyzed for the expression of lymphocyte antigens such as CD4, CD8 and CD56 to define the degree of Tumour Infiltrating Lymphocytes (TIL). Fig. 7 reports the descriptive statistical analysis and the differences found between the tissue areas analyzed. In particular, we observed within the PT tumour district a greater presence of TIL-CD4 positive compared with T and H ($p=0.016$ and 0.037, respectively).

Surface profile comparison between NSCL- cancer cells derived from liquid and tissue biopsy

To compare the surface profile of tissue and blood biopsies we characterized the NSCL-CTCs for CD133, CK7, CD29, CD45 cell surface expression. We found that the frequency of these antigens in blood biopsies was 1.44±0.1 (mean ± SEM) for $CD45^{-}CD133^{+}$, 11±1 for $CD45^{-}CK7^{+}$, 4.5±0.7 for $CD45^{-}$ $EpCAM^{+}$ and 4.7±0.8 for $CD45^{-}CD29^{+}$, as shown in Fig. 8 A, B. In particular, we also observed that the subset of CTCs with $CD45^{-}$ $EpCAM^{+}CD29^{++}$ phenotype was detectable from the second stage onwards with a mean of 2±0.2. Comparing the rate of cancer cells for each antigen investigated, a greater expression was found in the tumour tissue compared with the blood biopsy. The statistical comparison between H cells and the blood biopsy, revealed a higher amount in the blood of CD133 ($p<0.001$) and EpCAM ($p<0.01$). An inverse relationship was found for the CK7 expression ($p<0.001$). No statistically significant difference was reported for CD29 (Fig. 8 C).

In vitro NSCL-CTCs chemo-sensitivity and survival curves

NSCL-CTCs were cultivated *in vitro*, in order to develop a short-term culture suitable for testing the toxicity of chemotherapeutic agents. Fig. shows the pharmacological treatments of cancer cell cultures at zero (A), 24 (B) and 96 hours (C) of treatment. The graph shows the IC50 of anticancer chemotherapeutic agents able to induce 50% of apoptosis. We used Docetaxel with a dose ranging from 1.5 to 2 mg/ml. We used Adriblastina with a dose ranging from 1 to 2.5 mg/ml. These data shows a "gradient of chemo-resistance" within the same cancer cell population, in particular CD133>CD29>CK7.

Clinical and molecular data benchmarking in NSCLC patients (n=21) were also carried out for the expression of EpCAM (A) and CD29 (B) status (Fig. 10). The Kaplan–Meier plots demonstrate significant (Log rank = 10.208; $p = 0.001$) lower survival in NSCLC patients with an EpCAM high expression [green line (A)] and also in NSCLC with CD29 high expression [green line (B), Log rank = 13,94; $p < 0.001$].

DISCUSSION

We developed an *ex-vivo* bimodal approach to consider and study the NSCLC disease. Traditionally, tumours have been studied using a global survey approach to gain information content on the interacting populations of the human tissue. The global approach begins with a higher amount of starting material and is much less labour intensive. However, the disadvantage of this approach is related to the impossibility of determining the exact proportion of the diseased subpopulation represented by the tumour stem cells. Any molecular analysis of cancer cells in their native tissue environment provides the most accurate picture of the *in vivo* disease state. However, accomplishing this goal

is more difficult than just grinding up a piece of tissue. This is because tissues are complicated three-dimensional structures, composed of large numbers of interacting cell populations (18). To deal with this problem here we propose our multiple "macro dissection" approach to define the proportions for each subpopulation within fresh tumour using anatomic references such as the proximal branch of the bronchial tree. The sub-fraction was performed using a topographic map. The team designed the map in relation to the distance of the cancer lesion to proximal bronchial structure. The bronchus was used as an anatomic reference point because the embryogenic process of the lung starts from this structure (19). The cancer cell population distribution reflects the hierarchy stem differentiation evolution suggesting an orderly architecture rather than a disorganized mass. Within each tumour analyzed we found it possible to design a gradient of expression for every marker investigated. A part of tumour was detected, proximal to the bronchial structure that displayed a predominance of the $CD133^+$ cell population PT or "TSC niche". The same region was also analyzed for tumour infiltrating lymphocytes (TIL) to evaluate the host response to tumour lesion. We found that the $CD4^+$ cells are more present in PT compared with $CD8^+$ and $CD56^+$ cells. Woo et al. (20) showed that human lung tumours contain large numbers of $CD4^+$ cells that selectively inhibit the host immune response and therefore could contribute to the progression of lung cancer. Moreover, we considered the cancer cell population resident in PT area for the expression of CD29, EpCAM and CK7. Comparative statistical analysis highlighted the coexistence of cancer cells CD29 and EpCAM positive in PT with a significant higher expression compared with the other tumour district considered (T). The cell cycle phase analysis and the evaluation of the spontaneous apoptosis fraction of PT and T districts confirmed that PT can be considered a "hot zone" within the tumour mass. Its elevated S phase and apoptosis fraction suggest a higher cell production rate that can be transferred to the blood stream with greater probability than other tumour districts such as T. Our attention focused on the antigen profile of PT, and used this information as a guideline to identify corresponding NSCL-CTCs in liquid biopsies. The consideration of NSCL-CTCs in liquid biopsies showed a corresponding antigen profile. Comparative analysis highlighted greater expression in correspondent tumour districts for each antigen investigated in the blood. The greater difference in expression found comparing PT and blood compared with T leads us to believe that the circulating progeny result from PT is in response to a potential difference of concentration. Our attention focused on the antigen profile of PT, and used this information as guidelines to identify corresponding NSCL-CTCs in liquid biopsies. The consideration of NSCL-CTCs in liquid biopsies showed a corresponding antigen profile. Comparative analysis highlighted greater expression in correspondent tumour districts for each antigen investigated in the blood. The greater difference in expression found comparing PT and blood compared with T leads us to believe that the circulating progeny result from PT is in response to a potential difference of concentration. In fact, CTCs are a highly heterogeneous population of circulating progeny deriving from a primary tumour lesion (21) and it is restrictive to consider them only in the metastatic phase. Their circulation in the bloodstream is a bi-directional dynamic process because CTCs are released and attracted by the tumour mass that transiently recaptures and releases them independently of the stage of the disease (22). This dynamism guarantees a continuous CTC replacement in the bloodstream and a consideration of these cells could provide a detailed assessment of the dynamic changes occurring in tumour disease. Our results confirm the heterogeneous composition of the circulating progeny as a reflection of the heterogeneous composition of the primary lesion that generates them.

Finally, to enrich the purely experimental data with the patients' medical histories we developed *In vitro* CTCs expansion to provide dose-response data able to detect heterogenic response to drug sensitivity consistent with clinical experience. In our opinion this is a big improvement, able to differentiate the clean and sterile scientific approach from a translational approach, as reported in literature (23). The *in vitro* results in terms of cellular chemo-resistance are confirmed by the overall survival and disease-free survival results. The survival curves confirmed that a high expression of NSCL-CTCs $CD29^+$ can be considered as a negative prognostic factor as can the high expression of NSCL-CTCs

EpCAM+. Moreover, the subset of NSCL-CTCs-EpCAM $^{+}$CD29^{+} is detected only in late stage of disease suggesting a dynamic interplay between the resident cellular cancer population and its relative progeny in the blood. The better characterization of the NSCL-CTCs profile and *in vitro* expansion to evaluate chemical resistance, as a result of the methodology here presented, can be exported to other tumours, to redefine a personalized monitoring program. Our results suggest that a liquid biopsy can be considered an exhaustive tool for monitoring NSCLC disease because it is a reflection of the resident cancer cell population and of the dynamic evolution that characterizes the progression of this complicated disease.

ACKNOWLEDGEMENTS

This work was partially supported by the project PON "Nuove strategie nanotecnologiche per la messa a punto di farmaci e presidi diagnostici diretti verso cellule cancerose circolanti" (code: PON01_02782), the project Interregional Research Centre for Food Safety and Health (IRC_FSC) (cod. PON a3-00359) and the project ExChanger Share your Science (code: PON 04a3_00433).

REFERENCES

1. Alberg AJ, Ford JG, Samet JM . Epidemiology of lung cancer: ACCP evidence-based clinical practice guidelines. Chest 2007; 123:29S-55S.
2. Baccelli I, Schneeweiss A, Riethdorf S, et al. Identification of a population of blood circulating tumour cells from breast cancer patients that initiates metastasis in a xenograft assay. Nat Biotechnol 2013; 31:539-44.
3. Simone G, Malara N, Trunzo V, et al. Protein-carbohydrate complex reveals circulating metastatic cells in a microfluidic assay. Small 2013; 9:2152-61.
4. Koren A, Motain H, Cufer T. Lung cancer stem cells: a biological and clinical perspective. Cell Oncol 2003; 36:265-75.
5. Li L, Xie T. Stem cell niche: structure and function. Annu Rev Cell Dev Biol 2005; 21:605-31.
6. Eckfeldt, C.E. Mendenhall, E.M. Verfaillie, C.M. The molecular repertoire of the "almighty" stem cell. Nat Rev Mol Cell Biol 2005; 6:726-37.
7. Chauchereau A, Al Nakouzi N, Gaudin C, et al. Stemness markers characterize IGR-CaP1, a new cell line derived from primary epithelial prostate cancer. Exp Cell Res 2011; 317:262-75.
8. Shmelkov SV, St Clair R, Lyden D, Rafii S. AC-133/CD133/Prominin-1. Int J BiochemCell Biol 2002; 37:715-9.
9. Shuman Moss LA, Jensen-Taubman S, Stetler-Stevenson WG. Matrix metalloproteinases: changing roles in tumour progression and metastasis. Am J Pathol 2012; 181:1895-9.
10. Eramo A, Lotti F, Sette G, et al. Identification and expansion of the tumorigenic lung cancer stem cell population. Cell Death Differ 2008; 15:504-14.
11. Peck K, Sher YP, Shih JY, Roffler SR, Wu CW, Yang PC. Detection and quantification of circulating cancer cells in the peripheral blood of cancer patients. Cancer Res 1998; 58:2761-5.
12. Kreidberg JA, Donovan MJ, Goldstein SL, Rennke H, Shepherd K, Jones RC, Jaenisch R. Alpha3 beta1 integrin has a crucial role in kidney and lung organogenesis. Development 1998; 122:3537-47.
13. Hérard AL, Pierrot D, Hinnrasky J, Kaplan H, Sheppard D, Puchelle E, Zahm JM. Fibronectin and its alpha 5 beta 1-integrin receptor are involved in the wound-repair process of airway epithelium. Am J Physiol 1996; 271:L726-33.
14. Falcioni R, Cimino L, Gentileschi MP, D'Agnano I, Zupi G, Kennel SJ, Sacchi A. Expression of beta1, beta4, and beta5 integrins by human lung carcinoma cells of different histotypes. Exp Cell Res 1994; 210:113-22.
15. Kikkawa, Y.Sanzen, N. Sekiguchi, K. Isolation and characterization of laminin-10/11 secreted by human lung carcinoma cells. laminin-10/11 mediates cell adhesion through integrin alpha3 beta1. J Biol Chem 1998; 273:15854-9.
16. Malara NM, Sgambato A, Granone P, et al. Biological characterization of central and peripheral primary non small cell lung cancers (NSCLC). Anticancer Res 1999; 19(3B):2249-52.
17. Malara N, Focà D, Casadonte F, et al. Simultaneous inhibition of the constitutively activated nuclear factor kappaB and of the interleukin-6 pathways is necessary and sufficient to completely overcome apoptosis resistance of human U266 myeloma cells. Cell

Cycle 2008; 7(20):3235-45.
18. Liotta, L. Petricoin, E. Molecular profiling of human cancer. Nat Rev Genet 2000; 1:48-56.
19. Burri, P.H. Fetal and postnatal development of the lung. Annu Rev Physiol 1984; 46:617-28.
20. Woo, E.Y. Cutting edge: regulatory T cells from lung cancer patients directly inhibit autologous T cell proliferation. J Immunol 2002; 168:4272-76.
21. Powell AA, Talasaz AH, Zhang H, et al. Single cell profiling of circulating tumor cells: transcriptional heterogeneity and diversity from breast cancer cell lines. Plos One 2012; 7:e33788.
22. Kim MY, Oskarsson T, Acharyya S, Nguyen DX, Zhang XH, Norton L, Massagué J. Tumor self-seeding by circulating cancer cells. Cell 2009; 139:1315-1326.
23. Hunter EM, Sutherland LA, Cree IA, Dewar JA, Preece PE, Wood RA, Linder D, Andreotti PE. Heterogeneity of chemosensitivity in human breast carcinoma: use of an adenosine triphosphate (ATP) chemiluminescence assay. Eur J Surg Oncol 1993; 19:242-9.

INCREASED RISK OF OSTEOPOROSIS IN POSTMENOPAUSAL WOMEN WITH TYPE 2 DIABETES MELLITUS: A THREE-YEAR LONGITUDINAL STUDY WITH PHALANGEAL QUS MEASUREMENTS

C. NEGLIA[1], N. AGNELLO[1], A. ARGENTIERO[1], G. CHITANO[1], G. QUARTA[1], I. BORTONE[1], G. DELLA ROSA[1], A. CARETTO[2], A. DISTANTE[1], A. COLAO[3], C. DI SOMMA[4], A. MIGLIORE[5], R.S. AURIEMMA[6,7]and P. PISCITELLI[6,7]

[1]Euro Mediterranean Biomedical Scientific Institute, Brindisi, Italy; [2]Department of Endocrinology, Local Health Authority, ASL Brindisi, Brindisi, Italy; [3]Division of Endocrinology, Department of Clinical Medicine and Surgery, University of Naples Federico II, Naples, Italy; [4]IRCCS SDN Foundation, Naples, Italy; [5]Department of Rheumatology, Fatebenefratelli St. Peter's Hospital, Rome, Italy; [6]Division of Epidemiology, IOS, Southern Italy Hospital Institute, Naples, Italy; [7]Coleman LTD, Naples, Italy

Received July 7, 2014 – Accepted October 24, 2014

Type 2 diabetes mellitus (T2DM) is associated with a higher risk of fractures even in presence of normal or increased bone mineral density. The purpose of this three-year longitudinal study was to evaluate the risk of osteoporotic fractures by assessing the changes of Quantitative Ultrasound (QUS) parameters in a group of postmenopausal women with type 2 diabetes mellitus (T2DM) compared with non-diabetic controls. The measurements were taken on a group of 18 postmenopausal women affected by T2DM and 18 healthy age-matched controls, aged 55-70 years, referring to the Osteolab laboratory at the ISBEM Research Institute (Brindisi, Italy) between 2009 and 2013. Subjects had baseline and 3-year follow-up measurements with phalangeal QUS carried out by a DBM Sonic Bone Profiler 1200 (Igea®); medical history, current drug therapies and risk factors for fractures were recorded for each patient. The analyzed phalangeal QUS parameters were Amplitude-Dependent Speed of Sound (AD-SoS), Bone Transmission Time (BTT), Fast Wave Amplitude (FWA) and Signal Dynamic (SDy). At the baseline visit we found no statistically significant difference between T2DM and non-diabetic patients when looking at phalangeal QUS parameters. At the three-year follow-up visit, a significantly higher decrease of both BTT (P<0.001) and AD-SoS (P<0.001) parameters was found in the T2DM group. On the contrary, the decrease of FWA was significantly higher in non-diabetic controls (P<0.001). Our data confirm the ability of phalangeal QUS to detect differences in the risk of osteoporotic fractures in T2DM postmenopausal women compared to non-diabetic controls. The study suggests that T2DM women present a higher cortical porosity and increased trabecular bone density compared to non-diabetic controls, respectively shown by the higher decrease of both AD-SoS and BTT and the lower decrease of FWA.

Increasing evidence is available in medical literature concerning the association between diabetes and osteoporosis. Observational studies, carried out in Europe and the United States, have reported a

Key words: osteoporosis, quantitative ultrasound, Type 2 diabetes

Mailing address: Dr Prisco Piscitelli,
c/o Medicina Futura Group
Centro Direzionale, Isola E3, Palazzo Avalon
80143 Naples, Italy
Tel.: +39 081 7879520 Fax:+39 081 7879481
e-mail: prisco.piscitelli@tiscali.it

0393-974X (2014)

significantly increased risk of fracture in older adults affected by type 1 or type 2 diabetes mellitus (1). However, subjects with T1DM show a higher risk of fracture in presence of reduced bone mineral density (BMD) compared to controls (2), while patients affected by T2DM show a significantly higher risk of fractures both at hip and other skeletal sites even in the presence of normal or increased BMD (3). Currently, controversial results have been obtained in different studies concerning the association between T2DM, risk of fractures and BMD, with the majority of these studies reporting unchanged or paradoxically higher BMD values (2, 4). Several explanations for this have been proposed by different authors and involve two possible mechanisms (2): i) the increased frequency of falls in older women due to comorbidities associated with diabetes, such as impaired vision and balance, arthritis, cardiovascular diseases, depression and use of anxiolytics or other drugs active on the central nervous system; ii) a weaker bone structure caused by non-enzymatic glycation of collagen which leads to accumulation of advanced glycosilation end-products (AGEs) in the organic bone matrix (5).

The assessment of hip BMD by dual-energy x-ray absorptiometry (DEXA) has been demonstrated to be a strong predictor of risk of osteoporotic fractures (6). However, recent evidence has shown that - in women with diabetes - hip BMD measurements are not exhaustive in the evaluation of bone strength and in predicting fracture risk since bones can assume different internal geometries with a consequent wide variation of strength despite presenting the same BMD values (7). In experimental fatigue tests conducted on parallelepiped beams of trabecular tissue, realized with a micromilling machine, some authors found that the assessment of mineral content could only explain approximately 40% of the variance in the tissue modulus of bone, and that BMD measurements may leave residual errors in the estimation of bone strength in the range of 35-55 % (8).

Quantitative Ultrasound (QUS) can provide more information on the physical properties and quality of bone tissue, as compared with DXA. Phalangeal QUS, as demonstrated in several studies, are able to assess qualitative characteristics of the bone such as microarchitecture, geometry and elasticity (9). Phalangeal QUS parameters are not only related to BMD but also to other skeletal properties (10). QUS measurements performed at proximal phalanges are easily accessible. Furthermore, it has been demonstrated that phalanges contain both cortical and trabecular bone and they are sensitive to early changes in bone mass. Phalangeal QUS measurements have been used in the evaluation of osteoporotic fracture risk in several cross-sectional studies carried out on patients with T1DM, mostly young and pre-menopausal women (11). Tao et al. found that QUS measurements performed at three peripheral skeletal sites - including phalanges - are a useful tool for detecting the impaired bone quality in postmenopausal women with T2DM (12). In this context, we carried out a three-year longitudinal study aimed at investigating the changes in phalangeal QUS parameters occurring in a group of post-menopausal women diagnosed with T2DM compared to a group of age-matched non-diabetic controls.

MATERIALS AND METHODS

Eighteen consecutive post-menopausal women were visited at the Euro-Mediterranean Biomedical Scientific Institute (ISBEM) research centre under the Osteoporosis and Fractures Prevention Project (PROF) between November 2009 and May 2010. All patients underwent a baseline visit and a follow-up visit after three years. Inclusion criteria of this longitudinal study were: age between 55 and 70 years; diagnosis of T2DM confirmed by medical records or by the use of daily hypoglycemic drugs. The date of diagnosis and of the start-month of the hypoglycemic therapy were recorded. At baseline, patients were excluded from the study if they had a prior diagnosis of heart failure, cancer, kidney diseases and diseases affecting bone metabolism; we excluded from the study patients with prior use of drugs inducing osteoporosis (i.e. corticosteroids, cancer drugs, heparin, thyroid hormones), calcium and vitamin D supplementation and antiresorptive therapies. The control group consisted of 18 healthy age-matched postmenopausal women. At follow-up visit, the average values of glycosylated hemoglobin (HbA_{1c}) and fasting blood glucose, measured during the month prior to the visit, were also recorded. Hemoglobin A1c levels were not available for non-diabetic subjects since they had not been prescribed by the general practitioner. Written informed consent was obtained from each participant.

At the baseline and the follow-up visits, anthropometric

data were collected: the weights of all patients were recorded, with a tolerance of 0.5 kg; standing height was measured on the balance stadiometer to the nearest centimeter; Body Mass Index (BMI) was calculated as weight/height^2 (Kg/m^2).

Moreover, patients were interviewed by a physician to collect data concerning factors potentially influencing bone metabolism, daily intake of milk and dairy products, smoking and alcohol consumption habits; physical activity levels were assessed using the General Practice Physical Activity (GPPAQ) guideline. Medical history and use of medications were recorded for each patient.

Phalangeal QUS measurements were performed at baseline and at the 3-year follow-up visit in both groups. Ultrasound measurements were carried out for all subjects using a DBM Sonic Bone Profiler 1200 (Igea ®, Carpi, Italy). This device is based on the transmission of ultrasounds through proximal phalanges (II- V) of the fingers of the non-dominant hand. The transmitting and the receiving probes are applied to the lateral surface of each finger and the coupling of the probes with the skin is accomplished by a simple gel for ultrasound transmission. The measurements were performed by placing the probes at the distal metaphysis of the first phalanges, in the proximity of the condyles.

The device calculates the speed of sound (SoS, in meters per second) transmission through the phalanx by measuring the width of the finger (including soft tissues) divided by the time of flight, defined as the time from the emitted pulse to the received signal. It is important to underline that the measurement is performed only when the amplitude of the signal is greater than 2 mV, so that ultrasound velocity is finally evaluated as AD-SoS (Amplitude-dependent Speed of Sound) (9).

The measurements analyzed in this study were: AD-SoS (Amplitude-dependent Speed of Sound), and three parameters describing the graphic trace of the QUS signal as Bone Transmission Time (BTT, μs), Fast Wave Amplitude (FWA, mV) and Signal Dynamic (SDy, mV/μs^2).

BTT is the difference between the time when the first peak of the signal received reaches its maximum and the time when that signal would be measured in presence of only soft tissue between the transducers. FWA is the amplitude of the first wave of the graphic trace. SDy is the mean value of the second derivative of amplitude versus time of the first two peaks of the ultrasound signal. All the measurements were performed by a single operator. For ten subjects, we performed repeated measurements on different days, in order to detect the standard error of each measurement. The coefficient of variation of the measurements was calculated as the ratio between the standard deviation of the measurements and the average of the measurements, and it was expressed as a percentage. Coefficient of variation were: 2.08% for AD-SoS, 5.5% for BTT, 12.8% for FWA, and as much as 80% for SDy.

Statistical analysis

Statistical analyses were performed with STATA/SE 11 software for Windows (STATA® 11.0, Texas, USA). Baseline clinical characteristics of control and T2DM group were compared using two-sample *t*-test for continuous variables and Fisher's exact test for categorical variables. Percentages of use of medication during follow-up between the groups were compared using Fisher's exact test.

Analysis of covariance (ANCOVA) was performed to compare both groups regarding changes in anthropometric and phalangeal QUS values between baseline and follow-up measurements. For each value, we obtained a regression equation that can be summarized as follows:

$$\textit{Follow-up value} = \textit{constant} + ax_1\ \textit{baseline value} + bx_2\ \textit{group};$$

where *a* and *b* are estimated coefficient and group is a binary variable that assumes value 1 for the T2DM group and 0 for the control group. The changes of each anthropometric and phalangeal QUS measurement were calculated as difference between follow-up and baseline values.

RESULTS

Complete data at the beginning of the study and at the three-year follow-up were available for 36 postmenopausal women (18 with diagnosis of T2DM and 18 healthy control subjects). Clinical characteristics at baseline are shown in Table I.

At the baseline visit, the mean age was 62.2 years (SD: 4.5) for T2DM subjects and 60.2 years (SD: 4.7) for controls. No statistically significant differences were found between the two groups for age, anthropometric data (weight, height and BMI), risk factors for osteoporosis and prevalence of hypertension. Prevalence of dislipidemias resulted significantly different: 61.1% in T2DM and 22.2% in controls ($p<0.05$). No previous fractures had occurred in any subject.

The mean range of time to follow-up was 38 months. All medications taken by the patients during the follow-up period are shown in Table II. After the follow-up period, only 1 woman in the control group and 2 women in the T2DM group reported use of bisphosphonates. The frequency of use of aspirin and statins was higher in the T2DM group

with statistically significant differences ($p<0.02$ and $p<0.05$, respectively).

Among hypoglycemic drugs in the T2DM group, metformin and repaglinide were the most frequently used (with a frequency of 66.7 and 27.8, respectively).

At the follow-up visit, the mean values of fasting blood glucose and hemoglobin A1c levels in the T2DM patients (taken in the month prior to the visit) were 139.3 mg/dl (SD: 35.9) and 6.9% (SD: 0.7), respectively (Table III). In the control group, the value of fasting blood glucose was lower than 95.0 mg/dl for all subjects.

In each group, no changes in terms of comorbidities and no relevant differences concerning risk factors for osteoporosis were observed during the interval between the two visits. Moreover, no fractures were reported during the follow-up period. Phalangeal

Table I. *Baseline clinical characteristics of T2DM postmenopausal women and non-diabetic controls.*

Charateristics	Controls	T2DM	*p*
Demographic and anthropometric			
Age (years), mean ± SD	60.2 ± 4.7	62.2 ± 4.5	0.10
Weight (kg), mean ± SD	68.4 ± 10.4	74.3 ± 8.9	0.08
Height (cm), mean ± SD	154.0 ±6.3	153.4 ± 7.1	0.77
Body Mass Index (kg/m^2), mean ± SD	29.0 ± 4.8	31.6 ± 3.2	0.06
Risk factors of osteoporosis			
Age menopause (years), mean ± SD	49.2 ± 4.5	49.2 ± 5.5	0.97
Early menopause, yes (%)	4 (22.2)	3 (16.6)	1.00
Physical activity – moderately active, yes (%)	1 (5.6)	2 (11.1)	1.00
Physical activity – moderately inactive or inactive, yes (%)	17 (94.4)	15 (88.9)	1.00
Smoking cigarettes, yes (%)	2 (11.1)	1 (5.6)	1.00
Alcohol, yes (%)	10 (55.6)	8 (44.4)	0.74
Milk, yes (%)	10 (55.6)	14 (77.8)	0.29
Intake of Dairy products, yes (%)	15 (83.3)	15 (83.3)	1.00
Other diseases			
Hypertension, n (%)	12 (66.7)	15 (83.3)	0.44
Dyslipidemias n (%)	4 (22.2)	11 (61.1)	<0.05
Hypotiroidism, n (%)	4 (22.2)	5 (27.8)	1.00

Table II. *Medications taken during follow up period.*

	Controls	T2DM	*p*
Antiresorptive medications			
Calcium and Vitamin D	2 (11.1)	3 (17.6)	1.00
Bisphosphonates	1 (5.6)	2 (11.1)	1.00
Antihypertensive medications			
Diuretics	2 (11.1)	5 (27.8)	0.40
ACE inhibitors	1 (5.6)	1 (5.6)	1.00
Beta blockers	3 (17.6)	6 (33.3)	0.44
Sartans	6 (37.5)	10 (55.6)	0.32
Other medications			
Aspirin	3 (18.7)	11 (61.1)	<0.02
Antidepressants	1 (5.6)	4 (22.2)	0.34
Statins	4 (22.2)	10 (55.6)	<0.05
Hypoglycemic Medications			Daily Dosage (mg)
Acarbose	-	2 (11.1)	50
Glimepiride	-	4 (22.2)	2
Repaglinide	-	5 (27.8)	2.1 ± 1.7
Insulin	-	3 (16.7)	103.3 ± 95.0
Metformin	-	12 (66.7)	1107.7 ± 519.1
Pioglitazone	-	1 (5.6)	15

Table III. *Blood sample test at follow-up visit and duration of diabetes in T2DM group.*

Characteristics	
Hemoglobin A1c, %	6.9 ± 0.7
Fasting blood glucose, mg/dL	139.3 ± 35.9
Duration of diabetes, years	9.2 ± 9.5

QUS measurements taken at baseline and at the 3-year follow-up are reported in Table IV.

At baseline, all the four QUS parameters analyzed in the study were lower in the T2DM group (although no statistically significant differences have emerged). At the follow-up visit, only AD-SoS resulted significantly lower in the T2DM group. Analysis of

Table IV. *Phalangeal QUS measurements at baseline and at follow-up visit.*

	Baseline			*Follow-up*		
Phalangeal QUS parameter	*Controls*	*T2DM*	*p*	*Controls*	*T2DM*	*p*
AD –SoS, m/s	2010.3 ± 52.3	1973.7 ± 65.4	0.07	1971.1 ± 15.5	1916.61 ± 12.20	<0.01
BTT, µs	1.42 ± 0.20	1.36±.21	0.36	1.40 ± 0.23	1.22 ± 0.28	0.06
SDy, mV/µs2	-300.9 ± 143.4	-341.5 ± 250.6	0.55	-398.7 ± 200.0	-398.7 ± 153.5	0.99
FWA, mV	41.9 ± 9.5	38.1±5.6	0.14	30.3 ± 8.3	31.8 ±6.8	0.55

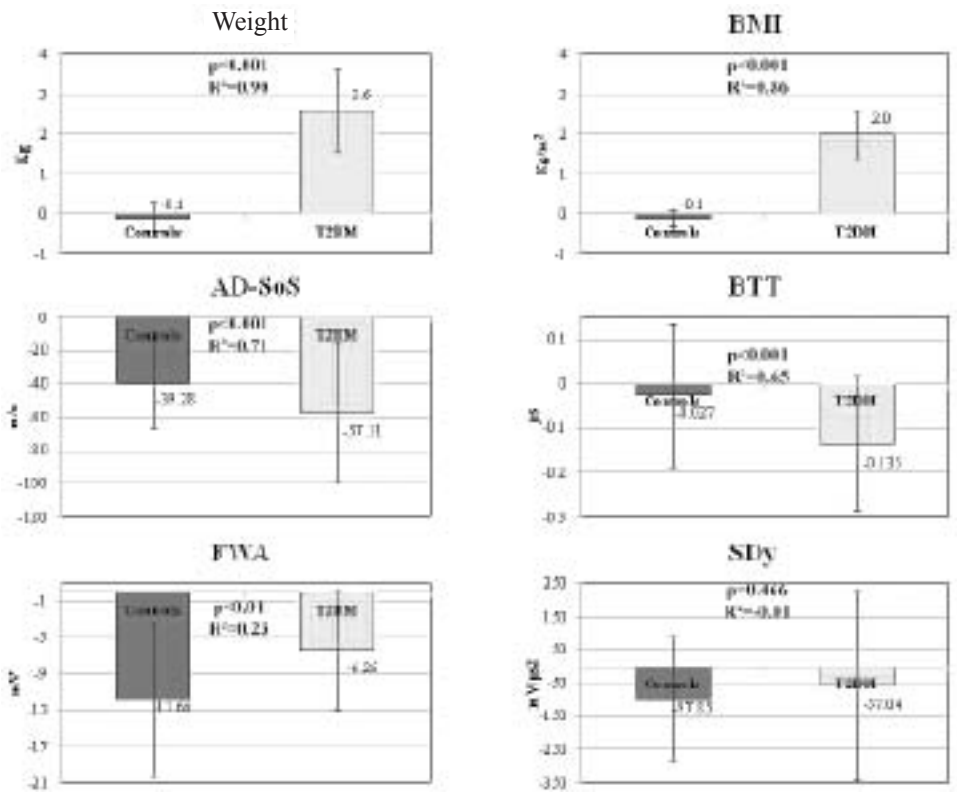

Fig. 1. *Changes of anthropometric measurements and QUS parameters during follow-up period. Changes are reported as mean difference between follow-up and baseline value ± SD. P value and R^2 are derived by regression analysis of follow-up value with baseline value and group as covariates.*

covariance (ANCOVA) was performed to compare the amount of the changes in anthropometric parameters and phalangeal QUS measurements between the baseline and follow-up visits (Fig. 1). There were significant differences between the two groups in respect to the weight and BMI ($p<0.001$): in the T2DM patients we found an increase in the average weight and BMI of 2.6 kg (SD: 4.2) and 1.9 kg/m^2 (SD: 0.6), respectively; whereas in the control group, the change in average weight was -0.2 kg (SD: 1.7) and the change in average BMI was -0.1 kg/m^2 (SD: 0.2).

When looking at the mean changes observed in phalangeal QUS parameters, we found a decrease of AD-SoS and BTT in both group. This variation was significantly higher in the T2DM group ($p<0.001$); on the contrary, the decrease of FWA was higher in the control group ($p<0.01$). Changes in SDy during the follow-up period did not show statistically significant differences between the two groups.

DISCUSSION

Most of the studies based on phalangeal QUS measurements are cross-sectional. Longitudinal studies using QUS to detect changes in bone quality have been conducted mainly on young subjects, pregnant and pre-menopausal women (13-15), and the very conducted on postmenopausal women evaluated only the effect of ageing and medications on bone loss (16, 17). To our knowledge, this is the first longitudinal study in which phalangeal QUS are used to asses changes in bone mineralization in T2DM postmenopausal women compared to non-diabetic controls.

In the T2DM patients, we found lower values of AD-SoS and BTT than in the non-diabetic controls both at baseline and the follow-up visit, but no statistically significant differences emerged (except for the AD-SoS at follow-up). These results are consistent with the findings of other studies where an increased risk of fracture in T2DM patients was shown (3). Moreover, our results are consistent with those of Tao et al. who found lower SOS (Speed Of Sound) in phalangeal QUS measurements concerning T2DM patients in a cross-sectional study comaparing T2DM and non-diabetic postmenopausal women.

This longitudinal study shows that both T2DM and non-diabetic postmenopausal women show decreased values of AD-SoS and BTT between the first and the second measurement (three years later); it is noteworthy that the decrease was significantly higher ($p<0.001$)in the T2DM group, as shown by the analysis of covariance (ANCOVA); this type of analysis adjusts each patient's follow-up value for the relative baseline value and it presents the advantage of not being affected by baseline differences between the two groups (18).

AD-SoS was shown to be significantly associated with area and porosity of the cortical bone (10): it increases with age before 30 years because of the increase in bone mineralization, but it decreases with ageing (19). In a three-year longitudinal study conducted on female subjects, the first decrease of AD-SoS was found after 40 years of age (16). Moreover, in the group of women who entered the menopause, a decrease in the AD-SoS of 56 m/s between the first and the second phalangeal QUS measurement was reported (16). Similarly, in our three-year longitudinal study, we found a decrease of 57 m/s in the T2DM group compared to 39 m/s in the non-diabetic controls, thus suggesting a negative impact of T2DM on cortical bone. These results are consistent also with recent evidence based on high-resolution peripheral quantitative computed tomography (HR-pQCT), that showed an increased cortical porosity at ultradistal and distal radius and tibia in postmenopausal women affected by T2DM (20, 21).

Unlike the AD-SoS, for which it is not possible to evaluate the influence of soft tissue of the phalanges, BTT is independent from the thickness of the soft tissue. BTT depends on the amount of bone inside the phalanxes and can be also considered sensitive to cortical bone density and cortical thinning and porosity (10). In our study, the decrease in BTT was significantly higher ($p<0.001$) in the T2DM group (–0.14 μs) than in the non-diabetic controls (-0.02 μs). A different porosity could be hypothesized between the two groups and a greater tendency to lose cortical thickness in the T2DM group.

Furthermore, studies carried out using phalangeal QUS measurements have shown that menopause is characterized not only by a decrease of AD-SoS and BTT (19, 22), but also by lower SDy and FWA, with a more evident reduction in SDy (19).

Our data on FWA and SDy are consistent with these findings since in both groups we found decreases of these values. The analysis of covariance on the difference between the value observed at follow-up and at baseline between the two groups showed no significant regression coefficients for SDy. On the contrary, a significant decrease was reported for FWA (R^2=0.23, p<0.01), which was significantly higher in the non-diabetic group. As FWA is positively correlated with trabecular separation and negatively with trabecular number (23), our results suggest that in T2DM women the trabecular structure was maintained more preserved than in the non-diabetic group; other evidence supports this finding, as an increase in trabecular bone density in addition to the cortical porosity of radio and tibia has been already demonstrated in other studies previously mentioned (20, 21). The same authors suggested that T2DM might be associated with an inefficient redistribution of bone mass, which would be a possible explanation for having observed a higher fracture risk and lower bone strength in T2DM patients compared to non-diabetic controls (20, 21). However, a recent two-year follow-up study on postmenopausal women (with and without T2DM) was carried out by using magnetic resonance imaging (MRI) of distal radius, finding no statistically significant differences in the percentage changes of trabecular bone between diabetic and non-diabetic patients (24).

There were no significant differences between the groups concerning SDy. We were unable to give a clear explanation of this finding because of the worse accuracy and the lower reproducibility of this parameter compared to the others.

The analysis of potential risk factors that may explain the differences of bone structure observed between the two groups must take into account the significant higher prevalence of dyslipidemia in the group of T2DM patients as well as the higher frequency of assumption of aspirin and statins detected in these subjects.

Dyslipidemia has been proposed as a risk factor for osteoporosis although the assumption of statins should have a compensatory effect. Much evidence demonstrates that the assumption of 3-hydroxy-3-methylglutaryl coenzyme A (HMG-CoA) reductase inhibitors (statins) is associated with increased bone formation and density, also in patients with type 2 diabetes (25). In a test conducted on rats it was shown that the oral administration of statins stimulated an increase of trabecular bone volume (26).

Moreover, relative to the effect of aspirin therapy on bone health, a sizeable amount of evidence documents a beneficial effect on trabecular and cortical bone of aged population (27).

The higher frequency of use of aspirin and statins could have represented a protective factor on trabecular bone in the T2DM subjects in our study, as shown by the results obtained with FWA parameter. However, the role that dyslipidemias could have had in the absence of specific therapy to lower their level remains to be clarified.

Coming to the assumption of hypoglycemic medications, exclusively used by the group of T2DM patients, several studies have documented only the negative effect of thiazolidinediones on bones. However, during the follow-up of our study, only one patient had taken this medication, so we could exclude this effect.

With regard to the significant increase in BMI (2 units up) during the follow-up period in the T2DM subjects, our data would suggest a role of weight and BMI increase on QUS parameter and therefore on micro-architectural structure. A lot of evidence, including that from the NORA study, reported that an increased BMI is associated to a BMD increase (28). A recent study, conducted on US adults over 50 years of age, reported a significant increase of BMD of about 0.0082 g/cm^2 per unit increase of BMI (29). Considering our results regarding the QUS parameters - that give information on bone mineral density as AD-SoS and BTT - it would seem that the increase in weight has a negative effect on bone density. Although this result is in conflict with previous scientific evidence, in recent studies a negative influence was shown of fat mass and BMI on bone health (30). The relationship between high fat mass and bone is quite complex. Further research is needed to investigate the effect on bone of a series of adipokines and cytokines secreted by adipose tissue, such as leptin, resistin, adiponectin, interleukin 6, and tumor necrosis factor-alpha. Under the conditions of our study, the real impact of weight gain of T2DM subjects on bone structure also remains to be clarified.

Some limitations affect the present study, as it was

not possible to collect data about biochemical bone turnover markers at baseline and at follow-up visits to combine them with phalangeal QUS parameters to have a more comprehensive assessment of bone formation and resorption balance. Moreover, it would have been relevant to have a more frequent testing of fasting blood glucose and Glycosilated hemoglobin (HbA_{1c}) levels during the follow-up period in the T2DM patients.

Our study shows significant differences in the changes of three QUS parameters (AD-SoS, BTT and FWA) between postmenopausal T2DM patients and non-diabetic age-matched controls over three years. These results confirm the ability of phalangeal QUS to detect differences in bone mass at proximal phalanges in T2DM postmenopausal women, possibly reflecting a higher cortical porosity and increased trabecular bone density compared to non-diabetic controls. Therefore, this non-invasive, radiation-free and low-cost methodology could have a specific role in the clinical practice for the diagnosis of alterations in bone micro-architecture in T2DM subjects, considering that femoral or lumbar DXA cannot detect them.

Moreover, further studies will be useful to understand whether the QUS parameters, examined in this study, can be used in premenopausal and younger women.

REFERENCES

1. Schwartz AV, Vittinghoff E, Bauer DC, et al. Association of BMD and FRAX score with risk of fracture in older adults with type 2 diabetes. JAMA 2011; 305:2184-92.
2. Vestergaard P. Discrepancies in bone mineral density and fracture risk in patients with type 1 and type 2 diabetes--a meta-analysis. Osteoporos Int 2007; 18:427-44.
3. de Liefde I, van der Klift M, de Laet CE, van Daele PL, Hofman A, Pols HA. Bone mineral density and fracture risk in type-2 diabetes mellitus: the Rotterdam Study. Osteoporos Int 2005; 16:1713-20.
4. Isidro ML, Ruano B. Bone disease in diabetes. Curr Diabetes Rev 2010; 6:144-55.
5. Kume S, Kato S, Yamagishi S, et al. Advanced glycation end-products attenuate human mesenchymal stem cells and prevent cognate differentiation into adipose tissue, cartilage, and bone. J Bone Miner Res 2005; 20:1647-58.
6. Johnell O, Kanis JA, Oden A, et al. Predictive value of BMD for hip and other fractures. J Bone Miner Res 2005; 20:1185-94.
7. Hamilton CJ, Jamal SA, Beck TJ, Khaled AS, Adachi JD, Brown JP, Davison KS, Canadian Multicentre Osteoporosis Study Research G. Evidence for impaired skeletal load adaptation among Canadian women with type 2 diabetes mellitus: insight into the BMD and bone fragility paradox. Metabolism 2013; 62:1401-5.
8. Choi K, Goldstein SA. A comparison of the fatigue behavior of human trabecular and cortical bone tissue. J Biomech 1992; 25:1371-81.
9. Cadossi R, de Terlizzi F, Cane V, Fini M, Wuster C. Assessment of bone architecture with ultrasonometry: experimental and clinical experience. Horm Res 2000; 54(S):9-18.
10. Sakata S, Barkmann R, Lochmuller EM, Heller M, Gluer CC. Assessing bone status beyond BMD: evaluation of bone geometry and porosity by quantitative ultrasound of human finger phalanges. J Bone Miner Res 2004; 19:924-30.
11. Catalano A, Morabito N, Di Vieste G, Pintaudi B, Cucinotta D, Lasco A, Di Benedetto A. Phalangeal quantitative ultrasound and metabolic control in pre-menopausal women with type 1 diabetes mellitus. J Endocrinol Invest 2013; 36:347-251.
12. Tao B, Liu JM, Zhao HY, Sun LH, Wang WQ, Li XY, Ning G. Differences between measurements of bone mineral densities by quantitative ultrasound and dual-energy X-ray absorptiometry in type 2 diabetic postmenopausal women. J Clin Endocrinol Metab 2008; 93:1670-5.
13. Di Iorgi N, Calandra E, Secco A, et al. Quantitative ultrasound detects bone changes following bone marrow transplantation in pediatric subjects with hematological diseases: a longitudinal study. J Endocrinol Invest 2010; 33:478-82.
14. Pluskiewicz W, Drozdzowska B, Stolecki M. Quantitative ultrasound at the hand phalanges in pregnancy: a longitudinal study. Ultrasound Med Biol 2004; 30:1373-8.
15. Hadji P, Ziller M, Maskow C, Albert U, Kalder M. The influence of chemotherapy on bone mineral density,

quantitative ultrasonometry and bone turnover in pre-menopausal women with breast cancer. Eur J Cancer 2009; 45:3205-12.
16. Mele R, Masci G, Ventura V, de Aloysio D, Bicocchi M, Cadossi R. Three-year longitudinal study with quantitative ultrasound at the hand phalanx in a female population. Osteoporos Int 1997; 7:550-7.
17. Agostinelli D, de Terlizzi F. QUS in monitoring raloxifene and estrogen-progestogens: a 4-year longitudinal study. Ultrasound Med Biol 2007; 33:1184-90.
18. Vickers AJ, Altman DG. Statistics notes: Analysing controlled trials with baseline and follow up measurements. BMJ 2001; 323:1123-4.
19. Wuster C, Albanese C, De Aloysio D, et al. Phalangeal osteosonogrammetry study: age-related changes, diagnostic sensitivity, and discrimination power. The Phalangeal Osteosonogrammetry Study Group. J Bone Miner Res 2000; 15:1603-14.
20. Patsch JM, Burghardt AJ, Yap SP, Baum T, Schwartz AV, Joseph GB, Link TM. Increased cortical porosity in type 2 diabetic postmenopausal women with fragility fractures. J Bone Miner Res 2013; 28:313-24.
21. Shu A, Yin MT, Stein E, Cremers S, Dworakowski E, Ives R, Rubin MR. Bone structure and turnover in type 2 diabetes mellitus. Osteoporos Int 2012; 23:635-41.
22. Albanese CV, Cepollaro C, de Terlizzi F, Brandi ML, Passariello R. Performance of five phalangeal QUS parameters in the evaluation of gonadal-status, age and vertebral fracture risk compared with DXA. Ultrasound Med Biol 2009; 35:537-44.
23. Cavani F, Fini M, de Terlizzi F, et al. Effect of trabecular orientation on mechanical resistance and ultrasound propagation in specimens of equine vertebrae. Ultrasound Med Biol 2003; 29:1777-85.
24. Pritchard JM, Giangregorio LM, Atkinson SA, et al. Changes in trabecular bone microarchitecture in postmenopausal women with and without type 2 diabetes: a two year longitudinal study. BMC Musculoskelet Disord 2013; 14:114.
25. Nakashima A, Nakashima R, Ito T, Masaki T, Yorioka N. HMG-CoA reductase inhibitors prevent bone loss in patients with Type 2 diabetes mellitus. Diabet Med 2004; 21:1020-4.
26. Mundy G, Garrett R, Harris S, et al. Stimulation of bone formation *in vitro* and in rodents by statins. Science 1999; 286:1946-9.
27. Carbone LD, Tylavsky FA, Cauley JA, Harris TB, Lang TF, Bauer DC, Barrow KD, Kritchevsky SB. Association between bone mineral density and the use of nonsteroidal anti-inflammatory drugs and aspirin: impact of cyclooxygenase selectivity. J Bone Miner Res 2003; 18:1795-802.
28. Siris ES, Miller PD, Barrett-Connor E, et al. Identification and fracture outcomes of undiagnosed low bone mineral density in postmenopausal women: results from the National Osteoporosis Risk Assessment. JAMA 2001; 286:2815-22.
29. Skrzek A, Koziel S, Ignasiak Z. The optimal value of BMI for the lowest risk of osteoporosis in postmenopausal women aged 40-88 years. Homo 2014; 65:232-9.
30. Zhao LJ, Liu YJ, Liu PY, Hamilton J, Recker RR, Deng HW. Relationship of obesity with osteoporosis. J Clin Endocrinol Metab 2007; 92:1640-6.

INHIBITORY EFFECTS OF DIFFERENT LACTOBACILLI ON *CANDIDA ALBICANS* HYPHAL FORMATION AND BIOFILM DEVELOPMENT

C.F. ORSI[1,2], C. SABIA[3], A. ARDIZZONI[2], B. COLOMBARI[2], R.G. NEGLIA[2], S. PEPPOLONI[2], G. MORACE[1] and E. BLASI[2]

[1]Department of Health Sciences, University of Milan, Milan, Italy; [2]Department of Diagnostic, Clinic and Public Health Medicine, University of Modena and Reggio Emilia, Modena, Italy; [3]Department of Life Sciences, University of Modena and Reggio Emilia, Modena, Italy

Received August 4, 2014 – Accepted November 4, 2014

The aim of this study was to investigate the effects of different species of Lactobacilli on hyphal formation and biofilm development by the opportunistic fungal pathogen *Candida albicans*. We employed 4 different Lactobacillus species, namely *L. rhamnosus*, *L. acidophilus*, *L. plantarum* and *L. reuteri*, and 2 *C. albicans* strains, the reference DAY286 and its isogenic *hwp1/hwp1* mutant, the FJS24 strain. As assessed by morphological analysis and quantitative colorimetric assays, Lactobacillus crude filtrate supernatant fluids (CFSF) affected Candida, impairing both hyphal formation and biofilm production. The CFSF-mediated phenomenon occurred in a dilution- and time-dependent manner and was consistently observed, irrespective of the *C. albicans HWP1* genotype.

Candida albicans is a commensal fungus frequently found as component of human cutaneous, oral and intestinal microbiota (1). Furthermore, *C. albicans* is a major human fungal pathogen, causing both mucosal and deep tissue infections, especially in certain categories of individuals, including critical patients and immunocompromised subjects, where it becomes responsible for life-threatening invasive infections with a high rate of mortality (2).

A well-known pathogenic trait of *C. albicans* is its ability to undergo transition from yeast-to-hyphal form, under certain predisposing conditions. Such a transition ultimately allows fungal penetration into host mucosa and, in turn, this causes tissue damage (3). Among the multitude of Candida genes involved in cell wall rearrangement, *HWP1*, *ECE1*, *HYR1*, *ALS3* and *ALS8* are amongst those specifically transcribed during hyphal development; accordingly, they have been recognized as hyphal form-related genes (4-5). In particular, *HWP1* gene encodes for a cell-wall protein (hyphal wall protein 1) involved in a variety of functions, including parietal assembly, intracellular signaling, binding to epithelial cells, resistance to macrophage-mediated killing and pathogenicity, as assessed by *in vitro* and *in vivo* studies (6-13).

Recent evidence indicates that Candida pathogenic potential also depends on its ability to produce biofilm on abiotic as well as living surfaces (14, 15). As detailed elsewhere (16), during early biofilm formation, yeast cells adhere and initiate germ tube formation; in the intermediate phase, hyphal elongation continues and extracellular matrix (ECM) is abundantly produced. Mature biofilm consists ultimately of a yeast base, with hyphal elements embedded in ECM, from where newly formed daughter yeast cells grow out

Key words: Candida albicans, Lactobacillus, probiotics, hypha, biofilm, hyphal wall protein 1

Mailing address: Prof. Elisabetta Blasi, Ph.D.
Department of Diagnostic, Clinical and Public Health Medicine,
University of Modena and Reggio Emilia,
Istituti Biologici, Via Campi 287,
41125 Modena, Italy
Tel.: +39 059 205 5468 Fax: 39 059 205 5483
e-mail: elisabetta.blasi@unimore.it

0393-974X (2014)

DISCLOSURE: ALL AUTHORS REPORT NO CONFLICTS OF INTEREST RELEVANT TO THIS ARTICLE.

and are released, seeding new niches for biofilm formation and/or infection. Interestingly, once organized in a biofilm structure, Candida also exhibits reduced susceptibility to host defenses and enhanced resistance to antimicrobial drugs (17). Taken together, these findings strongly emphasize the relevance of fungal biofilm in clinical settings. Accordingly, *Candida,* which is the fourth most common cause of bloodstream infections (2), is recognized as being responsible for an increasing number of device-related infections, mostly because of its high propensity to develop biofilms on the surfaces of almost any medical devices, such as stents, shunts, prostheses, implants and catheters (14, 18, 19).

Probiotic bacteria are defined as ''living microorganisms which, when administered in adequate amounts, confer a health benefit on the host''(20). According to this definition, they are suggested to play a role in health maintenance. Furthermore, probiotics may have a role in preventing human diseases, such as infections (either oral or urogenital) and intestinal barrier dysfunctions, including lactose intolerance, acute gastroenteritis, food allergy, and Crohn's disease (21-23). The vast majority of probiotic bacteria naturally occurs as part of human mucosal microbiota and mainly belong to *Lactobacillus, Bifidobacterium, Propionibacterium* and *Streptococcus* genera. In particular, several Lactobacillus species have been described as capable of preventing overgrowth of pathogens by producing acids, bacteriocins, biosurfactants, hydrogen peroxide and co-aggregation molecules (23-27). A better understanding of Lactobacilli effects on commensal and pathogenic microorganisms is mandatory to support their clinical application not only in the restoration of microbial equilibrium at the mucosal level, but also in the prevention and possibly in the therapeutical management of oral and uro-genital infections (20). Although *in vitro* studies or animal models are not adequate to directly prove the efficacy of probiotics, they can be used to identify and/or characterize the events involved in their action. In particular, correlations between *in vivo* experimental data and *in vitro* target-specific studies have facilitated and expanded the knowledge on bacterial strains to be considered for probiotic use in humans (28, 29).

The aim of the present study was to investigate the effects of secreted products from 4 different species of Lactobacilli, namely crude filtrate supernatant fluids (CFSF) from *L. acidophilus, L. rhamnosus, L. plantarum* and *L. reuteri* on the opportunistic fungal pathogen *C. albicans*. We found that both hyphal formation and biofilm development are affected by the CFSF to some extent, depending upon the CFSF dilution employed and the time of contact. Also, we provide evidence that such phenomenon consistently occurs, irrespective of the *C. albicans HWP1* genotype.

MATERIALS AND METHODS

Microbial strains and lactobacilli CFSF preparation

Two *C. albicans* laboratory strains were employed: the reference DAY286 (*HWP1/HWP1*) and its isogenic engineered counterpart, the null mutant FJS24 (*hwp1/hwp1*) (8); such strains were purchased from the Fungal Genetics Stock Center (Kansas City, Missouri, USA). The day before each experiment, a loop-full from frozen stock cultures was inoculated in Yeast Peptone Dextrose broth (YPD, Oxoid, Hampshire, UK) and incubated overnight in an orbital shaker at 30°C. Then, the yeast cells were washed twice with sterile phosphate-buffered saline (PBS, EuroClone, Whethereby, UK), counted and suspended in "complete medium", consisting of RPMI 1640 (Gibco, Grand Island, NY, USA), supplemented with 10% heat inactivated foetal bovine serum (Defined Hyclone, Logan, Utah, USA), 50 mg/ml gentamicin (EuroClone) and 2 mM L-glutamine (EuroClone). The yeast cell concentration of 10^6 cells/ml was employed. All the bacterial and fungal strains were maintained as stocks at -80°C, in glycerol solution 20% (v/v).

The following 4 species of lactobacilli were used: *L. acidophilus* ATCC 314*, L. plantarum* ATCC 8014, *L. rhamnosus* ATCC 7469 and *L. reuteri* ATCC 55730. Bacteria were grown on De Man Rogosa Sharpe agar (MRS Oxoid, Milan, Italy), at 37°C for 48 h in anaerobic conditions (Gas-Pak System, bioMérieux).

The Lactobacilli CFSF were prepared, as detailed elsewhere (27), by culturing each Lactobacillus strain in MRS broth (Oxoid, Milan, Italy), at 37°C for 24 h. The supernatant fluids were collected by centrifugation (10,000 x g for 10 min at 4°C), dialyzed against 30 mmol/l sodium acetate buffer (pH 5.3) and filtered with 0.45 µm pore-size filters (Millipore Corp., Bedfort, Mass, USA). The pH of each CFSF was adjusted to 7.0 with 1 M NaOH, prior to being used in the experiments.

Antifungal activity evaluation

The antifungal activity by Lactobacilli and their supernatants (CFSF) was assessed by two different

methods, the modified agar-spot deferred test and the well diffusion assay, as previously described with minor modifications (30).

The modified agar-spot deferred test was performed as follows. Overnight Lactobacilli cultures were spotted onto the surface of agar plates and incubated for 24 h at 30°C. Then, 7 ml of soft agar medium, containing Candida (1.5×10^5 CFU/ml), were poured onto those same plates, that were further incubated, anaerobically, for additional 24 h. Candida susceptibility to Lactobacilli was evaluated as fungal growth inhibition, which was quantitatively assessed by measuring the diameter of the growth inhibition zone around the Lactobacilli spots.

The well diffusion assay was carried out as follows. A pre-made plate with an agar base medium (1.5% agar) was overlaid with 7 ml of soft agar medium containing Candida (1.5×10^5 CFU/ml). Thereafter, 7 mm diameter wells were cut into the agar and 200 µl of Lactobacilli CFSF were placed into each well. Plates were then incubated for 24-48 h at 37°C; finally, the zones of growth inhibition were measured and their diameters (in mm) were recorded.

CFSF effect on C. albicans hyphal formation

C. albicans DAY286 and FJS24 (10^6 cells/ml in 3 ml of complete medium) were plated in 6 well plates and exposed to Lactobacilli CFSF (1 ml/well; 1:4 final dilution), for 1 or 3 h at 37°C, in 5% CO_2. At the end of the incubation times, the samples were examined for morphology, using the inverted microscope Nikon ECLIPSE TS100, equipped with Digital Sight DS-L3 microscope camera controller (Nikon Corporation, Tokyo, Japan). Microphotographs were obtained at 200x magnification. For each experimental condition, at least 100 cells were analyzed in order to quantify hyphal and yeast forms.

CFSF effect on C. albicans biofilm development

In order to assess the effect of CFSF on Candida biofilm formation, two different protocols (A and B) were employed. In both cases, experiments were performed in 96-well plates, using a starting yeast cell concentration of 10^6 cells/ml, in complete medium; incubations were performed at 37°C in the presence of 5% CO_2; each sample was assessed in 6-replicates.

Protocol A (24 h or 48 h): *C. albicans* yeast cells, suspended in "complete medium", were exposed to different dilutions of Lactobacilli supernatants (1:4; 1:8 and 1:16) or "complete medium" plus MRS broth (used as a control) and incubated at 37°C for either 24 or 48 h; then, the levels of biofilm produced were evaluated, as detailed below.

Protocol B (24 h + 24 h): a preformed *C. albicans* biofilm (24-h-old cultures in "complete medium") was exposed to different dilutions of Lactobacilli supernatants (1:4; 1:8 and 1:16) or "complete medium" plus MRS broth (used as a control) and incubated for additional 24 h. In parallel groups, as additional controls, Candida yeast cells were incubated in "complete medium" alone.

In both Protocols, A and B, the levels of fungal biofilm production were measured by crystal violet (CV) and 2,3-bis(2-methoxy-4-nitro-5-sulfophenyl)-2H-tetrazolium-5-carboxanilide (XTT, Sigma, St Louis, MO, USA) reduction assays, as detailed elsewhere (31). In particular, for the CV assay, absorbance was measured spectrophotometrically by the SunRise Microplate Reader (Sunrise, Tecan, Salzburg, Austria) at 540 nm (OD_{540}) and the colour intensity was proportional to biofilm biomass. For the XTT assay, the absorbance was measured at 450 nm and 620 nm; the results were expressed, according to the formula previously described (32), as percentage of fungal damage: $100 \times [1 - (OD_{Candida + CFSF} / OD_{Candida\ alone})]$.

Statistical analysis

Statistical analysis was performed by one way ANOVA test. The data in the Figures and Table are expressed as mean or median values ± standard deviations (SD) of three to five independent experiments, unless otherwise specified.

RESULTS

Antifungal activity by Lactobacillus species and their CFSF

Initially, the 4 Lactobacillus species were directly screened for anti-Candida activity by the agar-spot deferred test. Each of the 4 Lactobacilli exerted inhibitory effects against Candida: as shown in Fig. 1, left panel, the sizes of the inhibition zones were always > 10 mm. Subsequently, the effects of the 4 Lactobacilli CFSF against Candida were assessed by the agar well diffusion assay. As detailed in Fig. 1, right panel, the sizes of inhibition haloes were between 10 and 15 mm, irrespective of the CFSF-producing Lactobacilli species.

The results shown in Fig. 1 were obtained using the DAY286 Candida strain; similar sets of data were also observed when evaluating the FJS24 strain, for susceptibility to either Lactobacilli or CFSF (data not shown).

Effect of CFSF from different Lactobacillus species on C. albicans hyphal formation

To investigate the effect of Lactobacilli CFSF on yeast-to-hyphal form transition, morphological

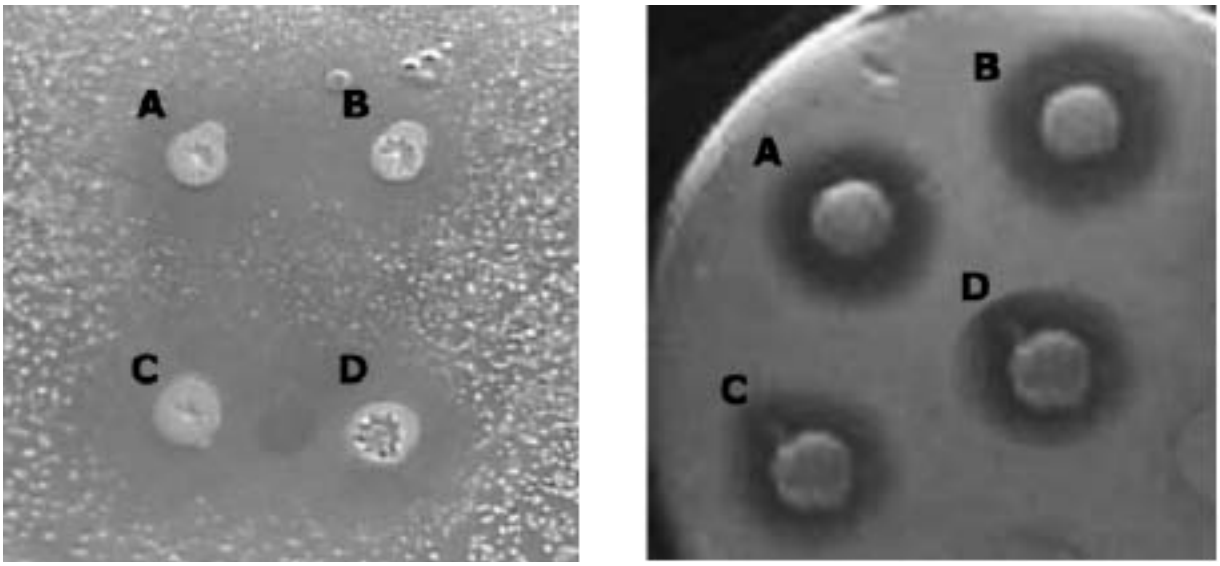

Fig. 1. *Anti-Candida activity by Lactobacilli and their CFSF. Left panel: the anti-Candida activity by L. acidophilus (A), L. plantarum (B), L. rhamnosus (C) and L. reuteri (D) was assessed by agar-spot deferred test. Right panel: the anti-Candida activity of CFSF from L. acidophilus (A), L. plantarum (B), L. rhamnosus (C) and L. reuteri (D) was evaluated by the agar well diffusion assay.*

analysis was carried out on Candida yeast cells exposed or not to CFSF for different times. As detailed in Fig. 2, images of Candida strain DAY286 incubated for 1 h in "complete medium" alone, as negative control (Fig. 2 A), revealed the presence of abundant germ tubes, that further elongated after 3 h of incubation (Fig. 2 B). When Candida was incubated in "complete medium" and MRS broth (3 and 1 ml, respectively), no differences were observed (Fig. 2, C and D). In contrast, when the yeast cells were incubated with the different CFSF (Fig. 2, E-L), for either 1 or 3 h, little or no germ tubes were detected, irrespectively of the experimental group considered. Similar results were observed when the mutant Candida strain FJS24 was employed (data not shown).

As detailed in Fig. 3, quantification of the yeast cells detectable in each experimental condition revealed that only about 10% of *C. albicans* still retained the yeast-like structure, both at 1 and 3 h, in the control groups (3 ml "complete medium" plus 1 ml MRS broth), while such a percentage ranged between 50% and 80% in parallel groups exposed to the CFSF (1:4 final dilution). In particular, the CFSF from *L. acidophilus*, *L. plantarum* and *L. reuteri* resulted more effective in preventing dimorphic transition (as indicated by the highest percent of yeast-like cells) with respect to *L. rhamnosus* CFSF. Once again, no appreciable differences were observed when comparing the two Candida strains.

Effect of CFSF from different Lactobacillus species on C. albicans biofilm development

In order to investigate the effect of lactobacilli CFSF on *C. albicans* biofilm development, the CV and the XTT assays were employed. Each CFSF was tested on Candida at different dilutions (1:4, 1:8 and 1:16) and according to different schedule times (yeast cells + 24 h; yeast cells + 48 h; 24-h-old biofilm + 24 h). As detailed in Table I, we found consistent inhibitory effects in all the cases, as shown by the reductions in the OD values, strictly related to the CFSF dilutions. In particular, as assessed by one-way ANOVA test, 3 out of 4 CFSF (i.e., those from *L. acidophilus*, *L. plantarum* and *L. reuteri*) caused significant OD reductions ($p<0.05$), always detectable at the 1:4 dilution, against both the DAY286 and FJS24 *Candida* strains, at 24 and 48 h. Furthermore, when used at the 1:8 dilution, CFSF from *L. plantarum* and *L. reuteri* significantly impaired *C. albicans* after 24-h incubation, whereas no significant effects were observed at 48-h

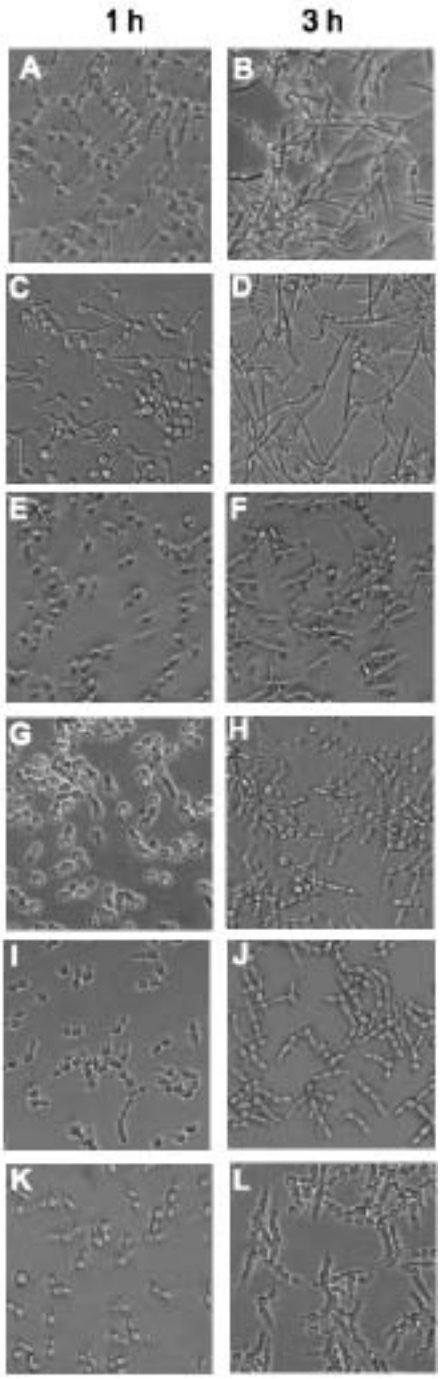

Fig. 2. *Morphology of C. albicans DAY286 reference strain exposed or not to CFSF from different Lactobacillus species. C. albicans (10^6 cells/ml) were incubated for 1 and 3 h, at 37°C in 5% CO_2, in "complete medium" as negative control (**A**, **B**) in "complete medium" plus MRS broth (1:4 dilution) (**C**, **D**), or in "complete medium" plus 1:4 dilution of CFSF from L. acidophilus (**E**, **F**), L. plantarum (**G**, **H**), L. rhamnosus (**I**, **J**) and L. reuteri (**K**, **L**). Optical microscope images were taken at magnification of 200x.*

incubation time. When the CFSF were added for 24 h to preformed biofilm (24 h + 24 h), only *L. acidophilus* and *L. reuteri* (but not *L. plantarum*) still retained the ability to significantly affect Candida biofilm development and the phenomenon occurred only at the 1:4 dilution. As reported in Table I, *L. rhamnosus* CFSF inhibited fungal growth in a dose-dependent manner but never to a significant extent. In no cases did we observe differences between the two strains of *C. albicans;* in particular, both were affected to similar extent by the CFSF, irrespective of the lactobacilli species and of the CFSF dilution tested.

In parallel groups, we performed the XTT assay and the results obtained were then expressed as percentage of fungal damage, according to previously established protocols (32). As detailed in Fig. 4, *L. acidophilus*, *L. plantarum* and *L. reuteri* CFSF (1:4 dilution) significantly impaired both the DAY286 and FJS24 strains, when employing either the 24-h or the 48-h protocol. Differently, when the CFSF were added to the preformed biofilm (24 h + 24 h), only *L. acidophilus* and *L. reuteri* (but not *L. plantarum*) still retained the ability to exert a significant influence on biofilm, and such effect was comparable in both *C. albicans* strains. *L. rhamnosus* never showed any significant inhibitory activity.

DISCUSSION

The present study investigates the effects of 4 Lactobacillus species (commonly employed as probiotics) against the opportunistic fungal pathogen *C. albicans*.

Increasing literature underlines that the use of broad spectrum antibiotics, anti-inflammatory therapies, and various types of implanted biomaterials, is associated with a notable incidence of fungal diseases; the latter are difficult to treat because of the persistence of biofilm and the increased antifungal resistance associated with it (17). Probiotics are gaining more and more interest as potential alternatives to antimicrobial drugs. Recent evidence indicates that clinical isolates from vulvovaginal candidiasis are indeed susceptible *in vitro* to the inhibitory effects by metabolites of Lactobacillus strains; moreover, clinical trials have shown that administration of Lactobacilli, given

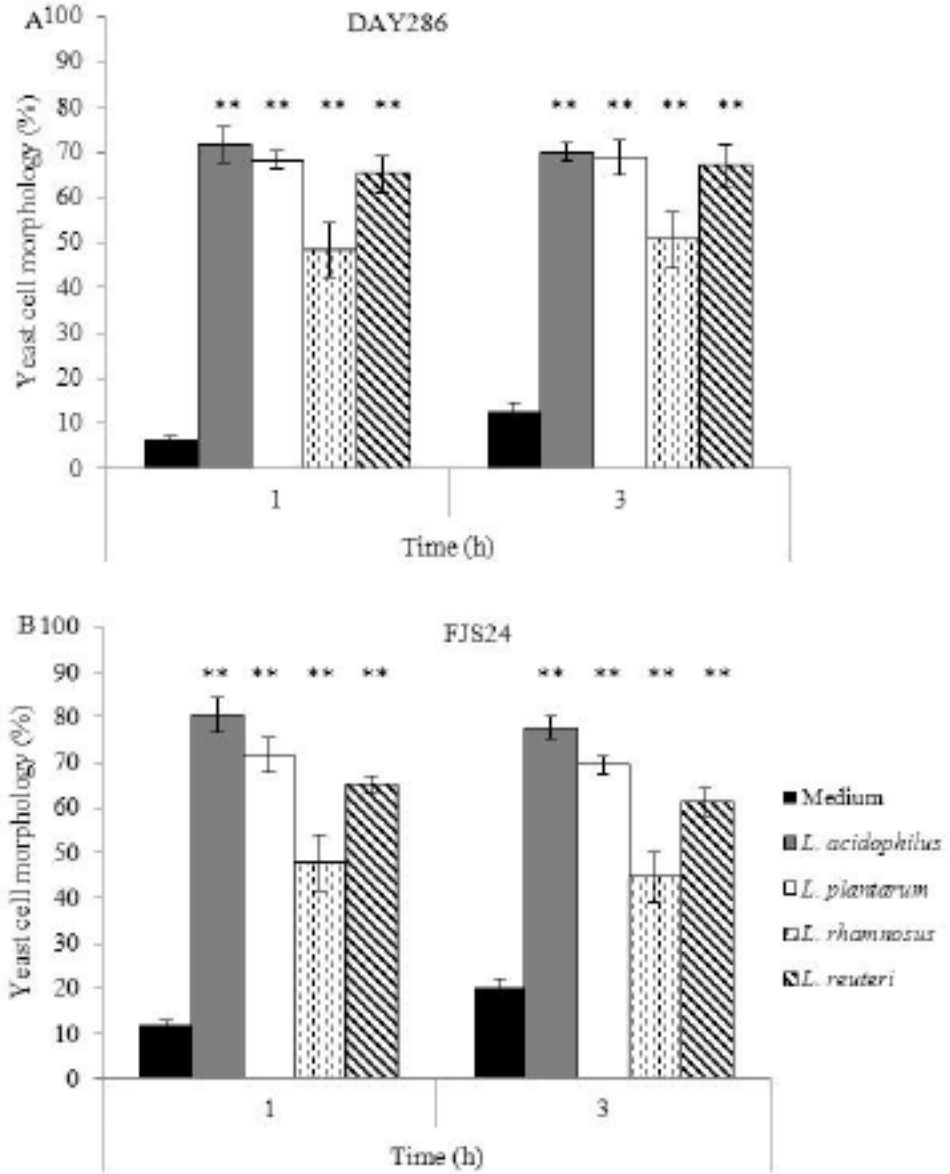

Fig. 3. *Percentage of yeast cells in C. albicans, DAY286 (reference) and FJS24 (mutant), exposed or not to CFSF from the 4 Lactobacillus species. C. albicans (10^6 cells/ml) was incubated for 1 and 3 h in the presence of "complete medium" plus MRS broth or CFSF from the 4 species of Lactobacillus (1:4 dilution). After 1 and 3 h incubation, samples were morphologically observed, by optical microscope, and the percentage of yeast cells in each sample was calculated. Asterisks indicate statistically significant differences (p-value < 0.01) between C. albicans treated with CFSF and untreated samples.*

as oral capsules or vaginal tablets, is effective as adjuvant in the treatment of vulvovaginal candidiasis as well as in the prevention of recurrences (33-36).

The present study shows that *L. plantarum*, *L. acidophilus*, *L. rhamnosus* and *L. reuteri*, and also their supernatants, have inhibitory effects on two *C. albicans* strains, the reference DAY286 and its isogenic counterpart FJS24 (*hwp1/hwp1* mutant strain). In particular, as documented here by morphological analysis, CFSF are able to impair yeast-to-hyphal transition. As established by *in vivo* and *in vitro* models (11-13), such dimorphic

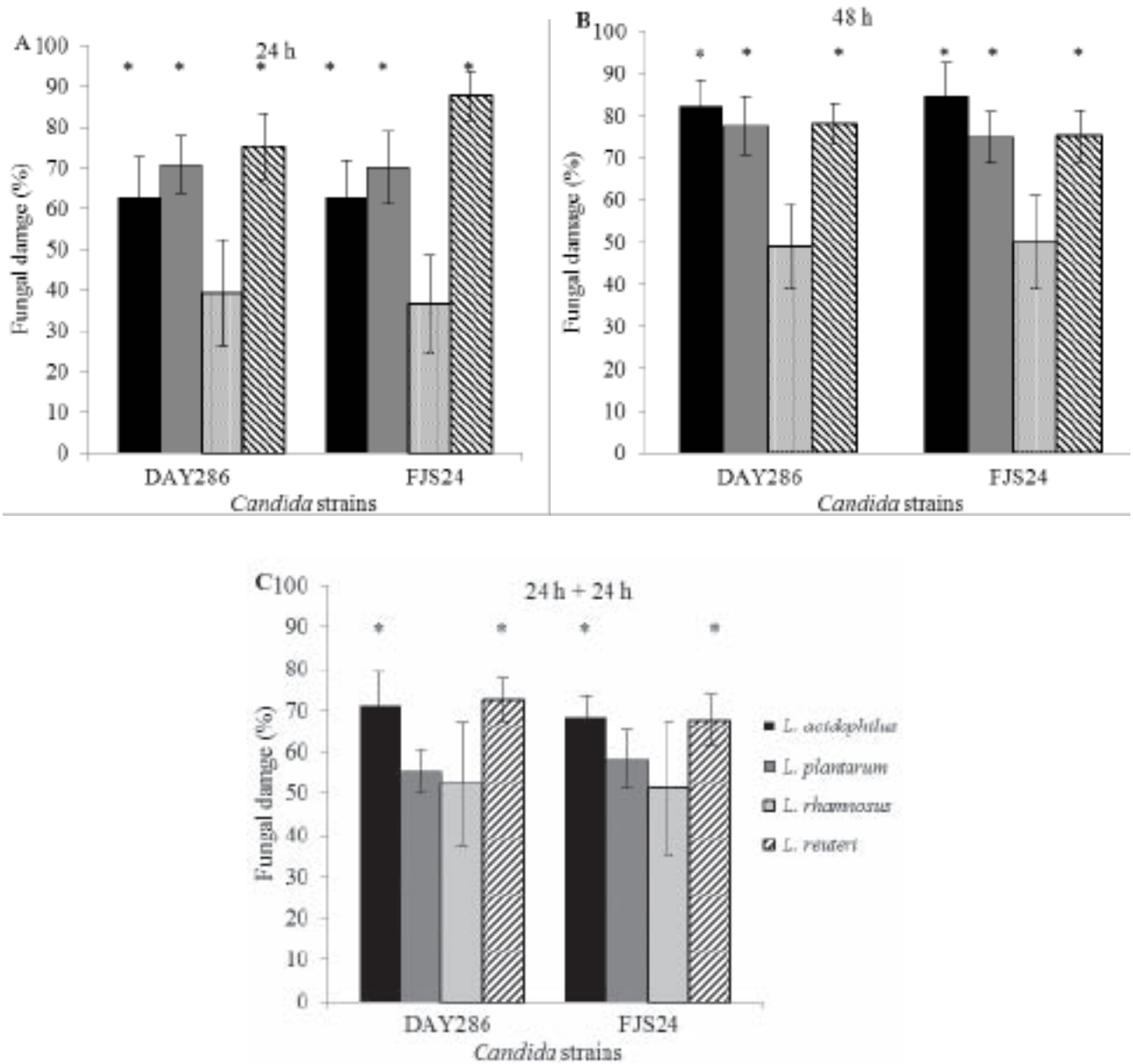

Fig. 4. *Fungal damage by CFSF from different Lactobacillus species, as assessed by XTT assay. Both DAY286 (reference) and FJS24 (mutant) strains (10^6 cells/ml), as yeast cells (panels A and B) or pre-formed biofilm (panel C), were exposed or not to CFSF from the 4 Lactobacillus species (1:4 dilution in "complete medium"). At the end of the incubation time (24 or 48 h), the XTT assay was performed and the results were expressed as % of fungal damage, as detailed in Materials and Methods. Asterisks indicate statistically significant differences (p-value < 0.05) between C. albicans treated with CFSF and untreated samples.*

transition enables *C. albicans* to avoid phagocytic clearance and to invade tissues, where virtually only hyphae are indeed found. In this respect, our data provide initial evidence of Lactobacilli ability to impair such an important virulence feature of *C. albicans.*

Next, we demonstrate that CFSF from Lactobacilli significantly affect fungal biofilm formation as well

Table I. *Inhibitory effects of CFSF from different Lactobacillus species on C. albicans biofilm.*

CFSF from	CFSF dilution in "complete medium"	OD levels in *C. albicans*					
		yeast cells + 24 h CFSF		yeast cells + 48 h CFSF		pre-formed biofilm + 24 h CFSF	
		DAY286	FJS24	DAY286	FJS24	DAY286	FJS24
medium	-	4.00	4.00	4.00	4.00	4.00	4.00
L. acidophilus	1:16	3.34 ± 1.14	3.63 ± 0.20	3.78 ± 0.01	3.80 ± 0.01	4.00 ± 0.00	3.95 ± 0.05
	1:8	1.62 ± 1.18	1.88 ± 1.40	2.00 ± 0.10	2.02 ± 0.81	3.98 ± 0.02	3.55 ± 0.32
	1:4	0.08 ± 0.02 *	0.09 ± 0.05 *	0.10 ± 0.01 *	0.11 ± 0.02 *	1.04 ± 0.24 *	1.59 ± 0.35 *
L. plantarum	1:16	3.22 ± 1.35	3.53 ± 0.42	3.80 ± 0.01	3.79 ± 0.02	4.00 ± 0.00	3.92 ± 0.08
	1:8	2.11 ± 1.48 *	1.65 ± 1.25 *	1.78 ± 0.00	1.83 ± 1.23	4.00 ± 0.00	3.70 ± 0.16
	1:4	0.12 ± 0.08 *	0.11 ± 0.07 *	0.10 ± 0.02 *	0.11 ± 0.02 *	2.37 ± 0.22	1.89 ± 0.79
L. rhamnosus	1:16	3.60 ± 0.70	3.56 ± 0.60	3.85 ± 0.02	3.81 ± 0.02	4.00 ± 0.00	3.97 ± 0.03
	1:8	2.36 ± 1.24	1.74 ± 1.34	2.75 ± 0.25	2.65 ± 0.69	3.91 ± 0.09	3.89 ± 0.11
	1:4	1.00 ± 1.85	1.08 ± 1.38	0.95 ± 0.85	0.97 ± 0.88	2.55 ± 1.45	2.40 ± 1.60
L. reuteri	1:16	3.66 ± 0.59	3.45 ± 0.83	3.77 ± 0.02	3.78 ± 0.01	3.86 ± 0.14	3.95 ± 0.01
	1:8	2.10 ± 1.47 *	1.67 ± 1.32 *	2.22 ± 0.02	2.17 ± 1.55	3.82 ± 0.09	3.58 ± 0.26
	1:4	0.19 ± 0.23 *	0.13 ± 0.05 *	0.15 ± 0.07 *	0.23 ± 0.15 *	1.55 ± 0.67 *	1.46 ± 0.13 *

C. albicans (10^6 cells /ml), as yeast cells or pre-formed biofilm (24 h-old cultures), were exposed or not to CFSF from L. acidophilus, L. plantarum, L. rhamnosus and L. reuteri at the indicated dilutions in "complete medium". After 24 or 48 h of incubation, biofilm was quantified by CV assay. Numbers represent the mean OD540 values of 6 replicates ± SD. Asterisks indicate statistically significant differences (p value < 0.05) between Candida treated with CFSF and untreated samples.

as pre-formed biofilm, though to a different extent, depending upon the Lactobacilli species involved. In particular, when using the CV and XTT assays, *L. plantarum*, *L. acidophilus* and *L. reuteri*, but not *L. rhamnosus*, significantly impair biofilm formation from freshly seeded yeast-like cells. In line with this finding, Thein and co-workers (22) have shown that *L. acidophilus* can impair Candida biofilm formation. Our present study provides a step forward, demonstrating the efficacy of Lactobacilli CFSF also against pre-formed biofilm; specifically, only *L. plantarum* and *L. reuteri* still retain the ability to significantly damage fungal cells embedded in a structure of well-known resistance. These *in vitro* results further strengthen the *in vivo* beneficial effects of Lactobacilli administration and indicate that the success of the treatment may also depend on the bacterial strains employed. Furthermore, the efficacy of CFSF on preformed biofilm encourages the use of Lactobacilli in clinical settings, where eradication of biofilm-associated infections represents a major problem.

Multiple roles have been ascribed to the *HWP1* gene in Candida behavior and pathogenesis (6-10). In this respect, we have recently shown that two Candida strains, *HWP1/HWP1* and its isogenic counterpart (*hwp1/hwp1*), are differently affected by macrophages (10), while, as shown here, dimorphic transition and biofilm development are impaired by Lactobacilli to a similar extent, irrespective of the fungal genetic background. Taken together, these findings underline the relevance of HWP1 genotype on host-pathogen interplay, while its involvement on other virulence traits, such as fungal transition and biofilm production, remains unlikely.

Overall, our data add novel insights on the impact of Lactobacilli on *C. albicans*: their ability to interfere with fungal virulence, through inhibition of morphological transition and biofilm production and, even more, their capacity to mediate fungal damage also on pre-formed biofilm, may account for the beneficial effects of Lactobacilli, both when used as adjuvants in therapeutic protocols against mucosal candidiasis and in preventing its recurrence.

REFERENCES

1. Rizzetto L, De Filippo C, Cavalieri D. Richness and diversity of mammalian fungal communities shape innate and adaptive immunity in health and disease.

Eur J Immunol 2014; doi:10.1002/eji.201344403
2. Pfaller MA, Diekema DJ. Epidemiology of invasive candidiasis: a persistent public health problem. Clin Microbiol Rev 2007; 20:133-63.
3. Naglik JR, Moyes D. Epithelial cell innate response to *Candida albicans*. Adv Dent Res 2011; 23:50-5.
4. Nobile CJ, Andes DR, Nett JE, et al. Critical role of Bcr1-dependent adhesins in *C. albicans* biofilm formation *in vitro* and *in vivo*. PLoS Pathog 2006; 2:e63.
5. Thomas DP, Bachmann SP, Lopez-Ribot JL. Proteomics for the analysis of the *Candida albicans* biofilm lifestyle. Proteomics 2006; 6:5795-804.
6. Staab JF, Bradway SD, Fidel PL, Sundstrom P. Adhesive and mammalian transglutaminase substrate properties of *Candida albicans Hwp1*. Science 1999; 283:1535-38.
7. Tsuchimori N, Sharkey LL, Fonzi WA, French SW, Edwards JE Jr, Filler SG. Reduced virulence of *HWP1*-deficient mutants of *Candida albicans* and their interactions with host cells. Infect Immun 2000; 68:1997-2002.
8. Nobile CJ, Nett JE, Andes DR, Mitchell AP. Function of *Candida albicans* adhesin *Hwp1* in biofilm formation. Eukaryot Cell 2006; 5:1604-10.
9. Sundstrom P, Balish E, Allen CM. Essential role of the *Candida albicans* transglutaminase substrate, hyphal wall protein 1, in lethal oroesophageal candidiasis in immunodeficient mice. J Infect Dis 2002; 185:521-30.
10. Orsi CF, Borghi E, Colombari B, Neglia RG, Quaglino D, Ardizzoni A, Morace G, Blasi E. Impact of *Candida albicans* hyphal wall protein 1 (*HWP1*) genotype on biofilm production and fungal susceptibility to microglial cells. Microb Pathog 2014; 70:20-27.
11. Borghi E, Romagnoli S, Fuchs BB, et al. Correlation between *Candida albicans* biofilm formation and invasion of the invertebrate host *Galleria mellonella*. Future Microbiol 2014; 9:163-73.
12. Scaringi L, Blasi E, Rosati E, Marconi P, Bistoni F. Fungicidal activity of *Candida albicans*-induced murine lymphokine-activated killer cells against *C. albicans* hyphae *in vitro*. J Gen Microbiol 1991; 137:2851-6.
13. Blasi E, Pitzurra L, Puliti M, Lanfrancone L, Bistoni F. Early differential molecular response of a macrophage cell line to yeast and hyphal forms of *Candida albicans*. Infect Immun 1992; 60:832-37
14. Harriott MM, Lilly EA, Rodriguez TE, Fidel PL Jr, Noverr MC. *Candida albicans* forms biofilms on the vaginal mucosa. Microbiology 2010; 156:3635-44.
15. Ramage G, Martínez JP, López-Ribot JL. *Candida* biofilms on implanted biomaterials: a clinically significant problem. FEMS Yeast Res 2006; 6:979-86.
16. Chandra J, Kuhn DM, Mukherjee PK, Hoyer LL, McCormick T, Ghannoum MA. Biofilm formation by the fungal pathogen *Candida albicans*: development, architecture, and drug resistance. J Bacteriol 2001; 183:5385-94.
17. Ramage G, Rajendran R, Sherry L, William G. Fungal biofilm resistance. Intl J Microbiol 2012; doi: 10.1155/2012/528521.
18. Samaranayake LP, Keung Leung W, Jin L. Oral mucosal fungal infections. Periodontol 2000 2009; 49:39-59 .
19. Ganguly S, Mitchell AP. Mucosal biofilms of *Candida albicans*. Curr Opin Microbiol 2011; 14:380-85.
20. FAO/WHO. Evaluation of health and nutritional properties of powder milk and live lactic acid bacteria. Food and Agriculture Organization of the United Nations and World Health Organization Expert Consultation Report. http://www.fao.org.es/ESN/Probio/probio.htm; 2001
21. Bonifait L, Chandad F, Grenier D. Probiotics for oral health: myth or reality? JCDA 2009; 75:585-90.
22. Thein ZM, Samaranayake YH, Samaranayake LP. Effect of oral bacteria on growth and survival of *Candida albicans* biofilms. Arch Oral Biol 2006; 51:672-80.
23. Köhler GA, Assefa S, Reid G. Probiotic interference of *Lactobacillus rhamnosus* GR-1 and *Lactobacillus reuteri* RC-14 with the opportunistic fungal pathogen *Candida albicans*. Infect Dis Obstet Gynecol 2012; doi: 10.1155/2012/636474.
24. Martinez RCR, Seney SL, Summers KL, Nomizo A, De Martinis EC, Reid G. Effect of *Lactobacillus rhamnosus* GR-1 and *Lactobacillus reuteri* RC-14 on the ability of *Candida albicans* to infect cells and induce inflammation. Microbiol Immunol 2009; 53:487-95.
25. Hasslöf P, Hedberg M, Twetman S, Stecksén-Blicks

C. Growth inhibition of oral mutans Streptococci and Candida by commercial probiotic Lactobacilli - an *in vitro* study. BMC Oral Health 2010; 10:18.

26. Gil1 NF, Martinez RCR, Gomes BC, Nomizo A, De Martinis EC. Vaginal Lactobacilli as potential probiotics against *Candida* spp. Braz J Microbiol Publ Braz Soc Microbiol 2010; 41:6-14.
27. Sabia C, Anacarso I, Bergonzini A, et al. Detection and partial characterization of a bacteriocin-like substance produced by *Lactobacillus fermentum* CS57 isolated from human vaginal secretions. Anaerobe 2014; 26:41-45.
28. Fijan S. Microorganisms with claimed probiotic properties: an overview of recent literature. Int J Environ Res Public Health. 2014; 11:4745-67.
29. Pham M, Lemberg DA, Day AS. Probiotics sorting the evidence from the myths. Med J Aust. 2008; 188:304-8.
30. Schillinger U, Lücke FK. Antibacterial activity of *Lactobacillus sake* isolated from meat. Appl Environ Microbiol 1989; 55:1901-6.
31. Pierce CG, Uppuluri P, Tristan AR, Wormley FL Jr, Mowat E, Ramage G, Lopez-Ribot JL. A simple and reproducible 96-well plate-based method for the formation of fungal biofilms and its application to antifungal susceptibility testing. Nat Protoc 2008; 3:1494-500.
32. Katragkou A, Kruhlak MJ, Simitsopoulou M, et al. Interactions between human phagocytes and *Candida albicans* biofilms alone and in combination with antifungal agents. J Infect Dis 2010; 201:1941-9.
33. Ogunshe AA, Omotoso MA, Bello VB. The i*n vitro* antimicrobial activities of metabolites from Lactobacillus strains on Candida species implicated in Candida vaginitis. Malays J Med Sci. 2011; 18:13-25.
34. Martinez RCR, Franceschini SA, Patta MC, Quintana SM, Candido RC, Ferreira JC, De Martinis ECP, Reid G. Improved treatment of vulvovaginal candidiasis with fluconazole plus probiotic *Lactobacillus rhamnosus* GR-1 and *Lactobacillus reuteri* RC-14. Lett Appl Microbio. 2009; 8:269-74.
35. Vicariotto F, Del Piano M, Mogna L, Mogna G. Effectiveness of the association of 2 probiotic strains formulated in a slow release vaginal product, in women affected by vulvovaginal candidiasis: a pilot study. J Clin Gastroenterol 2012; 46:S73-80.
36. Murina F, Graziottin A, Vicariotto F, De Seta F. Can *Lactobacillus fermentum* LF10 and *Lactobacillus acidophilus* LA02 in a slow-release vaginal product be useful for prevention of recurrent vulvovaginal candidiasis? A clinical study. J Clin Gastroenterol 2014; 48:S102-5.

JOURNAL OF BIOLOGICAL REGULATORS & HOMEOSTATIC AGENTS Vol. 28, no. 4, 753-766 (2014)

THE IMMUNOMODULATORY MOLECULE PIDOTIMOD INDUCES THE EXPRESSION OF THE NOD-LIKE RECEPTOR NLRP12 AND ATTENUATES TLR-INDUCED INFLAMMATION

M. FOGLI, F. CACCURI, ML. IARIA, C. GIAGULLI, S. CORBELLINI, F. CAMPILONGO, A. CARUSO and S. FIORENTINI

Section of Microbiology, Department of Molecular and Translational Medicine, University of Brescia

Received June 4, 2014 – Accepted November 12, 2014

Pidotimod (3-L-pyroglutamyl-L-thiaziolidine-4-carboxylic acid) (PDT) is a synthetic dipeptide with *in vitro* and *in vivo* immunomodulatory properties that is largely used for treatment and prevention of infections in paediatric and disease-prone patients. However, the effects of PDT on cellular immune responses are still poorly characterized and there is little information on the mechanism of action of this compound. It has been speculated that PDT action may be exerted through the interaction with a Pattern Recognition Receptor (PRR). Therefore, to gain a further understanding of the immune pathways involved by PDT, we first decided to investigate whether PDT could modify the immune response triggered by TLR ligands. Monocytic cells were exposed to PDT then stimulated with a panel of TLR agonists. Under these experimental conditions, we observed a significant decrease in the synthesis of key proinflammatory mediators in comparison to the production observed in TLR-stimulated cells that were not treated with PDT. Using RT² Profiler PCR Array we have observed that PDT specifically up-regulates the expression of the NOD-like receptor NLRP12 mRNA in the absence of any further co-stimulation. Increase of NLRP12 in cells treated with PDT was confirmed using specifically designed real-time quantitative PCR and western blotting assays where a clear increase in the amount of NLRP12 protein was detected. Furthermore, in myeloid/monocytic cells we demonstrated that PDT treatment counteracts the NLRP12 reduction induced by TLR agonists. Finally, the results obtained using NLRP12 silenced cells showed that down-regulation of the proinflammatory function occurring in PDT-treated cells upon interaction with TLRs is associated with the increased levels of NLRP12 induced by PDT. To our knowledge this is the first evidence of an immunomodulatory peptide that upregulates NLRP12 and, through this molecule, antagonizes the TLR-induced inflammatory response. These results pave the way for the development of innovative therapeutic approaches aimed at controlling different pathological settings such as tumorigenesis, systemic inflammatory processes and autoimmunity, where NLRP12 plays a crucial role.

Pidotimod (3-L-pyroglutamyl-L-thiaziolidine-4-carboxylic acid) (PDT), is an immunomodulatory synthetic thymic dipeptide introduced as supportive agent in the treatment of acute infections or

Key words: pidotimod, toll like receptors, immunoregulation, NLRP12

Mailing address: Prof. Simona Fiorentini, Section of Microbiology, Department of Molecular and Translational Medicine, University of Brescia, Piazzale Spedali Civili, 1 25123 Brescia, Italy
Tel.: +39 030 3996696 Fax: +39 030 395258
e-mail: simona.fiorentini@unibs.it

0393-974X (2014)

as prophylactic molecule in patients suffering from recurrent infections. In fact, PDT has been demonstrated to reduce the rate of recurrence of respiratory and urinary infections in children, as well as to shorten the time to recovery in paediatric patients hospitalized in acute phase of infection (15 days) with 2/3 days less of antibiotic therapy. Moreover, after recovery, PDT administrated for the following 2 months determined a significant reduction in relapses, successive hospitalization need and antibiotic treatment (1, 2). The same efficacy of PDT has been observed in disease-prone individuals such as Down children that are highly susceptible to acute respiratory tract infections (ARTI) (3).

Ex vivo studies performed on either cells derived from patients with RRIs or with recurrent urinary tract infections have shown that PDT administration leads to the normalization of neutrophilic functional parameters (i.e. chemotactic and phagocytic indexes) (1, 2). Furthermore, T lymphocytes from neoplastic patients who had undergone PDT administration, but had not been treated with specific anti-cancer therapy, showed a higher proliferative response to mitogens or to allogeneic lymphocytes compared to cells derived from patients not treated with PDT (4).

Immunomodulatory activity of PDT has been confirmed in murine experimental models. PDT treatment of mice increased, *ex vivo*, the cellular proliferative response to mitogens and natural killer cytotoxic activity (5). *In vivo,* our group has demonstrated that, upon intranasal administration of OVA, PDT favours the development of a specific antibody response and the generation of antigen-specific Th1 effector cells suggesting the possibility to use PDT as adjuvant molecule to promote an effective mucosal and systemic immune response (6).

Activity of PDT on the innate and the adaptive immune response has been better dissected by *in vitro* studies performed using either murine or human cells. PDT has been described to induce increased production of IFN-α and IFN-γ in mitogen-activated peripheral blood mononucleated cells (PBMCS) as well as to enhance cell proliferation and IL-2 production in PBMCs derived from cancer patients (4). Moreover, PDT treatment skews the Th1/Th2 phenotype in PBMCs from children with atopic asthma where it induces down-regulation of CD30 expression (7). Recent studies have shown that PDT promotes maturation of dendritic cells (DCs), an event that plays an important role in initiating the T-cell-mediated immune response (6-8).

Molecular targets and intracellular pathways engaged by PDT are not yet known. The ability of PDT to modulate different aspects of both innate and adaptive immune responses suggests that the dipeptide might exert its function through its interaction with Pattern Recognition Receptors (PRRs). PRRs are a big family of surface and intracellular receptors able to identify Pathogen-Associated Molecular Patterns (PAMPs) or rather small molecules derived from pathogens or from cellular stress. Among PRRs, Toll Like Receptors (TLRs) are evolutionarily conserved molecules that play a crucial role in early host defence against invading pathogens. Upon microbial molecule engagement, TLRs trigger intracellular signalling cascades ultimately culminating in the expression of a variety of proinflammatory molecules able to orchestrate the early response to infection. TLR activation is also a prerequisite for the subsequent activation and shaping of adaptive immunity. Individual TLR interacts with different combination of adapter proteins and activates various transcription factors such as NF-kB, AP-1 and interferon regulatory factors, driving specific immune response. However, the inflammatory cascade induced by TLR signalling may cause serious local and/or systemic disorders (9). Innate responses, therefore, are modulated by several endogenous inhibitors at various points in the 'downstream' pathways (10). In addition to TLRs, recent research has focused on the discovery and characterization of other receptors involved in regulating cellular activation after exposure to PAMPs. The nucleotide-binding domain and leucine-rich-repeat containing (NLR) family of genes have been largely characterized as activators of inflammation. For example, NLRP3, NLRC4, NAIP5, and NLRP6 are essential for inflammasome activation, and NOD1 and NOD2 are activators of NF-kB and MAPK transcription factors (11). Recently, several reports revealed NLRs that negatively regulate immune activation (12, 13). *In vitro* analysis of NLRP12 (Monarch 1) in human monocytic cell lines suggests that it is a negative regulatory protein that suppresses non-canonical

NF-kB activation and p52-dependent chemokine expression (14) and also has an effect on canonical NF-kB signaling (15).

In this study we sought to gain a further understanding of the immune pathways involved by PDT. In particular, we investigated whether PDT could interact with the TLR activation pathways. We found that PDT induces the expression of the NOD-like receptor NLRP12 and modulates the inflammatory cascade triggered by TLR ligands.

MATERIALS AND METHODS

Reagents

PDT (purity >99.6%) was a kind gift from Polichem SA (Lugano, Switzerland). For all experiments the same PDT stock solution was used (10 mg/ml in ultrapure endotoxin-free water, stored in aliquots at -20°C). Biological effects were evaluated using PDT at the final concentrations of 5 and 25 μg/ml. TLR ligands (Human TLR1-9 Agonist Kit) were purchased from InvivoGen (San Diego, CA, USA) and were used at concentrations suggested by the manufacturer: 100ng/ml Pam3CSK4 (TLR1/2L), 10^8cell/ml HKLM (TLR2L), 1μg/ml Poly(I:C) (TLR3L), 100ng/ml LPS (TLR4L), 100 ng/ml Flagellin (TLR5L), 100ng/ml FSL1 (TLR6/2L), 1 μg/ml Imiquimod (TLR7L), 1μg/ml ssRNA40 (TLR8L), and 5μM ODN2006 (TLR9L). All experiments were performed in endotoxin free-condition, and the absence of endotoxin contamination (<0.25 unit/500μg) in the PDT stock solution was assessed by Limulus amoebocyte assay (Associates of Cape Cod, MA, USA).

Cell culture and stimulation

PBMCs were obtained, under informed consent, from healthy donors selected within laboratory workers or from buffy coats (Centro Trasfusionale, Spedali Civili di Brescia, Italy). PBMCs were isolated by using Ficoll-Paque density gradient centrifugation, and cultured in RPMI 1640 added with 10% low endotoxin fetal calf serum (Lonza, Caravaggio, Italy), and with 2 mM L-glutamine (growth medium). Primary human monocytes were isolated from PBMCs by positive selection using a CD14 MicroBead kit (Miltenyi Biotec, Bologna, Italy) according to the manufacturer's protocol, then cultured in the standard growth medium. In each experiment cell purity was always greater than 97%, as determined by flow cytometry.

The Mono Mac6 (MM6) cell line was kindly provided by Prof. Sozzani (University of Brescia) and maintained in culture using the growth medium enriched with 1% OPI (oxaloacetate, pyruvate and insulin, Sigma Aldrich, San Louis, MO, USA), and 1X nonessential amino acids (Sigma Aldrich). All cells were cultured at 37°C in a 5% CO_2 humidified atmosphere.

Assessment of cell viability

Cell viability was first evaluated by microscopic observation of trypan blue dye exclusion (EuroClone, Milan, Italy), then using the Propidium Iodide (PI) (BD Biosciences, Milan, Italy) incorporation assay. Percentage of viable cells was calculated by flow cytometry enumerating the PI-negative events within the gated cell populations. In each experiment nonviable cells never exceeded 7%.

RT^2 Profiler PCR Array

Screening of gene expression induced by PDT was investigated using the human NF-kB Signaling Pathway RT^2 Profiler PCR Array (PAHS-025A; SABiosciences, Frederick, MD, USA) which profiles the expression of 84 key genes related to NF-kB -mediated signal transduction. MM6 cells were plated in quadruplicate in round-bottom 96-well plates at the concentration of 10^6 cells/ml and treated with or without PDT (25 μg/ml). After 16 h cells were harvested and RNA was isolated using the RNeasy Mini Kit (Qiagen, Hilden, Germany). Nucleic acid extracts were quantified by nanodrop technology (Fisher Thermoscientific, Waltham, MA, USA) then DNA was cleaned up by RQ1 RNase free DNase treatment (Promega). After RNA quantification, cDNA was generated from 1 μg of total RNA using the RT^2 qPCR Array First Strand Kit in accordance with the manufacturer's protocol (Qiagen SABiosciences). The template was combined with RT^2 SYBR Green/Fluorescein PCR master mix. An equal amount of this mixture (25 μl) was added to each well of the qPCR profiler plate containing the gene-specific primer sets. Amplification was performed using the ABI 7500 sequence detector (Applied Biosystems, Foster City, CA, USA) and data were evaluated with the aid of an Excel spreadsheet provided by the manufacturer containing algorithms based on the $2^{-\Delta\Delta Ct}$ formula. In each experimental sample, quantification of cDNA was normalized according to the GAPDH housekeeping gene expression.

Real-time PCR

For gene expression experiments, cells were seeded in triplicate at the concentration of 10^6 cells/ml in 96 round-bottom well plates, with or without PDT treatment, then subjected to stimulation with TLR agonists for 6 h. In each experiment unstimulated cells were used as control. After the appropriate treatment, cells were collected by centrifugation and dry pellets were stored at -80 °C until use. Analysis of gene transcription was determined by

quantitative real-time PCR (qRT-PCR). Automatic nucleic acid extraction was performed using the NucliSens Easymag device (Biomerieux, Firenze, Italy) and cDNA was synthesized with High Capacity cDNA Reverse Transcription Kit (Applied Biosystems).

The relative amounts of MCP-1, IL-1β, IL-8 and β-actin mRNAs were determined by TaqMan RT-PCR method. Amplification was carried out in a 25 µl reaction mix containing 12.5 µl 2X TaqMan universal PCR master mix and 1.25 µl of primer and FAM dye-labeled specific probe mix (Gene expression assays, Applied Biosystems).

The SYBR green qRT-PCR method (GoTaq qPCR technology, Promega, Madison, WI, USA). was used to determine the expression level of NLRP12 mRNA. For this evaluation home-designed primers (IDT, Castesano, Bologna, Italy) were used (NLRP12 for 5'-GTT GGT GCA GCT ACC AGA GAG-3', NLRP12 rev 5'-ACC TCT TCA GCC TCA GGT TCT-3; β-actin for 5'-CAA CTG GGA CGA CAT GGA-3', β-actin rev5'-GTT GG CTT GGG GTT CAG-3').

QRT-PCR assays were performed in triplicate on a 7500 qRT-PCR system (Applied Biosystems) and analyses of data were performed with the $2^{-\Delta\Delta Ct}$ method using the Relative Quantitation Study software (Applied Biosystems). Quantification of cDNA was normalized in each reaction according to the internal β-actin control.

Immunoprecipitation and western blot analysis

For immunoprecipitation assays and Western blot experiments, 10^7 MM6 cells per condition were cultured in T75 flasks, pre-treated with or without PDT (25 µg/ml) for 48 h, then stimulated or not with the TLR1/2 ligand Pam3CSK4. MM6 cells were then collected and cell pellets were lysed with 50 µl of Lysis Buffer (Hepes pH 7.9 10 mM, KCl 10 mM, $MgCl_2$ 1.5 mM, EDTA 0.5mM, EGTA 0.5mM, NP40 0.6%, Sigma Aldrich) added with 1X protease inhibitor cocktail (Roche, Basel, Swizerland). After a 20-min incubation on ice, samples were centrifuged and proteins were quantified by Bicinconic Acid assay (BCA, Sigma Aldrich, Milan, Italy). To perform a quantitative analysis under this experimental condition, NLRP12 was immunoprecipitated from equivalent amounts of different cellular extracts and an excess of immunoprecipitating antibody (Goat anti-human PYPAF7/NLRP12 N13 polyclonal antibody, Santa Cruz Biotechnology Dallas, TX, USA) was used. Immunoprecipitated NLRP12 was then recovered using the "Protein G Plus Agarose" reagent, according to the manufacturer's instructions (Santa Cruz Biotechnology). After extensive washing, samples were eluted by boiling them in reducing sample buffer (Laemmli buffer). Immunoprecipitated products were separated by SDS-PAGE, transferred to nitrocellulose and probed with a rabbit anti-human PYPAF7 polyclonal antibody (H-77, Santa Cruz Biotechnology) followed by a goat anti-rabbit IgG-HRP antibody (Pierce Thermo Scientific, Rockford, IL, USA). Membranes were developed with Luminol reagent (Promega) and results were acquired using the ChemiDoc MP imaging system and analysed by Gel-Pro Analizer 6.0 software (Biorad Italy, Milan).

ELISA

For ELISAs, cells were pretreated with PDT and stimulated for 24 h by TLR1/2L to allow the production and secretion of MCP-1, IL1-β and IL-8 cytokines. Culture plates were then centrifuged and supernatants were collected and stored at -70°C until use. Proinflammatory molecules were quantified in supernatants by commercial sandwich ELISAs (Quantikine human MCP-1, IL1-β and IL-8 immunoassay, R & D Systems, Minneapolis, MN, USA) following the manufacturer's instructions.

NLRP12 silencing

NLRP12 silencing was performed by nucleoeffective cells (Amaxa, Lonza) with PYPAF7/NLRP12 siRNA (Santa Cruz Biotechnology). Fluorescein-labeled irrelevant siRNAs (Block-IT Fluorescent oligonucleotides, Invitrogen) were used to assess specificity of the assay and to evaluate the efficiency of siRNA nucleoporation. The efficacy of NLRP12 silencing was evaluated by qRT-PCR analysis of the NLRP12 mRNA amounts, as previously described.

Silencing of NLRP12 expression was performed in MM6 cells treated for 24 h with PDT. Twenty-four h after nucleoporation, cells were stimulated with TLR1/2L and analysed for MCP-1 expression.

NLRP12 transient expression

MM6 cells (3×10^6) were nucleofected with 2 µg of a human NLRp12 expression plasmid (OriGene, Rockville, MD, USA) using the Amaxa Cell Line Nucleofector Kit V (Lonza). Nucleofection efficiency was evaluated using the EGFP-expressing plasmid provided with the nucleofection kit. Twenty-four h after transfection, cells were stimulated for 6 h with TLR1/2L. Unstimulated nucleofected cells were used as controls. Presence of overexpressed NLRP12 protein in cells nucleofected with NLRP12 expression plasmid was evaluated by Western blot analysis, carried out as described above.

Statistical analysis

Statistical evaluation was performed using the statistical software package GraphPad Prism (San Diego, CA, USA). Data obtained from multiple independent experiments were expressed as median and range or, in selected experiments, as mean ± standard deviation.

Significance was assessed using Mann Whitney test, Student *t*-test or Anova one way test when appropriate. Probability values (P) ≤0.05 were considered as statistically significant.

RESULTS

PDT inhibits TLR-induced production of MCP-1 in primary human peripheral blood cells

Because of its immunomodulatory function, we first decided to investigate whether PDT could modify the immune response triggered by TLR ligands. PBMCs derived from 5 healthy donors were treated with PDT at 5 and 25 μg/ml for 48 h and then stimulated with TLR ligands (TLR1-9L) for 6 h. Treatment with PDT did not affect cell viability during the treatment or upon TLR stimulation, as assessed by flow cytometric analysis of PI incorporation (data not shown). As expected, PBMC stimulation with TLR ligands led to a significant increase of MCP-1 mRNA in comparison to the unstimulated condition. However, PDT by itself did not induce a significant MCP-1 gene expression both at 5 and 25 μg/ml (Fig. 1A). Surprisingly, PDT treatment induced a significant reduction of the MCP-1 specific transcription triggered by TLR ligands (Fig. 1B). This effect was dose-dependent and a higher dose of PDT appears to be more efficient in controlling TLRs-triggered MCP-1 gene transcription (data not shown). Moreover, independently from the dose used, the inhibitory effect exerted by PDT was more pronounced when cells were stimulated with the TLR1/2L Pam3CSK4 (median percentage inhibition: 68%, range: 60-77%, P<0.001).

PDT counteracts TLR-induced inflammation in monocytic cells

Circulating blood monocytes express substantial amounts of TLRs and play a key role in the TLR-mediated inflammatory response to pathogens. Therefore, we sought to evaluate whether PDT could exert the modulatory effects observed on PBMCs also on purified circulating monocytes. Monocytes derived from the peripheral blood of 7 healthy donors were purified using anti-CD14 beads and stimulated with the TLR1-9 panel of agonists. These cells were even more responsive than PBMCs to most of the TLR ligands (Fig. 2A) with the exception of response to TLR3L and TLR7L. In fact, when monocytes were stimulated with Poly(I:C) or Imiquimod, no significant induction of MCP-1 transcripts was observed (data not shown).

Irrespective of the TLR triggered, monocytes pretreated for 48 h with PDT showed a dose-dependent suppressive trend, however, PDT differentially decreased MCP-1 transcripts induced by treatment with each TLR agonist. A striking inhibition was observed when cells were stimulated with TLR1/2L (median: 40%, range: 31-51%, P<0.005), and TLR8L (median: 59%, range: 38-73%, P<0.005), whereas PDT induced a slighter effect on monocyte activation triggered by TLR2, and TLR4 engagement (Fig. 2B).

In order to elucidate whether PDT counteracts the production of other key inflammatory molecules (i.e. IL-1β and IL-8) produced by monocytes upon TLR stimulation, primary CD14-positive cells were treated with or without PDT (25 μg/ml) for 48 h and then stimulated with TLR1/2L. PDT-treated monocytes showed a lowering of IL-1β and IL-8 mRNA levels, which was comparable to the effect observed for MCP-1 transcripts [median percentage inhibition: 34% (range: 17-97%, P<0.05) and 32% (range: 23-85%, P<0.05, respectively)] (Fig. 2C). Finally, ELISA assays were performed to measure the amount of MCP-1, IL-1β and IL-8 proteins detected in cell culture supernatants. Results obtained confirmed that PDT treatment significantly decreases the release of these inflammatory mediators when cells were stimulated by the TLR1/2 ligand (P<0.01 for MCP-1and IL-8, P<0.005 for IL-1β) (Fig. 2D).

PDT increases the expression of NOD-like receptor NLRP12

All TLR signalling pathways culminate in activation of the transcription factor NF-kB, which controls the expression of an array of inflammatory cytokine genes. In order to identify the molecular mechanism that enables PDT to inhibit the TLR function, we investigated the involvement of NF-kB-related molecules in PDT function.

MM6 represents the only mature human monocytic cell line available to date and is a powerful tool alternative to primary cells to analyse inflammatory processes. In our experimental setting, MM6 cells showed the same behaviour as primary cells. Indeed,

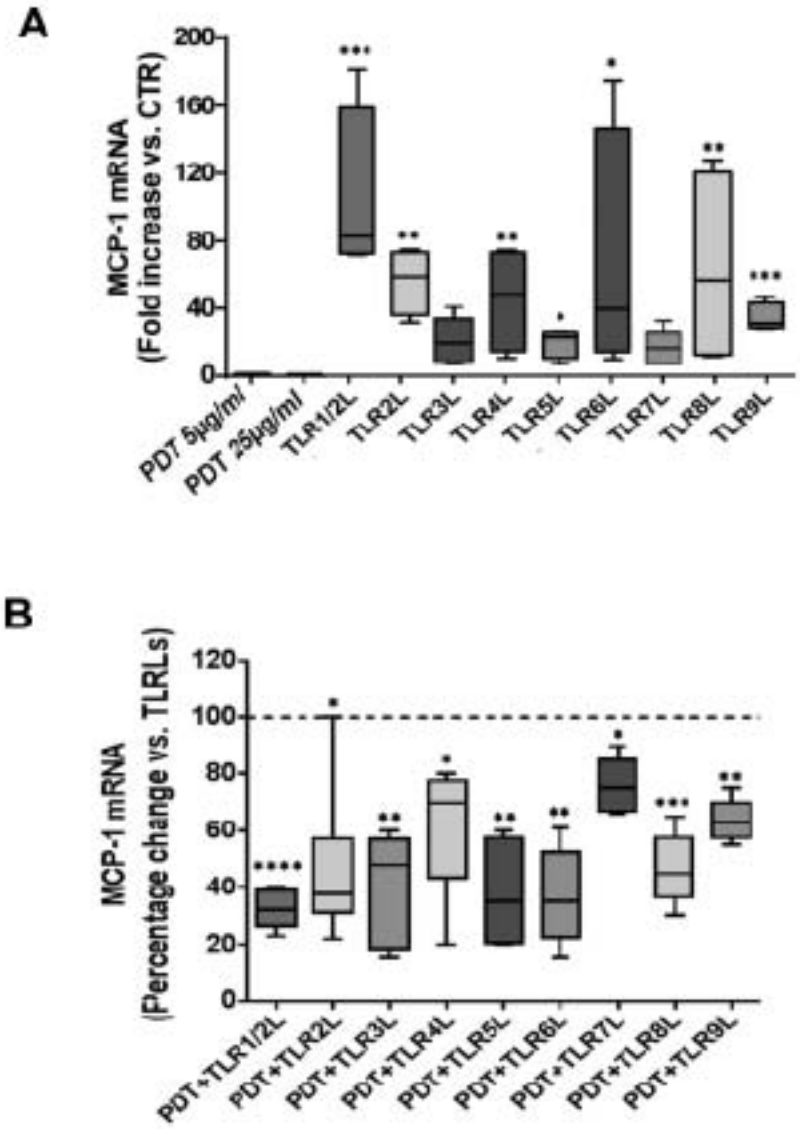

Fig. 1. *PDT reduces the MCP-1 expression induced by TLR activations in PBMCs. PBMCs from healthy donors were maintained in culture medium for 48 h in the absence or in the presence of PDT and then stimulated for 6 h with 9 TLR ligands at the concentrations described in the Materials and Methods section. QRT-PCRs were performed to evaluate the MCP-1 mRNA expression.* ***A)*** *Fold-increase of MCP-1 mRNA in PBMCs stimulated with PDT (5µg/ml and 25µg/ml) or TLR ligands versus unstimulated cells (calibrator sample).* ***B)*** *Percentage of MCP-1 mRNA level changes in PBMCs pre-treated with PDT and then stimulated with TLR ligands. The amount of transcripts induced by the corresponding TLR ligand in the absence of PDT was defined as 100% of MCP-1 mRNA expression (calibrator samples). Box-plots represent 5 independent experiments with medians, quarters, minimum and maximum values indicated. Comparison between treated and untreated cells was calculated using Mann-Whitney test. Significant differences are indicated. *: P<0.05; **: P<0.01; ***: P<0.005; ****: P<0.001*

PDT-treated MM6 cells compared to untreated cells showed a clear reduction in the increase of MCP-1 (median percentage inhibition: 43.5%; range 14-52%, P<0.05), IL1-β (median percentage inhibition: 55%; range 37-69%, P<0.01) and IL-8 (median percentage inhibition: 42%; range 31-50%, P<0.01) gene expression in response to TLR1/2L (Fig. 3A). The results obtained were confirmed by

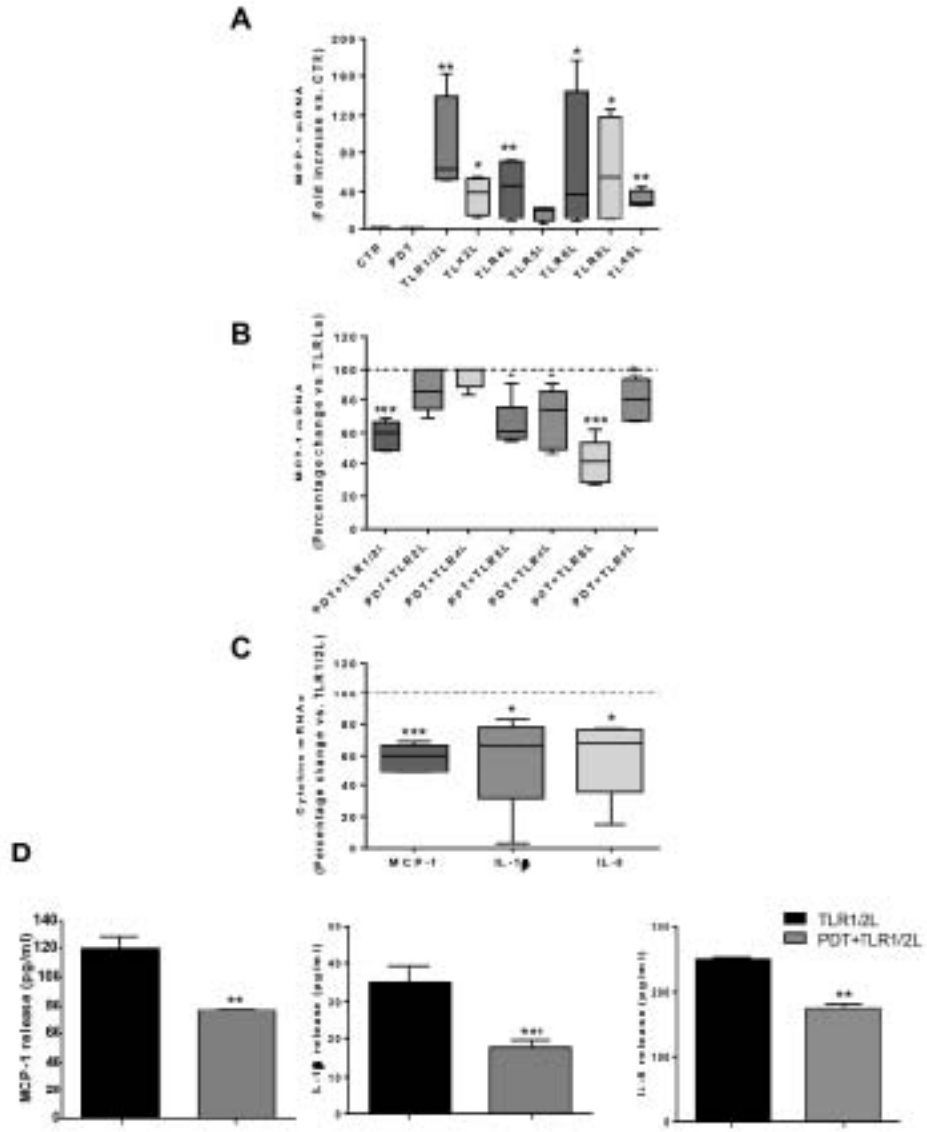

Fig. 2. *PDT reduces the MCP-1 expression induced by the TLR activation in primary monocytes. Purified primary monocytes were maintained in culture for 48 h in the absence or presence of PDT (25 μg/ml) and then stimulated with TLR ligands for 6 h. QRT-PCRs were performed to evaluate the MCP-1 mRNA expression.* ***A****) Fold-increase of MCP-1 mRNA in monocytes stimulated with TLR ligands versus unstimulated cells (calibrator sample).* ***B****) Percentage of MCP-1 mRNA level changes in PBMCs pre-treated with PDT (25 μg/ml) and then stimulated with TLR ligands. The amount of transcripts induced by the corresponding TLR ligand in the absence of PDT was defined as 100% of MCP-1 mRNA expression (calibrator samples). Box-plots represent the analysis of 7 independent experiments performed with different donor monocytes. Median, quarters, minimum and maximum values are indicated.* ***C****) Percentage change of MCP-1, IL-1β and IL-8 mRNA levels in monocytes pretreated with PDT and stimulated with a representative TLR ligand (Pam3CKS4, TLR1/2L). One hundred % value corresponds to the MCP-1, IL-1β and IL-8 mRNA expression in monocytes stimulated with TLR1/2L in the absence of PDT. Box-plots represent the medians, quarters, minimum and maximum values of 5 independent experiments performed with different donor monocytes.* ***D****) Secreted MCP-1, IL-1β and IL-8 quantified by capture ELISA. All experimental points were measured in triplicate for calculation of means and standard deviations (SD). Statistical analysis was calculated using Mann-Whitney test (panels A, B and C) and Student t-test (panel D). Significant differences are indicated. *: P<0.05, **: P<0.01, ***: P<0.005.*

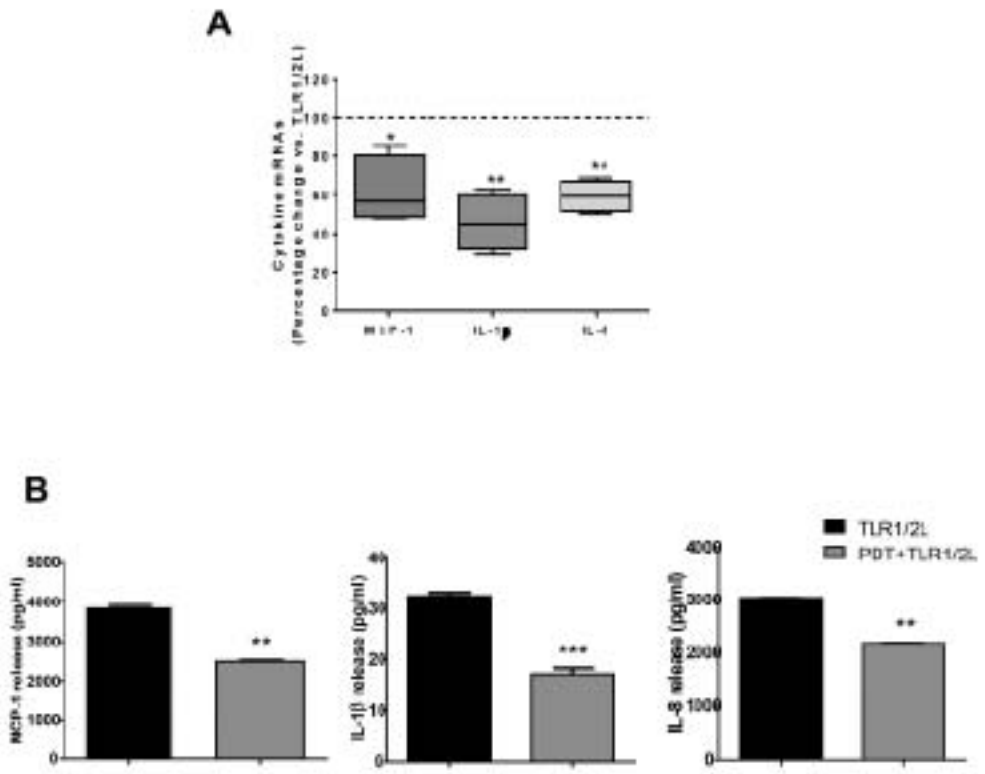

Fig. 3. *PDT reduces the cytokine expression induced by TLR activation in MM6 cells.* ***A****) MM6 cells were cultured for 48 h in the absence or presence of PDT 25μg/ml and then stimulated with TLR1/2L for 6 h. MCP-1, IL-1β and IL-8 mRNA changes induced by PDT were calculated in comparison to the amount of transcripts induced by TLR1/2L in the absence of PDT (calibrator sample, 100% of mRNA expression). Medians, quarters, minimum and maximum values from five independent experiments are shown.* ***B****) Secreted MCP-1, IL-1β and IL-8, were quantified by capture ELISA. All experimental points were measured in triplicate for calculation of means and SD. Comparison between PDT-treated and untreated cells was calculated using Mann-Whitney test (panel A) and Student t-test (panel B). Significant differences are indicated. *: P<0.05, **: P<0.01, ***: P<0.005.*

evaluating the release of inflammatory mediators in cell supernatants (Fig. 3B). Thus, NF-kB pathway modification induced by PDT was measured in MM6 cells using a gene expression array. PDT-treated cells showed modulation of few mRNA molecules and, interestingly, it induced a significant increase (2.2-fold increase) of NLRP12 specific mRNA (data not shown). NLRP12 molecule belongs to the NOD-like receptor family and has been recently characterized as an inhibitor of NF-kB activation (15). The array data were confirmed by qRT-PCR analysis of RNA extracted from MM6 cells cultured for 16 h in the absence or presence of PDT; indeed, there was a significant induction (1.51±0.5 fold-increase, P< 0.01) of NLRP12mRNA expression in response to PDT (Fig. 4A). When time course experiments were run, the peak of NLRP12 mRNA increase was observed 24 h after PDT treatment, and no relevant changes were observed at 6 h post-stimulation (Fig. 4B).

PDT-induced NLRP12 inhibits TLR-mediated MCP-1 synthesis

Previously published results have shown that NLRP12 is a negative regulator of TLR (especially TLR1/2) signalling in human monocytic-macrophage cell lines and that ablation of NLRP12

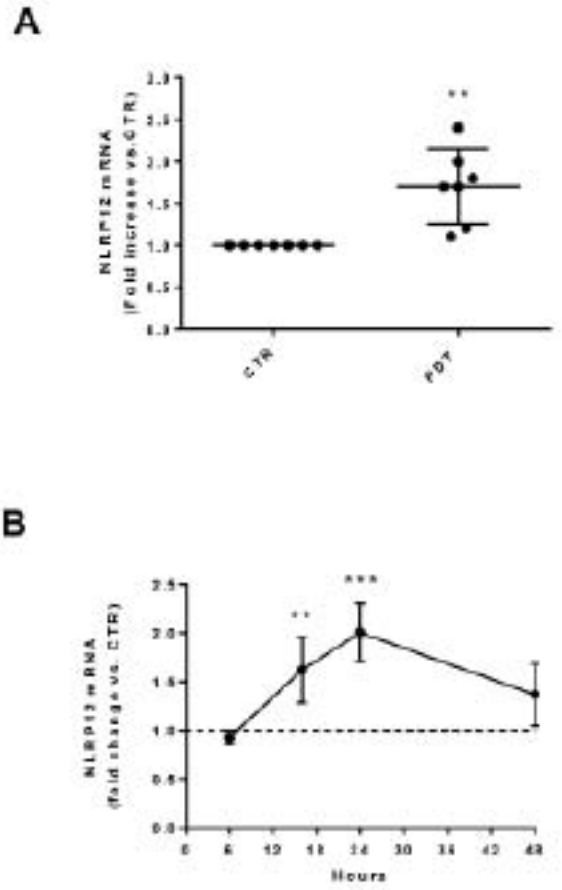

Fig. 4. *PDT increases the expression of NLRP12 mRNA in MM6 cells.* ***A)*** *NLRP12 mRNA expression was evaluated in MM6 after PDT treatment (25 μg/ml). Dot-plots represent the n-fold increase of NLRP12 in PDT-treated cells versus PDT-untreated cells (calibrator value, 1). Seven independent experiments are represented.* ***B)*** *Time course analysis of NLRP12 mRNA increase in PDT-treated MM6 cells (25 μg/ml). Results represent the mean ± SD of three independent experiments. Comparison between PDT-treated and untreated cells was calculated using Mann-Whitney test. Significant differences are indicated. **: P<0.01, ***: P<0.005.*

increases proinflammatory gene expression (15). Therefore, we wanted to determine if, up-regulating NLRP12, PDT was able to counteract the down-regulation of NLRP12 expression induced through TLR stimulation and consequently to attenuate the TLR-induced production of inflammatory mediators. Firstly, we analysed NLRP12 mRNA levels. As expected, when compared to unstimulated cells, PDT induced a higher expression of NLRP12 (median percentage increase: 80%; range: 10-110%) whereas stimulation of MM6 cells with TLR1/2L lowered the amount of NLRP12 transcripts (median percentage decrease: 30%; range: 20-60%). Interestingly, cells treated for 48 h with PDT and then stimulated with TLR1/2L showed a significant increase of NLRP12 mRNAs compared to cells stimulated with only TLR1/2L (median percentage increase: 40%, range: 20-70%, P<0.05) (Fig. 5A).

To better characterize the role of PDT in modulating NLRP12 expression upon TLR1/2 engagement, we sought to determine whether the results observed at transcriptional level were mirrored by changes in NLRP12 protein levels. MM6 cells were subjected to lysis and cell extracts were immunoprecipitated with anti-NLRP12 specific antibody. The need of immunoprecipitation step was due to the evidence that, as previously observed by other Authors (15), NLRP12 protein is not detectable in cell lysates by direct Western blot analysis.

In accordance with the results obtained in qRT-PCR, PDT treatment induced an increase of intracellular NLRP12 protein, and was also able to counteract the TLR1/2L-triggered NLRP12 down-regulation (Fig. 5B). Data obtained using MM6 cells were confirmed in primary monocytes. In fact, PDT induced a time-dependent increase in NLRP12 mRNA expression (median n-fold increase: 1.53; range: 1.4-2.0) in human monocytes that peaked at 24 h post-treatment (Fig. 5C and D), and significantly prevented the down-modulation of NLRP12 induced by the TLR1/2L (median percentage increase: 60%; range: 50-74%, P<0.01) (Fig. 5E).

Once we demonstrated the ability of PDT to up-regulate NLRP12 expression and antagonize its TLR ligand-induced down-regulation we asked whether the inhibition of TLR-triggered proinflammatory events induced by PDT was dependent on NLRP12 modulation. For this purpose we performed siRNA experiments in which MM6 cells were nucleofected with NLRP12 specific siRNA or control scrambled oligonucleotides (Block IT). The effects of siRNA on NLRP12 expression were evaluated by real-time PCR analysis. As shown in Fig. 6A, approximately 60% inhibition of NLRP12 transcripts was observed in MM6 24 h after nucleofection with NLRP12

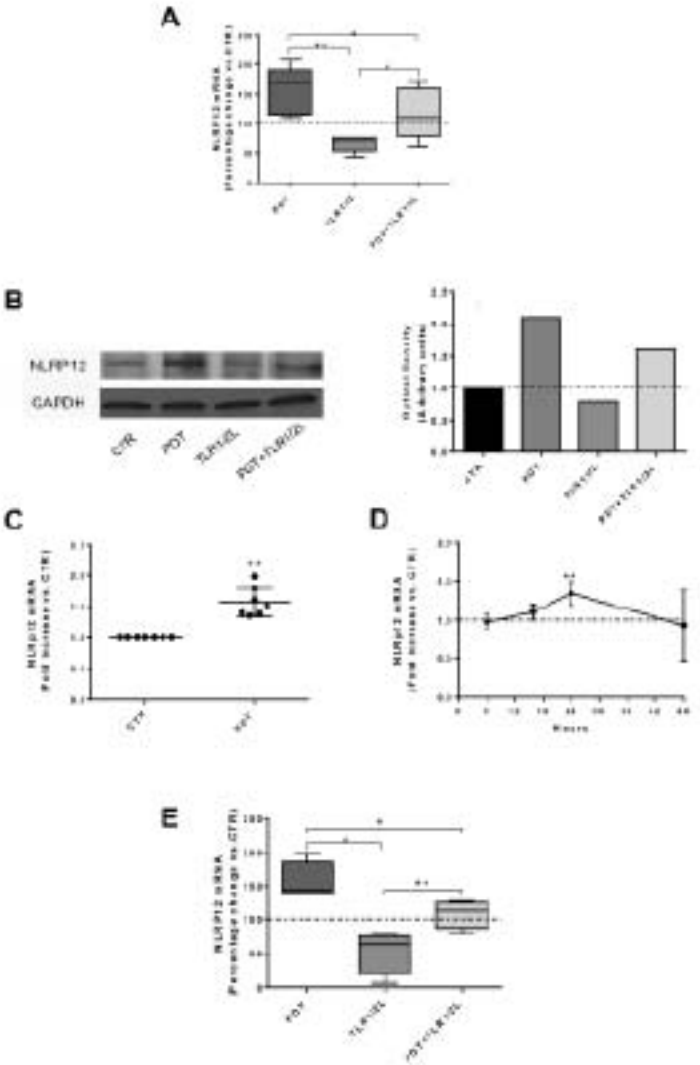

Fig. 5. *PDT increases the expression of NLRP12 in TLR stimulated monocytes.* ***A****) Changes in NLRP12 mRNA expression occurring in MM6 cells treated or not for 48 h with PDT and then stimulated for 6 h with the TLR1/2L. Untreated cells represent the calibrator sample (100% of mRNA expression). Box-plots represent medians, quartiles, minimum and maximum values of five independent experiments.* ***B****) MM6 cells, pretreated or not with PDT, were stimulated for 16 h with the TLR1/2. Cells were then lysed and NLRP12 protein was immunoprecipitated from equal amounts of protein extracts. Immunoprecipitated samples were then analyzed by Western blot and specific NLRP12 bands were quantified by densitometry. Western blot from 1 out of 6 independent experiments with similar results is shown. GAPDH analysis was used to relatively quantify NLRP12 protein amounts (left panel). Graph in the right panel represents the densitometric quantitation of NLRP12 protein detected upon different treatments. Untreated cells were used as control (Optical density = 1).* ***C****) Primary isolated monocytes were treated as in Fig. 4 and NLRP12 mRNA expression was evaluated. Dot-plots represent the n-fold increase of NLRP12 in PDT-treated cells compared to untreated cells (calibrator sample, fold increase = 1). Seven independent experiments, performed with different donor monocytes, are represented.* ***D****) Time course analysis of NLRP12 mRNA increase in PDT-treated monocytes. Results represent the mean ± SD of three independent experiments.* ***E****) Changes in NLRP12 mRNA expression occurring in monocytes treated or not for 24 h with PDT and then stimulated for 6 h with the TLR1/2L. Untreated cells represent the calibrator sample (100% of mRNA expression). Box-plots represent medians, quartiles, and minimum and maximum values of seven independent experiments are shown. Statistical significance was assessed by Mann Whitney test (panels C and D) and one way Anova test (panels A and E). *: P<0.05, **: P<0.01.*

siRNAs compared to cells nucleofected with Block IT siRNA. The biological consequence of NLRP12 silencing is shown in Fig. 6B. Upon transfection with NLRP12 siRNA, PDT-treated MM6 cells lost their ability to decrease TLR1/2L-induced MCP-1 synthesis, being the amount of MCP-1 transcripts produced by silenced cells comparable to levels present in untreated cells (left panel). Quantification of MCP-1 protein released in the supernatant mirrored the results observed at transcriptional levels (right panel). Finally, we observed that overexpression of NLRP12 in MM6 cells upon transfection with a

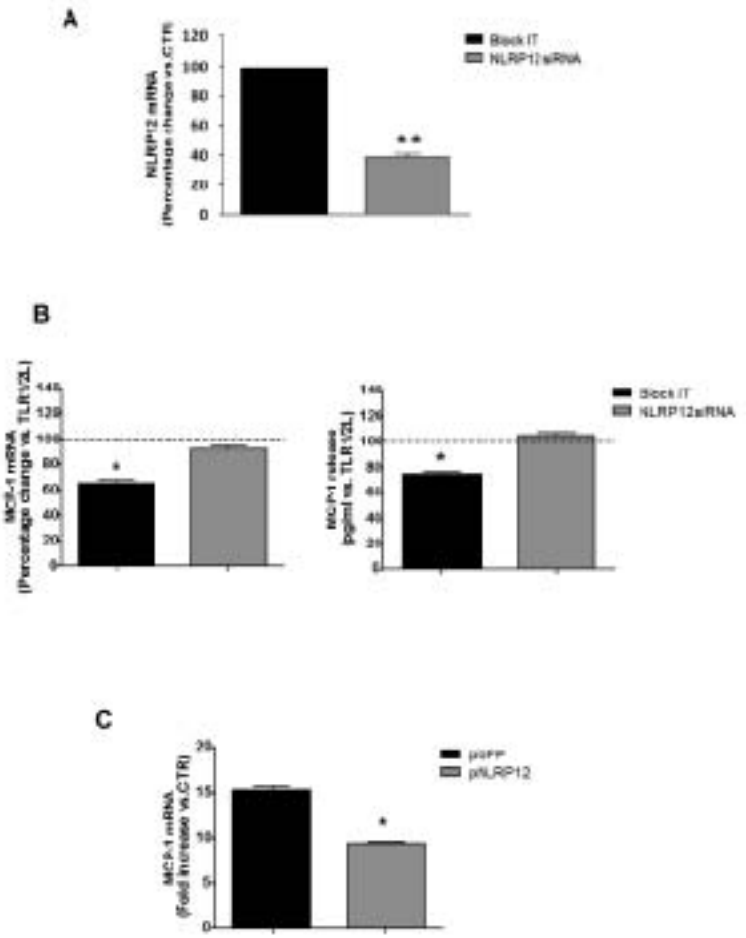

Fig. 6. *PDT-induced NLRP12 expression is responsible for the decrease in MCP-1 expression induced by TLR engagement. **A**) MM6 were nucleoporated with human NLRP12 siRNA or "Block-IT oligos" as irrelevant control reagent. Analysis of NLRP12 gene expression silencing was performed after 24 h using quantitative real-time PCR. One hundred % value corresponds to the NLRP12 mRNA expression in cells exposed to Block- IT oligos. **B**) MM6 cells were cultured in the presence or absence of PDT for 24 h and then transfected with human NLRP12 siRNA or "Block- IT oligos" as irrelevant control reagent. After 24 h, cells were stimulated with TLR1/2L and then analyzed for MCP-1 expression. Graph in the left panel represents MCP-1 mRNA changes in NLRP12-silenced PDT-treated MM6 cells in comparison to PDT-treated cells still capable of expressing NLRP12. PDT-untreated cells were used as calibrator sample (100% of mRNA expression). In the same experiments the release of MCP-1 protein was also evaluated (right panel). **C**) MM6 cells were nucleofected with a NLRP12-expressing plasmid or with an irrelevant GFP-expressing plasmid. After 48 h, MCP-1 mRNA expression upon TLR1/2 stimulation was analyzed. Graph represents the fold increase of MCP-1 transcription detected in cells overexpressing or not NLRP12. MM6 cells not stimulated with TLR1/2L were used as calibrator sample (fold increase = 1). One out of three independent experiments with similar results is shown. In each panel data are represented as mean ± SD of triplicate samples. Statistical significance was assessed by Student t-test. *: P<0.05, **: P<0.01.*

human NLRP12-expressing plasmid resembled the biological effect induced by PDT. Moreover, MM6 cells transiently transfected with the NLRP12 gene significantly controlled the MCP-1 transcriptional activity induced by TLR1/2L, thus confirming that this effect relies on NLRP12 levels (Fig. 6C).

DISCUSSION

The immunomodulatory molecule PDT has been shown to ameliorate different functions of the innate and adaptive immune response in both animals and humans, and this *in vitro* effect may, at least in part, explain its well-defined pharmacological activity against infections (1-3). However, few studies have attempted to characterize which kind of cellular receptors and intracellular pathways are engaged by the dipeptide (16-17).

Our data demonstrate a novel effect of PDT on innate immune sensing of microbial products. We show, for the first time, that PDT up-regulates NLRP12 expression in monocytes at the transcriptional and protein level. PDT-induced increase of NLRP12 was found to influence the expression profile of key inflammatory mediators after TLR-ligand interaction. In fact, treatment of monocytes with PDT led to a significant attenuation of MCP-1, IL-1β and IL-8 synthesis during the acute response to TLR agonist, and this effect was associated with the ability of PDT to counteract the NLRP12 downregulation induced by TLR engagement.

Since TLRs are key components in pathogen recognition and critical mediators in the early response to foreign microorganisms, attenuation of the inflammatory response to their agonists by PDT represents an important and novel immunomodulating effect. Proximal TLR1/2 agonist signalling is facilitated by accessory mechanisms that allow for a full inflammatory response to occur; specifically, the downregulation of NLRP12 expression after activation of myeloid cells seems to play a critical role (18). It is worth noting that, in contrast to most innate immune genes, human NLRP12 expression is present before immunostimulation and an adequate level of this protein helps to maintain a quiescent phenotype by inhibiting IRAK-1 phosphorilation and NIK activation (14-15). Expression of negative regulators of TLR signalling are usually TLR-induced and turn off the TLR activation downstream pathway once it is expressed (19). Therefore, it has been suggested that NLRP12 may play the unique role of modulating overzealous immune responses during states of infection and several observations support this hypothesis. Specific mutations in NLRP12 have been associated to different immune-based diseases leading to the definition of a new class of autoinflammatory diseases (20), while other studies have demonstrated that NLRP12 plays a crucial role in suppressing colon inflammation and tumorigenesis (21-22). It is therefore tempting to speculate that PDT may drive a finely tuned immune response by inhibiting inappropriate TLR activation where constitutive NLRP12 expression is altered. Other recent studies have highlighted that NLRP12 deficiency is a key step in the development of atopic dermatitis (23); and due to their common immunopathological features, it has been suggested that NLRP12 may be also critical in the development of asthmatic phenotype as well as in asthma exacerbation (24). These observations strengthen the possibility that PDT effects observed by Gourgiotis et al. (7) in atopic asthmatic children may be dependent on the up-regulation of NLRP12 expression *in vivo*. In this study the Authors observed that PDT was able to down-regulate the expression of CD30 molecule on cells from both atopic and normal subjects, raising the possibility that PDT is capable of affecting the Th1/Th2 balance in atopic asthma. Again, an important role of PDT in priming immune response toward a Th1 phenotype has been assessed by several research groups who highlighted the capability of PDT to induce DC maturation and help mount an adequate humoral response (3, 6, 25).

Growing evidence indicates that immunomodulation by bacteria or bacterial components plays a crucial role in immune protection versus pathogenic bacterial strains (26). Protective effects are mainly due to a significant reduction of the proinflammatory cascade triggered by the pathogen. A recent paper has shown that co-incubation of human DCs with *Salmonella* and *Lactobacillus paracasei* significantly reduced the ability of *Salmonella* to induce IL-6, IL-8 and TNF-α (27). Tezera et al. have demonstrated that *Neisseria lactamica* attenuates TLR1/2 cytokine response, suggesting that commensal-driven

attenuation protects the mucosal barrier integrity from inflammatory destruction during high levels of pathogen colonization while priming innate response remains enabled (26). In this scenario, treatment with PDT may provide a control of those clinical manifestations that are often a result of the excessive activation of the innate immune cells.

Our results demonstrated that PDT up-regulates NLRP12 expression and reduces MCP-1 synthesis. MCP-1 is a master regulator of inflammatory processes that are critically involved in the development or relapse of several immune-mediated pathologies (28). In particular, an overexuberant production of MCP-1 in the lungs of infants correlates with severity of viral bronchiolitis, suggesting that MCP-1 could be involved in worsening the virus-induced disease (29). Furthermore, severity of viral respiratory infections, as well as their recurrence, predisposes infants to develop an asthmatic phenotype (30). The epidemiological evidence that PDT reduces the symptoms of respiratory infections, as well as the rate of infection recurrence, suggests that PDT, lowering the amount of molecules like MCP-1 through NLRP12 up-regulation, may contribute to avoid a virus-induced abnormal inflammatory response and, eventually, the detrimental long-term consequence of severe viral-induced respiratory diseases.

In conclusion, in this study we demonstrated that PDT immunomodulatory peptide upregulates NRLP12 and antagonizes the TLR-induced inflammatory response. These results pave the way for the development of innovative therapeutic approaches for the control of many pathological settings in which NLRP12 is known to play a crucial role, such as tumorigenesis, inflammatory processes and autoimmunity.

ACKNOWLEDGEMENTS

This work was fully supported by VALEAS SpA - Industria Chimica e Farmaceutica, Milano, Italy. We wish to thank Erika Porter for critically revising the manuscript.

Conflicts of interest. Arnaldo Caruso and Simona Fiorentini are inventors in patents owned by Polichem S.A.. Silvia Corbellini received honoraria as scientific consultant from Polichem S.A..

All the other Authors declare no conflicts of interest.

REFERENCES

1. Clemente E, Solli R, Mei V, et al. Therapeutic efficacy and safety of pidotimod in the treatment of urinary tract infections in children. Arzneimittelforschung 1994; 44:1490-94.
2. Caramia G, Clemente E, Solli R, Mei V, Cera R, Carnelli V, Venturoli V, Corsini A. Efficacy and safety of pidotimod in the treatment of recurrent respiratory infections in children. Arzneimittelforschung 1994; 44:1480-84.
3. Zuccotti GV, Mameli C, Trabattoni D, Beretta S, Biasin M, Guazzarotti L, Clerici M. Immunomodulating activity of Pidotimod in children with Down syndrome. J Biol Regul Homeost Agents 2013; 27:253-58.
4. Di Renzo M, Pasqui AL, Bruni F, et al. The *in vitro* effect of Pidotimod on some immune functions in cancer patients Immunopharmacol Immunotoxicol 1997; 19(1):37-51.
5. Migliorati G, Nicoletti I, Riccardi C. Immunomodulating activity of pidotimod. Arzneimittelforschung 1994; 44:1421-24.
6. Giagulli C, Noerder M, Avolio M, Becker PD, Fiorentini S, Guzman CA, Caruso A. Pidotimod promotes functional maturation of dendritic cells and displays adjuvant properties at the nasal mucosa level. Int Immunopharmacol 2009; 9:1366-73.
7. Gourgiotis D, Papadopoulos NG, Bossios A, Zamanis P, Saxoni-Papageorgiou P. Immune modulator pidotimod decreases the *in vitro* expression of CD30 in peripheral blood mononuclear cells of atopic asthmatic and normal children. J Asthma 2004; 41:285-87.
8. Hu X, Zheng W, Wang L, Wan N, Wang B, Li W, Hua H, Shan F. The detailed analysis of the changes of murine dendritic cells (DCs) induced by thymic peptide: pidotimod (PDT), Hum Vaccin Immunother 2012; 8:1250-58.
9. Cook DN, Pisetsky DS, Schwartz DA. Toll-like receptors in the pathogenesis of human disease. Nat

Immunol 2004; 5:975-79.
10. O Neill LAJ. Fine tuning TLR signaling. Nature Immunol 2008; 9:459-61.
11. Inohara N, Nuñez G. NODs: intracellular proteins involved in inflammation and apoptosis. Nat Rev Immunol 2003; 3:371-82.
12. Liew FY, Xu D, Brint, EK, O'Neill LAJ. Negative regulation of toll-like receptor-mediated immune responses. Nat Rev Immunol 2005; 5:446-58.
13. Xia X, Cui J, Wang HY, et al. NLRX1 negatively regulates TLR-induced NF-κB signaling by targeting TRAF6 and IKK. Immunity 2011 24; 34:843-53.
14. Lich JD, Williams KL, Moore CB, Arthur JC, Davis BK, Taxman DJ, Ting P-Y. Cutting Edge: Monarch-1 suppress non-canonical NF-kB activation and p52-Dependent chemokine expression in monocytes. J Immunol 2007; 178:1256-60.
15. Williams KL, Lich JD, Duncan JA, et al. The CATERPILLAR protein Monarch-1 is an antagonist of Toll-like Receptor-, Tumor Necrosis Factor α, and Mycobacterium tuberculosis-induced pro-inflammatory signals. J Biol Chem 2005; 280:39914-24.
16. Carta S, Silvestri M, Rossi GA. Modulation of airway epithelial cell functions by Pidotimod: NFkB cytoplasmatic expression and its nuclear translocation are associated with an increased TLR-2 expression. Ital J Pediatr 2013; 39:29.
17. Riboldi P, Gerosa M, Meroni PL. Pidotimod: a reappraisal. Int J Immunopathol Pharmacol 2009; 22(2):255-62.
18. Lord CA, Savitsky D, Sitcheran R, Calame K, Wright JR, Ting JP, Williams KL. Blimp-1/PRDM1 mediates transcriptional suppression of the NLR gene NLRP12/Monarch-1. J Immunol 2009; 182:2948-58.
19. Pathak SK, Basu S, Bhattacharyya A, Pathak S, Kundu M, Basu J. Mycobacterium tuberculosis lipoarabinomannan-mediated IRAK-M induction negatively regulates Toll-like receptor-dependent interleukin-12 p40 production in macrophages. J Biol Chem 2005; 280:42794-800.
20. Jéru I, Duquesnoy P, Fernandes-Alnemri T, et al. Mutations in NALP12 cause hereditary periodic fever syndromes. Proc Natl Acad Sci USA 2008; 105:1614-9.
21. Allen IC, Wilson JE, Schneider M, et al. NLRP12 suppress colon inflammation and tumorigenesis through the negative regulation of noncanonical NF-kB signaling. Immunity 2012; 36:742-54.
22. Zaki H, Vogel P, Subbarao Malireddi RK, et al. The NOD-like Receptor NLRP12 attenuates colon inflammation and tumorigenesis. Cancer Cell 2011; 20:649-60.
23. Macaluso F, Nothnagel M, Parwez Q, Petrasch-Parwez E, Bechara FG, Epplen JT, Hoffjan S. Polymorphisms in NACHT-LRR (NLR) genes in atopic dermatitis. Exp Dermatol 2007; 16:692-8.
24. Allen IC, Lich JD, Arthur JC, Jania CM, Roberts RA, Callaway JB, Tilley SL, Ting JP. Characterization of NLRP12 during the development of allergic airway disease in mice. PLoS One 2012; 7:e30612.
25. Zhao Y, Huang B, Huang S, et al. Evaluation of the adjuvant effect of pidotimod on the immune protection induced by UV-attenuated Toxoplasma gondii in mouse models. Parasitol Res 2013; 112:3151-60.
26. Tezera LB, Hampton J, Jackson SK, Davenport V. Neisseria lactamica attenuates TLR-1/2-induced cytokine responses in nasopharyngeal epithelial cells using PPAR-γ. Cell Microbiol 2011; 13:554-68.
27. Bermudez-Brito M, Muñoz-Quezada S, Gomez-Llorente C, Matencio E, Bernal MJ, Romero F, Gil A. Human intestinal dendritic cells decrease cytokine release against Salmonella infection in the presence of *Lactobacillus paracasei* upon TLR activation. PLoS One 2012; 7:e43147.
28. Conti P. Role of TNF Alpha, IL-33 and CCL2/MCP-1 in Mast Cell Activity. Glob J Immunol Allerg Dis 2013; 1:35-43.
29. Welliver RC, Garofalo RP, Ogra PL. Beta-chemokines, but neither T helper type 1 nor T helper type 2 cytokines, correlate with severity of illness during respiratory syncytial virus infection. Pediatr Infect Dis J 2002; 21:457-61.
30. Busse WW, Lemanske RF Jr, Gern JE. Role of viral respiratory infections in asthma and asthma exacerbations. Lancet 2010; 376:826-34.

NITRIC OXIDE SYNTHASE EVALUATION IN ORAL PRECANCEROUS AND CANCEROUS LESIONS

F. MASTRANGELO[1], R. VINCI[2], G. FALCO[4], L. TETTAMANTI[3], S. TETÈ[1†], A. TAGLIABUE[3] and E. GHERLONE[2]

[1]Department of Oral Science, University of Chieti, Italy; [2]University of Vita e Salute Milano, Italy; [3]Department of Oral Science, Insubria University of Varese, Italy; [4]Self-employed professional, Lecce, Italy

Received August 8, 2014 – Accepted November 18, 2014

Nitric Oxide (NO) has been linked to several cardiovascular, neurological and immunological physiological and pathological functions. Several studies have shown that the eNOS, nNOS and iNOS effects on cancer cell growth and proliferation are related to the upregulation of the Wnt pathway and have a central role during metastasis development. Recent studies suggest that cancer cells undergo metabolic reprogramming, which drives cancer cell growth and progression. The aim of this study was to observe the NOS activity in the pathogenesis of oral precancerous and cancerous lesions. The results showed changes in eNOS activity levels, which increased from healthy oral mucosa to oral squamous cell carcinoma SCC, through different dysplasia levels. The iNOS activity levels increased in precancerous lesions compared to healthy mucosa, where iNOS was absent, while it decreased in SCC lesions. Moreover, a gradual increase of nNOS activity together with the progression of the lesions was also found. These results may suggest how NO could play a critical role during pathogenesis, growth and development of precancerous lesions to cancer degeneration.

Increasing evidence demonstrates that cancer cells undergo metabolic transformation during tumorigenesis, proliferation and dissemination through nutrients and growth factors available in tumor microenvironment. Altered metabolic functions further enhance tumor growth and progression. Recent studies have started to clarify the role of more molecules on the proliferation of cancer cells. One critical component to tumor growth is the metabolic reprogramming of nitric oxide (NO) pathways in cancer cell growth in some cancers, including lung (1), breast (2), thyroid (3) and ovarian (4).

Nitric Oxide (NO) is a related intracellular messenger in neurological, cardiovascular and immunogical functions (5, 6) during angiogenesis processes (7), tumor progression and, in relationship with CXCR (2), COX-24 and VEGF (8, 9) it plays a critical role in cell migration during metastasis and cancer dissemination. NO synthase (NOS) (3) is produced in three distinct isoforms: endothelial NO synthase (eNOS), neuronal NO synthase (nNOS) and inducible NO synthase (iNOS) (1). eNOS and nNOS are constitutive isoforms that can rapidly synthesize small amounts of NO after receptor stimulation (10, 11). iNOS is mainly involved in the inflammatory process also in dentistry,

Key words: nitric oxide synthase, nitric oxide, squamous oral carcinoma, oral hyperkeratosis, oral leukoplakia

Mailing address: Filiberto Mastrangelo, MD, DDS, PhD
Department of Oral Science,
University "G. d'Annunzio" – Chieti
Via dei Vestini 31, 66013 Chieti Scalo (CH), Italy
Tel.: +39 335 8390720
Fax : +39 0871 3554073
email: filibertomastrangelo@hotmail.com

0393-974X (2014)

in periapical inflammatory lesions (12). Furthermore, pro-inflammatory stimuli make resident or immigrant inflammatory cells able to induce iNOS7-35. After adequate stimulation, iNOS produces large amounts of NO for sustained periods of time, which is involved in non-specific immune responses, by acting as toxic agent during infections (5, 4, 13, 14). Nitric Oxide is also implicated in the carcinogenic process in various organs (15-17) such as the oral cavity, and in the development of distant metastasis from squamous cell carcinoma (18, 19). Moreover, Caneba showed NO as a cancer therapeutic agent by itself or as a target of cancer therapies. This may be because NO can act as a signaling molecule or as a source of oxidative and nitrosative stress. NO can stimulate mitochondrial biogenesis through a PGC-1-related coactivator and increase mitochondrial function (4). Kerezoudis hypothesized a correlation between NOS activity and the presence of NADPH-diaphorase in dental pulp, in periodontal ligament and in alveolar bone of the rat in physiological conditions (20). Czesnikiewicz-Guzik demonstrated how NO levels greatly increase in an organism under carcinoma, OLP (Oral Lichen Planus) and RAU (Regular Aphthous Ulcerations) had potential implications for immune regulation in high oxidative stress conditions (21-26). Moreover, Ohashi showed that most of the macrophages found in the inflammatory infiltrate of patients with OLP did not express iNOS (27). This could be explained by the complex immunogenic picture of OLP, which includes many immune cells, such as macrophages and T lymphocytes and a great number of cytokines, such as IL-2, IL-4, IL-10, TGF-β, and TNF-α, well-known inhibitors of iNOS induction (19). Therefore high concentrations of NO could induce cellular damage with consequent erosions and ulcerations of the oral mucosa, so that, high levels of NO in human saliva would have patho-physiologic implications for oral lichen planus and recurring acute oral ulceration (27, 28). The aim of the study was to evaluate eNOS, nNOS, and iNOS in normal oral mucosa, in hyperkeratosis, in leukoplakia and in SCC to find a relationship between NO expression and the development of precancerous and cancerous oral lesions (29, 30).

MATERIALS AND METHODS

Sixty-five patients (34 male and 31 female), aged 30-68 years, who came to our attention in the Department of Oral Surgery of the University of Chieti were included in this study after giving signed informed consent. Ten of these were afflicted with oral hyperkeratosis, 24 patients presented oral homogeneous leukoplakia, 23 were suffering from oral nodular leukoplakia and 8 patients from SCC. Healthy patients to be treated for impacted third molar extraction were also included in the study as a control group. After an accurate anamnesis and clinical examination, any possible relationship between the lesions and systemic or oral pathologies was excluded, and a valid biopsy from each lesion was carried out for histological and immunohystochemical assay in order to formulate a diagnosis. Five samples of healthy oral mucosa were removed during surgical extraction of impacted third molars, in order to compare them with pathological oral mucosa samples.

Experimental procedure

For histological analysis, sections were obtained from the bioptic tissues and stained with haematoxylin-eosin. For immunohystochemical analysis, the samples were immerged in a gelatinous substance, Bio-optica KILLIX, and then immediately frozen at -80°C for 24-48 hours. These specimens were sectioned with the aid of a cryostat (Reichert-Jung, Germany) into 7-micron thick sections, and positioned on the slides treated with a chrome alum gel at room temperature. Ten sections from each group were initially treated with a fixing agent containing 5% normal goat serum, 0.1% albumin serum in a solution of PBS at room temperature, in a humid room for 30 min. Subsequently, the sections were washed for 5 min with TRIS-HCl and incubated with rabbit anti-eNOS, anti-iNOS and anti-nNOS primary antibody (antibodies dilution 1:100 in PBS, Saint Cruz Biotech Inc., Santa Cruz, California, USA). These sections were incubated with secondary antibodies coming from goat anti-rabbit for 30 min, washed for 5 min in a saline solution of TRIS-HCl and then incubated with PAP complex (peroxidase anti-peroxidase) for 10 min. The presence of eNOS and iNOS was highlighted by pink-violet precipitate due to antigen antibody reaction blocked by haematoxylin (19).

Statistical evaluation

The sections were examined with an optical microscope (Leitz Dialux 22, LEICA, Heidelberg, Germany). Quantitative evaluation of the immune reaction was determined through the integral optic density (I.O.D.) by analysing the changes in the digital images. The evaluated areas came from a randomising of the slides; 5 slides for each group were appraised. For the analysis of the data a Sony video camera was connected to a LEICA Quantimet 500 plus (LEICA Cambridge Ltd, Cambridge, England)

Table I. *The evaluation of the integrated optic density resulted statistically significant for the immune reactivity of eNOS, nNOS and iNOS ($p < 0.05$).*

eNOS	Oral healthy mucosa	Hyperkeratosis	Leukoplakia	Squamous Cell Carcinoma
Immuno-histochemical analysis	32 ± 5	48 ± 3	70 ± 8	78 ± 5
Western Blot	2 ± 0.4	5.1 ± 0.2	5 ± 0.5	5 ± 0.5
RT-PCR	1 ± 0.05	2.5 ± 0.5	4.7 ± 0.2	5.4 ± 0.5
iNOS	**Oral healthy mucosa**	**Hyperkeratosis**	**Leukoplakia**	**Squamous Cell Carcinoma**
Immuno-histochemical analysis	0.8 ± 0.01	25 ± 5	80 ± 5	70 ± 5
Western-Blot	0.05	3 ± 0.2	5 ± 0.5	6 ± 0.2
RT-PCR	0.03	2.8 ± 0.3	4.5 ± 0.2	5.6 ± 0.3
nNOS	**Oral healthy mucosa**	**Hyperkeratosis**	**Leukoplakia**	**Squamous Cell Carcinoma**
Immuno-histochemical analysis	30 ± 5	50 ± 3	75 ± 5	78 ± 5
Western-Blot	5 ± 0.4	8 ± 0.2	7.5 ± 0.2	7.8 ± 0.5
RT-PCR	5 ± 0.05	7.5 ± 0.3	7 ± 0.2	7.2 ± 0.5

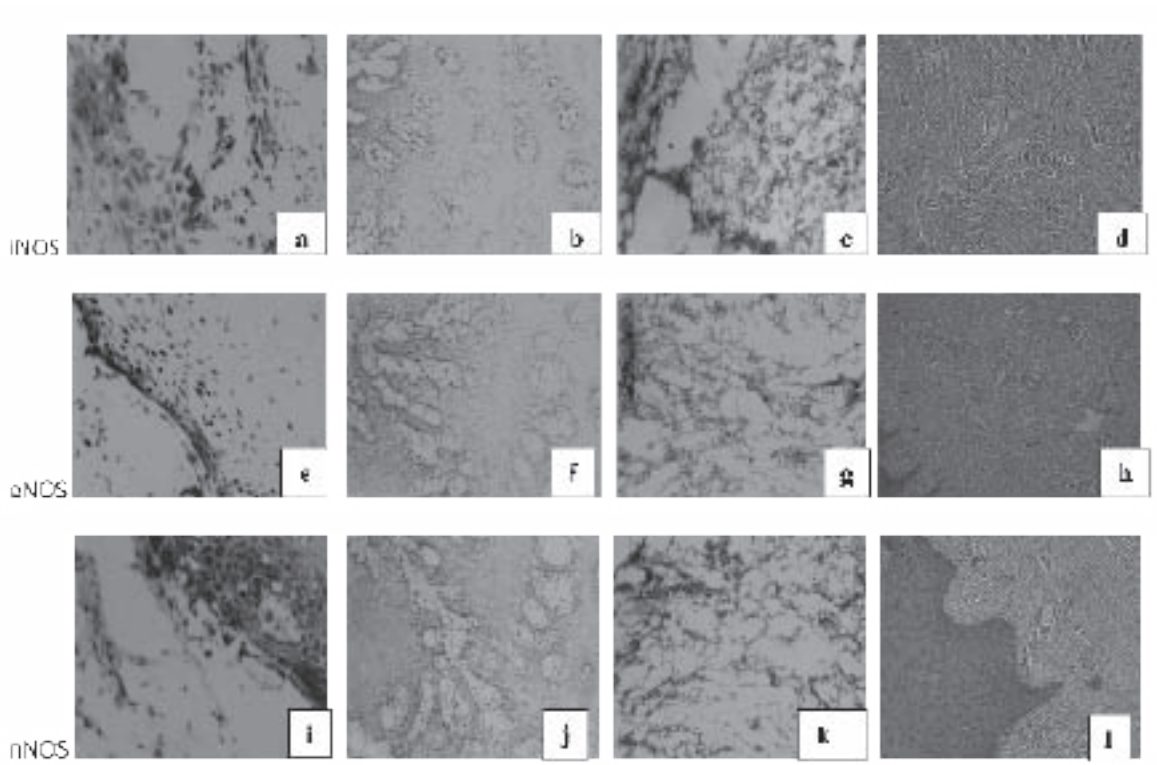

Fig. 1. ***a)*** *High levels of iNOS were found in all samples in the presence of an inflammatory infiltrate.* ***b)*** *High levels of iNOS were found around inflammation infiltrate in all samples.* ***c)*** *Lower levels of iNOS in SCC samples were visible compared to leukoplakia and hyperkeratosis specimens.* ***d)*** *Healthy oral mucosa.* ***e)****Hyperkeratosis showed high levels of eNOS around the vascular endothelium cells of the connective tissue compared to the healthy mucosa control group.* ***f)*** *Leukoplakia-founded low eNOS marker levels were observed around the vascular endothelium.* ***g)*** *Squamous cell carcinoma eNOS levels also resulted increased in all specimens.* ***h)*** *Healthy oral mucosa.* ***i)*** *Moderate positive levels of nNOS markers compared to the healthy control group.* ***j)*** *Moderate positive levels of nNOS markers compared to the healthy control group.* ***k)*** *Moderate positive levels of nNOS markers compared to the healthy control group.* ***l)*** *Healthy oral mucosa.*

and the changes in the I.O.D. were determined on a surface of 512x512 pixel, using a density of transmission standard ISO (Kodak CAT 152-3406, Eastman Kodak Company, Rochester, USA). The results were expressed through a media ± standard deviation (SD). Probability of null hypothesis of less than 5% was considered as statistically significant ($p < 0.05$).

Semi-quantitative reverse transcription-polymerase chain reaction for iNOS, eNOS and nNOS

Total RNA was extracted using 1 ml ULTRASPEC-RNA (Biotech, Lab., Inc. Huston, TX, USA), as recommended by the manufacturer. RNA was dissolved in diethyl pyrocarbonate (DEPC)-treated water and quantified spectrophotometrically at $_{260}$ nm. First-strand cDNA was generated by adding RNA (1 µg) to a mixture containing 1 mM deoxy-nucleoside- triphosphates (d-NTP), 1U/µl RNase inhibitor, 2.5 U/ µl moloney murine leukemia virus reverse transcriptase, 2.5 µM oligo-dt, 5 mM $MgCl_2$, 10x PCR buffer in a final volume of 20 µl. Reverse transcription was performed at 42°C for 1 h followed by heat inactivation of reverse transcriptase at 92°C for 10 min. 18S was amplified from the same amount of RNA to correct for variation of different samples. PCR amplification was performed using a Programmable Thermal Controller (MJ Research, Inc. Massachusetts, USA) at the following annealing temperatures: 58°C for 60 sec for eNOS, 56°C for nNOS and 55°C for iNOS. The PCR solution contained 10 µl of first-strand cDNA, 4 µl 10x PCR buffer, 2 mM $MgCl_2$. The following primer pairs were used: sense 5'-CTC TCC AGG CAC TTC AGG C-3' and antisense 5'-TGT CTG TCT GCT GCT CCT AG-3' for human eNOS, sense 5'-CGT TTG GCA TGG GGG AGT GAG $C^{-3'}$ and antisense 5'-TTG GGG GCC TGG GAT TTC $TGG^{-3'}$ for human nNOS and sense 5'-CGT AAA GAC CTC TAT GCC AA-3' and antisense 5'-AGC CAT GCC AAA TGT CTC AT-3' for human iNOS. 2 u.i. of Termophylus Acquaticus (Taq) DNA polymerase (Celbio, Milan, Italy), and water added to a final volume of 50 µl. PCR products were run on 2% agarose gel electrophoresis and photographed after ethidium bromide staining under UV light. Bands on the gel were scanned using a computerized densitometric system (Bio-Rad Gel Doc 1000, Milan, Italy).

Western blot analysis

Determination of eNOS, nNOS and iNOS proteins were performed in three series of protein extracts by Western blotting. Fifty mg cytoplasmatic proteins, quantified by spectrophotometric assay (HP 8452A, California, USA) using Lowry method, were separated by electrophoresis in a 7.5% sodium dodecyl sulfate-polyacrylamide gel (SDS-PAGE (BIO-RAD), Hercules, CA, USA) and transferred at 4°C to nitrocellulose membrane (BIO-RAD, Hercules, CA, USA) in glycine-methanol buffer. Nitrocellulose was then blocked in Tris-Buffered Saline (TBS)-milk and incubated, overnight, with various primary antibodies: anti-human-eNOS, nNOS, iNOS (Santa Cruz Biotech, Inc. Santa Cruz, CA, USA). The nitrocellulose was then washed in TBS, incubated with a secondary antibody conjugated with alkaline phosphatase for 2 h, washed again, and developed in an alkaline buffer with nitrobluetetrazolium (NBT) as substrate (Alkaline Phosphatase Conjugate Substrate Kit, BIO-RAD, Hercules, CA, USA). β-actin (Sigma, 1/10.000) was used as an internal standard. The densitometric analysis of Western blots was performed using a computerized densitometric system (Bio-Rad Gel Doc 1000, Milan, Italy).

RESULTS

All histological analysis confirmed clinical diagnosis of the samples. Immunohistochemical analysis detected NOS in all samples analyzed, however, there were different levels of expression linked to the molecules analyzed and the lesions (Table I). High levels of eNOS were found in hyperkeratosis specimens around the vascular endothelium cells of the connective tissue compared to the healthy mucosa control group (Fig. 1a). Low eNOS marker levels were observed in leukoplakia specimens around the vascular endothelium cells of the connective tissue (Fig. 1b). The eNOS levels also resulted increased in all oral carcinoma specimes (Fig. 1c). Moderate positive levels of nNOS markers were detected in all oral hyperkeratosis, leukoplakia and SCC samples (Fig. 1 d, e, f) compared to the healthy control group. High levels of iNOS were increased in hyperkeratosis (Fig. 1g) and leukoplakia specimens (Fig. 1h), in agreement with the literature, in presence of an inflammatory infiltrate. iNOS was also found in oral carcinoma samples (Fig. 1j), but at lower levels compared to leukoplakia and hyperkeratosis specimens. iNOS markers were not observed in healthy mucosa. The evaluation of the integrated optic density resulted statistically significant for the immune reactivity of eNOS, nNOS, iNOS ($p < 0.05$).

DISCUSSION

In several recent studies NO was related with pancreas, breast and ovarian cancer growth and

metastasis progression. However, there is still no unanimous consensus on the mechanisms of the pathogenesis development and cancer timing progression. Indeed, correlation was not found between eNOS expression and some significant clinical factors, as for example, TNM staging, grading, primitive site of the lesion or associated pathologies. In a recent study, Brennan investigated iNOS expression in bland, moderate and severe oral epithelial dysplasia (31). iNOS was not found in healthy mucosa but its expression progressively enhanced with the increasing severity of the dysplasia. In bland and moderate dysplasia, iNOS was confined to basal and suprabasal layers of the epithelium, while in severe cases it could be detected in its entire thickness and in the macrophages of the connective underlying tissue. The high levels of iNOS found in severe hyperplasia suggest that this enzyme expression begins to increase before the malignant degeneration of a dysplastic lesion, as according to Gavilanes (12, 20, 22-26, 29, 30, 32, 33), who stated that the high production of NO, from iNOS, is required in the first stages of tumour growth to activate angiogenesis, and to increase cell adhesion and permeability. Gavilanes also found that an increase of Ca++-dependent NOS activity, in a primary tumour site, corresponded to a decrease of Ca++-independent NOS activity (12, 20, 22-26, 29, 30, 32, 33). This suggests that NO probably plays a double role in tumour growth, as being responsible for cell death or as a promoter of cell proliferation. In fact, it is well known that NO released by macrophages promotes the death of cancer cells. On the other hand, NO is also responsible for cell proliferation by three main effects: promoting angiogenesis and vascularization, facilitating tumour cell adhesion to endothelial cells, and increasing vascular permeability. All these effects may favour the growth of a primary tumour and the development of secondary sites (18, 35). Also Scher investigated the role in the development of distant metastasis from head and neck squamous cell carcinoma and confirmed this role of NOS and IL-1 (34). Our results showed positive NOS activity in all samples examined, however, there are different levels of expression related to the lesions analyzed. Indeed, the eNOS levels were gradually increased from healthy mucosa to oral carcinoma samples. In hyperkeratosis and in leukoplakia specimens, the distribution of the eNOS was local and mainly confined to the connective tissue, while in SCC, because of the neo-angiogenic phenomena, its distribution loses its local feature to engage all the epithelium. The evaluation of nNOS, despite a statistically significant result, does not clarify the role of this enzyme in lesion progression. We also found that iNOS was not present in healthy mucosa and its positiveness increased with the progression of the dysplasia according to the recent literature. In hyperkeratosis a strong positive reaction was seen in basal and suprabasal layers, while in leukoplakia almost all the thickness of the epithelium was interested. iNOS was seen especially in the connective tissue, where most of the macrophages were found (35, 36). In our study, iNOS from SCC samples showed a small positive reaction compared to leukoplakia, and this can probably be explained with cell death. According to literature, we can state that iNOS plays a conclusive role in early tumour stages, while subsequently its release causes apoptosis and therefore an auto-limitation of its production (35). In conclusion, the results show nitric oxide determinant role in growth and development of oral dysplasia and confirm that oral squamous cell carcinoma is characterized by a dysregulated nitric oxide synthase system. Further studies are needed in order to characterize the role of nitric oxide synthase enzymes and the related mechanism in the pathogenesis of oral precancerous and cancerous lesions.

REFERENCES

1. Kisley LR, Barrett BS, Bauer AK, Dwyer-Nield LD, Barthel B, Meyer AM, Thompson DC, Malkinson AM. Genetic ablation of inducible nitric oxide synthase decreases mouse lung tumorigenesis. Cancer Res 2002; 62:6850-56.
2. Ohtsu N, Takaoka K, Segawa E. Antitumor effects of inhibitors of nitric oxide synthase or cyclooxygenase-2 on human KB carcinoma cells overexpressing COX-2. Oncol Rep 2010; 24(1):31-36.
3. Raharijaona M, Le Pennec S, Poirier J, et al. PGC-1-related coactivator modulates mitochondrial-nuclear crosstalk through endogenous nitric oxide in a cellular model of oncocytic thyroid tumours. PLoS One 2009; 4:e7964.
4. Caneba CA, Yang L, Baddour J, Curtis R, Win J,

Hartig S, Marini J, Nagrath D. Nitric oxide is a positive regulator of the Warburg effect in ovarian cancer cells. Cell Death Dis 2014; 5:e1302;
5. Nathan C. Nitric oxide as a secretory product of mammalian cells. FASEB J 1992; 6:3051-64.
6. Nathan C, Xie QW. Nitric oxide synthases: roles, tolls and controls. Cell 1994; 78:915-18.
7. Mei K, Cai XH, Du L. Effect of nitric oxide derived from endothelial nitric oxide synthase on tumor angiogenesis. Chin J Cancer 2010; 29(1):32-7.
8. Shang ZJ, Li JR. Expression of endothelial nitric oxide synthase and vascular endothelial growth factor in oral squamous cell carcinoma: its correlation with angiogenesis and disease progression. J Oral Pathol Med 2005; 34(3):134-9.
9. Tu YT, Tao J, Liu YQ. Expression of endothelial nitric oxide synthase and vascular endothelial growth factor in human malignant melanoma and their relation to angiogenesis. Clin Exp Dermatol 2006; 31(3):413-18.
10. Forstermann U, Kleinert H. Nitric oxide synthase: expression and expressional control of the three isoforms. Naunyn Schmiedebergs Arch Pharmacol 1995; 352(4):351-64.
11. Speranza L, Pesce M, Franceschelli S, et al. The role of inducible nitric oxide synthase and haem oxygenase 1 in growth and development of dental tissue. Cell Biochem Funct 2012; 30(3):217-23.
12. Felaco M, Di Nardo Di Maio F, De Fazio P, et al. Localization of the e-NOS enzyme in endothelial cells and odontoblasts of healthy human dental pulp. Life Sci 2000; 68(3):297-306.
13. Bredt DS, Snyder SH. Nitric oxide: a novel neuronal messenger. Neuron 1992; 8:3-11.
14. Farhad AR, Razavi SM, Nejad PA. The use of aminoguanidine, a selective inducible nitric oxide synthase inhibitor, to evaluate the role of nitric oxide on periapical healing. Dent Res J (Isfahan) 2011; 8(4):197-202.
15. Pervin S, Singh R, Hernandez E, Wu G, Chaudhuri G. Nitric oxide in physiologic concentrations targets the translational machinery to increase the proliferation of human breast cancer cells: involvement of mammalian target of rapamycin/eIF4E pathway. Cancer Res 2007; 67:289-99.
16. Hussain SP, Hofseth LJ, Harris CC. Radical causes of cancer. Nat Rev Cancer 2003; 3:276-85.
17. Lampson BL, Kendall SD, Ancrile BB, et al. Targeting eNOS in pancreatic cancer. Cancer Res 2012; 72(17):4472-82.
18. Brennan PA, Palacios-Callender M, Sinclair D, Spedding AV, Zaki GA. Does expression of inducible nitric oxide synthase correlate with severity of oral epithelial dysplasia? J Cranio-Maxillofac Surg 2000; 28:44-48.
19. Brennan PA, Callender MP, Zaki GA, Spedding AV, Langdon JD. Does Type II nitric oxide synthase expression correlate with cellular proliferation in oral squamous cell carcinoma and dysplasia? Head & Neck 2001; 23:217-22.
20. Kerezoudis NP, Olgart L, Fried K. Localization of NADPH-diaphorase activity in the dental pulp, periodontium and alveolar bone of the rat. Histochemistry 1993; 100:319-22.
21. Czesnikiewicz-Guzik M, Lorkowska B, Zapala J, Czajka M, Szuta M, Loster B, Guzik TJ, Korbut R. NADPH oxidase and uncoupled nitric oxide synthase are major sources of reactive oxygen species in oral squamous cell carcinoma. Potential implications for immune regulation in high oxidative stress conditions. J Physiol Pharmacol 2008; 59(1):139-52.
22. Connelly ST, Macabeo-Ong M, Dekker N, Jordan RC, Schmidt BL. Increased nitric oxide levels and iNOS over-expression in oral squamous cell carcinoma. Oral Oncol 2005; 41(3):261-67.
23. Ohshima H, Tatemichi M, Sawa T. Chemical basis of inflammation-induced carcinogenesis. Arch Biochem Biophys 2003; 417:3-11.
24. Kizilay A, Kalcioğlu MT, Ozuğurlu F, Ozyurt H, Aladağ I, Ozturan O, Akyol O. Serum nitric oxide levels in patients with head and neck squamous cell carcinoma. Kulak Burun Bogaz Ihtis Derg 2007; 17(3):148-51.
25. Shang ZJ, Li JR, Li ZB. Effects of exogenous nitric oxide on oral squamous cell carcinoma: an *in vitro* study. J Oral Maxillofac Surg 2002; 60(8):905-10.
26. Mastrangelo F, Grilli A, Tettamanti L, et al. Nitric oxide synthase isoenzyme expression in human oral lichen planus. J Biol Regul Homeost Agents 2013; 27(4):1069-75.
27. Ohashi M, Iwase M, Nagumo M. Elevated production of salivary nitric oxide in oral mucosal diseases.

J Oral Pathol Med 1999; 28:355-59.
28. Kawanishi S, Hiraku Y, Pinlaor S, Ma N. Oxidative and nitrative DNA damage in animals and patients with inflammatory diseases in relation to inflammation-related carcinogenesis. Biol Chem 2006; 387(4):365-72.
29. Clevers H. At the crossroads of inflammation and cancer. Cell 2004;118:671-4.
30. Bentz BG, Pelzer HJ, Hanson DG, Radosevich JA, Haines Iii GK, Lingen MW. Nitric oxide synthase type 3 is increased in squamous hyperplasia, dysplasia, and squamous cell carcinoma of the head and neck. Ann Otol Rhinol Laryngol 1999; 108:781-87.
31. Brennan PA, Umar T, Palacios-Callender M, Spedding AV, Mellor TK, Buckley J, Langdon JD. A study to assess inducible nitric oxide synthase expression in oral lichen planus. J Oral Pathol Med 2000; 29:249-54.
32. Gavilanes J, Moro MA, Lizasoain I, Lorenzo P, Perez A, Leza JC, Alvarez-Vicent JJ. Nitric oxide synthase activity in human squamous cell carcinoma of the head and neck. Laryngoscope 1999; 109:148-52.
33. Hobbs AJ, Higgs A, Moncada S. Inhibition of nitric oxide synthase as a potential therapeutic target. Ann Rev Pharmacol Toxicol 1999; 39:191-220.
34. Scher RL. Role of nitric oxide in the development of distant metastasis from squamous cell carcinoma. Laryngoscope 2007; 117(2):199-209.
35. Lejeune P, Lagadec P, Onier N, Pinard D, Ohshima H, Jeannin JF. Nitric oxide involvement in tumor-induced immunosuppression. J Immunol 1994; 152:5077-83.
36. Mastrangelo F, Grilli A, Tettamanti L, et al. J Biol Regul Homeost Agents 2013; 27(4):1069-75.

A NATURAL FORMULATION (IMOVIRAL™) INCREASES MACROPHAGE RESISTANCE TO LPS-INDUCED OXIDATIVE AND INFLAMMATORY STRESS *IN VITRO*

L. MENGHINI[1], L. LEPORINI[1], G. PINTORE[2], C. FERRANTE[1], L. RECINELLA[1], G. ORLANDO[1], M. VACCA[1] and L. BRUNETTI[1]

[1]*Dipartimento di Farmacia, Università "G. D'Annunzio" Chieti-Pescara, Chieti, Italy;*
[2]*Dipartimento Farmaco-Chimico-Tossicologico, Università di Sassari, Sassari, Italy*

Received October 16, 2012 – Accepted May 23, 2013

Imoviral™ is a natural product formulation containing a mixture of uncaria, shiitake and ribes extracts. All ingredients are recognized as antioxidant, anti-inflammatory agent and immunomodulant. In order to evaluate the rational basis of extract mixture as immunomodulatory agent, we tested the effect of Imoviral™ formulation on macrophage response to lipopolysaccharide (LPS)-induced stress. The effect was evaluated as variation of reactive oxygen species (ROS) and prostaglandin E_2 (PGE_2) production and as cytokine gene expression. The extract did not affect cell viability up to 250μg/ml. Treatment with extract (10-150μg/ml) reduced ROS and PGE_2 production as well as IL-8 and TNF-α gene expression. A pre-treatment with extract blunted LPS-induced production of ROS and PGE_2, markers of oxidative and inflammatory stress, as well as the gene expression of all cytokines tested, indicators, *in vitro*, of immune response activation. In conclusion, we demonstrated that Imoviral™ formulation could be a useful tool to modulate the immune function, reducing the oxidative and inflammatory markers related to bacterial attack. Experimental data suggest that Imoviral™ extract mixture could also represent a preventive pharmacological strategy to enhance cell resistance to bacterial infections.

Many plants and extracts from traditional medicine are healthy food and useful herbal medicine tools to treat a wide range of disorders. Interest in identification and research on extracts and preparations from natural sources as preventive agents for immunological complications of various organs is continuously increasing (1).

It has been proved that many herbal drugs have healthy effects by modulating both humoral and cellular immune functions. For many of these, the capacity to control the production of pro-inflammatory mediators involved in many inflammatory processes has been demonstrated. Activated macrophages, as well as other immunocompetent cells, are directly related to inflammation (2).

Macrophages are present in all body tissues and play a key role in the immune surveillance against endogenous and exogenous stimuli with variable and multifunctional activities. Macrophages respond to microenvironment, microbial attack and neoplasia by modulating the expression of cytokines and histocompatibility complex molecules, as well as acting as killer for pathogens and tumor cells (3). Therefore, the control of macrophage activities is

Key words: Immunomodulatory, Shiitake, Lentinula edodes, Uncaria tomentosa, cytokines, oxidative stress

Mailing address: Dr Luigi Menghini,
Dipartimento di Farmacia,
Università "G. D'Annunzio" Chieti-Pescara,
Via dei Vestini 31,
66100 Chieti, Italy
Tel.: +39 0871 3554655 Fax: +39 0871 3554912
e-mail: lmenghini@unich.it

0393-974X (2014)

an important strategy for the treatment of chronic inflammatory diseases. Macrophages secrete several pro-inflammatory gene products as well as modulating the levels of cytokines with anti-inflammatory effects.

Among different endogenous and exogenous stimuli, lipopolysaccharide (LPS) is a potent activator of the inflammatory response which, via different signaling pathways, induces the production of inflammatory cytokines, such as tumor necrosis factor-alpha (TNF-α), interleukin (IL)-6, IL-8 and other mediators such as prostaglandins and reactive oxygen species (ROS) (4).

In inflammatory sites, the conversion of arachidonic acid to prostaglandin E_2 (PGE_2) is regulated by the enzyme cyclooxygenase 2 (COX-2). One of the possible mechanisms for the anti-inflammatory activity of herbal drugs can involve the inhibition of COX-2, and consequent blockade of the production of inflammatory PGE_2 (5, 6).

Production of cytokines such as TNF-α, IL-6 and IL-8 from macrophage and other cells, as a response to endogenous and exogenous antigens, can trigger inflammation and modulate the effects at cellular and tissue levels. Therefore, the modulation of the production of such mediators can be regarded as a potential target for herbal drugs used for inflammatory disorders (7, 8).

A previous work from our laboratory showed that the extracts of shiitake, uncaria, ribes and their formulation have immunomodulatory functions (9). Single extract and their mixture showed no interference with cell viability, with promising efficacy in modulation of the immune system. In order to further evaluate the rational use of Imoviral™, an extract mixture marketed as food supplement, we tested its modulatory effects on inflammation and oxidative stress response in macrophages.

An important mechanism of the anti-inflammatory effects of herbal drugs can be related to their antioxidant and ROS scavenging effects (10, 11). Imoviral™ combines the immunomodulant and anti-inflammatory properties of uncaria and shiitake with the antioxidant properties of blackcurrant juice.

Uncaria extracts are used in modern phytotherapy to treat acute and chronic inflammatory disease, such as the common cold, limb pain, prostatitis and cystitis. It contains oxindole alkaloids and polyphenols that modulate cytokine production and immune cell activity (12, 13).

Shiitake is a mushroom used as food and as a medicinal fungus with immunomodulatory, antidiabetic and antihyperlipidemic activities. The main active fraction is lentinan, a complex polysaccharide fraction that, in macrophages, can modulate the production of cytokines involved in the immune response (14).

Blackcurrant has been used in phytotherapy for a long time, with a wide range of indications, such as antioxidant, anti-inflammatory, analgesic, venotonic, capillary protector, antiviral and antiallergy. The juice, and particularly the polysaccharide fraction CAssis PolySaccharide (CAPS) is proven to stimulate macrophage activity by inducing interleukins, particularly IL-1 (15, 16).

In the present study, we investigated the effects of the herbal formula Imoviral™ on macrophage (U937 cells) response both basally and after stimulation with LPS from *Escherichia coli*.

MATERIALS AND METHODS

Imoviral™ is formulated as a mixture of *Uncaria tomentosa* (dry extract, titolated for alkaloid content, 3%), shiitake (*Lentinula edodes*, dry extract, containing 6% of lentinan), β-glucan and blackcurrant (*Ribes nigrum*, dehydrated juice), in weight ratio 15/15/10/6. The quantity and standardized quality of each ingredient were confirmed by specific phytochemical analysis certificates.

Cell culture

U937 cells were cultured in DMEM (Euroclone) supplemented with 10% (v/v) heat-inactivated fetal bovine serum and 1.2% (v/v) penicillin G/streptomycin in 75cm^2 tissue culture flask (n=5 individual culture flasks for each condition). The cultured cells were maintained in a humidified incubator with 5% CO_2 at 37°C. For cell differentiation, U937 cell suspensions at a density of 1×10^6 cells/ml were treated with various doses (10, 50, and 100ng/ml) of phorbol myristate acetate (PMA, Fluka) for 48 h (induction phase). Thereafter, the PMA-treated cells were washed twice with ice-cold phosphate buffer saline to remove PMA and non-adherent cells, whereas the adherent cells were further maintained for 48 h (recovery phase). Morphology of cells was examined under an inverted phase-contrast microscope (17).

Viability test

To assess the basal cytotoxicity of Imoviral™, a

viability test was performed on 96 microwell plates, using 3-(4,5-Dimethylthiazol-2-yl)-2,5-Diphenyltetrazolium Bromide (MTT) test. Macrophages were incubated with extracts (ranging concentration 10-500µg/ml) for 24 h. About 10 µL of MTT (5mg/ml) was added to each well and incubated for 3 h. The formazan dye formed was extracted with dimethyl sulfoxide and absorbance recorded as previously described (18). Effects on cell viability were evaluated in comparison to the untreated control group.

Effect of Imoviral™ on LPS-induced oxidative stress

In order to detect the potential protective effect of Imoviral™ against LPS-induced oxidative stress (19), cells were pre-incubated for 24 h in presence of scalar sub-toxic concentration of herbal formula (10, 50, 150µg/ml) at 37°C in 5% CO_2. After incubation, the medium was changed and 2 h later added with LPS from *Escherichia coli* (1µg/ml). After a 24-h incubation, the supernatants were removed and were used for quantitative determinations of oxidative stress (PGE_2 and ROS), and cells were used for RNA extraction and RT-PCR quantification of IL-6, IL-8 and TNFα gene expression. Cells incubated in culture medium without extracts and treated with LPS were used as controls.

RNA extraction

Total RNA from cells was extracted using TRI Reagent (Sigma-Aldrich, St. Louis, MO, USA), as previously described (9). In brief, the cells were lysed in 1 ml of TRI reagent. After incubation at room temperature for 5 min, 0.2 ml of chloroform was added to each sample and centrifuged at 12000xg for 15 min at 4°C. The aqueous phase was removed and mixed with 0.5 ml of isopropyl alcohol. After centrifugation at 12000xg for 10 min at 4°C, the gel-like RNA pellet was washed with 1 ml of 75% ethanol and dissolved in RNase-free water. Contaminating DNA was removed using 2 units of RNase-free DNase 1 (DNA-free kit, Ambion, Austin, TX), according to the manufacturer's instructions. The RNA solution was quantified at 260 nm by spectrophotometer reading (BioPhotometer, Eppendorf, Hamburg, Germany) and its purity was assessed by the ratio at 260 and 280 nm readings. The quality of the extracted RNA samples was also determined by electrophoresis through agarose gel and staining with ethidium bromide, under UV light.

Reverse transcription and real-time reverse transcription polymerase chain reaction (real-time RT PCR)

One µg of total RNA extracted from each sample in a 20 µl reaction volume was reverse transcribed using High Capacity cDNA Reverse Transcription Kit (Applied Biosystems, Foster City, CA, USA) according to the manufacturer's manual. Reactions were incubated in a 2720 Thermal Cycler (Applied Biosystems, Foster City, CA, USA) initially at 25°C for 10 min, then at 37°C for 120 min and finally at 85°C for 5 s.

Gene expression was determined by quantitative real-time PCR using TaqMan probe-based chemistry (Applied Biosystems, Foster City, CA, USA). Reactions were performed in MicroAmp Fast Optic 96-well Reaction Plates (Applied Biosystems, Foster City, CA, USA) on an ABI PRISM 7900 HT Fast Real-Time PCR System (Applied Biosystems, Foster City, CA, USA). PCR primers and TaqMan probes were obtained from Applied Biosystems [Assays-on-Demand Gene Expression Products, Hs00985639_m1 for IL-6 gene, Hs00174103_m1 for IL-8 gene, Hs00174128_m1 for TNFα gene, Hs99999909 m1 for hypoxanthine phosphoribosyltransferase 1 (HPRT1) gene].

HPRT1 was used as the housekeeping gene. In accordance with the manufacturer's instructions, each amplification reaction was performed with 10 µl of TaqMan Fast Universal PCR Master Mix (2X), No AmpErase UNG (Applied Biosystems, Foster City, CA, USA), 1 µl of primer probe mixture, 1 µl of cDNA, 8 µl of nuclease-free water. The thermal cycling conditions (fast operational mode) were: 95°C for 20 s, followed by 40 cycles of amplification at 95°C for 1 s and 60°C for 20 s. The real-time PCR was carried out in triplicate for each cDNA sample in relation to each of the investigated genes. In addition to samples, individual runs included no-template controls (one for each Assay-on-Demand Gene Expression Product). Data were elaborated with the Sequence Detection System (SDS) software version 2.3 (Applied Biosystems, Foster City, CA, USA). The comparative $2^{-\Delta\Delta Ct}$ method was used to quantify the relative abundance of mRNA and then determine the relative changes in individual gene expression (relative quantification) (20).

This method uses a calibrator sample to enable a comparison of gene expression levels in different samples. The values obtained indicate the changes in gene expression in the sample of interest by comparison with the calibrator sample, after normalization to the housekeeping gene. For the comparison, 1.00 (calibrator sample) was considered the theoretical mean.

PGE_2 Radioimmunoassay (RIA)

Prostaglandin RIA was performed as previously reported (21). 100 µL of PGE_2 standard or sample were incubated overnight at 4°C with the ^{3}H-PGE_2 (3000 cpm/tube; NEN) and antibody (final dilution: 1:120000; kindly provided by prof. G. Ciabattoni), in a volume of 1.5 ml of 0.025 M phosphate buffer. Free and antibody-bound prostaglandins were separated by the addition of 100 µl 5% bovine serum albumin and 100 µl 3%

charcoal suspension, followed by centrifuging for 10 min at 4000xg at 5°C and decanting off the supernatants into scintillation fluid (Ultima Gold™, Perkin Elmer) for β emission counting. Sensitivity of the assay was 2 pg/ml; ED_{50} was 20 pg/ml. The PGE_2 production was expressed as picograms per ml.

ROS generation

ROS generation was assessed using a ROS-sensitive fluorescence indicator, DCFH-DA. When DCFH-DA is introduced to viable cells, it can penetrate the cell and become deacetylated by intracellular esterases to form 2',7'-dichlorodihydrofluorescein (DCFH), which can react quantitatively with ROS within the cell, and be converted to 2',7'-dichlorofluorescein (DCF), which is detected by a fluorescence spectrophotometer. To determine intracellular effects on ROS production, macrophages were seeded in a black 96-well plate ($2.0x10^4$ cells/well) in medium containing scalar concentration of extracts. Cells were treated with samples for 24 h and then stimulated with LPS. After cell incubation with DCFH-DA (20 μM) for 30 min, the fluorescence intensity was measured at an excitation wavelength of 485 nm and an emission wavelength of 530 nm, using a fluorescence microplate reader (22, 23).

Statistical analysis

Experiments were performed in triplicate. Data were calculated as means ± S.E.M. and evaluated by performing analysis of variance (ANOVA) followed by post-hoc Newman-Keuls multiple comparison test (Software GraphPad, Prism, version 5.01).

The differences were considered significant if the probability was associated with $p<0.05$.

RESULTS

Cell viability

MTT test revealed no significant effects of extracts on cell viability up to 250μg/ml (data not shown). In order to exclude possible interferences, a maximum dose of 150μg/ml was chosen for biochemical assays.

Oxidative stress

The effects of extracts on PGE_2 and ROS production are reported in Figs. 1 and 2, respectively. Pretreatment with extracts significantly reduced the release of ROS and PGE_2, but only at the higher tested dose, compare to control. LPS supplementation induced a marked increase of both ROS and PGE_2.

Pre-incubation of cells for 24 h with extracts increased cell resistance to LPS stimulation as revealed by marked and significant reduction of ROS and PGE_2 production compared to the LPS group alone. The effect is more consistent on PGE_2 release. Furthermore, ROS production was significantly reduced.

Cytokines

Macrophage incubation with Imoviral™ induced different modulating effects on basal cytokine production (Figs. 3-5). At all tested doses, the extract mixture induced a marked IL-6 gene expression, while TNF-α was significantly inhibited. In contrast, the extract mixture did not exert evident effects on IL-8 expression.

LPS induced a marked increase of all tested cytokines; on the other hand, Imoviral™ pre-incubation blunted this effect. Pre-treatment with extracts reduced the TNF-α gene expression induced by LPS. The effects of mixture pretreatment were more evident on LPS-induced IL-8 production. Also, IL-6 was significantly inhibited compared to the LPS

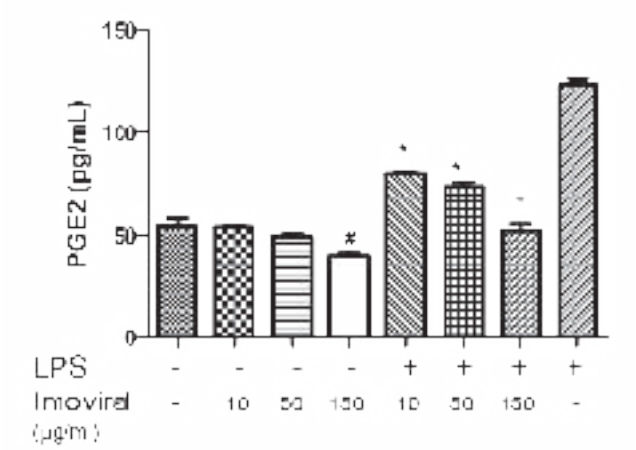

Fig. 1. *PGE_2 production on macrophage treated with herbal extract mixture. Data represent means ±S.E.M. of at least three experiments performed in triplicate. Results were analyzed by analysis of variance (ANOVA) followed by Newman-Keuls comparison multiple test. ANOVA $P<0.01$, $^{\#}P<0.01$ vs CTR; ANOVA $P<0.0001$, $*P<0.001$ vs LPS.*

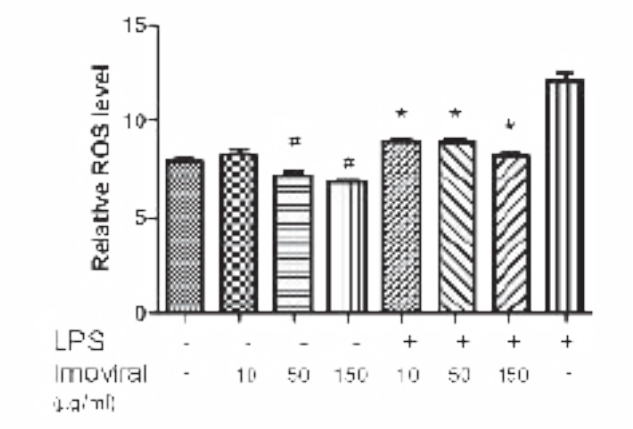

Fig. 2. *ROS production on macrophage treated with herbal extract mixture. Data represent means ±S.E.M. of at least three experiments performed in triplicate. Results were analyzed by analysis of variance (ANOVA) followed by Newman-Keuls comparison multiple test. ANOVA P<0.0001, #P<0.05 vs CTR; ANOVA P<0.0001, *P<0.001 vs LPS.*

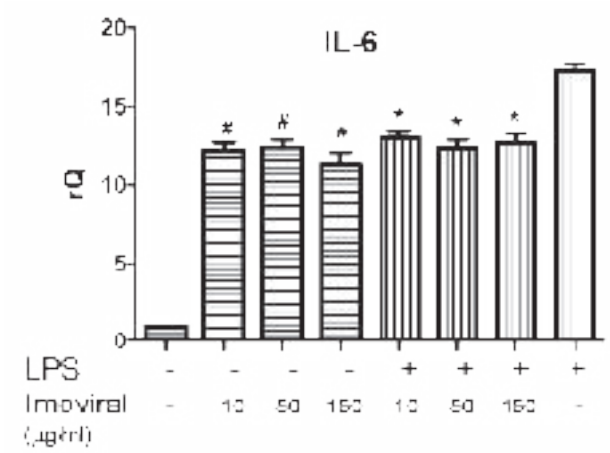

Fig. 3. *Relative gene expression of IL-6, determined by real-time RT PCR, on macrophages treated with herbal extract mixture. Data were calculated using the $2^{-\Delta\Delta Ct}$ method; they were normalized to HPRT1 mRNA levels and then expressed as relative to control group (calibrator sample, defined as 1.00). Values represent the means ± S.E.M. Results were analyzed by analysis of variance (ANOVA) followed by Newman-Keuls comparison multiple test. ANOVA P<0.0001, #P<0.001 vs CTR; ANOVA P<0.01, *P<0.05 vs LPS.*

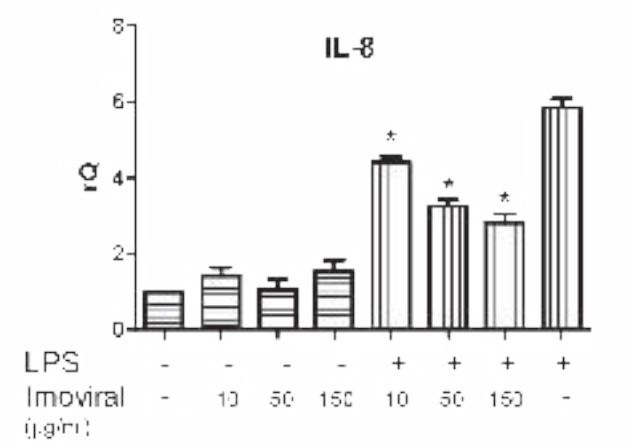

Fig. 4. *Relative gene expression of IL-8, determined by real-time RT PCR, on macrophages treated with herbal extract mixture. Data were calculated using the $2^{-\Delta\Delta Ct}$ method; they were normalized to HPRT1 mRNA levels and then expressed as relative to control group (calibrator sample, defined as 1.00). Values represent the means ± S.E.M. Results were analyzed by analysis of variance (ANOVA) followed by Newman-Keuls comparison multiple test. ANOVA P<0.0001, *P<0.001 vs LPS.*

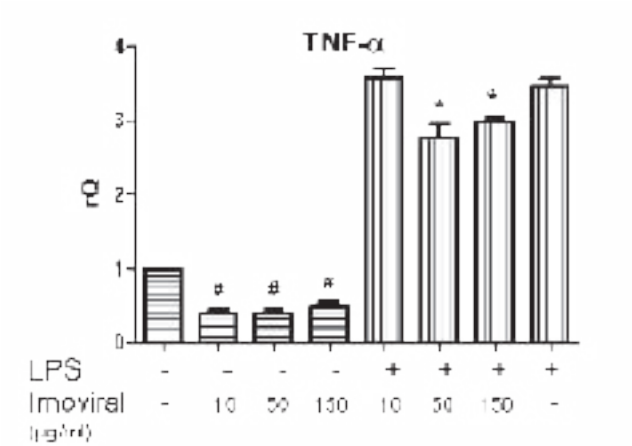

Fig. 5. *Relative gene expression of TNFα, determined by real-time RT PCR, on macrophages treated with herbal extract mixture. Data were calculated using the $2^{-\Delta\Delta Ct}$ method; they were normalized to HPRT1 mRNA levels and then expressed as relative to control group (calibrator sample, defined as 1.00). Values represent the means ± S.E.M. Results were analyzed by analysis of variance (ANOVA) followed by Newman-Keuls comparison multiple test. ANOVA P<0.001, #P<0.001 vs CTR; ANOVA P<0.01, *P<0.05 vs LPS.*

group.

DISCUSSION

The involvement of oxidative stress in degenerative processes, aging and immune response is well established. Macrophages play a pivotal role in modulating innate and adaptive immune response. Activated by external stimuli, they are able to

release pro-inflammatory cytokines, chemokines and cytotoxicity factors, such as ROS and PGE_2.

The involvement of each component of Imoviral™ herbal formula on oxidative stress is well documented. Lentinan, the active fraction of shiitake, demonstrated a protective role against hydrogen peroxide toxicity as well as modulatory activity on LPS-induced immune response (24, 25). The *in vitro* antitumor activity of uncaria extract is closely connected with antioxidant properties of this plant (26). Blackcurrant extract is a well known strong antioxidant, as demonstrated in chemical assays and in cellular models. Experimental data report scavenging properties, with no cell toxicity, and inhibitory activity on ROS production on different cell lines (27).

We can speculate that the effects of Imoviral™ on PGE_2 and ROS production that we found could be related to concomitance of different mechanisms, such as direct radical scavenging activity, inhibition of radical production and increased activity of detoxifying enzymes.

IL-6 is a multifunction cytokine involved in physiology and inflammation. It can stimulate synthesis of acute phase proteins, B cell maturation in antibody-producing plasma cells and T-cell activation and differentiation, with systemic or local effects, particularly focused on liver and the central nervous system (CNS). IL-6 can be regarded as a modulator of inflammation, regulating cytokine synthesis, particularly IL-2 and TNF-α (28).

TNF-α is a typical pro-inflammatory cytokine produced by monocytes and macrophages that acts as a modulator of immune response. Activated by different stimuli, it induces fever via increased PGE_2 synthesis by the vascular endothelium of the hypothalamus, or through increased IL-1 production. TNF-α is also induced by IL-6 in the acute phase and further stimulates IL-6 production in several cell types. On the other hand, an anti-inflammatory effect of IL-6 has been reported, possibly related to the inhibition of TNF-α production, providing a negative feedback loop to limit the acute inflammatory response (28, 29).

IL-8 is a pro-inflammatory cytokine involved in acute-phase reaction and showing chemotactic effects. It is responsible for migration and activation of neutrophils and other cell types (such as monocytes, lymphocytes, basophils, eosinophils and granulocytes) at sites of inflammation, and its activation can be instigated by TNF-α (28).

We found that in basal conditions Imoviral™ treatment did not affect IL-8 mRNA levels, while a significant decrease in TNF-α gene expression was observed that could be, at least in part, related to a marked increase of IL-6 gene expression. The present data highlight the dual role of IL-6 on inflammation acting either as an activator of inflammatory cascade or an anti-inflammatory agent, due to the negative feedback action on TNF-α gene expression (29).

As expected, after LPS pretreatment, a condition simulating bacterial challenge, an evident induction of cytokine gene expression was observed, and the tested natural mixture showed a modulatory role on cytokine gene expression, which is consistent with previous works on its immune system effects (30). We can speculate that the reduction of LPS-induced TNF-α and IL-8 production could be, at least in part, related to the modulator feedback effects of IL-6.

Our *in vitro* results confirm the effects of Imoviral™ extract mixture on the immune response, particularly on macrophage, during bacterial attack, modulating both the oxidative stress markers and the cytokine gene expression.

REFRENCES

1. Ernst E. Prevalence of use of complementary/ alternative medicine: a systematic review. Bull World Health Organ 2000; 78:252-7.
2. Spelman K, Burns J, Nichols D, Winters N, Ottersberg S, Tenborg M. Modulation of cytokine expression by traditional medicines: a review of herbal immunomodulators. Altern Med Rev 2006; 11:128-50.
3. Biswas SK, Sica A, Lewis CE. Plasticity of macrophage function during tumor progression: regulation by distinct molecular mechanisms, J Immunol 2008; 180:2011-17.
4. Heo SK, Yun HJ, Noh EK, Park WH, Park SD. LPS induces inflammatory responses in human aortic vascular smooth muscle cells via Toll-like receptor 4 expression and nitric oxide production. Immunol Lett 2008; 120:57-64.
5. Crofford LJ, Lipsky PE, Brooks P, Abramson SB,

Simon LS, van de Putte LB. Basic biology and clinical application of specific cyclooxygenase-2 inhibitors. Arthritis Rheum 2000; 43:4-13.

6. Wu SJ, Ng LT. Tetrandrine inhibits pro-inflammatory cytokines, iNOS and COX-2 expression in human monocytic cells. Biol Pharm Bull 2007; 30:59-62.
7. Kim MS, Yi JM, Kim SH, Hong SH, Kim HM. Madimadi, Korean folk medicine, blocks TNF--alpha, IL-1beta, and IL-8 production by activated human immune cells. Cytokine 2004; 25:179-86.
8. Plaeger SF. Clinical immunology and traditional herbal medicines. Clin Diag Lab Med 2003; 10:337-8.
9. Menghini L, Leporini L, Scanu N, et al. A multiherbal formulation influencing immune response *in vitro*. Minerva Med 2012; 103:13-21.
10. Kim DO, Lee KW, Lee HJ, Lee CY. Vitamin C equivalent antioxidant capacity (VCEAC) of phenolic phytochemicals. J Agric Food Chem 2002; 50:3713-7.
11. Eberhardt MV, Lee CY, Liu RH. Antioxidant activity of fresh apples. Nature 2000; 405:903-4.
12. Heitzman ME, Neto CC, Winiarz E, Vaisberg AJ, Hammond GB. Ethnobotany, phytochemistry and pharmacology of Uncaria (Rubiaceae). Phytochemistry 2005; 66:5-29.
13. Lemaire I, Assinewe V, Cano P, Awang DVC, Arnason JT. Stimulation of interleukin-1 and -6 production in alveolar macrophages by the neotropical liana, *Uncaria tomentosa* (Uña de Gato). J Ethnopharmacol 1999; 64:109-15.
14. Bisen PS, Baghel RK, Sanodiya BS, Thakur GS, Prasad GBKS. Lentinus edodes: A Macrofungus with Pharmacological Activities. Curr Med Chem 2010; 17:2419-30.
15. Takata R, Yamamoto R, Yanai T, Konno T, Okubo T. Immunostimulatory effects of a polysaccharide-rich substance with antitumor activity isolated from black currant (*Ribes nigrum* L.). Biosci Biotechnol Biochem 2005; 69:2042-50.
16. Garbacki N, Tits M, Angenot L, Damas J. Inhibitory effects of proanthocyanidins from *Ribes nigrum* leaves on carrageenin acute inflammatory reactions induced in rats. BMC Pharmacol 2004; 4:25.
17. Sintiprungrat K, Singhto N, Sinchaikul S, Chen ST, Thongboonkerd V. Alterations in cellular proteome and secretome upon differentiation from monocyte to macrophage by treatment with phorbol myristate acetate: insights into biological processes. J Proteomics 2010; 73:602-18.
18. Menghini L, Leporini L, Scanu N, Pintore G, La Rovere R, Di Filippo ES, Pietrangelo T, Fulle S. Effect of phytochemical concentrations on biological activities of cranberry extracts. J Biol Regul Homeost Agents 2011; 25:27-35.
19. Chiavaroli A, La VD, Orlando G, Menghini L, Epifano F, Grenier D. *Rhamnus alpinus* leaf extract suppresses lipopolysaccharide-induced, monocyte-derived macrophage chemokine. Inflammation 2008; 31:313-8.
20. Livak KJ, Schmittgen TD. Analysis of relative gene expression data using real-time quantitative PCR and the 2(-Delta Delta C(T)) Method. Methods 2001; 25:402-8.
21. Menghini L, Genovese S, Epifano F, Tirillini B, Ferrante C, Leporini L. Antiproliferative, protective and antioxidant effects of artichoke, dandelion, turmeric and rosemary extracts and their formulation. Int J Immunopathol Pharmacol 2010; 23:601-10.
22. Lebel CP, Bondy SC. Sensitive and rapid quantitation of oxygen reactive species formation in rat synaptosomes. Neurochem Int 1990; 17:435-40.
23. Heo SK, Ju SA, Lee SC, Park SM, Choe SY, Kwon B, Kwon BS, Kim BS. Light enhances the bactericidal activity of human monocytes and neutrophils via HVEM. J Leukoc Biol 2006; 79: 330-8.
24. Kuppusamy UR, Chong YL, Mahmood AA, Indran M, Abdullah N, Vikineswary S. *Lentinula edodes* (shiitake) mushroom extract protects against hydrogen peroxide induced cytotoxicty in peripheral blood mononuclear cells. Indian J Biochem Biophys 2009; 46:161-5.
25. Djordjevic B, Škugor S, Jørgensen SM, Øverland M, Mydland LT, Krasnov A. Modulation of splenic immune responses to bacterial lipopolysaccharide in rainbow trout (*Oncorhynchus mykiss*) fed lentinan, a beta-glucan from mushroom *Lentinula edodes*. Fish Shellfish Immunol 2009; 26:201-9.
26. Dreifuss AA, Bastos-Pereira AL, Avila TV, Soley BdA S, Rivero AJ, Aguilar JL, Acco A. Antitumoral and antioxidant effects of a hydroalcoholic extract of cat's claw (*Uncaria tomentosa*) (Willd. ex Roem. & Schult) in an *in vivo* carcinosarcoma model. J

Ethnopharmacol 2010; 130:127-33.
27. Tabart J, Franck T, Kevers C, Pincemail J, Serteyn D, Defraigne JO, Dommes J. Antioxidant and anti-inflammatory activities of *Ribes nigrum* extracts. Food Chemistry 2012; 131:1116-22.
28. Feghali CA, Wright TM. Cytokines in acute and chronic inflammation. Front Biosci 1997; 2:12-26.
29. Starkie R, Ostrowiski SR, Jauffred S, Febbraio M, Pedersen BK. Exercise and IL-6 infusion inhibit endotoxin-induced TNF-alpha production in humans. FASEB J 2003; 17:884-6.
30. Spelman K, Burns J, Nichols D, Winters N, Ottersberg S, Tenborg M. Modulation of cytokine expression by traditional medicines: a review of herbal immunomodulators. Altern Med Rev 2006; 11:128-50.

LETTER TO THE EDITOR

SARCOID-LIKE PATTERN IN A PATIENT WITH TUBERCULOSIS

A.A. CHOKOEVA[1], G. TCHERNEV[2], C. TANA[3,4], J. ANANIEV[5] and U. WOLLINA[6]

[1]Onkoderma- Policlinic for Dermatology and Dermatologic Surgery, General Skobelev 26, Sofia, Bulgaria; [2]Policlinic for Dermatology and Venereology, Saint Kliment Ohridski University, Medical Faculty, University Hospital Lozenetz, Sofia, Bulgaria; [3]Internal Medicine Unit, Guastalla Hospital, AUSL Reggio Emilia, Italy; [4]Unit of Internistic Ultrasound, Department of Medicine and Science of Aging, "G. d'Annunzio" University, Chieti, Italy; [5]Department of General and Clinical Pathology, Medical Faculty, Trakia University, Stara Zagora, Bulgaria; [6]Department of Dermatology and Allergology, Dresden Hospital and Friedrichstadt Academic Teaching Hospital of the Technical University of Dresden, Germany

Received October 24, 2014 – Accepted December 9, 2014

The first three authors equally contributed to this work

For several decades the "mystery" of sarcoidosis has continued to evade revelation. Nowadays, due to medical progress and the opportunity of performing highly specialized tests which assist the identification of this condition as a separate disease, the understanding of the eternal mystery appears closer. Nevertheless, many contemporary studies focus on the putative link between sarcoidosis and infectious antigens isolated from skin lesions. On the other hand, a golden rule to differentiate sarcoidosis from other conditions such as tuberculosis and sarcoid-like reactions is the sterility of granulomas. However, there are hypotheses which state that sarcoidosis could be related to tuberculosis and, in particular, to the Mycobacterium species. The similarities that many authors identify between the genetic signatures of the two conditions definitely raise concerns regarding: i) the inability to categorize every single case in a clear-cut way, namely in inflammatory/autoimmune or infectious; ii) the need of new criteria to clearly differentiate sarcoid-type reactions in the context of infectious diseases from sarcoidosis as an autonomous disease. We report the case of a 35-year-old male patient with histopathological evidence of sarcoid-like granulomas in cutaneous lesions on the face and imaging studies consistent with a systemic form of sarcoidosis. However, a positive QuantiFERON-TB Gold test and Ziehl-Neelsen staining was found, leading to the diagnosis of a rare case of TBC with histopathological evidence of sarcoid-like lesions. The following are also discussed: i) the potential role of tuberculosis antigens in the context of occult tuberculosis as generators of sarcoid-type of reaction; and ii) the necessity of additional diagnostic panels as a standard procedure in patients with suspected sarcoid granulomas of unknown origin.

Sarcoidosis can be defined as a granulomatous disease the histopathological substrate of which is the sterile epitelioid cell granuloma (1-4). The etiology still remains unknown, and Scadding et al. previously

Key words: sarcoidosis, tuberculosis, PCR, histopathology, infection

Mailing address: Assoc. Prof. Georgi Tchernev,
Policlinic for Dermatology and Venereology,
Saint Kliment Ohridski University,
Medical Faculty, University Hospital Lozenetz
Koziak street 1, 1407 Sofia, Bulgaria
Tel.: +359 885 588 424
e-mail: georgi_tchernev@yahoo.de

0393-974X (2014)

DISCLOSURE: ALL AUTHORS REPORT NO CONFLICTS OF INTEREST RELEVANT TO THIS ARTICLE.

emphasized the importance of the pathological features in the diagnosis of sarcoidosis (5). In their investigations these authors repeatedly focused their attention on the "sterility of sarcoid granulomas" and asserted that "sarcoidosis is a diagnosis of exclusion, in which no evidence for the presence of mycobacteria or any other organism exists"(5, 6). Many years later, however, several studies found new essential pieces in the eternal puzzle called "sarcoidosis" (7-9). In parallel with them, the focus shifted in searching for a connection between sarcoidosis and mycobacteria, propionibacteria and other immunogenic antigens isolated from sarcoid lesions. Thus, the paradigm of "the sterility of sarcoid granuloma" is displaced by theories that establish a possible relationship between these infectious agents (or their antigens) with sarcoidosis (10, 11).

We present the rare case of a patient with histologically proven epithelioid cell granulomas from cutaneous lesions, in the context of suspected systemic sarcoidosis and positive quantiferon gold test.

Case report

A 35-year-old male patient was admitted to the Lozenets University Hospital for evaluation of cutaneous lesions of the face, namely on the nose, cheeks and forehead, with a duration of 5-6 years, with recent changes in shape, size and color. There were no subjective symptoms related to the lesions. Recurrent infections of the upper respiratory tract (bronchitis, pharyngitis) were also reported in the last 5-6 years, without evidence of weight loss, fever or night sweats. Simultaneously with these complaints, the patient presented with bilaterally enlarged cervical lymph nodes for about one year, which failed to respond to several courses of antibiotic treatment, the last one about 3 weeks prior to hospitalization.

Clinical examination

Five to six erythematous plaques were identified with a non-symmetrical distribution predominantly on the central face (Fig. 1a). The plaques varied in size (Fig. 1b) and had a dark-brownish center with

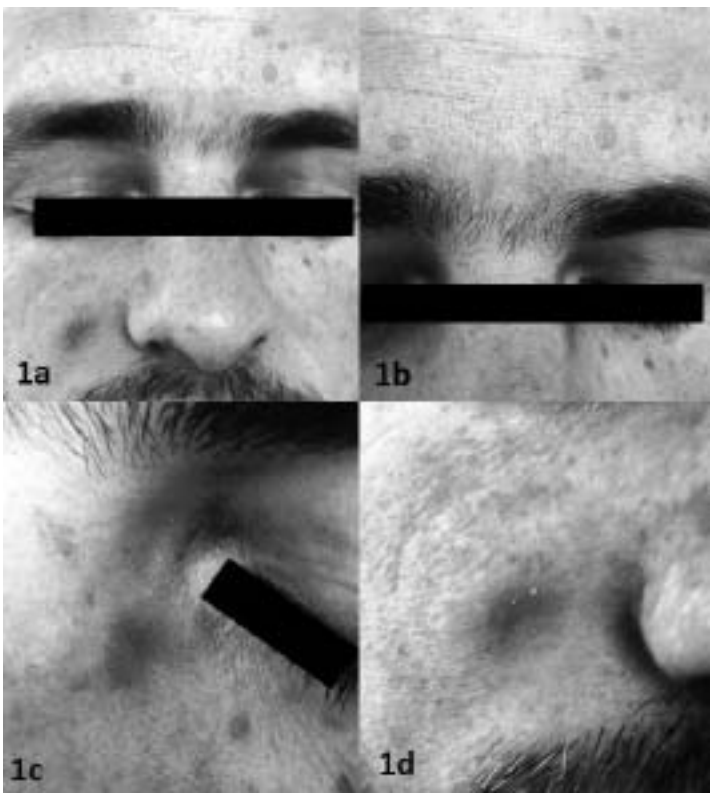

Fig. 1. ***a)*** *Asymmetrical erythematous plaques, located on the central face.* ***b,c,d)*** *Moderately infiltrated plaques of various sizes.* ***c,d)*** *Plaques unevenly colored, with a darker brownish center, lighter erythemous periphery and mild scaling.*

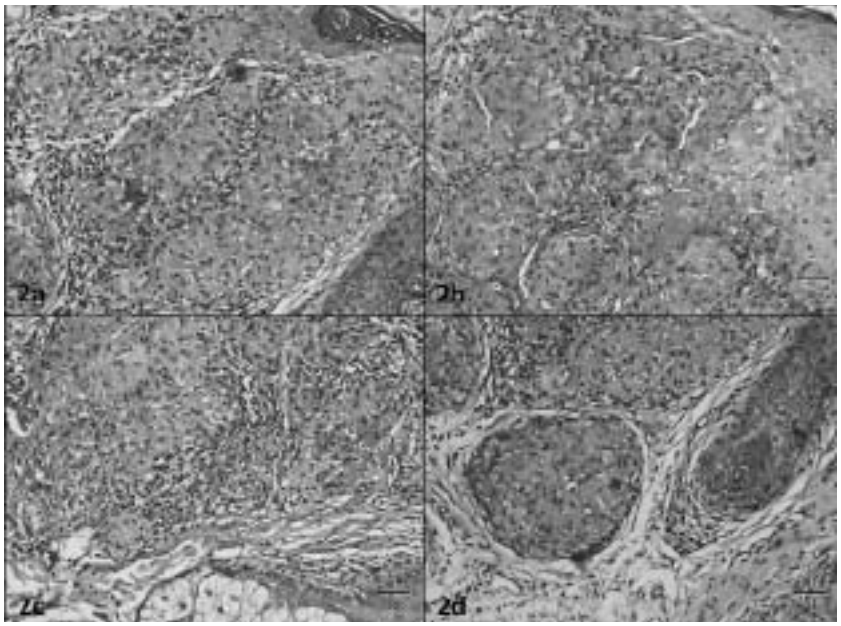

Fig. 2. ***a,b)*** *Histopathological findings of the cutaneous lesions: epidermal hyperplasia - acanthosis, focal hyper- and parakeratosis, hypergranulosis.* ***c,d)*** *Epithelioid cell granulomas forming focal aggregates in the dermis. Centrally located zones of irregular-shaped necrosis with Langhans cells present in some. Peripheral, irregularly distributed lymphocytes in all granulomas.*

a slightly erythematous periphery and mild scaling (Fig. 1c, d). Apple jelly-phenomenon was positive.

Bilateral cervical lymphadenomegaly, with nodes of 2 x 2 cm in size, was present. The nodes were non-adherent and painless. A single enlarged occipital lymph node of 1.5 x 1.5 cm was also found.

Cardiac and respiratory examination was not significant. Mild splenomegaly and hepatomegaly was noted.

Laboratory tests

Laboratory analysis of blood, biochemistry, glucose and urine were within normal range.

Parasitological evaluation for toxoplasmosis was negative (IgG, IgM), as were the virological tests for EBV and HBV/HCV (anti HBc-total, anti HBs, anti HCV). Interferon gamma releasing assay (QuantiFERON Gold) was positive.

Imaging investigation

Chest X-ray revealed enlarged hilar opacities, thickened bronchial walls and bilateral micronodular opacities located in the middle and the lower lung lobes, more pronounced on the right site, considered as a response to the resolving broncho-alveolar inflammation. No significant abnormalities of the cardiac silhouette were found.

CT identified diffuse lymphadenomegaly on both sides of the diaphragm. Multiple nodular lesions were observed in the lung parenchyma bilaterally, as well as nodular changes on the pleura. Mild and even interstitial reaction was present bilaterally. Enlarged lymph nodes were found also in both supraclavicular areas, axillas and on both sides of the trachea and hilus. No pleural effusions or pericardial changes were detected. In addition to the increased size of the spleen and liver, enlarged lymph nodes were also seen in their hilar regions. Enlarged lymph nodes from the celiac group were also present. No free fluid in the abdomen was found.

Abdominal ultrasound revealed slightly enlarged liver and spleen, extending approximately 2 cm beyond the rib arc, both hyper-echoic with homogeneous structure. The right kidney was normal in size, with presence of 2 concretions, 8-10 mm in size. Left kidney was also of normal size with 5-6 concretions of 5-10 mm in size.

Histological examination of the cutaneous lesions revealed acanthosis, focal hyperkeratosis, parakeratosis and hypergranulosis. (Fig. 2 a,b).

Epithelioid cell granulomas forming focal aggregates were found in the dermis (Fig. 2c). Centrally located zones of irregularly shaped minimal necrosis were seen in some of the granulomas. Only two of the granulomas contained Langhans-type giant cells, while peripheral, irregularly distributed lymphocytes were found in all of them. Rarely, peripheral vascular ectasia was observed (Figs. 2c,d).

DISCUSSION

Various studies detected nucleic acids and insoluble proteins from mycobacteria in sarcoid lesions, as well as specific T-cell immune responses to mycobacterial antigens (12, 13). One study established that even though the sarcoidosis gene expression signature is similar to TB, it is not identical. The authors suggest a role of TB-like immune response, rather than an infection per se, but only in some of the individuals who develop sarcoidosis (14). On one hand, this raises the question of how is it possible that two different conditions share a similar genetic signature, but not in all of the cases. On the other hand, infectious antigens were detected in sarcoid lesions in some cases, while the majority of the lesions remained sterile with the methods available for detection of infectious agents.

Thus, we are probably considering two different conditions: on the one hand sarcoidosis, and on the other sarcoid-like reactions as a response to immunogenic antigens that may be infectious or non-infectious. But regarding the cases of sarcoidosis, does that mean that predisposed individuals could respond to different antigens, or are they predisposed to develop sarcoidosis as an autonomous disease due to cross-reactivity with consequent development of a specific sarcoid-like reaction? Unfortunately, to date a more detailed differentiation between the genetic signature of sarcoidosis and sarcoid-like reactions has not yet been established (4).

Almost 30 years after Scadding's studies, many questions found their answer but many others have been raised. Keeping in mind the current knowledge, we report the case of a patient with suspected sarcoidosis with concomitant tuberculosis, and ask: is it possible?

We are considering a patient with suspected cutaneous sarcoidosis associated with a positive Quantiferon test, in which the pulmonary findings could correspond to either sarcoidosis or tuberculosis. Current diagnostic criteria of cutaneous sarcoidosis appear insufficient to differentiate it from sarcoid-type reactions to specific antigens (1, 4). As we already mentioned, as a rule, the sarcoid granuloma should be sterile, without evidence of infectious antigens (1-4), and the so-called naked sarcoidal granulomas (NSGs) are the characteristic histologic finding in sarcoidosis (16).

According to a study of 28 sarcoidosis specimens, classic NSGs were identified in 25 biopsies, as in four biopsies tuberculoid granulomas were seen, two with neutrophils suggesting infection (16). As additional histologic findings, birefringent foreign material was established in 14 biopsies (50%), as well as focal necrosis in 43%, elastophagocytosis in 39%, linear peri-neural granulomas resembling leprosy in 25%, increased dermal mucin in 18%, and lichenoid inflammation in 14% (16). The clinical presentation of the lesions suggested sarcoidosis in all but three of the cases (16). This clearly demonstrates that neither clinical presentation nor histologic evaluation alone can be considered enough to confirm the diagnosis of sarcoidosis. The epithelioid cell granuloma is not equivalent to sarcoidosis as it can be observed in numerous infectious and non-infectious disorders, and even in association with neoplastic diseases (3).

On the one hand, the absence of additional investigations could easily lead to misdiagnosis of leprosy, syphilis, other infectious granulomas, rosacea, granuloma annulare, necrobiosis lipoidica, and foreign body reaction, according to the reported cases (16). On the other, are we observing sarcoidosis or sarcoid-like reactions in general?

It has been reported that sarcoidosis and tuberculosis can very rarely occur simultaneously, but only few reports provided evidence of sterile granulomas by PCR analysis (2, 17). It seems that most of these combined cases should be considered as sarcoid-like reactions as a response to a specific disease (1, 4).

The understanding of the genetic signature of sarcoidosis as an autonomous disease could be helpful for the differentiation from these conditions (1, 4). However, it appears that gene expression profiles could be indicative of a persistent activation

of the immune system and chronic inflammatory pathology in active TB (12). According to a study by Maertzdorf et al. "definition of a biosignature with unique specificity for TB demands that identified profiles can differentiate diseases with similar pathology, like sarcoidosis". Their analysis revealed that "gene expression signatures in TB show highly similar patterns in sarcoidosis, with a common up-regulation of proinflammatory pathways and IFN signaling and close similarity to TB-related signatures" (12).

It was also demonstrated that "microRNA expression presented a highly similar pattern in both diseases, whereas cytokines in the serum of TB patients revealed a slightly elevated proinflammatory pattern compared with SARC [sarcoidosis] and controls" (12). An increased metabolic activity and significantly higher antimicrobial defense responses in TB is indicated to be one of the main differences between the two conditions, according to the same study, as well as overexpression of the gene matrix metallopeptidase 14, identified as the most distinctive marker of sarcoidosis (12).

CONCLUSION

This case has demonstrated the importance of additional diagnostic panels to avoid a misdiagnosis of sarcoidosis or sarcoid-like reactions alone. Indeed, a positive QuantiFERON-TB Gold test and Ziehl-Neelsen staining was found, leading to the diagnosis of a rare case of TBC with sarcoid appearance histopathologically.

Although highly similar, the genetic signatures of TB and sarcoidosis are not the same. However, at the current state of knowledge they would not be enough to differentiate between sarcoidosis and a sarcoid-like reaction in the present case.

Further investigations are still needed regarding the degree to which MMP14 is associated to or expressed in patients with sarcoid-like reactions. Considering the present case and other similar cases, this distinction would be of great value in the diagnosis and management of such patients.

REFERENCES

1. Tchernev G, Cardoso JC, Chokoeva AA, et al. The "mystery" of cutaneous sarcoidosis: facts and controversies. Int J Immunopathol Pharmacol 2014; 27(3):321-30.
2. Ahmad K, Powell FC. Cutaneous sarcoidal reaction in a patient with pulmonary tuberculosis. Ir Med J 2005; 98(6):182.
3. Tchernev G. Cutaneous sarcoidosis: the "great imitator": etiopathogenesis, morphology, differential diagnosis, and clinical management. Am J Clin Dermatol 2006; (6):375-82.
4. Tchernev G, Tana C, Schiavone C, Cardoso JC, Ananiev J, Wollina U. Sarcoidosis vs. sarcoid-like reactions: the two sides of the same coin? Wien Med Wochenschr 2014; 164(13-14):247-59.
5. Scadding JG, Mitchell D. Sarcoidosis, 2nd Edn. London, Chapman and Hall 1985; pp. 36–42.
6. Scadding JG. Prognosis of intrathoracic sarcoidosis in England. A review of 136 cases after five years' observation. Br Med J 1961; 2(5261):1165-72.
7. Bandyopadhyay D, Panchabhai TS, Mehta AC. Mycobacterium and sarcoidosis: Old wine in a new bottle. Lung India 2014; (3):205-7.
8. Tchernev G, Patterson JW, Nenoff P, Horn LC. Sarcoidosis of the skin--a dermatological puzzle: important differential diagnostic aspects and guidelines for clinical and histopathological recognition. J Eur Acad Dermatol Venereol 2010; (2):125-37.
9. Tana C, Giamberardino MA, Di Gioacchino M, Mezzetti A, Schiavone C. Immunopathogenesis of sarcoidosis and risk of malignancy: a lost truth? Int J Immunopathol Pharmacol 2013; 26(2):305-13.
10. Hance AJ. The role of mycobacteria in the pathogenesis of sarcoidosis. Semin Respir Infect 1998; 13(3):197-205
11. Yamada T, Eishi Y, Ikeda S, et al. In situ localization of *Propionibacterium acnes* DNA in lymph nodes from sarcoidosis patients by signal amplification with catalysed reporter deposition. J Pathol 2002; 198:541-7.
12. Maertzdorf J, Weiner J 3rd, Mollenkopf HJ, TBornotTB Network, Bauer T, Prasse A, Müller-Quernheim J, Kaufmann SH. Common patterns and disease-related signatures in tuberculosis and sarcoidosis. Proc Natl Acad Sci USA 2011; 109(20):7853-8.
13. Dubaniewicz A, Trzonkowski P, Dubaniewicz-Wybieralska M, Dubaniewicz A, Singh M, Myśliwski A. Comparative analysis of mycobacterial heat

shock proteins-induced apoptosis of peripheral blood mononuclear cells in sarcoidosis and tuberculosis. J Clin Immunol 2006; 26(3):243-50.

14. Dubaniewicz A, Dubaniewicz-Wybieralska M, Sternau A, et al. *Mycobacterium tuberculosis* complex and mycobacterial heat shock proteins in lymph node tissue from patients with pulmonary sarcoidosis. J Clin Microbiol 2006; 44(9):3448-51.
15. Koth LL, Solberg OD, Peng JC, Bhakta NR, Nguyen CP, Woodruff PG. Sarcoidosis blood transcriptome reflects lung inflammation and overlaps with tuberculosis. Am J Respir Crit Care Med 2011; 184(10):1153-63.
16. Ball NJ, Kho GT, Martinka M. The histologic spectrum of cutaneous sarcoidosis: a study of twenty-eight cases. J Cutan Pathol 2004; 31(2):160-8.
17. van Enschot JWT, van Balkom RHH. Sarcoidosis following *Mycobacterium tuberculosis* infection: Coincidence or consequence? Respir Med Case Rep 2013; 9(1):11-4.

LETTER TO THE EDITOR

MACROPHAGES AND DENDRITIC CELLS IN THE DEVELOPMENT OF LIVER INJURY LEADING TO LIVER FAILURE

J. ANANIEV[1], M. PENKOVA[2], G. TCHERNEV[3], A.A. CHOKOEVA[4], S. PHILIPOV[5], C. TANA[6], M. GULUBOVA[1] and U. WOLLINA[7]

[1]Department of General and Clinical Pathology and Forensic Medicine, Medical Faculty, Trakia University, Stara Zagora, Bulgaria; [2]Department of Internal medicine, Medical Faculty, Trakia University, Stara Zagora, Bulgaria; [3]Polyclinic for Dermatology and Venereology, Medical Faculty, University Hospital Lozenetz, Sofia University, Sofia, Bulgaria; [4]Onkoderma- Policlinic for Dermatology and Dermatologic Surgery, General Skobelev 26 Sofia, Bulgaria; [5]Department of General and Clinical Pathology, Medical Faculty, "Saint Kliment Ohridski University", Sofia, Bulgaria; [6]Unit of Internistic Ultrasound, Department of Medicine and Science of Aging, "G. d'Annunzio" University, Chieti, Italy; [7]Department of Dermatology and Allergology, Academic Teaching Hospital, Dresden-Friedrichstadt, Dresden, Germany

Received August 25, 2014 – Accepted September 30, 2014

Liver failure (LF) continues to be a serious problem due to different underlying disorders. Not only hepatocytes but Kupffer cells (KCs) and dendritic cells (DCs) are of importance in this instance. We wanted to investigate the possible role of KCs and liver DCs in the development of liver injury in patients with liver failure. Liver specimens from 23 patients who died after liver failure were examined for the presence and distribution of CD68-positive KCs and CD83-positive DCs by immunohistochemistry. The distribution of the CD83-positive DC in the sinusoidal and the periportal spaces was not even. While 39.1% of patients had a high sinusoidal density of CD83-positive cells, 60.9% demonstrated a high density of CD83-positive cells in the periportal tract. The number of CD83-positive DCs in periportal tracts in patients with advanced liver fibrosis (n = 5) were high, while those with mild liver fibrosis (n = 18) had low numbers of mature dendritic cells ($\chi 2=4.107$; p=0.043). In addition, all patients with intensive fibrosis had low counts of CD68-positive KC's in portal tracts *vs* patients with mild fibrosis of which 67% had high counts ($\chi 2=6.97$; p=0.008). In seven of the patients with moderate steatosis (87.5%) low numbers of CD68-positive KCs were found in sinusoids, in contrast to those with severe steatosis, where 12 patients (80%) had high KC counts ($\chi 2=13.4$; p<0.001). The distribution and number of CD68-positive KC and CD83-positive DC reflect the progression of liver fibrosis leading to liver failure.

Liver failure is defined by the American Association for the Study of Liver Diseases (AASLD) and the European Association for the Study of the Liver (EASL) as an "acute deterioration of pre-existing chronic liver disease usually related to a precipitating event and associated with

Key words: liver failure, Kupffer cells, dendritic cells

Mailing address: Prof. Georgi Tchernev,
Policlinic for Dermatology and Venereology,
Saint Kliment Ohridski University,
Medical Faculty, University Hospital Lozenetz,
Koziak street 1, 1407 Sofia, Bulgaria
Tel.: +359 885 588 424
e-mail: georgi_tchernev@yahoo.de

0393-974X (2014)

increased mortality at 3 months due to multisystem organ failure". Two features of liver damage are hyperbilirubinemia and coagulopathy. Risk factors for associated mortality include renal dysfunction and hepatic encephalopathy (1).

Various factors can lead to the development of hepatic insufficiency:

- viral infections (hepatitis A, B, C, D and E; coxsackie B; herpes simplex; varicella/ zoster; cytomegalovirus; measles, Epstein-Barr; Yellow fever);
- toxins (fungi, aflatoxins, cuprum, phosphorus; alcohol);
- medical drugs (antibiotics, anesthetics, hormones);
- others (Wilson's disease, autoimmune hepatitis etc.).

The importance of immune cells in the development of liver pathologies is well known. Dendritic cells (DCs), as antigen-representing cells, play a role in the initiation of immune response and its control with impact upon effector T-cells (2). Their activity and number may be affected by other factors such as the presence of infection or tissue damage (3). Mature DCs appear to be modulators of liver fibrosis, participating in the regulation of angiogenesis (4). DCs in the different phases of their development may exert variable effects on fibrogenesis (5, 6).

Kupffer cells (KCs) are a kind of specialized macrophages hosted in the liver tissue. They participate in immune response during chronic liver diseases as they are known to have pro- as well as antifibrogenic activity. Recently, considerable evidence for their participation in the development of fulminant hepatitis has been accumulated (7). With the help of experimental models it was found that KCs have immune modulating effects upon the inflammatory response realized by the pro-inflammatory cytokines and chemokines, such as tumor necrosis factor (TNF), interleukin-6 (IL-6), IL-1 etc. In this way they might influence T-lymphocytes, NK-cells, hepatocytes and, not the least, DC (8).

The aim of our investigation was to examine the distribution of KCs (CD68-positive cells) and mature liver DCs (CD83-positive) in the development of liver damage and to compare their presence with some clinical and morphological parameters in patients with liver failure as a result of viral hepatitis.

MATERIALS AND METHODS

Patients and materials

Autopsy material from 23 patients, who died in the University Hospital – Stara Zagora, was investigated. The group was composed of 14 men and 9 women, aged between 44 and 68 years (mean 59.2 years). The group of patients with liver failure was selected according to clinical, laboratory and morphological data.

All twenty-three patients suffered from chronic HBV or HCV infection. Liver failure was defined by the presence of hepatic encephalopathy, a change in the coagulation factors and monitoring of the cases less than 26 weeks to characterize as "acute liver failure". Some clinical and histological data for the patients were retrospectively collected (Table I). For the evaluation and staging of fibrosis and steatosis, it is important to know that scoring systems are not intended to replace the detailed, descriptive, pathology report, but we used the criteria published from Guido et al. (9). Steatosis is scored on a scale from 0 to 3, where: 0 = absent, 1 (mild) = ≤33%; 2 (moderate) = >33% to ≤ 66%; 3 (severe)= >66%, and fibrosis is assessed in more detail and the scale ranges from 0 to 6, making it more accurate in comparing paired biopsies. The system clearly distinguishes incomplete (i.e. "short" = scores 1 and 2) from complete septa formation, and keeps P-P and P-C septa separate. For our study and in relation to the number of the patients examined by us, we united three groups of fibrosis: no fibrosis, mild fibrosis and intensive fibrosis.

Permission to carry out the study was obtained from the hospital ethics committee.

Immunohistochemistry

Liver tissue specimens were processed for routine histology (staining with hematoxylin and eosin) and light microscopic immunohistochemistry. The samples were fixed in 10% formalin, included in paraffin and cut in 5-μm shears. After de-paraffination of the shears, the blocking of the endogenous peroxidase was accomplished according to the 5 minutes protocol with peroxidase blocking-agent. Three times jet washing with buffer was performed, followed by and incubation with initial antibody for 1 h. After washing three times, antibodies were incubated with marked polymer for 20 min and were washed again. In the last phase antibodies were incubated with DAB Substrate-chromogen, jet washed again and contra stained by hematoxylin of Mayer.

The following components were used for

immunohistochemical examination: antibodies - CD68 (M0718, DAKO, Denmark) diluted 1:100; CD83 (NCL-CD83, Leica Biosystems, UK) diluted 1:40; and detection system EnVision™ FLEX+, Mouse, High pH, (Link) (K8002, DAKO, Denmark). Immunohistochemical examination was accomplished according to manufacturers' instructions.

The number of CD68- and CD83-positive cells in the periportal spaces and sinusoidal was counted using 10 viewed fields and a magnification of 320, 0.74 mm^2 space.

Statistical analysis

The data received during the investigation were processed statistically by SPSS for Windows, Version 16 (SPSS, Inc., Chicago, IL, USA). Non-parametric analysis was made by Mann-Whitney U test. For comparison of the cell counts χ^2-test was used. Results $p<0.05$ were considered statistically significan.

RESULTS

The patients were divided into two groups: with low and high density of the macrophages and DC in the sinusoidal and periportal spaces on basis of 75th percentile (Table II). Fourteen of the cases (60.9%) had high numbers of CD68-positive macrophages in the sinusoidal and 12 (52.2%) in the periportal tract. The analysis of CD83-positive mature DCs in the sinusoidal and the periportal spaces demonstrated 9 patients (39.1%) with high counts of CD83-DCs in sinusoids, while 14 (60.9%) had high CD83-counts in the periportal tract. The number of CD83-positive DCs in periportal tracts in patients with advanced liver fibrosis (n = 5) were high, while those with mild liver fibrosis (n = 18) had low numbers of mature dendritic cells ($\chi2=4.107$; $p=0.043$). In addition, all patients with intensive fibrosis had low counts of CD68-positive KCs in portal tracts *vs* patients with mild fibrosis of which 67% had high counts ($\chi2=6.97$; $p=0.008$) (Fig. 1 a,b,c).

In seven patients (87.5%) of the cases with moderate steatosis, low numbers of CD68-positive KCs were found in sinusoids, in contrast to severe steatosis where 12 patients (80%) had high KC counts ($\chi2=13.4$; $p<0.001$)

Table I. ***D****emographic, laboratory and histological data of the patients.*

Parameter	Number (%)
Clinical and histological data	*(n=23)*
Age (years)	
median	59.2
(range)	(44-66)
Sex	
male	14 (60.9)
female	9 (39.1)
Chronic viral hepatitis	23 (100)
Steatosis	
absent	-
mild	-
moderate	8 (34.8)
severe	15 (65.2)
Fibrosis	
no	-
mild	18 (78.3)
intensive	5 (21.7)
Portal inflammation	
weak	18 (78.3)
strong	5 (21.7)
AST	38.6 (22.1-140.2)
ALT	35.9 (18.1-78)

Table II. *Distribution and density of CD68- and CD83-positive cells in liver sinusoids and portal tracts.*

a/ Density	Sinusoids	Periportal tracts
CD68		
- mean	39.2	20.3
- median	35.9	13.5
(Range)	(0.27-97)	(0.54-96)
75th percentille	49.7	27
CD83		
- mean	4.87	5
- median	4.05	2.7
(Range)	(0.27-11.9)	(0.3-24.6)
75th percentille	8.1	5.4
b/ Distribution (75th percentile)	**Sinusoids**	**Periportal tracts**
CD68		
low	9 (39.1)	11 (47.8)
high	14 (60.9)	12 (52.2)
CD83		
low	14 (60.9)	9 (39.1)
high	9 (39.1)	14 (60.9)

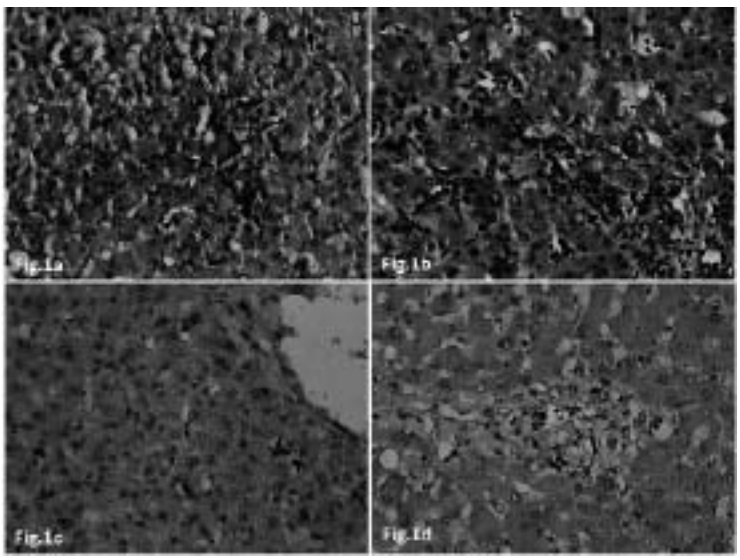

Fig. 1. ***a)*** *Expression of CD68-positive macrophages in liver sinusoids x400.* ***b)*** *Expression of CD68-positive macrophages in liver periportal spaces x400.* ***c)*** *Expression of CD83-positive DCs in liver sinusoids x400.* ***d)*** *Expression of CD83-positive DCs in liver periportal spaces x400.*

(Fig. 1d).

There was no statistical significance between distribution and density of DCs and KCs, and other clinicomorphological data.

DISCUSSION

Chronic hepatitis due to HBV and HCV pregresses with chronic inflammation and destruction of hepatocytes. KCs play a major role in this pathogenetic mechanism, which by the release of nitric oxide and oxidizing radicals has a direct cytotoxic effect on hepatocytes. Another mechanism of liver failure is associated with the production of different cytokines such as interleukins, TNF-α (10). Some authors found a correlation between KCs and the degree of liver failure (11, 12).

We demonstrate variable DC and KC counts in different parts of the liver in relation to fibrosis and steatosis.

Henning et al. carried out an animal study on non-alcoholic steatohepatitis (NASH). They postulated a major role of intrahepatic DC expansion for limiting the sterile inflammation and controlling both innate immune cells like KCs and CD8-positive T-lymphocytes. Furthermore, DCs are involved in clearance of apoptotic cells and cell debris (13). Our data shown that the number of KCs is high in patients with severe steatosis, but this finding is not clear, because our group consisted of patients with chronic hepatitis, but not with NASH or ASH.

Liver fibrosis and cirrhosis are considered as important complications of chronic hepatitis which leads to progressive liver dysfunction and liver failure. KCs are important players in the activation of the liver inflammasome that is necessary for a full fibrotic response. They become activated during this process (14).

Tissue injury causes damaged parenchymal cells, like hepatocytes, to undergo either apoptotic or necrotic cell death. Macrophages clear the dead cells in both cases; however, they typically repress inflammation when phagocytosing apoptotic cells and promote inflammation during necrotic cell removal (15, 16). Macrophages ingesting dying hepatocytes, and dead cells in general, lead to increased TGF-β1 secretion. In this case the phagocytic activity of macrophages is profibrogenic. However, macrophage phagocytosis can also aid in the regression or resolution of fibrosis because by clearing apoptotic myofibroblasts, hepatocytes, and cellular debris they often eliminate the stimuli inducing TGF-β1 and other profibrotic factors (17, 18). The macrophage-dependent proinflammatory response to necrotic cells similarly maintains both pro- and anti-fibrotic potential: firstly by recruiting inflammatory cells, which stimulate fibroblast activity and then by terminating inflammation by cleaning up tissue debris, including the dying inflammatory cells (19).

The role of DC in the development of fibroplastic process in the liver remains controversial (20). In the present study we observed that advanced fibrosis is associated with high numbers of CD83-positive DCs, which is a prerequisite for rapid progression to liver failure .

Our findings argue for a positive correlation of KC numbers in the sinusoidal spaces to the severity of steatosis. Szabo et al. emphasized the importance of the number of immune cells, such as KCs and DCs, in the inflammatory process and the degree of steatosis in murine models of alcoholic steatohepatitis (21). Data from non-alcoholic steatohepatitis argue in the same direction (22). Satoh et al. investigating the significance of KCs in the development of non-alcoholic fatty liver disease after gut-surgery found an up-regulation of different cluster Kupffer cells during this process (23).

In conclusion, our data suggest an active role of CD68-positive KCs and CD83-positive DCs in viral hepatitis associated steatosis, fibrosis and in the development of liver failure.

REFERENCES

1. Zamora Nava LE, Aguirre Valadez J, Chávez-Tapia NC, Torre A. Acute-on-chronic liver failure: a review. Ther Clin Risk Manag 2014; 10:295-303.
2. Tajiri K, Shimizu Y. Liver physiology and liver diseases in the elderly. World J Gastroenterol 2013; 19(46):8459-67.
3. Agrawal A, Sridharan A, Prakash S, Agrawal H. Dendritic cells and aging: consequences for autoimmunity. Expert Rev Clin Immunol 2012; 8(1):73-80.
4. Blois SM, Piccioni F, Freitag N, et al. Dendritic

cells regulate angiogenesis associated with liver fibrogenesis. Angiogenesis 2014; 17(1):119-28.
5. Rahman AH, Aloman C. Dendritic cells and liver fibrosis. Biochim Biophys Acta 2013; 1832(7):998-1004.
6. Lukacs-Kornek V, Schuppan D. Dendritic cells in liver injury and fibrosis: shortcomings and promises. J Hepatol 2013; 59(5):1124-26.
7. Zimmermann HW, Tacke F. Modification of chemokine pathways and immune cell infiltration as a novel therapeutic approach in liver inflammation and fibrosis. Inflamm Allergy Drug Targets 2011; 10(6):509-36.
8. Zimmermann HW, Trautwein C, Tacke F. Functional role of monocytes and macrophages for the inflammatory response in acute liver injury. Front Physiol 2012; 3:56.
9. Guido M, Mangia A, Faa G. Chronic viral hepatitis: the histology report. Dig Liver Dis 2011; 43(S):S331-43.
10. Kolios G, Valatas V, Kouroumalis E. Role of Kupffer cells in the pathogenesis of liver disease. World J Gastroenterol 2006; 12(46):7413-20.
11. McGuinness PH, Painter D, Davies S, McCaughan GW. Increases in intrahepatic CD68 positive cells, MAC387 positive cells, and proinflammatory cytokines (particularly interleukin 18) in chronic hepatitis C infection. Gut 2000; 46(2):260-9.
12. Tomita M, Yamamoto K, Kobashi H, Ohmoto M, Tsuji T. Immunohistochemical phenotyping of liver macrophages in normal and diseased human liver. Hepatology 1994; 20(2):317-25.
13. Henning JR1, Graffeo CS, Rehman A, et al. Dendritic cells limit fibroinflammatory injury in nonalcoholic steatohepatitis in mice. Hepatology 2013; 58(2):589-602.
14. Mehal WZ. The inflammasome in liver injury and non-alcoholic fatty liver disease. Dig Dis 2014; 32(5):507-15.
15. Hotchkiss RS, Strasser A, McDunn JE, Swanson PE. Cell death. N Engl J Med 2009; 361(16):1570-83.
16. Rock KL, Kono H. The inflammatory response to cell death. Annu Rev Pathol 2008; 3:99-126.
17. Iredale JP. Models of liver fibrosis: exploring the dynamic nature of inflammation and repair in a solid organ. J Clin Invest 2007; 117(3):539-48.
18. Iredale JP, Benyon RC, Pickering J, McCullen M, Northrop M, Pawley S, Hovell C, Arthur MJ. Mechanisms of spontaneous resolution of rat liver fibrosis. Hepatic stellate cell apoptosis and reduced hepatic expression of metalloproteinase inhibitors. J Clin Invest 1998; 102(3):538-49.
19. Wynn TA. Common and unique mechanisms regulate fibrosis in various fibroproliferative diseases. J Clin Invest 2007; 117(3):524-9.
20. Pradere JP, Kluwe J, De Minicis S, et al. Hepatic macrophages but not dendritic cells contribute to liver fibrosis by promoting the survival of activated hepatic stellate cells in mice. Hepatology 2013; 58(4):1461-73
21. Szabo G, Petrasek J, Bala S. Innate immunity and alcoholic liver disease. Dig Dis 2012; 1:55-60.
22. Bieghs V, Rensen PC, Hofker MH, Shiri-Sverdlov R. NASH and atherosclerosis are two aspects of a shared disease: central role for macrophages. Atherosclerosis 2012; 220(2):287-93.
23. Satoh D, Yagi T, Nagasaka T, Shinoura S, Umeda Y, Yoshida R, Utsumi M, Tanaka T, Sadamori H, Fujiwara T. CD14 upregulation as a distinct feature of non-alcoholic fatty liver disease after pancreatoduodenectomy. World J Hepatol 2013; 5(4):189-95.

LETTER TO THE EDITOR

ALEXITHYMIA AND ITS RELATIONSHIPS WITH ACUTE PHASE PROTEINS AND CYTOKINE RELEASE: AN UPDATED REVIEW

D. DE BERARDIS[1-2], C. CONTI[2], F. IASEVOLI[3], A. VALCHERA[4], M. FORNARO[5], M. CAVUTO[6], M. BRUCCHI[7], G. PERNA[8,9,10], M. POMPILI[11], A. MODABBERNIA[12], G. LUCIDI[13], M. MAZZA[14], G. MARTINOTTI[2] and M. DI GIANNANTONIO[2]

[1]Department of Mental Health, Psychiatric Service of Diagnosis and Treatment, Hospital "G. Mazzini", ASL 4 Teramo, Italy; [2]Department of Neurosciences and Imaging, University "G. D'Annunzio", Chieti, Italy; [3]Laboratory of Molecular Psychiatry and Psychopharmacotherapeutics, Section of Psychiatry, Department of Neuroscience, University School of Medicine "Federico II", Naples, Italy; [4]Hermanas Hospitalarias, FoRiPsi, Villa S. Giuseppe Hospital, Ascoli Piceno, Italy; [5]Department of "Scienze della Formazione", University of Catania, Italy, [6]IASM, L'Aquila, Italy, [7]National Health Service, U. O. S. D. Senology, Hospital "G. Mazzini", ASL 4, Teramo, Italy; [8]Hermanas Hospitalarias, FoRiPsi, Department of Clinical Neurosciences, Villa San Benedetto Menni, Albese con Cassano, Como, Italy; [9]Department of Psychiatry and Behavioral Sciences, Leonard Miller School of Medicine, University of Miami, USA; [10]Department of Psychiatry and Neuropsychology, University of Maastricht, The Netherlands; [11]Department of Neurosciences, Mental Health and Sensory Organs, Suicide Prevention Center, Sant'Andrea Hospital, Sapienza University of Rome, Italy; [12]Department of Psychiatry and Psychiatry Research Center, Roozbeh Hospital, Tehran University of Medical Sciences, Tehran, Iran; [13]Director, School of Nursing, MeSvA Department, University of L'Aquila, Italy; [14]Department of Life, Health and Environmental Sciences, University of L'Aquila, Italy

Received January 19, 2014 – Accepted August 26, 2014

The alexithymia construct is multidimensional and comprises several features: (a) difficulty in identifying and describing feelings, (b) difficulty in distinguishing feelings from the bodily sensations, (c) diminution of fantasy, and (d) concrete and poorly introspective thinking. Altered immune responses have been seen in some psychiatric disorders and several data suggest that analogous changes could also be observable in alexithymia. Hence, the aim of this review is to investigate the relationships between alexithymia and acute phase proteins and cytokines in psychiatric, psychosomatic and medical diseases. Several studies have reported an association between alexithymia and higher circulating levels of acute phase proteins, especially C-Reactive Protein. Moreover, in alexithymic subjects the pro-inflammatory and anti-inflammatory cytokine balance may be tuned toward a pro-inflammatory imbalance with a concomitant altered cell-mediated immunity. These findings may be consistent with the "stress-alexithymia hypothesis". Therefore, the screening of alexithymic traits and the administration of appropriate

Key words: alexithymia, acute phase proteins, C-Reactive protein, cytokines, stress, HPA, cortisol

Mailing adresss: Domenico De Berardis, MD, PhD.
National Health Service, Department of Mental Health,
Psychiatric Service of Diagnosis and Treatment,
"G. Mazzini" Hospital, p.zza Aldo Moro 1,
64100 Teramo, Italy
Tel.: +39 0861429708 Fax: +39 0861429706
e-mail: dodebera@aliceposta.it

0393-974X (2014)

DISCLOSURE: ALL AUTHORS REPORT NO CONFLICTS OF INTEREST RELEVANT TO THIS ARTICLE.

psychological and psychotherapeutical interventions should be integral parts of disease management programs. Supplying such interventions will probably help with prevention of the development of the disease and/or its exacerbation by improving the quality of life of alexithymic individuals.

The term "alexithymia" was introduced to designate a cluster of cognitive and affective characteristics that were observed among subjects with psychiatric and psychosomatic diseases and may be considered as a personality trait (1). The alexithymia construct is multidimensional and comprises four distinct features: (a) difficulty in identifying (DIF) and describing feelings (DDF), (b) difficulty in distinguishing feelings from the bodily sensations, (c) diminution of fantasy, and (d) concrete and poorly introspective thinking (2). Alexithymics may have affective dysregulation, the inability to self-appease and deal with emotions because of a lack of awareness of emotions (1). These cognitive characteristics have been ascribed to an impaired capability to elevate emotions from a sensorimotor level of experience to a representational level, where they can be used as signaling responses to internal or external events and modulated by psychological mechanisms (2). Because alexithymic subjects are psychologically poorly equipped, they generally demonstrate significantly higher levels of anxiety, depression and general psychological distress and are inclined to suffer both "functional" somatic symptoms and symptoms of emotional turmoil (2, 3).

Alexithymia is easily evaluated with the 20-item Toronto Alexithymia Scale (TAS-20), which is a widely used patient-rated instrument (4). The TAS-20 is composed of 20 items rated on a five-point Likert-type scale, ranging from "strongly disagree" (scored 1) to "strongly agree" (scored 5). Scores range from 20 to 100, with a score of 61 or higher considered indicative of the presence of alexithymic traits (2).

Altered immune responses are seen in psychiatric disorders and several data suggest that analogous changes could also be observable in alexithymia (5, 6), even in absence of comorbid diseases. Altered cell-mediated immunity in alexithymia has been reported. Todarello et al. (7) found that women with alexithymia had lower counts of almost all lymphocytic subsets when compared to women without alexithymia, whereas Dewaraja et al. (8) found that alexithymic men showed decreased cytotoxic lymphocyte count. The possible role of immune system as a mediator between personality and cancer may explain why emotional inhibition is related to greater cancer vulnerability (9). Indeed, the decreased cytotoxic lymphocytes may activate a mechanism that may partially explain the association between alexithymia and neoplasia (10).

The aim of this review was to investigate the relationships between alexithymia and levels of acute phase proteins and cytokines in psychiatric, psychosomatic and medical diseases.

MATERIALS AND METHODS

Searches of the Medline database from 1988 through August 2012 and the PsycInfo/Embase database from 1988 through August 2013 were carried out with the help of a professional librarian (M.C.), restricted to the English language. The search term "alexithymia" was combined with "inflammation", "C-Reactive Protein" (CRP), "cytokines", "interleukin", "anxiety", "depression", "schizophrenia" and "psychosomatic diseases" to identify relevant original research and review articles. All citations were screened, and the full texts of peer-reviewed journal articles considered to be relevant to the purposes of the review were obtained. Relevant articles in press were also included. Bibliographies were scanned to find additional relevant publications, even those prior to 1988.

Alexithymia and acute phase proteins

Several studies reported an association between the presence of alexithymia and higher circulating levels of acute phase proteins, especially CRP. De Berardis et al. (11) measured CRP levels in 145 drug-naïve adult outpatients suffering from major depression (MD) who were assessed using the Italian version of the TAS-20. Alexithymic patients showed higher CRP levels than non-alexithymics even after controlling for age, gender, BMI and smoking status. In a very interesting study on a large sample published in 2011, Honkalampi et al. (6) analyzed data of the Kuopio Depression (KUDEP) general population study (n=308), that focused on the psychological health of a general Finnish population of adults aged 25–64 years. Alexithymia was measured using the TAS-20 and depressive symptoms were assessed using the Beck Depression Inventory (BDI). The authors also measured

the serum levels of CRP and interleukin-6 (IL-6), as the latter seemed to be strongly associated with depression (12). Results showed that higher CRP concentrations were associated with an increased likelihood of alexithymia, even after adjustments for chronic inflammation-related disorders, use of inflammation-modulating medications and depressive symptoms.

Recently, in a very interesting study, Kojima et al. (13) evaluated 213 outpatients with rheumatoid arthritis (RA) using TAS-20, BDI and a visual analogue scale to quantify perceived pain. Moreover, CRP levels were measured to assess inflammation severity. Although no association was observed between pain severity and CRP among alexithymics, depressed patients with alexithymia reported severe pain even at low CRP levels.

Alexithymia and cytokines

Several studies have demonstrated that the presence of alexithymia may influence the cytokine production. Pedrosa Gil et al. (14) found a negative correlation between the severity of alexithymia (total TAS score) and the serum levels of soluble interleukin 2 receptor α (sIL-2 Rα) and IL-4 in subjects with somatoform disorders. A remarkable study was conducted by Corcos et al. (15), who evaluated the relationship between alexithymia and circulating levels of IL-1, IL-2 and IL-4 in healthy women and found a significant association between alexithymia (particularly with the DIF dimension of TAS-20) and serum levels of IL-4. Moreover, an association between alexithymia and increased TNF-alpha and IL-6 levels was found in patients with RA and systemic lupus erythematosus (16). In a study by Guilbaud et al. (17), women with alexithymia showed decreased IL-1b, IL-2 and IL-4 release with reduced ratios of Th1/Th2 (IL-2/IL-10) and of CD4/CD8, as well as reduced CD4 percentages, resembling the same pattern seen in individuals afflicted by chronic stress (18).

Recently, in a well conducted study, Mandarelli et al. (19) recruited 68 patients referred for routine diagnostic upper endoscopy, tested them with TAS-20 and evaluated serum levels of IL-1β, IL-4, IL-6, IL-10, TNF-α and IFN-γ. They found lower IL-4 and IL-6 concentrations in alexithymic patients than in non-alexithymic ones. Moreover, alexithymia predicted low IL-4 and IL-6 levels in the overall sample, independent of stress, anxiety, depression and other possible confounders. In another study on patients with non-inflammatory neurological disorders, increased levels of IL-8 in cerebrospinal fluid were found to be related to the presence of alexithymia and symptoms of anxiety (20). On the other hand, Honkalampi et al. (7) reported that alexithymic subjects had higher serum levels of IL-6 than non-alexithymic subjects, which independently explained approximately 1% of the variation in TAS-20 scores.

Moreover, in a sample of HIV-infected outpatients attending an HIV primary care clinic, alexithymia was related to decreased production of the anti-HIV b-chemokine MIP-1a, shifting the normal balance between pro- and anti-inflammatory cytokines toward the pro-inflammatory ones (21).

How alexithymia may influence inflammation and immune responses? The "Alexithymia-stress hypothesis"

Because several studies have shown a link between alexithymia and stress-related diseases, it has been suggested that the influence of alexithymia on the expression of stress-related pathological conditions might involve a chronic reduced resistance to stress (22). On this basis, the presence of alexithymia can be viewed as a psychological vulnerability factor that may predispose affected individuals to develop several psychiatric and psychosomatic disorders as well as medical diseases (23). The finding of higher CRP and pro-inflammatory cytokine levels among alexithymics may be consistent with the "stress-alexithymia hypothesis": patients with alexithymic traits may be suffering from chronic stress reaction that, on its own, can promote persistent and often subclinical increases in inflammatory factors such as CRP and cytokines (10, 19). Several researchers (7, 10, 24) have suggested that alexithymia is a condition characterized by a pronounced inflammatory state, and, therefore, should be considered a chronic state reaction to stressful situations.

The association of alexithymia with higher circulating cortisol levels suggests that it may chronically enhance sustained hypothalamus-pituitary-adrenal (HPA) axis reactivity to even mild to moderate life stressors (25). Chronic hyperactivation of the HPA-axis is linked to stress-related disorders and cortisol may enhance the release of interleukin-6, one of the major inducers of CRP, and IL-4. This might be responsible for impaired immune response and/or cytokine production observed in subjects with alexithymic traits.

Moreover, it has been demonstrated that cytokine production may be directly stimulated by negative emotions and conversely, cytokines may affect the function of the HPA and sympathetic–adrenal–medullary axis (SAM) systems (25). Substantial evidence of association between negative emotions and alexithymia (4, 5, 9, 13), may further support the presence of a vicious circle of HPA/SAM hyperactivation, chronic inflammatory state and altered immune responses.

Study limitations

Even if in all reviewed studies potential confounding factors such as smoking, substance abuse, fever, current infections, age and gender were considered (as covariates

in statistical analyses concerning smoking, age and gender or exclusion criteria in the case of substance abuse, fever or current infections), all of the studies included in this review had, at least, two major limitations.

In fact, alexithymia was routinely assessed by a self-rated questionnaire, the TAS-20, with possible biases due to the inherent nature of self-rating scales. The disadvantages of self-report questionnaires to measure alexithymia are: 1) reporting bias resulting in minimization or over-reporting of symptom severity, thus reducing validity, 2) the test may not be completed by some individuals, due to illiteracy or impaired cognitive functioning.

Moreover, all of the study settings were cross-sectional. As cross-sectional studies are carried out at one point or over a very short period of time, there are several disadvantages. In fact, the cross-sectional study design does not allow causal conclusions to be made on the relationships among acute phase proteins, depressive symptoms and alexithymia. Moreover, these studies represent only a snapshot of the patient's current status: the situation would have provided differing results if another time-frame had been chosen.

Conclusions and future directions

Alexithymia is associated with higher circulating levels of acute phase proteins, especially CRP. Moreover, in alexithymic subjects the pro-inflammatory and anti-inflammatory cytokine balance is shifted toward a pro-inflammatory state with a concomitant altered cell-mediated immunity. These findings may be consistent with the "stress-alexithymia hypothesis". Moreover, alexithymia may constitute a psychological vulnerability factor that could predispose individuals to several psychiatric and psychosomatic disorders as well as medical diseases. Therefore, the screening of alexithymic traits and the administration of appropriate psychological and psychotherapeutical interventions should be integral parts of disease management programs. Supplying such interventions will probably help with prevention of disease development and/or its exacerbation and with improvement of the quality of life of alexithymic individuals.

As far as the reviewed studies limitations are concerned, the definitive assessments of acute phase proteins, mood states and alexithymia in future studies require that patients should be followed longitudinally, with serial samplings over a specific time frame as well as after clinical remission and pharmacological treatment. Moreover, the availability of the clinician-administered Toronto Structured Interview for Alexithymia (TSIA) (3) may further improve the recognition of alexithimic subjects, bypassing the limitations of TAS-20, and should be routinely employed in future research.

ACKNOWLEDGEMENTS

This paper is dedicated to Prof. Rocco Pollice (1969-2014), a talented, smart and intelligent researcher whose premature death has left a great void in contemporary psychiatry.

The authors thank Mrs. Roberta Polimanti for checking and editing the English language.

REFERENCES

1. De Berardis D, Campanella D, Serroni N, et al. The impact of alexithymia on anxiety disorders: a review of the literature. Curr Psychiatry Rev 2008; 4:80-86.
2. De Berardis D, Campanella D, Gambi F, et al. Insight and alexithymia in adult outpatients with obsessive-compulsive disorder. Eur Arch Psychiatry Clin Neurosci 2005; 255:350-8.
3. De Berardis D, Campanella D, Serroni N, et al. Alexithymia, suicide risk and serum lipid levels among adult outpatients with panic disorder. Compr Psychiatry 2013; 54:517-22.
4. Verrocchio MC, Conti C, Fulcheri M. Deliberate self-harm in substance-dependent patients and relationship with alexithymia and personality disorders: a case-control study. J Biol Regul Homeost Agents 2010; 24:461-9.
5. Guilbaud O, Corcos M, Hjalmarsson L, Loas G, Jeammet P. Is there a psychoneuroimmunological pathway between alexithymia and immunity? Immune and physiological correlates of alexithymia. Biomed Pharmacother 2003; 57:292-5.
6. Honkalampi K, Lehto SM, Koivumaa-Honkanen H, Hintikka J, Niskanen L, Valkonen-Korhonen M, Viinamäki H. Alexithymia and tissue inflammation. Psychother Psychosom 2011; 80:359-64
7. Todarello O, Casamassima A, Daniele S, Marinaccio M, Fanciullo F, Valentino L, Tedesco N, Wiesel S, Simone G, Marinaccio L. Alexithymia, immunity and cervical intraepithelial neoplasia: replication. Psychother Psychosom 1997; 66:208-13.
8. Dewaraja R, Tanigawa T, Araki S, Nakata A, Kawamura N, Ago Y, Sasaki Y. Decreased cytotoxic lymphocyte counts in alexithymia. Psychother Psychosom 1997; 66:83-6.

9. Conti CM, Maccauro G, Fulcheri M. Psychological stress and cancer. Int J Immunopathol Pharmacol 2011; 24:1-5.
10. Todarello O, Casamassima A, Marinaccio M, La Pesa MW, Caradonna L, Valentino L, Marinaccio L. Alexithymia, immunity and cervical intraepithelial neoplasia: a pilot study. Psychother Psychosom 1994; 61:199-204.
11. De Berardis D, Serroni N, Campanella D, et al. Alexithymia and its relationships with C-reactive protein and serum lipid levels among drug naïve adult outpatients with major depression. Prog Neuropsychopharmacol Biol Psychiatry 2008; 32:1982-6.
12. Abbasi SH, Hosseini F, Modabbernia A, Ashrafi M, Akhondzadeh S. Effect of celecoxib add-on treatment on symptoms and serum IL-6 concentrations in patients with major depressive disorder: randomized double-blind placebo-controlled study. J Affect Disord 2012; 141:308-14.
13. Kojima M, Kojima T, Suzuki S, et al, Depression, inflammation and pain in patients with rheumatoid arthritis. Arthritis Care Res 2014; 66:679-86.
14. Pedrosa Gil F, Nickel M, Ridout N, Schwarz MJ, Schoechlin C, Schmidmaier R. Alexithymia and interleukin variations in somatoform disorder. Neuroimmunomodulation 2007; 14:235-42.
15. Corcos M, Guilbaud O, Paterniti S, et al. Correlation between serum levels of interleukin-4 and alexithymia scores in healthy female subjects: preliminary findings. Psychoneuroendocrinology 2004; 29:557-62.
16. Vadacca M, Bruni R, Cacciapaglia F, et al. Alexithymia and immunoendocrine parameters in patients affected by systemic lupus erythematosus and rheumatoid arthritis. Reumatismo 2008; 60:50-6.
17. Guilbaud O, Curt F, Perrin C, et al. Decreased immune response in alexithymic women: a cross-sectional study. Biomed Pharmacother 2009; 63:297-304.
18. Modabbernia A, Taslimi S, Brietzke E, Ashrafi M. Cytokine alterations in bipolar disorder: a meta-analysis of 30 studies. Biol Psychiatry 2013; 74:15-25.
19. Mandarelli G, Tarsitani L, Ippoliti F, Covotta F, Zerella MP, Mirigliani A, Biondi M. The relationship between alexithymia and circulating cytokine levels in subjects undergoing upper endoscopy. Neuroimmunomodulation 2011; 18:37-44.
20. Uher T, Bob P. Cerebrospinal fluid IL-8 levels reflect symptoms of alexithymia in patients with non-inflammatory neurological disorders. Psychoneuroendocrinology 2011; 36:1148-53.
21. Temoshok LR, Waldstein SR, Wald RL, Garzino-Demo A, Synowski SJ, Sun L, Wiley JA. Type C coping, alexithymia, and heart rate reactivity are associated independently and differentially with specific immune mechanisms linked to HIV progression. Brain Behav Immun 2008; 22:781-92.
22. Martin JB, Pihl RO. The stress-alexithymia hypothesis: theoretical and empirical considerations. Psychother Psychosom 1985; 43:169-76.
23. De Berardis D, Campanella D, Gambi F, et al. Alexithymia, fear of bodily sensations, and somatosensory amplification in young outpatients with panic disorder. Psychosomatics 2007; 48:239-46.
24. Uher T. Alexithymia and immune dysregulation: a critical review. Act Nerv Super 2010; 52:40-44.
25. de Timary P, Roy E, Luminet O, Fillée C, Mikolajczak M. Relationship between alexithymia, alexithymia factors and salivary cortisol in men exposed to a social stress test. Psychoneuroendocrinology 2008; 33:1160-64.

JOURNAL OF BIOLOGICAL REGULATORS & HOMEOSTATIC AGENTS Vol. 28, no. 4, 801-807 (2014)

LETTER TO THE EDITOR

EXPRESSION OF POLY(ADP-RIBOSE) POLYMERASE IN BONE REGENERATION

L. LO MUZIO[1], G. PANNONE[1], A. SANTARELLI[2,3], L. LO RUSSO[1], A. DE LILLO[1], C. RUBINI[4], F. BAMBINI[2,3], P. BUFO[1], M. DIOGUARDI[1] and M. PROCACCINI[2,3]

[1]Department of Department of Clinical and Experimental Medicine, Foggia University, Foggia, Italy; [2]Department of Clinic Specialistic and Stomatological Sciences, Marche Polytechnic University, Ancona, Italy; [3]Odontostomatologic Clinic, National Institute of Care and Research on Ageing, Ancona, Italy; [4]Department of Pathologic Anatomy and Histopathology, Marche Polytechnic University, Ancona, Italy

Received September 9, 2013 Accepted October 2, 2014

Poly(ADP-ribose) polymerase (PARP) is a 116kDa enzyme catalysing the synthesis of ADP-ribose polymers from NAD+. PARP is activated in response to DNA strand breaks and plays a critical role in the maintenance of genomic integrity. However, considering its role also in transcription, proliferation as well as apoptosis in biological process, in the present study the role of PARP in bone regeneration was evaluated, in particular in bone cell proliferation and differentiation processes. Thus, formalin fixed paraffin embedded specimens of 10 human bone samples after sinus lift were collected and investigated by immunohistochemistry using a mouse monoclonal anti-human PARP antibody. PARP was expressed in cells with morphological features of osteoblasts in the areas of new bone formation at the junction between mineralized and unmineralized tissue, between osteoid tissue and bone. Few osteoclasts were observed and showed only focal nuclear expression of PARP, while osteocytes showed no positivity for PARP. Our data showed an overall involvement of PARP enzyme in human bone tissues, in particular during bone regeneration process.

Poly(ADP-ribose) polymerase (PARP) is a 116kDa nuclear DNA-binding protein involved in the transfer of long, branched ADP-ribose chains to either itself or different classes of target nuclear proteins involved in chromatin condensation, DNA replication, DNA repairing, and gene expression (1). ADP-ribosylation by PARP plays an important role in several cellular processes, such as apoptosis, necrosis, cell differentiation, and malignant transformation (2). PARP is usually activated in response to DNA strand breaks and plays a critical role in the maintenance of genomic integrity.

PARP is also involved in the regulation of transcription, mediating ADP ribosylation of the transcription factors TATA-binding protein and/or enhancing activator-dependent transcription. PARP has been shown to activate transcription of genes involved in cell proliferation (3).

PARP has an important role also in apoptosis process. During apoptosis CPP32, a proteinase with properties like those of interleukin-1b converting enzyme (ICE), cleaves the death substrate PARP into a stable 85kDa fragment containing the carboxyl terminal and a 25kDa fragment (4). Major fragment

Key words: bone, regeneration, apoptosis, PARP, Poly(ADP-ribose) polymerase

Mailing address:
Prof. Lorenzo Lo Muzio,
Via Rovelli, 48
71122 Foggia, Italy
Tel.: +39 0881 588090
Fax: +39 0881 588081
e-mail: l.lomuzio@unifg.it

0393-974X (2014)

DISCLOSURE: ALL AUTHORS REPORT NO CONFLICTS OF INTEREST RELEVANT TO THIS ARTICLE.

(85kDa) goes into cytoplasm from nucleus (5). This cleavage is the downstream effect in the caspase-dependent programmed cell death. Overexpression of ICE in rat cells causes cell death with overexpression of a functionally related protein Nedd-2, which is a protein similar to the product of the Caernorhabditis elegans cell death gene Ced-3 and the mammalian IL1b converting enzyme (6)The apoptotic effect of these proteins may be suppressed by human bcl-2.

The final goal of this study is to evaluate the expression of PARP in bone processes, in particular in cell proliferation and differentiation during regeneration.

MATERIALS AND METHODS

Formalin-fixed paraffin-embedded specimens of 10 human bone samples taken after sinus lift were collected and examined by immunohistochemistry. PARP protein staining was performed by the avidin-biotin peroxidase method.

Ten patients who needed important maxillary sinus lifts were selected. All patients gave their informed consent to be involved in the study. General exclusion criteria from the study were: uncontrolled diabetes, all the immunosuppressive conditions and systemic diseases that may prevent the intervention. Further exclusions were: chemotherapy and radiation therapy to the head and neck region, during the previous 12 months, sepsis and severe general debilitation. On the local level, the following exclusion criteria were applied: active sinusitis or a history of persistent sinus infections, the presence of maxillary cyst, tumours or the displacement of dental roots, the presence of sinus septa, and active periodontal disease. Complete examinations of soft and hard oral tissue were performed on all patients. In all cases, the site analysis was performed with orthopantomography, intraoral radiograms and axial computerized tomography (dentascan).

After an initial preparation, the sinus lift procedures were performed. In all cases, autologous bone, harvested from omolateral maxillary tuber or from the chin, was used as grafting material. All surgical operations were performed under local anaesthesia. At 1 month after the sinus lift, patients had samples taken by trephine drill and the bone carrots were placed in 4% paraformaldehyde + 0.1% gluteraldehyde buffered with 0.1 m sodium phosphate, ph 7.2, and fixed for 24 h at 4C°. Then washed in 0.1 M phosphate buffer and decalcified for 6 h. The decalcified specimens were washed in PBS buffer, dehydrated in ethanol and embedded in paraffin. Dental implants were positioned four months after sinus grafts and, at this time, a second sample was taken.

Serial 4-micron thick sections were obtained. After antigen retrieval, endogenous peroxidase was inhibited with 3% hydrogen peroxide, and non-specific binding sites were blocked with normal goat serum. Slides were incubated with the primary antibody anti-PARP (mouse monoclonal anti-human PARP antibody against the Carboxyl terminus of the human PARP protein, at 1:100 dilution, overnight, Santa Cruz biotechnology) and then with biotinylated goat anti-mouse (Vector-Quick kit). Slides were washed and incubated for 30 min at room termperature with horseradish-peroxidase-conjugated streptavidin (Dako; 1:1000 dilution). Peroxidase activity was visualized by the application of 3-3'diaminobenzidine (DAB, Sigma Chemical) dissolved in 10 ml of tris buffer and 0.03% H_2O_2 or alternatively with Vector-VIP substrate giving rise to a purple end product. Some sections were then counterstained with haematoxylin. Positive (normal oral epithelium) and negative (by substituting primary antibody with normal goat serum) controls were performed.

Evaluation

The number of PARP-expressing cells was evaluated as a percentage of the final number of 300 cells of each case, and scored in two categories: + <50%, ++ >50% independently of the topographical staining pattern (nuclear or cytoplasmatic).

RESULTS

Interestingly, the bone tissues examined showed very high levels of PARP expression. In particular, concerning the bone regeneration process, we found that PARP was expressed in cells with morphological features of osteoblasts in the areas of new bone formation, at the junction between mineralized and un-mineralized tissue, between osteoid tissue and bone (Figs. 1 and 2). Osteocytes, cells located in lacunae of mature mineralized bone and involved in maintenance of bone vitality, showed no positivity for PARP (Fig. 1).

PARP+ osteoblast count showed a mean of 80%; PARP+ osteocyte count showed a mean <5%.

Few osteoclasts, identified as large multinucleated cells derived from monocytes with abundant acidophilic cytoplasm, showed only focal nuclear expression of PARP.

Comparing data of the two samples for each patient, the cases characterized by a high level of PARP expression in osteoblasts after 1 month

Table I. *Expression of PARP in osteoblasts.*

Case	PARP expression	
	1° month	4° month
1	++	+
2	+	+
3	+	-
4	++	+
5	++	-
6	++	+
7	++	+
8	++	+
9	+	+
10	++	+

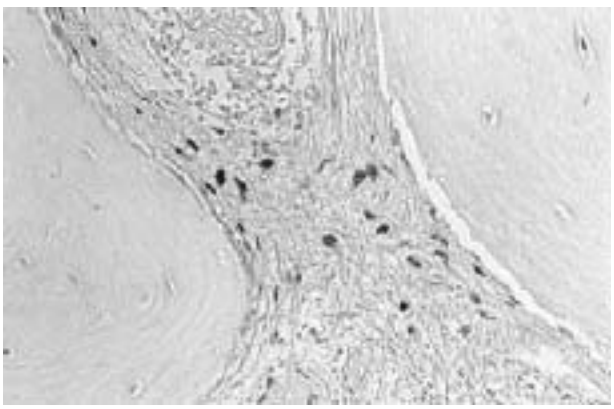

Fig. 1. *Area of new bone formation showing high expression of PARP in the osteoblasts at the junction between mineralized and un-mineralized tissue; osteocytes show no positivity for PARP (400X).*

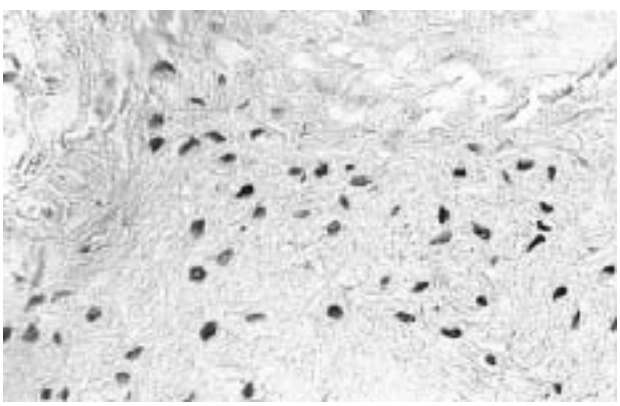

Fig. 2. *Osteoid tissue showing high expression of PARP in osteoblasts synthetizing bone components (400X).*

showed a high grade of bone maturation after 4 months (Table I). After 1 month, 3 cases showed low/moderate PARP expression (+) and 7 high expression (++), after 4 months 8 cases showed low/moderate expression (+) and 2 no expression. Dividing the cases into two groups, A with low/moderate expression (3 cases), and B with high expression of PARP (7 cases), group A showed PARP positivity in 2/3 cases (66%) after 4 months and a lower grade of bone maturation at histological exam compared to group B, while group B showed PARP positivity in 6/7 cases (86%) after 4 months and a more enhanced grade of bone maturation at histological exam than group A. The better grade of bone maturation was detected in the cases showing high PARP expression after the first month and no expression after the third month.

DISCUSSION

The prosthetic rehabilitation of the edentulous posterior maxilla by dental implants has always been a difficult challenge for clinicians the world over (7, 8). In fact, there is often a limited amount of bone between the sinus floor and the alveolar ridge for the placement of a dental implant (9). Anatomic limitations have led to the continual development of surgical tecniques to improve bone quantity and quality. One of these techniques is called "Sinus Grafting", a type of inlay augmentation of the maxillary sinus in order to create more bone height in the edentulous maxilla, which is for the placement of dental implants of sufficient length (10). To date, an ideal bone substitute has not been identified (10). Autologous bone, due to its biological properties, appears to be the best option, hence the term "Gold or Golden Standard" (10). In fact it is the only material that may promote all three bone healing mechanisms: osteogenesis, osteoconduction, osteoinduction (11). However, a recent review suggested that there is no reason to prefer autogenous bone over bone substitutes (11). Indeed, other forms of human bone grafts have been widely used in sinus augmentation techniques, such as fresh frozen bone allograft (FFBA), freeze-dried bone allograft (FDBA) and demineralized freeze-dried bone allograft (DFDBA). Thanks to newer protocols, these materials have been demonstrated to be safe while conservating osteoinduc-

tive properties (11).

However, every material can induce two predominant events in bone: 1) tissue irritation, 2) neohistogenesis and bone regeneration (12). Several studies have examined bone processes during regeneration. However, several mechanisms involved in this physiological process are still unknown.

Our findings demonstrate an overall involvement of PARP enzyme in human bone tissues and in particular during regeneration.

PARP is a 116kDa enzyme catalysing the synthesis of ADP-ribose polymers from NAD+. PARP catalyzes the poly(ADP-ribosyl)ation of nuclear proteins only when bound to single- or double-stranded DNA ends (13) and cycles on and off the DNA ends during DNA repair *in vitro* (14). In addition to undergoing automodification, PARP catalyzes the poly(ADP-ribosyl)ation of such nuclear proteins such as histones, topoisomerases I and II (15), SV40 large T antigen (16), DNA polymerase alpha, proliferating cell nuclear antigen (PCNA) and 15 protein components of the DNA synthesome (17).

PARP is expressed in several cell populations, such as differentiated epithelial (hepatocytes, keratinocytes, and adrenocytes) and connective tissue cells (osteoblasts and fibroblasts) (18).

This protein is certainly involved in cell proliferation processes, as demonstrated by its expression in the basal layers of the epithelium lining skin and oral mucosa (data not shown); it has been suggested that PARP activates the transcription of genes involved in cell proliferation (3).

However, the difference in PARP expression among different tissues indicates that this protein has also other functions than cell proliferation. In fact, PARP is highly expressed in human embryonic tissues in periods in which the normal cell-cycle check-point mechanisms have not yet been activated (19). In this period, characterised by an active cell proliferation, PARP could play a fundamental role in the maintenance of genomic integrity, since it is activated when strand breaks of DNA occur.

PARP is involved also in the apoptosis process and in its inhibition (20, 21)and subsequent late apopain-mediated suppression, of poly(ADP-ribose. Indeed, it has been shown that p53 undergoes extensive poly-(ADP-rybosyl)ation early during the apoptotic program in osteosarcoma cells. Subsequent degradation of poly(ADP-rybose) attached to p53 by PAR-glycohydrolase, seems to be concomitant with the activation of caspase-3 as well as with the induction of expression of the p53 responsive genes bax and fas when cells are irreversibly committed to death (21). Caspase-3-mediated cleavage of 116 kDa PARP protein in a stable 85kDa fragment containing the C-terminus and a smaller 25 kDa fragment is one of the downstream events determining the apoptotic cell death. The poly(ADP-ribosyl)ation of p53 is an early event in apoptosis (21). Co-localization of PARP and p53 in the vicinity of large DNA breaks and their physical association (22) suggest that poly(ADP-ribosyl)ation may regulate the DNA binding ability and, consequently, the function of p53 (21). Poly(ADP-ribosyl)ation of p53 by PARP-1 during early apoptosis in osteosarcoma cells also inhibited p53 interaction with its DNA consensus sequence; thus, poly(ADP-ribosyl)ation may represent a novel mean for regulating transcriptional activation by p53 *in vivo* (23).

Moreover, it is reported that when PARP is cleaved its cellular level of expression rapidly decreased and the resulting fragment was undetectable with anti-PARP antibody (24).

Furthermore, other authors reported that cells expressing bcl-2 and Mcl-1 proteins, in which the process of programmed cell death is inhibited, also express PARP, lamin B and topoisomerase II-alpha nuclear proteins; whereas cells negative for bcl-2 and Mcl-1 showed also loss of the nuclear protein, presence of phosphatidylserine flip and TUNEL positivity, demonstrating activation of the apoptotic cascade (25).

However, we aim to demonstrate that immunohistochemical detection of high level of PARP protein does not indicate activation of programmed cell death, but active cell proliferation in bone.

First of all, we observed that the pattern of PARP expression in human bone is approximately overlapping to that of PCNA expression (data not shown) and, therefore, it does not correspond to the limited areas of induced apoptosis. Proliferating Cell Nuclear Antigen (PCNA) is a KD36 acid nuclear protein involved directly in DNA synthesis, reaching an expression peak during the S phase of cellular cycle

and playing a role in cellular proliferation (26, 27). The gene for human PCNA is transcribed effectively both in quiescent and proliferating cells, but mRNA for PCNA accumulates normally only in proliferating cells. In other words, PCNA immunoreactivity shows the "proliferating compartment" on routinely fixed and processed tissues, providing useful kinetic information.

Our observation of co-expression of PCNA and PARP proteins in regions where an extensive apoptosis is not demonstrated represents further evidence that PARP protein shows a high level of expression in proliferating cells where the apoptotic pathway is inhibited by bcl-2 activation. These findings in human foetal tissues, where p53 check-point protein was undetectable, are in agreement with a previous observation on a fundamental role played in cell proliferation during mice development. In fact, Menisser-de Murcia et al. showed a functional synergy between PARP-1 and ATM (a protein that interacts with double-strand break repair pathways and induces signals resulting in the control of the cell cycle-coupled checkpoints) during a period of mice embryogenesis when cell cycle cheekpoints are not active and the embryo is particularly sensitive to DNA damage (19). Moreover, it was demonstrated that activated poly(ADP-ribose) polymerase 1 (PARP-1) promoted cell proliferation by inhibiting Sp1-mediated checkpoint proteins, such as p21 and p27 (28).

These data and our results seem to demonstrate that the major role of PARP is related to cell proliferation and DNA repairing processes, suggesting that PARP plays a fundamental role in DNA surveillance and cell survival.

Our data showed a marked positivity for PARP in pre-osteoblasts and osteoblasts, bone cells able to proliferate, differentiate and synthesize bone components, while osteocytes, inactive bone cells, showed a very low positivity. This could be due to the different levels of proliferation activity giving an evidence that PARP has an important role in the proliferation and differentiation of bone cells. Specimens characterized by high level of PARP expression in osteoblasts after 1 month showed high grade of bone maturation after 4 months. As expected, these cases showed also reduced PARP expression after 4 months. It is probably due to the fact that in mature bone osteoblasts become surrounded by matrix and mature in osteocytes. Moreover, it is interesting to notice that PARP expression in early stage of bone forming process was required for bone maturation.

Furthermore, a recent paper displayed that PARP-1 activation was required for the inhibition of the brain-type cytoplasmic creatine kinase (Ckb) expression, demonstrating that PARP-1 is a negative regulator of the Ckb expression and that down-regulation of PARP-1 is responsible for the up-regulation of Ckb during RANKL-induced osteoclastogenesis (29).

On the basis of this data we could put PARP forward as a marker to detect bone regeneration. Detecting PARP in bone samples by immunohistochemistry after sinus lift could be an interesting new method to check whether bone grafting has been successful.

Moreover, it is known that osteoblasts differentiate from preostoblasts deriving from stem cells and that these differentiation processes are induced by BPM protein. It would be of scientific interest to study the relationship between BMP expression and PARP expression during the cascade of bone formation ending with the mineralizing osteoblasts.

ACKOWLEDGEMENTS

This work was all or in part supported by the National Scientific Research Programme PRIN 2008 number 20087BNE3K_003.

REFERENCES

1. Lindahl T. Recognition and processing of damaged DNA. J Cell Sci 1995; 19(S):73-77.
2. Lindahl T, Satoh MS, Poirier GG, Klungland A. Post-translational modification of poly(ADP-ribose) polymerase induced by DNA strand breaks. Trends Biochem Sci 1995; 20:405-11.
3. Cervellera MN, Sala A. Poly(ADP-ribose) polymerase is a B-MYB coactivator. J Biol Chem 2000; 275:10692-96.
4. Yuan J, Shaham S, Ledoux S, Ellis HM, Horvitz HR. The C. elegans cell death gene ced-3 encodes a protein similar to mammalian interleukin-1 beta-converting enzyme. Cell 1993; 75:641-52.
5. Soldani C, Lazze MC, Bottone MG, Tognon G, Big-

giogera M, Pellicciari CE, Scovassi AI. Poly(ADP-ribose) polymerase cleavage during apoptosis: when and where? Exp Cell Res 2001; 269:193-201.
6. Miura M, Zhu H, Rotello R, Hartwieg EA, Yuan J. Induction of apoptosis in fibroblasts by IL-1 beta-converting enzyme, a mammalian homolog of the C. elegans cell death gene ced-3. Cell 1993; 75:653-60.
7. Jensen OT, Shulman LB, Block MS, Iacono VJ. Report of the Sinus Consensus Conference of 1996. Int J Oral Maxillofac Implants 1998; 13(S):11-45.
8. Bambini F, Greci L, Memè L, Santarelli A, Carinci F, Pezzetti F, Procaccini M, Lo Muzio L. Raloxifene covalently bonded to titanium implants by interfacing with (3-aminopropyl)-triethoxysilane affects osteoblast-like cell gene expression. Int J Immunopathol Pharmacol 2006; 19:905-14.
9. Bambini F, Pellecchia M, Memè L, Santarelli A, Emanuelli M, Procaccini M, Lo Muzio L. Anti-inflammatory cytokines in peri-implant soft tissues: A preliminary study on humans using cDNA microarray technology. Eur J Inflamm 2007; 5:121-27.
10. Geurs NC, Wang IC, Shulman LB, Jeffcoat MK. Retrospective radiographic analysis of sinus graft and implant placement procedures from the Academy of Osseointegration Consensus Conference on Sinus Grafts. Int J Periodontics Restorative Dent 2001; 21:517-23.
11. Nkenke E, Stelzle F. Clinical outcomes of sinus floor augmentation for implant placement using autogenous bone or bone substitutes: a systematic review. Clin Oral Implants Res 2009; (S)4:123-33.
12. Bauer TW, Muschler GF. Bone graft materials. An overview of the basic science. Clin Orthop 2000; 371:10-27.
13. Cope JB, Samchukov ML, Muirhead DE. Distraction psteogenesis and histogenesis in beagle dogs: the effect of gradual mandibular osteodistraction on bone and gingiva. J Periodontol 2002; 73:271-82.
14. Gradwohl G, Menissier de-Murcia JM, Molinete M, Simonin F, Koken M, Hoeijimakers JH, de Murcia G. The second zinc-finger domain of poly(ADP-ribose) polymerase determines specificity for single-stranded breaks in DNA. Proc Natl Acad Sci USA 1990; 87:2990-4.
15. Smulson ME, Pang D, Jung M, et al. Irreversible binding of poly(ADP-ribose) polymerase cleavage product to DNA ends revealed by atomic force microscopy: possible role in apoptosis. Cancer Res 1998; 58:3495-98.
16. Kasid UN, Halligan B, Liu LF, Dritschilo A, Smulson M. Poly(ADPribose)-mediated post-translational modification of chromatin-associated human topoisomerase I. Inhibitory effects on catalytic activity. J Biol Chem 1989; 264:18687-92.
17. Baksi K, Alkhatib H, Smulson ME. *In vivo* characterization of the poly(ADP-ribosyl)ation of SV40 chromatin and large T antigen by immunofractionation. Exp Cell Res 1987; 172:110-23.
18. Simbulan-Rosenthal CMG, Rosenthal DS, Hilz H, et al. The expression of poly(ADPribose) polymerase during differentiation-linked DNA replication reveals that this enzyme is a component of the multiprotein DNA replication complex. Biochemistry 1996; 35:11622-33.
19. Dal Pra I, Tognana E, Guerriero C, Armato U. Investigations into mechanisms modulating proliferation, differentiation, and apoptosis in cultured liver, adrenal, skin, and bone cells. Ital J Anat Embryol 1997; 102:9-119.
20. Menisser-de Murcia J, Mark M, Wendling O, Wynshaw-Boris A, de Murcia G. Early embryonic lethality in PARP-1 Atm double-mutant mice suggests a functional synergy in cell proliferation during development. Mol Cell Biol 2001; 21:1828-32.
21. Lo Muzio L, Sartini D, Santarelli A, et al. Expression and prognostic significance of apoptotic genes in oral squamous cell carcinoma. Mol Carcinog 2014; 53:264-71.
22. Simbulan-Rosenthal CM, Rosenthal DS, Luo R, Smulson ME. Poly(ADP-ribosyl)ation of p53 during apoptosis in human osteosarcoma Cells. Cancer Research 1999; 59:2190-94.
23. Vaziri H, West M, Allsop R, Davison T, Wu Y, Arrowsmith C, Poirier G, Benchimol S. ATM-dependent telomere loss in aging human diploid fibroblasts and DNA damage lead to the posttranslational activation of p53 protein involving poly(ADP-ribose) polymerase. EMBO J 1997; 16:6018-33.
24. Simbulan-Rosenthal CM, Rosenthal DS, Luo RB, Samara R, Jung M, Dritschilo A, Spoonde A, Smulson ME. Poly(ADP-ribosyl)ation of p53 *in vitro* and *in vivo* modulates binding to its DNA consensus se-

quence. Neoplasia 2001; 3:179-88.
25. Alexandre S, Rast C, Nguyen-Ba G, Poirier GG, Vasseur P. PARP degradation in apoptotic Syrian hamster embryo (SHE) cells compared to HL60 cell line. Biochimie 2000; 82:1115-22.
26. Lo Muzio L, Santarelli A, Orsini G, et al. MG63 and MC3T3-E1 osteoblastic cell lines response to raloxifene. Eur J Inflamm 2013; 4:757-64
27. Waseem NH, Lane DP. Monoclonal antibody analysis of the proliferating cell nuclear antigen (PCNA), structural conservation and the detection of a nucleolar form. J Cell Science 1990; 96:121-29.
28. Yang L, Huang K, Li X, et al. Identification of poly(ADP-ribose) polymerase-1 as a cell cycle regulator through modulating Sp1 mediated transcription in human hepatoma cells. PLoS One 2013; 8:e82872.
29. Chen J, Sun Y, Mao X, Liu Q, Wu H, Chen Y. RANKL Up-regulates brain-type creatine kinase via Poly(ADP-ribose) Polymerase-1 during osteoclastogenesis. J Biol Chem 2010; 285:363156-21.

ERRATA CORRIGE

Vol. 28 No. 1, Page 107, in the article entitled: "Olea europea-derived phenolic products attenuate antinociceptive morphine tolerance: an innovative strategic approach to treat cancer pain" the authors and affiliations should read as follows:

C. MUSCOLI[1,2,3], F. LAURO[1,2,3], C. DAGOSTINO[1,2,3], S. ILARI[1,2,3], L.A. GIANCOTTI[4], M. GLIOZZI[1,2], N. COSTA[1], C. CARRESI[1,2], V. MUSOLINO[1,2], F. CASALE[1], D. VENTRICE[4], M. OLIVERIO[1], E. PALMA[1], S. NISTICÒ[1], A. PROCOPIO[1], M. RIZZO[5] and V. MOLLACE[1,2,3]

[1]Department of Health Sciences, University "Magna Graecia", Germaneto, Catanzaro, Italy; [2]Interregional Research Center for Food Safety and Health (IRC-FSH), Germaneto, Catanzaro, Italy; [3]Drug Center, IRCCS San Raffaele Pisana, Roma, Italy; [4]CETA, ArpaCal, Catanzaro, Italy; [5]Department of Pharmacology, University of Catania, Italy

Vol. 12, No 3, September - December 2014

ISSN 1721-727X

2011
IMPACT
FACTOR
0.990

European Journal of Inflammation

Cima da Conegliano *"Madonna con il Bambino"*

Published by
Biolife

www.biolifesas.org

Vol. 27, No 4, October - December 2014

ISSN 0394-6320/2014

2013
IMPACT
FACTOR
2.507

International Journal of Immunopathology and Pharmacology

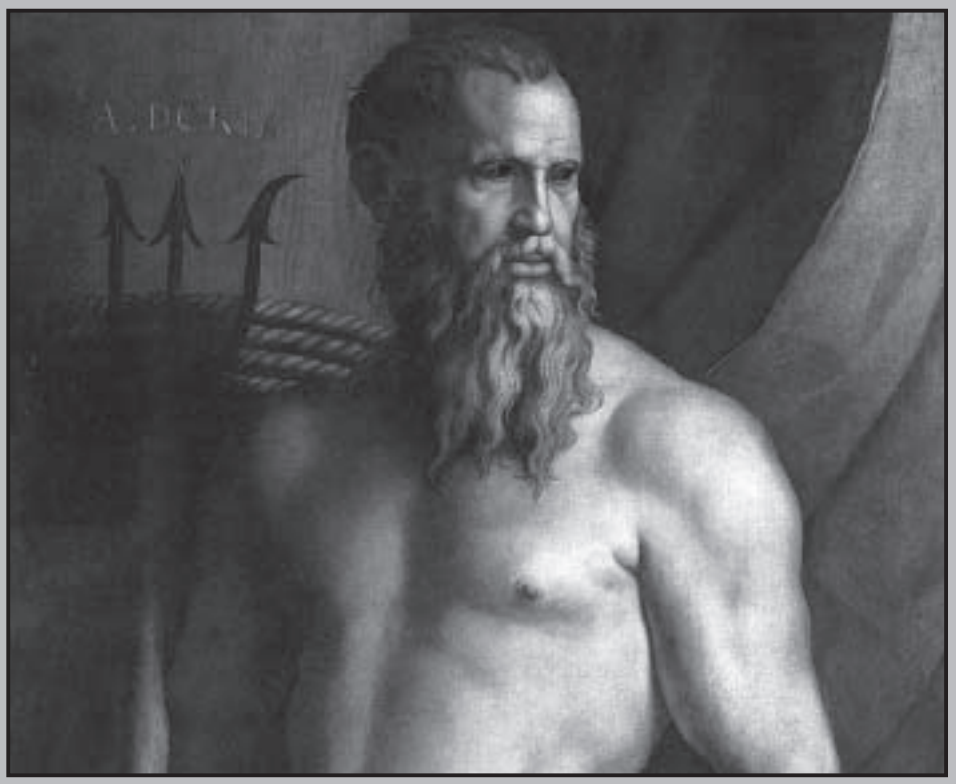

Agnolo Bronzino *"Ritratto di Andrea Doria nelle vesti di Nettuno" (Detail)*

Published by
Biolife

www.biolifesas.org